RHIZOSPHERE FUNCTIONING AND STRUCTURAL DEVELOPMENT AS COMPLEX INTERPLAY BETWEEN PLANTS, MICROORGANISMS AND SOIL MINERALS

EDITED BY: Carsten W. Mueller, Andrea Carminati, Christina Kaiser, Jens-Arne Subke and Caroline Gutjahr

PUBLISHED IN: Frontiers in Environmental Science, Frontiers in Plant Science and Frontiers in Microbiology

frontiers Research Topics

frontiers

ISSN 1664-8714
ISBN 978-2-88963-207-7
DOI 10.3389/978-2-88963-207-7

About Frontiers

Frontiers is more than just an open-access publisher of scholarly articles: it is a pioneering approach to the world of academia, radically improving the way scholarly research is managed. The grand vision of Frontiers is a world where all people have an equal opportunity to seek, share and generate knowledge. Frontiers provides immediate and permanent online open access to all its publications, but this alone is not enough to realize our grand goals.

Frontiers Journal Series

The Frontiers Journal Series is a multi-tier and interdisciplinary set of open-access, online journals, promising a paradigm shift from the current review, selection and dissemination processes in academic publishing. All Frontiers journals are driven by researchers for researchers; therefore, they constitute a service to the scholarly community. At the same time, the Frontiers Journal Series operates on a revolutionary invention, the tiered publishing system, initially addressing specific communities of scholars, and gradually climbing up to broader public understanding, thus serving the interests of the lay society, too.

Dedication to Quality

Each Frontiers article is a landmark of the highest quality, thanks to genuinely collaborative interactions between authors and review editors, who include some of the world's best academicians. Research must be certified by peers before entering a stream of knowledge that may eventually reach the public - and shape society; therefore, Frontiers only applies the most rigorous and unbiased reviews.
Frontiers revolutionizes research publishing by freely delivering the most outstanding research, evaluated with no bias from both the academic and social point of view. By applying the most advanced information technologies, Frontiers is catapulting scholarly publishing into a new generation.

What are Frontiers Research Topics?

Frontiers Research Topics are very popular trademarks of the Frontiers Journals Series: they are collections of at least ten articles, all centered on a particular subject. With their unique mix of varied contributions from Original Research to Review Articles, Frontiers Research Topics unify the most influential researchers, the latest key findings and historical advances in a hot research area! Find out more on how to host your own Frontiers Research Topic or contribute to one as an author by contacting the Frontiers Editorial Office: researchtopics@frontiersin.org

RHIZOSPHERE FUNCTIONING AND STRUCTURAL DEVELOPMENT AS COMPLEX INTERPLAY BETWEEN PLANTS, MICROORGANISMS AND SOIL MINERALS

Topic Editors:
Carsten W. Mueller, Technical University of Munich, Germany
Andrea Carminati, University of Bayreuth, Germany
Christina Kaiser, University of Vienna, Germany
Jens-Arne Subke, University of Stirling, Scotland
Caroline Gutjahr, Technical University of Munich, Germany

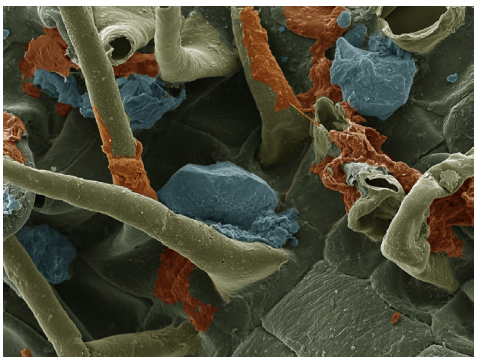

Image: Carsten W. Mueller

"Rhizoplane with attached soil minerals and microbial residues"

The rhizosphere, the soil volume, which is directly affected by root activity, is an important hot spot for a multitude of biotic and abiotic processes. Carbon transfer from plants to microorganisms and to soil takes place in these small volumes around living roots, creating chemical gradients and zones of microbial activity over distinct temporal and spatial scales. Hydraulic and biogeochemical properties of the rhizosphere and the formation of complex three-dimensional structures such as micro- and macroaggreates in turn, result from complex feedbacks between physical, chemical and biological processes. The aim of this Research Topic is to advance our understanding of rhizosphere interactions by collating 16 original contributions across disciplines, including original research, reviews and specific methods on the processes taking place in the rhizosphere, to shed new light on one of the most important interfaces for the diversity of life on earth.

Citation: Mueller, C. W., Carminati, A., Kaiser, C., Subke, J.-A., Gutjahr, C., eds. (2019). Rhizosphere Functioning and Structural Development as Complex Interplay between Plants, Microorganisms and Soil Minerals. Lausanne: Frontiers Media. doi: 10.3389/978-2-88963-207-7

Table of Contents

frontiers in Environmental Science

EDITORIAL
published: 10 September 2019
doi: 10.3389/fenvs.2019.00130

Editorial: Rhizosphere Functioning and Structural Development as Complex Interplay Between Plants, Microorganisms and Soil Minerals

Carsten W. Mueller[1]*, *Andrea Carminati*[2], *Christina Kaiser*[3], *Jens-Arne Subke*[4] and *Caroline Gutjahr*[5]

[1] Chair of Soil Science, TUM School of Life Sciences Weihenstephan, Technical University of Munich, Munich, Germany, [2] Department of Soil Physics, Bayreuth Center of Ecology and Environmental Research, University of Bayreuth, Bayreuth, Germany, [3] Division of Terrestrial Ecosystem Research, Department of Microbiology and Ecosystem Science, University of Vienna, Vienna, Austria, [4] Biological and Environmental Sciences, University of Stirling, Stirling, Scotland, [5] Plant Genetics, TUM School of Life Sciences Weihenstephan, Technical University of Munich, Munich, Germany

Keywords: arbuscular mycorrhizal fungi, soil structure, aggregation, hot spot, mucilage, rhizodeposition, root exudation, hyphosphere

Editorial on the Research Topic

Rhizosphere Functioning and Structural Development as Complex Interplay Between Plants, Microorganisms and Soil Minerals

OPEN ACCESS

Edited and reviewed by:
Balwant Singh,
University of Sydney, Australia

***Correspondence:**
Carsten W. Mueller
carsten.mueller@wzw.tum.de

Specialty section:
This article was submitted to Soil Processes, a section of the journal Frontiers in Environmental Science

Received: *06 August 2019*
Accepted: *22 August 2019*
Published: *10 September 2019*

Citation:
Mueller CW, Carminati A, Kaiser C, Subke J-A and Gutjahr C (2019) Editorial: Rhizosphere Functioning and Structural Development as Complex Interplay Between Plants, Microorganisms and Soil Minerals. Front. Environ. Sci. 7:130. doi: 10.3389/fenvs.2019.00130

The rhizosphere, the soil volume, which is directly affected by root activity (Hinsinger et al., 2009), is an important hot spot for a multitude of biotic and abiotic processes (Lambers et al., 2009). Carbon transfer from plants to microorganisms and to soil takes place in these small volumes around living roots, creating chemical gradients and zones of microbial activity over distinct temporal and spatial scales. Hydraulic and biogeochemical properties of the rhizosphere and the formation of complex three-dimensional structures such as micro- and macroaggreates in turn, result from complex feedbacks between physical, chemical and biological processes. The aim of this Research Topic is to advance our understanding of rhizosphere interactions by collating 16 original contributions across disciplines, including original research, reviews and specific methods on the processes taking place in the rhizosphere, to shed new light on one of the most important interfaces for the diversity of life on earth.

Growing roots are at the core of the rhizosphere and dynamically impact soil structure through the spatial rearrangement of mineral soil particles due to the physical pressure exerted by their growth. Continued growth and branching resulting in constantly changing root architectures that continuously alter the spatial extent of the rhizosphere. To account for these constant spatiotemporal changes, Schlüter et al. developed a new method to model root architecture and estimate rhizosphere volume via a combination of time-lapse μCT imaging, image registration and root distance modeling. Besides exerting pressure, roots also secrete mucilage from their tips, which impacts the physical properties of the rhizosphere microenvironment (Carminati et al., 2011). Haas et al. used gel-like model substances to understand the behavior of mucilage in soils. They found that the capacity of these substances to stabilize soil particles depends on their deformation capacity. In addition, mucilage dynamically modifies mechanical properties of the soil matrix such as the penetration

resistance (Haas and Horn) and hydraulic properties of the soil solution (Benard et al., 2019). While the importance of mucilage for rhizosphere hydration and root growth is well-recognized (Carminati et al., 2011), direct measurements of mucilage in intact soils remain challenging. Holz et al. present a promising approach using infrared spectroscopy to measure the distribution of mucilage in the rhizosphere, making use of the C-H signals of mucilage fatty acids. By the application of exudate mixtures via artificial rhizospheres to top- and sub-soils, Baumert et al. demonstrate that higher levels of root exudates lead to an increased macro-aggregation of subsoil material. The authors thus demonstrate soil structure formation driven by root exudation in a soil compartment that was previously thought to be determined mainly by physical rather than biological processes. However, the mechanisms of root exudation of primary metabolites are not yet fully understood. In a comprehensive review, Canarini et al. propose that root exudation rates are regulated via source-sink driven dynamic processes, rather than occurring as a passive leaking of exudates.

Growing roots and hyphae of mycorrhizal fungi release tremendous amounts of organic carbon derived from photosynthesis into soil compartments at depths that otherwise receive only small amounts of dissolved organic matter leached from litter. The exudation of organic compounds into the rhizosphere can prime the decomposition of previously stabilized inherited soil organic matter (Baumert et al.). In addition to the roots themselves, mycorrhiza fungi function as vectors for plant derived organic matter into the root free bulk soil, where the "hyphosphere" fosters nutrient acquisition, soil aggregation and the allocation of initially plant derived organic matter into more stable organo-mineral associations (Gorka et al.; Vidal et al.). Although being structurally different to the rhizosphere, the mycorrhizal hyphosphere thus may extend some of the rhizosphere's functions, including soil structure formation and the sequestration of initially plant derived organic carbon.

Mycorrhiza fungi not only facilitate carbon flow into the soil but their primary function for plants seems to be aid in the uptake of mineral nutrients. Arbuscular mycorrhiza fungi (AMF) especially provide the host plant with phosphate. Using a tomato—*Rhizophagus irregularis* (AMF) model system grown in pure sand or sand mixed with goethite Andrino et al. show that plants have to invest more carbon for per unit of fungal-delivered phosphate, when the phosphate is strongly adsorbed to a substrate such as goethite. This implies that mycorrhiza-mediated carbon flow into the rhizosphere may be co-determined by soil physico-chemical properties. Molecular processes underlying arbuscular mycorrhizal nutrient exchange are mainly studied under laboratory conditions, although application of the symbiosis will happen in the field. In his review, Kobae summarizes the current knowledge on arbuscular mycorrhizal phosphate uptake and advocates for more research toward understanding arbuscular mycorrhizal phosphate uptake under complex field conditions. The complexity of plant-fungal-soil interactions is exemplified by Paymaneh et al., who show that the growth of strongly AMF-dependent plant *Antropogon gerardii* is inhibited by the addition of biochar to soil, while growth can be partially recovered after the addition of AMF, the extend of which is dependent on the acidity or alkalinity of the soil. Using split root systems, Henkes et al. show that AMF alter the N-uptake and -allocation patterns facilitated by protists in wheat; and that mycorrhiza and protists together determine the rhizosphere microbial community in a systemic manner.

Volatile organic compounds (VOC) emitted by soil microbes are known to modulate root growth (Sharifi and Ryu, 2018). Schenkel et al. exhibit another example for the complexity of biotic interactions in the soil by demonstrating that several *Fusarium* isolates, reduced VOC emissions from soils thereby allowing increased elongation of Arabidopsis primary roots.

A better understanding of roots and rhizosphere functioning under drought is critical to adaptations to rapid climate change and frequent occurrences of climate extremes. Soil management and plant breeding needs to aim for increasing efficiency in plant water acquisition and for keeping water in the soil. Breeding efforts for producing drought resistant cultivars can lead to distinct alterations in the rhizosphere bacterial communities as demonstrated by Li et al. for drought and insect resistant rice cultivars. As reviewed by Yu and Hochholdinger different plant genotypes also develop different root systems and produce different chemical cocktails in their root exudate, which can determine the physical and chemical properties of the rhizosphere and the species composition of its inhabiting microbiota. They state that the resolution of conventional sampling strategies used to describe root endosphere and rhizosphere microbiota communities is too coarse to capture such differences, and emphasize laser capture microdissection in combination with next-generation sequencing as a promising route to elucidate plant microbe interactions in the future. Interestingly, in grafted cultivated plants such a wine, the endosphere and rhizosphere community differs in function of the rootstock (D'Amico et al.).

Since the rhizosphere is hidden in the soil matrix it was previously difficult to extensively explore its complex interactions. To study intact soil environments like the rhizosphere, different imaging techniques play a crucial role, as for instance approaches to trace enzyme activities like the *in-vivo* imaging of phosphatase activity along intact root systems (Dinkelaker and Marschner, 1992). With the advent of high resolution spectromicroscopic imaging techniques it is now possible to directly study plant-microorganism-soil interactions using a wide array of visualization techniques from infrared spectroscopy to nanoscale secondary ion mass spectrometry (Gorka et al.; Holz et al.; Vidal et al.). As demonstrated by Gorka et al. it is vital to get down to micro and nanoscale measurements to gain a more complete understanding of water and nutrient supply and microbial activity at the relevant process scale. The complex nature of active rhizosphere thus asks for a combined approach of chemical, biological and physical concepts and methods (Gorka et al.; Vidal et al.). Gaining a deeper understanding of the rhizosphere as a driving force in ecosystem functionality, can be fostered by interdisciplinary collaborations involving soil physics, microbiology, plant physiology, and

biogeochemistry disciplines (Baumert et al.; Haas et al.; Vidal et al.).

This Research Topic highlights the rapid rate of advancements in rhizosphere research. Continuous improvements in imaging methods together with the combination of interdisciplinary approaches aiming at linking physical, chemical, and biological processes is fostering new understanding of the belowground interactions between soil, microorganisms and plants, as well as of the significance of these processes for plant performance and adaptation to biotic and abiotic stresses.

AUTHOR CONTRIBUTIONS

All authors listed have made a substantial, direct and intellectual contribution to the work, and approved it for publication.

ACKNOWLEDGMENTS

We acknowledge the financial support in the frame of the DFG priority program Rhizosphere Spatiotemporal Organisation—a Key to Rhizosphere Functions (SPP 2089; MU 3021/11-1).

REFERENCES

Benard, P., Zarebanadkouki, M., Brax, M., Kaltenbach, R., Jerjen, I., Marone, F., et al. (2019). Microhydrological niches in soils: how mucilage and EPS alter the biophysical properties of the rhizosphere and other biological hotspots. *Vadose Zone J.* 18, 1–10. doi: 10.2136/vzj2018.12.0211

Carminati, A., Schneider, C. L., Moradi, A. B., Zarebanadkouki, M., Vetterlein, D., Vogel, H. J., et al. (2011). How the rhizosphere may favor water availability to roots. *Vadose Zone J.* 10, 988–998. doi: 10.2136/vzj2010.0113

Dinkelaker, B., and Marschner, H. (1992). *In vivo* demonstration of acid-phosphatase-activity in the rhizosphere of soil-grown plants. *Plant Soil* 144, 199–205.

Hinsinger, P., Bengough, A. G., Vetterlein, D., and Young, I. M. (2009). Rhizosphere: biophysics, biogeochemistry and ecological relevance. *Plant Soil* 321, 117–152. doi: 10.1007/s11104-008-9885-9

Lambers, H., Mougel, C., Jaillard, B., and Hinsinger, P. (2009). Plant-microbe-soil interactions in the rhizosphere: an evolutionary perspective. *Plant Soil* 321, 83–115.

Sharifi, R., and Ryu, C. M. (2018). Sniffing bacterial volatile compounds for healthier plants. *Curr. Opin. Plant Biol.* 44, 88–97. doi: 10.1016/j.pbi.2018.03.004

Conflict of Interest Statement: The authors declare that the research was conducted in the absence of any commercial or financial relationships that could be construed as a potential conflict of interest.

frontiers in Plant Science

ORIGINAL RESEARCH
published: 24 July 2018
doi: 10.3389/fpls.2018.01084

Quantification of Root Growth Patterns From the Soil Perspective via Root Distance Models

Steffen Schlüter[1]*, *Sebastian R. G. A. Blaser*[1], *Matthias Weber*[2], *Volker Schmidt*[2] and *Doris Vetterlein*[1,3]

[1] Department of Soil System Science, Helmholtz-Centre for Environmental Research – UFZ, Halle, Germany, [2] Institute of Stochastics, Ulm University, Ulm, Germany, [3] Soil Science, Martin-Luther-University Halle-Wittenberg, Halle, Germany

The rhizosphere, the fraction of soil altered by plant roots, is a dynamic domain that rapidly changes during plant growth. Traditional approaches to quantify root growth patterns are very limited in estimating this transient extent of the rhizosphere. In this paper we advocate the analysis of root growth patterns from the soil perspective. This change of perspective addresses more directly how certain root system architectures facilitate the exploration of soil. For the first time, we propose a parsimonious root distance model with only four parameters which is able to describe root growth patterns throughout all stages in the first 3 weeks of growth of *Vicia faba* measured with X-ray computed tomography. From these models, which are fitted to the frequency distribution of root distances in soil, it is possible to estimate the rhizosphere volume, i.e., the volume fraction of soil explored by roots, and adapt it to specific interaction distances for water uptake, rhizodeposition, etc. Through 3D time-lapse imaging and image registration it is possible to estimate root age dependent rhizosphere volumes, i.e., volumes specific for certain root age classes. These root distance models are a useful abstraction of complex root growth patterns that provide complementary information on root system architecture unaddressed by traditional root system analysis, which is helpful to constrain dynamic root growth models to achieve more realistic results.

Keywords: x-ray tomography, euclidean distance, root system architecture, time-lapse imaging, parametric model

OPEN ACCESS

Edited by:
Jens-Arne Subke,
University of Stirling, United Kingdom

Reviewed by:
Kris Vissenberg,
University of Antwerp, Belgium
Tony Pridmore,
University of Nottingham, United Kingdom
Katherine Sinacore,
University of New Hampshire, United States

***Correspondence:**
Steffen Schlüter
steffen.schlueter@ufz.de

Specialty section:
This article was submitted to Plant Microbe Interactions, a section of the journal Frontiers in Plant Science

Received: *08 February 2018*
Accepted: *05 July 2018*
Published: *24 July 2018*

Citation:
Schlüter S, Blaser SRGA, Weber M, Schmidt V and Vetterlein D (2018) Quantification of Root Growth Patterns From the Soil Perspective via Root Distance Models. Front. Plant Sci. 9:1084. doi: 10.3389/fpls.2018.01084

INTRODUCTION

Root-soil interactions are an essential part of global matter cycles as all water and nutrients taken up by the plant have to be transported through the rhizosphere (York et al., 2016). Roots have to fulfill a range of different functions at the same time, resulting in the plasticity of the root system, with individual root segments changing their function during ontogeny (Vetterlein and Doussan, 2016; Morris et al., 2017). The consortium of root segments comprising the root system can thus adapt to heterogeneity in resource availability and demand in time and space (Carminati and Vetterlein, 2012). The actual root system architecture is both a manifestation of genetic predisposition and environmental factors (De Smet et al., 2012). There is a genotype specific regulation of root development (Atkinson et al., 2014). However, this program is modified by soil traits like bulk density, soil structure, water distribution or nutrient supply (Drew, 1975; Passioura, 1991; Robinson, 1994; Malamy, 2005; Hodge et al., 2009; Smith and De Smet, 2012; Giehl and von Wiren, 2014).

The rhizosphere, i.e., the zone of soil modified by the roots, is closely related to root system architecture. The spatial arrangement of root segments determines the fraction of the soil volume directly altered by roots with respect to a specific process. An even distribution of root segments may be advantageous, and cost effective in terms of carbon investment as well as for the acquisition of resources that have a high fluctuation over time like water. However, clustering of roots may be beneficial for resource acquisition that requires alteration of biochemical properties (Ho et al., 2005; Lynch and Ho, 2005).

Methods to quantify root system architecture—the three-dimensional distribution of the root system from a single plant within the soil volume—have so far mainly focused on the plant perspective (Danjon and Reubens, 2008; Iyer-Pascuzzi et al., 2010; Clark et al., 2011; Flavel et al., 2017). Traditionally, destructive sampling is carried out, separating the roots from soil by washing and detecting roots visually (Tennant, 1975) or by semi-automatic detection with a flat scanner and analysis with WinRHIZO (Regent Instruments, Canada). Results are presented as root length density, root surface or root volume distributed over a certain sampling depth, occasionally, specified for certain root diameter classes. Alternatively root system architecture in the field has been described by tedious and only semi-quantitative root profile methods and drawings as in Kutschera (1960).

The rise of non-invasive imaging methods like X-ray computed tomography (X-ray CT) and magnetic resonance imaging (MRI) has enabled the analysis of undisturbed root system architecture (Helliwell et al., 2013; Schulz et al., 2013). This has brought about additional insights into root networks like branching patterns (Flavel et al., 2017), root-soil contact (Carminati et al., 2012; Schmidt et al., 2012) and root growth response to localized application of e.g., phosphorus (Flavel et al., 2014). In addition, it enables repeated sampling to analyze root growth dynamics (Koebernick et al., 2014, 2015; Helliwell et al., 2017). However, these approaches focus on the plant perspective and are not able to describe all spatial aspects of root-soil interactions. Complementary information on root growth patterns is provided instead by a shift toward the soil perspective. That is, the root growth patterns are not characterized solely based on root traits, but based on consequences that these patterns have for the exploration of soil. For any soil voxel, the distance to the closest root voxel can be determined by employing the so-called Euclidean distance transform on segmented 3D root images. The concept has been suggested by van Noordwijk et al. (1993), however, at the time they could only apply it to a stack of 2D slices from resin embedded samples and calculations were very tedious. This might explain why the concept has not been adopted more widely, despite the fact that numerous studies have shown that alterations of soil properties by the root in the rhizosphere extend to a distance which is specific for the process in question (Hinsinger et al., 2009). We suggest to use distance maps not only as a tool to approximate travel distances in radial transport to and from the root, but also as a genuine alternative to describe root system architecture. To our knowledge the only study in this regard was reported by Koebernick et al. (2014). They showed that the frequency distribution of root distances integrated over all soil voxels, from now on denoted as root distance histogram (RDH), typically exhibits a shift from long to short root distances as the root network develops and explores the soil.

We will compare the information which can be derived from this new approach, to the classical half-mean distance parameter. Half-mean distance is used as an approximation in many modeling approaches, when real spatial information is missing. We show that the average distance to root segments estimated from an RDH can be linked to the root length density R_L [$\frac{L}{L^3}$, e.g., cm/cm^3] through the theoretical half-mean distance HMD [L]

$$HMD = (\pi R_L)^{\frac{-1}{2}} \tag{1}$$

a formula which has been derived for equidistant ensembles of cylindrical roots (Gardner, 1960; Newman, 1969; de Parseval et al., 2017). However, it is unclear whether this relationship still holds for a natural, more complex root system, since experimental studies on such a comparison are lacking.

The objective of the present paper is to advocate the use of root distance histograms as complementary information on root system architecture, which remains unaddressed by traditional metrics focused on root density and morphology. We will show that root distance histograms evolve in a very regular manner, which can be predicted by means of a simple model with only four parameters. The experimental dataset to calibrate and validate the model stems from a recent study about radiation effects on early root development in *Vicia faba* (Blaser et al., 2018).

THEORETICAL BACKGROUND

To better understand the nature of the distribution of the Euclidean distance from a randomly chosen point in soil to the nearest root voxel, we take a closer look at two synthetic test cases (**Figure 1**). For both test cases considered, we fix a cylindrical region of interest (ROI) in line with sample geometries used in X-ray tomography analysis. First, we create one vertical root, typical for the tap root of a dicotyledonous plant (black). We assume that the horizontal coordinates of the root are not aligned with the center of the soil column, as it is frequently observed in real pot experiments. Calculating the Euclidean distance transform inside the cylinder leads to a roughly triangular-shaped distance distribution, whose probability density function is given by

$$f_p^{\Delta}(d) = \begin{cases} \frac{d}{p^2}, \ if\ 0 \le d \le p, \\ \frac{2p-d}{p^2}, \ if\ p < d \le 2p, \\ 0, \ if\ d > 2p, \end{cases} \tag{2}$$

where d [L] denotes the radial distance from the vertical root. This distribution has only one parameter, p [L], reflecting the distance between the vertical root and the wall. The linearity in the left slope follows from the linear relationship between radial distance and perimeter. The exact slope depends on the ROI diameter and the exact position of the root. The tailing

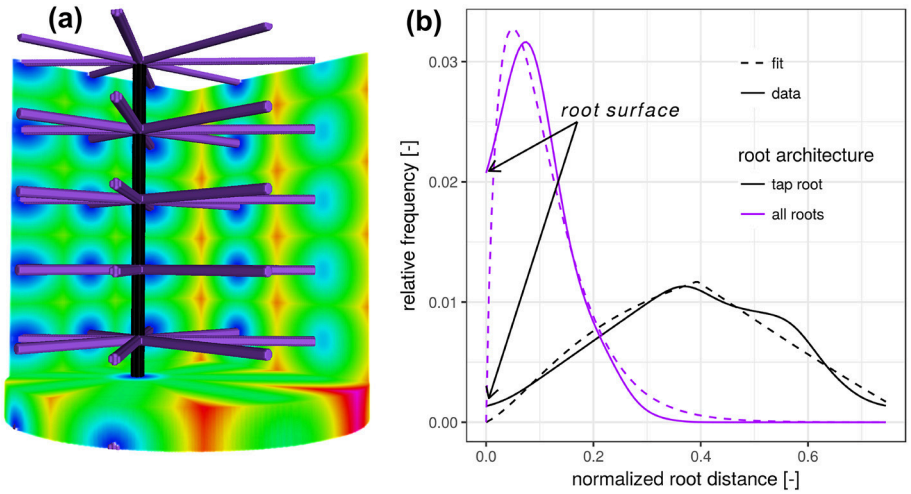

FIGURE 1 | (a) Synthetic test image of a vertical tap root only (black) and a fully developed root architecture including the tap root and lateral roots at various depths (purple). **(b)** The root distance histogram (RDH) of the single, vertical tap root follows a triangular distribution, whereas the addition of lateral roots changes the RDH toward a Gamma distribution.

toward larger distances is a result of the random horizontal root position. For young tap roots the right tailing can also be caused by incomplete vertical exploration of the soil, which contributes larger distances to the RDH that originate from the unexplored lower ROI layer (not shown).

The addition of lateral roots (purple) to the tap root changes the RDH toward a Gamma distribution with density

$$f_{k,\theta}^{\Gamma}(d) = d^{k-1}\frac{\exp\left(\frac{-d}{\theta}\right)}{\theta^{k}\Gamma(k)},\ for\ all\ d \geq 0 \tag{3}$$

with distance d $[L]$, scaling parameter θ $[L]$ and dimensionless shape parameter k. Here, Γ denotes the Gamma function, i.e., $\Gamma(k) = \int_0^\infty x^{k-1}e^{-x}dx$. The shape parameter k has two special cases, the exponential distribution for $k = 1$ and the Gaussian distribution for $k = \infty$. While the scaling parameter θ is likely to reflect the general exploration of soil by roots, the shape parameter k is more likely to reflect the balance between the frequency of minimal distances and most frequent distances, depicted in blue and green in **Figure 1a**. In this synthetic test case the expected Euclidean root distance $\left\langle f_{k,\theta}^{\Gamma}(d)\right\rangle = k\theta$ is mainly governed by the vertical separation distance between laterals. In this particular example the variance $var\left(f_{k,\theta}^{\Gamma}(d)\right) = k\theta^2$ is mainly governed by the ratio between sample diameter and the vertical separation distance between laterals. The intercept with the y-axis at zero distance is increased because there are more soil voxels located directly at the root surface. The combination of Equations (2) and (3) leads to the proposed root distance model, the so-called mixed triangular-gamma distribution with density

$$f_{c,k,\theta,p}(d) = cf_{k,\theta}^{\Gamma}(d) + (1-c)f_{p}^{\Delta}(d),\ for\ all\ x \geq 0 \tag{4}$$

which has one additional parameter, $c \in [0, 1]$, the dimensionless weighting factor for linear mixing of both densities. This mixed triangular-gamma distribution will be used to model intermediate structural scenarios between a vertical tap root only and a fully developed root architecture including the tap root and lateral roots at various depths.

MATERIALS AND METHODS

The present paper is based on the data obtained in a study on radiation effects on early root development in faba bean (Blaser et al., 2018). The experimental setup is briefly summarized here. *Vicia faba* plants (L., cv. "Fuego") were grown in cylindrical columns (250 mm height, 35 mm radius, 5 mm wall thickness) filled with sieved (<2 mm) silty clay loam with a bulk density of 1.2 g/cm^3 and a constant volumetric water content of 27%. Root growth during the first 17 days after planting (DAP) was detected via X-ray CT. Two treatments (with 5 biological replicates each) were considered for this study, differing in frequency of X-ray CT scanning. In the high radiation treatments, from now on denoted as frequent scanning (FS), samples were scanned every second day and exposed to an estimated, total radiation of 7.8 Gy. In the low radiation treatment, from now on denoted as moderate scanning (MS), samples were only scanned every fourth day resulting in an estimated total dose of 4.2 Gy. Doses were calculated with the Rad Pro Calculator Version 3.26 (McGinnis, 2009). For both treatments the first application of X-ray CT was performed at 4 DAP. The X-ray CT images were filtered with Gaussian smoothing and segmented with semi-automated region growing. Registration of segmented images of consecutive time steps of the same sample was performed in order to achieve the best visualization of growth dynamics (**Figure 2**) and to enable subsequent analysis of distances related to root age. A root age image was computed using simple

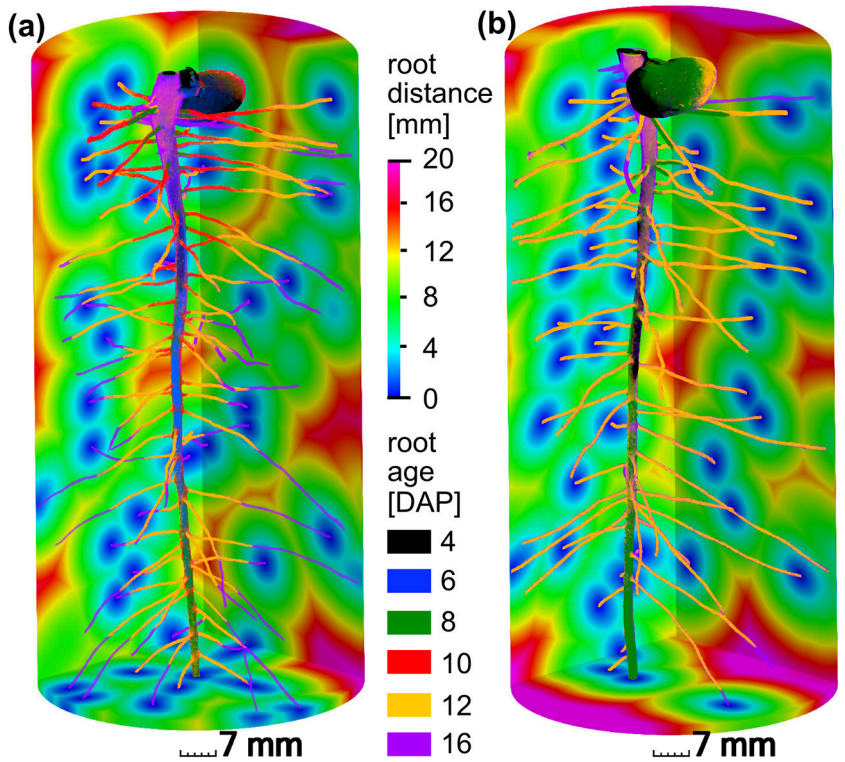

FIGURE 2 | Different root growth dynamics of *Vicia faba* in two radiation treatments: **(a)** frequent scanning (FS) every second day exposed to an estimated total dose of 7.8 Gy, **(b)** moderate scanning (MS) every fourth day exposed to an estimated total dose of 4.2 Gy. Accordingly, time step (6 DAP, blue) and (10 DAP, red) are only available for frequent scanning **(a)**. The main difference between both treatments is the slower growth of laterals around 12 days after planting (DAP) in the FS treatment. The root distances in the soil are depicted for the final time step at 16 DAP.

image arithmetic, i.e., a gray value represents the time step, when a voxel was assigned to the root class for the first time. By means of a skeletonization algorithm the root network was analyzed with respect to total root length density and individual root length densities of tap roots and lateral roots. Detailed information about the growth conditions, X-ray CT scan settings and all image processing steps can be retrieved from Blaser et al. (2018). For each treatment, examples of a root network with age information and root distances in the soil matrix are depicted in **Figure 2**.

RESULTS

Root Distance Histograms

The experimental root distance histograms in the frequent scanning treatments exhibit a clear transition from triangular distributions (4–8 days after planting) to left skewed gamma distributions (12–16 days after planting) (**Figure 3a**). Data for 14 DAP are left out as it barely differs from the final state at 16 DAP. The root system at 10 DAP is in a transitional stage, during which the lateral roots are already developed in the upper part of the column but still absent at the lower part. The mixed triangular-gamma model is capable of fitting all growth stages very well. The temporal evolution of all model parameters displays some consistent trends (**Figure 3b**). The weighting factor c of the gamma distribution is increasing monotonically with the development of laterals. The scale parameter θ and the shape parameter k are only meaningful when c clearly differs from zero, i.e., $c > 0.15$. In that case, θ decreases with increasing exploration of soil by laterals. The shape parameter k, in turn, fluctuates around 2 during all development stages, i.e., the ratio between the volume fraction of soil voxels with minimal root distance and most frequent root distance remains rather constant. The tap root-wall distance parameter p of the triangular model decreases while the tap root is still expanding vertically and loses meaning as c approaches one.

Parameter profiles for each time step reveal vertical differences in the development of laterals as already discussed above for the root network at 10 DAP (**Figure 4**). In fact, only for this sampling date a steep transition in the weighting factor c exists within the soil column, i.e., from a gamma model at the top to a triangular model in the lower part. The shape parameter k is rather stable across all soil layers and time points except for cases when roots are generally absent (4–6 DAP, lower ROI). Apparently the value of k is characteristic for *Vicia faba* during all development stages, perhaps reflecting the rather constant separation distance of laterals along the tap root and the absence of secondary lateral roots in this study. The scaling parameter θ varies with depth during the transitional stages

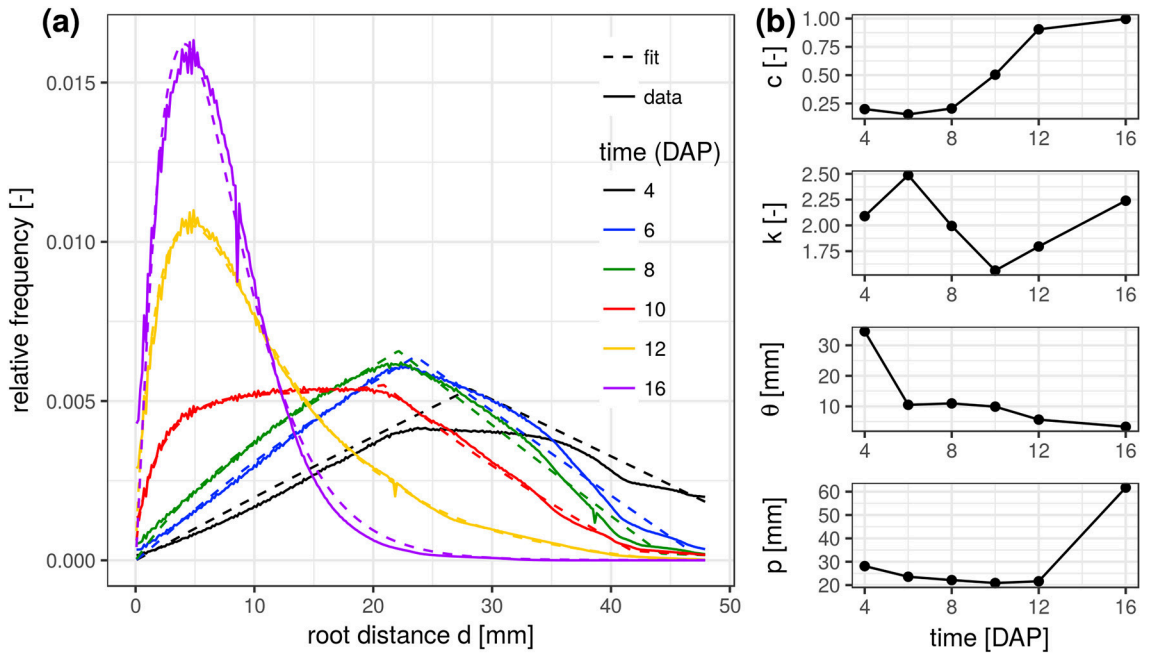

FIGURE 3 | (a) Root distance histograms for all time steps in the FS treatment including the fitted mixed triangular-gamma models (Equation 4). **(b)** Time series of the four parameters of the mixed triangular-gamma model: c, weighting factor; k, shape parameter; θ, scaling parameter; p, tap root-wall distance.

(10–12 DAP) and reflects the uneven exploration of the soil further away from the tap root. Obviously, the tap root-wall distance parameter p is almost constant across all depths for a constant ROI diameter and a vertically oriented tap root. The parameter p loses meaning when $c > 0.85$ and starts to fluctuate. Differences between FS and MS radiation treatment are also depicted in **Figure 4**. In line with visual inspection, the largest differences emerge at the joint sampling date 12 DAP. The MS treatment has already reached its final RDH everywhere except for the lowest layers (depth $>$ 100 mm), whereas the FS treatment has reached this final state only at the very top (depth $<$ 30 mm).

This congruency of space and time is further demonstrated for two soil depths and scanning dates of the FS treatment. The RDH at 10 DAP in a shallow depth range of 29–45 mm (**Figure 5a**) is very similar to the RDH at 12 DAP in a larger depth range of 93–109 mm (**Figure 5d**). The RDH at 12 DAP in the shallow soil layer has already fully turned into a Gamma distribution (**Figure 5c**), a stage that is only reached at 16 DAP in the deeper soil layer (not shown). The RDH at 10 DAP in the deeper soil layer, in turn, is still dominated by the triangular distribution (**Figure 5b**). The mixed triangular-gamma distribution is suitable to fit the experimental RDH in all cases considered. Note, however, that this congruency of space and time is characteristic for *Vicia faba* in the radiation experiment considered in the present paper, but not necessarily the case for other plant species and growth stages beyond those studied. Potentially this is a typical phenomenon observed in tap rooted plant species but more studies are needed to proof this hypothesis.

Rhizosphere Volumes

The relative frequency value of a certain root distance in the RDH represents the volume fraction of voxels with a given Euclidean distance to the nearest root voxel. Integrating the RDH over all distances smaller than a maximum rhizosphere extent accordingly results in the volume fraction of the rhizosphere. The extent of the rhizosphere depends on the considered process. It can be large for water depletion by root water uptake as the resulting gradient in water potential around roots drives water flow toward the roots, which stretches the zone of water depletion far into the bulk soil (Carminati et al., 2011). The capacity for this water redistribution depends on the unsaturated conductivity and water retention of the surrounding soil. The extent of the rhizosphere is much smaller for strongly adsorbed nutrients like ammonium and phosphate which are less mobile (Hinsinger et al., 2009). Substances released by the roots, like enzymes and mucilage, are also only present in a small volume of soil for their susceptibility to microbial attack (Carminati and Vetterlein, 2012). Furthermore, they are not released uniformly by the entire root network but mainly by young root segments (Vetterlein and Doussan, 2016). This variability of the rhizosphere extent in time and space can be accounted for with root age dependent RDHs as shown in **Figure 6**. The top row demonstrates the increase in total rhizosphere volume for both radiation treatments and two hypothetical rhizosphere extents. Approximately 2% of the soil columns are explored by the roots after 16 days in both treatments, when a rhizosphere extent of 0.5 mm is assumed. This increases to approximately 40% if the extent is enlarged to 5 mm. The differences in the growth dynamics between both radiation treatments is fully

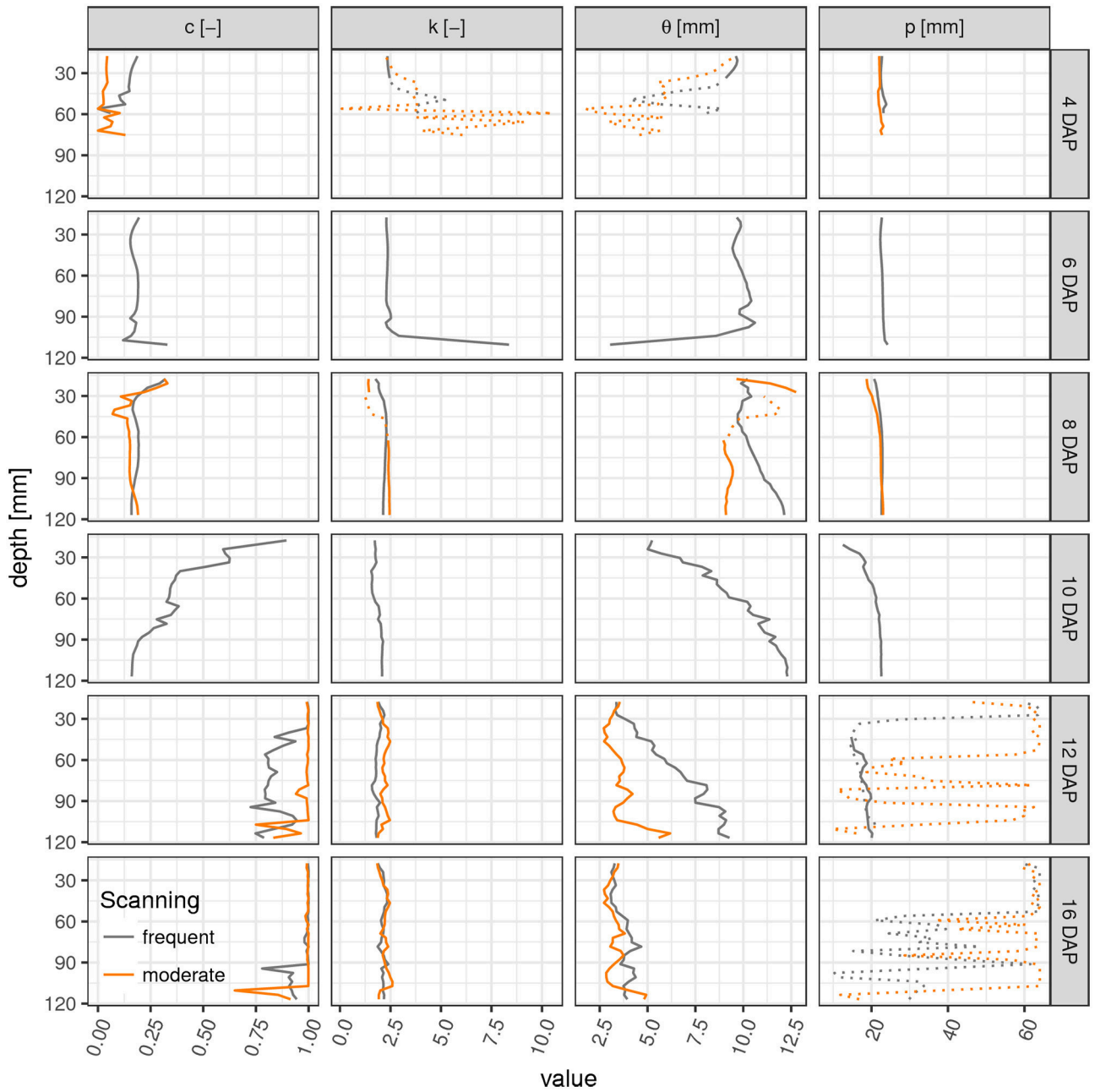

FIGURE 4 | Parameter profiles (c, weighting factor; k, shape parameter; θ, scaling parameter; p, tap root-wall distance) of the mixed triangular-gamma model at each scan time (days after planting) in equidistant, 5 mm thick slices. Dashed lines indicate uncertain values due to imbalanced mixing of the two models in Equation (4) ($c < 0.15$ or $c > 0.85$).

developed 12 days after planting and significant for 5 mm rhizosphere extent but has vanished at 16 DAP because root growth only occurs outside the ROI by then. This is also confirmed by the rhizosphere volume fraction of young roots only, i.e., root segments that have grown since the last scan time 4 days earlier (**Figures 6c,d**). Until 12 DAP, this restricted rhizosphere volume develops in line with the total rhizosphere volume. The differences between radiation treatments become significant after 12DAP. The gap in absolute values between the two rhizosphere volume fractions (young vs. total) increases with decreasing rhizosphere extent. At 16 DAP, there are less young roots in the ROI and hence their rhizosphere volume fraction decreases. Note that this decline is not an inevitable consequence of pot experiments but a manifestation of the root system architecture of *Vicia faba* in this experiment, which largely lacked the development of second order laterals that could have

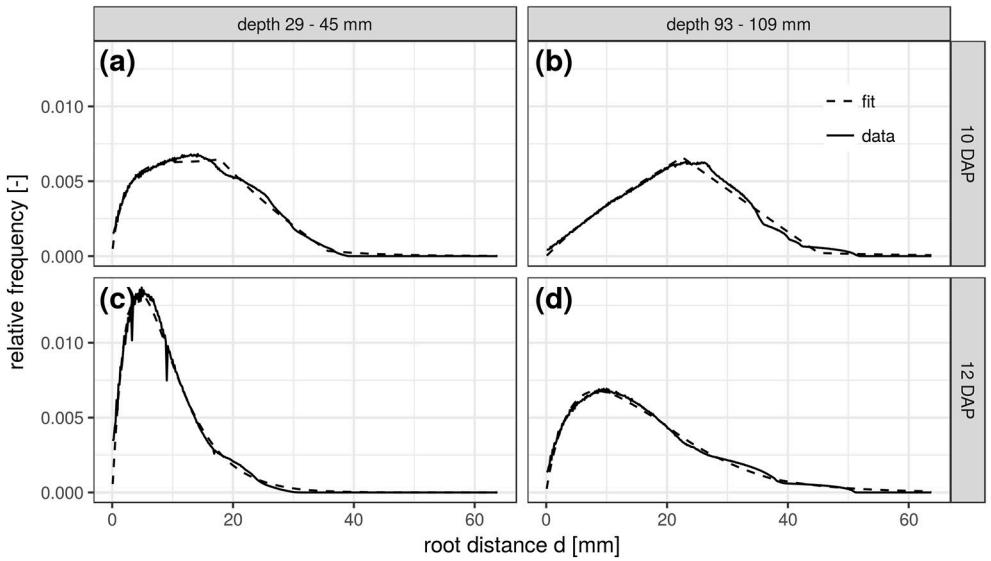

FIGURE 5 | Root distance histograms in two different soil depths (**a,c**: 29–45 mm; **b,d**: 93–109 mm) at two scanning times (**a,b**: 10DAP; **c,d**: 12DAP; DAP, days after planting) of the frequent scanning (FS) radiation treatment.

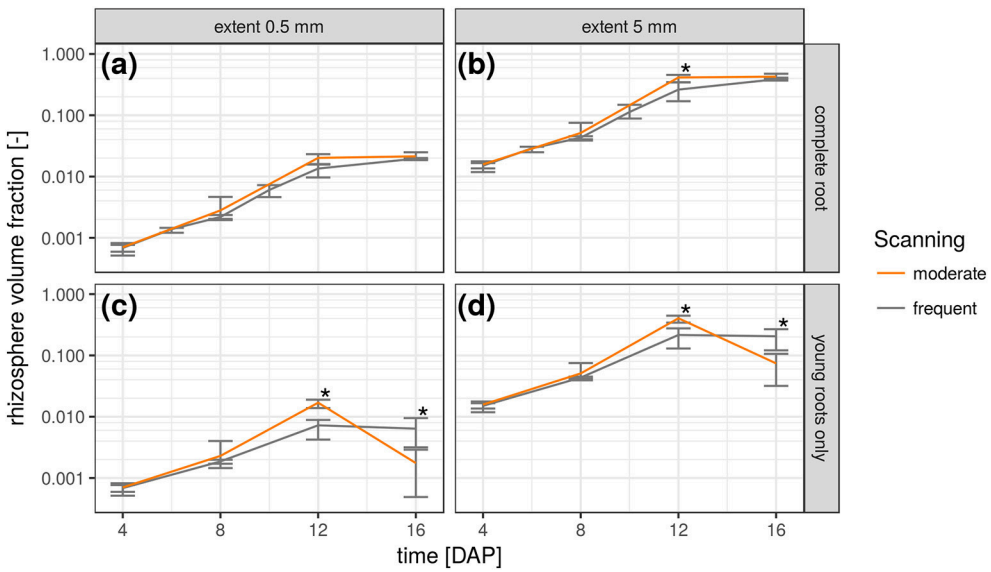

FIGURE 6 | Temporal change of rhizosphere volume fraction in both radiation treatments for two hypothetical rhizosphere radii (0.5 and 5 mm) and shown separately for the complete root network **(a,b)** and only the young roots that have grown since the previous scan time **(c,d)**. Error bars refer to minimum and maximum for five biological replicates of each treatment and asterisk refers to significant differences tested at $p < 0.05$.

entered the space between the first order laterals at that growth stage.

DISCUSSION

Root Perspective vs. Soil Perspective

The results presented so far describe spatial patterns in root-soil interactions from the soil perspective through distance distributions in soil and volume fractions of soil explored by roots. Traditional approaches to describe root system architectures are focused on the root perspective, e.g., by quantifying root length densities and branching patterns. We therefore discuss the question if this change in perspective provides complementary information or merely redundant information. This is assessed by comparing features of the root distance histogram with results obtained by skeletonization analysis of the segmented root network (Blaser et al., 2018) summarized in **Figure** 7.

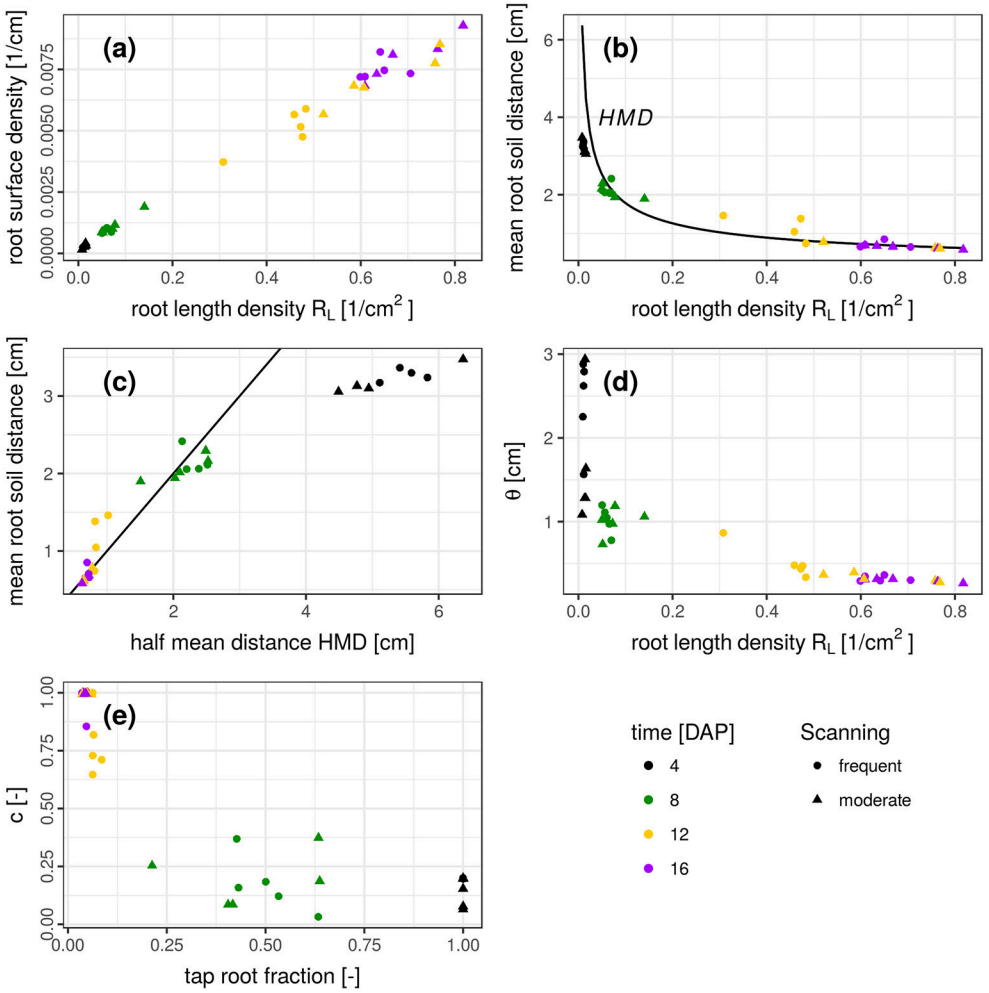

FIGURE 7 | (a-e) Relationship between several root system traits derived from a skeleton analysis (root length density, half mean distance, tap root fraction) and root distance traits derived from mixed triangular-gamma models (relative root surface, mean root-soil distance, i.e., first central moment of the root distance histogram, and the parameters θ and c). Root system traits are shown on the abscissa and root distance traits on the ordinate. In **(b)**, the half mean distance derived from root length density is added as a reference for comparison (black line). In **(c)**, the 1:1 line is added.

There is a close, linear relationship ($R^2 = 0.991$) between root length density R_L [cm/cm^3] and root surface density [cm^2/cm^3], derived from the frequency of the smallest root distance (**Figure 7a**). This very good agreement is not surprising and only confirms the reliability of the complimentary approaches to estimate two highly correlated metrics. Another characteristic metric of the root distance histogram is the mean root-soil distance, i.e., its first central moment,

$$\langle RDH \rangle = \sum_{i=1}^{d_{\max}} f_i d_i \tag{5}$$

with distance d_i and relative frequency f_i. The relationship between R_L and mean root-soil distance $\langle RDH \rangle$ is non-linear (**Figure 7b**) with a huge reduction in mean distance by a relatively small R_L that is only composed of the tap root in the first week after planting. Note that $\langle RDH \rangle$ is bounded by $p \approx 3.5$ cm, when the ROI is reduced to the maximum depth of the tap root (**Figure 3b**), as then p is simply the horizontal distance between the tap root and the ROI perimeter. The theoretical half mean distance HMD derived from R_L (Equation 1) and the measured mean root-soil distance $\langle RDH \rangle$ show good agreement (**Figure 7b**) which has already been reported previously (Koebernick et al., 2014). Note that HMD refers to root-root distances, whereas $\langle RDH \rangle$ refers to root-soil distances. The relationship between both entities depends on the spatial distribution of roots. This is shown by the following example.

For a bundle of equidistant roots on a hexagonal lattice $\langle RDH \rangle$ amounts to 69% of the HMD (**Figure 8a**). For a random distribution of roots in two-dimensional cross sections it amounts to 89% of the theoretical HMD derived from R_L (**Figure 8b**). Evidently, the branching and clustering of roots changes the root distance histogram in characteristic ways

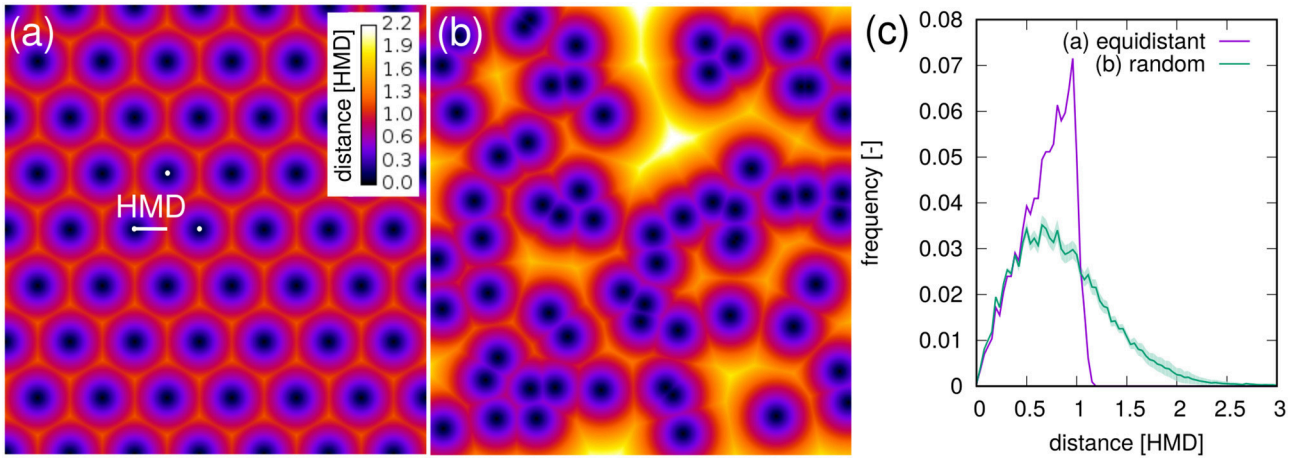

FIGURE 8 | Root-soil distances in **(a)** an equidistant, hexagonal root bundle and **(b)** for a random pattern of roots in a two-dimensional cross section. The distances are normalized by the half-mean distance between roots. The root length density is the same in both point patterns. **(C)** The root distance histograms for both point patterns. Shaded areas for random point patterns represent standard deviation of ten realizations.

(**Figure 8c**): (1) Short distances directly at the root surface ($d < 0.5HMD$) are just as abundant and mainly imprinted by the root length density itself. (2) Intermediate root distances ($0.5HMD < d < HMD$) are less frequent, when neighboring roots approach each other in the randomly distributed example (**Figure 8b**). That is, the local root length density increases by a factor of two, but not the volume fraction of intermediate distances between them. (3) Long distances beyond the equidistant spacing ($d > HMD$) can only occur in random point patterns. Taken together this leads to a higher $\langle RDH \rangle$ than what would be theoretically expected for a bundle for parallel roots with the same root length density. Note that these relations between root-root distances and root-soil distances are constant for a given pattern and do not depend on the actual spacing between roots (data not shown).

It turns out that for real root networks of *Vicia faba*, the $\langle RDH \rangle$ is in fact even larger than for random point patterns and amounts to 97% of the theoretical *HMD* derived from R_L. This is also indicated by a 1:1 relationship in **Figure 7c** for all dates within 8-16 DAP, whereas the relationship starts to become non-linear and flattens out around $\langle RDH \rangle \approx 2$ cm or $R_L < 0.08$ cm/cm^3 due to the incomplete exploration of the full ROI depth by the young tap root at 4 DAP. In a previous experiment with *Vicia faba* by Koebernick et al. (2014) the $\langle RDH \rangle$ amounted to a similar value of 93% of the theoretical *HMD* and the linear relationship between $\langle RDH \rangle$ and *HMD* started to flatten out around $R_L < 0.12$ cm/cm^3 due to the same limitations in soil exploration by young roots. Real three-dimensional root networks differ from two-dimensional random point patterns in that they are continuous, i.e., they cannot emerge everywhere but have to branch and grow to explore the soil. This immanent alignment and clustering causes larger unexplored areas for the same root density in two-dimensional sections. As a consequence the normalized $\langle RDH \rangle$ is larger in real root networks of *Vicia faba* than in random root configurations. Future studies will show whether differences in root system architecture between different plant species lead to characteristic differences in the relationship between the introduced metrics for root length density and soil exploration.

The weighting factor c should be inversely related to the tap root fraction, which is confirmed by **Figure 7e**. There is some scatter in the data, which is presumably due to some correlation in the parameter set of the mixed triangular-gamma model leading to an equally good fit of the model to the RDH for a range of c values. Finally, the scaling parameter θ decreases as the root length density increases (**Figure 7d**). The relationship is mildly non-linear for 8–16 DAP, since an additional increase in root length density beyond 0.6 cm/cm^3 does not lead to a proportional reduction in root distances for this root system architecture presumably due to the lack of secondary laterals. The large θ-values at 4 DAP are not reliable, since the weighting factor c is rather small, which renders the model fit insensitive to the θ-parameter.

In summary, the root distance traits reveal information that cannot be derived from conventional root system traits based on a skeleton analysis of the root network. The exact relationship between parameters derived from the root perspective (root network traits) and the soil perspective (root distance traits) hints to characteristic root growth patterns. An in-depth analysis of such scaling relations is out of scope of this study, as it would require a set of different plant species to compare different root system architectures.

Strengths and Limitations of Soil Perspective

The quantitative analysis of root growth patterns via root distance models has several advantages over traditional approaches based on root network analysis: (1) It is a more direct assessment of which soil volume is accessible to roots. (2) It can take

into account variable extents of the rhizosphere with respect to different elements and processes (water uptake, nutrient uptake, rhizodeposits, etc.). (3) The proposed combination of root distance histograms and root age, obtained by differential imaging of registered X-ray CT datasets, enables a dedicated analysis of soil exploration by young roots. (4) Root distance analysis is more robust against image segmentation problems, as it is virtually insensitive to root surface roughness and small gaps, which are notorious problems for skeleton analysis of the root network.

Similar to dynamic root growth models based on root network traits (Leitner et al., 2010) the mixed triangular-gamma model proposed in the present paper lends itself to interpolation between sampling dates, since its parameters either change monotonically or remain rather constant. Especially during intermediate growth stages it might be necessary to carry out interpolation for different depths separately.

There are also some limitations of the description of root growth patterns from the soil perspective: (1) Branching angles, hierarchical ordering of laterals, length distributions of root segments and related traits of root networks cannot be assessed with root distance models. This is the reason why a combined analysis from the root perspective and the soil perspective may provide a more comprehensive representation of root growth patterns (2) Even though the mixed triangular-gamma model is versatile enough to model RDHs at all growth stages with only four parameters which have an easily conceivable, geometrical meaning, there is the downside that some parameters become unconstrained and start to fluctuate when the weighting factor of the corresponding model becomes too small or too large.

CONCLUSIONS AND OUTLOOK

We have introduced the mixed triangular-gamma model to describe root distance histograms, i.e., frequency distributions of Euclidean distances from soil to root, at several growth stages of *Vicia faba*. This new approach to assess root growth patterns from the soil perspective delivers complementary information to the traditional plant perspective based on root network analysis and facilitates a more direct assessment on rhizosphere processes.

In future work, the approach needs to be extended to further plant species, differing in root architecture. In particular the method needs to be tested for adventitious root architectures of grass species and in general for older plants. A prerequisite for such tests is obtaining 3D time resolved datasets with sufficient resolution to capture all roots, including fine roots. This is still a challenge for many grass species if the pot size is chosen to enable unrestricted root growth at least for the seedling stage. Another approach could be the extraction of undisturbed soil cores from the field, which enables the study of older plants with the trade-off of introducing field heterogeneity into the investigations. Finally, the approach can also be applied to root system architectures for a suite of plant species derived from dynamic root growth models like CRootBox (Schnepf et al., 2018). The benefits are two-fold. Metrics derived from root distance histograms may complement established skeleton-based metrics in high-throughput phenotyping. In addition, comparing parameter sets derived by model fitting to root distance histograms from plant species with vastly different root system architectures is helpful to scrutinize the physical meaning of each parameter in the proposed model.

AUTHOR CONTRIBUTIONS

All authors conceived the project and wrote the manuscript. SS and MW carried out the analysis. SB and SS provided the underlying data.

ACKNOWLEDGMENTS

The experimental work providing the CT-data sets was supported by SKW Stickstoffwerke Piesteritz. The collaboration between the authors was promoted by the establishment of the DFG priority program 2089 Rhizosphere spatiotemporal organization—a key to rhizosphere functions.

REFERENCES

Atkinson, J. A., Rasmussen, A., Traini, R., Voß, U., Sturrock, C., Mooney, S. J., et al. (2014). Branching out in roots: uncovering form, function, and regulation. *Plant Physiol.* 166, 538–550. doi: 10.1104/pp.114.245423

Blaser, S. R. G. A., Schlüter, S., and Vetterlein, D. (2018). How much is too much?-Influence of X-ray dose on root growth of faba bean (Vicia faba) and barley (Hordeum vulgare). *PLoS ONE* 13:e0193669. doi: 10.1371/journal.pone.0193669

Carminati, A., Schneider, C. L., Moradi, A. B., Zarebanadkouki, M., Vetterlein, D., Vogel, H. J., et al. (2011). How the rhizosphere may favor water availability to roots. *Vadose Zone J.* 10, 988–998. doi: 10.2136/vzj2010.0113

Carminati, A., and Vetterlein, D. (2012). Plasticity of rhizosphere hydraulic properties as a key for efficient utilization of scarce resources. *Ann. Bot.* 112, 277–290. doi: 10.1093/aob/mcs262

Carminati, A., Vetterlein, D., Koebernick, N., Blaser, S., Weller, U., and Vogel, H. J. (2012). Do roots mind the gap? *Plant Soil* 367, 651–661. doi: 10.1007/s11104-012-1496-9

Clark, R. T., MacCurdy, R. B., Jung, J. K., Shaff, J. E., McCouch, S. R., Aneshansley, D. J., et al. (2011). Three-dimensional root phenotyping with a novel imaging and software platform. *Plant Physiol.* 156, 455–465. doi: 10.1104/pp.110.169102

Danjon, F., and Reubens, B. (2008). Assessing and analyzing 3D architecture of woody root systems, a review of methods and applications in tree and soil stability, resource acquisition and allocation. *Plant Soil* 303, 1–34. doi: 10.1007/s11104-007-9470-7

de Parseval, H., Barot, S., Gignoux, J., Lata, J. C., and Raynaud, X. (2017). Modelling facilitation or competition within a root system: importance of the overlap of root depletion and accumulation zones. *Plant Soil* 419, 97–111. doi: 10.1007/s11104-017-3321-y

De Smet, I., White, P. J., Bengough, A. G., Dupuy, L., Parizot, B., Casimiro, I., et al. (2012). Analyzing lateral root development: how to move forward. *Plant Cell* 24, 15–20. doi: 10.1105/tpc.111.094292

Drew, M. (1975). Comparison of the effects of a localised supply of phosphate, nitrate, ammonium and potassium on the growth of the seminal root system, and the shoot, in barley. *New Phytol.* 75, 479–490. doi: 10.1111/j.1469-8137.1975.tb01409.x

Flavel, R. J., Guppy, C. N., Rabbi, S. M., and Young, I. M. (2017). An image processing and analysis tool for identifying and analysing complex plant root systems in 3D soil using non-destructive analysis: root1. *PLoS ONE* 12:e0176433. doi: 10.1371/journal.pone.0176433

Flavel, R. J., Guppy, C. N., Tighe, M. K., Watt, M., and Young, I. M. (2014). Quantifying the response of wheat (*Triticum aestivum* L) root system architecture to phosphorus in an Oxisol. *Plant Soil* 385, 303–310. doi: 10.1007/s11104-014-2191-9

Gardner, W. R. (1960). Dynamic aspects of water availability to plants. *Soil Sci.* 89, 63–73. doi: 10.1097/00010694-196002000-00001

Giehl, R. F., and von Wirén, N. (2014). Root nutrient foraging. *Plant Physiol.* 166, 509–517. doi: 10.1104/pp.114.245225

Helliwell, J. R., Sturrock, C. J., Mairhofer, S., Craigon, J., Ashton, R. W., Miller, A. J., et al. (2017). The emergent rhizosphere: imaging the development of the porous architecture at the root-soil interface. *Sci. Rep.* 7:14875. doi: 10.1038/s41598-017-14904-w

Helliwell, J., Sturrock, C., Grayling, K., Tracy, S., Flavel, R., Young, I., et al. (2013). Applications of X-ray computed tomography for examining biophysical interactions and structural development in soil systems: a review. *Eur. J. Soil Sci.* 64, 279–297. doi: 10.1111/ejss.12028

Hinsinger, P., Bengough, A. G., Vetterlein, D., and Young, I. M. (2009). Rhizosphere: biophysics, biogeochemistry and ecological relevance. *Plant Soil* 321, 117–152. doi: 10.1007/s11104-008-9885-9

Ho, M. D., Rosas, J. C., Brown, K. M., and Lynch, J. P. (2005). Root architectural tradeoffs for water and phosphorus acquisition. *Funct. Plant Biol.* 32, 737–748. doi: 10.1071/FP05043

Hodge, A., Berta, G., Doussan, C., Merchan, F., and Crespi, M. (2009). Plant root growth, architecture and function. *Plant Soil* 321, 153–187. doi: 10.1007/s11104-009-9929-9

Iyer-Pascuzzi, A. S., Symonova, O., Mileyko, Y., Hao, Y., Belcher, H., Harer, J., et al. (2010). Imaging and analysis platform for automatic phenotyping and trait ranking of plant root systems. *Plant Physiol.* 152, 1148–1157. doi: 10.1104/pp.109.150748

Koebernick, N., Huber, K., Kerkhofs, E., Vanderborght, J., Javaux, M., Vereecken, H., et al. (2015). Unraveling the hydrodynamics of split root water uptake experiments using CT scanned root architectures and three dimensional flow simulations. *Front. Plant Sci.* 6:370. doi: 10.3389/fpls.2015.00370

Koebernick, N., Weller, U., Huber, K., Schlüter, S., Vogel, H. J., Jahn, R., et al. (2014). *In situ* visualization and quantification of three-dimensional root system architecture and growth using X-ray computed tomography. *Vadose Zone J.* 13, 1–10. doi: 10.2136/vzj2014.03.0024

Kutschera, L. (1960). *Wurzelatlas Mitteleuropäischer Ackerunkräuter und Kulturpflanzen DLG*. Frankfurt: DLG-Verlag.

Leitner, D., Klepsch, S., Bodner, G., and Schnepf, A. (2010). A dynamic root system growth model based on L-Systems. *Plant Soil* 332, 177–192. doi: 10.1007/s11104-010-0284-7

Lynch, J. P., and Ho, M. D. (2005). Rhizoeconomics: carbon costs of phosphorus acquisition. *Plant Soil* 269, 45–56. doi: 10.1007/s11104-004-1096-4

Malamy, J. (2005). Intrinsic and environmental response pathways that regulate root system architecture. *Plant Cell Environ.* 28, 67–77. doi: 10.1111/j.1365-3040.2005.01306.x

McGinnis, R. (2009). *Rad Pro Calculator*. Available online at: http://www.radprocalculator.com/

Morris, E. C., Griffiths, M., Golebiowska, A., Mairhofer, S., Burr-Hersey, J., Goh, T., et al. (2017). Shaping 3D root system architecture. *Curr. Biol.* 27, R919–R930. doi: 10.1016/j.cub.2017.06.043

Newman, E. I. (1969). Resistance to water flow in soil and plant. I. Soil resistance in relation to amounts of root: theoretical estimates. *J. Appl. Ecol.* 6, 1–12. doi: 10.2307/2401297

Passioura, J. (1991). Soil structure and plant growth. *Soil Res.* 29, 717–728. doi: 10.1071/SR9910717

Robinson, D. (1994). Tansley review no. 73. The responses of plants to non-uniform supplies of nutrients. *New Phytol.* 127, 635–674. doi: 10.1111/j.1469-8137.1994.tb02969.x

Schmidt, S., Bengough, A. G., Gregory, P. J., Grinev, D. V., and Otten, W. (2012). Estimating root-soil contact from 3D X-ray microtomographs. *Eur. J. Soil Sci.* 63, 776–786. doi: 10.1111/j.1365-2389.2012.01487.x

Schnepf, A., Leitner, D., Landl, M., Lobet, G., Mai, T. H., Morandage, S., et al. (2018). CRootBox: a structural–functional modelling framework for root systems. *Ann. Bot.* 121, 1033–1053. doi: 10.1093/aob/mcx221

Schulz, H., Postma, J. A., Van Dusschoten, D., Scharr, H., and Behnke, S. (2013) "Plant root system analysis from MRI images," in *Computer Vision, Imaging and Computer Graphics. Theory and Application*, eds G. Csurka, M. Kraus, R. S. Laramee, P. Richard, and J. Braz (Berlin; Heidelberg, Springer), 411–425.

Smith, S., and De Smet, I. (2012). Root system architecture: insights from Arabidopsis and cereal crops. *Philos. Trans. R. Soc. Lond. B Biol. Sci.* 367, 1441–1452. doi: 10.1098/rstb.2011.0234

Tennant, D. (1975). A test of a modified line intersect method of estimating root length. *J. Ecol.* 63, 995–1001. doi: 10.2307/2258617

van Noordwijk, M., Brouwer, G., and Harmanny, K. (1993). Concepts and methods for studying interactions of roots and soil structure. *Geoderma* 56, 351–375. doi: 10.1016/0016-7061(93)90122-2

Vetterlein, D., and Doussan, C. (2016). Root age distribution: how does it matter in plant processes? A focus on water uptake. *Plant Soil* 407, 145–160. doi: 10.1007/s11104-016-2849-6

York, L. M., Carminati, A., Mooney, S. J., Ritz, K., and Bennett, M. J. (2016). The holistic rhizosphere: integrating zones, processes, and semantics in the soil influenced by roots. *J. Exp. Bot.* 67, 3629–3643. doi: 10.1093/jxb/erw108

Conflict of Interest Statement: The authors declare that the research was conducted in the absence of any commercial or financial relationships that could be construed as a potential conflict of interest.

frontiers in Environmental Science

ORIGINAL RESEARCH
published: 10 August 2018
doi: 10.3389/fenvs.2018.00090

Impact of Small-Scaled Differences in Micro-Aggregation on Physico-Chemical Parameters of Macroscopic Biopore Walls

Christoph Haas [1,2]* *and Rainer Horn* [1,2]

[1] *Institute for Plant Nutrition and Soil Science, Christian-Albrechts-Universität zu Kiel, Kiel, Germany,* [2] *Institute of Soil Landscape Research, Leibniz Centre for Agricultural Landscape Research, Müncheberg, Germany*

Macroscopic biopores, like earthworm burrows or channels which remain after a root decayed, act as preferential flow paths for water, gas, and heat transport processes, and viewing at agricultural production, as preferential elongation paths for plant roots. These processes result in intense alterations of the soil volume and its composition that surrounds the pores. The effects of these processes were analyzed at small-scale and physico-chemical soil parameters, i.e., relative oxygen diffusion coefficient (D_s/D_O), oxygen partial pressure pO_2, Eh and pH of biopore walls, were measured. The analyses were carried out on undisturbed soil samples with different colonization history, excavated from a haplic Luvisol derived from loess. Soil resistance to penetration was determined simultaneously with D_s/D_O and pO_2 using a coupled, self-developed approach, and four matric potentials (namely, $\Psi_m = -1$ kPa; -3 kPa; -6 kPa or -30 kPa) were considered. We hypothesized that physico-chemical soil parameters in biopore walls were altered due to differing influences on the soil aggregation. Aggregation was visualized with scanning electron microscopy, classified and used to explain differences in–soil properties. Plant roots and earthworms altered aggregation next to biopore surfaces in a contrasted way, either by enhancing aggregates diversity or homogenizing it. Roots led to the formation of subpolyeders while earthworms formed subplates. Pore functions of microaggregates were comparable to those of larger scale, and subpolyeders showed much more favorable soil properties in terms of soil aeration (Ds/Do, pO2). Replicates of all parameters scattered intensely and showed deviations up to several orders of magnitude in case of D_s/D_O underlining the large variability of soil properties in biopore walls.

Keywords: diffusion, oxygen partial pressure, pH, redox potential, biopores, root channel, earthworm burrow

OPEN ACCESS

Edited by:
Andrea Carminati,
University of Bayreuth, Germany

Reviewed by:
Frédéric Rees,
Institut National de la Recherche Agronomique Centre Montpellier, France
Martin Leue,
Leibniz-Zentrum für Agrarlandschaftsforschung (ZALF), Germany

***Correspondence:**
Christoph Haas
c.haas@soils.uni-kiel.de

Specialty section:
This article was submitted to Soil Processes, a section of the journal Frontiers in Environmental Science

Received: *04 May 2018*
Accepted: *20 July 2018*
Published: *10 August 2018*

Citation:
Haas C and Horn R (2018) Impact of Small-Scaled Differences in Micro-Aggregation on Physico-Chemical Parameters of Macroscopic Biopore Walls. Front. Environ. Sci. 6:90. doi: 10.3389/fenvs.2018.00090

INTRODUCTION

Preferential elongation paths for plant roots (Passioura, 2002; McKenzie et al., 2009) and preferential flow paths like earthworm burrows and root channels (Jarvis, 2007) are hot spots of soil microorganisms (Hoang et al., 2016; Banfield et al., 2017), for nutrient turnover (Hoang et al., 2016) and exchange processes within the plant-soil-atmosphere-continuum. The surrounding soil volumes of these biopores differ not only in a linguistic way from the soil matric but biologically,

chemically, and physically alterations are known. The *drilosphere* is a 1–2 mm thick layer (Bouché, 1975; reviewed by Brown et al., 2000) that surrounds earthworm burrows. The formation of soil linings, which are rich in organic carbon (Don et al., 2008; Banfield et al., 2017) and dark in color, caused by deposed earthworm casts make the alteration of this soil volume visible to the naked eye. Biologically, chemically, and physically alterations in the aggregation of the soil become even more obvious when visualized with the help of scanning electron microscopy (SEM). SEM micrographs give general information about textural and mineralogical properties, particle shape and surface roughness and can be used as a supplemental, visualizing method to interpret and understand microstructural changes (Baumgarten et al., 2013). Biologically alterations show in elevated populations of e.g., nitrifying bacteria (Parkin and Berry, 1999) and result in enhanced nitrogen turnover rates. Since decades, research focuses on the *rhizosphere* that is the region of soil in the vicinity of plant roots in which the chemistry and microbiology is influenced by their growth, respiration, and nutrient exchange. Most plants live together with other microorganisms (e.g., in symbiosis) leading to elevated numbers of many microorganisms groups while there are specialized microorganisms causing the decay of the root. The soil microbial community is not the only soil property that is heavily altered next to living (*Rhizosphere*) or decaying roots (*Detritusphere*) in soils, because these biological alterations go along with chemical and physical alterations (schematized in **Figure 1**). For example, decreased oxygen partial pressures (pO_2) caused by the consumption of oxygen (O_2) by aerobic soil microorganisms coincides with the release of carbon dioxide (CO_2). This results in a decrease in pH because of the reaction of CO_2 with water to carbonic acid (H_2CO_3). Beside these biologically and chemically alterations, roots and earthworms release and incorporate organic matter into the soil volume that surrounds the cavities. Thereby they alter e.g., the chemical composition in terms of the ratio of hydrophobic and hydrophilic functional groups (C–H/C=O ratio), even after the root decayed completely (Haas et al., 2018) or the replenishment of earthworm casts stopped. The alteration of the C–H/C=O ratio goes along with changes in contact angles (Fér et al., 2016; Haas et al., 2018), resulting in altered in water contents (**Figure 1**). The latter one has a large impact on e.g., the oxygen diffusion coefficient of soils due to the 10,000 times higher diffusion coefficient of oxygen in air, compared to that one in water (Glinski and Stepniewski, 1985), resulting in a complex system of chemical, physical, and biological interactions (**Figure 1**). The dynamic of the system "soil" becomes obvious by considering direct physical alterations of the drilosphere and the rhizosphere/detritusphere, which can have biological, chemical or physical causes. Earthworms move via peristalsis, which is a radially symmetrical contraction and relaxation of muscles propagating in a waveform along the body of the earthworm. In consequence of the muscles contraction the hydrostatic skeleton expands radially, thereby anchoring to the wall of the burrow, leading to mechanical stress application on the pore wall of the earthworm burrow. Plant roots apply even higher radial stresses [in between 2.4 MPa (Bengough and Mullins, 1990) and 0.06–0.195 MPa (Keudel and Schrader, 1999)]. Two kinds of physical processes need to be distinguished. (I) Shearing occurs when mechanical stresses are applied in non-rectangular direction to the surface of stress application. Shearing occurs with both, the moving action of an earthworm through its cavity or with the formation of a root channel by a growing root. Aggregates disrupt with exceeding the shear resistance leading to the formation of smaller aggregates and shear cracks which are low in tortuosity and high in connectivity, leading to an increased soil volume well-connected to the biopore. (II) If the stress application is rectangular to the surface of e.g., the biopore wall, no shear forces occur. Here, two kinds of deformation processes can occur in soils, namely, elastic deformation (the internal soil rigidity is not exceeded, the deformation is reversible), and plastic deformation. The latter one is characterized by exceeding the internal soil rigidity which coincides with aggregate failure, and an irreversible loss of pore volumes and functions. Consequently, a decreased hydraulic and air conductivity or a decreased biological activity is known due to the loss of pore volumes (for more details see Horn and Fleige, 2003 or Haas et al., 2016).

Plastic soil deformation is needed to permanently expand the cavity of the earthworm, or to form the root channel even if it coincides with the blockage of lateral side pores (Pagenkemper et al., 2013). Plastic deformation can be expected to be more intense in the drilosphere, compared with the rhizosphere, caused by the much faster movement of earthworms (Ruiz et al., 2015). Repeated mechanical stress application in vertical biopores can result in the formation of vertically orientated platy structures with relatively well-connected pores. Platy structures are formed when initial plastic deformation is followed by finally elastic deformation.

However, soil compaction also leads to a shift in pore-space distribution (Becher, 1994; Riggert et al., 2017) whereby positive water pressures can be observed (Fazekas and Horn, 2005). Positive water pressures combined with shearing forces which occur due to the cone-shaped tip of the body of earthworms lead to a completely homogenization of soil aggregates, followed by swelling, and the blockage of smaller lateral side-pores. With the reduction of positive water pressures the soil begins to shrink again because the beforehand shear stress induced a mostly homogenized grain size distribution with proportional shrinkage behavior. Continuous but water-saturated pores are formed during such shrinkage. In general, these processes occur in the rhizosphere, too.

Crack-forming processes enhance the soil development also next to biopores, by swelling and shrinkage. In the rhizosphere the number of swelling and shrinkage cycles is enhanced by the hydraulic lift (Vetterlein and Marschner, 1993), which is a redistribution of water from wet to drier soil volumes. The water uptake of plant roots can dry the soil to a matric potential of approximately −1,500 kPa, leading to the formation of shrinkage-induced very rigid cracks. Fine root hairs, which penetrate the soil, result in the creation of new, and highly connected, lateral side pores. Furthermore, whenever a new surface is created, swelling pressures can occur, leading to the formation of new cracks after the pressure dissipated. Thus, crack forming processes result in highly connected pores, with a low tortuosity, altered pore geometry and pore size distribution.

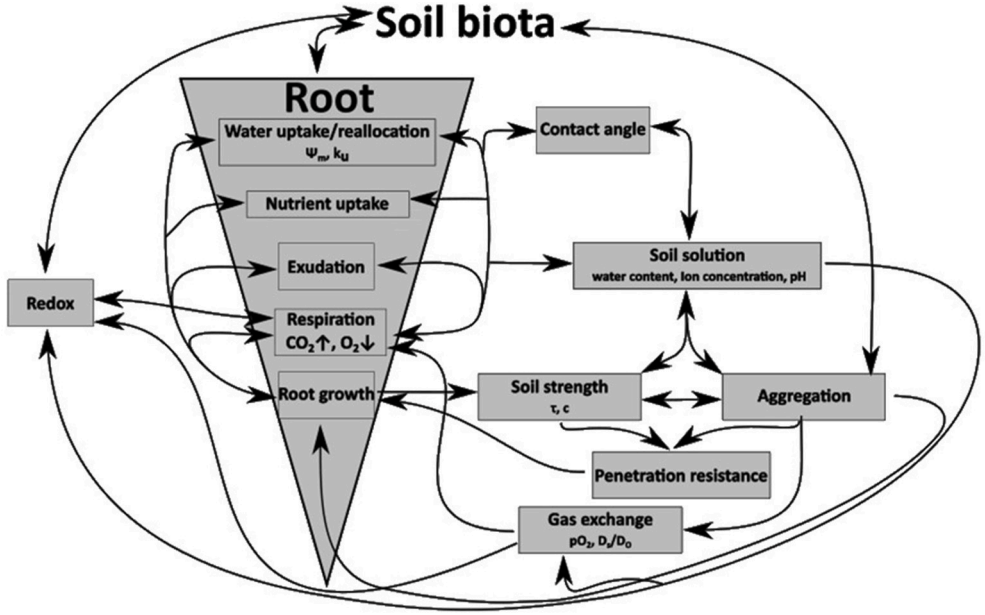

FIGURE 1 | Schematic diagram of the interactions between roots, growth processes, and interactions with the mineral soil phase and their influence of physico-chemical soil properties.

These alterations directly influence physico-chemical parameters like the aeration (in terms of pO_2 and oxygen diffusivity) or to related parameters like Eh and pH and the penetration resistance (**Figure 1**). The microbiological community of biopore walls, for example, depends on the history of the biopore (Banfield et al., 2017), thus an indirect influence on soil development (aggregation) can be expected, since soil biota is linked to aggregate dynamics (see a review of Six et al., 2004).

We therefore formulated the following hypotheses:

- Soil next to biopore walls shows altered physical properties (soil aggregation and penetration resistance) along with altered physico-chemical soil properties (i.e., altered oxygen diffusivity, pO_2, Eh, and pH values).
- These alterations depend on the history of the biopore (e.g., root or earthworm induced or colonized) and, with a view to earthworm burrows, on the duration of the colonization of the biopore [short-time (<6 months) or long-time].

The objective of this paper is to quantify the alteration of physico-chemical parameters like oxygen diffusivity, pO_2, Eh, and pH of biopore walls to better understand exchange and mass transport processes in soils.

To investigate these alterations, small-scaled analyses are conducted. (I) Combining a micromanipulator and a force sensor resulted in a (completely automated) measurement system enabling us to determine oxygen diffusivities or concentrations (pO_2) with coupled measurements of the soil penetration resistances in increments of 100 μm in distance from the biopore surface. (II) An enhanced approach of Uteau et al. (2015) enabled us to determine both, pH and Eh, with a spatial resolution of 100 μm by using a computer numerical controlled (CNC) mill for small-scaled soil displacement. (III) Differences in aggregation were visualized with the help of a scanning electron microscope and the soil structure was classified.

MATERIALS AND METHODS

Soil Material

In total 96 soil cores (3 cm in diameter, 10 cm in height) were excavated in September 2014 from two layers (Bt-1 from 0.45 to 0.55 m and Bt-2 from 0.55 to 0.65 m) from a haplic Luvisol (IUSS Working Group WRB, 2006) in four repetitions (i.e., from four pits) of a totally randomized trial (Kautz et al., 2014) at the experimental area of the Campus Klein-Altendorf (50°37′9″ N 6°59′29″ E, University of Bonn, Germany). The site is characterized by a maritime climate with temperate humid conditions (9.6°C mean annual temperature, 625 mm annual rainfall). Main soil properties are listed in **Table 1**. The Bt horizon is characterized by accumulated clay, leached from the A-horizon (0–0.27 m) and the E horizon (0.27–0.41 m).

Chicory (*Cichorium intybus* L. "Puna," 5 kg ha^{-1} seeding rate) had been grown in these trials for the last 3 years. With its herringbone or monopodial branching root systems *C. intybus* L. penetrates deeply into the subsoil exploring for water and nutrient supply (Kautz et al., 2012). Macroscopic biopores remained in the soil after the roots decayed. Biopores with three different histories were considered: the type of the biopore was classified with the help of an endoscopice. Herefore, a videoscope (Karl Storz GmbH, Tuttlingen, Germany, outer diameter of 3.8 mm, with a 0° direction of view and a flare angle of 80°) was carefully inserted into the macroscopic biopore (Athmann et al., 2013; Kautz et al., 2014). For more details about the used equipment see Athmann et al. (2013). Biopore walls differed visually in dependency to their "history:"

TABLE 1 | Sand, silt, clay, as well as, soil organic carbon (SOC) contents in g kg^{-1} soil, as well as, pH, and electrical conductivity (eC) in $\mu S\ cm^{-1}$ of the four pits where soil cores were excavated from a loess-derived Luvisol, Klein-Altendorf near Bonn, Germany.

Pit	Depth	Sand	Silt	Clay	SOC	pH	eC
	m		g kg^{-1}			–	$\mu S\ cm^{-1}$
24	0.45–0.55	71.4	780	149	4.0	7.0	83
24	0.55–0.65	66.1	730	204	5.8	7.03	74
40	0.45–0.55	54.7	650	295	4.5	6.99	100
40	0.55–0.65	44.8	710	245	3.4	7.11	83
57	0.45–0.55	59.8	770	170	3.9	7.02	81
57	0.55–0.65	44.6	740	215	4.1	7.0	71
74	0.45–0.55	58.9	660	281	4.0	6.98	104
74	0.55–0.65	40.0	700	260	3.8	7.02	77

- Macroscopic biopores colonized and/or created by a plant root [*C. intybus* L., (**R**)] contained residues of decayed roots (<1 mm), frequently showed a very porous filling (macropore root soil), and/or had a very porous pore wall with root residues.
- Biopores colonized and/or created by an earthworm [long-term colonization *of Lumbricus terrestris*, (**EW**)] showed wavy surfaces created by the peristaltic movement of the earthworm. Fresh or slightly decayed plant residues were visible and/or the wall appeared to be very dark in color due to carbon enrichment.
- Classification of biopores colonized and/or created by a plant root followed by short-term (<6 months) colonization of *L. terrestris*, (**REW**) was ensured by classifying R pores, followed by the artifical colonization with *L. terrestris, the feeding with rye residues, and a periodic monitoring of the feeding reception.*

Only macroscopic biopores with diameters of >5 mm sufficient for measurements were considered as sampling object. Biopores were discarded whenever the history could not be determined exactly. Furthermore, the videoscope was not inserted into the investigated soil layer but was inserted several centimeters above. The orientation of the biopores were assumed to be vertical. Not all samples could be investigated because some biopores ended within a few centimeters or due to samples failure at the final cutting process in the laboratory, or due to the occurrence of larger numbers of coarse particles (stones) making measurements with glass electrodes impossible. The number of investigated samples is shown in **Table 2**.

Soils were drained to defined matric potentials ($\Psi_m = -30$ kPa), scanned with the help of a μ-CT (μCT Nanotom© 180; GE Sensing & Inspection Technologies GmbH, Wunstorf, Germany), saturated again and drained to defined matric potentials ($\Psi_m = -1$ kPa; −3 kPa; −6 kPa or −30 kPa) for measurements of oxygen diffusivities or oxygen concentration profiles and coupled penetration resistance. In case of pH and Eh the samples were drained to $\Psi_m = -1$ kPa. After drainage samples were cut vertically into two halves creating two sample sets. While set A was used in this study, set B was used for relating soil organic matter composition to soil water repellency (Haas et al., 2018).

TABLE 2 | Number of investigated samples of biopores colonized and/or created by chicory (*Cichorium intybus L.*) roots (R), colonized and/or created by *Lumbricus terrestris* (EW), and biopores colonized and/or created by a plant root followed by colonization of *L. terrestris* (REW) for samples from Bt-1 (0.45–0.55 m soil depth) and Bt-2 (0.55–0.65 m soil depth) for defined matric potential (kPa).

Matric potential (kPa)	R		EW		REW	
	Bt-1	Bt-2	Bt-1	Bt-2	Bt-1	Bt-2
−1	3	3	3	2	2	2
−3	3	3	2	2	2	2
−6	3	3	3	3	3	3
−30	3	3	2	3	3	2

Shown numbers refer to samples used for D_s/D_o or pO_2. The double number of samples was used for PR. Three replicates were measured on each sample.

Coupled Measurement of Penetration Resistance and O_2 Diffusivity or O_2 Distribution

The measurement system is schematized in **Figure 2**. Clark-Type O_2 microelectrodes (OX-100, UNISENSE A/S, Aarhus, Denmark) connected to a 16 bit AD-converter (4 channel Multimeter, UNISENSE A/S, Aarhus, Denmark) were used to measure the oxygen partial pressure (pO_2), and to determine the relative oxygen diffusion coefficient (D_s/D_O), defined as the ratio of the oxygen diffusion coefficient in the soil (D_s) to that one of oxygen in free air ($D_O = 0.201\ cm^2\ s^{-1}$) at given temperature and atmospheric pressure conditions (Glinski and Stepniewski, 1985). Data were normalized to laboratory conditions (20°C and 101.25 kPa atmospheric pressure).

A motorized micromanipulator (*MM33, MC-232, and MMS, UNISENSE A/S, Aarhus, Denmark*) was used to place O_2 electrodes in defined distances from the biopore wall. Instead of mounting the O_2 electrode directly to the micromanipulator a customized mount was milled. That mount holds the electrode penetrating the soil (bottom) and a threated bar (top) which is connected to a S-shaped force sensor with strain gauge (*KD24s, ME-measurement systems GmbH, Germany*). The latter one is connected to the micromanipulator and to a 16-bit A/D-converter (GSV-1, *ME-measurement systems GmbH, Germany*) which is connected to the measuring PC. The force sensor showed with increasing forces a linear loss in height (2 mm at 10 N). That loss in height was automatically corrected by self-developed software, written in Python 2.7 scripting language (Python Software Foundation, 2017) to ensure that the measurements were performed in correct distance from the biopore wall. To automatize the measurement the reading of the sensor was fetched using PySerial (a python package, Python Software, Python Software Foundation, 2017). The soil penetration resistance (PR) was calculated according to Equation (1):

$$PR_x = F_x \cdot A_x^{-1} \quad (1)$$

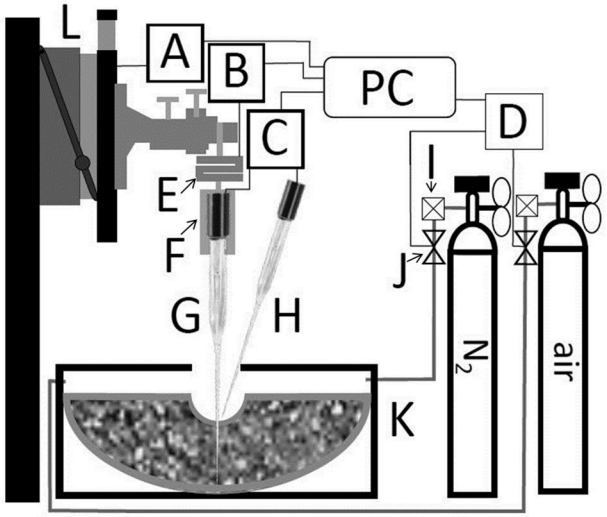

FIGURE 2 | Schematic representation of coupled measurement of penetration resistance and either oxygen diffusivity or oxygen distribution. Motorized micromanipulator (L) with motor driver (A). S-shaped force sensor (E) with A/D-converter (B). Customized mount (F) with electrode 2 (G) placed in soil. Electrode 1 (H) placed at soil surface. Both electrodes were connected to UniSense multimeter (C). Microcontroller board (D) controlled magnet valves (J). The outflow of gas bottles is regulated with flowmeter (I). (A), (B), (C), and (D) are connected to a personal computer (PC) with UniSense software controlled by self-developed software.

with soil penetration resistance PR (Pa), the measured force f (N) and the area of the penetrating electrode A (m^2) in each distance from the biopore surface x. Microscopy images of the tips of the electrodes were used to determine the diameter in increments of 100 µm in distance from the electrodes tip.

By penetrating the soil, air in the electrode tip gets compressed. Therewith, a temporarily peak in O_2 concentration can be observed, whenever the electrode proceeds to the next measurement depth. This behavior of the electrode can be used to find the samples surface: Whenever the tip of an electrode hits the surface of the soil sample a temporarily peak in O_2 concentration can be observed followed by a sharp decrease in O_2 concentration. This occurrence is linked with the air-filled volume in the sensor tip which fades off depending on the local air permeability. The peak usually occurred for <10 s. Because of differences in water-saturation we found 30 s to be long enough for stable and reliable measurement readings.

Oxygen diffusivities for (un-)saturated soil were determined according to Equation 2 (Rappoldt, 1995):

$$D_s \cdot D_O^{-1} = \frac{(\omega \cdot d^2)}{2} \cdot \varepsilon \cdot D_O^{-1} \quad (2)$$

with D_S = diffusion coefficient of O_2 in soil (m^2 s^{-1}); D_O = diffusion coefficient in air (m^2 s^{-1}); ε = gas-filled porosity (m^3 m^{-3}); ω angular frequency(s^{-1}); d = damping depth (m, see Equation 3). For determining the O_2 diffusivity, a one-dimensional O_2 concentration wave is applied at the surface of the soil sample. This is achieved by periodically flushing the measurement chamber with either nitrogen or air. Magnetic valves had been used to control the outflow of gas containers and to alternate the O_2 concentration in the measurement chamber. Two gases were used: N_2 (*AlphaGaz 1, Air Liquide*) for lowering the O_2 concentration or synthetic air (20.5 ± 0.5% O_2 in N_2, *AlphaGaz 1, Air Liquide*) to rise pO_2 to (more or less) atmospheric pO_2. Each valve (12 V) was operated by using a simple circuit containing a NPN-transistor (TIP 120), a resistor (10 k Ω) and a microcontroller board (*Arduino Uno)*. The *Arduino Uno* was programmed using the *Arduino software* in a way where it opens valve 1, valve 2 or none of both valves after it received a defined signal by the self-developed software using PySerial (a python package, Python Software Foundation, 2017). With the help of two O_2 electrodes (*electrode 1* is placed at the soil surface, and *electrode 2* is placed in defined distances from the biopore surface) a phase shift ϕ(x) between the concentration waves can be observed, showing a delay in depth × relative to the surface wave (Rappoldt, 1995). In general, the amplitude of the concentration wave decreases exponentially with increasing distance from the biopore, whereas the phase shift increases linearly. Equation (3) was used to calculate the *damping depth d* (Rappoldt, 1995):

$$d = x\phi(x)^{-1} \quad (3)$$

With phase shift $\phi(x)$ in depth x. Once d is known, Equation (2) is used to calculate the diffusivity D_S.

PyAutoIT (Xu, 2017) is a python module which needs AutoIt v3 (Bennett and the AutoIt Team, 2017), a freeware BASIC-like scripting language designed for automating the Windows GUI and general scripting. *PyAutoIT* was used to completely automatize the measurement by simulating keystrokes and mouse movements for controlling the software (*Sensor Trace Pro)* of the UniSense multimeter with highest precision in time domain. *NumPy* (NumPy developers, 2017)[1] was used for data evaluation and the calculation of the phase shift $\phi(x)$. This setup enabled us to determine both parameters (D_s/D_O and pO_2) within 0–3,500 µm in distance from the biopore surface in increments of 100 µm, or for PR with a spatial resolution of ≤5 µm. Values of PR are presented as means for each increment (0–100 µm; 100–200 µm, …, 3,400–3,500 µm).

Air-filled porosities (ε) were calculated by subtracting the weight of the saturated sample of the weight of the drained sample followed by division with the corrected sample volume calculated from x-ray microtomography. In this study, the corrected sample volume is defined by the difference of the total sample volume and the volume of the macroscopic biopore (calculated from CT-data by Wittig et al., unpublished).

Redox Potentials and pH Measurements

For measuring pH and Eh the manual approach applied by Uteau et al. (2015) was refined to a semi-automatic procedure using a computer numerical controlled (CNC) mill to which a twisted drill was attached. Therewith, we were able to scrape

[1] Available online at: http://www.numpy.org/

off the uppermost soil material with a high spatial resolution (increments of the used stepper motors equals 8 μm).

Calibration of Micro-Electrodes and Mirco-Sensors

A two point calibration was applied for all used micro-electrodes and micro-sensors. For Clark type O_2 electrodes the zero point (0 kPa) was reached with an anoxic solution (2 g sodium ascorbate diluted in 100 mL of 0.1 M NaOH), while $pO_2 = 20.95$ kPa were assumed for a well aerated (by bubbling ambient air into the water) aqueous calibration solution. Eh and pH microelectrodes were calibrated by placing both, the reference electrode and the redox microelectrode tips to quinhydrone redox buffers (pH 4 equal to 470 mV and pH 7 equal to 295 mV at 20°C).

Scanning Electron Microscope (SEM) and Description of the Soils Structure

Scanning electron microscopy (SEM) was performed with CamScan CS 44 (CamScan Ltd., Cambridgeshire, UK). SEM micrographs were obtained at 15 keV. Monochrome photographs were taken with an integrated reflex camera. A detailed description of SEM, microanalysis with 200 or 700 magnification factors and their applications are given in Goldstein (2003). The soil structure was described using a system (Babel et al., 1995) which is based on soil physical theory and can be applied on various scales. Four levels are needed to describe aggregate properties (size, shape, movement, packing and surface). The fifth level describes further soil properties like the pore water pressure.

Statistical Analyses

The statistical software R (R Core Team, 2017) was used to evaluate the data. The data evaluation started with the definition of an appropriate statistical mixed model (Laird and Ware, 1982; Verbeke and Molenberghs, 2000) for the logarithmized D_s/D_O-values. The assumption that logarithmized D_s/D_O-values were normally distributed distributed and homoscedastic are based on a graphical residual analysis.

The statistical model included the history of the biopore (referred as history, as shown in section Material and Methods), the sampling depth (0.45–0.55 m and 0.55–0.65 m) and the distance from the biopore surface (0–3,500 μm), as fixed factors according to the following equation:

$$Ds/Do_{ij} = e^{a_{ij}*\Psi_{mij}} * e^{b_{ij}*dist} * e^{c_{ij}} \quad (4)$$

with *a*, *b*, and *c* as fitting parameter, e is Euler's number, *i* and *j* for the histories of the biopores and the depths, and *dist* for the distance from the biopore surface (10^{-3} m). Model for penetration resistance and O_2 partial pressure behaved analogously to D_S/D_O. All regression coefficients are shown in **Table 3**. The covariates (and potential interaction effects) are based on a model selection. Assuming a split-plot design random effects were defined by the pits and suitable interaction effects with the history of the biopore, the sampling depths and with the soil core. Based on this model, a pseudo-R^2 was calculated (Nakagawa and Schielzeth, 2013) and an analysis of covariances (ANCOVA) was conducted (Cochran, 1957).

RESULTS AND DISCUSSION

Differences in aggregation were confirmed by scanning electron microscope (SEM) micrographs, shown in **Figure 3**. For R pores (i.e., colonized and/or created by a plant root), a very porous surface can be observed in comparison with surfaces of EW or REW (colonized and/or created by *L. terrestris* for long-term or short-term, respectively). Round-shaped lateral pores (marked with "a") are visible for all pore types and at both magnification factors (namely, 200 and 700) and are possibly created by lateral side roots (Roose et al., 2016) or soil fauna. Shrinkage induced cracks can be observed next to these round-shaped pores and for very plane and homogenous surfaces of REW. With a magnification factor of 700 the first and second crack generation becomes visible (marked with "b"). These soil systems are biologically altered by e.g., fungal hyphae ("c"). Platy structures are marked with "d." SEM micrographs underline the very different soil structure for biopore with differing histories and are helpful to explain the results of coupled measurement of penetration resistance and O2 diffusivity or O2 distribution.

Following the soil structure classification system by Babel et al. (1995) first the size of the aggregate is defined by the amount of occurring cracks. Biopore walls of R and EW were classified as *microaggregated* because two or more cracks were found within a distance of 100 μm (**Figure 3**), while REW was classified as *microcoherent* were no or one crack showed within a distance of 100 μm. The second level defines the shape of the aggregates. Micro-aggregates at the surfaces of R showed subpolyeders (all three axes are of approximately equal length with mostly rounded edges and some planes), while those of EW and REW showed micro-aggregates where two axis are larger than the third one. Micro-aggregates of EW and REW were classified as *subplates* (edges rounded, planes visible) and *plates* (aggregate sharp edged), respectively. With the third level the movement and packing of aggregates is considered: R and REW were classified as *original*, because aggregates were not rearranged after the formation of stress and shear induced cracks. EW aggregates were classified as rearranged, due to the repeated earthworms moving action. Within the fourth level the surface of the aggregates is described. The porosity decreased in the order R > EW > REW. R and EW were classified as *porous* [with both, biological and physical induced cracks (by shrinkage and swelling)]. REW showed *dense* surfaces, with cracks caused by two shrinkage and swelling-cycles, which resulted in the formation of primary and (rectangular to these cracks) secondary cracks (**Figure 3**). Surfaces of R consisted of randomly arranged particles (classified as *rough*). REW showed oriented particles (classified as *smooth*). A new class was needed to describe the surfaces of EW. Here, orientated particles formed porous surfaces EW (namely, *porous and rough*). Two other parameters which refer to the grain size distribution or the color were not considered. The pore water pressure at time of observation is classified as *dry* (namely $pF \geq 3.5$) for all types, since SEM was performed on air-dried samples. For the same reason the strength of the micro-aggregates can be classified as *strong*, because the soil can only be deformed at high forces.

TABLE 3 | Regression coefficients according to Equation (4) for penetration resistance (PR, Pa), relative oxygen diffusion coefficient (D_S/D_O) and oxygen partial pressure (pO_2) for biopores colonized and/or created by chicory (*Cichorium intybus L.*) roots (R), colonized and/or created by *Lumbricus terrestris* (EW), and biopores colonized and/or created by a plant root followed by colonization of *L. terrestris* (REW) for samples from Bt-1 (0.45–0.55 m soil depth) and Bt-2 (0.55–0.65 m soil depth).

		R		EW		REW	
	Regression coefficient	**Bt-1**	**Bt-2**	**Bt-1**	**Bt-2**	**Bt-1**	**Bt-2**
PR (Pa)	a	−5,908.6	−1,282.7	−12,230.0	−2,468.1	−3,515.4	−2,149.2
	b	−527.9	1,074.4	−283.9	99.6	218.5	162.9
	c	51,571.7	29,044.6	30,910.7	48,652.5	266,363.7	73,627.0
DS/DO (–)	a	−0.072	−0.138	−0.035	−0.052	−0.008	−0.095
	b	−0.017	0.025	0.055	0.045	0.072	0.047
	c	−3,973	−7,303	−5,645	−6,454	−5,532	−7,680
pO_2 (kPa)	a	0.054	−0.078	0.109	−0.051	−0.033	0.104
	b	0.000	0.000	−0.001	0.000	0.000	0.000
	c	13,049	13,991	15,321	14,553	14,329	11,385

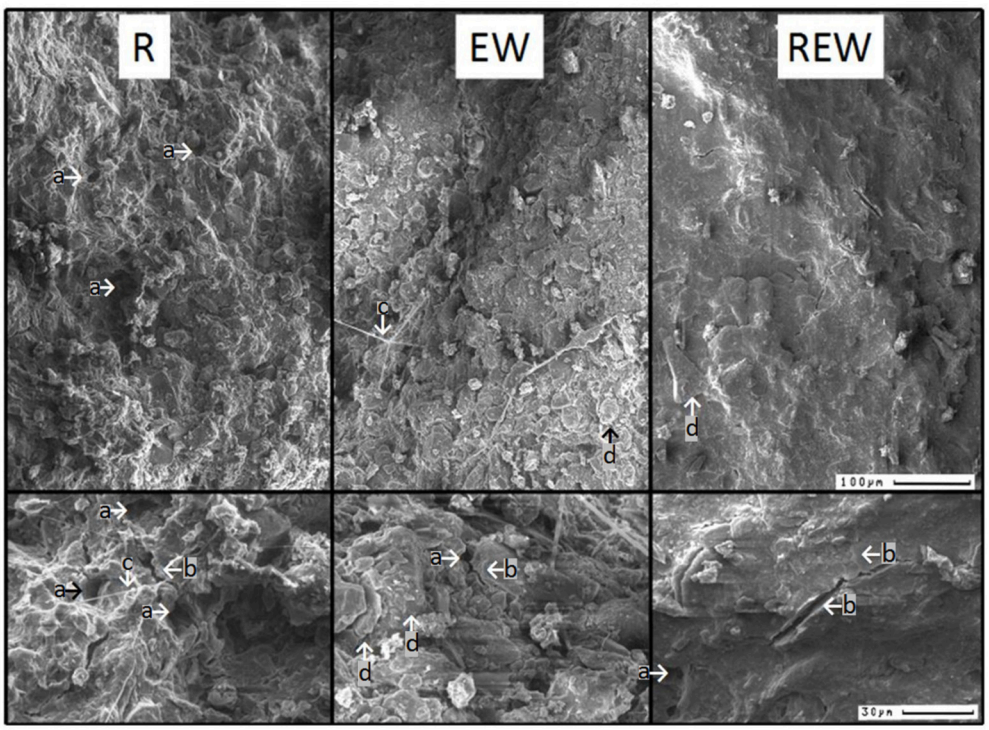

FIGURE 3 | Exemplary scanning electron microscope images of biopore walls [pore colonized by root (R), colonized by *L. terrestris* (EW), and (REW) just like R but followed by short-term (<6 months) colonization of *L. terrestris*]. Using a magnification factor of 200 (upper-row) or 700 (lower row), a very porous surface for R can be observed in comparison with surfaces of EW or REW. Exemplary pores, created by lateral side roots are marked with "a," exemplary shrinkage-induced cracks (due to root water uptake or initial shrinkage) with "b." Fungal hyphae networks are indicated by "c." Platy structures are clearly visible for EW (d).

The model output of the statistical analysis for the penetration resistance as a measure of soil stability is shown in **Figure 4**. PR showed highly significant ($p < 0.001$) interactions with the history of the pore, the matric potential, the distance from the biopore surface and the sampled depth. Interestingly, the chemical composition (in terms of hydrophobic and hydrophilic functional groups) of these biopore walls showed highly significant ($p < 0.001$) interactions with the history of the pore, the matric potential, the distance from the biopore surface and the sampled depth, as also mentioned by Haas et al. (2018). PR increased with increasing drainage (more negative matric potential, **Figure 4**, **Table 3**). This is especially distinctive for the upper depth (Bt-1, 0.45–0.55 m), and reflects the more pronounced aggregate development caused by swelling and shrinkage (Becher, 1991, 1994) at this depth compared to the deeper one. Values for PR of earthworm colonized pore walls (R) exceed the maximum pressure *L. terrestris* is able to apply to soils (195 kPa according to Keudel and Schrader, 1999). This increased

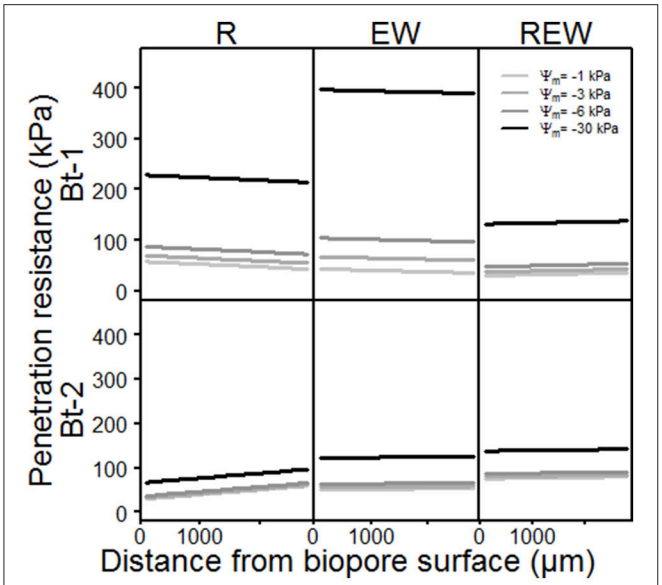

FIGURE 4 | Model output of the statistical analysis of penetration resistance of biopore walls [pore colonized by root (R), colonized by *L. terrestris* (EW) and (REW) just as R but followed by short-term (<6 months) colonization of *L. terrestris*] as a function of matric potential.

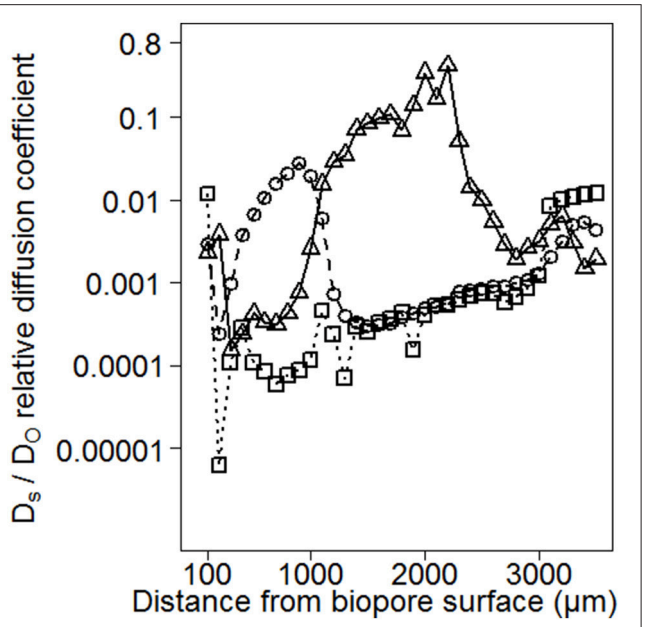

FIGURE 5 | Consequences of small-scaled differences in aggregation for D_S/D_O exemplarily for three replicated measurements within the same biopore wall. Deviations up to several orders of magnitude are observed for the replicates.

PR is possibly caused by calcite, released from specialized esophageal glands of *L. terrestris* (Lankester, 1865). Calcite can influence PR not only by enhancing the soil development by altering the biological activity in soils (Mordhorst et al., 2017) but also by forming crusts on the aggregate surface and by coagulating primary particles. Biological crusts also may have caused these altered PR (Chamizo et al., 2015). This intensified aggregate development led to highest PR for the surface of the biopore (distance = 0 µm), indicated by the negative slope of the curve (EW, Bt-1). The negative slope which is also found for R (Bt-1) reflects the intensified aggregate development, caused by both, an intensified shrinkage caused by root water-uptake, and an increased number of swelling-and-drying-cycles caused by hydraulic lift (Vetterlein and Marschner, 1993). The PR of REW in Bt-1 and of all types of biopores in Bt-2 behaved in an opposite way: The lowest PR was found at the surface of the biopore wall possibly caused by homogenization and the coinciding loss of soil strength at higher water contents. Further possible explanations are the generally increasing water contents with depth at field condition (for Bt-2) or with increased water content caused by exudates (REW, Bt-1). Gerard et al. (1982) computed regression models (stepwise) for both, root growth and soil strength, as dependent variables, using soil type, soil depth, clay content, bulk density, voids, and water content as independent variables. The considered soil types were a sandy loam and a clay loam. Soil strength was significantly influenced by voids, and clay content, while root growth was additionally influenced by volumetric water content, whereas decreasing soil strength were found with increasing clay content, voids and water content or decreasing soil depth. In this study, the statistical analysis of PR only confirms the influence of water contents on soil strength on the micro scale. This is caused by but the lack of information about small scaled differences in clay content and total or air-filled porosity which were assumed to be homogeneous within a single sample. Small scaled differences in pore volumes or textural differences can be determined with the help of micro X-ray computed tomography (Peth et al., 2010; Rogasik et al., 2014) or infrared spectroscopy (Leue et al., 2010; Stenberg et al., 2010), respectively.

Consequences of small-scaled differences in aggregation for D_S/D_O are shown exemplarily for three replicated measurements within the same biopore wall (**Figure 5**). This earthworm burrow showed deviations up to several orders of magnitude for the replicates of D_S/D_O. The minimum value of 6×10^{-6} indicates a water-filled (Glinski and Stepniewski, 1985) and/or a tortuous or not well-connected pore system while the maximum value of 0.14 is higher than those measured on soil cores by Mordhorst et al. (2017).

Consequences of differences in aggregation on pore functions are shown in **Figures 6A,B** and **Table 3** for D_S/D_O, and for pO_2, for biopore walls and their surrounding soils in dependency of the considered matric potentials ($\Psi_m = -1$ kPa; -3 kPa; -6 kPa and -30 kPa). Both parameters (D_S/D_O and pO_2) showed highly significant ($p < 0.001$) interactions with the history of the biopore, the matric potential, the distance from the biopore surface and the sampled depth. In general, D_S/D_O increases with decreasing (more negative) matric potential, and whenever the pore wall had been influenced by an earthworm, higher D_S/D_O values can be observed for Bt-1 compared to Bt-2. Biopore walls that had been colonized by a plant root (R) showed the highest

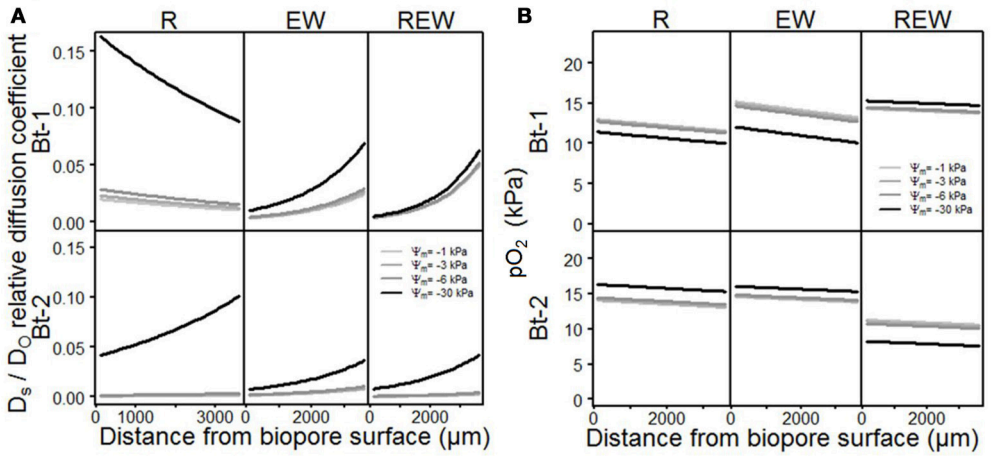

FIGURE 6 | Model output of the statistical analysis for **(A)** relative diffusion coefficient D_S/D_O ratio of soil oxygen diffusion coefficient (D_S) to air (D_O) and **(B)** oxygen partial pressure pO_2, of biopore walls [pore colonized by root (R), colonized by *L. terrestris* (EW) and (REW) just as R but followed by short-term (<6 months) colonization of *L. terrestris*] as a function of matric potential.

values for D_s/D_O which can be found in 0 mm distance from the biopore surface (Bt-1), or within 0–3,500 µm (Bt-2).

In the sphere of plant roots, root water uptake and root water redistribution enhanced the aggregation leading to the formation of highly connected shrinkage cracks. The pore-size distribution is also altered by decaying lateral side roots and fine roots whereas highly-connected coarse are created. This effect is especially visible in Bt-1 (R). The shift of pore functionality is especially distinctive for REW where further drainage from −1 to −6 kPa had almost no influence on already high values of D_s/D_O for the wettest condition ($\Psi_m = -1$ kPa) proving the alteration of pore functions by earthworms. For R in Bt-1 a more pronounced influence of the drainage can be observed by a more pronounced increase of D_s/D_O with more negative matric potential (e.g., from $\Psi_m = -1$ to -3 kPa) if compared with the deeper depth or with the other biopore types. This reflects an increased pore function for pores >300 µm to 50 µm (corresponding to the drainage to $\Psi_m = -1$ and to $\Psi_m = -6$ kPa) and follows the root length density as measured after 2 years of *C. intybus* (Perkons et al., 2014). The higher D_s/D_O of Bt-1 compared with Bt-2 can be explained by the intensified soil structure development with decreasing depth, providing a more continuous pore system.

The influence of earthworms on aggregation, which include processes like homogenization of the surrounding soil volume by shearing, smearing and therewith occurring blockage of smaller lateral side pores (see also Pagenkemper et al., 2013), is also reflected by alterations in pore functions (Horn and Fleige, 2003). It can be confirmed for the micro-scale by reduced values for D_s/D_O for biopores of EW and REW-type, as well as aggregation of biopore walls of the REW-type which was more homogenous than that of the R-type (**Figure 3**).

These altered pore functions alter the gas composition, consequently. The oxygen partial pressure (pO_2) decreased with increasing distance from the biopore surface (**Figure 6B**) and decreased with increasing water content (REW in Bt-1, R and EW in Bt-2). This is in accordance with Zausig and Horn (1992) and can be explained by the lower diffusion coefficient for O_2 in water compared to air. The remaining variants (R and EW in Bt-1 and REW in Bt-2) behaved contrarily. Here, lower pO_2 was found with decreasing water content (more negative matric potential). This can also be found when studying some literature attentively (e.g., Zausig et al., 1993) but has never been discussed so far. A possible explanation is: If a micro sensor is inserted into an almost water-saturated soil the degree of water-saturation can increase because an additional volume is added to the soil. With the resulting shift in pore-space distribution larger pores become thinner due to compaction (Becher, 1994; Riggert et al., 2017) and positive water pressure can occur. Furthermore, due to the cone-shaped tip shearing occurred leading to the homogenization of soil aggregates and with that to swelling. The following reduction of the positive water pressure results in the formation of coarser and continuous interaggregate pores. The soil solution that is found in these regions, saturated with water but poor in O_2, is mixed with soil solution of the aggregates' exterior, where higher pO_2 is expected (Horn, 1994). These processes will not occur if the water content is lower ($\Psi_m = -30$ kPa), because of the larger aggregate stability. This results in lower values for pO_2 with lower water contents.

Ecological Impact of Altered Pore Functions and Gas Composition

How far changes in aggregation, the arrangement of particles within the pore wall and differences in pore size distribution interact with the kind and intensity of the living organisms or the decaying roots can be elucidated with the Eh and pH pattern. Exemplary results for Eh and pH are shown in **Figure 7**. For both parameters, there were only weak ($0.05 \leq p \leq 0.1$) statistical interactions with the distance from the biopore surface, the history of the biopore and the depth. Representative results

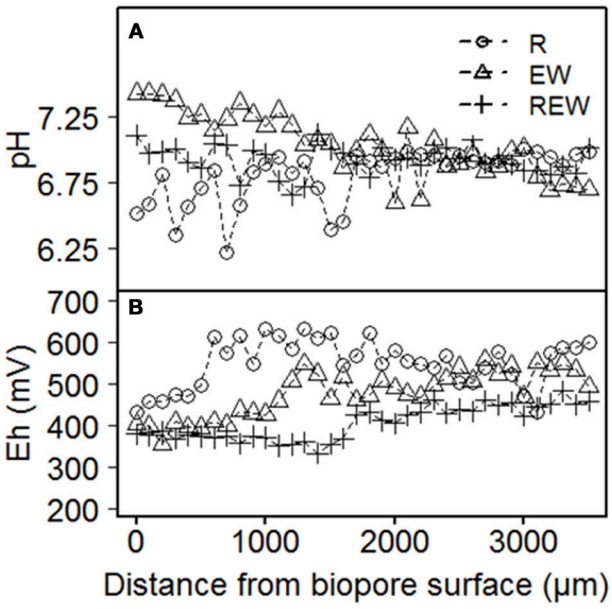

FIGURE 7 | Exemplary results of **(A)** pH and **(B)** Eh of biopore walls [pore colonized by root (R), colonized by *L. terrestris* (EW) and (REW) equal to R but followed by colonization of *L. terrestris*]. Samples drained to $\Psi_m = -1$ kPa.

show that pH of the biopore wall decreases from EW to REW to R (**Figure 7A**). In distances >1,000 µm from the biopore wall, differences between the histories could not be found. The pH values next to R-type biopores showed an intense scattering in the range from 6.2 to 7.1. Higher pH values may be caused by released calcite by earthworms, while lower pH values next to R-type biopores are caused by the plants release of H^+.

Eh-values for biopore surfaces (=0 µm) were in a close range (380–430 mV) and increased tendentially with increasing distance from the biopore surface. Thus, Eh-values can be classified (Zhi-Guang, 1985) as oxidizing (>400 mV; O_2 predominant) or weakly reducing (400 mV to 200 mV; O_2, nitrate-N and Mn(II, IV) reduced). An expected decrease of Eh with increasing distance from the biopore surface (caused by weaker aeration) was not found within 3,500 µm in distance from the biopore surface. Shown values were not corrected for pH. R-type biopores showed the highest values for Eh and increased within a distance <1,000 µm from the biopore surface, whereas those of the EW-type biopore increased after approximately 1,000 µm and those of the REW-type biopore within 1,500 µm. Such a pattern may reflect the increased organic carbon content next to biopore surfaces and the increased aeration due to lateral side roots (in case of R-type biopore).

Redox potentials were in the same range as those of Zausig et al. (1993) who investigated soil rich in clay, namely an Udert and an Udifluvent soil. Zausig et al. (1993) found anoxic aggregate centers that were not always accompanied by a decrease in redox potential and assumed that these effects are induced by different microbial activities as well as by differing redox buffering systems of the investigated soils. If we consider the dynamics in the drilosphere much lower redox potentials were expected, because of the disruption of aggregates, the following release of organic carbon and the subsequent oxidation of these molecules.

Under consideration of further methodological limitations which may affect the actual *in situ* aeration and redox reactions we may include the disadvantage of the applied pO_2 and Eh measuring procedure under laboratory conditions with the relatively high pO_2 and Eh-values due to (a) the removal of soil and therewith decreased distances for diffusion and (b) the increased pO_2 under laboratory conditions, compared with the pO_2 under field conditions. The effect of these parameters need further research in order to quantify such side effects.

CONCLUSIONS

This study aimed at quantifying the effects of micro-aggregation within macroscopic biopore walls on physico-chemical parameters such as oxygen diffusivity, oxygen partial pressure, Eh, and pH. The conclusions are as follows:

(I) The refined measurement approach allowed the coupled determination of penetration resistance with either oxygen diffusivity or oxygen partial pressure. The automation improved the measurement system by controlling the precision of spatial and temporal resolution of the measurement steps. The use of cylindrical-shaped electrodes was found superior over cone-shaped electrodes because of the lower shearing.

(II) Biopore history-dependent differences in the morphology of micro-aggregates were confirmed with the help of scanning electron microscopy. Both, plant roots and earthworms alter soil structure next to biopore surfaces with contradictory impact: soil structure formation is enhanced by roots while aggregates are homogenized by earthworms with a consecutive reformation.

(III) Differences in aggregation were found to result in differences in pore functions. The observed alterations in structure by roots and earthworms impact on pore functions responsible for water flow and gas transport processes (i.e., pore-size distribution, tortuosity, connectivity, and pore geometry). While these relationships were already known for the mesoscale (cm-to-m), they were confirmed here for the microscale (µm-to-mm).

(IV) The Eh and pH mm-scale patterns can be used as indicator for interactions of microbial colonization, soil structure, and soil rooting conditions.

The results improved understanding of interactions between soil physico-bio-chemical properties at the scale of micro-aggregates or macropore walls.

AUTHOR CONTRIBUTIONS

All authors listed have made a substantial, direct and intellectual contribution to the work, and approved it for publication.

ACKNOWLEDGMENTS

This study was funded by the German Research Foundation (DFG), Bonn, under grants PAK 888. We thank Timo Kautz and the staff of the Institute of Organic Agriculture in Bonn for assistance with the field work. Many thanks to the reviewers for their very helpful comments.

REFERENCES

Athmann, M., Kautz, T., Pude, R., and Köpke, U. (2013). Root growth in biopores–evaluation with *in situ* endoscopy. *Plant Soil* 371, 179–190. doi: 10.1007/s11104-013-1673-5

Babel, U., Benecke, P., Hartge, K. H., Horn, R., and Wiechmann, H. (1995). "Determination of soil structure at various scales," in *Soil Structure, Its Development and Function*, eds K. H. Hartge, and B. A. Stewart (Boca Raton, FL: CRC Press), 1–10.

Banfield, C. C., Dippold, M. A., Pausch, J., Hoang, D. T. T., and Kuzyakov, Y. (2017). Biopore history determines the microbial community composition in subsoil hotspots. *Biol. Fertil. Soils* 9, 54 doi: 10.1007/s00374-017-1201-5

Baumgarten, W., Dörner, J., and Horn, R. (2013). Microstructural development in volcanic ash soils from South Chile. *Soil Till. Res.* 129, 48–60. doi: 10.1016/j.still.2013.01.007

Becher, H. H. (1991). Observations on soil aggregates following measurements of penetration resistance. *Soil Tech.* 4, 351–362. doi: 10.1016/0933-3630(91)90013-D

Becher, H. H. (1994). Soil compaction around a small penetrating cylindrical body and its consequences. *Soil Tech.* 7, 83–91. doi: 10.1016/0933-3630(94)90009-4

Bengough, A., and Mullins, C. (1990). Mechanical impedance to root growth: a review of experimental techniques and root growth responses. *J. Soil Sci.* 41, 341–358. doi: 10.1111/j.1365-2389.1990.tb00070.x

Bennett, J., and the AutoIt Team. (2017). *AutoIt*. Available online at: https://www.autoitscript.com/site/autoit/

Bouché, M. B. (1975). "Action de la faune sur les etats de la matiere organique dans les ecosystemes," in *Humification et Biodegradation*, eds G. Kilbertius, O. Reisinger, A. Mourey and J. A. C. da Fonseca (Sarreguemines: Pierron), 157–168.

Brown, G. G., Barois, I., and Lavelle, P. (2000). Regulation of soil organic matter dynamics and microbial activity in the drilosphere and the role of interactions with other edaphic functional domains. *Eur. J. Soil Biol.* 36, 177–198. doi: 10.1016/S1164-5563(00)01062-1

Chamizo, S., Rodríguez-Caballero, E., Cantón, Y., Asensio, C., and Domingo, F. (2015). Penetration resistance of biological soil crusts and its dynamics after crust removal: relationships with runoff and soil detachment. *Catena* 126, 164–172. doi: 10.1016/j.catena.2014.11.011

Cochran, W. G. (1957). Analysis of covariance–its nature and uses. *Biometrics* 13, 261–281.

Don, A., Steinberg, B., Schöning, I., Pritsch, K., Joschko, M., and Gleixner, G. (2008). Organic carbon sequestration in earthworm burrows. *Soil Biol. Biochem.* 40, 1803–1812. doi: 10.1016/j.soilbio.2008.03.003

Fazekas, O., and Horn, R. (2005). Zusammenhang zwischen hydraulischer und mechanischer Bodenstabilität in Abhängigkeit von der Belastungsdauer. *J. Plant Nutr. Soil Sci.* 168, 60–67. doi: 10.1002/jpln.200421381

Fér, M., Leue, M., Kodešová, R., Gerke, H. H., and Ellerbrock, R. H. (2016). Droplet infiltration dynamics and soil wettability related to soil organic matter of soil aggregate coatings and interiors. *J. Hydrol. Hydromech.* 64, 111–120. doi: 10.1515/johh-2016-0021

Gerard, C. J., Sexton, P., and Shaw, G. (1982). Pyhsical factors influencing soil strength and root growth. *Agron J.* 74, 875–879. doi: 10.2134/agronj1982.00021962007400050025x

Glinski, J., and Stepniewski, W. (1985). *Soil Aeration and its Role for Plants*. Boca Raton, FL: CRC Press.

Goldstein, J. I. (2003). *Scanning Electron Microscopy and X-ray Microanalysis*, *3rd Edn*. New York, NY: Kluwer Academic/Plenum Publishers.

Haas, C., Gerke, H. H., Ellerbrock, R. H., Hallett, P. D., and Horn, R. (2018). Relating soil organic matter composition to soil water repellency for soil biopore surfaces different in history from two Bt horizons of a Haplic Luvisol. *Ecohydrology* 2018:e1949. doi: 10.1002/eco.1949

Haas, C., Holthusen, D., Mordhorst, A., Lipiec, J., and Horn, R. (2016). Elastic and plastic soil deformation and its influence on emission of greenhouse gases. *Int. Agrophys.* 30, 173–184. doi: 10.1515/intag-2015-0088

Hoang, D. T. T., Pausch, J., Razavi, B. S., Kuzyakovam, I., Banfield, C. C., and Kuzyakov, Y. (2016). Hotspots of microbial activity induced by earthworm burrows, old root channels, and their combination in subsoil. *Biol. Fertil. Soils* 52, 1105–1119. doi: 10.1007/s00374-016-1148-y

Horn, R. (1994). "Effect of aggregation of soils on water, gas and heat transport," in *Flux Control in Biological Systems*, ed E. D. Schulze (San Diego, CA: Academic Press), 335–364.

Horn, R., and Fleige, H. (2003). A method for assessing the impact of load on mechanical stability and on physical properties of soils. *Soil Till. Res.* 73, 89–99. doi: 10.1016/S0167-1987(03)00102-8

IUSS Working Group WRB (2006). *World Reference Base for Soil Resources*, World Soil Resources Reports No 103. Rome: FAO.

Jarvis, N. J. (2007). A review of non-equilibrium water flow and solute transport in soil macropores: principles, controlling factors and consequences for water quality. *Eur. J. Soil Sci.* 58, 523–546. doi: 10.1111/j.1365-2389.2007.00915.x

Kautz, T., Amelung, W., Ewert, F., Gaiser, T., Horn, R., Jahn, R., et al. (2012). Nutrient acquisition from arable subsoils in temperate climates: a review. *Soil Biol. Biochem.* 57, 1003–1022. doi: 10.1016/j.soilbio.2012.09.014

Kautz, T., Lüsebrink, M., Pätzold, S., Vetterlein, D., Pude, R., Athmann, M., et al. (2014). Contribution of anecic earthworms to biopore formation during cultivation of perennial ley crops. *Pedobiologia* 57, 47–52. doi: 10.1016/j.pedobi.2013.09.008

Keudel, M., and Schrader, S. (1999). Axial and radial pressure exerted by earthworms of different ecological groups. *Biol. Fertil. Soils* 29, 262–269.

Laird, N. M., and Ware, J. H. (1982). Random-effects models for longitudinal data. *Biometrics* 38, 963–974.

Lankester, E. R. (1865). The anatomy of the earthworm. *J. Cell Sci.* s2–5, 99–116.

Leue, M., Ellerbrock, R. H., Bänninger, D., and Gerke, H. H. (2010). Impact of soil microstructure geometry on DRIFT spectra: comparisons with beam trace modelling. *Soil Sci. Soc. Am. J.* 74, 1976–1986. doi: 10.2136/sssaj2009.0443

McKenzie, B. M., Bengough, A. G., Hallett, P. D., Thomas, W. T. B., Forster, B., and McNicol, J. W. (2009). Deep rooting and drought screening of cereal crops: a novel fieldbased method and its application. *Field Crops Res.* 112, 165–171. doi: 10.1016/j.fcr.2009.02.012

Mordhorst, A., Zimmermann, I., Fleige, H., and Horn, R. (2017). Changes in soil aeration and soil respiration of simulated grave soils after quicklime application. *J. Plant Nutr. Soil Sci.* 180, 53–164. doi: 10.1002/jpln.201600351

Nakagawa, S., and Schielzeth, H. (2013). A general and simple method for obtaining R2 from generalized linear mixed-effects models. *Methods Ecol. Evol.* 4, 133–142. doi: 10.1111/j.2041-210x.2012.00261.x

Pagenkemper, S. K., Peth, S., Uteau Puschmann, D., and Horn, R. (2013). "Effects of root-induced biopores on pore space architecture investigated with industrial X-ray computed tomography," in *Soil-Water-Root Processes: Advances in Tomography and Imaging*, eds S. H. Anderson and J. W. Hopmans (Madison, WI: American Society of Agronomy), 69–96.

Parkin, T. B., and Berry, E. C. (1999). Microbial nitrogen transformations in earthworm burrows. *Soil Biol. Biochem.* 31, 1765–1771. doi: 10.1016/S0038-0717(99)00085-1

Passioura, J. B. (2002). Soil conditions and plant growth. *Plant Cell Environ.* 25, 311–318. doi: 10.1046/j.0016-8025.2001.00802.x

Perkons, U., Kautz, T., Uteau, D., Peth, S., Geier, V., Thomas, K., et al. (2014). Root-length densities of various annual crops following crops with contrasting root systems. *Soil Till. Res.* 137, 50–57. doi: 10.1016/j.still.2013.11.005

Peth, S., Nellesen, J., Fischer, G., and Horn, R. (2010). Non-invasive 3D analysis of local soil deformation under mechanical and hydraulic stresses by μCT

and digital image correlation. *Soil Till. Res.* 111, 3–18. doi: 10.1016/j.still.2010.02.007

Python Software Foundation. (2017). *Python Language Reference, Version 2.7*. Available online at: www.python.org

Rappoldt, C. (1995). Measuring the millimetre-scale oxygen diffusivity in soil using microelectrodes. *Eur. J. Soil Sci.* 46, 169–177. doi: 10.1111/j.1365-2389.1995.tb01824.x

R Core Team. (2017). *R: A Language and Environment for Statistical Computing*. Vienna: R Foundation for Statistical Computing. Available online at: http://www.R-project.org/

Riggert, R., Fleige, H., Kietz, B., Gaertig, T., and Horn, R. (2017). Dynamic stress measurements and the impact of timber harvesting on physical soil properties. *Aust. Forestry* 80, 255–263. doi: 10.1080/00049158.2017.1347981

Rogasik, H., Schrader, S., Onasch, I., and Gerke, H. H. (2014). Micro-scale dry bulk density variation around earthworm (*Lumbricus terrestris* L.) burrows based on X-ray computed tomography. *Geoderma* 213, 417–477. doi: 10.1016/j.geoderma.2013.08.034

Roose, T., Keyes, S. D., and Daly, K. R. (2016). Challenges in imaging and predictive modeling of rhizosphere processes. *Plant Soil* 407, 9–38. doi: 10.1007/s11104-016-2872-7

Ruiz, S., Or, D., and Schymanski, S. J. (2015). Soil penetration by earthworms and plant roots—mechanical energetics of bioturbation of compacted soils. *PLoS ONE* 10:e0128914. doi: 10.1371/journal.pone.0128914

Six, J., Bossuyt, H., Degryze, S., and Denef, K. (2004). A history of research on the link between (micro)aggregates, soil biota, and soil organic matter dynamics. *Soil Till. Res.* 79, 7–31. doi: 10.1016/j.still.2004.03.008

Stenberg, B., Rossel, R. A. V., Mouazen, A. M., and Wetterlind, J. (2010). Visible and near infrared spectroscopy in soil science. *Adv. Agron.* 107, 163–215. doi: 10.1016/S0065-2113(10)07005-7

Uteau, D., Hafner, S., Pagenkemper, S. K., Peth, S., Wiesenberg, G. L. B., Kuzyakov, Y., et al. (2015). Oxygen and redox potential gradients in the rhizosphere of alfalfa grown on a loamy soil. *J. Plant Nutr. Soil Sci.* 178, 278–287. doi: 10.1002/jpln.201300624

Verbeke, G., and Molenberghs, G. (2000). *Linear Mixed Models for Longitudinal Data*. New York, NY: Springer.

Vetterlein, D., and Marschner, H. (1993). Use of a microtensiometer technique to study hydraulic lift in a sandy soil planted with pearl millet (*Pennisetum americanum* (L.) Leeke). *Plant Soil* 149, 275–282. doi: 10.1007/BF00016618

Xu, J. (2017). *PyAutoIt 0.3*. Available online at: https://pypi.python.org/pypi/PyAutoIt/0.3

Zausig, J., and Horn, R. (1992). Soil water relations and aeration status of single soil aggregates, taken from a gleyic vertisol. *Z. Pflanz. Bodenkunde* 155, 237–245.

Zausig, J., Stepniewski, W., and Horn, R. (1993). Oxygen concentration and redox potential gradients in unsaturated model soil aggregates. *Soil Sci. Soc. Am. J.* 57, 908–916. doi: 10.2136/sssaj1993.03615995005700040005x

Zhi-Guang, L. (1985). "Oxidation-reduction potential," in *Physical Chemistry of Paddy Soils*, ed Y. Tian-ren (Berlin: Springer), 1–26.

Conflict of Interest Statement: The authors declare that the research was conducted in the absence of any commercial or financial relationships that could be construed as a potential conflict of interest.

frontiers in Environmental Science

METHODS
published: 17 August 2018
doi: 10.3389/fenvs.2018.00087

Spatial Distribution of Mucilage in the Rhizosphere Measured With Infrared Spectroscopy

Maire Holz[1], Martin Leue[2], Mutez A. Ahmed[3], Pascal Benard[3], Horst H. Gerke[2] and Andrea Carminati[3]*

[1] Department of Agricultural Soil Science, University of Göettingen, Göttingen, Germany, [2] Leibniz Centre for Agricultural Landscape Research (ZALF), Group of Hydropedology, Müncheberg, Germany, [3] Division of Soil Physics, University of Bayreuth, Bayreuth, Germany

Mucilage is receiving increasing attention because of its putative effects on plant growth, but so far no method is available to measure its spatial distribution in the rhizosphere. We tested whether the C-H signal related to mucilage fatty acids is detectable by infrared spectroscopy and if this method can be used to determine the spatial distribution of mucilage in the rhizosphere. Maize plants were grown in rhizoboxes filled with soil free of organic matter. Infrared measurements were carried out along transects perpendicular as well as axially to the root channels. The perpendicular gradients of the C-H proportions showed a decrease of C-H with increasing distance: 0.8 mm apart from the root center the C-H signals achieved a level near zero. The measured concentrations of mucilage were comparable with results obtained in previous studies, which encourages the use of infrared spectroscopy to quantitatively image mucilage in the rhizosphere.

Keywords: rhizosphere extension, root mucilage, DRIFT spectroscopy, maize (*Zea mays* L.), soil hydrophobicity

OPEN ACCESS

Edited by:
Luiz Fernando Wurdig Roesch, Federal University of Pampa, Brazil

Reviewed by:
Akifumi Sugiyama, Kyoto University, Japan
Paul Knox, University of Leeds, United Kingdom

****Correspondence:***
Maire Holz
maire.holz@forst.uni-goettingen.de

Specialty section:
This article was submitted to Soil Processes, a section of the journal Frontiers in Environmental Science

Received: *31 January 2018*
Accepted: *20 July 2018*
Published: *17 August 2018*

Citation:
Holz M, Leue M, Ahmed MA, Benard P, Gerke HH and Carminati A (2018) Spatial Distribution of Mucilage in the Rhizosphere Measured With Infrared Spectroscopy. Front. Environ. Sci. 6:87. doi: 10.3389/fenvs.2018.00087

INTRODUCTION

The rhizosphere is the soil volume around the roots and plays a crucial role for nutrient and water acquisition by plants (Gregory, 2006; Neumann et al., 2009). Organic compounds (rhizodeposits) are released through the root into the rhizosphere in different chemical forms and they may have positive effects on plant growth (Jones et al., 2009). Mucilage is one of those compounds and makes up 2–12% of total rhizodeposition (Dennis et al., 2010 and references therein). Mucilage is a gel-like substance and is released from the root-cap cells (**Figure 1**). Its main components are polysaccharides (∼ 94%), proteins (1–5%) and phospholipids (Oades, 1978; Bacic et al., 1986; Read et al., 2003; Jones et al., 2009; Carminati and Vetterlein, 2013).

Mucilage provides several benefits for plant growth, such as the lubrication during root penetration (Iijima et al., 2004) or the stabilization of aggregates (Morel et al., 1991; Traoré et al., 2000). Recently it has been shown that mucilage increases rhizosphere water content (Carminati et al., 2010) due to the high water-holding capacity of the contained polysaccharides (McCully and Boyer, 1997) and it may therefore facilitate root water uptake (Ahmed et al., 2014). The extent of such benefits depends on the spatial distribution of mucilage around roots. To date, there is no experimental method to non-invasively and quantitatively image mucilage in soils and our knowledge of mucilage spatial distribution remains largely speculative.

FIGURE 1 | Mucilage around the root tips of a 3 day old wheat seedling.

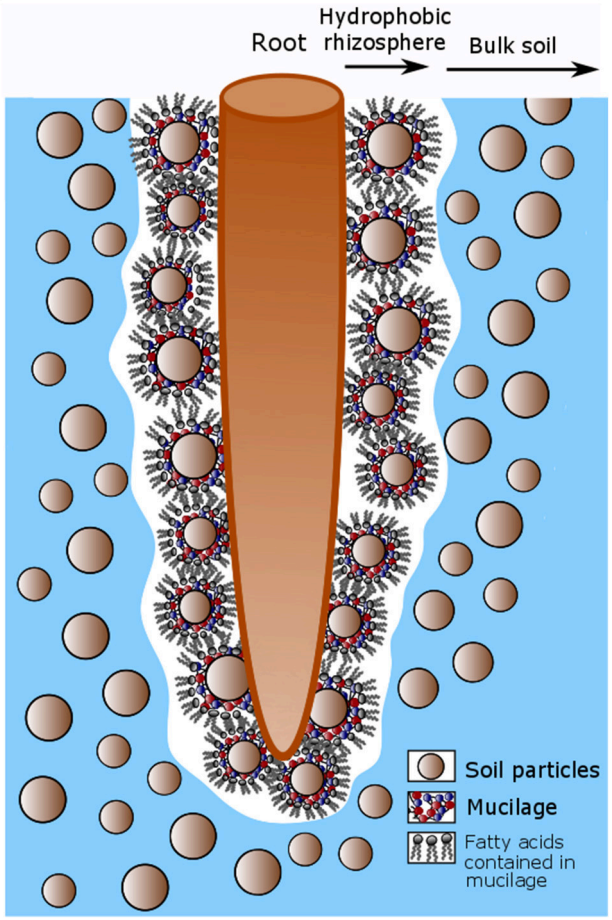

FIGURE 2 | Conceptual model describing the hydrophobicity around root after soil drying caused by fatty acids contained in mucilage. Mucilage is released by the root tip and accumulates around soil particles in the rhizosphere. Upon soil drying the fatty acids contained in mucilage turn their hydrophobic tails outwards so that the soil around the root becomes hydrophobic.

Among the many effects of mucilage on soil properties, one spectacular effect is the rhizosphere water repellency (Hallett, 2003; Whalley et al., 2004; Moradi et al., 2012). While the polysaccharides contained in mucilage have a very high water holding capacity (McCully and Boyer, 1997), the lipids which are also contained (Read et al., 2003), can have a reverse effect when mucilage dries. It is therefore likely that mucilage is responsible for the observed rhizosphere hydrophobicity (Carminati, 2013; Ahmed et al., 2015; Benard et al., 2017). Fatty acids are composed of a hydrophilic and a hydrophobic tail of nonpolar fatty acid chains (C-H groups). Upon soil drying these hydrophobic tails probably turn outwards. Hereby they reduce soil wettability and cause a hydrophobic region around the root as indicated in **Figure 2**.

Diffuse reflectance infrared Fourier transform (DRIFT) spectroscopy can be used to map functional groups such as C-H groups at intact soil surfaces at the mm-scale (Leue et al., 2010, 2015). In combination with microscopic techniques, DRIFT spectroscopy can be used to determine organic functional groups also at the µm-scale. The aim of this study was to use the C-H groups of the fatty acids contained in mucilage as a proxy for mucilage distribution in the rhizosphere. Although the main compound of mucilage is polysaccharides, we used fatty acids as a proxy for mucilage because the C-H groups are specific for mucilage, while no functional group specifically for polysaccharides exists. Although C=O or O-H groups can be measured by IR spectroscopy, those groups are not specifically for polysaccharides because they are also present in sugar monomers or amino acids, which are present in the rhizosphere as they are released as root exudates.

We used DRIFT spectroscopy and Fourier-transform infrared spectroscopy (FTIR) microscopy to map the distribution of fatty acids from mucilage in soil. Maize plants were grown in rhizoboxes and the signal of the C-H groups was recorded with a high spatial resolution along the roots as well as perpendicular to the roots.

MATERIALS AND METHODS

Plant Growth and Mucilage Extraction

Quartz material consisting of 70% quartz sand [collected from Duingen (Germany), particle size: 0.1–0.2 mm] and 30% quartz powder (*Carl Roth*, particle size: < 0.125 mm) was used for the calibration and as a growth medium free of soil organic matter. For the calibration, maize root mucilage was extracted as described in Zickenrott et al. (2016) in a slightly modified way. A mesh of stainless steel (2 mm diameter mesh size) was hanged into a plastic box 15 cm above surface of the box. The box had a size of 30 × 40 × 30 cm and was filled with water to a height of approximately 6 cm (**Figure 3A**). An aquarium diffuser was placed into the water in the box and connected to a plastic tube which was plugged to pressurized air. The air

was circulated though the diffuser which creates tiny air bubbles which increased the humidity in the box. Maize seeds were sterilized in 10% H_2O_2 solution for 10 min and placed on the mesh and the box was closed with a plastic lid to maintain high air humidity. After 3–4 days root tips were growing trough the mesh and showed small drops of hydrated mucilage at the tips due to the high humidity in the box (**Figure 3A**). The mucilage was collected from the tips once a day till the roots reached the water surface after approximately 3 days. The collection of mucilage was done with a syringe by applying negative pressure. Per box and day we collected approximately 6 mg of dry mucilage.

For the calibration, dried quartz material was mixed with different amounts of previously collected mucilage at concentrations of 0.0, 0.025, 0.05, 0.1, 0.25, 0.5, and 1 mg/g (gram of dry mucilage per gram of dry soil). The mixtures were applied on object slides in four replicates and were air-dried. For the mapping of the spatial distribution of mucilage across root channels, maize (*Zea mays* L.) plants (KWS 2376) were grown in rhizoboxes with an inner size of 10 × 20 × 1.5 cm filled with the same quartz substrate as used for the calibration. Before germination, maize seeds were immersed in a 10% H_2O_2 solution for 10 min to avoid seed-borne diseases. Prior to plant growth the following nutrients were added per kg of soil: NH_4NO_3-N: 0.3 g, $Ca(H_2PO_4)_2$-P: 0.06 g, K_2SO_4-K: 0.03 g, $CaSO_4$-Ca: 0.05 g, $MgSO_4$-Mg: 0.05 g, H_3BO_4-B: 2 mg, $CuSO_4$-Cu: 0.03 mg, $MnSO_4$-Mn: 1.5 mg, $(NH_4)_2MoO_4$-Mo: 0.03 mg, $ZnCl_2$-Zn: 1.2 mg, FeNaEDTA-Fe: 3.6 mg. During plant growth, the water content was adjusted to 20%. Soil water content was checked gravimetrically each day and lost water was added from the top with a syringe. The rhizoboxes were kept at an angle of approximately 55° to make sure that the roots were growing close to the lower side of the rhizoboxes. The temperature in the climate chamber was 25°C during day and 22°C during night, the photoperiod was 14 h and the light intensity was 300 μmol m^{-2} s^{-1}. After 4 weeks of growth, plant shoots were cut and the soil samples were dried at 35°C. A low temperature of 35°C was chosen for drying to allow for a drying process close to natural conditions and to avoid physical and chemical changes of mucilage. After drying, the roots were removed from the soil manually so that the channel were root had been growing in remained as a depression in the otherwise even soil surface (**Figure 4**).

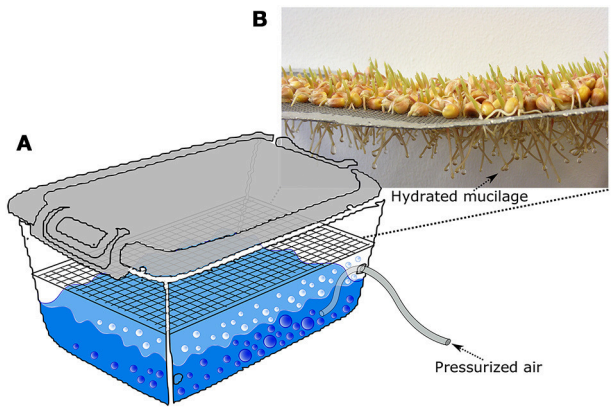

FIGURE 3 | Sketch, describing the procedure of mucilage collection. A tray covered with maize seeds is placed in a closed plastic box. The box is partly filled with deionized water. An aquarium diffuser is placed into the water and pressurized air is pumped through it so that tiny bubbles are produced **(A)**. Hereby the humidity of the air is increased so that the mucilage stays hydrates and forms small drops around the roots tips **(B)**. The mucilage drops are once a day with a syringe by applying negative pressure.

Diffuse Reflectance Infrared Spectroscopy

Diffuse reflectance infrared spectroscopy (DRIFT) measurements in the mid-infrared range (wavelength: 2.5–25 μm, wave numbers (WN): 4,000–400 cm^{-1}) was applied to the calibration samples at the object slides using a BioRad® FTS 135 spectrometer (Cambridge, Massachusetts, USA). Each DRIFT spectrum was recorded by 16 co-added scans with a

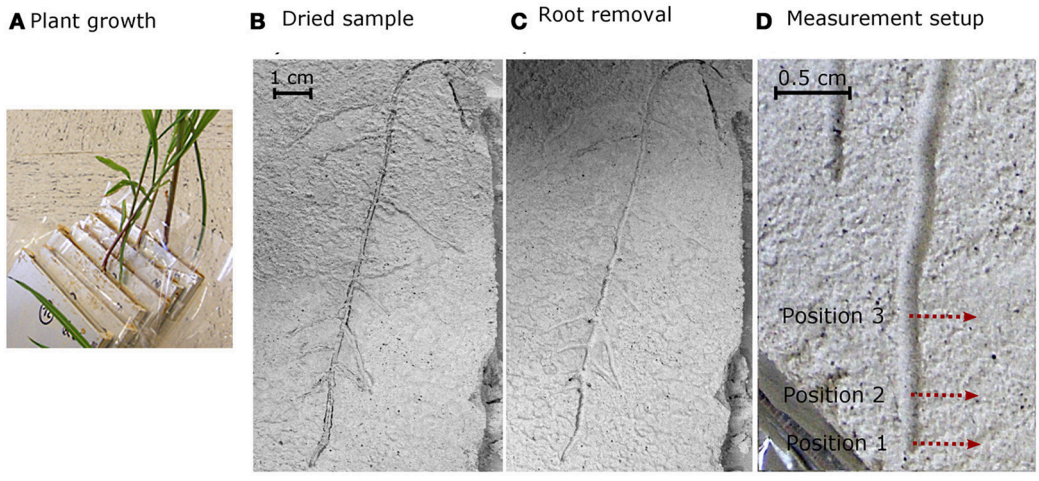

FIGURE 4 | Plant growth **(A)** and rhizobox with dried soil and plants before **(B)** and after **(C)** the roots were excavated from the soil. Measurements were conducted after removing the roots at three position (0, 1, and 3 cm behind the tip) perpendicular to the root channel as indicated by the red arrows **(D)**.

spectral resolution of 4 cm^{-1} against a gold background (Leue et al., 2015). At the intact root channels and surrounding substrate, DRIFT spectra were conducted using an Agilent Cary series 600 FTIR microscope (Agilent Cary series 600, Agilent Technologies, Inc., Santa Clara, CA, USA). The measurements were done at three positions, (a) directly at the root tip, 1 cm behind the root tip and 3 cm behind the root tip. Measurement at each position started in the center of the root channel. From there, IR spectra were recorded each 100 µm perpendicular to the root channel till a distance of 13 mm from the root channel center was reached (**Figures 4**, **5**). The measurements within the root channel (soil that had been in direct contact with the root) are referred to as "root channel" while measurements beyond the root channel border are referred to as "rhizosphere." The spectra were recorded as 64 co-added scans at a spectral resolution of 4 cm^{-1} in steps of 100 µm from sample areas of 0.1 × 0.1 mm. For the rhizosphere samples, one root was chosen per plant and spectra were measured at three positions along each root (0, 1, and 3 cm behind the tip). After preprocessing of the spectra (Ellerbrock et al., 2009; Leue et al., 2010), the local peak heights of the C-H bands were normalized for the absolute peak height of the SiO_2 band at WN 1,350 cm^{-1}. The relationship between mucilage content and C-H signal intensities obtained from the calibration samples was used to quantify the mucilage content in the rhizosphere of the maize roots. After calibration, the background signal (i.e., the average signal in the bulk soil where no mucilage was expected) was subtracted from each measured value.

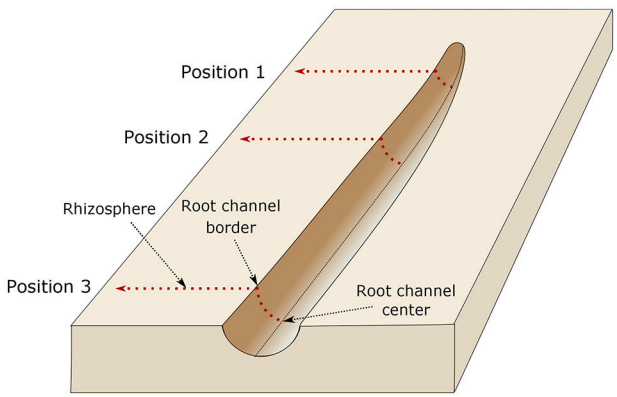

FIGURE 5 | Illustration of the measurement setup. The dried roots were carefully removed from the sample and IR measurements were done at three positions, directly at the root tip (position 1), 1 cm behind the root tip (position 2), and 3 cm behind the root tip (position 3). Measurement at each position started in the center of the root channel. From there, IR spectra were recorded each 100 µm perpendicular to the root channel till a distance of 13 mm from the root channel center was reached. The border of the root channel is defined as the position were the intact soil sample (i.e., rhizosphere) starts.

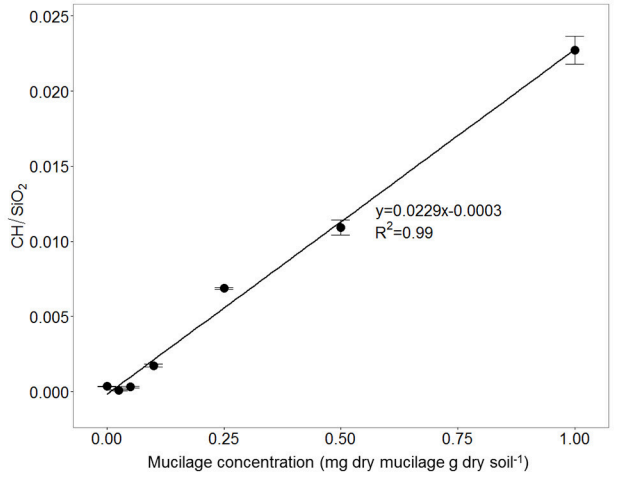

FIGURE 6 | Ratio between CH and SiO2 signal for soil mixed with different maize-mucilage concentrations collected from maize seedlings ranging from 0 to 1 mg dry mucilage per g dry soil.

STATISTICS

To test for differences between soil regions and root positions we applied a one-way ANOVA ($p < 0.05$) followed by a *post-hoc* test. Statistical analysis were done in R 3.3.1.

RESULTS

The calibration measurements on the object slides revealed a linear relationship between mucilage concentration and the C-H/SiO_2 ratio The fit of the linear equation war good and resulted

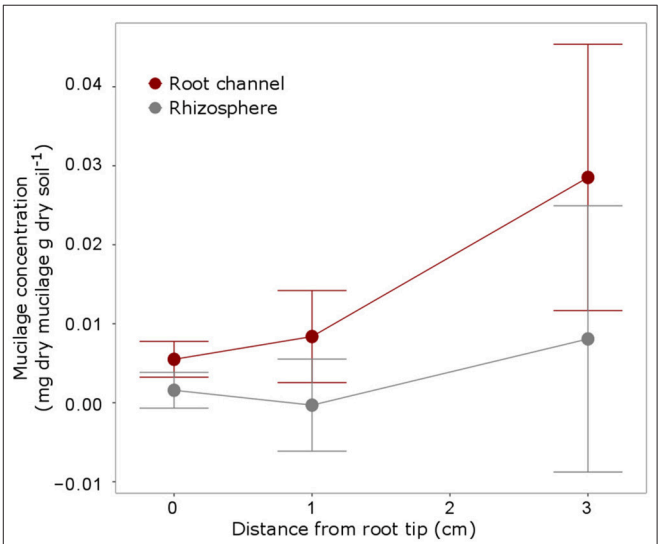

FIGURE 7 | Mucilage concentration (mg dry mucilage per g dry soil) for the 3 positions were measurements were taken i.e., at the root tip, 1 cm behind the tip and 3 cm behind the tip as indicated in **Figure 4**. The measurements within the root channel (soil that had been in direct contact with the root) were averaged and compared to the measurements beyond the root channel with was defined as rhizosphere soil [10 measurements (=1 mm) beyond the root channel border, corresponding to the region defined as "rhizosphere" in **Figure 5**]. The displayed values are the means of 5 replicates (i.e., plants). Variation is given as standard error. Differences between the positions and the soil regions were not significant ($p < 0.05$).

in an R^2 of 0.99 (**Figure 6**). The calibration equation was applied to the IR measurements at the root channels to obtain mucilage concentration (mg/g).

The IR measurements at the 3 root positions showed that mucilage concentration slightly increased with increasing distance from the root tip (i.e., increasing root age), however, differences between the positions were not statistically significant (**Figure 7**). Mucilage concentration in the rhizosphere was lower compared to the root channel for all 3 positions but these differences were likewise not statistically different probably due to very high variation between the samples.

The highest mucilage concentrations of 0.02 mg/g were found in the center of the root channel (**Figure 8**). Toward the border of the root channel this concentration decreased to around 0.01 mg/g. The radial gradients of mucilage from the center of the root channel toward rhizosphere dropped rapidly and decreased to approximately 0 mg/g at a distance of around 0.8 mm from the center of the root channel (**Figure 8**). Averaging the mucilage concentration in the root channel for all 3 measured root positions resulted in a mucilage concentration of 0.017 mg/g. The rhizosphere reached on average a much lower concentration of 0.003 mg/g mucilage (**Figure 9**). Differences between both measurements were not different statistically, presumably because of the high variation in the root channel measurements.

DISCUSSION

This pilot experiment showed that infrared spectroscopy can in principle be applied to detect gradients of mucilage around roots grown in soil. Although not significant, the measurements of mucilage at different root positions showed an increase in C-H groups (i.e., hydrophobicity) with increasing root age (**Figure 7**). This is in agreement with Carminati (2013) who found that rhizosphere hydrophobicity was enhanced with increasing root age. This observation was explained by an increased stiffening of mucilage either due to (a) repeated drying and rewetting, (b) interaction between mucilage and solutes such as Ca^{2+} present in soil solution or (c) microbial decomposition of mucilage (Carminati, 2013; Carminati and Vetterlein, 2013). The first two processes cannot explain an increase in C-H groups that we observed. However, it is possible that mucilage was exposed to microbial decomposition. This could cause a change in the ratio of fatty acids to other compounds such as polysaccharides

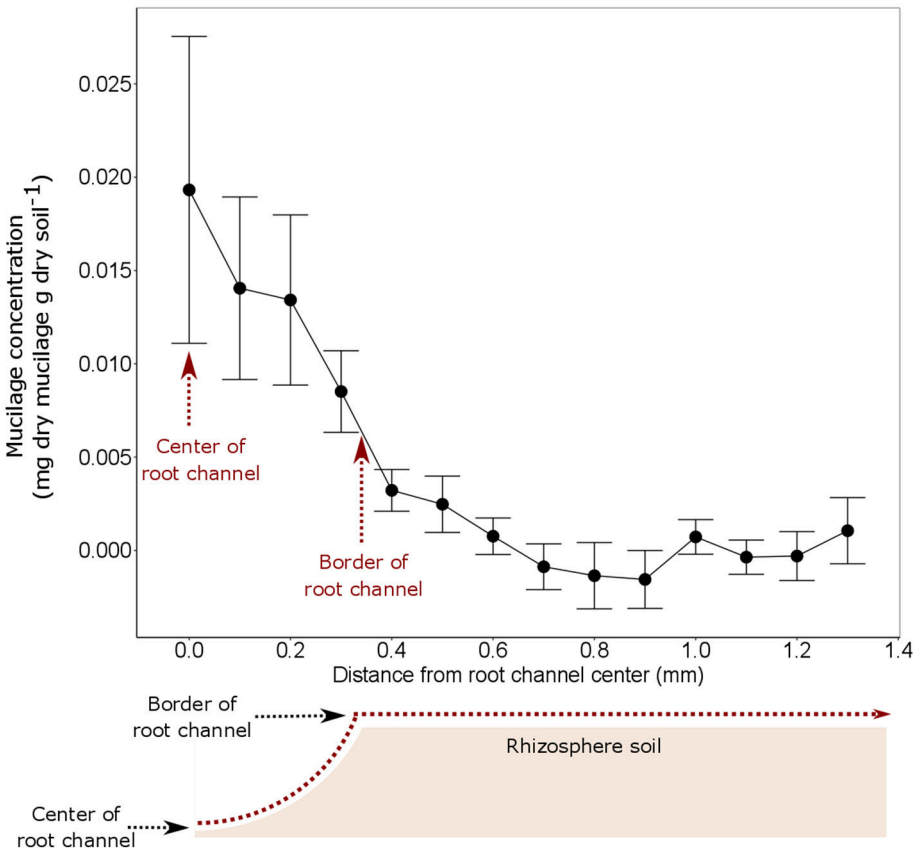

FIGURE 8 | Mucilage concentration (mg dry mucilage per g dry soil) starting from the root channel center in radial direction toward the bulk soil. The measurements from the 3 different root positions were averaged because they did not reveal any statistical difference (**Figure 6**). The displayed values are the means of 5 replicates (i.e., plants). Variation is given as standard error. x = 0 equals to the position of the center of the root channel as indicated in the sketch below the figure. The average extend of the root channel (r = 0.34 mm) is indicated as border of root channel.

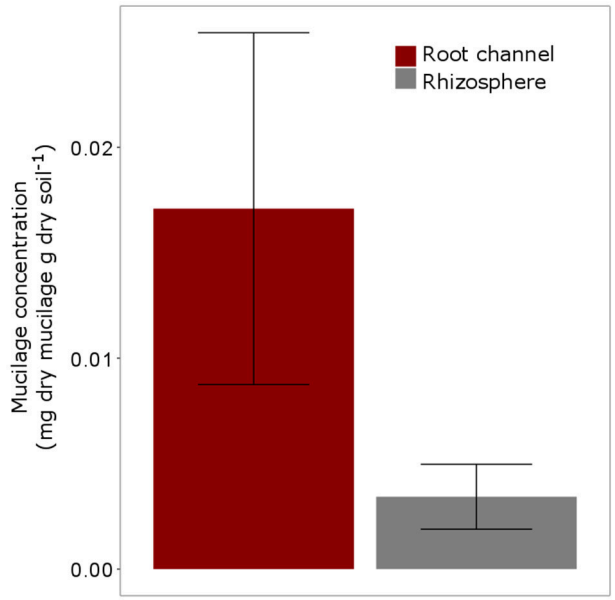

FIGURE 9 | Average Mucilage concentration (mg dry mucilage per g dry soil) for all measured positions (=3) and all plants (5 replicates). "Root channel" refers to the measurements within the root channel (soil that had been in direct contact with the root). "Rhizosphere" refers to the soil 1 mm (=10 measurements) beyond the root channel border, corresponding to the region defined as "rhizosphere" in **Figure 3**). Variation is given as standard error. Differences between Root channel and rhizosphere were not statistically different ($p < 0.05$).

or may increase the amount of fatty acids. A change in mucilage composition due to aging would be problematic for the interpretation of our results. As the measurements were calibrated with maize root mucilage, a prerequisite for this approach is that the chemical composition of mucilage used in the calibration is similar to those found in the soil around roots.

The fact that we found a trend of increasing C-H signal with increasing root age but no statistical differences, can have two reasons. First, natural variability between plants may be high. This could be solved by a higher number of replicates. Second, the measured root channel segments at distances of 0, 1, and 3 cm behind the tip may have been too young to show differences in mucilage concentration and distribution. Probably longer time intervals (i.e., older root segments) would be necessary to detect changes in mucilage quantity or quality due to decomposition.

The radial gradients of mucilage were relatively steep: at 0.6 mm distance from the border of the root channel, mucilage content decreased below the limit of detection. The extent of the rhizosphere affected by mucilage (0.6 mm) was smaller compared to results obtained from ^{14}C imaging analyses. Holz et al. (2017) showed that overall root exudates diffused up to 1 mm into the bulk soil. The fact that mucilage did not move as far from the root surface as compared to overall exudates may be explained by the higher viscosity of mucilage compared to root exudates (Read and Gregory, 1997) and reduced diffusion coefficient of mucilage compared to root exudates.

We found contents of up to 0.02 mg dry mucilage per g dry soil in the center of the root channel and average values of around 0.017 mg dry mucilage per g dry soil in the root channel (**Figures 8**, **9**). Based on the literature, we can expect a mucilage exudation rate of 15 $\mu g\ d^{-1}$ per root tip (Chaboud, 1983). Assuming a maximum diffusion length of 1 mm into the soil, a mean root radius of 0.5 mm, a soil bulk density of 1.43 g cm^{-3} as for our samples and a root elongation of 3 cm d^{-1} we expect a mucilage concentration in the rhizosphere of 0.056 mg dry mucilage per g dry soil. This theoretical value is 3-times higher than the values obtained by DRIFT spectroscopy; however, they still appear comparable.

One opportunity for increasing the precision of the DRIFT measurements could be the use of the same DRIFT spectrometer (here: FTIR microscope) for both, the calibration and intact sample measurements. The use of a finer substrate to optimize the application of the DRIFT technique could improve the spectral analysis of the mucilage and the identification resolution. However, plant growth may be difficult in even finer substrates.

CONCLUSIONS

The results suggest that DRIFT spectroscopy and FTIR microscopy can be applied to quantify the spatial distribution of mucilage in the rhizosphere. The measured mucilage contents and the spatial extent of the mucilage-affected rhizosphere were slightly lower but comparable to calculated and published values. This technique can in principle be applied to any other plant species that produces mucilage.

A few aspects have to be considered when applying the method:

- Our results showed a high variability which resulted in a lack of statistical differences even though trends of increasing mucilage with root age were observed (**Figure 7**). The high standard error is probably caused by a high variability between the plants. An increase in sample size would probably solve this problem.
- The IR measurements have to be calibrated to obtain the mucilage content in soil. As such, it needs to be ensured that the chemical composition of mucilage used for the calibration is similar to mucilage around roots in soil. This may be true for mucilage close to the root tip but may be problematic at older root sections where mucilage was exposed to microbial decomposition which might have changed its chemical composition.
- This approach is restricted to dried samples and soil materials with no organic matter because any C-H signal from native soil organic matter would overlay the comparatively low C-H signal of mucilage. Therefore, the transfer of results to natural conditions is limited. While the texture of the material we used is comparable to a natural soil, chemical and biological conditions may differ.

Bearing those aspects in mind, IR spectroscopy can be applied to measure the spatial distribution of mucilage in soil. Future studies could investigate the effect of factors such as: root hairs, root age, root type, plant species, soil texture, and soil water content on the spatial distribution of mucilage in the rhizosphere.

AUTHOR CONTRIBUTIONS

MH, ML: planning and conducting the experiment, data analysis, writing manuscript; MA, PB: planning and conducting experiment; HG: planning experiment, providing facilities for IR measurements; AC: planning experiment, providing funding.

ACKNOWLEDGMENTS

We acknowledge the DFG for funding (Projects CA 921/3-1, KU 1184/33-1, and LE3177/1-2) and ev. Studienwerk Villigst for funding the position of MH. We thank KWS for providing the seeds for the experiment and we acknowledge support by the Open Access Funds of the University of Göttingen.

REFERENCES

Ahmed, M. A., Holz, M., Woche, S. K., Bachman, J., and Carmintati, A. (2015). Effect of soil drying on mucilage exudation and its water repellency: a new method to collect mucilage. *J. Plant Nutr. Soil Sci.* 178, 1–4. doi: 10.1002/jpln.201500177

Ahmed, M. A. A., Kröner, E., Holz, M., Zarebanadkouki, M., and Carminati, A. (2014). Mucilage exudation facilitates root water uptake in dry soils. *J. Funct. Plant Biol.* 41, 1129–1137. doi: 10.1071/FP13330

Bacic, A., Moody, S. F., and Clarke, A. E. (1986). Structural analysis of secreted root slime from maize (*Zea mays* L.). *Plant Physiol.* 80, 771–777. doi: 10.1104/pp.80.3.771

Benard, P., Zarebanadkouki, M., Hedwig, C., Holz, M., Ahmed, M. A., and Carmintati, A. (2017). Pore-scale distribution of mucilage affecting water repellency in the rhizosphere. *Vadose Zo. J.* 7:170013. doi: 10.2136/vzj2017.01.0013

Carminati, A. (2013). Rhizosphere wettability decreases with root age: a problem or a strategy to increase water uptake of young roots? *Front. Plant Sci.* 4:298. doi: 10.3389/fpls.2013.00298

Carminati, A., Moradi, A. B., Vetterlein, D., Vontobel, P., Lehmann, E., Weller, U., et al. (2010). Dynamics of soil water content in the rhizosphere. *Plant Soil* 332, 163–176. doi: 10.1007/s11104-010-0283-8

Carminati, A., and Vetterlein, D. (2013). Plasticity of rhizosphere hydraulic properties as a key for efficient utilization of scarce resources. *Ann. Bot.* 112, 277–290. doi: 10.1093/aob/mcs262

Chaboud, A. (1983). Isolation, purification and chemical composition of maize root cap slime. *Plant* 73, 395–402. doi: 10.1007/BF02184316

Dennis, P. G., Miller, A. J., and Hirsch, P. R. (2010). Are root exudates more important than other sources of rhizodeposits in structuring rhizosphere bacterial communities? *FEMS Microbiol. Ecol.* 72, 313–327. doi: 10.1111/j.1574-6941.2010.00860.x

Ellerbrock, R. H., Gerke, H. H., and Böhm, C. (2009). *In situ* drift characterization of organic matter composition on soil structural surfaces. *Soil Sci. Soc. Am. J.* 73, 531–540. doi: 10.2136/sssaj2008.0103

Gregory, P. J. (2006). Roots, rhizosphere and soil: the route to a better understanding of soil science? *Eur. J. Soil Sci.* 57, 2–12. doi: 10.1111/j.1365-2389.2005.00778.x

Hallett, P. (2003). Plant influence on rhizosphere hydraulic properties: direct measurements using a miniaturized infiltrometer. *New Phytol.* 157, 597–603. doi: 10.1046/j.1469-8137.2003.00690.x

Holz, M., Zarebanadkouki, M., Kuzyakov, Y., Pausch, J., and Carminati, A. (2017). Root hairs increase rhizosphere extension and carbon input to soil. *Ann. Bot.* 121, 61–69. doi: 10.1093/aob/mcx127

Iijima, M., Higuchi, T., and Barlow, P. W. (2004). Contribution of root cap mucilage and presence of an intact root cap in maize (zea mays) to the reduction of soil mechanical impedance. *Ann. Bot.* 94, 473–477. doi: 10.1093/aob/mch166

Jones, D. L., Nguyen, C., and Finlay, R. D. (2009). Carbon flow in the rhizosphere: carbon trading at the soil–root interface. *Plant Soil* 321, 5–33. doi: 10.1007/s11104-009-9925-0

Leue, M., Ellerbrock, R. H., and Gerke, H. H. (2010). DRIFT mapping of organic matter composition at intact soil aggregate surfaces. *Vadose Zo. J.* 9, 317–324. doi: 10.2136/vzj2009.0101

Leue, M., Gerke, H. H., and Godow, S. C. (2015). Droplet infiltration and organic matter composition of intact crack and biopore surfaces from clay-illuvial horizons. *J. Plant Nutr. Soil Sci.* 178, 250–260. doi: 10.1002/jpln.201400209

McCully, M. E., and Boyer, J. S. (1997). The expansion of maize root-cap mucilage during hydration. 3. changes in water potential and water content. *Physiol. Plant.* 99, 169–177. doi: 10.1111/j.1399-3054.1997.tb03445.x

Moradi, A. B., Carminati, A., Lamparter, A., Woche, S. K., Bachmann, J., Vetterlein, D., et al. (2012). Is the rhizosphere temporarily water repellent? *Vadose Zone J.* 11. doi: 10.2136/vzj2011.0120

Morel, J. L., Habib, L., Plantureux, S., and Guckert, A. (1991). Influence of maize root mucilage on soil aggregate stability. *Plant Soil* 136, 111–119. doi: 10.1007/BF02465226

Neumann, G., George, T. S., and Plassard, C. (2009). Strategies and methods for studying the rhizosphere-the plant science toolbox. *Plant Soil* 321, 431–456. doi: 10.1007/s11104-009-9953-9

Oades, J. M. (1978). Mucilages at the root surface. *J. Soil Sci.* 29, 1–16. doi: 10.1111/j.1365-2389.1978.tb02025.x

Read, D. B., Bengough, A. G., Gregory, P. J., Crawford, J. W., Robinson, D., Scrimgeour, C. M., et al. (2003). Plant roots release phospholipid surfactants that modify the physical and chemical properties of soil. *New Phytol.* 157, 315–326. doi: 10.1046/j.1469-8137.2003.00665.x

Read, D. B., and Gregory, P. J. (1997). Surface tension and viscosity of axenic maize and lupin root mucilages. *New Phytol.* 137, 623–628. doi: 10.1046/j.1469-8137.1997.00859.x

Traoré, O., Groleau-Renaud, V., Plantureux, S., Tubeileh, A., and Boeuf-Tremblay, V. (2000). Effect of root mucilage and modelled root exudates on soil structure. *Eur. J. Soil Sci.* 51, 575–581. doi: 10.1046/j.1365-2389.2000.00348.x

Whalley, W., Leeds-Harrison, P., Leech, P., Riseley, B., and Bird, N. (2004). The hydraulic properties of soil at root-soil interface. *Soil Sci.* 2, 90–99. doi: 10.1097/01.ss.0000117790.98510.e6

Zickenrott, I.-M., Woche, S. K., Bachmann, J., Ahmed, M. A., and Vetterlein, D. (2016). An efficient method for the collection of root mucilage from different plant species–a case study on the effect of mucilage on soil water repellency. *J. Plant Nutr. Soil Sci.* 179, 294–302. doi: 10.1002/jpln.201500511

Conflict of Interest Statement: The authors declare that the research was conducted in the absence of any commercial or financial relationships that could be construed as a potential conflict of interest.

frontiers in Environmental Science

ORIGINAL RESEARCH
published: 02 October 2018
doi: 10.3389/fenvs.2018.00110

Biological Alteration of Flow Properties of Soil Samples From Two Bt Horizons of a Haplic Luvisol Determined With Rheometry

Christoph Haas[1,2]*, *Dörthe Holthusen*[3] *and Rainer Horn*[1]

[1] *Institute for Plant Nutrition and Soil Science, CAU Kiel, Kiel, Germany,* [2] *Institute of Soil Landscape Research, Leibniz Centre for Agricultural Landscape Research, Müncheberg, Germany,* [3] *Department of Soil Science, Federal University of Santa Maria, Santa Maria, Brazil*

Flow properties of soils are helpful to describe the soils' response on mechanical loading, which occurs naturally (e.g., caused by growing roots or drilling earthworms) or anthropenically (e.g., in the course of management practices like tillage) In order to determine the effect of bacterial or plant exudation induced changes of soil strength and soil's flow behavior soil samples of the Bt horizons of a haplic Luvisol were saturated with pure water or with aqueous solutions of biological model substance. We chose xanthan gum as a bacterial exudate which represents the chemical alteration of soil microorganism, while polygalacturonic acid has been used as a root's mucilage analog. Surface tension and viscosity of these aqueous solutions were determined, and soil samples' flow properties were obtained with the help of rheometry. By applying amplitude sweep tests to the soil samples soil stability related parameters were determined [loss (G″) and storage (G′) moduli, representing the plasticity or elasticity of soils, respectively] or calculated [namely, the loss factor (ratio of G″ and G′), Integral Z (a strain-stress dependent sum-parameter) and the linear viscoelastic range (where no changes in soil structure occur)]. We hypothesized that (I) flow properties of used model substances differ from those of pure water and, (II) biological model substances influence the water content at defined matric potential caused by e.g., altered surface tension, thus influencing parameters that were related to soil stability. Furthermore, (III) the impact of biological model substance depends on the shear rate that is applied to achieve the soil's deformation because some biological model substances show non-Newtonian flow. So far and to our knowledge this is the first rheological work on soils that evaluates the effect of differing shear rates on elastic and plastic deformation statistically. We found the impacts of biological model substances on soils' flow properties to be not only dependent of origin (plan or bacterial), concentration and matric potential, but also on deformation intensities. Due to chemical particularities of PGA a deformation induced soil stabilization was observed. Leading to the conclusion that deformation processes e.g., in the rhizosphere are much more complex than previously thought.

Keywords: amplitude sweep test, polygalacturonic acid, xanthan, rheology, viscosity, surface tension

OPEN ACCESS

Edited by:
Andrea Carminati,
University of Bayreuth, Germany

Reviewed by:
Thomas Keller,
Swedish University of Agricultural Sciences, Sweden
Muhammad Naveed,
University of the West of Scotland, United Kingdom

***Correspondence:**
Christoph Haas
c.haas@soils.uni-kiel.de

Specialty section:
This article was submitted to Soil Processes, a section of the journal Frontiers in Environmental Science

Received: *14 March 2018*
Accepted: *07 September 2018*
Published: *02 October 2018*

Citation:
Haas C, Holthusen D and Horn R (2018) Biological Alteration of Flow Properties of Soil Samples From Two Bt Horizons of a Haplic Luvisol Determined With Rheometry. Front. Environ. Sci. 6:110. doi: 10.3389/fenvs.2018.00110

INTRODUCTION

Biological processes like plant roots' or soil microorganisms' exudation result in chemically and physically alterations of soil properties. For example, plant roots' mucilage exudation (Tisdall and Oades, 1979) or biological reallocation or transformation (e.g., caused by earthworms or microorganisms, Hoang et al., 2016; Banfield et al., 2017) of organic compounds results in changes in chemical parameters [e.g., $CaCO_3$ production, SOC accumulation (Jones et al., 2009), changes in pH and redox (Uteau et al., 2015) or in altered ion concentrations (Carvalhais et al., 2011)], and coincides with altered physical properties, like aggregation (Six et al., 2004). These physical alterations result in,

(I) decreased soil stability, for example, caused by microorganisms that oxidize gluing compounds (like particulate organic matter, Six et al., 2004) or neutralize cementing agents (like $CaCO_3$) by H^+ release or by applying shear stresses to the soil at moist conditions, for example caused by a growing root.

(II) increased stabilities directly caused by the exudation, likegluing effects or an increased surface tension of the soil solution and therewith indirect effects on wetting properties which diminishes the disrupting impact of swelling (Hallett and Young, 1999; Chenu et al., 2000) Two exemplary substances for cementing and gluing are Xanthan gum and polygalacturonic acid. The former is an anionic polysaccharide that is often used as a food additive (Zhang et al., 2008). It is produced by fermentation or by exudation of Xanthomonas campestris bacterium. The basic chemical structure of Xanthan gum ($C_{35}H_{49}O_{29}$) is a linear linked ß-D glucose backbone with a trisaccharide side chain on every other glucose. A well-known characteristic is its pseudo-plasticity (i.e., shear thinning). Acid sugars are found on root surfaces and on cells walls. They occur as monomers or polymers. One polymer, for example, is polygalacturonic acid (PGA), which occurs as chains and is the main constituents of root mucilage (Manunza et al., 1997). For example, PGA-chains linked by Ca^{2+} act as model of the soil root interface, because it exhibits a fibrillary structure similar to that of natural mucilage (Manunza et al., 1997). Both substances form gels, having the potential to alter the pore-size distribution in soils. Furthermore, since both substances are negatively charged at most soil conditions (not too acidic soil) they are bond to negative charged clay particles by polyvalent cations like Ca^{2+} and Mg^{2+}.

Soil stability defines not only the trafficability of soils (Riggert et al., 2017) but also plant root growth processes (Bengough and Mullins, 1990). As shown by Markgraf et al. (2006), rheometry delivers a set of parameters that are related to microstructural soil stability of which the most important are (**Figure 1**): The shear stress, which is required for soil deformation and which represents the capability of the soil to withstand the deformation. The storage modulus, G′, which is a measure for the elasticity of a soil. It represents the energy that is available to reverse the gradual increase of soil distortion, while the loss modulus G″ equals the dissipated energy (Mezger, 2014). The deformation where G′ equals G″ is called cross-over. With deformations larger than the cross-over the viscous behavior of the samples overweighs the elastic component. The samples' structural integrity is irreversibly destroyed which may result in creeping or flowing, depending on the water content of the sample (Markgraf and Horn, 2006; Holthusen et al., 2010; Mezger, 2014). Markgraf et al., 2012 introduced a semi-quantitative parameter which is calculated according to Equation (1) and named Integral z, abbreviated to I_z in this manuscript.

$$I_Z = \int_{0.001}^{cross-over} (1 - G''G'^{-1})dy \quad (1)$$

Since Iz is integrated over the deformation, the flow behavior at small deformations is mostly neglected but influenced by larger strains which leading to higher similarity of values for Iz (Holthusen et al., 2017). The linear viscoelastic (LVE) region, and Iz are derived parameters from G′ and G″. Within the LVE region there are no significant changes in the structure of the sample. Soil stability is linked to hydraulic capacities like the pore-size distribution or the water content (Riggert et al., 2017) and to intensities like (un-)saturated hydraulic conductivity (Fazekas and Horn, 2005; Riggert et al., 2017).

Alterations of flow properties (e.g., viscosity and surface tension) of the soil solution potentially result in altered hydraulic capacities and intensities (Holthusen et al., 2012) influencing not only the soil strength but the plant-roots' water uptake, and consequently, the productivity of agriculturally used soils. For example, the surface tension influences the amount of plant-available water, and, due to adhesive forces also the soil stability. The viscosity influences intensities like the (un-) saturated hydraulic conductivity: The flow of water is described by Darcy's law. The volume of water that flows in a defined time through a given area decreases linearly with increasing viscosity, and vice versa. An increased viscosity results in decreased plant water uptake per unit of time.

The aim of this study was to quantify biological alterations of flow properties and of parameters related to microstructural soil stability as derived from amplitude sweep tests.

We hypothesized that (I) flow properties of used model substances differ from those of pure water and, (II) biological model substances influence the water content at defined matric potentials caused by altered flow properties, and with that, parameters related to soil stability as derived from amplitude sweep tests. Furthermore, (III) the impact of biological model substance depends on the shear rate that is applied to achieve the soils' deformation because some biological model substances show non-Newtonian flow. So far and to our knowledge this is the first rheological work on soils that evaluates the effect of differing shear rates on elastic and plastic deformation (represented as loss factor) statistically.

MATERIALS AND METHODS

Soil Material

Disturbed soil material was excavated in September 2014 from two layers (Bt-1 from 0.45 to 0.55 m, and Bt-2 from 0.55 to

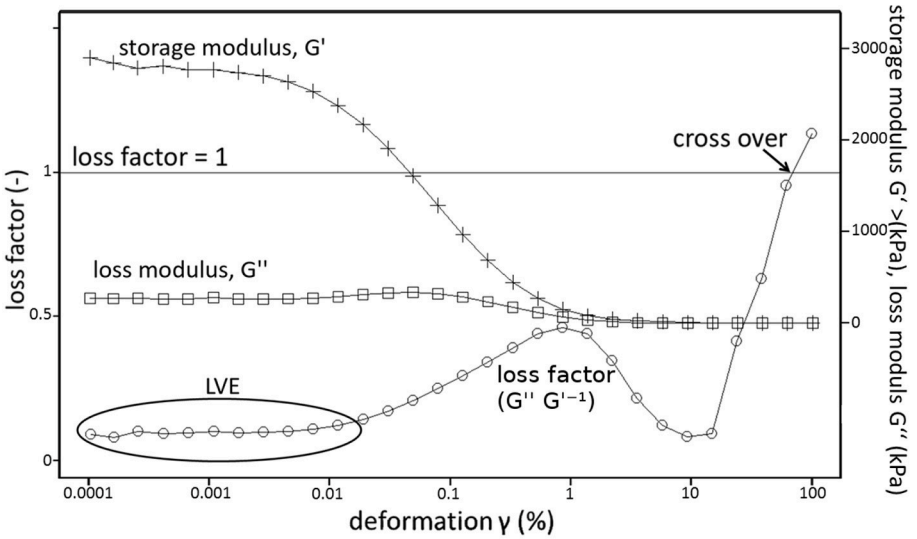

FIGURE 1 | Exemplary curves for linear viscoelastic range (LVE), storage modulus (G′), loss modulus (G″), and their ratio (loss factor, G″ G'^{-1}) as well as the cross over.

TABLE 1 | Sand, silt, clay, as well as, soil organic carbon (SOC) contents in g kg^{-1} soil, as well as, pH, and electrical conductivity (eC) in μS cm^{-1} of the four pits where soil cores were excavated from a loess-derived Luvisol, Klein-Altendorf near Bonn, Germany.

Pit	Depth	Sand	Silt	Clay	SOC	pH	eC
	m	g kg^{-1}				–	μS cm^{-1}
24	0.45–0.55	71.4	780	149	4.0	7.0	83
24	0.55–0.65	66.1	730	204	5.8	7.03	74
40	0.45–0.55	54.7	650	295	4.5	6.99	100
40	0.55–0.65	44.8	710	245	3.4	7.11	83
57	0.45–0.55	59.8	770	170	3.9	7.02	81
57	0.55–0.65	44.6	740	215	4.1	7.0	71
74	0.45–0.55	58.9	660	281	4.0	6.98	104
74	0.55–0.65	40.0	700	260	3.8	7.02	77

0.65 m) of a Bt horizon from a haplic Luvisol (IUSS Working Group WRB, 2006) in four repetitions (i.e., from four pits) of a totally randomized trial (Kautz et al., 2014) at the experimental area of Campus Klein-Altendorf (50°37′9″ N 6°59′29″ E, University of Bonn, Germany). The site is characterized by a maritime climate with temperate humid conditions (9.6°C mean annual temperature, 625 mm annual rainfall). Main soil properties are listed in **Table 1**. The Bt horizon is characterized by accumulated clay, leached from the A-horizon (0–0.27 m) and the E horizon (0.27–0.41 m). Chicory (Cichorium intybus L. "Puna," 5 kg ha^{-1} seeding rate) had been grown in these trials for the last three years. With its herringbone or monopodial branching root systems Cichorium intybus L. penetrates deep into the subsoil exploring for water and nutrient supply (Kautz et al., 2012).

Determination of Flow Properties of Aqueous Solutions of Biological Model Substances

Dynamic viscosity of aqueous solutions of biological model substances and of water were determined with a rheometer (MCR300, Anton Paar, Stuttgart, Germany) and a standardized cone-plate measuring system (0.5° cone angle, gap size = 50 μm) with a shear rate ramp ranging from 10 to 1,000 s^{-1}. Within this shear rate rampe 29 sampling points were considered. Viscosity was calculated using the rheometers' software RheoPlus (Anton Paar, Stuttgart, Germany). The samples' volume was 400 μl. Surface tensions were determined with the help of a microtensiometer (Krüsstensiometer, Kruess, Hamburg, Germany) and the Wilhelmy-plate method (with a platinum plate) as described by Mohamed et al. (2010). The sample volume was 50 ml. The platinum plate was inserted (2 mm) into the fluid. Ten sampling points were consideredwhile the plate was pulled out of the fluid. The test duration was 60 s. All measurements were performed at laboratory conditions (T = 293.15 K) with n = 5. The temperature was checked using a thermometer.

Biological Model Substances and Sample Preparation for Amplitude Sweep Test

Soil was sieved to ≤ 2 mm and refilled to small cylinders, 0.9 cm in height, and 3.6 cm in diameter (V = 9.2 cm^3). Aqueous solutions of two biological model substances were used to saturate the samples and to determine biological alterations of biopore walls: (I) Polygalacturonic acid [abbreviated PGA; $(C_6H_8O_6)_n$, ∼95% (enzym.), Fluka BioChemika 81325, EC No. 2116826, Gillingham, United Kingdom] which was identified as a model root exudate (Morel et al., 1987; Gessa and Deiana, 1992; Gessa et al., 1997; Czarnes et al., 2000; Traoré et al., 2000; Grimal et al., 2001; Zhang et al., 2008). PGA was solubilized by adding

0.51 ml of 1 M KOH for 100 mg PGA and diluted with double-distilled water. (II) Xanthan gum from Xanthomonas campestris (Sigma-Aldrich, G1253, EC No. 234-394-2) was mixed with double-distilled water using a magnetic stirrer. Three defined concentrations from model substances were tested, namely, 1, 2, and 3 gL^{-1}. Three samples per pit, depths, model substance, as well as concentration and five control samples (0 gL^{-1}) were saturated by capillary rise. Measurements were performed at four matric potentials [namely, $\Psi_m = -1$, -3, and -6 kPa (drained with the help of sand beds) or -30 kPa (drained on ceramic suction plates)].

Amplitude Sweep Test (AST) and Volumetric Water Contents

A profiled parallel plate measurement system, 0.025 m in diameter, was used to perform the AST with a rheometer MCR300 (Anton Paar, Stuttgart, Germany). The soil samples (9 mm in height) were cut in halves horizontally. The lower half of the sample was placed on the lower plate of the rheometer. The upper half of the sample was used to determine volumetric water contents (= before measurement). The lower plate is fixed while the upper one is moving in an oscillating manner with successively increasing amplitudes at a constant frequency of 0.5 Hz. Controlled shear deformation ranged from 10^{-4} to 100% related to the measuring gap (4 mm). More detailed information can be obtained from Markgraf et al. (2006). The remaining soil was recovered from the lower plate in order to determine the volumetric water content (= after measurement). The storage modulus (G′), the loss modulus (G″), and the linear viscoelastic range (LVE) were calculated using the rheometers' software RheoPlus (Anton Paar, Stuttgart, Germany), while cross-over and Integral Z were calculated manually from raw data.

Statistical Analyses

The statistical software R (R Development Core Team, 2017) was used to evaluate the data. (I) The data evaluation started with the definition of an appropriate statistical mixed model (Laird and Ware, 1982; Verbeke and Molenberghs, 2000), including the sampling depths (qualitative: 0.45–0.55 m; 0.55–0.65 m), the concentrations of aqueous solutions [0 gL^{-1} (for water), 1, 2, and 3 gL^{-1}], the matric potentials (quantitative: $\Psi_m = -1$, -3, -6, or -30 kPa) and corresponding interaction effects, also with the biological model substances (polygalacturonic acid, Xanthan gum), as fixed factors. The investigated pits and further nested

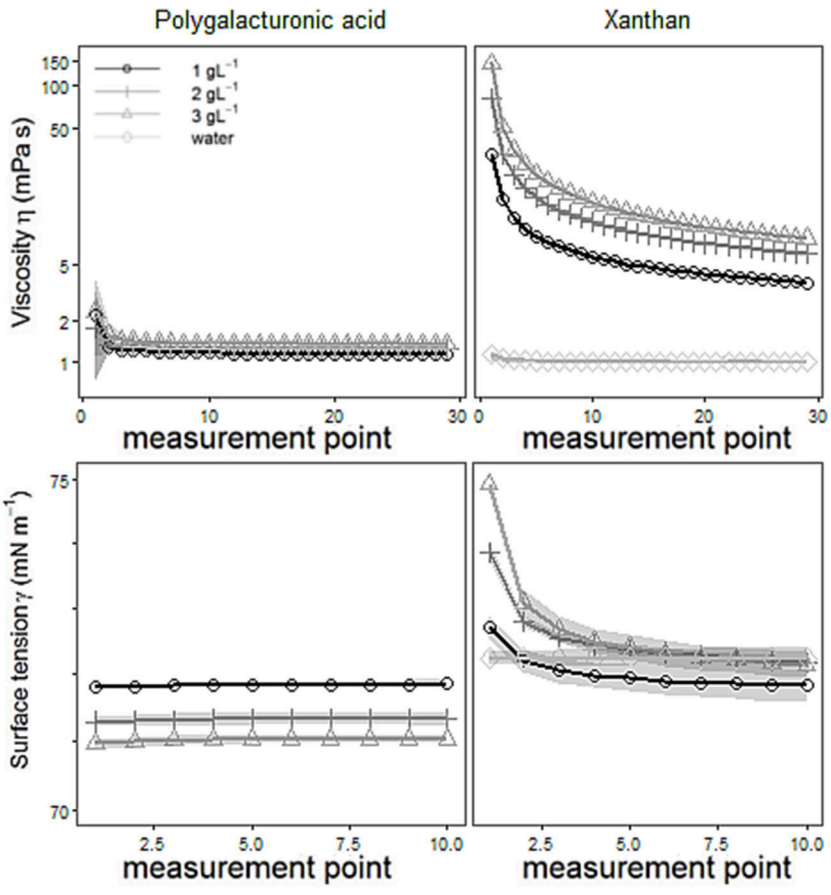

FIGURE 2 | Means with standard deviations (shadowed) of viscosity (upper row) or of surface tension (lower row) of aqueous solutions with 1, 2, or 3 gL^{-1} of polygalacturonic acid (left-hand side) or of Xanthan gum (right-hand side) or of double-distilled water. $n = 5$.

effects were regarded as random factors. The data were assumed to be normally distributed and to be heteroscedastic due to the different levels of the matric potential. These assumptions are based on a graphical residual analysis. Based on this initial model, a model selection (forward selection) based on AIC values (Akaike, 1973; Sakamoto et al., 1986) was conducted to decide which covariates can be used for prediction. After that, covariates with a variance inflation factor (VIF) of 10 or higher were removed stepwise. Finally, non-significant covariates were omitted, based on an analysis of covariances (Cochran, 1957). For the final model, a Pseudo R^2 was calculated (Nakagawa and Schielzeth, 2013). The used covariates were soil organic carbon content, electrical conductivity, pH and the texture (sand, silt or clay content). (II) Single point evaluation: Here, the measurement points (1–30) were added to the statistical model to evaluate the impact of differing shear rates (named as single point evaluation, abbreviated as SPE in this manuscript). The normal force was added, additionally, beside those covariates already used for (I).

RESULTS AND DISCUSSION

Dynamic viscosity (η) for shear rates ranging from 10 to 1,000 s^{-1}, and surface tensions (γ) of aqueous solutions of biological model substances, and double-distilled water are shown in **Figure 2**. The addition of polygalacturonic acid (PGA) or Xanthan gum (Xanthan) increased the viscosity of double-distilled water. The more PGA or Xanthan had been added the more pronounced the change in viscosity. Considering shear rates ≥ 187 s^{-1} (=equals measurement point 6) Newtonian flow was found for PGA and double-distilled water (indicated by a constant viscosity over the applied shear rates). However, increased viscosities were found for both fluids for very small shear rates. This contradicts the fact, that pure water is a Newtonian fluid, while Stoddart et al. (1969) found PGA to be shear thinned even for larger shear rates. Thus, we have to take into account that flow behavior of water is caused by impurities of the double distilled water. For Xanthan an intense shear thinning was found, which is characterized by an under proportional increase of shear stress that is required for fluid deformation with increasing shear rates. These findings are in agreement with those described by Pettitt et al. (1995). Small amounts of Xanthan increased the viscosity disproportionally as indicated by the intercept of the regression line shown in **Figure 3**, presenting the relative change of both, viscosity and surface tension caused by the addition of PGA or Xanthan (=concentration effect). Here, values for viscosity are gathered for maximum shear rates (=1,000 s^{-1}), whereas those of the surface tension were obtained from the last measurement point. The change in viscosity is much more pronounced than the change in surface tension. The change in viscosity is much more pronounced for Xanthan (up to ∼700%, blank symbols) compared to PGA (filled symbols). The surface tension of aqueous solutions of PGA decreased with increasing concentration and showed smaller values than those for pure water. The surface tension of Xanthan remained (more or less) unchanged for 2 or 3 gL^{-1} but the addition of

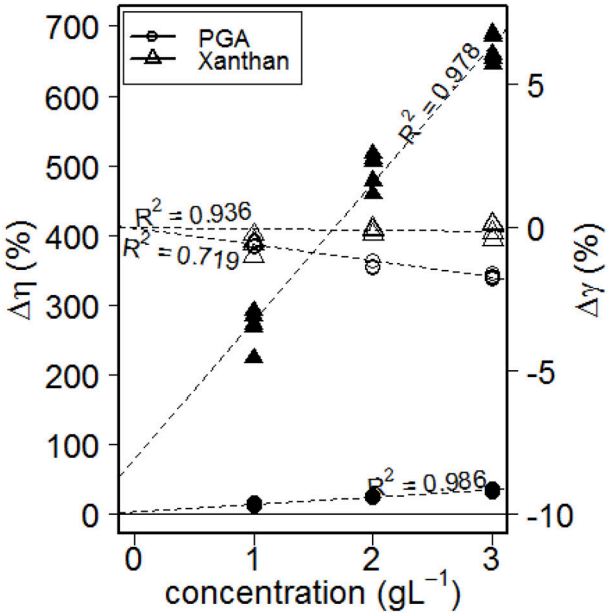

FIGURE 3 | Relative change of viscosity (scale to the left-hand side) and of surface tension (scale to the right hand-side) for aqueous solutions with 1, 2, or 3 gL^{-1} of polygalacturonic acid (PGA) or Xanthan gum. Viscosity is represented by filled symbols (axis to the left-hand side), blank symbols represent surface tension (axis to the right-hand side).

1 g PGA L^{-1} decreased surface tension. These changes seem to follow linear trends, as indicated by high values of R^2. Read and Gregory (1997) determined the surface tension and the viscosity of mucilage gathered from Zea mays L. They found non-Newtonian flow behavior and a viscosity of 2.1 mPa s (diluted in 70 % w/w H_2O, measured at 20°C). This is confirmed by measurements presented in this study. With a view to surface tension results of this study contradict Read and Gregory (1997) who found heavily decreased values (<48 mN m^{-1}). PGA and mucilage differ not only in flow properties. Mucilage contains protein (Morel et al., 1986) and several different types of e.g., sugars (Morel et al., 1986; Read and Gregory, 1997) while pure PGA is protein-free and contains only one type of (an acidic) sugar (galacturonic acid). Thus we have to come to a critical statement about PGA as mucilage analog: PGA and mucilage differ in chemical and physical parameters.

The influence of drainage to defined matric potentials (namely, $\Psi_m = -1, -3, -6$, or -30 kPa) on water content of soil saturated with water or saturated with aqueous solutions of polygalacturonic acid (PGA) or Xanthan gum (Xanthan) is shown in **Figure 4**. Means of water contents of soil samples saturated with water or with aqueous solutions of 1 gL^{-1} PGA showed similar values for $\Psi_m = -1$ kPa and-30 kPa, but increased means in water content for $\Psi_m = -3$ and -6 kPa, indicating (I) the impact of altered flow properties of the soil solution (the viscosity of used biological model substances exceeds that of pure water), or (II) alterations of the pore size

distribution. The latter one might have had several causes: (a) soil loosening (due to decreased surface tension, resulting in lowered menisci forces) and therewith changes in aggregation, (b) the physical blockage of pores (Hallett et al., 2003), (c) gelation of biological model substance (and the coinciding formation of a secondary pore system) or (d) electrostatic interactions of anionic model substances and the soil matrix (caused by Ca^{2+} "bridge" formation or hydrogen bonding; Chang et al., 2015). The statistical evaluation supports the theory of an alternated pore system, because no significant differences between PGA and Xan were found for the volumetric water content before rheometry (**Table 2**, θ_{before}), which would be expected if the fluids viscosity would be of importance.

After rheometry, the water content depended on the fluid- (**Table 2**, θ_{PGA} and θ_{XAN}). Differences in water contents are more distinct for sample where positive water pressures were more pronounced and are caused by differing amounts of water that were squeezed out of pores which could be explained by differences in soil pore elasticity or by increased viscosities for Xanthan. The decrease in (recovered) volumetric water content for PGA exceeds that one of Xan by a factor of ~2.6 (−0.37/−0.14) with increasing concentration. Differences in regression coefficients for the concentration further support the theory of changes in the pore system because less water was recovered with increasing concentration which is in contradiction to the effect caused by viscosity (which increased with increasing concentration). Although the concentration of the fluid is of less importance for Xan compared with PGA (**Table 2**, θ_{PGA} and θ_{XAN}, coeffienct c) more water can be recovered from samples of Xan. Due to altered water

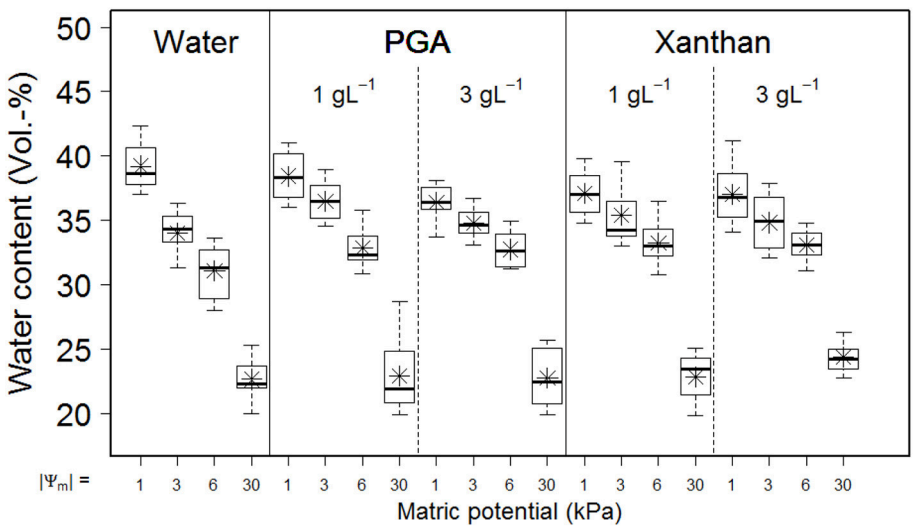

FIGURE 4 | Boxplot with means (✳) of exemplary results of volumetric water contents for soil samples saturated with pure water or aqueous solutions of two defined concentrations ($1gL^{-1}$ or $3gL^{-1}$) of biological model substances [namely, polygalacturonic acid (PGA) or xanthan gum (Xanthan)] in dependency to the absolute value of the matric potential ($|\Psi_m|$). Pits and depths are pooled for graphical representation. $n = 40$ for water. $n = 24$ for PGA and Xanthan. Values represent the volumetric water content prior to the application of rheometry (="before measurement").

TABLE 2 | Regression coefficients (with standard error in brackets) and *p*-value for selected rheological parameters as derived from analysis of covariance.

parameter	coefficient			*p*-value		
	a	b	c	a	b	c
θ_{before} (vol.-%)	38.78 (0.78)	0.48 (0.01)	−0.64 (0.01)	<0.0001	<0.0001	<0.0001
θ_{PGA} (vol.-%)	37.04 (0.72)	0.46 (0.01)	−0.37 (0.11)	<0.0001	<0.0001	<0.0001
θ_{Xan} (vol.-%)	37.04 (0.72)	0.46 (0.01)	−0.14 (0.11)	<0.0001	<0.0001	0.22
LVE_{PGA} (%)	0.008 (0.0006)	$4.5*10^{-5}$ ($2.0*10^{-6}$)	$4.0*10^{-4}$ ($22.3*10^{-5}$)	<0.001	0.023	0.083
LVE_{Xan} (%)	0.008 (0.0006)	$4.5*10^{-5}$ ($2.0*10^{-6}$)	$-11.8*10^{-4}$ ($22.3*10^{-5}$)	<0.001	0.023	<0.0001
LVE_{PGA} (Pa)	27.82 (11.81)	−14.49 (1.4)	14.23 (4.9)	0.128	<0.0001	0.005
LVE_{Xan} (Pa)	27.82 (11.81)	−5.98 (1.7)	−11.14 (5.3)	0.128	0.0004	0.041
I_Z	7.15 (0.55)	−1.04 (0.05)	−1.20 (0.23)	0.001	<0.0001	<0.0001
Cross $over_{PGA}$	21.4 (1.15)	−1.59 (0.11)	−2.85 (0.55)	<0.001	<0.0001	<0.0001
Cross $over_{Xan}$	21.4 (1.15)	−0.53 (0.11)	−0.71 (0.59)	<0.001	<0.0001	0.23

Coefficient a represents the y-intercept, b the influence of the matric potential (Ψ_m), and the concentration effect (gL^{-1} PGA or Xan).

contents we would expect a higher soil rigidity for Xan samples, caused by a more rarely occurrence of positive pore water pressures, which lead to a larger amount of recovered water. This was found for cross over values (**Table 2**) but not for LVE or I_z.

The linear viscoelastic region (LVE, soil samples remain stable) can be described with maximal values for the deformation **Figure 6**, **Table 2**, LVE_{PGA} (%) and LVE_{Xan} (%) and the corresponding shear stress [**Table 2**, LVE_{PGA} (Pa) and LVE_{Xan} (Pa)].

The statistical analysis showed in both cases significant influences of the matric potential [=increase with a more negative matric potential, fluid independent for LVE (%) or fluid dependent for LVE (Pa)] and of the concentration (fluid dependent). LVE increases with increasing concentrations of PGA but decreases with increasing concentrations of Xan. This contradicts Hallett et al. (2003) who assumed soil loosening with PGA at low deformation ranges. However, further statistical analyses enabled a more detailed evaluation of the results, and are shown in the second part of Results and Discussion. Different regression coefficients for matric potential [LVE (Pa)] prove a much more pronounced soil stabilizing effect with increasing drainage for PGA compared to Xan.

The soil samples structural failure can be described with I_Z or with crossover (%) (**Table 2**).

The statistical analysis showed an effect of the matric potential and a fluid independent (I_Z) or fluid dependent [crossover (%)] effect for the concentration. Both parameters increase with progressing drainage, indicating an increased soil stability, or decrease with increasing concentrations of the model substances (**Figure 6**). For crossover, both effects are less pronounced for Xanthan than for PGA, indicating reduced soil rigidity for samples saturated with Xan. The less intense effect for matric potential (3-fold = 1.59/0.53) of Xan is possibly caused by an altered pore size distribution (wetter with more negative matric potentials), while the 4-fold (2.85/0.71) higher concentration effect of PGA is caused by more pronounced soil loosening effects of PGA. This proves an effect of PGA contradicting to Hallett et al. (2003) (= a soil loosening effect for increased concentrations of PGA at higher deformations/shear rates).

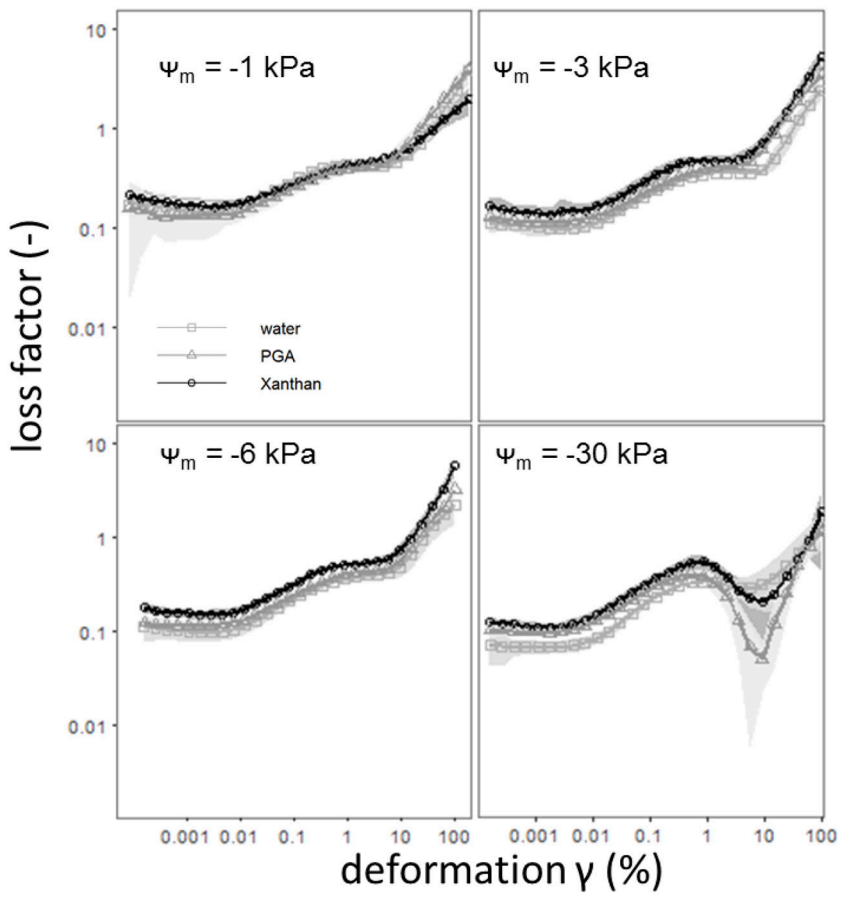

FIGURE 5 | Means with standard deviations (shadowed) of the loss factor [defined as the ratio of loss (G″) and storage modulus (G′)] as derived from amplitude shear tests for the complete deformation range (0.001–100 %) for soil saturated with pure water (□) or for soil saturated with aqueous solutions of polygalacturonic acid (3 gL^{-1} PGA, △) or of Xanthan gum (3 gL^{-1} Xanthan, ⊖) for defined matric potentials, namely $\Psi_m = -1$ kPa,−3 kPa,−6 kPa or−30 kPa. Pits and depths are pooled for graphical representation. $n = 40$ for water. $n = 24$ for PGA and Xanthan.

However, since the parameters (Iz) are sensitive for larger shear rates (Holthusen et al., 2017) we need to take into account that flow behavior is deformation dependent, which has been shown in several studies, but has never been evaluated statistically. **Figure 5** shows differing flow behavior for soils mixed with various biological model substances and for differing deformations. Means with standard deviations of the loss factor as derived from amplitude sweep tests for the complete deformation range (0.001–100 %) for soil mixed with water and for soil mixed with 3 gL^{-1} of polygalacturonic acid (PGA, circles or) or 3 gL^{-1} of Xanthan for $\Psi_m = -1$, -3, -6, or -30 kPa are shown in **Figure 5**. Here, general trends can be observed: At very low deformation intensities (0.001%) the loss factor decreases with increasing drainage (more negative matric potential), independently from the used fluid (water, PGA, Xanthan). While for $\Psi_m = -1$ kPa all fluids showed similar values for the loss factor, a treatment-dependent effect can be observed with $\Psi_m = -3$ kPa and $\Psi_m = -6$ kPa. Here, a shift to larger values of the loss factor over the complete deformation range can be observed with the addition of Xanthan. This can be caused by lowered soil stability, due to increased water contents [**Figure 4** and **Table 2** (θ_{before} vs. θ_{PGA} or θ_{XAN}), (Riggert et al., 2017)] or by the occurrence of positive water pressures (Fazekas and Horn, 2005) due to an increased viscosity of the soil solution (**Figure 2**). Remarkably are the curves for the driest matric potential ($\Psi_m = -30$ kPa): All flow curves showed a local peak for the loss factor (between 0.1 and 1% deformation), followed by a decrease of the loss factor for deformations around 10%. This decrease is less pronounced for samples saturated with water and most pronounced for samples saturated with PGA. For PGA an absolute minimum for the loss factor can be found. Furthermore, the occurrence of this minimum is achieved with a less pronounced deformation if water was used for saturation compared to PGA or Xanthan. Baumgarten et al. (2013) stated, that the curve's progression is influenced by many soil properties like soil texture, clay mineralogy, particle shape, organic matter compounds, (micro)- aggregate stability and other physicochemical properties. We found out that water

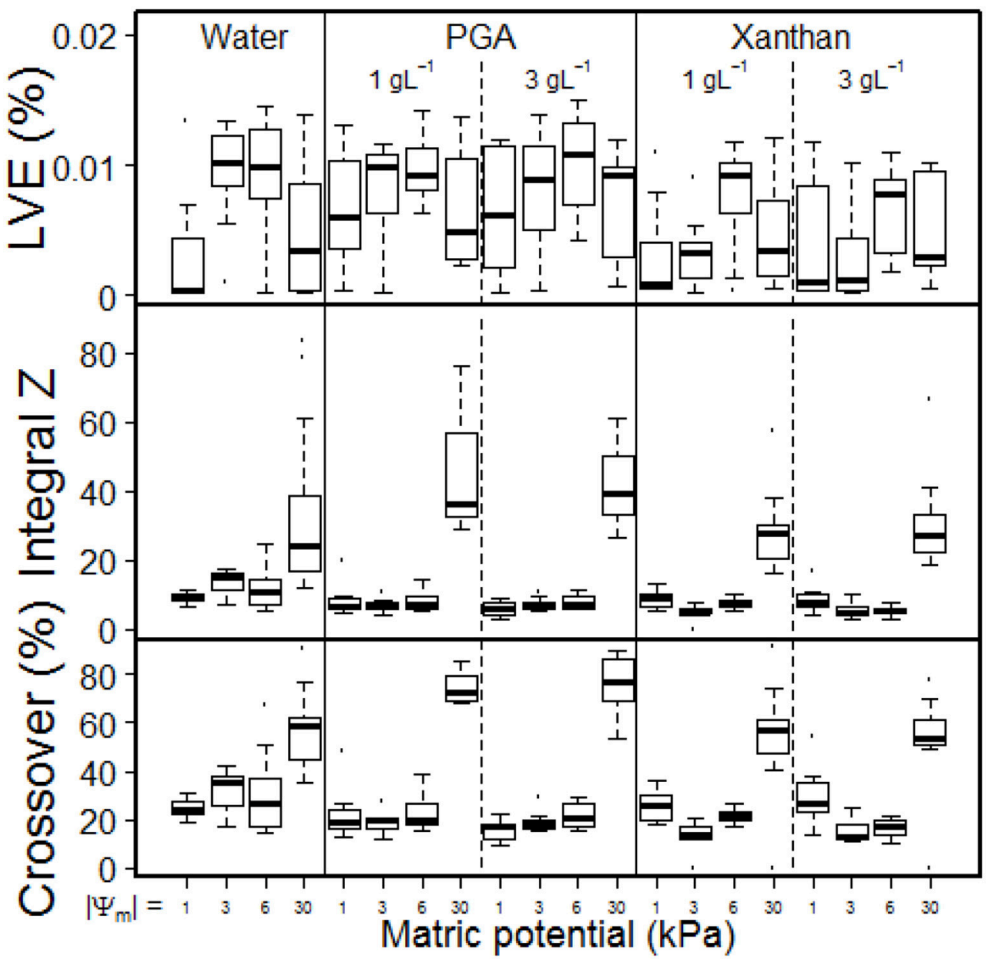

FIGURE 6 | Boxplot for linear viscoelastic range [LVE (% Deformation)], Integral Z and Crossover (%, G′ = G″) as derived from amplitude shear tests for soil saturated with water or for soil saturated with aqueous solutions with 1 or 3 gL^{-1} of polygalacturonic acid (PGA) or 1 or 3 gL^{-1} of Xanthan gum (Xanthan) for defined matric potentials, namely $\Psi_m = -1$, -3, -6, or -30 kPa. Pits and depths are pooled for graphical representation. $n = 40$ for water. $n = 24$ for PGA and Xanthan.

content is the most important parameter on the progression of the curve as it has indeed an influence on (micro)- aggregate stability. It is mandatory, to measure the water content, as a standard parameter, and thus, most appropriate as an input factor to describe the flow behavior of soils. In this study it was found to influence the deformation behavior significantly, while SOC, texture, pH and eC did not. Curves with a locale maximum in loss factors can be found with other soils, for example for several Andisols from Chile (Baumgarten et al., 2013), for salic tidalic fluvisols or fluvi-calcic gleysols (Baumgarten et al., 2012) but until now, a massive decrease like that one shown in **Figure 3** ($\Psi_m = -30$ kPa) has never been observed but indicates soil stabilization processes caused by deformation: Aggregates disrupt, even if the deformation is mostly elastic (loss factor <1). Polyvalent cations (especially Ca^{2+}, Santos et al., 1997) are released from the aggregate's interior, agglomerating negatively charged primary clay particles to each other, or leading to the formation of clay-organic associations with negatively charged organic anions like Xanthan or PGA. The fact that Mg^{2+} shows no cooperativity between single PGA chains while Ca^{2+} leads to the formation of PGA-PGA associations (Malovikova et al., 1994) supports this hypothesis, since the ratio Ca^{2+} to Mg^{2+} increases from aggregate's exteriors to aggregate's interiors (Santos et al., 1997). Another proof is that this behavior is only found with low degrees in water saturation, because otherwise the amount of released cations might be diluted in the soil solution. The shift in deformation (%) where the local minimum occurred may be caused by a less intense aggregate disruption with low deformations due to the aggregate's stabilizing effect of PGA and Xanthan. The statistical analysis proved both, the dependency of the loss factor on differing shear rates [expressed in differing deformation-intensities (%)] and the stabilization of soil with its deformation.

Results and Discussion (Single Point Evaluation)

The statistical results of the single point evaluation (SPE) delivered regression functions for each measurement point (MP, 1–30) which had been applied in the course of the amplitude sweep test. It was used to evaluate the loss- and storage-modulus, the loss factor and the shear stress. The normal force influences significantly storage- and loss-moduli but had no impact on loss factors or shear stresses. The impact of the normal forces was tenfold more pronounced for storage- than for loss moduli (data not shown). All parameters were significantly influenced by interaction effects for the depths and the MP (data not shown). Depth dependent regression parameters for storage moduli are shown in **Figure 7**. The concentration of PGA significantly influenced the storage module up to MP 14 (T0, 0.45–0.55 m) or MP 13 (T1, 0.55–0.65 m), resulting in increasing storage moduli with increasing concentrations. Here, a significant influence for the concentration of Xan was not found. With PGA, the matric

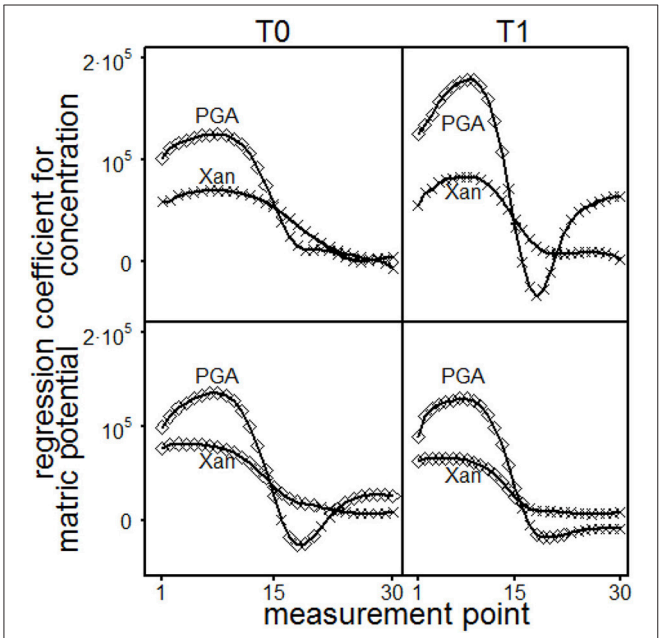

FIGURE 7 | Results of the single point evaluation for soil material excavated from T0 (0.45 to 0.55 m, left-hand side) or T1 (0.55 to 0.65 m, right-hand side) and saturated with Xanthan gum (Xan) or polygalacturonic acid (PGA): Regression coefficients for storage modulus. Concentration effect: regression coefficients for each measurement point and depth (upper row). Effect of matric potential: regression coefficients for each measurement point and depth (lower row). ◊ marks a significant influence of the regression coefficient ($p \leq 0.05$) on storage modulus, while × represenst $p > 0.05$.

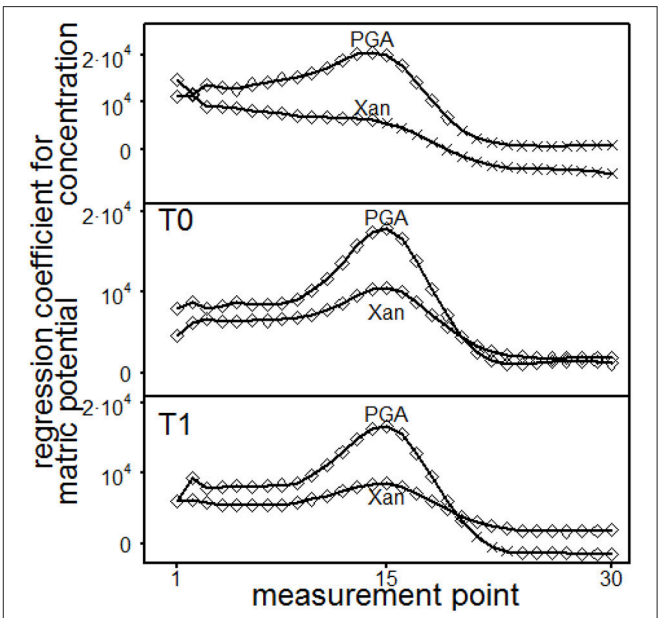

FIGURE 8 | Results of the single point evaluation for soil material excavated from T0 (0.45 to 0.55 m) or T1 (0.55 to 0.65 m) and saturated with Xanthan gum (Xan) or polygalacturonic acid (PGA): Regression coefficients for loss modulus. Concentration effect: regression coefficients for each measurement point (top). Effect of matric potential: regression coefficients for each measurement point and depth (T0, middle; T1, bottom). ◊ marks a significant influence of the regression coefficient ($p \leq 0.05$) on loss modulus, while × represents $p > 0.05$.

potential ($|\Psi_m|$) increased the storage moduli at low (MP < 17) and high (MP > 21) deformation rates but decreased the storage moduli at intermediate deformation rates for T0 (due to negative regression coefficients). The increasing effect at high deformation rates was not found with T1. The storage moduli significantly increased with increasing matric potential for Xanthan at low deformation rates (up to MP 21 for T0 or up to MP 17 for T1). The concentration effect of the loss-moduli (**Figure 8**) was not depth-dependent but reflects an significantly increase in loss moduli with increasing concentrations for Xanthan (MP < 15) and PGA (MP < 20). The effect of matric-potential significantly increased the loss moduli for Xanthan saturated samples in both depths over the complete deformation range. A significantly increasing effect was also found for PGA (MP 1-30) but T1 showed a more differentiated pattern: Here, increases in $|\Psi_m|$ (=absolute values) resulted in significantly increased values up to MP 21, but significantly decreased values for MP > 24. The loss factor for PGA increased independently of the depths with increasing concentration at high deformation rates (MP 27–28) or for MP 1–27 for Xanthan but decreased for MP 29 (**Figure 9**). Increasing matric potentials resulted in a reduced loss factor in both depths and for both fluids at low deformation rates but the loss factor increased with increasing Xanthan concentrations (MP 17–21 for T0 or MP 19–21 for T1). These results support the theory of (I) soil homogenization in the course of the deformation, and (II) increasing soil stability due to the establishment of PGA-PGA associations caused by the release of Ca^{2+} as a consequence of soil homogenization. This is reflected in the absence of a (significant) concentration effect for PGA at low deformation rates but a positive influence at high deformation rates, which was not found for Xanthan.

The shear stress was depth-dependent influenced by the concentration, whereas shear stress increased with increasing Xanthan concentrations, a peak was found with PGA for intermediate deformation rates (**Figure 10**). Increasing matric potential resulted in significantly increased shear stresses for Xan (MP 1–28) or PGA (1–30). The effect was more pronounced for Xanthan at low deformation rates (MP ≤12) and more pronounced for PGA at higher deformation rates. These results are contradictory to Mohr-Coulombs failure criterion because of the missing influence of the normal force and point out the dependency of shear stresses on deformation rates and furthermore, underline differing impacts of different biological model substances or in general of SOC on soil stability and on the flow behavior of soils.

The presented results underline that plant root growth processes depend not only on physical soil properties (surely driven by a biological process) because these parameters are chemically altered by biological processes with consequences for plant root growth. However, the results point out, that the definition of thresholds (e.g., penetration resistance) for plant-root growth are not appropriate because barriers of plant root

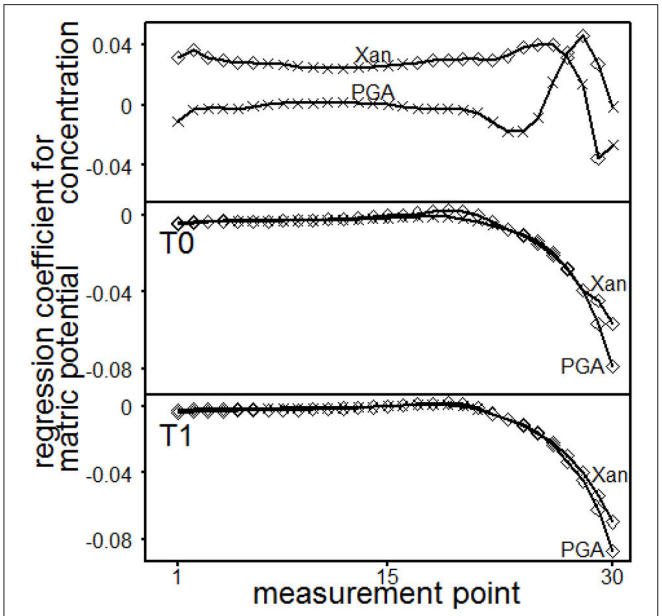

FIGURE 9 | Results of the single point evaluation for soil material excavated from T0 (0.45 to 0.55 m) or T1 (0.55 to 0.65 m) and saturated with Xanthan gum (Xan) or polygalacturonic acid (PGA): Regression coefficients for loss factor. Concentration effect: regression coefficients for each measurement point (top). Effect of matric potential: regression coefficients for each measurement point and depth (T0, middle; T1, bottom). ◊ marks a significant influence of the regression coefficient ($p \leq 0.05$) on loss modulus, while × represents $p > 0.05$.

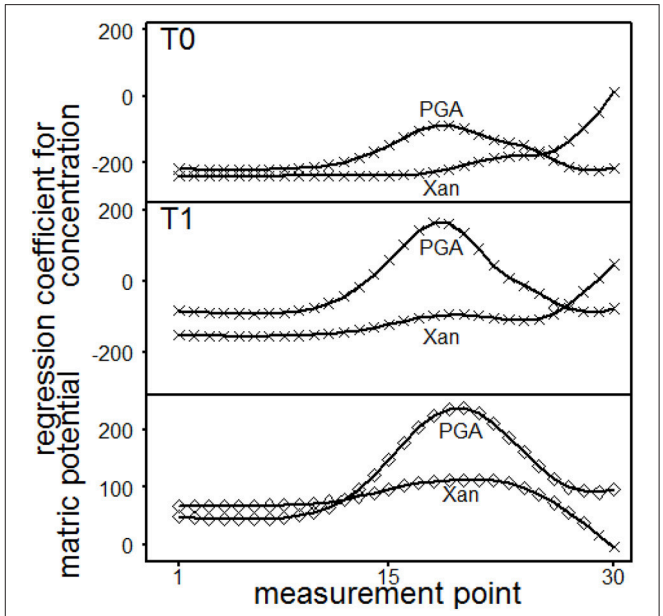

FIGURE 10 | Results of the single point evaluation for soil material excavated from T0 (0.45 to 0.55 m) or T1 (0.55 to 0.65 m) and saturated with Xanthan gum (Xan) or polygalacturonic acid (PGA): Regression coefficients for shear stress. Concentration effect: regression coefficients for each measurement point and depth (T0, top; T1, middle). Effect of matric potential: regression coefficients for each measurement point (bottom). ◊ marks a significant influence of the regression coefficient ($p \leq 0.05$) on shear stress, while × represents $p > 0.05$.

growth can be encountered by naturally altered shear rates, due to slower root growth or by altered water regimes, due to concentration effects of organic compounds exuded at the root's tip resulting in altered shear resistances and altered rheological properties like storage-, loss-moduli and loss factors. These results point out again the complexity of processes occurring in the rhizosphere, in which not only chemicals [like humic acids (Asli and Neumann, 2010), or inorganic salts (Holthusen et al., 2012)] influence e.g., the hydraulic conductivity and thus the plants development. Additionally indirect influences induced by plants or microorganisms occur like an altered root growth due to altered soil stability caused by altered physico-chemical properties like viscosity or surface tension.

CONCLUSION

All hypotheses were supported by the data, shedding a new light on soil stability and therewith on plant root growth processes in the rhizosphere. The results underline the biological alteration of physical properties, e.g., in the vicinity of biological hot spots like root or earthworm channels or particulate organic matter. Biological model substances alter flow properties and parameters related to microstability of soils, like the loss factor, the LVE or Iz. The intensity of the effects depends of the type of biological model substance and on its concentration. The single point evaluation proved that e.g., PGA can both, stabilize or destabilize soils, depending on the applied deformation.

AUTHOR CONTRIBUTIONS

All authors listed have made a substantial, direct and intellectual contribution to the work, and approved it for publication.

ACKNOWLEDGMENTS

This study was funded by the German Research Foundation (DFG), Bonn, under grants PAK 888. We thank MSc. Phillip Lange (LANUV NRW, Leibnizstr. 10, 45659 Recklinghausen) for the determination of flow properties of soil samples saturated with water. Many thanks to the reviewers for their helpful comments.

REFERENCES

Akaike, H. (1973). "Information theory and an extension of the maximum likelihood principle," in *Proceedings of the Second International Symposium on Information Theory,* eds B. N. Petrov and F. Csaki (Budapest: Akademiai Kiado), 267–281.

Asli, S., and Neumann, P. M. (2010). Rhizosphere humic acid interacts with root cell walls to reduce hydraulic conductivity and plant development. *Plant Soil* (2010) 336, 313–322. doi: 10.1007/s11104-010-0483-2

Banfield, C. C., Dippold, M. A., Pausch, J., Hoang, D. T. T., and Kuzyakov, Y. (2017). Biopore history determines the microbial community composition in subsoil hotspots. *Biol. Fertil. Soils* 9:54. doi: 10.1007/s00374-017-1201-5

Baumgarten, W., Dörner, J., and Horn, R. (2013). Microstructural development in volcanic ash soils from South Chile. *Soil Till Res.* 129, 48–60. doi: 10.1016/j.still.2013.01.007

Baumgarten, W., Neugebauer, T., Fuchs, E., and Horn, R. (2012). Structural stability of Marshland soils of the riparian zone of the Tidal Elbe River. *Soil Till* 125, 80–88. doi: 10.1016/j.still.2012.06.002

Bengough, A., and Mullins, C. (1990). Mechanical impedance to root growth: a review of experimental techniques and root growth responses. *Eur. J. Soil Sci.* 41, 341–358. doi: 10.1111/j.1365-2389.1990.tb00070.x

Carvalhais, L. C., Dennis, P. G., Fedoseyenko, D., Hajirezaei, M.-R.,Borriss, R., and von Wirén, N. (2011). Root exudation of sugars, amino acids, and organic acids by maize as affected by nitrogen, phosphorus, potassium, and iron deficiency. *J. Plant Nutr. Soil Sci.* 2010, 1–9. doi: 10.1002/jpln.201000085

Chang, I., Im, J., Prasidhi, A. K., and Cho, G.-C. (2015). Effects of xanthan gum biopolymer on soil strengthening. *Constr. Building Mat.* 74, 65–72. doi: 10.1016/j.conbuildmat.2014.10.026

Chenu, C., Le Bissonnais, Y., and Arrouays, D. (2000). Organic matter influence on clay wettability and soil aggregate stability. *Soil Sci. Soc. Am. J.* 64, 1479–1486. doi: 10.2136/sssaj2000.6441479x

Cochran, W. G. (1957). Analysis of covariance-Its nature and uses. *Biometrics* 13, 261–281. doi: 10.2307/2527916

Czarnes, S., Hallett, P. D., Bengough, A. G., and Young, I. M. (2000). Root- and microbioal-derived mucilages affect soil structure and water transport. *Eur. J. Soil Sci.* 51, 435–443. doi: 10.1046/j.1365-2389.2000.00327.x

Fazekas, O., and Horn, R. (2005). Zusammenhang zwischen hydraulischer und mechanischer bodenstabilität in Abhängigkeit von der Belastungsdauer. *J. Plant Nutr. Soil Sci.* 168, 60–67. doi: 10.1002/jpln.200421381

Gessa, C., and Deiana, S. (1992). Ca-polygalacturonate as a model for a soil-root interface. II. Fibrillar structure comparison with natural root mucilage. *Plant Soil* 140, 1–13. doi: 10.1007/BF00012801

Gessa, C., Deiana, S., Premoli, A., and Ciurli, A. (1997). Redox activity of caffeic acid towards iron (III) complexed in a polygalacturonate network. *Plant Soil* 190, 289–299. doi: 10.1023/A:1004295719046

Grimal, J. Y., Frossard, E., and Morel, J. L. (2001). Maize root mucilage decreases adsorption of phosphate on goethite. *Biol. Ferti. Soils* 33, 226–230. doi: 10.1007/s003740000312

Hallett, P. D., Gordon, D. C., and Bengough, A. G. (2003). Plant influence on rhizosphere hydraulic properties: direct measurements using a miniaturized infiltrometer. *N. Pythol.* 157, 597–603. doi: 10.1046/j.1469-8137.2003.00690.x

Hallett, P. D., and Young, I. M. (1999). Changes to water repellence of soil aggregates caused by substrate-induced microbial activity. *Eur. J. Soil Sci.* 50, 35–40. doi: 10.1046/j.1365-2389.1999.00214.x

Hoang, D. T. T., Pausch, J., Razavi, B. S., Kuzyakova, I., Banfield, C. C., and Kuzyakov, Y. (2016). Hotspots of microbial activity induced by earthworm burrows, old root channels, and their combination in subsoil. *Biol. Fertil. Soils* 52, 1105–1119. doi: 10.1007/s00374-016-1148-y

Holthusen, D., Haas, C., Peth, S., and Horn, R. (2012). Are standard values the best choice? a critical statement on rheological soil fluid properties viscosity and surface tension. *Soil Till. Res.* 125, 61–71. doi: 10.1016/j.still.2012.07.007

Holthusen, D., Pértile, P., Reichert, J. M., and Horn, R. (2017). Controlled vertical stress in a modified amplitude sweep test (rheometry) for the determination of soil microstructure stability under transient stresses. *Geoderma* 295, 129–141. doi: 10.1016/j.geoderma.2017.01.034

Holthusen, D., Peth, S., and Horn, R. (2010). Impact of potassium concentration and matric potential on soil stability derived from rheological parameters. *Soil Till. Res.* 111, 75–85. doi: 10.1016/j.still.2010.08.002

IUSS Working Group WRB (2006). *World Reference Base for Soil Resources,* World Soil Resources Reports No 103 (Rome).

Jones, D. L., Nguyen, C., and Finlay, R. D. (2009). Carbon flow in the rhizosphere: carbon trading at the soil-root interface. *Plant Soil* 321:5–33. doi: 10.1007/s11104-009-9925-0

Kautz, T., Amelung, W., Ewert, F., Gaiser, T., Horn, R., Jahn, R., et al. (2012). Nutrient acquisition from arable subsoils in temperate climates: a review. *Soil Biol. Biochem*. 57, 1003–1022. doi: 10.1016/j.soilbio.2012.09.014

Kautz, T., Lüsebrink, M., Pätzold, S., Vetterlein, D., Pude, R., Athmann, M., et al. (2014). Contribution of anecic earthworms to biopore formation during cultivation of perennial ley crops. *Pedobiologia* 57, 47–52. doi: 10.1016/j.pedobi.2013.09.008

Laird, N. M., and Ware, J. H. (1982). Random-effects models for longitudinal data. *Biometrics* 38, 963–974. doi: 10.2307/2529876

Malovikova, A., Rinaudo, M., and Milas, M. (1994). Comparative interactions of magnesium and calcium counterions with polyfalacturonic acid. *Biopolymers* 34, 1059–1064. doi: 10.1002/bip.360340809

Manunza, B., Deiana, S., Pintore, M., and Gessa, C. (1997). A molecular dynamics investigation on the occurrence of helices in polygalacturonic acid. *J. Mol. Struct*. 419, 169–172. doi: 10.1016/S0166-1280(97)00247-9

Markgraf, W., and Horn, R. (2006). Rheological-stiffness analysis of K^+-treated and $CaCO_3$-rich soils. *J. Plant Nutr. Soil Sci*. 169, 411–419. doi: 10.1002/jpln.200521934

Markgraf, W., Horn, R., and Peth, S. (2006). An approach to rheometry in soil mechanics - structural changes in bentonite, clayey and silty soils. *Soil Till. Res*. 91, 1–14. doi: 10.1016/j.still.2006.01.007

Markgraf, W., Moreno, F., and Horn, R. (2012). Quantification of microstructural changes in salorthidic fluvaquents using rheological and particle charge techniques. *Vadose Zone J*. 11, 1–11. doi: 10.2136/vzj2011.0061

Mezger, T. (2014). *The Rheology Handbook: for Users of Rotational and Oscillatory Rheometers*. Hannover: Vincentz Network

Mohamed, A., Trickett, K., Chin, S. Y., Cummings, S., Sagisaka, M., Hudson, L., et al. (2010). Universal surfactant for water, oils, and CO_2. *Langmuir* 26, 13861–13866. doi: 10.1021/la102303q

Morel, J., Andreux, F., Habib, L., and Guckert, A. (1987). Comparison of the adsorption of maize root mucilage and polygalacturonic acid on montmorillonite homoionic to divalent lead and cadmium. *Biol. Ferti. soils* 5, 13–17. doi: 10.1007/BF00264339

Morel, J. L., Mench, M., and Guckert, A. (1986). Measurement of Pb^{2+}, Cu^{2+} and Cd^{2+} binding with mucilage exudates from maize (*Zea mays* L) Roots. *Biol. Fertil. Soils* 2, 29–34. doi: 10.1007/BF00638958

Nakagawa, S., and Schielzeth, H. (2013). A general and simple method for obtaining R2 from generalized linear mixed-effects models. *Methods Ecol. Evol.* 4, 133–142. doi: 10.1111/J.2041-210x.2012.00261.X

Pettitt, D. J., Wayne, J. E. B., Renner Nantz, J., and Shoemaker, C. F. (1995). Rheological Properties of Solutions and Emulsions Stabilizied with Xanthan Gum and Propylene glycol Alginate. *J. Food. Sci. Vol*. 60, 528–531. doi: 10.1111/j.1365-2621.1995.tb09819.x

R Development Core Team (2017). *R: A Language and Environment for Statistical Computing. R Foundation for Statistical Computing, Vienna, Austria*. Available online at: http://www.R-project.org

Read, D. B., and Gregory, P. J. (1997). Surface tension and viscosity of axenic maize and lupin root mucilages. *N. Phytol.* 137, 623–628. doi: 10.1046/j.1469-8137.1997.00859.x

Riggert, R., Fleige, H., Kietz, B., Gaertig, T., and Horn, R. (2017). Dynamic stress measurements and the impact of timber harvesting on physical soil properties *Aust. Forestry* 80, 255–263. doi: 10.1080/00049158.2017.1347981

Sakamoto, Y., Ishiguro,M., and Kitagawa, G. (1986). *Akaike Information Criterion Statistics*. Dordrecht: D. Reidel Publishing Company.

Santos, D., Smucker, A. J. M., Murphy, S. L. S., Taubner, H., and Horn, R. (1997). Uniform separation of concentric surface layers from soil aggregates. *Soil Sci. Soc. Am. J.* 61, 720–724. doi: 10.2136/sssaj1997.03615995006100030003x

Six, J., Bossuyt, H., Degryze, S., and Denef, K. (2004). A history of research on the link between (micro)aggregates, soil biota, and soil organic matter dynamics. *Soil Till. Res*. 79, 7–31. doi: 10.1016/j.still.2004.03.008

Stoddart, R. W., Spires, I. P. C., and Tipton, K. F. (1969). Solution properties of polygalacturonic acid. *Biochem. J.* 114, 863–870. doi: 10.1042/bj1140863

Tisdall, J. M., and Oades, J. M. (1979). Stabilization of soil aggregates by the root systems of ryegrass. *Soil Res.* 17, 429–441. doi: 10.1071/SR9790429

Traoré, O. V., Groleau-Renaud, S., Plantureux, A., Tubeileh, and Boeuf-Tremblay, V. (2000). Effect of root mucilage and modelled root exudates on soil structure. *Eur. J. Soil Sci.* 51, 575–581. doi: 10.1046/j.1365-2389.2000.00348.x

Uteau, D., Hafner, S., Pagenkemper, S. K., Peth, S., Wiesenberg, G. L. B., Kuzyakov, Y., et al. (2015). Oxygen and redox potential gradients in the rhizosphere of alfalfa grown on a loamy soil. *J. Plant Nutr. Soil Sci*. 178, 278–287. doi: 10.1002/jpln.201300624

Verbeke, G., and Molenberghs, G. (2000). *Linear Mixed Models for Longitudinal Data*. New York, NY: Springer.

Zhang, B., Hallett, P. D., and Zhang, G. (2008). Increase in the fracture toughness and bond energy of clay by a root exudate. *Eur. J. Soil Sci.* 59, 855–862 doi: 10.1111/j.1365-2389.2008.01045.x

Conflict of Interest Statement: The authors declare that the research was conducted in the absence of any commercial or financial relationships that could be construed as a potential conflict of interest.

frontiers in Environmental Science

ORIGINAL RESEARCH
published: 09 February 2018
doi: 10.3389/fenvs.2018.00009

Linking 3D Soil Structure and Plant-Microbe-Soil Carbon Transfer in the Rhizosphere

Alix Vidal[1], Juliane Hirte[2], S. Franz Bender[3], Jochen Mayer[2], Andreas Gattinger[4,5], Carmen Höschen[1], Sebastian Schädler[6], Toufiq M. Iqbal[7] and Carsten W. Mueller[1]*

[1] Lehrstuhl für Bodenkunde, Technische Universität München, Munich, Germany, [2] Plant-Soil Interaction Group, Division, Agroecology and Environment, Agroscope, Zurich, Switzerland, [3] Department of Land, Air and Water Resources, University of California, Davis, Davis, CA, United States, [4] Departement für Bodenwissenschaften, FiBL, Frick, Switzerland, [5] Organic Farming, Justus-Liebig-Universität Giessen, Giessen, Germany, [6] Global Applications Support Crossbeam, Carl Zeiss Microscopy GmbH, ZEISS Group, Oberkochen, Germany, [7] Department of Agronomy and Agricultural Extension, University of Rajshahi, Rajshahi, Bangladesh

Plant roots are major transmitters of atmospheric carbon into soil. The rhizosphere, the soil volume around living roots influenced by root activities, represents hotspots for organic carbon (OC) inputs, microbial activity, and carbon turnover. Rhizosphere processes remain poorly understood and the observation of key mechanisms for carbon transfer and protection in intact rhizosphere microenvironments are challenging. We deciphered the fate of photosynthesis-derived OC in intact wheat rhizosphere, combining stable isotope labeling at field scale with high-resolution 3D-imaging. We used nano-scale secondary ion mass spectrometry and focus ion beam-scanning electron microscopy to generate insights into rhizosphere processes at nanometer scale. In immature wheat roots, the carbon circulated through the apoplastic pathway, via cell walls, from the stele to the cortex. The carbon was transferred to substantial microbial communuties, mainly represented by bacteria surrounding peripheral root cells. Iron oxides formed bridges between roots and bigger mineral particles, such as quartz, and surrounded bacteria in microaggregates close to the root surface. Some microaggregates were also intimately associated with the fungal hyphae surface. Based on these results, we propose a conceptual model depicting the fate of carbon at biogeochemical interfaces in the rhizosphere, at the forefront of growing roots. We observed complex interplays between vectors (roots, fungi, bacteria), transferring plant-derived OC into root-free soil and stabilizing agents (iron oxides, root and microorganism products), potentially protecting plant-derived OC within microaggregates in the rhizosphere.

Keywords: rhizosphere, microorganisms, iron oxides, organo-mineral associations, NanoSIMS, FIB-SEM, undisturbed samples, ^{13}C enrichment

OPEN ACCESS

Edited by:
Maria Luz Cayuela, Centro de Edafología y Biología Aplicada del Segura (CSIC), Spain

Reviewed by:
Eoin L. Brodie, Lawrence Berkeley National Laboratory (LBNL), United States
Lukas Van Zwieten, New South Wales Department of Primary Industries, Australia

****Correspondence:***
Alix Vidal
alix.vidal@wzw.tum.de

Specialty section:
This article was submitted to Soil Processes, a section of the journal Frontiers in Environmental Science

Received: *17 November 2017*
Accepted: *26 January 2018*
Published: *09 February 2018*

Citation:
Vidal A, Hirte J, Bender SF, Mayer J, Gattinger A, Höschen C, Schädler S, Iqbal TM and Mueller CW (2018) Linking 3D Soil Structure and Plant-Microbe-Soil Carbon Transfer in the Rhizosphere. Front. Environ. Sci. 6:9. doi: 10.3389/fenvs.2018.00009

INTRODUCTION

Soils harbor a huge fraction of the global terrestrial carbon (C) pool. While belowground C transfer by plants represents a major pathway of atmospheric C into the soil, soils also represent a major source of atmospheric C. Understanding the complex interactions that govern C storage in and release from soils is a major challenge to develop strategies to mitigate climate change (Lal, 2004).

Soils are composed of a wide diversity of organic and mineral compounds, forming a complex mosaic of microenvironments (Ranjard and Richaume, 2001). The volume of soil directly affected by living roots, i.e., the rhizosphere, represents an important hotspot for microbial activity, organic carbon (OC) inputs, and C turnover in soils (Hinsinger et al., 2009; Philippot et al., 2013; Finzi et al., 2015). Root products (mucilage, exudates, cell fragments) and dead roots, represent a major source of OC in soils (Rasse et al., 2005; Bardgett et al., 2014). Around 30% of the photosynthetically fixed C is transferred below ground, but this proportion can vary widely depending on environmental conditions, plant species, and the plant growing stage (Kuzyakov and Domanski, 2000). While half of the C transferred below ground is allocated to the root biomass, around one-third is respired in the rhizosphere (Jones et al., 2009), in equal proportions by roots and microorganisms (Kuzyakov and Larionova, 2005). Finally, more than 10% of the C transported below ground is allocated to soil microorganisms and soil organic matter (Jones et al., 2009; Kaiser et al., 2015). Alive or dead, microorganisms inhabiting the rhizosphere represent a major sink for plant-derived C and foster the development of soil microstructures (Liang and Balser, 2011; Kallenbach et al., 2016; Lehmann et al., 2017). These microorganisms include arbuscular mycorrhizal (AM) fungi, soil fungi that form symbiotic associations with the majority of land plants, including wheat (Van der Heijden et al., 1998; Dickie et al., 2013). These fungi can receive up to 20% of a plant's photosynthetic C intake in return for delivery of nutrients to the plant (Jakobsen and Rosendahl, 1990). Specific surface binding properties of organic soil components (roots, plant-derived compounds, and microorganisms) together with adsorption capacities of soil minerals are drivers of the formation of complex organo-mineral assemblages as microaggregates (Baldock and Skjemstad, 2000; Bronick and Lal, 2005). The association of OC in complex microaggregate structures stabilizes C against degradation and reduces its turnover in soil, hence representing a pathway of C sequestration (Kögel-Knabner and Amelung, 2014). Rhizosphere processes have a determinant impact on the global soil C pool that is still not fully understood (Schmidt et al., 2011; Pett-Ridge and Firestone, 2017). Enhancing rhizosphere processes, such as C transfer from roots to microorganisms and soil, can increase soil C storage (White et al., 2013; Lange et al., 2015), one of the challenges of the Twenty-firstt century to mitigate climate change (Lal, 2004; Lehmann, 2007).

The complexity of biogeochemical processes occurring in the rhizosphere requires observations at process-relevant scales, i.e., at the interface of root cells, microorganisms, and soil (Hallett et al., 2013; Oburger and Schmidt, 2016). The microscopic observation of intact soil structures as embedded thin sections has been applied since the 1930s (Kubiena, 1938; Alexander and Jackson, 1954) and has enabled the observation of the rhizosphere at the scale of organism interactions (Martin and Foster, 1985). Despite the descriptive quality of such imaging approaches, the absence of techniques to trace specific elements and isotopes hampered the direct *in situ* study of C allocation at biogeochemical interfaces in the rhizosphere. Since then, strong efforts have been made to observe undisturbed soil-root-microorganism assemblages at the microscale under controlled laboratory conditions, in some cases using ^{13}C and ^{15}N tracers (Nunan et al., 2001; Li et al., 2003; Castorena et al., 2016; Vidal et al., 2016). In the present study, we collected undisturbed rhizosphere samples in an agricultural field and considered *in situ* interactions of plants, microorganisms, and soil mineral particles at the microscale.

We qualitatively explored the pathway of photosynthetically fixed C from roots to microorganisms and soil, as well as how roots determine the structural and compositional 3D architecture of the rhizosphere at nanometer resolution. To meet this objective, we combined 2D elemental and isotopic information (nano-scale secondary ion mass spectrometry-NanoSIMS) with 3D structural information (Focused ion beam-scanning electron microscopy-FIB-SEM) highlighting biogeochemical interfaces and processes in the rhizosphere. We expected the highest enrichment in the close vicinity of roots, as well as a transfer of plant-derived C to microorganisms surrounding roots and forming intimate associations with minerals.

MATERIALS AND METHODS

In Situ ^{13}C-Labeling and Sampling

Samples were collected in 2015 on winter wheat (*Triticum aestivum*, var. Wiwa) plots of the Swiss long-term field trial "DOK" (Therwil, CH) (Mayer et al., 2015). Two microplots (stainless steel tubes, 0.35 m diameter, 0.55 m length) were inserted into the soil to 0.5 m depth to segregate wheat sub-populations (approximately 50 plants in two rows) from surrounding field populations below ground. The first microplot corresponded to a full-fertilized bio-organic management system (i.e., in compliance with the subsidiary scheme "Bio Suisse"). The second microplot corresponded to a full-fertilized conventional management system (i.e., in compliance with the subsidiary scheme "Proof of Ecological Performance"). The wheat was fertilized according to Swiss standards for the respective managements (Flisch et al., 2009). The present study did not aim at comparing organic and conventional treatments but at depicting rhizosphere processes through qualitative microscale observations. Thus, the samples collected from these two microplots were not separated by treatments for NanoSIMS analyses. In order to keep labeled plants as undisturbed as possible, the use of multiple-pulse labeling was chosen instead of a more invasive method (Kuzyakov and Domanski, 2000). From advanced tillering to maturity (beginning of April to end of June according to Zadoks et al., 1974), the headspace over each microplot was enclosed with a gas-tight Plexiglas® hood once per week and plants were exposed to 99 atom-% ^{13}C-CO_2 (**Figure 1**). Before the labeling campaign, the necessary amount of label, the number of pulse events during the vegetation period, and the duration of each pulse event were calculated. For this purpose, three parameters were considered: the strength of the label (99%), the daily assimilation rate of wheat, and the targeted bulk soil enrichment. The gas was injected in repeated pulses during 4 h between late morning and early afternoon while the CO_2 concentration was regularly tracked using a portable LI-COR (LI820, re-calibrated for ^{13}C-sensitivity) and allowed to

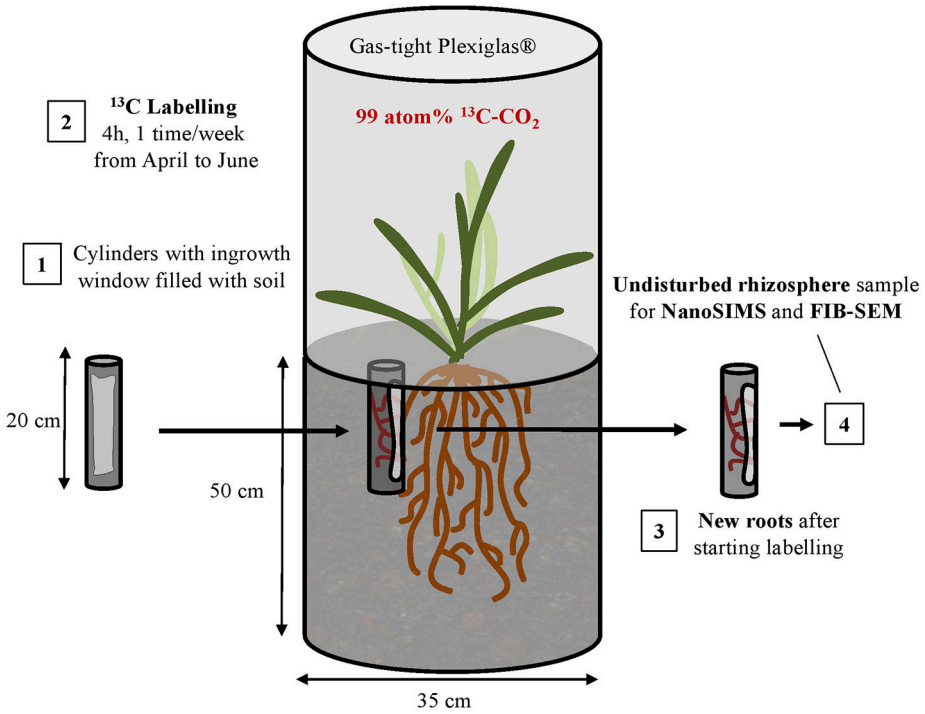

FIGURE 1 | Simplified representation of the experimental design applied to obtain undisturbed rhizosphere samples for NanoSIMS and FIB-SEM analyses. The cylinder represents a microplot. Numbers indicate the sequence of steps to obtain samples.

fluctuate between 150 and 800 ppm. Closed ventilation by PC fans and cooling with 4 kg ice packs ensured similar climatic conditions inside and outside the labeling hoods. The microplot plants received approximately 9.5 g ^{13}C over the entire labeling period. Considering the qualitative microscale approach of the present study, we did not include a bare fallow control to account for the autotrophic CO_2 fixation. Indeed, we focused on rhizosphere processes and assumed autotrophic microorganisms to be negligible compared to heterotrophic ones (Kuzyakov and Larionova, 2005). For minimal destruction of microplots by the root and soil sampling before plant maturity, one root-ingrowth cylinder (PVC tubes, 30 mm diameter, 200 mm length) was inserted into the topsoil of each microplot (cylinder 1 and 2, for the organic and conventional treatments, respectively). Cylinders had an ingrowth window of 150*30 mm on one side and were covered with a 1 mm mesh on openings. Sieved and homogenized topsoil was filled into the cylinders and re-compacted to a density of 1.3 g.cm^{-3}, which was estimated from the cylinder volume and the fresh soil mass. At the beginning of the labeling period, one hole per microplot was drilled in 20–30 mm distance from the wheat rows by means of a gouge auger (30 mm diameter; Eijkelkamp, Netherlands). The two ingrowth cylinders were gently pushed inside the holes so that the bottom and side walls were in close contact with the surrounding soil and the ingrowth windows faced wheat rows. Only new wheat roots that grew after the beginning of the labeling period could thereby enter ingrowth cylinders. Plants were labeled 10 times with the last labeling being conducted 3 days before sampling. At anthesis (Zadoks' scale 69; Zadoks et al., 1974, mid-June), the cylinders were removed from the soil, transported to the laboratory, and immediately processed or deep-frozen for further analyses.

Sample Processing

The two ingrowth cylinders were opened at the top and bottom and the complete soil core within the cylinder was removed. Soil was carefully broken by hand into several pieces. Larger soil aggregates including root fragments (approximately 1 cm^{-3}) were sampled. Two samples from each cylinder, i.e., four samples in total, were chemically fixed using Karnovsky fixative (Morris, 1965) and dehydrated in graded acetone series and embedded in araldite resin (Araldite 502) until complete polymerization, according to the method described by Mueller et al. (2012). Samples were cut and polished to obtain intact rhizosphere cross sections. In order to analyze the fine soil fraction containing microaggregates and fungal hyphae, a fungal hypha was extracted from cylinder 1, which showed a higher percentage of hyphal root colonization (**Table 1**). This sample was prepared on a silica wafer according to Mueller et al. (2012). Briefly, 1 mg of dried soil from the chemically fixed and dried rhizosphere was dispersed in 10 mL of analytical water ACS. A 100 µL drop was deposited on a silica wafer and dried overnight.

The remaining soil from cylinders was separated from roots and other organic materials by 0.5 mm wet-sieving, oven-dried at 80°C and analyzed for total C and ^{13}C abundance using an elemental analyzer coupled with an isotope ratio mass spectrometer (EA 1110; Carlo Erba; coupled with Delta

TABLE 1 | General characteristics of soil and colonization with arbuscular mycorrhizal fungi of roots extracted from the two cylinders, considered as replicated in the present study and used for the NanoSIMS and FIB-SEM analyses.

	Cylinder 1	Cylinder 2
SOIL CHARACTERISTICS		
Soil texture (% sand-silt-clay)	12-72-16	12-72-16
SOC (%)	1.34	1.23
$\delta^{13}C$ (‰)	−18.1	−22.7
$\delta^{13}C$ excess (‰)	9.3	4.4
ROOT LENGTH COLONIZED BY ARBUSCULAR MYCORRHIZAL FUNGI		
Hyphae (%)	63	30
Vesicles (%)	2	1
Arbuscles (%)	4	8

S; Thermo Finnigan). The root colonization by AM fungi was assessed by microscopy using a modified line-intersection method for 100 intersections after clearing and staining with an ink-vinegar mixture as described by Wagg et al. (2011). The general characteristics of the soil are presented in **Table 1** for the two cylinders, as well as the percentage of root length colonized by AM fungal hyphae, vesicles, and arbuscles.

NanoSIMS Analyses

We analyzed intact rhizosphere sections (four transversal and longitudinal sections) and a rhizosphere derived fungal hypha with NanoSIMS. At first, the scanning electron microscope (SEM in backscatter mode; JEOL JSM 5900LV, Garching, Germany) was used to identify areas for subsequent NanoSIMS analyses. Areas of interest corresponded to intact rhizosphere area containing root cells, microorganisms, and soil minerals/microaggregates. The sample surface was sputtered by a Cs^+ beam to obtain 30 × 30 μm^2 images (acquired using a NanoSIMS 50L Cameca, Germany) at 256 × 256 pixels. Secondary ion images of ^{12}C, ^{13}C, ^{16}O, $^{12}C^{14}N$, and $^{56}Fe^{16}O$ were obtained and 20 planes were accumulated for each final image, with a dwell time of 1 ms.pixel^{-1}. Measurements on the sample dispersed on the silica wafer were realized in the same manner, recording 22 planes. Higher resolution images were obtained acquiring 40 × 40 μm^2 images at 512 × 512 pixels for ^{12}C, ^{13}C, $^{12}C^{14}N$, and ^{16}O secondary ions. Measurements were processed using the ImageJ software (Abràmoff et al., 2004). OpenMIMS and MosaicJ plugins (Thévenaz and Unser, 2007) were used to display images and create mosaics, respectively. For RGB mosaic images, images were first uploaded individually, composite RGB images were created ($^{56}Fe^{16}O$ in red, $^{12}C^{14}N$ in green, ^{16}O in blue) and adjusted to remove the resin contribution using the color adjustment. Images were then uploaded in the MosaicJ plugin for mosaic creation. Mosaics including 3–32 NanoSIMS measurements were created. The ^{13}C:^{12}C ratio images were generated to follow the distribution of ^{13}C enrichment. The enrichment was estimated by comparing ^{13}C:^{12}C ratio values to the approximate soil natural abundance (0.011). For ^{13}C:^{12}C ratio mosaic images, images were first uploaded individually to obtain the ^{13}C:^{12}C ratio distribution and uploaded in the MosaicJ plugin for the mosaic creation. The interactive regions of interest (ROIs) definition tool of Look@NanoSIMS program (Polerecky et al., 2012) was used to draw ROIs on selected $^{12}C^{14}N$ images, in order to obtain their isotopic composition. ROIs were drawn either by using the threshold function according to $^{12}C^{14}N$ counts (microbes and hyphae), the freehand drawing option (plant cell walls) or by drawing ellipses (resin spots). The resin, which presented a ^{13}C:^{12}C ratio equal to the soil natural abundance was considered as natural background.

FIB-SEM Analyses

FIB-SEM imaging was performed using a Zeiss Crossbeam 550 L microscope with a primary beam operated at a landing energy of 1.8 keV. Backscattered electrons were recorded at an energy-selective backscattered electron detector with the grid voltage set to 1,000 V. The Carl Zeiss ATLAS 5 package was used for the identification of the adequate sample position by precise spatial correlation of sample stage coordinates to the previously acquired NanoSIMS analysis, and for the control of the FIB-SEM acquisition. Images were collected at 15 µs dwell time, at 10 nm pixel resolution, and at slice intervals of 10 nm. EDS maps were collected at 40 nm pixel resolution at a Z interval of 160 nm.

For the FIB sample preparation, first a 1.5 µm thick protective platinum layer was deposited on the surface of the sample's volume of interest using a 3 nA FIB beam current. The characteristic ATLAS 3D tracking marks, which are used to dynamically correct for drifts of the sample with respect to the SEM beam in x- and y-directions, and for drifts of the sample with respect to the FIB milling in z-direction, were milled into this platinum layer with a 50 pA FIB beam, filled in with a layer of C (100 pA FIB beam current) and then covered with a 1 µm thick C pad (3 nA FIB beam current). The cross-section in front of the volume of interest was opened using a 30 nA FIB beam current and then polished using a 7 nA FIB beam current.

During the collection of the imaging dataset, the FIB (3 nA beam current) and the SEM (1.8 kV, 1.0 nA) were operated simultaneously. FIB-SEM imaging was paused and the SEM ramped to analytical conditions (6 kV, 2 nA) at z intervals of 160 nm for the acquisition of EDS maps.

The 3D data set was created from the datasets using ORS Dragonfly software. Images were not aligned after the acquisition because the quality of the alignment achieved during the acquisition of the dataset was considered sufficient. The direction of image acquisition for both the FIB-SEM dataset and EDS maps is perpendicular to that for the NanoSIMS analysis and 2D surface imaging. To highlight the volumes of interest without additional segmentation steps, window levels of the images were adjusted and saturated black values made transparent in the volume view.

Statistical Analyses

The R software, version × 64 3.3.2 (R Core Team, 2017), was used for boxplot representations of ROI ^{13}C:^{12}C ratio values of NanoSIMS images and statistical analyses. The application of Shapiro–Wilk test revealed that data were not normally distributed. Thus, the non-parametric Kruskal–Wallis test was performed, followed by multiple pairwise comparisons with Dunn test. Statistical significance was set as $\alpha = 0.05$ for all tests.

RESULTS

Arrangement of Organic and Mineral Structures in Roots and Rhizosphere

We analyzed an immature wheat root close to the root tip (**Figures 2**, **3**, and Supplementary Figure 1) as this is the location of highest activity in terms of mucilage production and effects on soil structure due to pressure of the growing roots. The root tip has a stele diameter of less than 100 μm and no identifiable phloem and xylem cells. The cortex cells, located at the periphery of the root and in direct contact with the soil particles, present a marked deformation (**Figure 2**). This phenomenon is also observed on a longitudinal section of another root (Supplementary Figure 2).

Organic structures surrounding the root (**Figures 2**, **3A**) are mainly represented by unicellular microorganisms (bacteria or archaea) and particulate organic matter (POM). We were able to detect the round shape of microorganisms with an approximate diameter of 1 μm and high nitrogen content reflected by the $^{12}C^{14}N$ clearly indicating its microbial origin

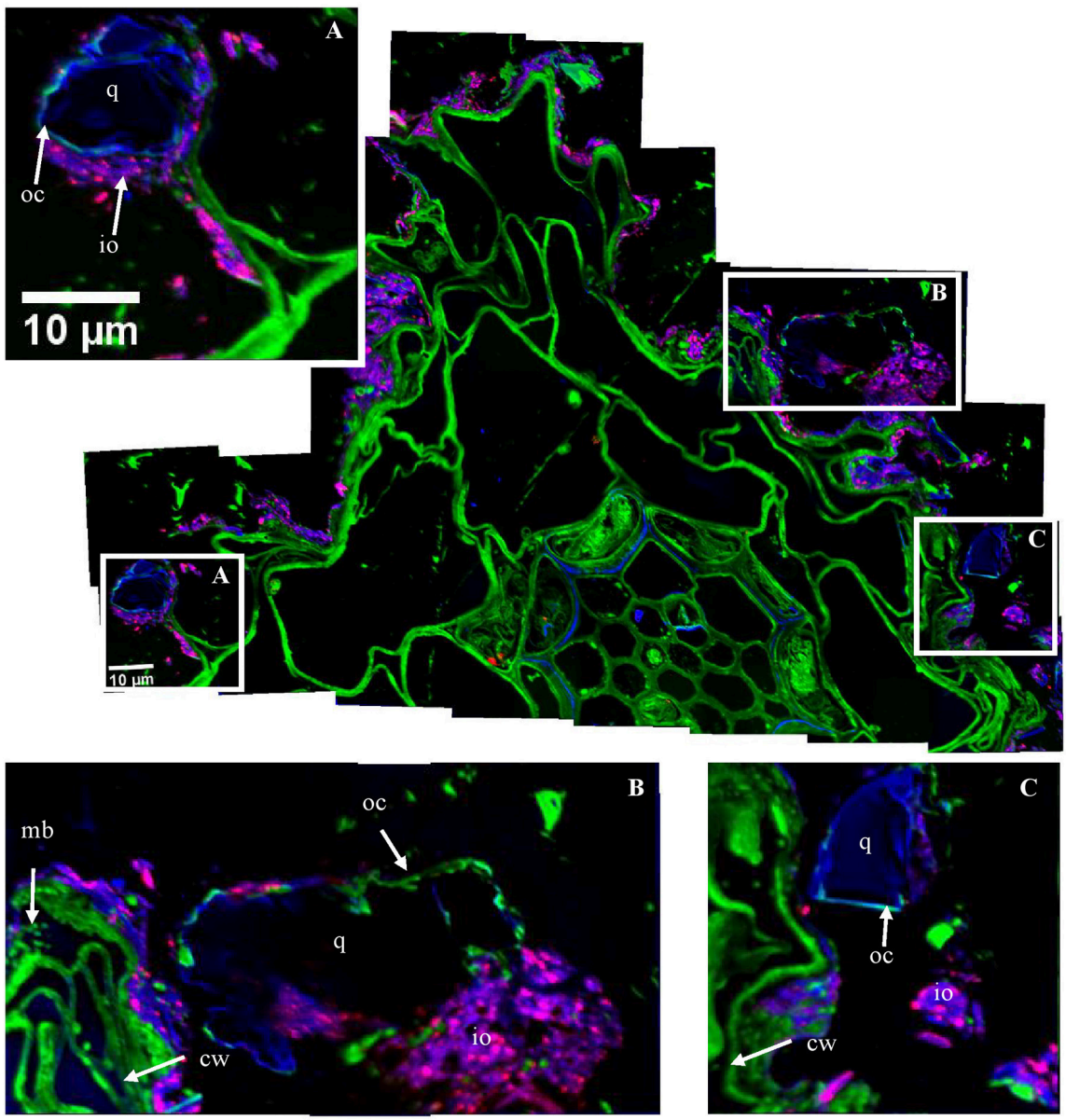

FIGURE 2 | Organo-mineral associations surrounding the root cells. Mosaic of NanoSIMS composite images of the area indicated in Supplementary Figure 1A; with $^{12}C^{14}N$ in green, ^{16}O in blue, $^{56}Fe^{16}O$ in red. The mosaic was built up from 32 NanoSIMS measurements (one image −30 × 30 μm, 256 × 256 pixels, 20 planes, 1 ms.pixel^{-1}). **(A–C)** Illustrate the intimate association between large mineral particles (>10 μm) (i.e., q, quartz grain); io, iron oxides; cw, plant cell walls; mb, microorganisms; and oc, organic coating. The black area represents the resin. White squares correspond to the areas used to obtain the boxplot in **Figure 8**.

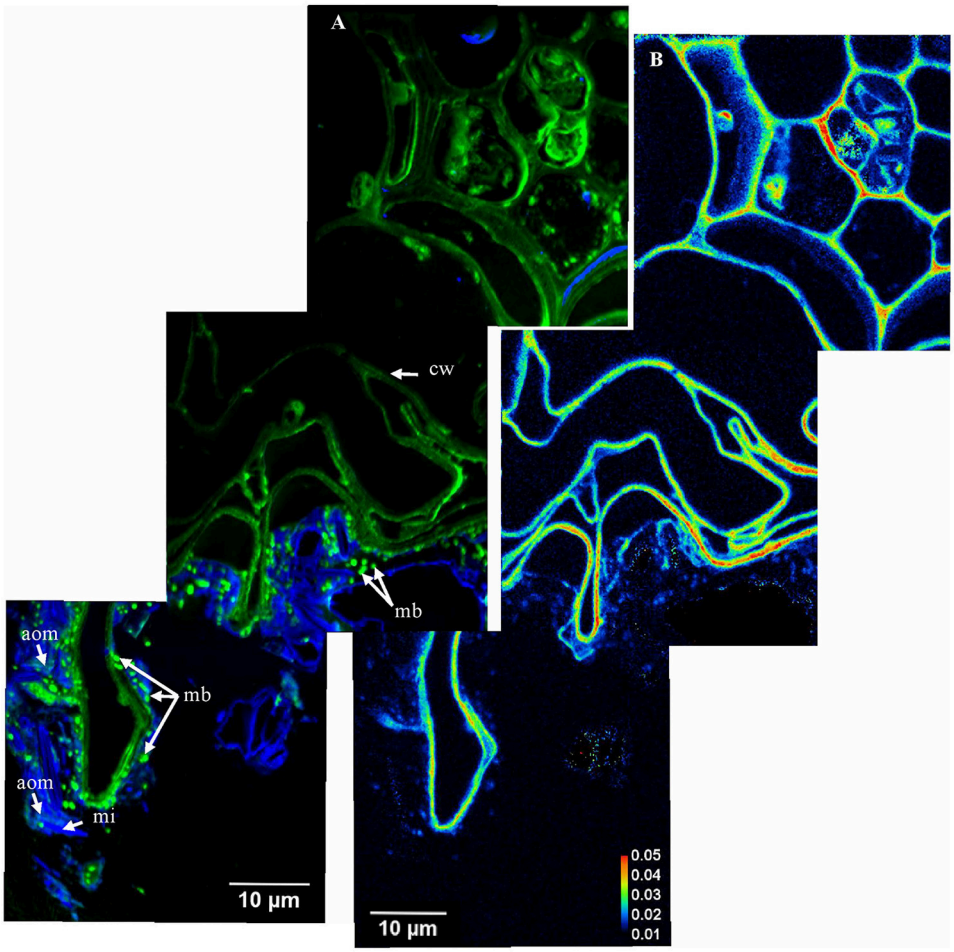

FIGURE 3 | From stele to cortex and rhizosphere–carbon transfer and organo-mineral associations. **(A)** Mosaic of NanoSIMS composite images of the area indicated in Supplementary Figure 1B; with $^{12}C^{14}N$ in green and ^{16}O in blue; aom, amorphous organic matter; cw, plant cell walls; mb, microorganisms; mi, mineral particle. The mosaic was created from 3 NanoSIMS images (one image- 40 × 40 µm, 512 × 512 pixels, 20 planes, 1 ms.pixel^{-1}); **(B)** The ^{13}C:^{12}C ratio of the same area presented in **(A)**.

(**Figure 3A**). The microorganisms are mainly concentrated at the close surrounding of peripheral root cells and/or in direct contact with root cell walls (**Figures 3A**, **4D**). From some micrometer distance to the rhizoplane, microorganisms, as well as laces of N rich POM, are identified in soil microaggregates (**Figures 2**, **5B**). These microorganisms appear as separated cells (**Figure 2**) or forming microbial cell assemblages (**Figure 5B**) at the surrounding of roots or within soil aggregates. By using FIB-SEM we were able to demonstrate the direct association of microbial cells with clay sized soil minerals forming microaggregate precursors directly at the rhizoplane (**Figure 4C**). Microbial cells forming the microbial assemblage are directly bound to the root cell surface on one side and enclosed within a dense layer of mineral soil constituents.

We also extracted a fungal hypha from the rhizosphere soil to study the direct effect of fungi on microaggregate assemblages in the rhizosphere (**Figure 6**). Microaggregates (high ^{16}O and $^{56}Fe^{16}O$ signals) are directly attached to the hyphal surface.

Inorganic structures are represented both by larger mineral particles (>5 µm), with high ^{16}O content (**Figures 2A–C**, **4E**, and Supplementary Figure 3C), assignable to quartz grains and iron oxides, with high $^{56}Fe^{16}O$ content (**Figure 2**). Clay sized minerals are oriented tangentially along the rhizoplane (**Figures 4A,D**). Some quartz grains are connected to root cells via iron oxides (**Figures 2A**, **4E**). Quartz grains located at the periphery of root cells and close to microbes are frequently surrounded by an organic coating (**Figures 2A–C**). Amorphous organic matter, reflected by its $^{12}C^{14}N$ content (**Figure 3**), was also identified close to root cells and surrounding mineral particles.

Carbon Transfer at the Root-Rhizosphere Vicinity

Root cell walls are highly enriched in ^{13}C (**Figures 3B**, **7A–C**, **8**), with a mean ^{13}C:^{12}C ratio of 0.024 (SD = 0.004). Within the same section, the ^{13}C:^{12}C ratio measured in root cell walls varies from

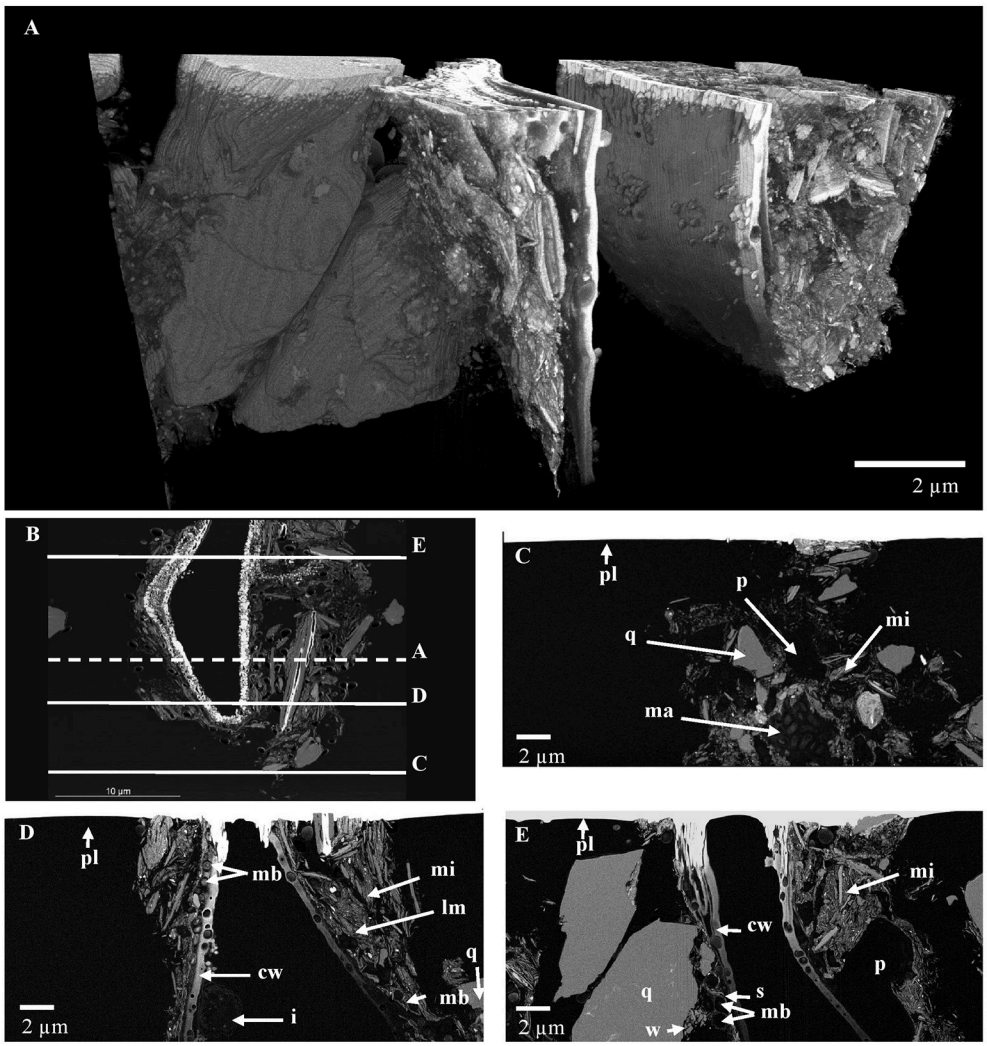

FIGURE 4 | Structural assembly of the intact rhizosphere at a subcellular resolution- FIB-SEM (area indicated in Supplementary Figure 1C). **(A)** Volume visualization of the FIB-SEM dataset representing the interaction between mineral particles and a root cell; **(B)** Virtual perpendicular slice through the FIB-SEM 3D dataset. Letters indicate the position of the selected images; **(C)** Microaggregate at the root periphery; **(D)** Intimate organo-mineral associations; **(E)** Larger mineral particles at the root periphery; cw, cell wall; i, inner cell organic structure; lm, laminar microaggregate; mi, mineral particle; ma, microbial cell assemblage; mb, microorganisms; p, pore; pl, platinum layer; q, quartz grain; s, space between the root cell wall and mineral particles; w, weathering of quartz grain. The overlay of EDS images corresponding to **(C–E)** images are presented in Supplementary Figure 3.

0.018 to 0.032 (**Figure 8**). The enrichment is not homogeneously distributed in the root, as other areas presented a lower ^{13}C:^{12}C ratio, varying between 0.015 and 0.020 (Supplementary Figure 2).

The mean ^{13}C:^{12}C ratio of microorganisms is highly variable (0.010-0.029). It is significantly higher than the natural background but lower than the ^{13}C:^{12}C ratio of plant cell walls, which is 0.016 (SD = 0.004) (**Figures 3B**, **7A,B**, **8**). The fungal hypha detected in the soil suspension is, on average, slightly ^{13}C enriched (mean ^{13}C:^{12}C ratio: 0.012), with a significantly higher ^{13}C:^{12}C ratio compared with the natural background (**Figure 6C**). A highly labeled spot, potentially a hypha-associated microbe, is observed (^{13}C:^{12}C ratio: 0.024) (**Figure 6D**). The OC forming a coating around quartz grains is on average not ^{13}C enriched (mean ^{13}C:^{12}C ratio: 0.011), with a slight enrichment in a distinct spot (^{13}C:^{12}C ratio: 0.015; **Figure 8A**).

DISCUSSION

The Apoplastic Pathway of Carbon at the Root Tip

Some root cell walls are highly enriched in ^{13}C compared with other organic soil compartments (e.g., microorganisms; **Figures 3B**, **7**, **8**). This illustrates that in the immature root tip, the C transfer is achieved through cell walls, as previously shown at the lab scale by Kaiser et al. (2015). At the root tips, the absence of a Casparian strip enables the flow of recently fixed C (McCully and Canny, 1985) from the stele toward the cortex

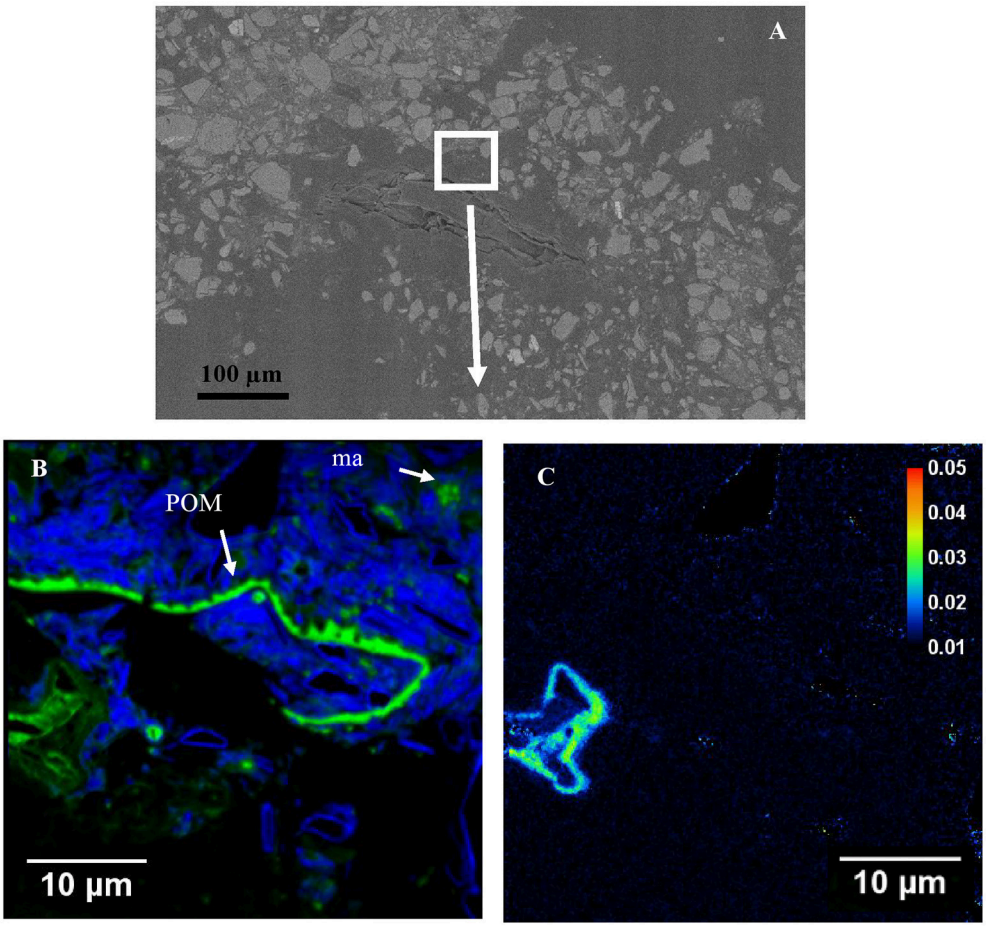

FIGURE 5 | Organo-mineral aggregates surrounding a ^{13}C enriched root cell. **(A)** SEM image of a root surrounded by microaggregates. This image was used to identify areas for subsequent NanoSIMS analyses represented in **(B,C)** images; **(B)** NanoSIMS composite image (40 × 40 µm, 512 × 512 pixels, 20 planes, 1 ms.pixel^{-1}); with $^{12}C^{14}N$ in green and ^{16}O in blue; POM, particulate organic matter; ma, microbial cell assemblage. **(C)** The ^{13}C:^{12}C ratio of the same area presented in **(B)**.

via the apoplastic pathway, i.e., along cell walls (Farrar et al., 2003; Jones et al., 2009; Kaiser et al., 2015). The C translocated to the rhizosphere by roots, e.g., root exudates, can be used as substrates by rhizosphere microbial communities (Bertin et al., 2003; Kuzyakov and Blagodatskaya, 2015). In the present study, we focused on root tips described as maximal exudate loss areas along the roots (Jones et al., 2009). It has to be noted that root elongation zones and root hairs are also important locations for root exudation (Rovira, 1973; Sauer et al., 2006).

Active Microbial Communities Close to Root Cells

Microbes surrounding or residing at the rhizoplane were highly enriched in photosynthate-derived ^{13}C (**Figures 3B**, **7**, **8**), although lower than root cells. This observation supports our hypothesis that microorganisms surrounding roots incorporated plant-derived C. The lower ^{13}C enrichment observed for microorganisms, compared with root cells reflects a parallel consumption of native soil OC (natural abundance ^{13}C) by microorganisms in the rhizosphere (Kuzyakov and Blagodatskaya, 2015), resulting in the dilution of ^{13}C in bacteria cells. During this process, plant cell walls, which are structural plant components, remained highly ^{13}C enriched (Cotrufo et al., 2015; Vidal et al., 2016). Root-derived C taken up by soil microorganisms is either assimilated, released as metabolites, or respired (Six et al., 2006). Marx et al. (2007) showed in an incubation experiment with root exudates from labeled wheat and maize plants, that more than 50% of the retrieved exudate C was respired as CO_2 by microorganisms. Thus, the lower ^{13}C enrichment observed for microbes may also have resulted from the release of the plant-derived ^{13}C in form of $^{13}CO_2$ and /or other metabolic products.

The transfer of C to microorganisms is highly dependent on the position of microorganisms in relation to root cells, forming a gradient of foraging on rhizodeposition. As expected, ^{13}C labeled microbes were located at a few micrometers from the root cells (**Figures 3B**, **7**). More distant microbes did not present any enrichment (**Figure 5**), which is in accordance with

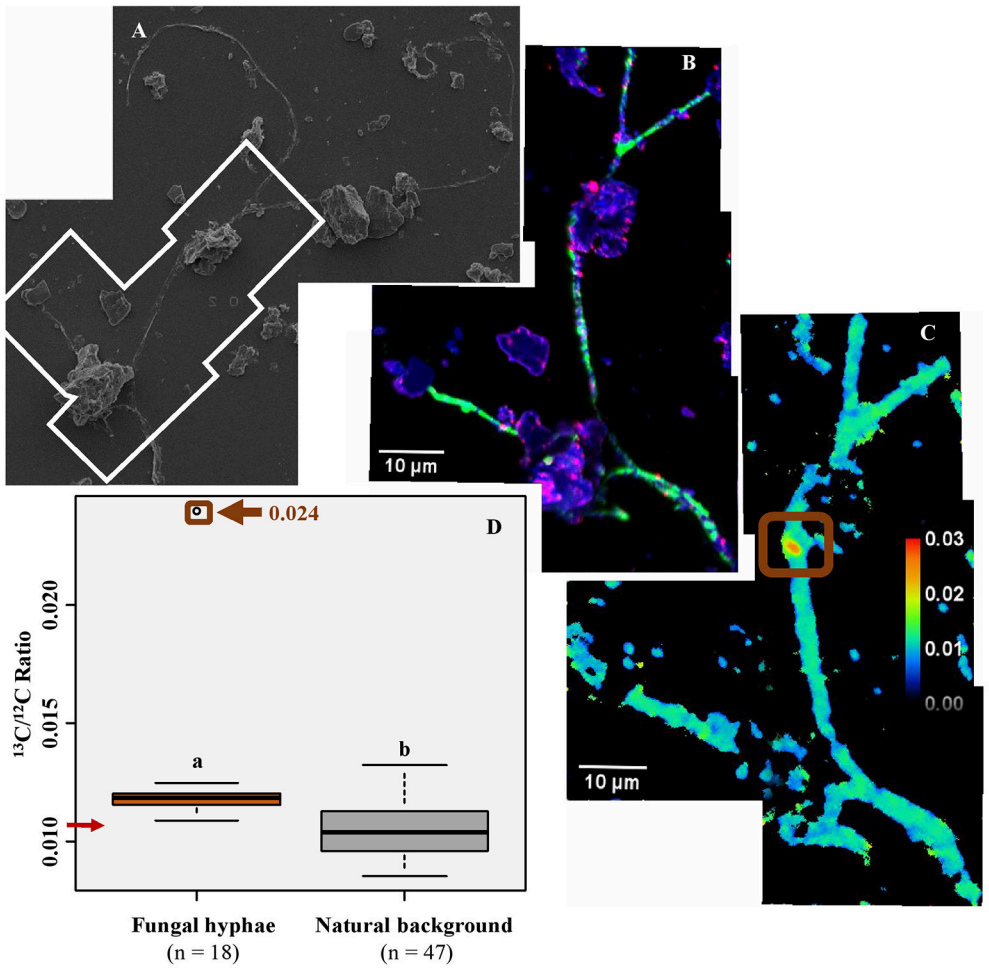

FIGURE 6 | Suspension of soil particles associated with the fungal hypha. The suspension was deposited on a silica wafer, observed with scanning electron microscopy **(A)** and NanoSIMS **(B,C)**; **(B)** Mosaic of NanoSIMS composite images; with $^{12}C^{14}N$ in green, ^{16}O in blue, $^{56}Fe^{16}O$ in red; The mosaic was created from 4 images (one image- 30 × 30 µm, 256 × 256 pixels, 22 planes, 1 ms.pixel^{-1}); **(C)** The ^{13}C:^{12}C ratio of the same area; the brown square indicates a ^{13}C enriched spot on the fungal hyphae. **(D)** The ^{13}C:^{12}C ratio for the fungal hypha–Regions of interest (ROIs) was obtained on $^{12}C^{14}N$ images, either by using the thresholding function (fungal hypha) or drawing ellipses (natural background); n indicates the number of ROIs drawn. The letters above boxes represent statistical results of Dunn test. The red arrow indicates the ^{13}C:^{12}C ratio corresponding to natural abundance. The brown square corresponds to the structure highlighted in **(C)**. Boxplots represent the third quartile, the median, the first quartile range of the data, and data outliers.

previous work on microbial communities in the rhizosphere of beech trees (Esperschütz et al., 2009). It has been reported that microbes of the rhizosphere are generally located within a dozen micrometers of the root surface, directly at the rhizoplane or at its close surrounding (Watt et al., 2006a). This distance parameter is directly related to the time of diffusion of a solute from roots to microorganisms (e.g., glucose diffusivity in soil: around 20 µm^2.s^{-1}) (Watt et al., 2006b).This indicates that the closer microbes are to root cells, the higher their chance to receive C-containing substrates.

Fungal Hyphae in the Rhizosphere

The extracted hypha presented a significantly higher ^{13}C:^{12}C ratio compared with the natural background. This illustrates the role of fungal hyphae as vectors for plant-derived OC into the bulk soil. However, the ^{13}C enrichment was lower compared with plant cell walls and bacteria cells, with the exception of a ^{13}C enriched spot (**Figure 6C**). The lower ^{13}C:^{12}C ratio might result from the ^{13}C dilution process, as described for bacteria cells. It has been shown that most of the plant C allocated to AM fungal hyphae is lost through respiration within 24 h (Johnson et al., 2002; De Deyn et al., 2011). Therefore, the fungal hypha might have been ^{13}C enriched in the past and the ^{13}C enriched signal was probably rapidly diluted by new, non-enriched C coming from the root (De Deyn et al., 2011). We assume that the highly enriched spot represents bacterial cells bound to the fungal hypha. Such strong association of bacterial cells to the hyphal surface was shown before (Artursson et al., 2006; Scheublin et al., 2010; Worrich et al., 2017). As the turnover rate of bacteria is generally considered to be higher compared to fungi (Rousk and Bååth, 2011), the bacteria or group of bacteria might have been transferred to the fungal hypha. It has been shown that bacteria

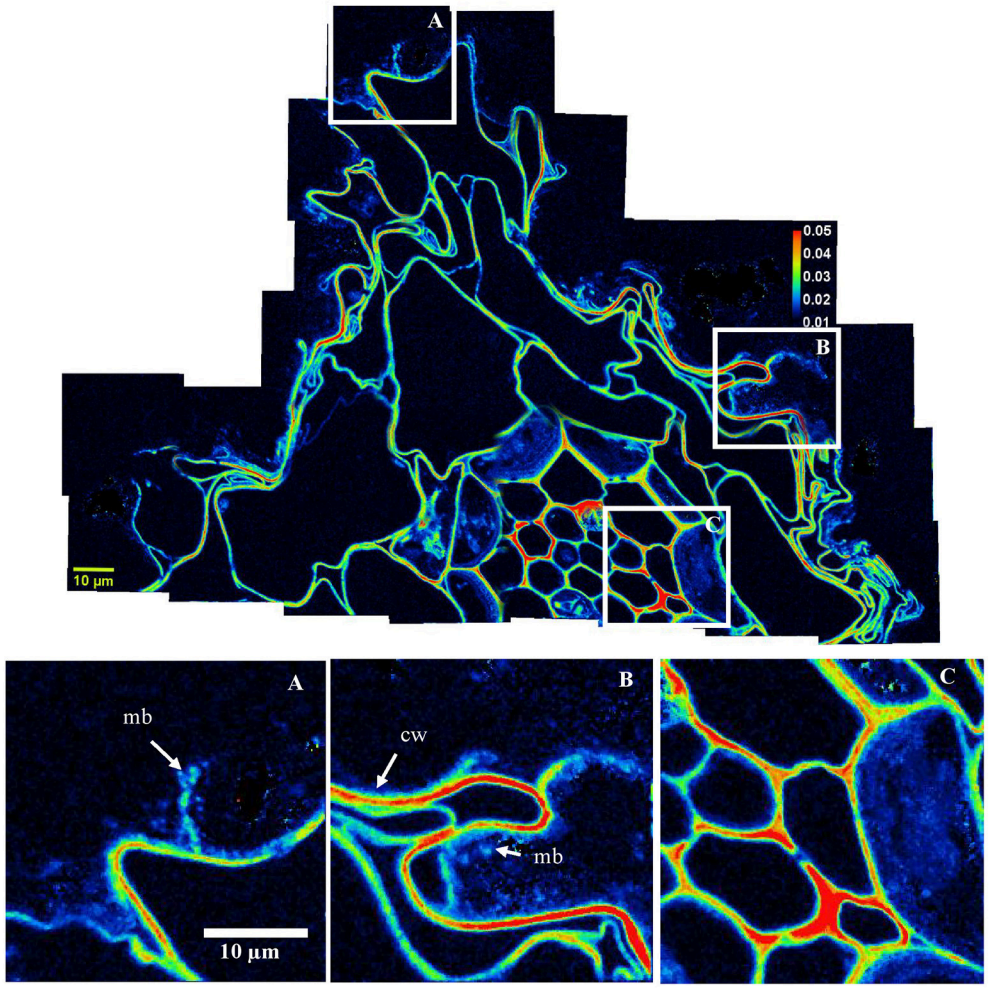

FIGURE 7 | Carbon transfers occurring in the rhizosphere–NanoSIMS images of ^{13}C:^{12}C ratio of areas highlighted in **Figure 2**. The scale ranges from natural abundance (0.011; dark blue) to highly enriched (0.050; red). The mosaic was created from 32 NanoSIMS images. Three areas (indicated with white scares on the mosaic) are represented below the mosaic for closer observation; **(A,B)**- highlight the transfer of carbon from roots toward the microbial community, intimately associated with the cortex root cells; cw, plant cell walls; mb, microbes. **(C)** Underlines the enrichment of stele cells.

are able to move on fungal hyphae thanks to the production of biofilms (Warmink et al., 2011), the so called "fungal highway."

The key role of fungal activity in soils is demonstrated by the presence of numerous microaggregates intimately associated with the hyphal surface (**Figure 6B**). We highlight the direct effect of fungal hyphae on the soil microstructure formation, a process which is still poorly understood (Rillig and Mummey, 2006; Lehmann et al., 2017). Mycorrhizal fungi strongly influence soil structure formation through biological (enhancing microbial activity), physical (exerting pressure on the mineral particles), and biochemical (excretion of hyphal products) processes (Chenu, 1989; Rillig and Mummey, 2006; Lehmann et al., 2017). Thus, the mycorrhizal fungal hyphae extend the rhizosphere volume into the root-free bulk soil, acting as a vector for plant-derived OC and fostering soil structure development in root-free bulk soil.

Binding Agents at the Root Surface

The observation of NanoSIMS and FIB-SEM images confirmed our expectations of intimate interactions between mineral particles, microorganisms, and root cells. The deformation of cortex root cells (**Figure 2**) was associated with the tangential orientation of mineral particles along these cells (**Figures 4A,D**). This illustrated the physical compression of soil occurring around roots during the root growth (Foster and Rovira, 1976; Jones et al., 2004). While growing, microorganisms can also exert a pressure on mineral particles at their surroundings, which participate to mediate mineral orientation around microbial aggregates (Foster and Rovira, 1976), as observed in the present study (**Figure 5C**). Thus, the root and microbial growth enhance the intimate association of OC with minerals, probably leading to an increased sorption of OC to mineral surfaces. There is evidence of the association between exudates and soil particles forming a rhizosheath, an

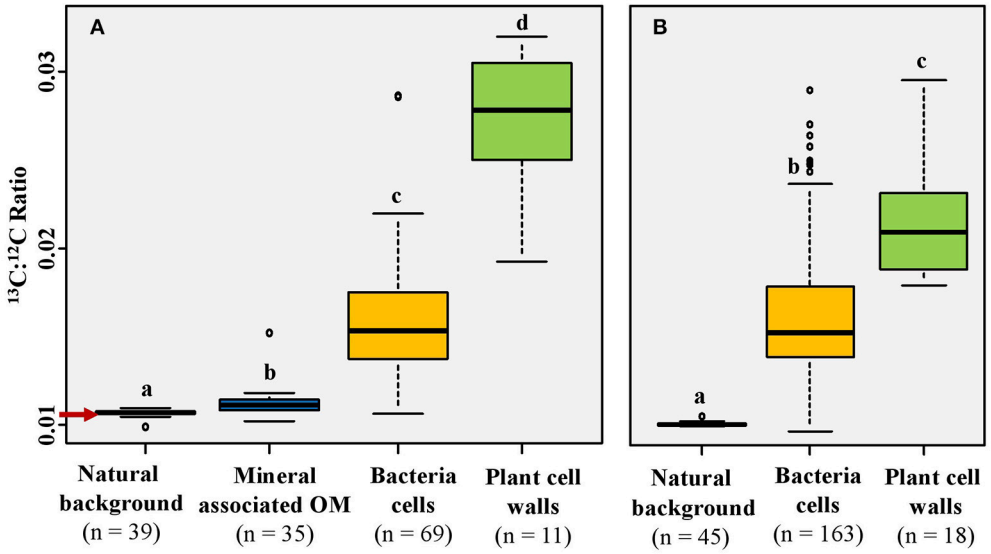

FIGURE 8 | The ^{13}C:^{12}C ratio distribution according to the type of organic matter. **(A)** ^{13}C:^{12}C values from areas indicated as white squares in **Figure 2**; **(B)** ^{13}C:^{12}C values from areas depicted in **Figure 3A**. Regions of interest (ROIs) were obtained on $^{12}C^{14}N$ images, either by using the thresholding function (mineral associated OM and bacteria cells), by drawing ellipses (natural background), or by freehand drawing (plant cell walls); n indicates the number of ROIs drawn. The letters above boxes represent statistical results of Dunn test. The red arrow indicates the ^{13}C:^{12}C ratio corresponding to natural abundance (0.011). Boxplots represent the third quartile, the median, the first quartile range of the data, and data outliers.

aggregated layer around the roots which remains physically stable (Ghezzehei and Albalasmeh, 2015). This process enhances the residence time of OC in the soil, which may contribute to OC sequestration (Rasse et al., 2005; Schmidt et al., 2011).

We assume that the amorphous $^{12}C^{14}N$ observed in between the mineral particles close to root cells (**Figure 3**) represents remnants of mucilage, a layer of highly bioavailable C surrounding root tips and acting as a binding agent for soil minerals at the root surface (Jones et al., 2009).This layer can also be seen in the FIB-SEM sections (**Figure 4**), highlighting microbial cells surrounded by a layer of presumably extracellular polymeric substances. Interestingly, most of the microbial cells were found within soil microaggregates, dominated by iron oxides (**Figure 2**). A counteracting process was proposed by Keiluweit et al. (2015) with a dissolution of iron (hydr)oxides and thus release and loss of mineral-associated OM due to the exudation of relatively high amounts of organic acids in artificial rhizospheres. In contrast, our data indicate the presence of iron (hydr)oxides, at natural exudate concentrations, under oxic soil conditions in the vicinity of roots. Oxidizing conditions in the rhizosphere can indeed contribute to the formation of an iron layer made of iron oxidation products, i.e., ferric hydroxide precipitates, at the root surface (Emerson et al., 1999; Kölbl et al., 2017). Ferrous ions, which represent the essential source for iron oxidation, were probably produced in anaerobic microsites created in the rhizosphere (Keiluweit et al., 2016). The large surface area and the high sorption capacity of iron (hydr)oxides, compared with larger particles such as quartz, facilitates the fixation and protection of microbes within microaggregates (Kögel-Knabner et al., 2008), thus creating a favorable environment for bacteria, which can be found in soil pores not bigger than 1 μm (Watt et al., 2006b), i.e., the typical size of a bacterium.

In the present study, iron oxides were identified as significant binding agents at the root-soil interface by (1) forming bridges between quartz grains and root cells (**Figure 2A**) and (2) being building constituents of organo-mineral microaggregates in the rhizosphere (**Figure 2**). The binding of organic matter to mineral surfaces, including oxides, has been reviewed in the literature (Kögel-Knabner et al., 2008) and more recently directly observed at the microscale (Xiao et al., 2015; Mueller et al., 2017). Iron oxides also represent an essential source of iron for plants and microorganisms in the rhizosphere. Specific mechanisms, such as acidification, reduction, and/or chelation increase iron dissolution and bioavailability in the rhizosphere (Robin et al., 2008). Thus, iron oxides were identified as key components of the rhizosphere, serving as binding agent as well as a potential source of iron for plants and microorganisms. Interestingly, quartz grains, normally described as minor agents for organo-mineral associations, showed patches of organic coatings at their surroundings (**Figures 2A–C**). Those patches had ^{13}C:^{12}C ratios close to natural abundance with a single spot slightly enriched in ^{13}C (**Figure 8**). Thus, most of the mineral associated OC is represented by native OC rather than derived from the labeled wheat root. This observation supports the idea that most of the C released by the plant is directly transferred to the living microbial community without being directly sorbed to the mineral phase (Kaiser et al., 2015). This indicates a lag phase between the release

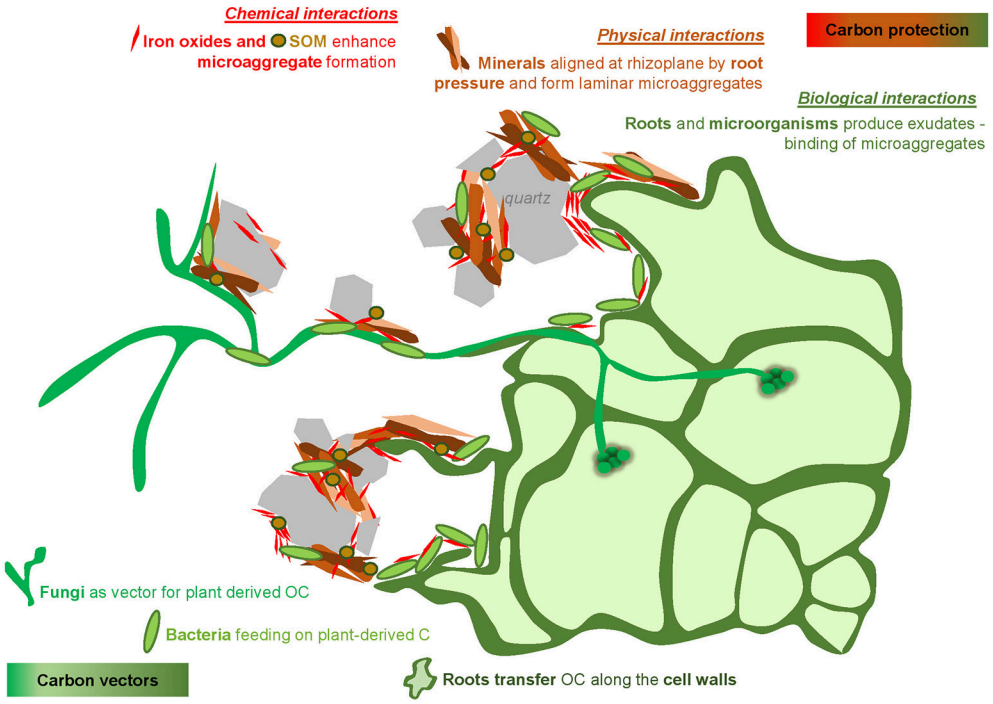

FIGURE 9 | Conceptual model illustrating the complex interplay between **vectors** (roots, fungi, bacteria) leading to a transfer of plant-derived OC into root-free soil and **stabilizing agents** (iron oxides, root and microorganism products) which protect plant-derived OC in the rhizosphere.

of OC by rhizodeposition and the allocation of microbial-derived OC into organo-mineral associated OC in the rhizosphere.

We confirmed that photosynthesis-derived OC was transferred to microorganisms located in the direct root vicinity. As expected, microorganisms, together with soil particles, especially iron oxides, formed microaggregates close to the root surface. We are proposing a conceptual model depicting the fate of carbon at biogeochemical interfaces in the rhizosphere at the forefront of the growing root (**Figure 9**). There is a complex interplay between stabilizing agents which protect plant-derived OC in the rhizosphere, and vectors leading to a transfer of plant-derived OC into root-free soil. Vectors of carbon are represented by (1) **roots**, transferring the carbon through their cell walls, (2) **fungi**, extending the root exploration space, and (3) **microorganisms**, including bacteria, feeding on plant-derived C at the root surface and participating to form a favorable environment for carbon protection in soil microstructures. These **microstructures** arise from the intimate association of organic substances (e.g., bacteria and their exudates, rhizodeposits) and mineral particles (e.g., quartz grains, clay particles, iron (hydr)oxides). **Iron (hydr)oxides** located around roots have a tremendous role in the rhizosphere by closely associating with microorganisms enclosed within microaggregates and by forming bridges with larger mineral particles. Thus, iron oxides can be assumed to have a stabilizing effect on the soil structure in natural rhizospheres. These processes, favoring the transfer and the potential protection of carbon in soil microstructures, are magnified by the physical pressure exerted by roots, enhancing the close contact of soil minerals and soil organic compartments.

AUTHOR CONTRIBUTIONS

AV collected and analyzed nanoSIMS data, wrote the manuscript, and insured the exchange between all co-authors. JH designed and performed field experimentation and wrote the paper, JH and SFB designed sampling procedures and processed samples, TI processed and analyzed samples, JM and AG supervised the field experiment from which the samples were collected. CH performed nanoSIMS analyses and gave technical support. SS conducted FIB-SEM analyses and output data. CM prepared the samples for nanoSIMS, supervised the analyses, and wrote the manuscript. All authors discussed the results and commented on the manuscript.

FUNDING

Funding by the Swiss National Science Foundation (SNSF), grant No. 406840-143060, as part of the National Research Program NRP68 "Soil as a Resource" is greatly acknowledged. SFB was funded with the latter program [grant no. 143097] and TI was funded by an International short visit grant of the SNSF [grant no. IZK0Z3_164397]. The work was also funded by the Deutsche Forschungsgemeinschaft (DFG), grant No.: MU3021-4/2, as part of the research unit "FOR1806: The Forgotten Part of Carbon Cycling: Organic Matter Storage and Turnover in Subsoils." We

also thank the DFG for funding the nanoSIMS instrument [KO 1035/38-1].

ACKNOWLEDGMENTS

We thank Barbara Orth and Swidran Kanapathipillai for support during field work. Johann Lugmeier is acknowledged for the assistance on the NanoSIMS analyses. We thank Andreas Pfeifer for giving us the access to the FIB-SEM at the ZEISS Microscopy Customer Center Europe in Oberkochen.

SUPPLEMENTARY MATERIAL

The Supplementary Material for this article can be found online at: https://www.frontiersin.org/articles/10.3389/fenvs.2018.00009/full#supplementary-material

REFERENCES

Abràmoff, M. D., Magalhães, P. J., and Ram, S. J. (2004). Image processing with imagej. *Biophoton. Int.* 11, 36–42. Available online at: https://dspace.library.uu.nl/handle/1874/204900

Alexander, F. E., and Jackson, R. M. (1954). Examination of soil micro-organisms in their natural environment. *Nature* 174, 750–751. doi: 10.1038/174750b0

Artursson, V., Finlay, R. D., Jansson, J. K., Artursson, V., Finlay, R. D., and Jansson, J. K. (2006). Interactions between arbuscular mycorrhizal fungi and bacteria and their potential for stimulating plant growth. *Environ. Microbiol.* 8, 1–10. doi: 10.1111/j.1462-2920.2005.00942.x

Baldock, J., and Skjemstad, J. (2000). Role of the soil matrix and minerals in protecting natural organic materials against biological attack. *Org. Geochem.* 31, 697–710. doi: 10.1016/S0146-6380(00)00049-8

Bardgett, R. D., Mommer, L., and De Vries, F. T. (2014). Going underground: root traits as drivers of ecosystem processes. *Trends Ecol. Evol.* 29, 692–699. doi: 10.1016/j.tree.2014.10.006

Bertin, C., Yang, X., and Weston, L. A. (2003). The role of root exudates and allelochemicals in the rhizosphere. *Plant Soil* 256, 67–83. doi: 10.1023/A:1026290508166

Bronick, C. J., and Lal, R. (2005). Soil structure and management: a review. *Geoderma* 124, 3–22. doi: 10.1016/j.geoderma.2004.03.005

Castorena, E. V. G., del Carmen Gutiérrez-Castorena, M., Vargas, T. G., Bontemps, L. C., Martínez, J. D., Méndez, E. S., et al. (2016). Micromapping of microbial hotspots and biofilms from different crops using digital image mosaics of soil thin sections. *Geoderma* 279, 11–21. doi: 10.1016/j.geoderma.2016.05.017

Chenu, C. (1989). Influence of a fungal polysaccharide, scleroglucan, on clay microstructures. *Soil Biol. Biochem.* 21, 299–305. doi: 10.1016/0038-0717(89)90108-9

Cotrufo, M. F., Soong, J. L., Horton, A. J., Campbell, E. E., Haddix, M. L., Partonet, W. J., al. (2015). Formation of soil organic matter via biochemical and physical pathways of litter mass loss. *Nat. Geosci.* 8, 776–779. doi: 10.1038/ngeo2520

De Deyn, G., Quirk, H., Oakley, S., Ostle, N., and Bardgett, R. D. (2011). Rapid transfer of photosynthetic carbon through the plant-soil system in differently managed species-rich grasslands. *Biogeosciences* 8, 1131–1139. doi: 10.5194/bg-8-1131-2011

Dickie, I. A., Martínez-García, L. B., Koele, N., Grelet, G.-A., Tylianakis, J. M., Peltzer, D. A., et al. (2013). Mycorrhizas and mycorrhizal fungal communities throughout ecosystem development. *Plant Soil* 367, 11–39. doi: 10.1007/s11104-013-1609-0

Emerson, D., Weiss, J. V., and Megonigal, J. P., Emerson, D., Weiss, J. V., and Megonigal, J. P. (1999). Iron-oxidizing bacteria are associated with ferric hydroxide precipitates (fe-plaque) on the roots of wetland plants. *Appl. Environ. Microbiol.* 65, 2758–2761.

Esperschütz, J., Buegger, F., Winkler, J. B., Munch, J. C., Schloter, M., and Gattinger, A. (2009). Microbial response to exudates in the rhizosphere of young beech trees (fagus sylvatica l.) after dormancy. *Soil Biol. Biochem.* 41, 1976–1985. doi: 10.1016/j.soilbio.2009.07.002

Farrar, J., Hawes, M., Jones, D., and Lindow, S. (2003). How roots control the flux of carbon to the rhizosphere. *Ecology* 84, 827–837. doi: 10.1890/0012-9658(2003)084[0827:HRCTFO]2.0.CO;2

Finzi, A. C., Abramoff, R. Z., Spiller, K. S., Brzostek, E. R., Darby, B. A., Kramer, M. A., et al. (2015). Rhizosphere processes are quantitatively important components of terrestrial carbon and nutrient cycles. *Glob. Chang. Biol.* 21, 2082–2094. doi: 10.1111/gcb.12816

Flisch, R., Sinaj, S., Charles, R., and Richner, W. (2009). Grundlagen für die düngung im acker- und futterbau. *Agrarforschung* 16, 6–31. Available online at: https://www.agrarforschungschweiz.ch/archiv_11de.php?id_artikel=1449

Foster, R., and Rovira, A. (1976). Ultrastructure of wheat rhizosphere. *New Phytol.* 76, 343–352. doi: 10.1111/j.1469-8137.1976.tb01469.x

Ghezzehei, T. A., and Albalasmeh, A. A. (2015). Spatial distribution of rhizodeposits provides built-in water potential gradient in the rhizosphere. *Ecol. Modell.* 298, 53–63. doi: 10.1016/j.ecolmodel.2014.10.028

Hallett, P. D., Karim, K. H., Glyn Bengough, A., and Otten, W. (2013). Biophysics of the vadose zone: from reality to model systems and back again. *Vadose Zone J.* 12:vzj2013.05.0090. doi: 10.2136/vzj2013.05.0090

Hinsinger, P., Bengough, A. G., Vetterlein, D., and Young, I. M. (2009). Rhizosphere: biophysics, biogeochemistry and ecological relevance. *Plant Soil* 321, 117–152. doi: 10.1007/s11104-008-9885-9

Jakobsen, I., and Rosendahl, L. (1990). Carbon flow into soil and external hyphae from roots of mycorrhizal cucumber plants. *New Phytol.* 115, 77–83. doi: 10.1111/j.1469-8137.1990.tb00924.x

Johnson, D., Leake, J. R., Ostle, N., Ineson, P., and Read, D. J. (2002). *In situ*$^{13}co_2$ pulse-labelling of upland grassland demonstrates a rapid pathway of carbon flux from arbuscular mycorrhizal mycelia to the soil. *New Phytol.* 153, 327–334. doi: 10.1046/j.0028-646X.2001.00316.x

Jones, D. L., Hodge, A., and Kuzyakov, Y. (2004). Plant and mycorrhizal regulation of rhizodeposition. *New Phytol.* 163, 459–480. doi: 10.1111/j.1469-8137.2004.01130.x

Jones, D. L., Nguyen, C., and Finlay, R. D. (2009). Carbon flow in the rhizosphere: carbon trading at the soil–root interface. *Plant Soil* 321, 5–33. doi: 10.1007/s11104-009-9925-0

Kaiser, C., Kilburn, M. R., Clode, P. L., Fuchslueger, L., Koranda, M., Cliff, J. B., et al. (2015). Exploring the transfer of recent plant photosynthates to soil microbes: mycorrhizal pathway vs direct root exudation. *New Phytol.* 205, 1537–1551. doi: 10.1111/nph.13138

Kallenbach, C. M., Frey, S. D., and Grandy, A. S. (2016). Direct evidence for microbial-derived soil organic matter formation and its ecophysiological controls. *Nat. Commun.* 7:13630. doi: 10.1038/ncomms13630

Keiluweit, M., Bougoure, J. J., Nico, P. S., Pett-Ridge, J., Weber, P. K., and Kleber, M. (2015). Mineral protection of soil carbon counteracted by root exudates. *Nat. Clim. Chang.* 5, 588–595. doi: 10.1038/nclimate2580

Keiluweit, M., Nico, P. S., Kleber, M., and Fendorf, S. (2016). Are oxygen limitations under recognized regulators of organic carbon turnover in upland soils? *Biogeochemistry* 127, 157–171. doi: 10.1007/s10533-015-0180-6

Kögel-Knabner, I., and Amelung, W. (2014). "12.7-Dynamics, chemistry, and preservation of organic matter in soils," in *Treatise on Geochemistry, 2nd Edn.*, eds K. Turekian and H. Holland (Oxford: Elsevier), 157–215. doi: 10.1016/B978-0-08-095975-7.01012-3

Kögel-Knabner, I., Guggenberger, G., Kleber, M., Kandeler, E., Kalbitz, K., Scheu, S., et al. (2008). Organo-mineral associations in temperate soils: integrating biology, mineralogy, and organic matter chemistry. *J. Plant Nutr. Soil Sci.* 171, 61–82. doi: 10.1002/jpln.200700048

Kölbl, A., Schweizer, S. A., Mueller, C. W., Höschen, C., Said-Pullicino, D., Romani, M., et al. (2017). Legacy of rice roots as encoded in distinctive microsites of oxides, silicates, and organic matter. *Soils* 1:2. doi: 10.3390/soils1010002

Kubiena, W. L. (1938). *Micropedology*. Ames, IA: Collegiate Press, Inc.

Kuzyakov, Y., and Blagodatskaya, E. (2015). Microbial hotspots and hot moments in soil: concept and review. *Soil Biol. Biochem.* 83, 184–199. doi: 10.1016/j.soilbio.2015.01.025

Kuzyakov, Y., and Domanski, G. (2000). Carbon input by plants into the soil. *Rev. J. Plant Nutr. Soil Sci.* 163, 421–431. doi: 10.1002/1522-2624(200008)163:4<421::AID-JPLN421>3.0.CO;2-R

Kuzyakov, Y., and Larionova, A. A. (2005). Root and rhizomicrobial respiration: a review of approaches to estimate respiration by autotrophic and

heterotrophic organisms in soil. *J. Plant Nutr. Soil Sci.* 168, 503–520. doi: 10.1002/jpln.200421703

Lal, R. (2004). Soil carbon sequestration impacts on global climate change and food security. *Science* 304, 1623–1627. doi: 10.1126/science.1097396

Lange, M., Eisenhauer, N., Sierra, C. A., Bessler, H., Engels, C., Griffiths, R. I., et al. (2015). Plant diversity increases soil microbial activity and soil carbon storage. *Nat. Commun.* 6:6707. doi: 10.1038/ncomms7707

Lehmann, A., Zheng, W., and Rillig, M. C. (2017). Soil biota contributions to soil aggregation. *Nat. Ecol. Evol.* 1, 1828–1835. doi: 10.1038/s41559-017-0344-y

Lehmann, J. (2007). A handful of carbon. *Nature* 447, 143–144. doi: 10.1038/447143a

Li, Y., Dick, W. A., and Tuovinen, O. H. (2003). Evaluation of fluorochromes for imaging bacteria in soil. *Soil Biol. Biochem.* 35, 737–744. doi: 10.1016/S0038-0717(02)00196-7

Liang, C., and Balser, T. C. (2011). Microbial production of recalcitrant organic matter in global soils: implications for productivity and climate policy. *Nat. Rev. Microbiol.* 9, 75–75. doi: 10.1038/nrmicro2386-c1

Martin, J., and Foster, R. (1985). A model system for studying the biochemistry and biology of the root-soil interface. *Soil Biol. Biochem.* 17, 261–269. doi: 10.1016/0038-0717(85)90058-6

Marx, M., Buegger, F., Gattinger, A., Zsolnay, Á., and Munch, J. C. (2007). Determination of the fate of 13c labelled maize and wheat exudates in an agricultural soil during a short-term incubation. *Eur. J. Soil Sci.* 58, 1175–1185. doi: 10.1111/j.1365-2389.2007.00911.x

Mayer, J., Gunst, L., Mäder, P., Samson, M.-F. Carcea, M., Narducci, V., et al. (2015). Productivity, quality and sustainability of winter wheat under long-term conventional and organic management in switzerland. *Eur. J. Agron.* 65, 27–39. doi: 10.1016/j.eja.2015.01.002

McCully, M., and Canny, M. (1985). Localisation of translocated 14c in roots and root exudates of field-grown maize. *Physiol. Plant.* 65, 380–392. doi: 10.1111/j.1399-3054.1985.tb08661.x

Morris, J. K. (1965). A formaldehyde glutaraldehyde fixative of high osmolality for use in electron microscopy. *J. Cell Biol.* 27, 137.

Mueller, C. W., Hoeschen, C., Steffens, M., et al. (2017). Microscale soil structures foster organic matter stabilization in permafrost soils. *Geoderma* 293, 44–53. doi: 10.1016/j.geoderma.2017.01.028

Mueller, C. W., Kölbl, A., Hoeschen, C., Hillion, F., Heister, K., Herrmann, A. M., et al. (2012). Submicron scale imaging of soil organic matter dynamics using nanosims - from single particles to intact aggregates. *Org. Geochem.* 42, 1476–1488. doi: 10.1016/j.orggeochem.2011.06.003

Nunan, N., Ritz, K., Crabb, D., Harris, K., Wu, K., Crawford, J. W., et al. (2001). Quantification of the *in situ* distribution of soil bacteria by large-scale imaging of thin sections of undisturbed soil FEMS Microbiology. *Ecology* 37, 67–77. doi: 10.1111/j.1574-6941.2001.tb00854.x

Oburger, E., and Schmidt, H. (2016). New methods to unravel rhizosphere processes. *Trends Plant Sci.* 21, 243–255. doi: 10.1016/j.tplants.2015.12.005

Pett-Ridge, J., and Firestone, M. K. (2017). Using stable isotopes to explore root-microbe-mineral interactions in soil. *Rhizosphere* 3(Pt 2), 244–253. doi: 10.1016/j.rhisph.2017.04.016

Philippot, L., Raaijmakers, J. M., Lemanceau, P., and van der Putten, W. H. (2013). Going back to the roots: the microbial ecology of the rhizosphere. *Nat. Rev. Microb.* 11, 789–799. doi: 10.1038/nrmicro3109

Polerecky, L., Adam, B., Milucka, J., Musat, N., Vagner, T., and Kuypers, M. M. (2012). Look@nanosims–a tool for the analysis of nanosims data in environmental microbiology. *Environ. Microbiol.* 14, 1009–1023. doi: 10.1111/j.1462-2920.2011.02681.x

Ranjard, L., and Richaume, A. (2001). Quantitative and qualitative microscale distribution of bacteria in soil. *Res. Microbiol.* 152, 707–716. doi: 10.1016/S0923-2508(01)01251-7

Rasse, D. P., Rumpel, C., and Dignac, M.-F. (2005). Is soil carbon mostly root carbon? Mechanisms for a specific stabilisation. *Plant Soil* 269, 341–356. doi: 10.1007/s11104-004-0907-y

R Core Team (2017). *R: A Language and Environment for Statistical Computing*. Vienna: R Foundation for Statistical Computing. Available online at: www.R-project.org

Rillig, M. C., and Mummey, D. L. (2006). Mycorrhizas and soil structure. *New Phytol.* 171, 41–53. doi: 10.1111/j.1469-8137.2006.01750.x

Robin, A., Vansuyt, G., Hinsinger, P., Meyer, J. M., Briat, J. F., and Lemanceau, P. (2008). Iron dynamics in the rhizosphere: consequences for plant health and nutrition. *Adv. Agron.* 99, 183–225. doi: 10.1016/S0065-2113(08)00404-5

Rousk, J., and Bååth, E. (2011). Growth of saprotrophic fungi and bacteria in soil. *FEMS Microbiol. Ecol.* 78, 17–30. doi: 10.1111/j.1574-6941.2011.01106.x

Rovira, A. D. (1973). Zones of exudation along plant roots and spatial distribution of micro-organisms in the rhizosphere. *Pest Manag. Sci.* 4, 361–366. doi: 10.1002/ps.2780040313

Sauer, D., Kuzyakov, Y., and Stahr, K. (2006). Short communication spatial distribution of root exudates of five plant species as assessed by 14c labeling. *J. Plant Nutr. Soil Sci.* 169, 360–362. doi: 10.1002/jpln.200621974

Scheublin, T. R., Sanders, I. R., Keel, C., van der Meer, J. R., and Scheublin, T. R. (2010). Characterisation of microbial communities colonising the hyphal surfaces of arbuscular mycorrhizal fungi. *ISME J.* 4, 752–763. doi: 10.1038/ismej.2010.5

Schmidt, M. W., Torn, M. S., Abiven, S., Dittmar, T., Guggenberger, G., Janssens, I. A., et al. (2011). Persistence of soil organic matter as an ecosystem property. *Nature* 478, 49–56. doi: 10.1038/nature10386

Six, J., Frey, S., Thiet, R., and Batten, K. M. (2006). Bacterial and fungal contributions to carbon sequestration in agroecosystems. *Soil Sci. Soc. Am. J.* 70, 555–569. doi: 10.2136/sssaj2004.0347

Thévenaz, P., and Unser, M. (2007). User-friendly semiautomated assembly of accurate image mosaics in microscopy. *Microsc. Res. Tech.* 70, 135–146. doi: 10.1002/jemt.20393

Van der Heijden, M. G., Klironomos, J. N., Ursic, M., Moutoglis, P., Streitwolf-Engel, R., Boller, T., et al. (1998). Mycorrhizal fungal diversity determines plant biodiversity, ecosystem variability and productivity. *Nature* 396, 69–72. doi: 10.1038/23932

Vidal, A., Remusat, L., Watteau, F., Derenne, S., and Quenea, K. (2016). Incorporation of 13c labelled shoot residues in lumbricus terrestris casts: a combination of transmission electron microscopy and nanoscale secondary ion mass spectrometry. *Soil Biol. Biochem.* 93, 8–16. doi: 10.1016/j.soilbio.2015.10.018

Wagg, C., Jansa, J., Stadler, M., Schmid, B., and van der Heijden, M. G. (2011). Mycorrhizal fungal identity and diversity relaxes plant-plant competition. *Ecology* 92, 1303–1313. doi: 10.1890/10-1915.1

Warmink, J. A., Nazir, R., Corten, B., and van Elsas, J. D. (2011). Hitchhikers on the fungal highway: the helper effect for bacterial migration via fungal hyphae. *Soil Biol. Biochem.* 43, 760–765. doi: 10.1016/j.soilbio.2010.12.009

Watt, M., Hugenholtz, P., White, R., and Vinall, K. (2006a). Numbers and locations of native bacteria on field-grown wheat roots quantified by fluorescence *in situ* hybridization (fish). *Environ. Microbiol.* 8, 871–884. doi: 10.1111/j.1462-2920.2005.00973.x

Watt, M., Silk, W. K., and Passioura, J. B. (2006b). Rates of root and organism growth, soil conditions, and temporal and spatial development of the rhizosphere. *Ann. Bot.* 97, 839–855. doi: 10.1093/aob/mcl028

White, P. J., George, T. S., Gregory, P. J., Bengough, A. G., Hallett, P. D., and McKenzie, B. M. (2013). Matching roots to their environment. *Ann. Bot.* 112, 207–222. doi: 10.1093/aob/mct123

Worrich, A., Stryhanyuk, H., Musat, N., König, S., Banitz, T., Centler, F., et al. (2017). Mycelium-mediated transfer of water and nutrients stimulates bacterial activity in dry and oligotrophic environments. *Nat. Commun.* 8:15472. doi: 10.1038/ncomms15472

Xiao, J., Wen, Y., Li, H., Hao, J., Shen, Q., Ran, W., et al. (2015). *In situ* visualisation and characterisation of the capacity of highly reactive minerals to preserve soil organic matter (som) in colloids at submicron scale. *Chemosphere* 138, 225–232. doi: 10.1016/j.chemosphere.2015.05.089

Zadoks, J. C., Chang, T. T., and Konzak, C. F. (1974). A decimal code for the growth stages of cereals. *Weed Res.* 14, 415–421. doi: 10.1111/j.1365-3180.1974.tb01084.x

Conflict of Interest Statement: There are no personal, professional or financial relationships that could potentially be construed as a conflict of interest in the present study.

frontiers in Microbiology

ORIGINAL RESEARCH
published: 26 February 2019
doi: 10.3389/fmicb.2019.00168

Rapid Transfer of Plant Photosynthates to Soil Bacteria via Ectomycorrhizal Hyphae and Its Interaction With Nitrogen Availability

Stefan Gorka[1], Marlies Dietrich[1], Werner Mayerhofer[1], Raphael Gabriel[1†], Julia Wiesenbauer[1], Victoria Martin[1], Qing Zheng[1], Bruna Imai[1], Judith Prommer[1], Marieluise Weidinger[2], Peter Schweiger[1], Stephanie A. Eichorst[1], Michael Wagner[1,3], Andreas Richter[1,3], Arno Schintlmeister[1,3], Dagmar Woebken[1] and Christina Kaiser[1]**

[1] Department of Microbiology and Ecosystem Science, Research Network "Chemistry meets Microbiology", University of Vienna, Vienna, Austria, [2] Core Facility Cell Imaging and Ultrastructure Research, University of Vienna, Vienna, Austria, [3] Large-Instrument Facility for Advanced Isotope Research, University of Vienna, Vienna, Austria

Plant roots release recent photosynthates into the rhizosphere, accelerating decomposition of organic matter by saprotrophic soil microbes ("rhizosphere priming effect") which consequently increases nutrient availability for plants. However, about 90% of all higher plant species are mycorrhizal, transferring a significant fraction of their photosynthates directly to their fungal partners. Whether mycorrhizal fungi pass on plant-derived carbon (C) to bacteria in root-distant soil areas, i.e., incite a "hyphosphere priming effect," is not known. Experimental evidence for C transfer from mycorrhizal hyphae to soil bacteria is limited, especially for ectomycorrhizal systems. As ectomycorrhizal fungi possess enzymatic capabilities to degrade organic matter themselves, it remains unclear whether they cooperate with soil bacteria by providing photosynthates, or compete for available nutrients. To investigate a possible C transfer from ectomycorrhizal hyphae to soil bacteria, and its response to changing nutrient availability, we planted young beech trees (*Fagus sylvatica*) into "split-root" boxes, dividing their root systems into two disconnected soil compartments. Each of these compartments was separated from a litter compartment by a mesh penetrable for fungal hyphae, but not for roots. Plants were exposed to a ^{13}C-CO_2-labeled atmosphere, while ^{15}N-labeled ammonium and amino acids were added to one side of the split-root system. We found a rapid transfer of recent photosynthates via ectomycorrhizal hyphae to bacteria in root-distant soil areas. Fungal and bacterial phospholipid fatty acid (PLFA) biomarkers were significantly enriched in hyphae-exclusive compartments 24 h after ^{13}C-CO_2-labeling. Isotope imaging with nanometer-scale secondary ion mass spectrometry (NanoSIMS) allowed for the first time *in situ* visualization of plant-derived C and N taken up by an extraradical fungal hypha, and in microbial cells thriving on hyphal surfaces. When N was added to the litter compartments, bacterial biomass, and the amount of incorporated ^{13}C strongly declined. Interestingly, this effect was also observed in adjacent soil compartments where added N was only available for

OPEN ACCESS

Edited by:
Tim Daniell,
James Hutton Institute,
United Kingdom

Reviewed by:
Rodica Pena,
University of Göttingen, Germany
Gary D. Bending,
University of Warwick,
United Kingdom
Katie Field,
University of Leeds, United Kingdom

***Correspondence:**
Christina Kaiser
christina.kaiser@univie.ac.at
Dagmar Woebken
woebken@microbial-ecology.net

†Present Address:
Raphael Gabriel,
Biological Systems and Engineering Division, Lawrence Berkeley National Laboratory, Berkeley, CA, United States

Specialty section:
This article was submitted to Terrestrial Microbiology, a section of the journal Frontiers in Microbiology

Received: *10 August 2018*
Accepted: *22 January 2019*
Published: *26 February 2019*

Citation:
Gorka S, Dietrich M, Mayerhofer W, Gabriel R, Wiesenbauer J, Martin V, Zheng Q, Imai B, Prommer J, Weidinger M, Schweiger P, Eichorst SA, Wagner M, Richter A, Schintlmeister A, Woebken D and Kaiser C (2019) Rapid Transfer of Plant Photosynthates to Soil Bacteria via Ectomycorrhizal Hyphae and Its Interaction With Nitrogen Availability. Front. Microbiol. 10:168. doi: 10.3389/fmicb.2019.00168

bacteria through hyphal transport, indicating that ectomycorrhizal fungi were acting on soil bacteria. Together, our results demonstrate that (i) ectomycorrhizal hyphae rapidly transfer plant-derived C to bacterial communities in root-distant areas, and (ii) this transfer promptly responds to changing soil nutrient conditions.

Keywords: ectomycorrhiza, hyphal carbon transfer, hyphosphere bacteria, mycorrhizosphere, hyphosphere priming, PLFAs, NanoSIMS

INTRODUCTION

Plants allocate considerable amounts of recently photoassimilated carbon (C) to their belowground biomass. A substantial fraction of this C is further transferred into the adjacent soil, either via direct root exudation (Walker et al., 2003; Dilkes et al., 2004; Bahn et al., 2009), or mycorrhizal fungi (Leake et al., 2001; Johnson et al., 2002; Simard et al., 2003). Root exudation is thought to trigger *rhizosphere priming*, that is, the acceleration of microbial soil organic matter (SOM) decomposition by increased availability of labile microbial substrates (Kuzyakov, 2002). The release of low-molecular-weight C compounds by plant roots increases the capability of otherwise energy-limited saprotrophic soil microbes to produce extracellular enzymes for degradation of high-molecular-weight organic compounds. This in turn results in increased availability of labile organic and inorganic nitrogen (N) and phosphorus (P) to both soil microbes and plants.

When plants are in mycorrhizal symbioses, however, a substantial proportion of plant photosynthates is allocated to mycorrhizal fungi (Hobbie, 2006; Smith and Read, 2008), which deliver nutrients in return. Mycorrhizal hyphae produce extensive extraradical mycelia (Agerer, 2001), which increase the plant's accessible soil volume substantially, making resources from distant soil regions available for plants. The two most prevalent mycorrhizal types, arbuscular mycorrhiza (AM) and ectomycorrhiza (ECM), differ fundamentally regarding their nutrient acquisition strategies (Chapman et al., 2005; Phillips et al., 2013). AM fungi have no or only limited capabilities to produce extracellular enzymes for degrading complex organic matter (Smith and Read, 2008), yet they have been shown to promote decomposition of organic material and utilize thereby released N (Hodge et al., 2001). Consequently, it has been suggested that AM fungi rely on associated saprotrophic microorganisms to gain access to nutrients bound in organic matter (Hodge et al., 2010; Jansa et al., 2013). Transfer of plant-derived C to bacteria via AM hyphae has been shown in a range of studies (Toljander et al., 2007; Drigo et al., 2010; Cheng et al., 2012; Kaiser et al., 2015; Paterson et al., 2016), indicating that *hyphosphere priming* with plant photosynthates by AM hyphae may be a relevant process for C cycling in AM-dominated ecosystems (Talbot et al., 2008).

In contrast to AM fungi, ECM fungi are known to produce a range of extracellular enzymes to degrade complex organic compounds (Read et al., 2004; Talbot et al., 2008). However, to what extent they possess saprotrophic capabilities (Bruns et al., 1998), and if the involved genes are expressed when the fungus is in a mycorrhizal symbiosis (Pellitier and Zak, 2017) is not fully understood. Specific ECM fungal lineages, depending on their enzymatic repertoire, may or may not depend on free-living saprotrophs for SOM nutrient liberation. Thus, while AM fungi are likely to cooperate with free-living soil saprotrophs by supplying them with plant-derived C, and receiving nutrients in return, the hyphospheric interactions of ECM fungi are much less clear.

Interactions between symbiotic partners have been suggested to be reciprocal as this ensures evolutionary stability (Noë and Hammerstein, 1995; Kiers and Van der Heijden, 2006). Hence, if mycorrhizal fungi rely on free-living saprotrophs for nutrient acquisition, their resource exchange would likely be reciprocal, where the amount of resource provided depends on the amount of resources received. In this sense, mycorrhizal fungal hyphae, which are able to explore the soil's pore space, may supply increased amounts of labile C to soil saprotrophs at spots with higher availability of nutrient-rich breakdown products or inorganic nutrients in order to further stimulate decomposition of a potential organic matter point source. Given that organic matter most likely exhibits a patchy distribution at the soil's microscale, this may be a viable strategy for nutrient exploration by adjusting the extent of C exudation to the amount of organic matter available at certain spots in the soil.

As a first step toward a better understanding of the interaction of ECM fungi and free-living soil saprotrophs and to elucidate whether hyphosphere priming is an integral process in ECM systems, it needs to be clarified (i) whether there is a transfer of recently photoassimilated plant C to soil bacteria via ECM hyphae, and (ii) whether this transfer is controlled by soil nutrient conditions.

To address these questions we investigated the short-term flow of plant-assimilated C and fungal-obtained soil N through an ECM system. For this purpose, we conducted a dual stable isotope labeling experiment with young beech (*Fagus sylvatica* L.) trees. Plants were grown in "split-root" pots consisting of two soil compartments, dividing the root system into two parts (Bever et al., 2009). Each of the soil compartments was connected to a root-inaccessible litter compartment, which was accessible by mycorrhizal hyphae only. Plant canopies were exposed to a ^{13}C-CO_2 labeled atmosphere for several hours ("pulse-chase experiment"). This setup allowed us to trace the flow of recently photoassimilated C from plants via ECM hyphae to soil bacteria using phospholipid fatty acid (PLFA) stable isotope probing as well as nano-scale secondary ion mass spectrometry (NanoSIMS) isotope imaging. Furthermore, we added a mixture of ^{15}N labeled ammonium and amino acids to one of the two litter

compartments to investigate the influence of N availability on the relationship between ECM hyphae and soil bacteria. We hypothesized that (i) ECM fungi transfer plant-derived C to associated hyphosphere bacteria and that (ii) a higher local availability of labile N compounds in soil increases hyphal exudation of plant C.

MATERIALS AND METHODS

Experimental Setup: Split-Root System With Hyphae-Exclusive Compartment

We collected 3- to 4-year-old beech (*Fagus sylvatica* L.) trees in a temperate beech forest site *ca.* 40 km south-west of Vienna, Austria (510 m above sea level) in July 2014. Additionally, we sampled soil (uppermost 5 cm, A horizon) and beech litter. The soil at this site is a dystric cambisol (over flysh) with a pH of 4.5–5.1 (Kaiser et al., 2010, 2011). Soil was sieved for homogenization (4 mm) and mixed with perlite (soil:perlite = 8:1, v/v) to enhance aeration, a method that has been shown to improve growing conditions for ECM fungi (Peter Schweiger, unpublished data). The litter was carefully homogenized by hand. Mycorrhization of the collected plants was confirmed by visual inspection under stereo microscopes.

Plants were potted in "split-root"-boxes (each 114 × 60 × 125 cm), which allowed to divide and subsequently manipulate the root system in separated soil compartments. In order to ensure an even distribution of roots in the two compartments, each plant was first freed of soil, and its root system was carefully investigated. If the plant had a dominant primary root, it was cut allowing the root system to be split evenly above the cut surface. If its primary root was bifurcating, the roots were pruned below the branch, thus creating root systems of comparable size. To compensate for the considerable loss of roots, the trees were trimmed below the first aboveground stem branch, resulting in leafless trees. We then transplanted the trees into the split-root boxes, carefully dividing the root system into the two compartments, which were filled with 750 ml of the aforementioned soil-perlite mixture, and the stems were stabilized by attaching a cylinder filled with sterile quartz sand (**Figure 1**). Each soil compartment was connected to another compartment (10 × 60 × 125 cm) filled with homogenized leaf litter (26 g compartment^{-1}). These "litter" compartments were separated from the respective soil compartments by a mesh (35 μm) which could be penetrated by fungal hyphae but acted as a barrier to plant roots (**Figure 1**). There was no connection between the two litter compartments. Plants were allowed to grow in the split-boxes for 12 months in a glasshouse under natural sunlight, temperature, and otherwise controlled conditions. The glasshouse was equipped with a movable ceiling, which remained open unless rain or strong winds were registered. Soil and litter compartments were watered regularly and equally on both sides of the boxes.

Dual Isotope Labeling Experiment

To trace plant N uptake via the mycorrhizal pathway, 12 ml of a ^{15}N-labeled solution of ammonium (98 atom% ^{15}N-NH_4Cl, Sigma Aldrich, Vienna, Austria; 54.5 mg/l, i.e., 1 mM N) and amino acids (Algal Amino Acid mixture, U-^{15}N 98 atom%, Cambridge Isotope Laboratories, Cambridge, UK; 140 mg/l, *ca.* 1 mM N based on an assumed average amino acid molar weight of 140 g/mol), dissolved in water, were added to one of the two litter compartments on average 48 h prior to sampling. This time period was selected based on preliminary tests. To ensure equivalent conditions, 12 ml of water was added to the other litter compartments. Diffusion between the soil and litter compartments was prevented by the structure of the mesh, which consisted of two membranes with an intermediate air-filled space. Elevating the "split-root" boxes on wooden blocks prevented water transfer between plant boxes.

Twenty-four hours after ^{15}N addition, aboveground plant parts were incubated in a ^{13}C-CO_2 enriched atmosphere (∼90 atom% ^{13}C; 1,500 ppm) for 6 h 20 min using a gas-tight acrylic glass incubation chamber (1,350 × 545 × 320 cm; **Figure S1**). The chamber is mounted on four vertically positioned acrylic glass plates (545 × 190 cm) so that pots can be placed beneath it. The top cover of the cuboid chamber can be lifted from the bottom plate. Lengthwise, the bottom plate consists of three separate parts, so that the outer parts can be removed by sliding them outwards. Opposite half-circle cutouts at the interface between middle and outer plates allow to fit in plant stems before closing the plates. Remaining gaps around the stems were sealed with Terostat® adhesive before the chamber was closed by mounting the top cover. Thus, plant canopies were exclusively exposed to chamber atmosphere, while soil and litter compartments were isolated from the incubation chamber. Additionally, any potential photosynthesis in the split-root boxes was inhibited by wrapping the boxes with black plastic bags (**Figure S1**).

^{13}C-CO_2-labeling took place under natural daylight conditions (cloudy, partly sunny) on 16th June 2015. Plants were arranged as described above, and the chamber was closed at noon. Inside chamber temperature stayed between 21 and 24°C in the course of the labeling procedure. Two small fans installed inside the chamber ensured a homogeneous atmosphere. Initial CO_2 concentrations were monitored using an infrared gas analyzer (EGM-4, PP systems, Hitchin, UK) connected to the chamber, showing that CO_2 was decreasing rapidly inside the chamber due to photosynthetic activity. Sixty milliliters of ^{13}C-CO_2 (99 atom%, Sigma-Aldrich, Vienna, Austria), corresponding to 255 ppm in the chamber volume, were injected with a gas-tight syringe via built-in septa every 30 min. This approach repeatedly replenished CO_2 withdrawn by plant photosynthesis, leading to a quick rise of ^{13}C enrichment of CO_2 in the chamber. Gas samples were drawn from the chamber at regular intervals starting 1.5 h after chamber closure, and later analyzed by a headspace gas sampler (GasBench II, Thermo Fisher Scientific, Bremen, Germany) interfaced to continuous-flow isotope ratio mass spectrometry (Delta Advantage V, Thermo Electron, Bremen, Germany) to determine total CO_2 concentration and ^{13}C enrichment in the chamber during the course of the experiment (85.5 ± 1.8 atom% ^{13}C (average ± SE), 875 to 3,300 ppm CO_2).

After the ^{13}C-CO_2-labeling, plants were kept overnight in the dark and harvested in a random sequence within a timeframe of

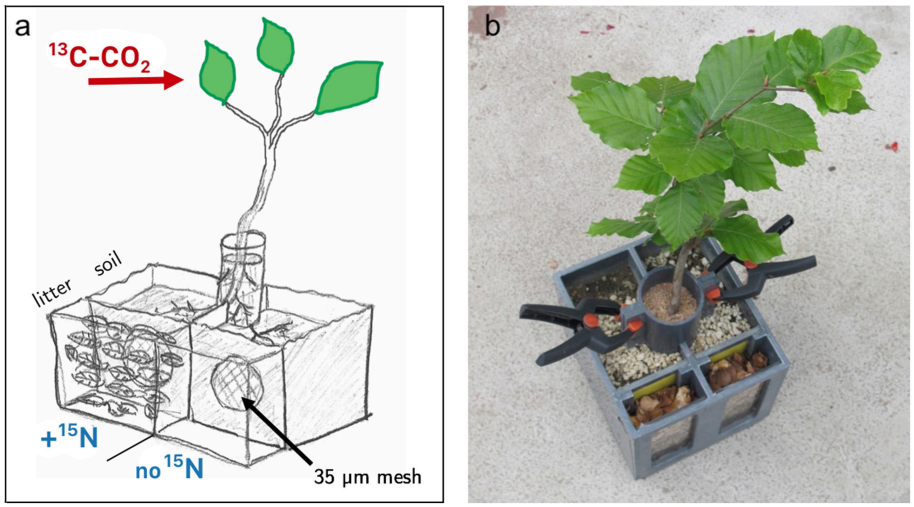

FIGURE 1 | Design of split–root boxes. Plants grew in two separated soil compartments where the root system was divided into two halves. Stems were stabilized in a cylinder filled with quartz sand. Each soil compartment was connected to a leaf litter compartment, separated by a mesh (35 µm) which is penetrable by fungal hyphae, but not by roots. Plant canopies were exclusively exposed to a ^{13}C-CO$_2$ enriched atmosphere. A mixture of ^{15}N-labeled ammonium and amino acids was added to only one litter compartment per box. **(a)** Schematic drawing of the setup. One of the two litter compartments is drawn without litter to illustrate the chamber design with the separating mesh. For the experiment both outer compartments were filled with beech litter. **(b)** Photo of a plant used in the labeling experiment.

10 h over the following day (i.e., 19–29 h after the start of the 6 h labeling period, referred to as *ca.* 24 h after labeling from now on). Here, we distinguished between leaves, stem, roots, rhizosphere soil, bulk soil (soil compartment), and litter (litter compartment). Bulk soil was defined as the soil remaining in the split-root boxes upon the removal of the plants, including soil which fell off the roots when shaking the plant gently. Consequently, rhizosphere soil was defined as the soil that remained attached to the roots after shaking, and was carefully removed by hand. Meshes were checked for intactness and root breakthrough.

Eight plants received ^{15}N- and ^{13}C-CO$_2$-treatments, four plants only the ^{13}C-CO$_2$-treatment, four plants were unlabeled controls, and four unlabeled boxes were kept without plants. One of the double-labeled plants had to be excluded from all analyses, because root-biomass on one side was extremely low ($n = 7$, **Table S1**). PLFA analysis was carried out on a subset of 6 replicates of the valid double-labeled plants ($n = 6$). Unlabeled controls plants served as a natural abundance control, and were used to calculate ^{13}C excess values. Plants that were only ^{13}C-labeled and unplanted boxes were used to rule out a systematic error in differences between the two litter compartments caused by other factors than N addition. Data from these samples are not explicitly shown. Unplanted boxes were also used as a control for assessing the mycorrhizal fungal community in litter compartments that originated from mycorrhizal fungi associated with plants in the planted boxes (see section *Mycorrhization and Identification of Fungal Communities via Sequencing of Internal Transcribed Spacer 1 (ITS1) Region*).

In order to assess the flow of photoassimilated ^{13}C through soil and hyphae-exclusive litter, we measured ^{13}C of dissolved organic carbon (DOC), microbial biomass, and PLFAs in the respective compartments. Unlabeled control plants served as natural abundance control. Comparison of the two split-root box sides of plants only labeled with ^{13}C-CO$_2$ ensured that equivalent conditions were present.

Mycorrhization and Identification of Fungal Communities Via Sequencing of Internal Transcribed Spacer 1 (ITS1) Region

Immediately after plant harvest, roots from each soil compartment were split into up to five parts (depending on the size of the root) which were analyzed under stereo microscopes for their degree of mycorrhization. Due to time-constraints during harvest (all plants needed to be processed within a few hours to ensure similar residence times of labeled C and N) mycorrhization (i.e., percentage of root tips colonized by ECM fungi) was roughly estimated based on visual screening of each of the root parts with the stereo microscope. The aim of this approach was not to get an accurate measure of mycorrhizal colonization, but a confirmation that roots of each plant were largely colonized (on average, estimations were at 85%). Roots were additionally scanned to allow documentation of their mycorrhizal status (for one example, see **Figure S2**).

Rhizosphere samples for downstream molecular analysis were sampled by cutting root pieces from the root after shaking off the bulk soil. Root pieces were transferred into 50 ml tubes containing 1x phosphate-buffered saline (pH = 8). After 30 min of shaking, the root was transferred into a fresh tube and the remaining slurry was centrifuged (4 min at 8,000 x g). The supernatant was discarded and the pellet (considered rhizosphere soil) was stored at −80°C until extraction. For sequencing of ITS1 regions, DNA was extracted from 400 mg of litter and rhizosphere soil samples using a phenol-chloroform protocol (Angel, 2012) and quantified using the Quant-iT™ PicoGreen® dsDNA Assay Kit (Thermo Fisher, Waltham, USA). The ITS1

region was amplified from these DNA samples via polymerase chain reaction (PCR) using multiplexed barcoded amplicon sequencing on the Illumina MiSeq platform (Illumina, San Diego, USA), as described by Herbold et al. (2015). The fungal ITS1 region was amplified in triplicate reactions using 30 cycles with primers ITS1F (5′ CTT GGT CAT TTA GAG GAA GTA A 3′, Gardes and Bruns, 1993) and ITS2 (5′ GCT GCG TTC TTC ATC GAT GC 3′, White et al., 1990, used as the reverse primer). Each 20 µl PCR reaction contained 13.95 µl nuclease free water, 2 µl 10x DreamTaq Green Buffer, 2 µl 2 mM dNTP mix, 0.125 µl BSA (0.1 µg μl^{-1}), 0.125 µl of 1.25U DreamTaq Green DNA Polymerase, 0.4 µl 0.2 µM of each primer, and 1 µl DNA template (*ca*. 10 ng per reaction). The following thermocycling conditions were utilized for the first step PCR: 94°C for 3 min, 94°C for 45 s, 52°C for 60 s, 72°C for 90 s, and a final step of 72°C for 10 min. The triplicate PCR products were pooled, assessed for the correct product size by gel electrophoresis visualized with GelRed Nucleic Acid Stain (Biotium Inc., Fremont, USA) and purified using the ZR-96 DNA Clean-up kitTM (Zymo Research, Irvine, USA). A second PCR reaction (additional 8 cycles) with the purified first step PCR product along with primers containing sample-specific barcodes was used for subsequent pooling prior to sequencing (Herbold et al., 2015). The second step PCR was carried out in 50 µl reactions containing 32.5 µl nuclease free water, 5 µl 10x DreamTaq Green Buffer, 5 µl 2 mM dNTP mix, 0.25 µl BSA (0.1 µg μl^{-1}), 0.25 µl of 1.25U DreamTaq Green DNA Polymerase, 4 µl of barcode (0.8 µM), and 3 µl of the purified first step PCR reaction. The correct product size was verified by gel electrophoresis as described above and purified using the ZR-96 Clean-Up Kit (Zymo Research). Final products were quantified by Quant-iT^{TM} PicoGreen® dsDNA Assay Kit and pooled equimolarly to 20 x 10^9 copies per sample library.

Sequencing was performed at Microsynth AG (Balgach, Switzerland). The TruSeq Nano DNA Library Prep Kit (Illumina, San Diego, USA; Protocol Illumina, FC-121-4003-excluding the fragmentation step) was used for the adaptor ligation. The MiSeq Reagent kit v3 (Illumina) was used with a run configuration of 2 x 300 cycle.

Paired MiSeq reads were split into sample datasets as described previously (Herbold et al., 2015). The paired-end raw fungal ITS1 MiSeq reads were extracted from raw amplicon data using ITSx (Bengtsson-Palme et al., 2013) and singletons were removed. Fungal OTUs were identified according to 99% sequence similarity threshold and the taxonomic classification was implemented by a Naïve Bayesian sequence classifier (Wang et al., 2007) using the Warcup training set version2 (Deshpande et al., 2016) at a confidence cutoff of 80%. Reads related to ECM fungi were identified based on literature (https://mycorrhizas.info/ecmf.html; Tedersoo and Smith, 2013). The sequence data were deposited in the NCBI Short Read Archive under study accession number PRJNA518765.

Tracing Plant-Derived Carbon and Hyphal-Assimilated Nitrogen in Bulk Pools

$^{13}C/^{12}C$ and $^{15}N/^{14}N$ isotopic ratios in bulk pools were measured with an elemental analyzer (EA 1110 elemental analyzer, CE Instruments, Milan, Italy) coupled to an isotope-ratio mass spectrometer (Finnigan MAT DeltaPlus, Thermo Finnigan, Bremen Germany).

^{13}C, Carbon and Nitrogen in Microbial Biomass and Dissolved Pools

To determine DOC, total dissolved N (TDN) and C and N in microbial biomass, 1.5 g of fresh soil and litter samples were extracted with 15 ml of 0.5 M K_2SO_4 before and after chloroform fumigation extraction (CFE; Brookes et al., 1985; Vance et al., 1987). Aliquots of the extracts were measured on a TOC/TN analyzer (TOC-V CPH/TMN-1, Shimadzu, Japan). Microbial biomass was calculated as the difference between fumigated and unfumigated samples. We did not include biomass conversion factors into our calculations. ^{13}C in DOC of fumigated and unfumigated samples was measured on a high performance liquid chromatography system (ICS-3000 Single Pump SP-1, Dionex, Sunnyvale, CA, USA) interfaced with an isotope ratio mass spectrometer (Finnigan Delta-V, Thermo Electron, Germany) through an LC-Isolink (Thermo Electron, Germany). We injected directly (i.e., without column) at a flow of 0.5 ml ultrapure water min^{-1} (Millipore, Vienna, Austria). ^{13}C in microbial biomass was calculated as the difference in atom% ^{13}C between fumigated and unfumigated samples. ^{13}C–enrichment was calculated as the difference in relative isotopic enrichment between labeled and unlabeled control samples as atom% excess ^{13}C (Kaiser et al., 2015).

Phospholipid Fatty Acids

Total lipids were extracted from soil and litter samples with a mixture of chloroform, methanol and citrate buffer (1:2:0.8, v/v/v; Bligh and Dyer, 1959). After fractionation on silica columns, collected phospholipids were derivatized to methyl esters via alkaline methanolysis (Frostegård et al., 1991) and dried under a constant stream of N_2. Dry fatty acid methyl esters (FAMEs) were re-dissolved in iso-octane and subsequently measured on a gas chromatograph (Trace GC Ultra, Thermo Scientific, Germany) coupled to a mass spectrometer (ISQ, Thermo Scientific, Germany) for PLFA identification, and on a Trace GC-Ultra (Thermo Fisher Scientific, Milan, Italy) coupled to a Delta V Advantage isotope ratio MS (Finnigan Delta-V, Thermo Fisher Scientific, Bremen, Germany) via a GC IsoLink (Thermo Fisher Scientific, Bremen, Germany) for quantification of the relative abundance and determination of isotopic $^{13}C/^{12}C$ ratios of PLFAs. Non-adecanoic acid (FAME 19:0) was added to samples prior to methylation and used as an internal standard for quantification. Bacterial and fungal fatty acid methyl esters (BAME CP mix, Supelco; 37 Component FAME mix, Supelco) were used as qualitative standards. ^{13}C enrichment was corrected for the isotope ratio of methanol-C added with methanolysis.

PLFAs were assigned to phylogenetic groups as reported by Ruess and Chamberlain (2010) unless noted otherwise. The PLFAs i15:0, a15:0, i16:0, i17:0, a17:0 were used as indicators for Gram-positive bacteria in general, 10Me17:0 (Zelles, 1999) for Actinobacteria specifically, 16:1ω5, 16:1ω7, cy17:0, and cy19:0 for Gram-negative bacteria, 17:0 (Hill et al., 2000; Koranda et al., 2011; Schnecker et al., 2012) and the sum of the above for bacteria

in general, cis18:1ω9, trans18:1ω9 and 18:2ω6,9 for fungi, and 16:0 and 18:0 for general PLFAs (Zelles, 1999; Leckie, 2005). The PLFA 16:1ω5 is also known to occur in AM fungi (Olsson, 1999). However, since *F. sylvatica* is not known to associate with AM fungi, 16:1ω5 represents most likely a biomarker for Gram-negative bacteria in this experiment (Phillips et al., 2002). The fungal PLFAs 18:1ω9 and 18:2ω6,9 were analyzed separately since they can vary considerably between fungal species (Zelles, 1997; Olsson, 1999).

We calculated isotopic enrichment in individual PLFAs as the difference in relative ^{13}C-enrichment of labeled samples to unlabeled controls as atom% excess ^{13}C (Kaiser et al., 2015). To calculate the relative ^{13}C content in respective microbial groups, relative ^{13}C-enrichment was weighted by the mean abundance (in μg C in PLFAs g^{-1} dry soil) of individual PLFAs.

Scanning Electron Microscopy and NanoSIMS

Scanning electron microscopy (SEM) was used to evaluate preparation strategies for optimum structural preservation of hyphae collected from the litter compartments, and to screen individual hyphal samples for their suitability for NanoSIMS measurements. SEM images, representing the signal intensity distribution of secondary electrons, were acquired with a SEM Jeol IT 300 (JEOL, Freising, Germany). Several combinations of different fixation and drying techniques were tested to find the optimum preparation procedure aimed at preserving the structure of the hyphae and sustaining attachment of associated microorganisms. In these tests, unfixed or chemically fixed (using formaldehyde or glutaraldehyde-osmiumtetroxide) hyphae were either air dried, dehydrated for critical point drying or treated with hexamethyldisilazane as a drying agent. These tests showed that air-drying yielded best results in preserving the structure of hyphae and the association of attached microorganisms. As air drying is also advantageous in terms of minimizing loss of diffusible compounds (transport forms of recent photosynthates and N in ECM hyphae are most likely sugars and amino acids; Martin and Botton, 1993; Taylor et al., 2004) compared to chemical fixation, we chose this preparation method for combined SEM and NanoSIMS analysis of fungal hyphae.

Hyphae were sampled and prepared for NanoSIMS analysis as follows: Litter compartments (from boxes exposed to stable-isotope labeled substrates as well as unlabeled control boxes) were screened for hyphae utilizing stereo microscopes. Per compartment, three to five hyphal bundles attached to leaves were collected with tweezers. Hyphal bundles were carefully and quickly dipped in H_2O_{MQ} to remove soil particles. One to two single hyphae were placed in fresh H_2O_{MQ} droplets spotted on Vectabond^{TM} (Vector Laboratories Inc., Burlingame, USA) reagent-coated, antimony-doped silicon wafer platelets (7.1 × 7.1 × 0.75 mm, Active Business Company, Brunnthal, Germany) and air-dried. Samples were sputter-coated with gold at 80 mA for 100 s using a High Resolution Fine Coater JFC-2300 HR (JEOL, Freising, Germany), yielding thin gold films of ∼20 to 40 nm thickness.

Fungal hyphae were critically screened by SEM to identify regions appropriate for NanoSIMS analysis. To measure the isotope content within the fungal hyphae (i.e., in the cell lumen), we screened for single, plane hyphae exhibiting a clean surface devoid of soil particles and microbial cells, located preferentially in the center of the silicon wafer platelets. For the NanoSIMS analysis of hypha-colonizing microorganisms, samples were screened by SEM for plane hyphal surfaces containing attached microorganisms. From 20 screened fungal hyphae, one was chosen representative for each sample type. Due to the labor-intensive nature of NanoSIMS analysis on these specific samples, we only had the chance to acquire data from one hypha per sample type. Consequently, we do not claim that these are representative measurements, but instead consider them as supporting data embracing spatial structure and thus providing topochemical information.

NanoSIMS measurements were performed on a NanoSIMS 50L (Cameca, Gennevilliers, France) at the Large-Instrument Facility for Advanced Isotope Research at the University of Vienna. In order to minimize degradation of the mass resolving power (MRP) due to topography, samples were mounted with a preferentially horizontal alignment of fungal hyphae inside the NanoSIMS analysis chamber. Prior to data acquisition, analysis areas were pre-sputtered utilizing a high-intensity, slightly defocused Cs^+ ion beam (100 pA beam current, ∼1 μm spot size). Data were acquired as multilayer image stacks by sequential scanning of a finely focused Cs^+ primary ion beam (*ca.* 80 nm probe size at 2 pA beam current) over areas between 40 × 40 and 52 × 52 μm^2 at 512 × 512 pixel image resolution and a primary ion beam dwell time of 15 to 20 msec/(pixel*cycle). For enhancement of the measurement efficiency, imaging of individual hyphae with horizontal alignment was performed under vertical confinement of the scanning area. $^{12}C^-$, $^{13}C^-$, $^{12}C^{12}C^-$, $^{12}C^{13}C^-$, $^{12}C^{14}N^-$, $^{12}C^{15}N^-$, $^{31}P^-$ secondary ions as well as secondary electrons were detected simultaneously.

Images based on NanoSIMS measurement data were generated using the Open MIMS plugin (Poczatek et al., 2009) in the FIJI package based on ImageJ (Schindelin et al., 2012). C isotope composition images displaying the $^{13}C/(^{12}C+^{13}C)$ isotope fraction, designated as atom% ^{13}C, were inferred from the C^- and C_2^- secondary ion signal intensity distribution images via per-pixel calculation of $^{13}C^-/(^{12}C^-+^{13}C^-)$ and $^{13}C^{12}C^-/(2\cdot{}^{12}C^{12}C^-+^{13}C^{12}C^-)$ intensity ratios. N isotope composition images displaying the $^{15}N/(^{14}N+^{15}N)$ isotope fraction, designated as atom% ^{15}N, were inferred from the $^{12}CN^-$ secondary ion signal intensity maps via per-pixel calculation of $^{12}C^{15}N^-/(^{12}C^{15}N^-+^{12}C^{14}N^-)$ intensity ratios. For visualization of relative phosphorus and nitrogen elemental distributions, C (i.e., matrix) associated secondary ion signals were utilized as reference signals. As such, relative phosphorus-to-carbon ratios, designated as $(P/C)_{rel.}$ given in arbitrary units [a.u.], were inferred from C^- normalized $^{31}P^-$ signal intensities via $^{31}P^-/(^{12}C^-+^{13}C^-)$. Correspondingly, relative nitrogen-to-carbon elemental ratios, designated as $(N/C)_{rel.}$ given in arbitrary units [a.u.], were obtained from C_2^- normalized CN^- signal intensities.

Overlay images, combining morphological with chemical information, were assembled using GIMP 2.10.4 (GNU Image Manipulation Program, https://www.gimp.org/). SEM (secondary electron) images where utilized for representation of the sample morphology prior to NanoSIMS analysis. For visualization of the sample morphology evolving during NanoSIMS imaging, C^- signal intensity distribution images were used.

Region of interest (ROI) specific numerical data evaluation was conducted using the WinImage software package (version 2.0.8) provided by Cameca. ROIs, referring to individual microbial cells (**Figure 7**), were manually defined based on the relative N/C and P/C elemental ratio maps (serving as indicators for biomass) and cross-checked by the morphological appearance in the C^- secondary ion intensity distribution and SEM images (**Figure S3**). Within the fungal lumen (**Figure 5**), ROIs were defined according to the isotope enrichment patterns since it was not possible to identify characteristic cellular features. This was likely because luminal regions were accessed via depth-profiling, which is less suited for visualization of cellular (ultra)structure than e.g., cross-sectional analysis of resin embedded samples. C and N isotope compositions were calculated from the accumulated intensities of $^{12}C^{12}C^-$ and $^{12}C^{13}C^-$ and $^{12}C^{14}N^-$ and $^{12}C^{15}N^-$ secondary ion signals detected within each ROI. The isotopic composition values summarized in the boxplot shown in **Figure 6** were determined by averaging over the individual images of the multilayer stack (ranging from 16 to 24 individual cycles). A more detailed description of the NanoSIMS measurement approach, including the concepts for data evaluation and visualization, is provided in the **Supplementary Methods**.

Statistical Analysis

R (version 3.4.3) was used for all statistical analyses (R Core Team, 2017), with the packages "ggplot2" for plotting (Wickham, 2009) and "vegan" for multivariate analysis (Oksanen et al., 2018). Means or medians were considered to be significantly different from each other when $p < 0.05$. Since data transformations did not result in normal distribution or homogeneity of variance in all samples, non-parametric tests were used in all statistical analyses. Labeled samples were compared to unlabeled controls with the Mann-Whitney *U*-test to validate significant ^{13}C-enrichment. Since N-treated and untreated plant box sides were under the influence of roots from the same plant for >1 year, they violated the independence assumption of many statistical tests; thus, plant box sides were compared with the Mann-Whitney *U*-test for paired samples. Pools were compared with the Kruskal-Wallis rank sum test optionally followed by Dunn's *post-hoc* test of multiple comparisons with Bonferroni correction.

ROI data extracted from NanoSIMS isotope composition images were tested for normal distribution using the Kolmogorov-Smirnov test and significance of enrichment in comparison to the natural abundance control was tested using the Welch *t*-test.

RESULTS

Evidence of Ectomycorrhizal Fungi Occurrence in Litter and Rhizosphere Compartments

ITS1 libraries of the litter (derived from 7 planted boxes and 4 unplanted boxes) and rhizosphere ($n = 7$) samples contained a total of 148,156 reads separated into 4,721 OTUs. These OTUs were comprised of Ascomycota and Basidiomycota spanning a variety of different orders, such as Dothideomycetes, Sordariomycetes, Leotiomycetes (Ascomycota) and Agaricomycetes, Tremellomycetes (Basidiomycota) among others. The Zygomycota were mainly represented by members of the order Mortierellales. Among the total fungal reads, members of the ECM fungi were detected in both, the rhizosphere and litter samples of planted boxes, at considerable proportions (19.87 ± 2.26% (average ± SE) and 9.04 ± 1.26%, respectively (**Figure 2**). Furthermore, 73% of the OTUs detected in the litter ECM fungal communities (excluding singletons) were detected in the rhizosphere ECM fungal communities. In contrast, the ECM fungi only comprised 0.8 ± 0.04% of the fungal communities in the litter samples of unplanted boxes. The average proportion of the orders in the ECM fungal communities are depicted in **Figure 2**. Members of the order Thelephorales were the dominating ECM fungi in our system, followed by Pezizales, Cantharellales, Agaricales, Russulales, Boletales, and Atheliales. Thelephorales constituted on average 87% of the ECM fungal communities in litter samples derived from planted boxes, compared to 44% in unplanted boxes and 75% in the rhizosphere. The proportion of Agaricales, Cantharellales and Pezizales in the ECM fungal community was highest in litter samples of unplanted boxes (up to 22%) compared to planted boxes, while the proportion of the Russulales and Boletales was highest in rhizosphere samples.

Bidirectional Transfer of Recently Photoassimilated C and N Taken Up by Ectomycorrhizal Hyphae

Our experimental setup allowed the simultaneous tracing of photoassimilated C and N available for fungal hyphae in an ECM symbiosis, demonstrating a rapid exchange of these resources between the symbiotic partners. Twenty-four hours after the start of the 6-h ^{13}C-CO_2 exposure a significant fraction (11.74%) of the ^{13}C photoassimilated by the plants had been transferred belowground into soil and litter pools (**Table 1**, **Figure 3A**). Moreover, a substantial fraction (3.0%) of the total ^{13}C allocated outside the plant roots was delivered to the root-inaccessible litter compartment. In addition, microbial biomass, based both on CFE (**Table 2**) and fungal and bacterial PLFA biomarkers, was significantly ^{13}C enriched in this compartment (**Figure 4**, **Table S2**), indicating a rapid hyphal transport. Interestingly, the two fungal-specific PLFAs 18:1ω9 and 18:2ω6,9 differed in their incorporation of ^{13}C between rhizosphere, bulk soil and litter pools: while isotopic enrichment of ^{13}C was similar for

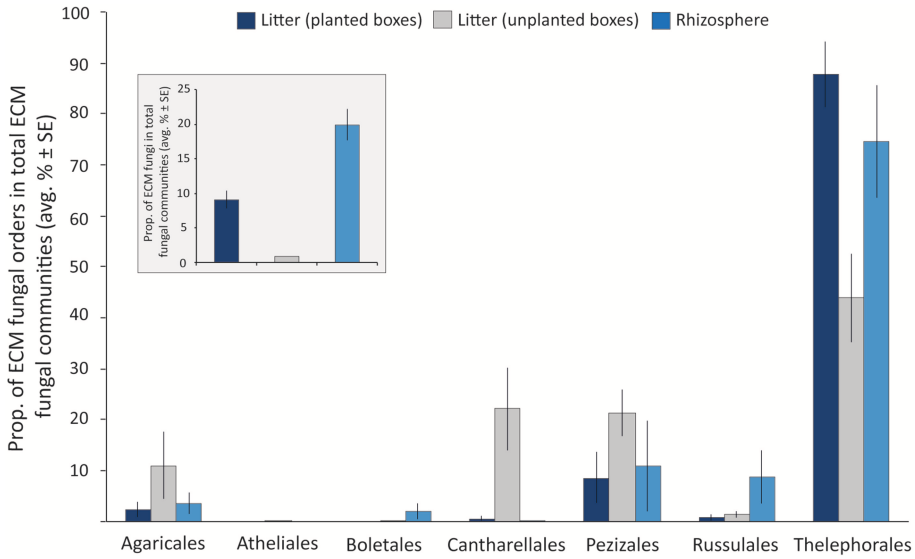

FIGURE 2 | Bar graph illustrating the proportion of ECM fungal orders in total ECM fungal communities in litter samples derived from planted (dark blue) and unplanted boxes (gray), as well as from the rhizosphere soil (light blue) as average proportion of the libraries ± standard error (SE). The insert graph depicts the proportion of ECM fungi in the total fungal communities (average proportion of the libraries ± SE).

TABLE 1 | Total C, ^{13}C, N, and ^{15}N per box (in absolute values), percent of total ^{13}C and ^{15}N showing allocation of recent photosynthates and N from the litter compartment in bulk pools, and C/N ratio of bulk pools.

Pool	C (g)	^{13}C excess (mg)	% ^{13}C of total ^{13}C	N (g)	^{15}N excess (μg)	% ^{15}N of total ^{15}N	C/N
Leaves	0.49 (0.05)	4.4 (0.64)	20.86 (2.74)	0.03 (0.00)	0.32 (0.14)	0.10 (0.05)	19.01 (0.49)
Stem	2.07 (0.19)	7.41 (0.48)	35.92 (2.21)	0.03 (0.00)	3.72 (1.73)	1.21 (0.58)	62.74 (4.09)
Roots	0.88 (0.14)	6.57 (0.74)	31.47 (3.04)	0.02 (0.00)	16.11 (4.66)	5.71 (1.99)	36.98 (1.37)
Plant biomass	3.44 (0.31)	18.37 (1.10)	88.26 (1.35)	0.08 (0.01)	20.15 (5.09)	7.02 (2.12)	-
Rhizosphere soil	6.70 (1.29)	0.96 (0.22)	4.35 (0.76)	0.53 (0.10)	13.22 (3.41)	4.25 (1.12)	12.46 (0.14)
Bulk soil	25.64 (1.88)	1.52 (0.34)	7.04 (1.25)	2.05 (0.16)	35.77 (13.48)	10.25 (3.07)	12.51 (0.06)
Litter	6.23 (0.15)	0.08 (0.03)	0.36 (0.13)	0.24 (0.00)	250.48 (18.46)	78.48 (3.56)	25.7 (0.39)
Soil + Litter	38.57 (1.72)	2.56 (0.43)	11.74 (1.35)	2.83 (0.13)	299.46 (26.07)	92.98 (2.12)	-
Total	42.01 (1.88)	20.93 (1.48)	100	2.91 (0.14)	319.62 (8.47)	100	-

^{13}C and ^{15}N values are in excess, i.e., the natural abundance control was subtracted. Standard errors are shown in brackets; n = 7.

18:1ω9, it decreased significantly from rhizosphere soil to litter for 18:2ω6,9.

Concurrently, 7% of the total added ^{15}N were transferred from the litter compartment to the plant within 48 h (**Table 1**). Significant ^{15}N enrichment was measured in stems and plant roots of the N-treated side, and a small but significant enrichment was found in roots of the untreated side (**Figure 3B**), which can be explained by plant-internal re-distribution of N. In contrast, ^{15}N enrichment of bulk and rhizosphere soil on the N-treated side was very low [δ^{15}N of 9.8 ± 2.4‰ and 17.7 ± 4.2‰, respectively (average ± SE)] compared to those of litter and roots (δ^{15}N of 540.9 ± 45.2‰ and 393.5 ± 165.7‰, respectively). This demonstrates the effectiveness of the double-layer mesh containing an air-filled space in the middle as a diffusion barrier, and indicates that N was mainly transferred directly via fungal hyphae from the litter to the roots. Soil of the N untreated side was not enriched in ^{15}N.

This symbiotic, bi-directional transport of recent photosynthates and added N was confirmed by NanoSIMS investigation of a fungal hypha retrieved from the litter compartment. The measurement was conducted at a depth below the hyphal surface, illustrating the incorporation of C and N isotopes inside the hypha (**Figure 5**, **Animation S1**). A carry-over of ^{13}C and ^{15}N atoms through the NanoSIMS measurement process (e.g., by atomic mixing) from surface-associated microbial cells can be ruled out, as overlay of the isotope composition images with the SEM image shows that regions of high isotopic enrichment within

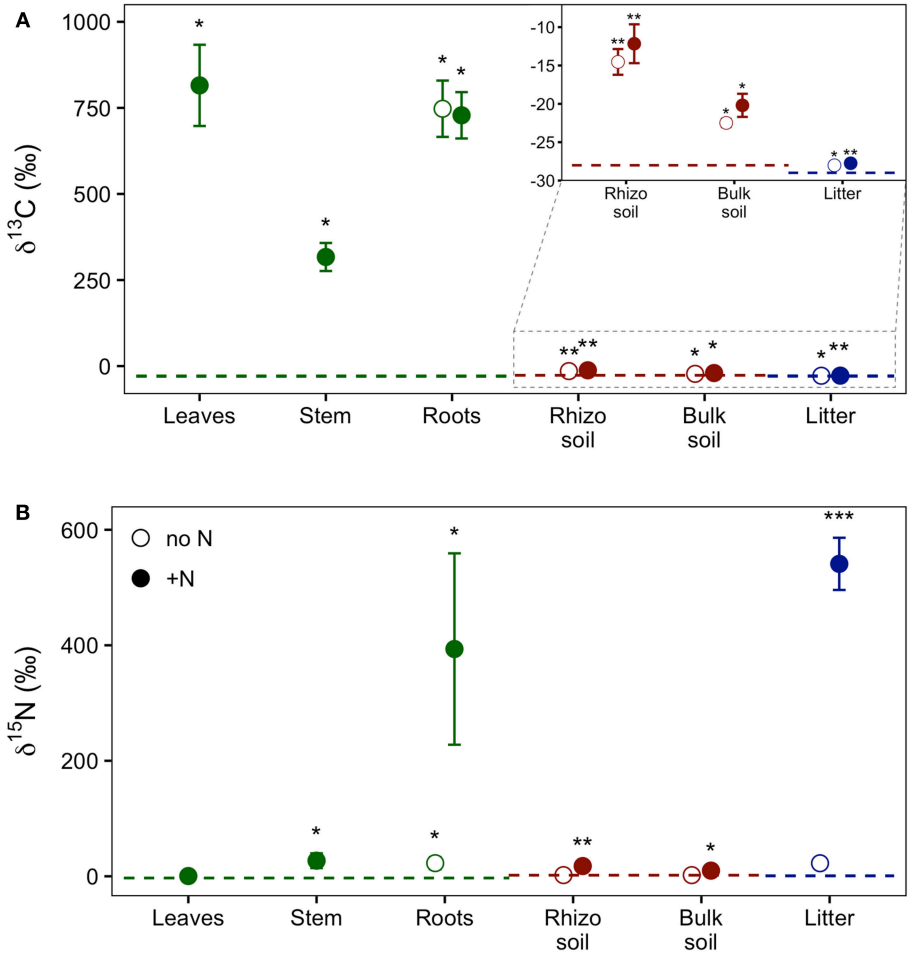

FIGURE 3 | Relative enrichment of **(A)** ^{13}C and **(B)** ^{15}N isotopes in plant, soil, and litter samples 24 h after ^{13}C-CO_2 labeling of plants and 48 h after addition of ^{15}N-labeled NH_4 and amino acids to litter compartments, indicating transfer of these supplies through the experimental system. Colors indicate the experimental system parts, i.e., plant (green), soil (red), and litter (blue). Dashed lines represent natural abundance values (mean of the respective system part). Symbols show results from dual-labeled (^{13}C and ^{15}N) plant boxes. Open circles, untreated side of the box; closed circles, N-treated side. This "side" designation refers only to roots, litter, and soil, as aboveground plant parts (i.e., leaves and stem) are connected to both sides. Error bars represent standard error. Asterisks indicate significant difference from natural abundance (*$p < 0.05$, **$p < 0.01$, ***$p < 0.001$; Mann-Whitney U-test; $n = 7$).

the lumen correspond to areas on the hyphal surface that were devoid of microbial cells (**Figure S4**). Region of interest (ROI) specific data evaluation of NanoSIMS images revealed that the fungal hypha was significantly enriched in both ^{13}C and ^{15}N ($p < 0.001$) compared to the natural abundance control. The isotopic signature of individual ROIs ranged from 1.5 to 2.6 atom% ^{13}C and from 0.46 to 0.56 atom% ^{15}N (**Figure 6**).

Transfer of Photoassimilated Carbon to Soil Microbes via Mycorrhizal Hyphae

Our results demonstrate a transfer of recently photoassimilated C to bacteria in both the rhizosphere and the hyphosphere. The sum of bacteria-specific PLFAs as well as specific bacterial groups (Gram-positive, Gram-negative, Actinobacteria) were significantly enriched in ^{13}C in the litter compartment and the rhizosphere soil compared to natural abundance controls (Mann-Whitney U-test, $p < 0.05$), which is illustrated by positive atom% excess values in **Figure 4**. In bulk soil, in contrast, only Gram-positive bacterial PLFAs were significantly enriched (**Figure 4**, **Table S2**). All individual PLFA biomarkers were significantly enriched in atom% ^{13}C in the litter compartment of the side that did not receive N (**Table S2**). We found no preferential ^{13}C transfer to specific bacterial groups, although the actinobacterial PLFA was slightly less enriched compared to other Gram-positive bacterial PLFAs, and Gram-negative bacterial PLFAs. All bacterial groups were similarly ^{13}C enriched in all pools (in atom% ^{13}C) except for Gram-positive bacteria which were more enriched in litter compared to bulk soil (**Figure 4**). Furthermore, dissolved organic carbon (DOC) was significantly enriched in ^{13}C in the litter compartment, in addition to bulk and rhizosphere soil (**Table 2**).

TABLE 2 | ^{13}C, C, and N in dissolved organic matter and microbial biomass. C_{mic}, N_{mic}, DOC, and TDN are means in μg g^{-1} dry weight, and $^{13}C_{mic}$ and ^{13}C in DOC are atom% excess.

Pool		C_{mic}	N_{mic}	DOC	TDN	$^{13}C_{mic}$	^{13}C in DOC	$(C/N)_{mic}$
Rhizosphere soil	no N	610.28 (15.95)	142.12 (4.69)	154.68 (6.27)	27.62 (3.16)	0.47* (0.05)	0.17* (0.06)	4.31 (0.10)
	+N	665.6 (24.63)	141.96 (5.94)	139.26 (3.79)	29.98 (7.4)	0.61* (0.06)	0.15* (0.06)	4.70 (0.12)
Bulk soil	no N	655.13 (30.75)	126.36 (6.05)	145.35 (25.47)	25.97 (3.3)	0.20* (0.02)	0.03* (0.01)	5.26 (0.34)
	+N	620.07 (18.81)	132.21 (7.75)	179.85 (11.92)	36.2 (7.86)	0.18* (0.04)	0.03* (0.01)	4.77 (0.24)
Litter	no N	1725.91 (137.64)	286.29 (33.68)	2867.67 (112.47)	811.58 (45.18)	0.10* (0.05)	0.01* (0.00)	6.22 (0.44)
	+N	1822.26 (206.47)	259.31 (39.96)	3004.41 (95.22)	857.49 (110.57)	0.09* (0.03)	0.01* (0.00)	7.53 (0.68)

C_{mic}, C in microbial biomass; $^{13}C_{mic}$, ^{13}C in microbial biomass; N_{mic}, N in microbial biomass; DOC, dissolved organic C; TDN, total dissolved N; $(C/N)_{mic}$, C/N ratio in microbial biomass. Standard error is shown in brackets. Asterisks indicate significant difference to control ($p < 0.05$) in atom% ^{13}C (comparison via Mann-Whitney U-test for equal medians; $n = 7$). No significant differences were detected between +N/noN compartments (comparison via Mann-Whitney U-test for equal medians; $n = 7$).

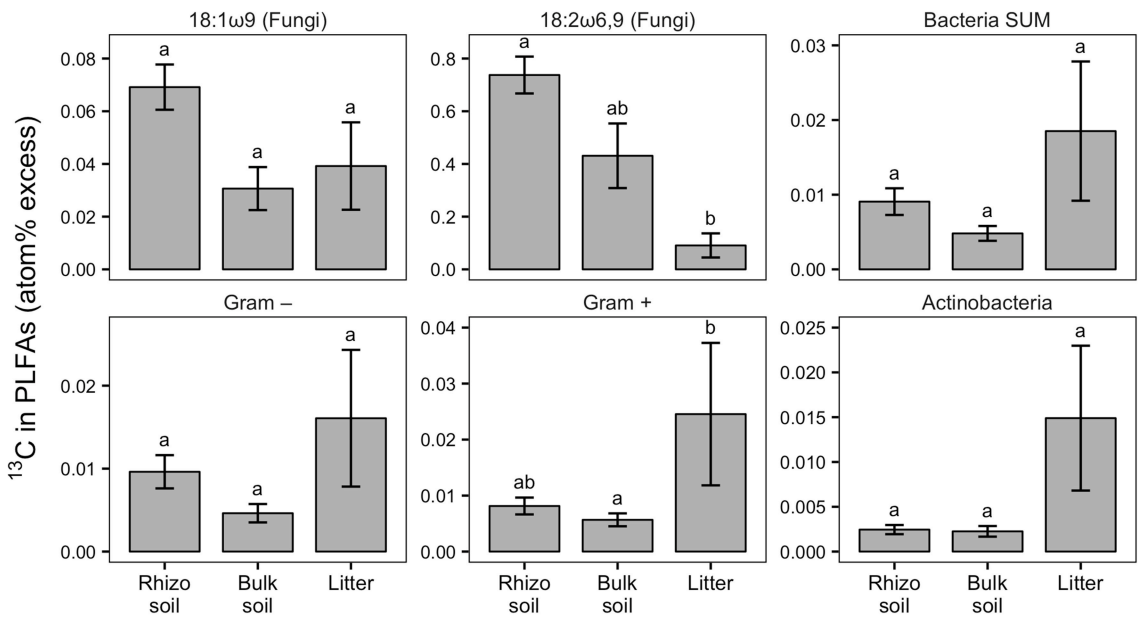

FIGURE 4 | Relative enrichment of ^{13}C in fungal-specific (18:1ω9 and 18:2ω6,9) and bacteria-specific PLFAs in rhizosphere, bulk soil, and litter pools shown as atom% excess ^{13}C (calculated by subtracting the natural abundance atom% value of the respective PLFA biomarkers). Bars show the weighted mean of each pool from N-treated and untreated sides from dual-labeled (^{13}C and ^{15}N) plant boxes. This format was chosen to emphasize general trends of relative ^{13}C enrichment in fungal and bacterial groups across the different pools irrespective of N addition. No significant differences in atom% excess ^{13}C could be detected between the N-treated and the untreated sides (+N/noN; Mann-Whitney *U*-test for paired samples). For visualization of differences between +N/noN box sides see **Figure S5**. Litter compartment enrichment indicates allocation of ^{13}C via ECM hyphae to root-distant bacteria. Error bars represent the standard error; $n = 6$. Differences in pools were analyzed with the Kruskal-Wallis rank sum test. Significant tests ($p < 0.05$) were followed by Dunn's *post-hoc* test of multiple comparisons with Bonferroni correction (adj. $p < 0.05$); significant differences are indicated by lowercase letters. All microbial groups were significantly enriched in ^{13}C in all pools, except for 18:2ω6,9, Gram-negative bacteria and Actinobacteria, each in bulk soil (comparison of atom% ^{13}C values via Mann-Whitney *U*-test, $p < 0.05$; not shown).

NanoSIMS imaging revealed a spatial pattern of ^{13}C and ^{15}N hotspots on the surface of the fungal hyphae collected from the litter compartment resembling the size and distribution of microbial cells. Chemical composition (such as the NanoSIMS-visualized relative contents of phosphor and nitrogen) and structural information (provided by SEM imaging and the NanoSIMS C$^-$ secondary signal intensity distribution) supported their identification as hyphosphere microbial cells (**Figure 7**, **Figure S3**). These microbial cells were significantly enriched in ^{13}C and ^{15}N ($p < 0.001$) compared to a natural abundance control, with ROI specific isotopic contents ranging from 1.2 to 1.4 atom% ^{13}C and from 0.40 to 0.47 atom% ^{15}N (**Figure 6**).

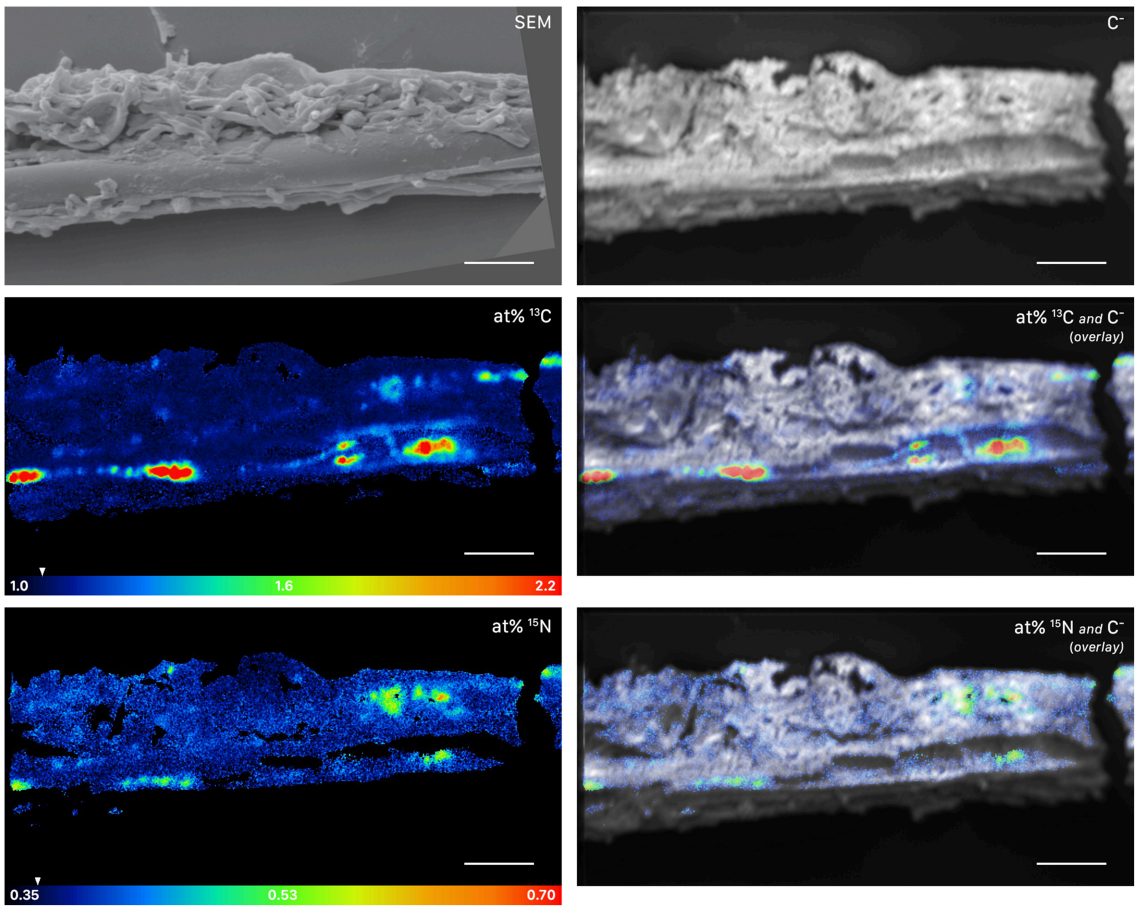

FIGURE 5 | NanoSIMS and SEM images of a root-distant fungal hypha extracted from a litter compartment of a dual-labeled plant box, depicting ^{13}C and ^{15}N labeled regions within the hypha. The SEM image shows the morphology of the sample prior to NanoSIMS measurement. NanoSIMS images were acquired at an erosion depth below the hyphal surface, visualizing the presence of isotopically enriched compounds inside the hypha. Isotopic label contents are displayed as atom%. The white arrows at the color-scales indicate the natural isotopic abundance values, determined on the unlabeled control (1.08 atom% ^{13}C and 0.37 atom% ^{15}N). The upper limit of the atom% ^{13}C scale is set to 2.2; however, maximum local values, extracted from individual cycles, range up to 3.6 atom% ^{13}C. Secondary ion signal intensity thresholds were set to 62 and 60 counts/(sec*pixel) for $^{12}C^{13}C^-$ and $^{12}C^{15}N^-$, respectively. SEM, scanning electron microscopy image (secondary electrons); C^-, accumulated $^{12}C^-$ and $^{13}C^-$ secondary ion signal intensity distribution images, indicating the morphology of the sample during NanoSIMS analysis; at% ^{13}C, carbon isotope composition image; at% ^{15}N, nitrogen isotope composition image. Overlay images are composites of the C^- and isotope images. NanoSIMS images consist of accumulated z-stacks obtained from 19 consecutive scans (displayed in **Animation S1**). Scale bars, 5 µm.

Effect of Nitrogen Addition on Soil Microbes and Belowground Carbon Flux

Microbial Reaction to Nitrogen Addition

PLFA analysis showed that several microbial groups significantly declined in response to N addition (**Figure 8**, **Table S3**). This effect of N was particularly pronounced in Actinobacteria and Gram-positive bacteria in general, but also Gram-negative bacteria and the fungal PLFA 18:1ω9 slightly declined. Surprisingly, the effect on Gram-positive bacteria was not restricted to the litter compartment to which N was added, but also occurred in the bulk soil and rhizosphere of the adjacent soil compartments (**Figure 8**). In line with this, correspondence analysis of PLFAs showed that microbial community composition differed not only between litter and soil, but also changed in response to N addition (**Figure 9**). Again, N addition resulted in a shift in community structure not only in the litter compartment to which N was added, but also in the adjacent soil compartment.

To rule out that this difference in microbial communities was caused by a systematic discrepancy between the compartments of the split-root boxes, we analyzed PLFAs in both litter compartments of plant boxes that did not receive N at all ($n = 4$, data not shown). We found no difference between box sides in these plant boxes, nor in boxes without plants, which also did not receive a N treatment ($n = 3$, data not shown).

In contrast to the PLFAs, microbial biomass C based on CFE was unaffected by N addition (**Table 2**).

Nitrogen Availability Affects Carbon Transfer to Soil Microbes

Based on PLFA analysis, N addition to the litter compartment significantly decreased ^{13}C transfer to Actinobacteria and other

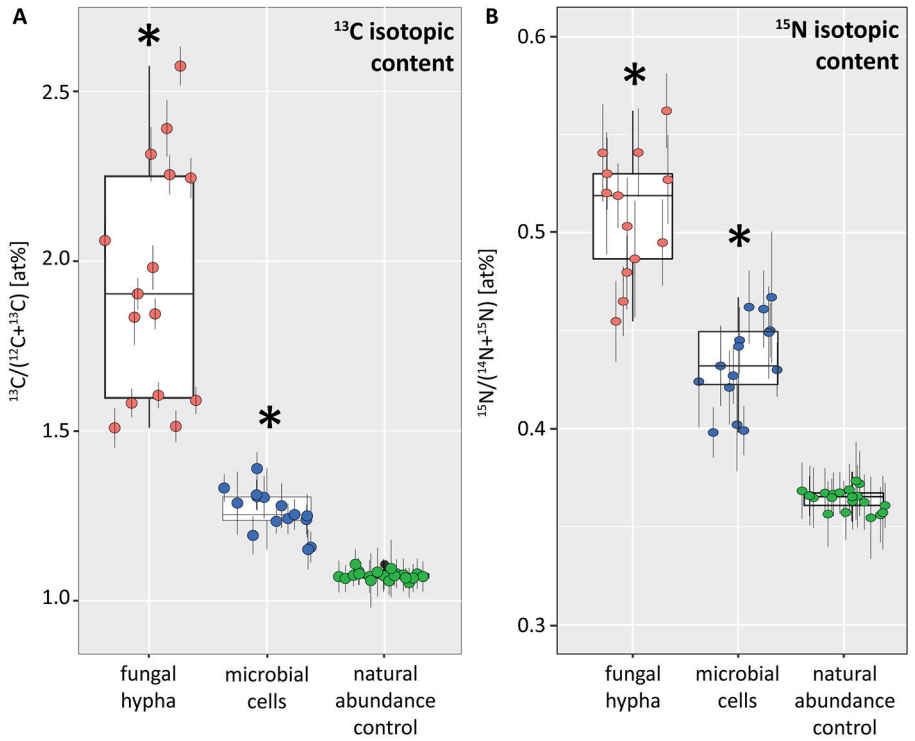

FIGURE 6 | Boxplots depicting the ^{13}C **(A)** and ^{15}N **(B)** isotopic content (in atom%) for a fungal hypha (displayed in **Figure 5**) and hyphosphere microorganisms (displayed in **Figure 7**) from dual-labeled plant-boxes, along with the values obtained from measurement on the natural abundance control. Each data point represents an individual region of interest (ROI) extracted from NanoSIMS images depicted in **Figures 5**, **7**, error bars refer to the estimated analytical uncertainty (1σ) due to counting statistics (see section Materials and Methods). Significant levels of isotopic enrichment ($p < 0.001$) are indicated with an asterisk (*). Data for the natural abundance control were obtained from microbial cells associated to the surface of a hypha extracted from a non-labeled control box. With respect to the values of the fungal hypha it should be noted that these refer to the averages over 19 consecutive scans. Owing to the observed variation of enrichment within the z-stack (see **Animation S1**), the displayed maxima rather represent conservative estimates.

Gram-positive bacteria, on a per g dry weight basis (**Figure 10**). This is caused by a reduction in biomass of the respective groups (**Figure 8**) combined with a constant or decreased relative enrichment of ^{13}C (**Figure S5**, **Table S2**). This indicates that, in addition to a loss of biomass, N treatment also affected the transfer of recent photosynthates to hyphosphere bacteria.

Relative isotopic enrichment (atom% excess ^{13}C) in PLFAs specific for bacteria and the fungal-specific PLFA 18:1ω9 tended to decrease (although not significantly) in litter after N addition (**Figure S5**). However, correspondence analysis shows no effect of N addition on relative ^{13}C enrichment (**Figure S6**). Moreover, we did not observe a significant effect of N addition on relative ^{13}C enrichment in microbial biomass based on CFE (**Table 2**).

DISCUSSION

The release of recent plant photosynthates into the soil has been shown to accelerate microbial decomposition of soil organic matter (Kuzyakov et al., 2000; Cheng et al., 2014), which has been identified as a strong driver for terrestrial C and nutrient cycling (Heimann and Reichstein, 2008). While research has traditionally focused on the effect of direct root exudation, recent studies highlight the contribution of an alternative "mycorrhizal pathway," demonstrating a transfer of plant-derived C via AM mycorrhizal fungi to soil bacteria (Toljander et al., 2007; Drigo et al., 2010; Cheng et al., 2012; Kaiser et al., 2015; Paterson et al., 2016). Very little, however, is known about a possible transfer of recent photosynthates to soil via ECM fungi, and interactions of ECM fungi with soil bacteria. Here, we provide evidence that plant-photoassimilated C is rapidly transferred to root-distant soil bacteria via ECM hyphae, indicating that ECM fungi readily share this resource with soil saprotrophs. Contrary to our hypothesis, however, the addition of labile N did not result in increased hyphal C transfer to bacteria. Instead, bacterial biomass and its incorporation of recent photosynthates declined with N addition not only in the litter compartment to which N was added, but also in adjacent untreated soil compartments, indicating a complex response of fungal-bacterial interactions to changing N availabilities.

Ectomycorrhizal Fungi Transfer Recent Photosynthates to Root-Distant Areas

Recent photosynthates were transferred to root-inaccessible areas in our system within hours. This transport of plant-derived C into litter compartments was most likely restricted to fungal hyphae, as our experimental design prevented

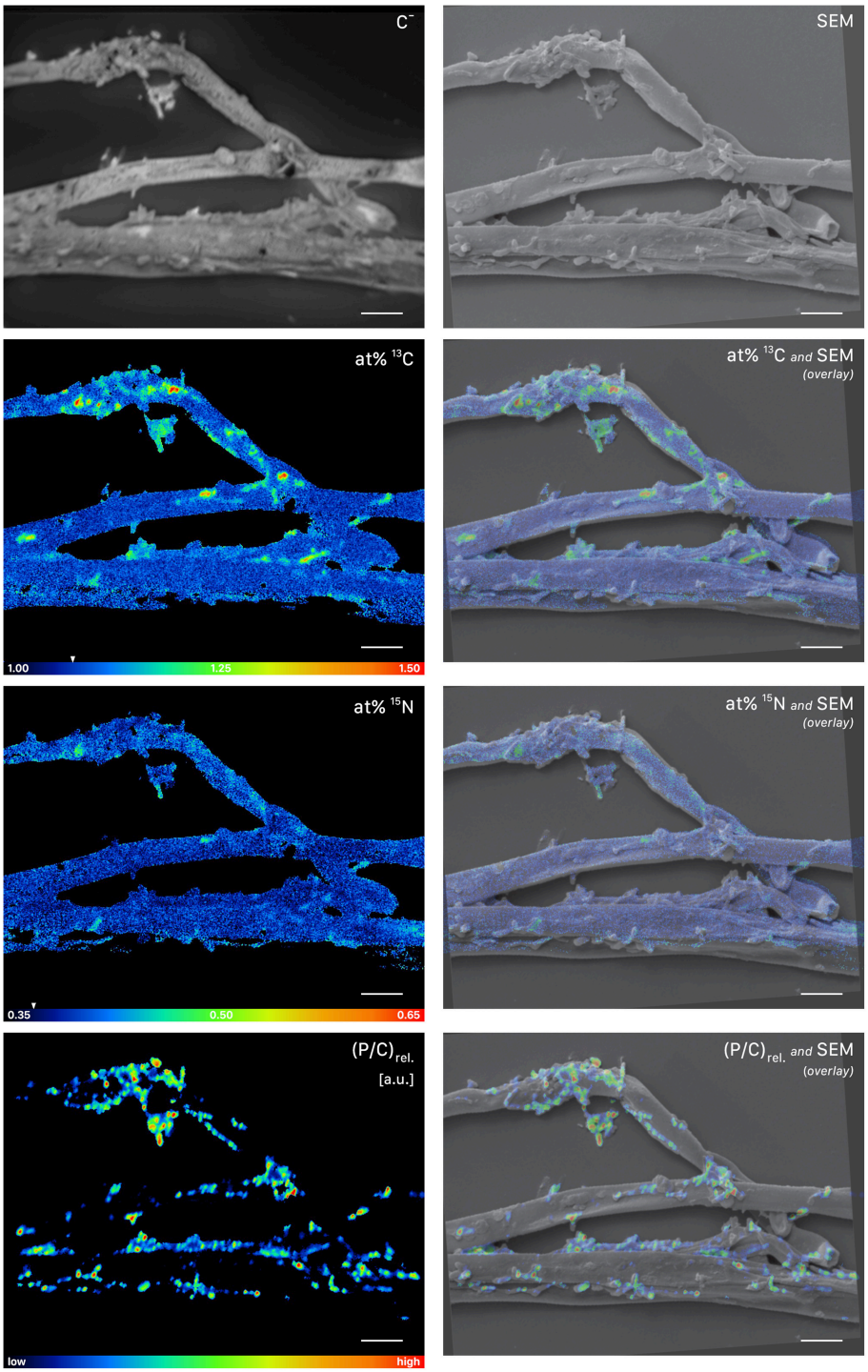

FIGURE 7 | NanoSIMS and SEM imaging of cells attached to root-distant fungal hyphae extracted from a litter compartment of a dual-labeled (^{13}C and ^{15}N) plant-box. SEM, scanning electron microscopy image (secondary electrons); C^-, accumulated $^{12}C^-$ and $^{13}C^-$ secondary ion signal intensity distribution images, indicating the morphology of the sample during NanoSIMS analysis; at% ^{13}C, carbon isotope composition image, showing ^{13}C enrichment in microbial cells on the surface of the hyphae; at% ^{15}N, nitrogen isotope composition image. Isotopic label contents are displayed as atom%. The white arrows at the color-scales indicate the natural isotopic abundance values, determined on the unlabeled control (1.08 atom% ^{13}C and 0.37 atom% ^{15}N). The upper limit of the atom% ^{13}C scale is set to 1.50, maximum values range up to 1.56 atom%. Secondary ion signal intensity thresholds were set to 119, 51 and 58 counts/(sec*pixel) for $^{12}C^{13}C^-$, $^{12}C^{15}N^-$, and $^{31}P^-$ respectively. $(P/C)_{rel.}$, relative phosphor-to-carbon elemental ratio image as inferred from C^- normalized $^{31}P^-$ secondary ion signal intensities, indicating the presence of microbial cells on hyphal surfaces. Overlay images are composites of the SEM and NanoSIMS images. NanoSIMS images consist of accumulated z-stacks obtained from 24 consecutive scans. Scale bars, 5 μm.

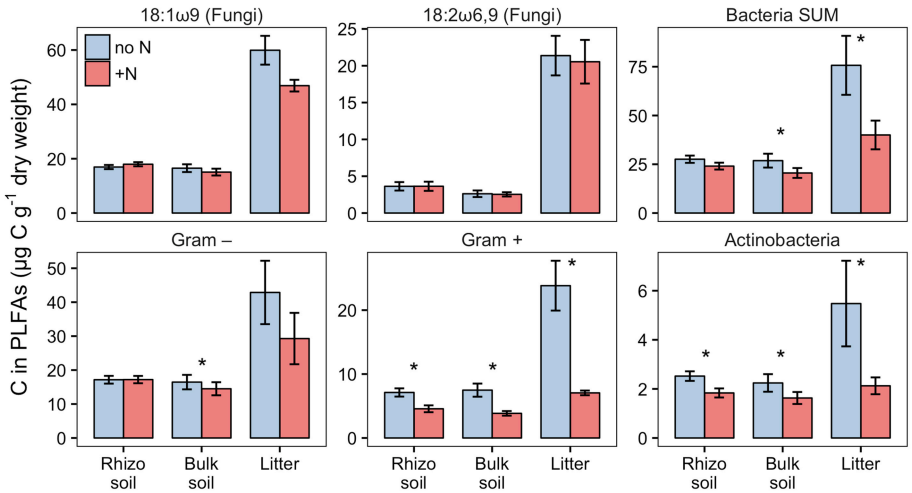

FIGURE 8 | Biomass of fungi and bacterial groups in rhizosphere, bulk soil and litter pools of N-treated and untreated sides of dual-labeled (^{13}C and ^{15}N) plant boxes, represented by PLFA biomarkers. Biomass of Actinobacteria and Gram-positive bacteria (excluding the Actinobacterial PLFA) declined significantly in both litter and soil compartments with N addition (i.e., to the litter compartment). Significant differences between N-treated (+N) and untreated side (no N) are indicated with asterisks (Mann-Whitney *U*-test for paired samples; $p < 0.05$; $n = 6$). Although not statistically significant, the adverse effect of N addition is also present in Gram-negative bacteria in litter, and the fungal PLFA 18:1ω9 in litter and bulk soil ($p < 0.01$). Error bars represent the standard error. Differences between soil and litter pools of the untreated side were analyzed with the Kruskal-Wallis rank sum test. Significant test results ($p < 0.05$) were followed by Dunn's *post-hoc* test of multiple comparisons with Bonferroni correction (adj. $p < 0.05$). Rhizosphere soil and litter, as well as bulk soil and litter, were significantly different in all groups except for Actinobacteria (not shown).

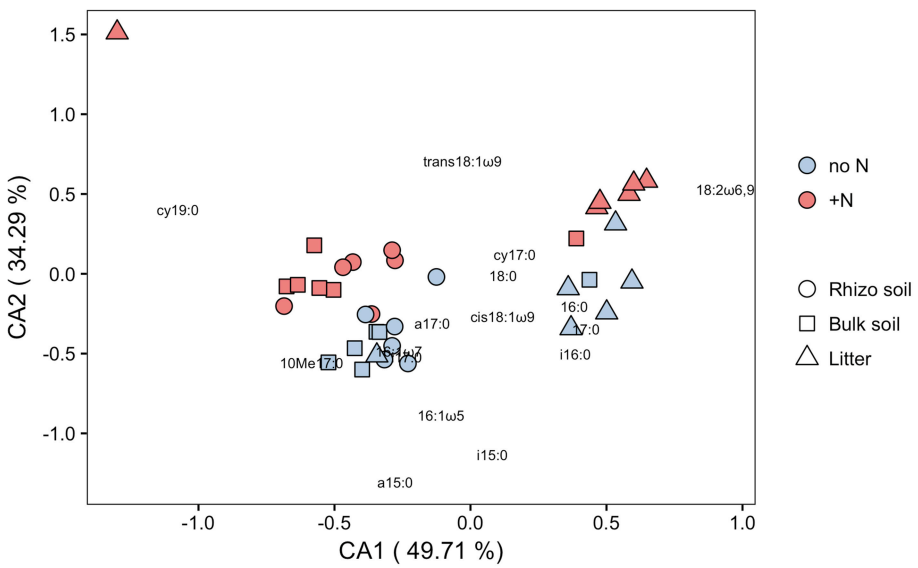

FIGURE 9 | Correspondence analysis (CA) of C in PLFAs (µg C g^{-1} dry weight) in N-treated and untreated compartments of dual-labeled (^{13}C and ^{15}N) plant boxes. Close distances between individual PLFAs (depicted as text) and soil/litter-pools of individual split-root boxes (depicted as symbols) indicate higher abundance of respective PLFAs in concerned pools. Axes notations give the proportion of variance explained on each coordinate in percent. Colors refer to box-sides with untreated (no N) and N-treated (+N) litter compartments. ANOSIM analysis shows significant difference between pools ($R = 0.566$, $p = 0.001$) as well as between N-treatments ($R = 0.103$, $p = 0.011$). This analysis indicates (i) a distinctly different microbial community between soil pools (rhizosphere soil, bulk soil) and litter, and (ii) that N addition affects not only community structure in hyphae-only litter compartments, but also in soil compartments (cf. **Figure 8**).

diffusion and penetration of roots into the litter compartment by means of a double-layer mesh with an air-filled gap that could only be penetrated by hyphae. Hyphal transport of recently photoassimilated C is supported by significant ^{13}C-enrichment in microbial biomass based on CFE (**Table 2**) as well as fungal- and bacterial-specific PLFAs in the litter compartment (**Figure 4**, **Table S2**). Furthermore, NanoSIMS imaging provided evidence of significant ^{13}C enrichment inside a fungal hypha obtained from the litter compartment (**Figure 5**).

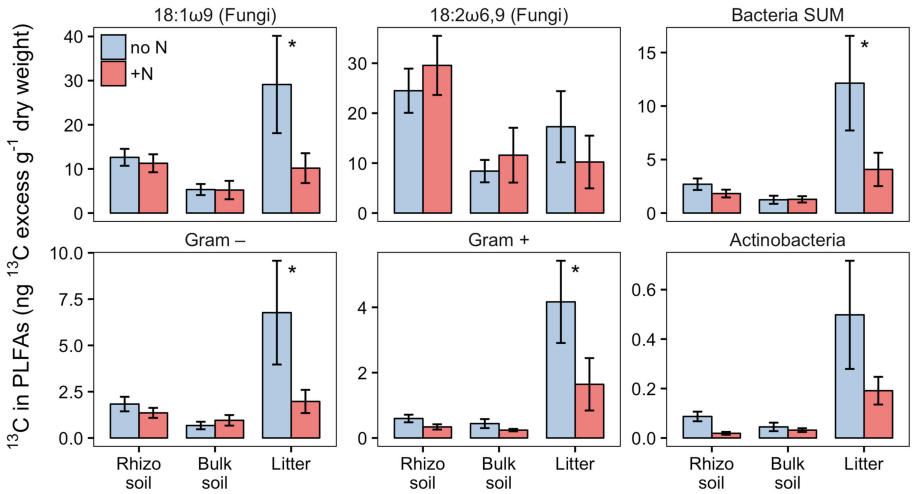

FIGURE 10 | ^{13}C-excess in PLFAs per g dry weight in N-treated and untreated compartments of dual-labeled (^{13}C and ^{15}N) plant boxes. Enrichment of bacteria-specific PLFAs in the litter compartment indicates allocation of photoassimilated ^{13}C via ECM hyphae to root-distant bacteria. Significant differences between untreated (no N) and N-treated side (+N) are indicated with asterisks (Mann-Whitney *U*-test for paired samples; $p > 0.05$; $n = 6$). Error bars represent the standard error.

The similarity of ECM fungal communities in rhizosphere and litter compartments, together with the near absence of ECM fungal communities in litter compartments of unplanted boxes (**Figure 2**), strongly indicates a vital connection between plant roots and associated litter compartments by mycorrhizal hyphae. While some transfer of recently plant-assimilated ^{13}C to the litter compartment via saprotrophic fungi cannot be ruled out, it is considered to be negligible because of the high degree of mycorrhization (which likely prevents high rates of root exudation) and the short time scales considered. Saprotrophic fungi are known to use complex organic matter as their main C source, rendering them unlikely to introduce substantial amounts of labile root exudates into the litter compartment within short time scales. We therefore assume that C transport via ECM hyphae accounted for the largest fraction of ^{13}C allocated to the litter compartment. In particular, the interior of the hypha investigated by NanoSIMS was highly enriched in ^{13}C (up to 2.6 atom% excess ^{13}C, **Figure 5**), clearly exceeding ^{13}C enrichment of the microbial biomass in the rhizosphere (up to 0.74 atom% excess ^{13}C), and also the ^{13}C enrichment of fine roots (0.88 atom% excess ^{13}C), with the latter representing a potential source of C for saprotrophic fungi. While it is impossible to identify its phylogenetic identity, this strongly indicates that this hypha was mycorrhizal, as other, not plant-associated fungi would not be able to acquire that much plant-photoassimilated C in such a short time.

Soil Bacteria Receive Recent Photosynthates From Ectomycorrhizal Fungi

Providing free-living saprotrophs with low-molecular-weight C compounds to supplement their energy demand is a potentially viable strategy for ECM fungi to accelerate decomposition of recalcitrant organic matter. We provide evidence for a direct, short-term transfer of recent photosynthates (i.e., shorter than 29 h) via fungal hyphae to hyphosphere bacteria. This is supported by significant ^{13}C-enrichment not only of (a) bacteria-specific PLFAs in a compartment only accessible by fungal hyphae (**Figures 4**, **10**), but also (b) hyphae-attached microbial cells as visualized by NanoSIMS (**Figure 7**). Together with the fact that DOC was significantly ^{13}C-enriched, this indicates consumption of ^{13}C-enriched exudates by hyphae-associated microbes and incorporation of this C into cellular biomass. This study is the first one visualizing the incorporation of stable isotope labeled plant-derived C from ECM fungal hyphae into hyphae-associated microorganisms.

Another explanation for the ^{13}C enrichment of bacteria in litter compartments could be the acquisition of ^{13}C by saprotrophic microbes feeding on ECM hyphal necromass. This appears however likely negligible within the short period between the onset of ^{13}C-CO_2 pulse labeling and harvest, since the turnover rate estimates for ECM hyphae in natural systems range from weeks to several months (Ekblad et al., 2013).

Unexpectedly, there was no preference in C transfer to specific bacterial groups, neither in the rhizosphere nor in the litter compartment as far as the resolution of the PLFA method allowed to trace this. This somewhat contrasts previous studies in which Gram-negative bacteria preferentially utilized plant-derived compounds in the rhizosphere (Kramer and Gleixner, 2006, 2008; Esperschütz et al., 2009; Pickles et al., 2016).

Interestingly, the relative ^{13}C enrichment of bacterial PLFA biomarkers was as high, or even higher in the litter compartment than in rhizosphere or bulk soil, while relative ^{13}C enrichment of the fungal biomarker 18:2w6,9 strongly decreased from rhizosphere soil to the litter compartment. Furthermore, bacteria incorporated the highest absolute amounts of ^{13}C in the litter compartment (untreated side in **Figure 10**). Together,

this suggests higher hyphal C exudation in litter compared to soil compartments, indicating that bacteria received more C via the mycorrhizal hyphal pathway in the litter compartment than via combined root and mycorrhizal hyphal exudation in the rhizosphere. ECM fungal hyphae are known to increase branching and growth when they reach organic-rich substrates (Agerer, 2001, 2006), which may have happened in our litter compartments. Such a growth pattern would tremendously increase the mycelial surface area and number of hyphal tips (Katz et al., 1972), which could, particularly under the assumption that ECM hyphal exudation concentrates on hyphal tips (Unestam and Sun, 1995; Sun et al., 1999), explain the higher total rate of ^{13}C transfer to bacteria that we observed in the litter compartments.

Evidence of hyphal C translocation to bacteria is missing in ECM systems and is scarce even for AM systems, where it is most often based on DNA and PLFA stable isotope probing (SIP) methods, which lack a spatial context. Here, we demonstrate the transfer of labeled compounds from fungi to soil microbes in an ECM system by a spatially explicit approach, which provides insight into the local aspects of this interaction, and allows the *in situ* visualization of the stable isotope composition of microbial cells associated with fungal hyphae via NanoSIMS analysis. While NanoSIMS represents a promising topochemical analysis technique to study C and nutrient transfer in fungal-bacterial interactions, it has only been used in a few studies for this purpose so far. Worrich et al. (2017), for example, investigated fungal-bacterial interactions in a synthetic microbial ecosystem, demonstrating a direct transfer of water and nutrients from hyphae of the oomycete *Phytium ultimum* to bacterial cells of *Bacillus subtilis*. In a pioneering effort of visualizing microscale rhizosphere C flow through an undisturbed plant-soil system, Vidal et al. (2018) repeatedly exposed wheat, an AM plant, to ^{13}C-CO_2 over a time period of 10 weeks and subsequently analyzed the distribution of ^{13}C in undisturbed rhizosphere samples using NanoSIMS. They found, amongst other results, a ^{13}C enriched spot, presumably a bacterial cell, on a fungal hypha associated with a wheat root. However, due to the long-term labeling approach, this finding can't be attributed to a hyphal transfer of recently assimilated plant C to microbial cells (which was also not the aim of that study), but may reflect accumulation of plant-derived organic C in soil bacteria over various pathways and longer time scales.

Relationship Between Ectomycorrhizal Hyphae and Associated Bacteria

The addition of ^{15}N-labeled labile N compounds affected microbial community structure within days, causing a loss of biomass of certain bacterial groups. Actinobacteria and other Gram-positive bacteria declined strongest ($p < 0.05$), but Gram-negative bacteria and the fungal PLFA 18:1ω9 tended to decline as well ($p < 0.1$; **Figure 8**). Only the fungal PLFA 18:2ω6,9 remained unaffected by the treatment. The two fungal-specific PLFA biomarkers also differed in their absolute abundance and ^{13}C incorporation: while 18:1ω9 was more abundant than 18:2ω6,9 (**Figure 8**), it was relatively less enriched in ^{13}C (**Figure 4**). Together with their different response to N addition, this could indicate that in our system 18:1ω9 is more indicative of fungi in general, including free living saprotrophs, while 18:2ω6,9 could be more specific for ECM fungi.

In contrast to the PLFAs, microbial biomass C based on CFE was unaffected by N addition (**Table 2**). Potential reasons for this could be (i) the higher precision of PLFA analysis compared to CFE or (ii) differences in the target of the two methods. Phospholipids mainly occur in cell membranes, thus emphasizing cell surface areas in PLFA measurements, while CFE lyses cells with the lysate being proportional to cell volumes. For example, if a deteriorating effect on microbial biomass affected small microbial cells (e.g., small bacteria) more than larger cells (e.g., fungi or larger bacteria), surface areas (PLFAs) would decrease stronger than volume (CFE-based biomass). This possibility is indirectly supported by PLFA analysis which also indicated a community shift in response to N addition.

The strong and very rapid negative effect of labile N on bacterial biomass seems counter-intuitive, as we would rather expect a positive effect of N on bacterial growth. The amount of N we have added (0.168 mg NH_4-N, and 0.168 mg N as amino acids) makes up for around 5% of the total dissolved N in the litter compartment, representing a moderate increase in the concentration of labile N compounds. However, the negative effect on microbial biomass was not restricted to the litter compartments, which received labile N inputs, but it also significantly affected the soil compartments separated from them by the hyphal-penetrable mesh.

Our ^{15}N measurements indicate that around 10% of the added N was transferred from the litter to the soil in total (**Table 1**), which would yield an enhancement of total dissolved N in this compartment by 0.5% (data not shown). As this represents only a negligible increase, we can rule out a direct effect of enhanced N availability on microbial biomass and community structure. As the effect however clearly took place not only in the litter, but also in the adjacent soil compartments, we can only speculate that it must have been caused by a systemic reaction of the fungi or the plant to altered local availability of N. If it was a fungal reaction it would be restricted to those fungi growing in the N-treated side of the box, i.e., those which connect the N-treated litter compartment with the plant roots in the mesh-separated soil compartment. If it was a plant reaction, it needed to have been directed toward the part of the root system that received more N.

One possible mechanism could be that when ECM fungi were exposed to easily available N in excess, their interaction with associated bacteria drastically changed from cooperative to competitive. As a consequence, ECM fungi may have taken up the main part of the added ^{15}N, transferring it toward plant roots, while impairing bacterial growth along the whole hyphal "supply line" (i.e., not only in the litter compartments, but also in the adjacent soil compartments). The latter could have happened in different ways, for example by reducing the input of labile C, which may be vital for parts of the bacterial community, or by

actively employing allelopathic strategies, such as the production of antibiotics.

In fact, fungi are known to produce a plethora of bacterial and fungal antibiotics (Keller et al., 2005), and to use them in competition against saprotrophic fungi (Fernandez and Kennedy, 2015). Furthermore, bacteria of the genus *Streptomyces* (Actinobacteria), which is the largest antibiotic-producing bacterial genus known (Watve et al., 2001) have been found to live in close association with ECM fungi (Schrey et al., 2005; Seipke et al., 2012). ECM fungi thus seem to have the potential to take allelopathic actions against bacterial saprotrophs when they switch to a competitive situation. To test if this actually happens goes however beyond the scope of this study and warrants further research.

As another option, ECM fungi may have reduced the transfer of plant-derived C to their bacterial competitors. This is supported by our results, which show a significant decline in the absolute amount of ^{13}C incorporated into bacterial PLFAs and the fungal PLFA 18:1ω9 after N addition (**Figure 10**). As bacterial and fungal PLFA biomarkers received significantly lower amounts of ^{13}C, but ^{13}C enrichment in DOC was unchanged, we conclude that in total less ^{13}C was transferred via mycorrhizal hyphae to the litter compartment after addition of N (**Table 2**). An analogous reaction is often observed in plants, where C allocation to the rhizosphere decreases with N fertilization (Kuzyakov and Domanski, 2000). The question remains whether a decrease in labile C input could have led to such a rapid decline in bacterial biomass, which seems unlikely to be caused just by starvation of bacterial cells. The hyphosphere, however, may be—similar to the rhizosphere—a microbial "hotspot," i.e., a spatially restricted soil volume with exceptionally high abundances and turnover rates of microbes, caused by high rates of labile C input (Kuzyakov and Blagodatskaya, 2015). High turnover rates are defined as fast growth rates balanced by high mortality rates. In an environment not limited by substrate availability, mortality is likely driven by density dependent mechanisms, such as predation, virus activity, or negative bacterial interactions (West et al., 2007; Ratzke et al., 2018). It is thus possible that diminishing substrate input decreases bacterial growth rates, but mortality rates may stay high until population density has substantially decreased, which may also explain the rapid decline in microbial biomass.

While our results indicate that N availability affects the relationship of mycorrhizal fungi and soil microbes, it has to be kept in mind that we added only easily available forms of N, and only at a single concentration. The system may have responded in a different way if other quantities or qualities of N, such as complex organic N, were added. While this would be interesting to investigate, it goes beyond the scope of this study.

CONCLUSIONS

Our results show a transfer of recent photosynthates via ECM hyphae to associated soil microbes in root-inaccessible areas within hours, supporting the hypothesis of priming in an ECM hyphosphere as a potential mechanism to increase access to nutrients from soil organic matter for ECM fungi and their host plants.

Contrary to our expectations, elevated local availability of labile N compounds did not result in higher hyphal exudation rates. Instead, we found a strong decline in biomass of Actinobacteria and other Gram-positive bacteria in response to N addition. This decline seems to have been caused by ECM fungi acting on soil bacteria, as the effect was observed in soil compartments where fertilized N would only be available for bacteria through hyphal transport.

Based on our observations, we suggest the relation between ECM hyphae and soil bacteria to be on a "razors edge," tilting between mutualistic and antagonistic interactions depending on environmental conditions. It is likely that fungi occupy the more sustained position in such an opportunistic mutualism, by controlling C flow to bacteria. Accordingly, hyphosphere priming may be a highly controlled process with hyphal exudation being rapidly adjusted to changing soil nutrient availabilities.

AUTHOR CONTRIBUTIONS

CK conceived and coordinated the study. CK, AR, and DW designed the experiment. WM, RG, JW, VM, QZ, JP, MD, and SG did the experimental work, supervised by CK, PS, AR, and DW. JW, VM, SG and BI did the PLFA analysis. MD did the hyphal sample preparation, SEM analyses and ITS sequencing and analysis under supervision of MWe, SE, and DW. AS performed the NanoSIMS analysis in collaboration with MD and DW. MWa contributed to NanoSIMS method development. SG and SE analyzed the data. SG wrote the manuscript in close collaboration with CK and AS, with contribution of all co-authors.

FUNDING

This work was partly supported by an Austrian Science Fund FWF project [P 30339-B29] to CK, as well as by an Austrian Science Fund FWF project grant [P26392-B20] to DW and SE, FWF DK Plus [W1257-B20] to DW and an ERC Starting grant (grant agreement number 636928, to DW) from the European Research Council (ERC) under the European Union's Horizon 2020 research and innovation program.

ACKNOWLEDGMENTS

SEM and other microscopy work was carried out at Core Facility Cell Imaging and Ultrastructure Research, and NanoSIMS imaging at the Large-Instrument Facility for Advanced Isotope Research, both at the University of Vienna. We thank Heinz Pfeiffer from the workshop of the Faculty of Life Sciences, University of Vienna, for building the split-root boxes and the labeling chamber, Margarete Watzka and Ludwig Seidl for technical support, Florian Strasser and Daniela Gruber for help in SEM preparation and Irene

Lichtscheidl, Siegfried Reipert and Peta Clode for helpful discussions about the experimental setup and NanoSIMS sample preparation techniques. We thank the three reviewers for constructive comments which helped to improve the quality of the manuscript.

SUPPLEMENTARY MATERIAL

The Supplementary Material for this article can be found online at: https://www.frontiersin.org/articles/10.3389/fmicb.2019.00168/full#supplementary-material

REFERENCES

Agerer, R. (2001). Exploration types of ectomycorrhizae. *Mycorrhiza* 11, 107–114. doi: 10.1007/s005720100108

Agerer, R. (2006). Fungal relationships and structural identity of their ectomycorrhizae. *Mycol. Prog.* 5, 67–107. doi: 10.1007/s11557-006-0505-x

Angel, R. (2012). *Total Nucleic Acid Extraction from Soil. Protocol Exchange*. Available online at: https://www.nature.com/protocolexchange/protocols/2484

Bahn, M., Schmitt, M., Siegwolf, R., Richter, A., and Brüggemann, N. (2009). Does photosynthesis affect grassland soil-respired CO_2 and its carbon isotope composition on a diurnal timescale? *New Phytol.* 182, 451–460. doi: 10.1111/j.1469-8137.2008.02755.x

Bengtsson-Palme, J., Ryberg, M., Hartmann, M., Branco, S., Wang, Z., Godhe, A., et al. (2013). Improved software detection and extraction of ITS1 and ITS2 from ribosomal ITS sequences of fungi and other eukaryotes for analysis of environmental sequencing data. *Methods Ecol. Evol.* 4, 914–919. doi: 10.1111/2041-210X.12073

Bever, J. D., Richardson, S. C., Lawrence, B. M., Holmes, J., and Watson, M. (2009). Preferential allocation to beneficial symbiont with spatial structure maintains mycorrhizal mutualism. *Ecol. Lett.* 12, 13–21. doi: 10.1111/j.1461-0248.2008.01254.x

Bligh, E. G., and Dyer, W. J. (1959). A rapid method of total lipid extraction and purification. *Can. J. Biochem. Physiol.* 37, 911–917. doi: 10.1139/y59-099

Brookes, P. C., Landman, A., Pruden, G., and Jenkinson, D. S. (1985). Chloroform fumigation and the release of soil nitrogen: a rapid direct extraction method to measure microbial biomass nitrogen in soil. *Soil Biol. Biochem.* 17, 837–842. doi: 10.1016/0038-0717(85)90144-0

Bruns, T. D., Szaro, T. M., Gardes, M., Cullings, K. W., Pan, J. J., Taylor, D. L., et al. (1998). A sequence database for the identification of ectomycorrhizal basidiomycetes by phylogenetic analysis. *Mol. Ecol.* 7, 257–272. doi: 10.1046/j.1365-294X.1998.00337.x

Chapman, S. K., Langley, J. A., Hart, S. C., and Koch, G. W. (2005). Plants actively control nitrogen cycling: uncorking the microbial bottleneck. *New Phytol.* 169, 27–34. doi: 10.1111/j.1469-8137.2005.01571.x

Cheng, L., Booker, F. L., Tu, C., Burkey, K. O., Zhou, L., Shew, H. D., et al. (2012). Arbuscular mycorrhizal fungi increase organic carbon decomposition under elevated CO_2. *Science* 337, 1084–1087. doi: 10.1126/science.1224304

Cheng, W., Parton, W. J., Gonzalez-Meler, M. A., Phillips, R., Asao, S., McNickle, G. G., et al. (2014). Synthesis and modeling perspectives of rhizosphere priming. *New Phytol.* 201, 31–44. doi: 10.1111/nph.12440

Deshpande, V., Wang, Q., Greenfield, P., Charleston, M., Porras-Alfaro, A., Kuske, C. R., et al. (2016). Fungal identification using a Bayesian classifier and the warcup training set of internal transcribed spacer sequences. *Mycologia* 108, 1–5. doi: 10.3852/14-293

Dilkes, N. B., Jones, D. L., and Farrar, J. (2004). Temporal dynamics of carbon partitioning and rhizodeposition in wheat. *Plant Physiol.* 134, 706–715. doi: 10.1104/pp.103.032045

Drigo, B., Pijl, A. S., Duyts, H., Kielak, A. M., Gamper, H. A., Houtekamer, M. J., et al. (2010). Shifting carbon flow from roots into associated microbial communities in response to elevated atmospheric CO_2. *Proc. Natl. Acad. Sci. U.S.A.* 107, 10938–10942. doi: 10.1073/pnas.0912421107

Ekblad, A., Wallander, H., Godbold, D. L., Cruz, C., Johnson, D., Baldrian, P., et al. (2013). The production and turnover of extramatrical mycelium of ectomycorrhizal fungi in forest soils: role in carbon cycling. *Plant Soil* 366, 1–27. doi: 10.1007/s11104-013-1630-3

Esperschütz, J., Buegger, F., Winkler, J. B., Munch, J. C., Schloter, M., and Gattinger, A. (2009). Microbial response to exudates in the rhizosphere of young beech trees (*Fagus sylvatica* L.) after dormancy. *Soil Biol. Biochem.* 41, 1976–1985. doi: 10.1016/j.soilbio.2009.07.002

Fernandez, C. W., and Kennedy, P. G. (2015). Revisiting the 'Gadgil effect': do interguild fungal interactions control carbon cycling in forest soils? *New Phytol.* 209, 1382–1394. doi: 10.1111/nph.13648

Frostegård, Å., Tunlid, A., and Bååth, E. (1991). Microbial biomass measured as total lipid phosphate in soils of different organic content. *J. Microbiol. Methods* 14, 151–163. doi: 10.1016/0167-7012(91)90018-L

Gardes, M., and Bruns, T. D. (1993). ITS primers with enhanced specificity for basidiomycetes - application to the identification of mycorrhizae and rusts. *Mol. Ecol.* 2, 113–118. doi: 10.1111/j.1365-294X.1993.tb00005.x

Heimann, M., and Reichstein, M. (2008). Terrestrial ecosystem carbon dynamics and climate feedbacks. *Nature* 451, 289–292. doi: 10.1038/nature06591

Herbold, C. W., Pelikan, C., Kuzyk, O., Hausmann, B., Angel, R., Berry, D., et al. (2015). A flexible and economical barcoding approach for highly multiplexed amplicon sequencing of diverse target genes. *Front. Microbiol.* 6:731. doi: 10.3389/fmicb.2015.00731

Hill, G., Mitkowski, N., Aldrich-Wolfe, L., Emele, L., Jurkonie, D., Ficke, A., et al. (2000). Methods for assessing the composition and diversity of soil microbial communities. *Appl. Soil Ecol.* 15, 25–36. doi: 10.1016/S0929-1393(00)00069-X

Hobbie, E. A. (2006). Carbon allocation to ectomycorrhizal fungi correlates with belowground allocation in culture studies. *Ecology* 87, 563–569. doi: 10.1890/05-0755

Hodge, A., Campbell, C. D., and Fitter, A. H. (2001). An arbuscular mycorrhizal fungus accelerates decomposition and acquires nitrogen directly from organic material. *Nature* 413:297. doi: 10.1038/35095041

Hodge, A., Helgason, T., and Fitter, A. H. (2010). Nutritional ecology of arbuscular mycorrhizal fungi. *Fungal Ecol.* 3, 267–273. doi: 10.1016/j.funeco.2010.02.002

Jansa, J., Bukovská, P., and Gryndler, M. (2013). Mycorrhizal hyphae as ecological niche for highly specialized hypersymbionts or just soil free-riders? *Front. Plant Sci.* 4:134. doi: 10.3389/fpls.2013.00134

Johnson, D., Leake, J. R., and Read, D. J. (2002). Transfer of recent photosynthate into mycorrhizal mycelium of an upland grassland: short-term respiratory losses and accumulation of 14C. *Soil Biol. Biochem.* 34, 1521–1524. doi: 10.1016/S0038-0717(02)00126-8

Kaiser, C., Fuchslueger, L., Koranda, M., Gorfer, M., Stange, C. F., Kitzler, B., et al. (2011). Plants control the seasonal dynamics of microbial N cycling in a beech forest soil by belowground C allocation. *Ecology* 92, 1036–1051. doi: 10.1890/10-1011.1

Kaiser, C., Kilburn, M. R., Clode, P. L., Fuchslueger, L., Koranda, M., Cliff, J. B., et al. (2015). Exploring the transfer of recent plant photosynthates to soil microbes: mycorrhizal pathway vs direct root exudation. *New Phytol.* 205, 1537–1551. doi: 10.1111/nph.13138

Kaiser, C., Koranda, M., Kitzler, B., Fuchslueger, L., Schnecker, J., Schweiger, P., et al. (2010). Belowground carbon allocation by trees drives seasonal patterns of extracellular enzyme activities by altering microbial community composition in a beech forest soil. *New Phytol.* 187, 843–858. doi: 10.1111/j.1469-8137.2010.03321.x

Katz, D., Goldstein, D., and Rosenberger, R. F. (1972). Model for branch initiation in *Aspergillus nidulans* based on measurements of growth parameters. *J. Bacteriol.* 109, 1097–1100.

Keller, N. P., Turner, G., and Bennett, J. W. (2005). Fungal secondary metabolism from biochemistry to genomics. *Nat. Rev. Microbiol.* 3, 937–947. doi: 10.1038/nrmicro1286

Kiers, E. T., and Van der Heijden, M. G. (2006). Mutualistic stability in the arbuscular mycorrhizal symbiosis: exploring hypotheses of evolutionary cooperation. *Ecology* 87, 1627–1636. doi: 10.1890/0012-9658(2006)87[1627:MSITAM]2.0.CO;2

Koranda, M., Schnecker, J., Kaiser, C., Fuchslueger, L., Kitzler, B., Stange, C. F., et al. (2011). Microbial processes and community composition in the rhizosphere of European beech – the influence of plant C exudates. *Soil Biol. Biochem.* 43, 551–558. doi: 10.1016/j.soilbio.2010.11.022

Kramer, C., and Gleixner, G. (2006). Variable use of plant- and soil-derived carbon by microorganisms in agricultural soils. *Soil Biol. Biochem.* 38, 3267–3278. doi: 10.1016/j.soilbio.2006.04.006

Kramer, C., and Gleixner, G. (2008). Soil organic matter in soil depth profiles: distinct carbon preferences of microbial groups during carbon transformation. *Soil Biol. Biochem.* 40, 425–433. doi: 10.1016/j.soilbio.2007.09.016

Kuzyakov, Y. (2002). Factors affecting rhizosphere priming effects. *J. Plant Nutr. Soil Sci.* 165, 382–396. doi: 10.1002/1522-2624(200208)165:4<382::AID-JPLN382>3.0.CO;2-%23

Kuzyakov, Y., and Blagodatskaya, E. (2015). Microbial hotspots and hot moments in soil: concept & review. *Soil Biol. Biochem.* 83, 184–199. doi: 10.1016/j.soilbio.2015.01.025

Kuzyakov, Y., and Domanski, G. (2000). Carbon input by plants into the soil. Review. *J. Plant Nutr. Soil Sci.* 163, 421–431. doi: 10.1002/1522-2624(200008)163:4<421::AID-JPLN421>3.0.CO;2-R

Kuzyakov, Y., Friedel, J. K., and Stahr, K. (2000). Review of mechanisms and quantification of priming effects. *Soil Biol. Biochem.* 32, 1485–1498. doi: 10.1016/S0038-0717(00)00084-5

Leake, J. R., Donnelly, D. P., Saunders, E. M., Boddy, L., and Read, D. J. (2001). Rates and quantities of carbon flux to ectomycorrhizal mycelium following ^{14}C pulse labeling of *Pinus sylvestris* seedlings: effects of litter patches and interaction with a wood-decomposer fungus. *Tree Physiol.* 21, 71–82. doi: 10.1093/treephys/21.2-3.71

Leckie, S. E. (2005). Methods of microbial community profiling and their application to forest soils. *For. Ecol. Manage.* 220, 88–106. doi: 10.1016/j.foreco.2005.08.007

Martin, F., and Botton, B. (1993). *Nitrogen Metabolism of Ectomycorrhizal fungi and Ectomycorrhiza. Advances in Plant Pathology*. Available online at: http://agris.fao.org/agris-search/search.do?recordID=US201301510038 (Accessed August 9, 2018)

Noë, R., and Hammerstein, P. (1995). Biological markets. *Trends Ecol. Evol.* 10, 336–339. doi: 10.1016/S0169-5347(00)89123-5

Oksanen, J., Blanchet, F. G., Friendly, M., Kindt, R., Legendre, P., McGlinn, D., et al. (2018). *Vegan: Community Ecology Package*. Available online at: https://CRAN.R-project.org/package=vegan.

Olsson, P. A. (1999). Signature fatty acids provide tools for determination of the distribution and interactions of mycorrhizal fungi in soil. *FEMS Microbiol. Ecol.* 29, 303–310. doi: 10.1111/j.1574-6941.1999.tb00621.x

Paterson, E., Sim, A., Davidson, J., and Daniell, T. J. (2016). Arbuscular mycorrhizal hyphae promote priming of native soil organic matter mineralisation. *Plant Soil* 408, 243–254. doi: 10.1007/s11104-016-2928-8

Pellitier, P. T., and Zak, D. R. (2017). Ectomycorrhizal fungi and the enzymatic liberation of nitrogen from soil organic matter: why evolutionary history matters. *New Phytol.* 217, 68–73. doi: 10.1111/nph.14598

Phillips, R. L., Zak, D. R., Holmes, W. E., and White, D. C. (2002). Microbial community composition and function beneath temperate trees exposed to elevated atmospheric carbon dioxide and ozone. *Oecologia* 131, 236–244. doi: 10.1007/s00442-002-0868-x

Phillips, R. P., Brzostek, E., and Midgley, M. G. (2013). The mycorrhizal-associated nutrient economy: a new framework for predicting carbon-nutrient couplings in temperate forests. *New Phytol.* 199, 41–51. doi: 10.1111/nph.12221

Pickles, B. J., Wilhelm, R., Asay, A. K., Hahn, A. S., Simard, S. W., and Mohn, W. W. (2016). Transfer of 13C between paired Douglas-fir seedlings reveals plant kinship effects and uptake of exudates by ectomycorrhizas. *New Phytol.* 214, 400–411. doi: 10.1111/nph.14325

Poczatek, C., Kaufman, Z., and Lechene, C. (2009). *OpenMIMS ImageJ Plugin Guide*. Boston, MA: Harvard Medical School.

R Core Team (2017). *R: A Language and Environment for Statistical Computing*. Vienna: R Foundation for Statistical Computing. Available online at: https://www.R-project.org/

Ratzke, C., Denk, J., and Gore, J. (2018). Ecological suicide in microbes. *Nat. Ecol. Evol.* 2, 867–872. doi: 10.1038/s41559-018-0535-1.

Read, D. J., Leake, J. R., and Perez-Moreno, J. (2004). Mycorrhizal fungi as drivers of ecosystem processes in heathland and boreal forest biomes. *Can. J. Bot.* 82, 1243–1263. doi: 10.1139/b04-123

Ruess, L., and Chamberlain, P. M. (2010). The fat that matters: soil food web analysis using fatty acids and their carbon stable isotope signature. *Soil Biol. Biochem.* 42, 1898–1910. doi: 10.1016/j.soilbio.2010.07.020

Schindelin, J., Arganda-Carreras, I., Frise, E., Kaynig, V., Longair, M., Pietzsch, T., et al. (2012). Fiji: an open-source platform for biological-image analysis. *Nat. Methods* 9, 676–682. doi: 10.1038/nmeth.2019

Schnecker, J., Wild, B., Fuchslueger, L., and Andreas, Richter (2012). A field method to store samples from temperate mountain grassland soils for analysis of phospholipid fatty acids. *Soil Biol. Biochem.* 51, 81–83. doi: 10.1016/j.soilbio.2012.03.029

Schrey, S. D., Schellhammer, M., Ecke, M., Hampp, R., and Tarkka, M. T. (2005). Mycorrhiza helper bacterium Streptomyces AcH 505 induces differential gene expression in the ectomycorrhizal fungus *Amanita muscaria*. *New Phytol.* 168, 205–216. doi: 10.1111/j.1469-8137.2005.01518.x

Seipke, R. F., Kaltenpoth, M., and Hutchings, M. I. (2012). Streptomyces as symbionts: an emerging and widespread theme? *FEMS Microbiol. Rev.* 36, 862–876. doi: 10.1111/j.1574-6976.2011.00313.x

Simard, S. W., Jones, M. D., and Durall, D. M. (2003). "Carbon and nutrient fluxes within and between mycorrhizal plants," in *Mycorrhizal Ecology*, eds M. G. A. van der Heijden and I. Sanders (Berlin, Heidelberg: Springer), 33–74.

Smith, S. E., and Read, D. (2008). *Mycorrhizal symbiosis*, 3rd Edn. New York, NY: Academic Press.

Sun, Y.-P.-., P., Unestam, T., Lucas, S. D., Johanson, K. J., Kenne, L., and Finlay, R. (1999). Exudation-reabsorption in a mycorrhizal fungus, the dynamic interface for interaction with soil and soil microorganisms. *Mycorrhiza* 9, 137–144. doi: 10.1007/s005720050298

Talbot, J. M., Allison, S. D., and Treseder, K. K. (2008). Decomposers in disguise: mycorrhizal fungi as regulators of soil C dynamics in ecosystems under global change. *Funct. Ecol.* 22, 955–963. doi: 10.1111/j.1365-2435.2008.01402.x

Taylor, A. F. S., Gebauer, G., and Read, D. J. (2004). Uptake of nitrogen and carbon from double-labelled (^{15}N and ^{13}C) glycine by mycorrhizal pine seedlings. *New Phytol.* 164, 383–388. doi: 10.1111/j.1469-8137.2004.01164.x

Tedersoo, L., and Smith, M. E. (2013). Lineages of ectomycorrhizal fungi revisited: Foraging strategies and novel lineages revealed by sequences from belowground. *Fungal Biol. Rev.* 27, 83–99. doi: 10.1016/j.fbr.2013.09.001

Toljander, J. F., Lindahl, B. D., Paul, L. R., Elfstrand, M., and Finlay, R. D. (2007). Influence of arbuscular mycorrhizal mycelial exudates on soil bacterial growth and community structure. *FEMS Microbiol. Ecol.* 61, 295–304. doi: 10.1111/j.1574-6941.2007.00337.x

Unestam, T., and Sun, Y.-P. P. (1995). Extramatrical structures of hydrophobic and hydrophilic ectomycorrhizal fungi. *Mycorrhiza* 5, 301–311. doi: 10.1007/BF00207402

Vance, E. D., Brookes, P. C., and Jenkinson, D. S. (1987). An extraction method for measuring soil microbial biomass C. *Soil Biol. Biochem.* 19, 703–707. doi: 10.1016/0038-0717(87)90052-6

Vidal, A., Hirte, J., Bender, S. F., Mayer, J., Gattinger, A., Höschen, C., et al. (2018). Linking 3D soil structure and plant-microbe-soil carbon transfer in the rhizosphere. *Front. Environ. Sci.* 6:9. doi: 10.3389/fenvs.2018.00009

Walker, T. S., Bais, H. P., Grotewold, E., and Vivanco, J. M. (2003). Root exudation and rhizosphere biology. *Plant Physiol.* 132, 44–51. doi: 10.1104/pp.102.019661

Wang, Q., Garrity, G. M., Tiedje, J. M., and Cole, J. R. (2007). Naïve bayesian classifier for rapid assignment of rRNA sequences into the new bacterial taxonomy. *Appl. Environ. Microbiol.* 73, 5261–5267. doi: 10.1128/AEM.00062-07

Watve, M. G., Tickoo, R., Jog, M. M., and Bhole, B. D. (2001). How many antibiotics are produced by the genus Streptomyces? *Arch. Microbiol.* 176, 386–390. doi: 10.1007/s002030100345

West, S. A., Diggle, S. P., Buckling, A., Gardner, A., and Griffin, A. S. (2007). The social lives of microbes. *Annu. Rev. Ecol. Evol. Syst.* 38, 53–77. doi: 10.1146/annurev.ecolsys.38.091206.095740

White, T. J., Bruns, T., Lee, S., and Taylor, J. (1990). Amplification and direct sequencing of fungal ribosomal RNA genes for phylogenetics. *PCR Protoc.* 18, 315–322. doi: 10.1016/B978-0-12-372180-8.50042-1

Wickham, H. (2009). *ggplot2: Elegant Graphics for Data Analysis*. New York, NY: Springer-Verlag.

Worrich, A., Stryhanyuk, H., Musat, N., König, S., Banitz, T., Centler, F., et al. (2017). Mycelium-mediated transfer of water and nutrients stimulates bacterial activity in dry and oligotrophic environments. *Nat. Commun.* 8:15472. doi: 10.1038/ncomms15472

Zelles, L. (1997). Phospholipid fatty acid profiles in selected members of soil microbial communities. *Chemosphere* 35, 275–294. doi: 10.1016/S0045-6535(97)00155-0

Zelles, L. (1999). Fatty acid patterns of phospholipids and lipopolysaccharides in the characterisation of microbial communities in soil: a review. *Biol. Fertil. Soils* 29, 111–129. doi: 10.1007/s003740050533

Conflict of Interest Statement: The authors declare that the research was conducted in the absence of any commercial or financial relationships that could be construed as a potential conflict of interest.

frontiers in Plant Science

REVIEW
published: 21 February 2019
doi: 10.3389/fpls.2019.00157

Root Exudation of Primary Metabolites: Mechanisms and Their Roles in Plant Responses to Environmental Stimuli

Alberto Canarini[1], Christina Kaiser[1], Andrew Merchant[2], Andreas Richter[1] and Wolfgang Wanek[1]*

[1] Terrestrial Ecosystem Research, Department of Microbiology and Ecosystem Science, Research Network 'Chemistry Meets Microbiology', University of Vienna, Vienna, Austria, [2] Faculty of Science, Sydney Institute of Agriculture, The University of Sydney, Sydney, NSW, Australia

Root exudation is an important process determining plant interactions with the soil environment. Many studies have linked this process to soil nutrient mobilization. Yet, it remains unresolved how exudation is controlled and how exactly and under what circumstances plants benefit from exudation. The majority of root exudates including primary metabolites (sugars, amino acids, and organic acids) are believed to be passively lost from the root and used by rhizosphere-dwelling microbes. In this review, we synthetize recent advances in ecology and plant biology to explain and propose mechanisms by which root exudation of primary metabolites is controlled, and what role their exudation plays in plant nutrient acquisition strategies. Specifically, we propose a novel conceptual framework for root exudates. This framework is built upon two main concepts: (1) root exudation of primary metabolites is driven by diffusion, with plants and microbes both modulating concentration gradients and therefore diffusion rates to soil depending on their nutritional status; (2) exuded metabolite concentrations can be sensed at the root tip and signals are translated to modify root architecture. The flux of primary metabolites through root exudation is mostly located at the root tip, where the lack of cell differentiation favors diffusion of metabolites to the soil. We show examples of how the root tip senses concentration changes of exuded metabolites and translates that into signals to modify root growth. Plants can modify the concentration of metabolites either by controlling source/sink processes or by expressing and regulating efflux carriers, therefore challenging the idea of root exudation as a purely unregulated passive process. Through root exudate flux, plants can locally enhance concentrations of many common metabolites, which can serve as sensors and integrators of the plant nutritional status and of the nutrient availability in the surrounding environment. Plant-associated micro-organisms also constitute a strong sink for plant carbon, thereby increasing concentration gradients of metabolites and affecting root exudation. Understanding the mechanisms of and the effects that environmental stimuli have on the magnitude and type of root exudation will ultimately improve our knowledge of processes determining soil CO_2 emissions, ecosystem functioning, and how to improve the sustainability of agricultural production.

Keywords: root exudates, soil micro-organisms, root architecture, nutrient sensing, priming effect, mycorrhiza

OPEN ACCESS

Edited by:
Davide Bulgarelli, University of Dundee, United Kingdom

Reviewed by:
Tanja Mimmo, Free University of Bozen-Bolzano, Italy
Ulrike Mathesius, Australian National University, Australia
Feth-el-Zahar Haichar, Microbial Ecology, France

****Correspondence:***
Alberto Canarini
alberto.canarini@univie.ac.at

Specialty section:
This article was submitted to Plant Microbe Interactions, a section of the journal Frontiers in Plant Science

Received: *01 September 2018*
Accepted: *29 January 2019*
Published: *21 February 2019*

Citation:
Canarini A, Kaiser C, Merchant A, Richter A and Wanek W (2019) Root Exudation of Primary Metabolites: Mechanisms and Their Roles in Plant Responses to Environmental Stimuli. Front. Plant Sci. 10:157. doi: 10.3389/fpls.2019.00157

INTRODUCTION

The process of carbon (C) allocation and its adaptability is vitally important for plants to successfully respond to changing environmental conditions. Indeed, maximizing the trade-offs between investments and returns in terms of energy, water, C and nutrients will ultimately determine a plant's growth, survival, and interaction with its microbiota. External stresses such as competition, nutrient, and/or water limitation cause a series of responses in plants that modify C allocation to maximize the gain of limiting resources. A plethora of research has shown that plant belowground C allocation is tightly connected to water and nutrient cycles (Cheng et al., 2010; McCormack et al., 2015; Gill and Finzi, 2016; Ledo et al., 2018). Yet, a major component of belowground C allocation, namely the process of root exudation, remains poorly understood. It remains unclear why and how plants invest up to 20–40% of their photosynthetically fixed C in root exudates (Badri and Vivanco, 2009). Current ecological theories link root exudation to a benefit for plants *via* stimulation of beneficial micro-organisms (e.g., symbionts), promoting nutrient acquisition and enabling recognition between self-roots and neighbor-roots (Ortíz-Castro et al., 2009; Dijkstra et al., 2013; Yin et al., 2013; Depuydt, 2014; Mommer et al., 2016; Meier et al., 2017). However, while some root exudates, such as bioactive secondary compounds, are actively exuded from roots through energy-consuming primary or secondary active transporters (Sasse et al., 2018), the majority of them are represented by primary metabolites (mainly sugars, amino acids, and organic acids) in which many studies suggest to be passively lost from the root at the meristematic root apex (McCully and Canny, 1985; Darwent et al., 2003; Jones et al., 2009). In this context, several fundamental questions emerge:

1. What is the mechanism driving root exudation of primary metabolites?
2. Do plants have control over this process through adjustments in plant source-sink dynamics and efflux carrier expression and what are the consequences for root growth?
3. Can plants sense the concentrations of exuded and/or soil-borne metabolites?
4. Are these metabolites somehow involved in nutrient foraging through root exudation?

In this manuscript, we propose a conceptual framework built upon recent advances in different disciplines of ecology and biology linking plants with the soil environment. Here, we focus on primary metabolites that are exuded to the soil (sugars, amino acids, and organic acids) and for which specific concentration gradients influence their root exudation. The transient concentrations of these metabolites in the root tip serve as a cue for environmental sensing by plants and signaling between roots and shoots to modify root growth and carbon allocation. Our framework suggests that root exudates are used by the plant to complement the function of nutrient transporters in sensing nutrient availability and in signaling nutrient supply relative to demand. This process therefore optimizes root growth to facilitate effective nutrient foraging and possibly to sense competing neighbors. Also, given that a vast proportion of root exudation is driven by diffusion, soil micro-organisms will play an important role in driving concentration gradients outside the root tip, thus affecting exudation rates. We will utilize examples from studies on root exudation and plant nutrient acquisition strategies to support our framework and then analyze ecosystem scale impacts to highlight the relevance of the proposed mechanism in contributing to soil organic matter decomposition and CO_2 emissions, plant community assemblage processes, and plant productivity.

FACILITATED DIFFUSION-DRIVEN ROOT EXUDATION AND THE ROLE OF MICRO-ORGANISMS

The majority of root exudation is localized at the root tip (McCully and Canny, 1985; Jaeger et al., 1999; Doan et al., 2017; Sasse et al., 2018). The root tip is the first plant part to explore new soil environment and plays a crucial role in root responses to environmental stimuli. We will now illustrate how primary metabolites can be released from the root tip and how microbes interact with this process. While this manuscript will cover primary metabolites, it is important to highlight that roots also exude a wide range of secondary metabolites and further release high molecular weight compounds into the soil through rhizodeposition, most importantly root border cells and mucilage. These types of rhizodeposits can serve important functions in the soil. For example, they represent an important nutrient source for rhizosphere microbes and influence root-microbe and root-symbiont relations (for example, Hawes et al., 2002, 2016; el Zahar Haichar et al., 2014; Ahmed et al., 2018).

Release of Primary Metabolites at the Root Tip

Root exudation is a complex phenomenon encompassing processes that drive C transport to roots and exudation from roots to soil. The long distance transport of C produced in source organs takes place in the phloem, through the widely accepted Munch's pressure-driven mechanism of phloem flow (Münch, 1930). According to this mechanism, phloem metabolites are transported by a difference in turgor between sink and source organs generated by concentration gradients, which are determined by source-sink activities (De Schepper et al., 2013). Recent experiments support this hypothesis (Knoblauch et al., 2016) and have shed light on how metabolites are unloaded from the phloem to the actively growing root tip (Ross-Elliott et al., 2017), knowledge which is essential to understand root exudation. Specifically, Ross-Elliott et al. (2017) showed that in *Arabidopsis,* phloem unloading occurs through plasmodesmata in a convective way (combination of mass flow and diffusion). During unloading, low-molecular-weight solutes and proteins are diverted into the phloem-pole pericycle, a tissue connected to the protophloem by a unique class of "funnel plasmodesmata" (**Figure 1**). While proteins are released in discrete pulses (referred to as "batch unloading") and remain restricted to the phloem-pole pericycle, low-molecular-weight organic solutes are unloaded without

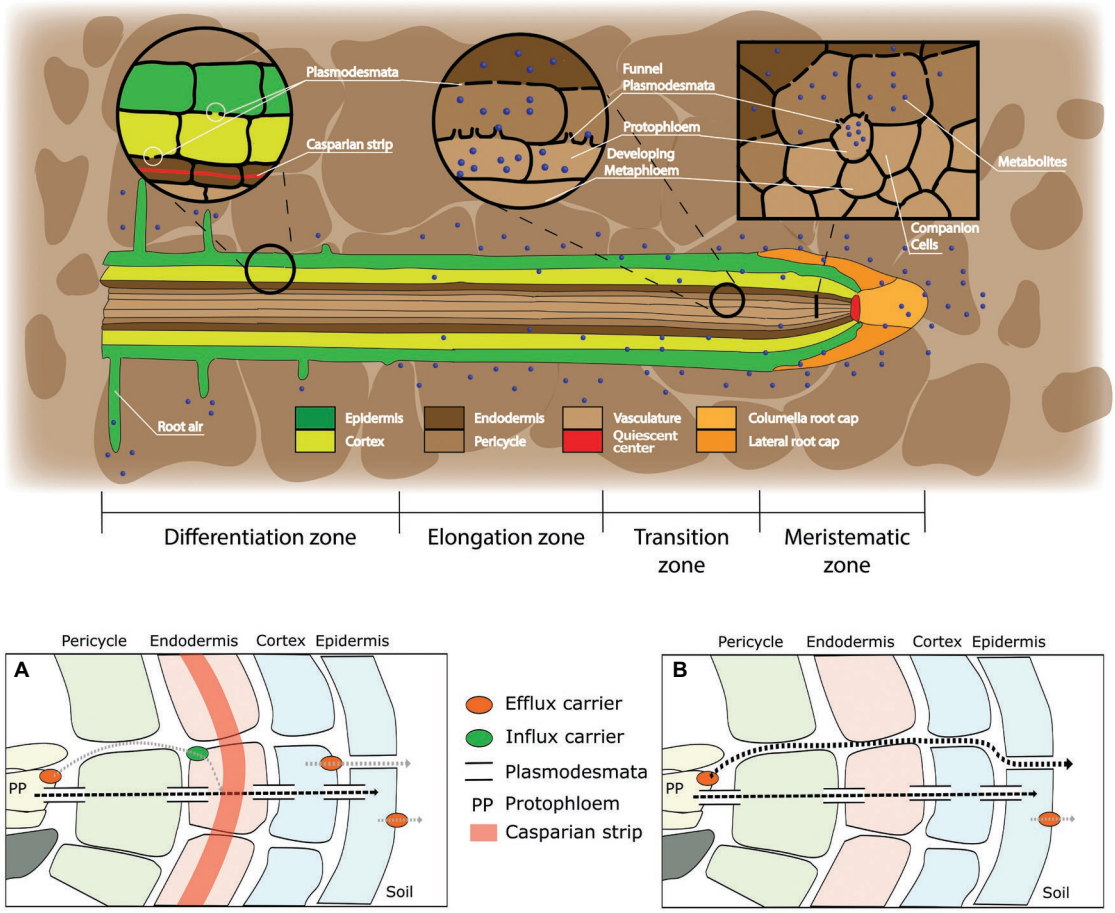

FIGURE 1 | Root structure and areas of root exudation. The upper figure represents the longitudinal section of a root. Tissues are indicated in different colors for the different zones of the root (listed at the bottom). The two circles focus on two distinct zones, a differentiated vs. an undifferentiated area, to show the presence of a Casparian strip and low abundance of plasmodesmata in the differentiated area (left circle), and the presence of funnel plasmodesmata in the undifferentiated area (right circle). The square represents a cross section close to the meristematic area where root exudation is the highest. The lower figures represent a schematic representation of solute movement sites from phloem unloading to the soil environment, either in the differentiation zone **(A)** or in the undifferentiated root tip **(B)**. **(A)** Solutes move both through the symplastic and apoplastic pathways, but then they are re-uptaken into the cytoplasm as the Casparian strip limits the apoplastic pathway. Only the cortex and epidermis are responsible for the flux of metabolites into the apoplast and consecutively into the soil (root exudation). Cortex and epidermis represents the major control point for root exudation. **(B)** At the phloem unloading site, both symplastic and apoplastic pathways are used. Because of the lack of a Casparian strip solutes can move out of the root (root exudation) through both the apoplastic and the symplastic pathway.

restrictions and move out of the phloem-pole pericycle. The discovery made by Ross-Elliott et al. (2017) is very important in connection to root exudation at the root tip. Indeed, they demonstrate that this area is the principal route for all solutes to be unloaded and that they will move toward the surrounding cells through diffusion (Ross-Elliott et al., 2017) because of the high degree of plasmodesmatal connections in this area (**Figure 1**; Rutschow et al., 2011).

Movement of Primary Metabolites Outside the Root Tip

While metabolites can move quite freely through the symplastic pathway, in order to be excreted to the soil environment, they need to pass through at least one plasma membrane to reach the apoplast. The plasma membrane is permeable to gas and to small molecules (such as urea or glycerol), while it is virtually impermeable against larger, uncharged polar molecules (e.g., glucose) and against all charged molecules including ions (Yang and Hinner, 2015). Therefore, these molecules only transit the plasma membranes through specific transmembrane proteins, which form small pores through the lipid bilayer, allowing polar or charged molecules to cross the membrane without interacting with the hydrophobic fatty acid chains of the membrane phospholipids (Sasse et al., 2018).

It was recently discovered that the efflux of sugars, organic acids, and amino acids is mediated through specific efflux carriers and channels that may allow a fine tuning of the exudation flux through up/downregulation of their gene expression or at the level of post-translational modification (Badri et al., 2008). Some of these efflux transporters of primary metabolites

have been characterized, e.g., for amino acids [UMAMIT transporters (Okumoto and Pilot, 2011; Moe, 2013; Besnard et al., 2016; Dinkeloo et al., 2017), CAT transporters (Yang et al., 2010), GDU transporters (Pratelli et al., 2010)], sugars [probably belonging to the SWEET transporter family (Williams et al., 2000; Chen et al., 2015; Manck-Götzenberger and Requena, 2016)], and organic acids [ALMT/malate and MATE/citrate transporters (Meyer et al., 2010; Mora-Macías et al., 2017)]. Most of these transporters are not primary or secondary active and therefore are not directly coupled to ATP hydrolysis or to ATP-dependent H^+ pumps and H^+ antiports (see **Figure 2**). The exception to this is the ATP-dependent ABC transporters

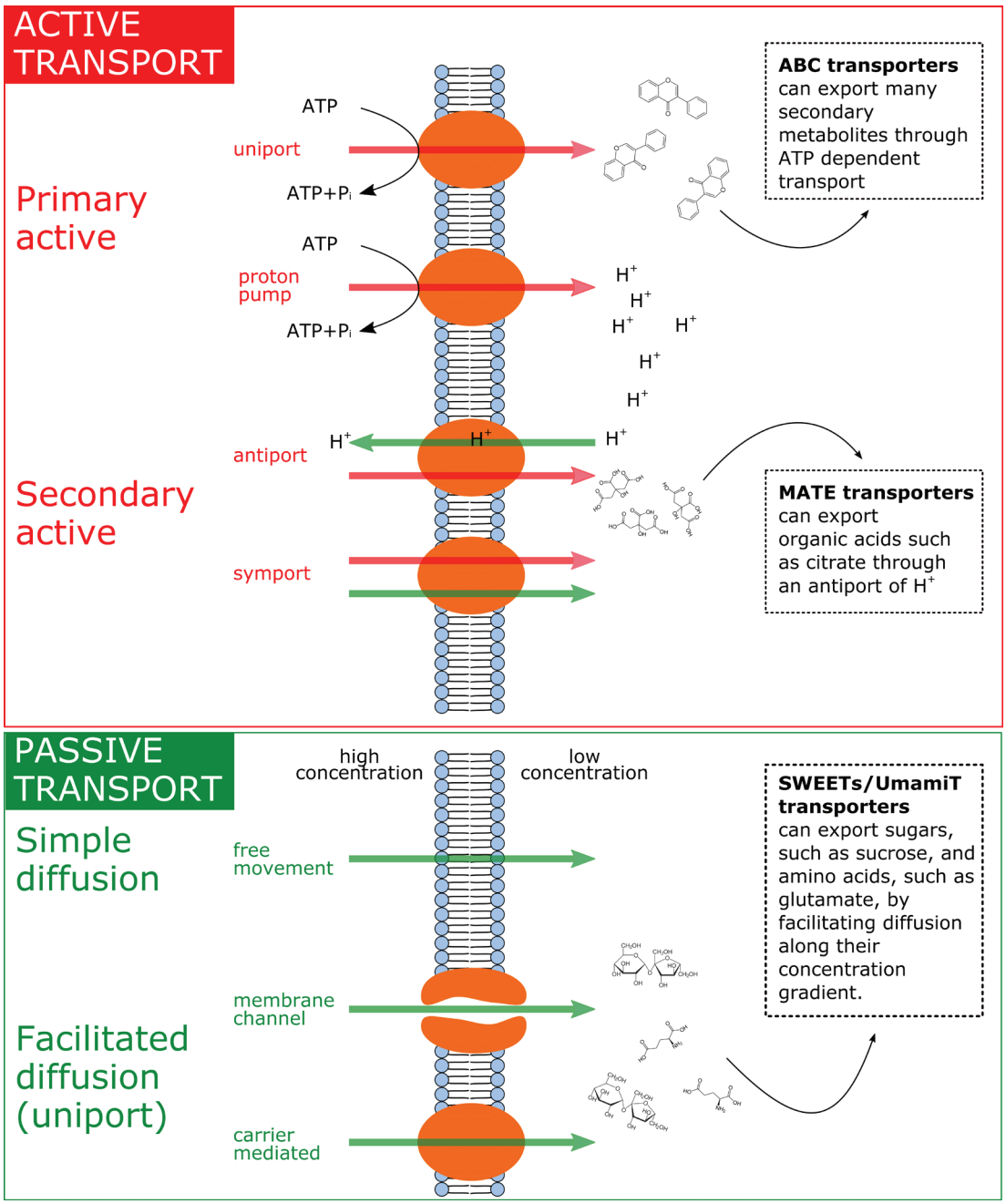

FIGURE 2 | Summary of the main exudation mechanisms through the plasmamembrane at the root tip. The top panel represents active transport mechanisms, either primary active (direct consumption of ATP) or secondary active (e.g. coupled to H^+ pumps that actively consume ATP). The bottom panel represents passive transport mechanisms, which allow diffusion following electrochemical gradients. Red arrows represent movement of solutes against their electrochemical gradient, while green arrows represent movement following their electrochemical gradient. On the right side of the figure, examples of membrane transporters allowing movement of primary metabolites are provided.

for secondary compounds (Badri et al., 2009) and MATE/citrate transporters that possess H^+-coupled antiport activity (Meyer et al., 2010). All other transporters were shown not to be coupled to ATP hydrolysis or to H^+ cotransport. The common denominator of most of the primary metabolite transporters is that they are substrate-specific facilitators, facilitating the diffusion of primary metabolites across the plasma membrane *via* transmembrane carriers along the concentration gradient, i.e., from high intracellular to low extracellular concentrations. The exact genes governing the synthesis and abundance of the UMAMIT and SWEET transporters involved in root amino acid and sugar exudation have not yet been identified, and relatively little is currently known regarding the plant demand for nutrients and environmental and edaphic factors that regulate their gene transcription. Only recently, pathogen-driven activation of SWEET expression was shown to increase glucose efflux into the root apoplast (Chen et al., 2015), and Al^{3+} toxicity or P deficiency triggers exudation of malate by ALMT upregulation in roots (Ma et al., 2001; Kochian et al., 2005; Mora-Macias et al., 2017). Identifying the responsible efflux carriers for the most abundant primary metabolite components of the exudates at the root-soil interface will revolutionize our understanding of the regulation of root exudation (Sasse et al., 2018).

Once metabolites have moved out of the phloem cell plasma membrane, and they may follow the apoplastic transport pathway. Indeed, a recent study suggests that in immature wheat roots, carbon containing compounds would circulate from the stele to the cortex through an apoplastic pathway and then be used by microbes in the soil environment (Vidal et al., 2018). In the apoplast, the diffusion process would regulate the flux from roots to the soil environment, without any obstacle represented by plasma membranes. This could be very important at the root tip. Indeed, while at distance from the meristem, in the differentiation zone, endodermis cells develop a barrier against apoplastic diffusion (Naseer et al., 2012; Somssich et al., 2016), the meristem lacks an apoplastic barrier ("Casparian strip"; **Figure 1**). Also, epidermis cell walls in the mature area of root tip of Arabidopsis showed more than 10 times slower apoplastic diffusion rates as compared to the elongation zone (Kramer et al., 2007). It would therefore be interesting to investigate the presence of a root hot spot, where carbon containing compounds are released to the apoplast (**Figure 1**). If indeed a hot spot could be identified close to the area in which phloem unloading occurs, this would indicate that the apoplastic pathway is a major contributor to root exudation and establishes a close link between the phloem and the soil environment. Indications of an apoplastic pathway are provided by studies showing that bacteria mostly distribute along the axial grooves in between neighboring root epidermal cells (Watt et al., 2006; Schmidt et al., 2018). However, these results could not exclude a direct loss from epidermal cells (Jones et al., 2009) or could indicate that grooves simply represent areas of physical protection for micro-organisms (Schmidt et al., 2018). Indeed, the specific pathway by which solutes move from the unloading area to the external medium is still matter of debate, and a switch from symplastic to apoplastic pathways with root development was also shown (Godt and Roitsch, 2006). More studies on the spatial and temporal dynamics of solute fluxes at the root tip are therefore necessary to improve our understanding of the plant control over the root exudation process.

From reasons outlined above, we therefore postulate that the anatomy of the root tip promotes the diffusion of metabolites (or offer less resistance) from the root apex to the external soil environment and thereby ultimately determines the concentration gradient-dependent outward flux of solutes, i.e., the rate of root exudation. Root tip exudation will be highly dependent on diffusion rates and therefore on concentration gradients between rhizodermal cells and the soil environment. This process will ultimately draw metabolites from the phloem and indicate a close coupling between photosynthetic activity and root exudation, which is strongly influenced by the consumption and transformation of metabolites by microbes in the rhizosphere. This hypothesis is supported by empirical studies showing: (1) localized exudation at the root tip level (McCully and Canny, 1985; Jaeger et al., 1999; Doan et al., 2017); (2) correlation between exudates and root growth (Lucas García et al., 2001); (3) coupling of exudation and photosynthesis (Kuzyakov et al., 2003; Mencuccini and Hölttä, 2010); and (4) reduction of root exudation when plants are allocating resources to reproductive organs instead of root growth (Prikryl and Vancura, 1980; Badri and Vivanco, 2009).

However, it is important to acknowledge two facts. First, many compounds are also exuded by active transport against the concentration gradient (citrate and secondary compounds). Second, while facilitated diffusion-driven root exudation is "passive" in its nature following the concentration gradient from high cytoplasmic to low external concentrations in the soil solution (because diffusion does not require plants to spend energy), plants can still control this process in different ways:

1. Induction/repression of gene expression and post-translational modification of efflux carriers for sugars, amino acids, and organic acids;
2. Possible re-uptake of exuded organic solutes and inorganic nutrients through uptake transporters and their regulation as in (1);
3. Changes in source/sink dynamics including processes at phloem loading sites, import of solutes into root cells and compartmentalization within root epidermal cells (vacuolar loading/sequestration of solutes), and changes in meristematic activity (e.g., root meristem exhaustion).

The above-mentioned mechanisms come at an energy cost for the plant, through secondary active re-uptake of metabolites and by energy-intensive biosynthesis of the efflux and influx carrier proteins. Therefore, we suggest to avoid the use of "passive exudation" to define the root exudation process.

The Role of Micro-organisms in Facilitated-Diffusion Driven Root Exudation

Based on the diffusive nature of the exudation process as described above, we also propose that microbial utilization and metabolism play a pivotal role in modulating concentration

gradients right outside root tips, thereby constituting a soil sink and promoting root exudation. Indeed, it was found that when micro-organisms were present in plant growth solution, exudation was enhanced as compared to axenic solutions (Biondini et al., 1988; Jones and Darrah, 1993; Meharg and Killham, 1995; Groleau-Renaud et al., 2000; Phillips et al., 2004; Vranova et al., 2013; Pii et al., 2015b). Some studies concluded that concentration gradients drew solutes out of the roots, although re-absorption of metabolites has also been indicated (Jones and Darrah, 1993; Warren, 2015, 2016). Enhancement of exudation was also observed in the absence of micro-organisms but through reduction of the external concentration in axenic solution by using pure water to collect exudates (Groleau-Renaud et al., 2000; Valentinuzzi et al., 2015) or by simulating the effect of removal of metabolites by regularly changing the growth solution. Additionally, the presence of micro-organisms in the growth solution altered plant C allocation to roots and root/shoot ratios (Jones and Darrah, 1993; Groleau-Renaud et al., 2000). In a more recent experiment, activated charcoal was used to evaluate the removal of exudates from the growth medium, showing that the absence of root exudates from the root surroundings caused a re-programming of the whole root system architecture in *Arabidopsis* (Caffaro et al., 2011). It is known that there is a tight relationship between root exudates and microbial diversity (Eisenhauer et al., 2017), but it is still unknown at what level they influence each other. Microbial diversity is affected by exuded primary metabolites (Shi et al., 2011; Steinauer et al., 2016), and at the same time, it affects specific concentration gradients outside the root through preferential microbial utilization of plant exudates. Also, soil microbes can release compounds such as 2,4-diacetylphloroglucinol and zearalenone that stimulate root exudation of primary metabolites, such as amino acids (Phillips et al., 2004). It was suggested that current models depicting C pools/fluxes and vegetation dynamics are mainly structured as "source driven" models. It was argued that the control of environmental cues (e.g., temperature, water, and nutrient availability) on meristematic activity (sink capacity) are pivotal because they mostly become limiting to plant growth before the source capacity represented by photosynthesis responds (Fatichi et al., 2014; Körner, 2015). While source-sink dynamics are increasingly recognized as fundamental in understanding plant C allocation, micro-organisms should also be considered as a strong sink of plant photosynthates, thereby promoting root exudation (Farrar and Jones, 2000; Savage et al., 2016).

Interactions Between Mycorrhizal Associations and Root Exudates

While our knowledge on both the function and magnitude of root system architecture, nutrient sensing, and root exudation has significantly increased, it remains unclear how mycorrhizae are involved in these processes. Indeed most laboratory studies on root exudation did not include mycorrhizal associations, while mycorrhizal fungi colonize the roots of about 90% of all land plant species. The establishment of mycorrhizal association is mediated by controlled exudation and sensing of specific secondary metabolites by the roots (Parniske, 2008; Bonfante and Requena, 2011; Martin et al., 2017). However, once the association is established, the major flow of C from plants to the fungus consists of recently photoassimilated sugars and fatty acids transferred across the symbiotic interface. Whether or not this major diversion of belowground C flow alters root exudation rates of plants qualitatively or quantitatively is not known.

In the colonization phase, plant roots communicate in a complex way with their potential mycorrhizal partners *via* exchange of chemical signals. Different mechanisms exist for arbuscular mycorrhizae (AM), which are the most widespread form of mycorrhizal association (formed by 74% of all vascular plant species), and ectomycorrhizal (EM) symbiosis, which is dominant in temperate and boreal forest ecosystems (for more information, see, for example, Parniske, 2008; Smith and Read, 2008; Brundrett, 2009; Smith and Smith, 2011; Gutjahr and Parniske, 2013). In either case, once the mycorrhizal association has been formed, mycorrhizal fungi receive a substantial fraction of the plant belowground C flux as their sole energy and C source while delivering nutrients to the plant in return (Van Der Heijden et al., 2015). How and where this C is transferred from plant roots to their mycorrhizal partners differs strongly between different types of mycorrhizal association. In the AM symbiosis, fungal hyphae grow and form arbuscules inside cells of the root cortex along the entire length of plant fine roots. A substantial amount of recently assimilated C is diverted from the phloem and allocated into intraradical hyphae and arbuscules and further into the fungal extraradical hyphal network (Drigo et al., 2010; Kaiser et al., 2015; Paterson et al., 2016). Whether this pathway, which represents a substantial drawing of C "upstream" of the root tip, consequently reduces root exudations at the tip is not known. It has been shown, however, that AM colonization increases plant photosynthetic rates (Grimoldi et al., 2006; Johnson et al., 2015), which may reflect increased demand from increased belowground C transfer to the fungi. Also AM colonized plants show increased sugar transport to roots. It has therefore been suggested that this increased sugar flux may cause lateral root formation (as discussed in "The role of organic acids and sugars in P acquisition strategies" section for P sensing), which is typical of AM colonized plants (Fusconi, 2014). Ectomycorrhizal fungal hyphae, in contrast, do not grow inside root cells but form a tight mantle completely covering the root tips, with fungal hyphae growing in between the outer layers of root epidermal cells, forming the Hartig Net (Smith and Read, 2008). Within the Hartig Net, plant and fungal cells are separated by an apoplastic space that serves as an exchange zone for C released by plant cells and nutrients released by the fungus (Nehls, 2008). This highlights the potential of plant cells to use the apoplastic space in the root cortex as exudation zone, as opposed to direct exudation from epidermal cells (Jones et al., 2009). In contrast to AM and other endomycorrhizal associations, EM may effectively reduce or even stop root exudates from being transferred into the soil due to the formation of the tight hyphal mantle "sealing" the root tip. A recent study has shown that exudation rates

of AM vs. EM-colonized roots only changed when plants were drought stressed (Liese et al., 2018). To what extent EM may affect root exudations compared to AM or if part of the plant-derived C is exuded from the fungal cells at the outside of the hyphal mantle is still not known.

Plant-derived C transferred to the plant's mycorrhizal partner is quickly transported into the hyphal network extending into the soil. *In vitro* studies have shown hyphal exudation of carbohydrates and amino acids (Bharadwaj et al., 2012; Zhang et al., 2018). Therefore, it has been hypothesized that fungal hyphae exude this labile C at root-distant places into the soil, where it may stimulate decomposition of organic matter by free-living soil saprotrophs and consequently increases nutrient availability (Jansa et al., 2013; Kaiser et al., 2015; Meier et al., 2015; Paterson et al., 2016). In other words, hyphal exudation could trigger (analogous to the rhizosphere priming effect) a hyphosphere priming effect. Indications for hyphosphere priming and actual transfer of recently photoassimilated C *via* mycorrhizal hyphae to soil bacteria has been shown for AM associations (Toljander et al., 2007; Drigo et al., 2010; Cheng et al., 2012; Kaiser et al., 2015; Paterson et al., 2016) and hyphal-bacterial transfer of plant-derived C recently also for EM associations (Gorka et al., 2019).

Despite the overwhelming presence of mycorrhiza in terrestrial ecosystems, they are neglected in most root exudate research. One reason for them being overlooked may be attributed to common model plants, like *Arabidopsis*, belonging to the 5–10% of vascular plant species that do not form mycorrhizal associations. Studies that integrate mycorrhizae into "traditional" rhizosphere research are urgently needed to close this research gap and improve our understanding of the interactions between mycorrhiza, root exudation, and rhizospheric processes.

SENSING AND SIGNALING OF NUTRIENTS BY CONCENTRATION GRADIENTS

It is not a new concept that root exudates are used to sense and interact with the abiotic and biotic components of the soil environment (Mommer et al., 2016; Martin et al., 2017) and to aid in nutrient acquisition (Dakora and Phillips, 2002; Ström et al., 2002). However, studies of such interactions often addressed only specific compounds (e.g., secondary metabolites) and therefore leave unexplained possible functions of the largest proportion of root exudates, i.e., primary metabolites. We propose that this efflux from the actively growing root cells regulates the temporal concentrations of primary metabolites inside the root tip, many of which have the double function of metabolite and signaling molecule (Häusler et al., 2014). Any changes that modify the influx and/or the efflux of metabolites at the root tip can have cascading effects on the root system architecture, with the latter being defined as the spatial configuration of the root system. Root system architecture is a key factor in determining the ability of a plant to respond to nutrient hotspots, thereby maximizing the acquisition of soil resources (Khan et al., 2016). It is well known that root architecture is genetically determined, but that the chemical and physical characteristics of the soil environment ultimately shape root growth, especially in response to soil nutrients (Lynch, 1995; López-Bucio et al., 2003). Recent advancements in studies of nutrient uptake and root system architecture responses to nutrient-rich patches have strongly advanced our understanding of the fine tuning between roots and shoots to control root growth. Here, we highlight examples of how common metabolites present in root exudates can be sensed by the root to modify root system architecture responses to environmental cues. We place particular focus on the two main nutrients limiting plant growth: nitrogen (N) and phosphorus (P).

The Role of Amino Acids in N Acquisition Strategies

Plants are highly flexible in adapting to changing conditions of soil N availability (Giehl and von Wirén, 2014), which implies that they can sense N in the soil. The main examples of this flexibility come from studies on nitrate (NO_3^-) uptake and sensing. Nitrate possesses the strongest signaling effects on root system architecture, which seems to be even more important than its nutritional function (Sun et al., 2017). For example, under low NO_3^- supply, plants tend to adopt a "foraging strategy" with lateral root proliferation to enhance nutrient access. Root responses to NO_3^- are mediated by a family of transporters (mainly NRT2 and NRT1), which can modulate the transport of auxin (and other plant hormones and signal molecules) to regulate the development of root system architecture. The regulatory network connecting nitrate transporters to changes in root system architecture is complex in nature due to the multi-stage root branching process, the dependence on nitrate levels in soil (high or low) and sometimes demonstrating antagonism between signaling pathways. We refer the reader to more in-depth reviews on this topic (see, Sun et al., 2017; Forde, 2014). While in high fertility soil microsites, NO_3^- tends to dominate the available soil N pool, and in low fertility soil microsites, amino acids become dominant (Schimel and Bennett, 2004; Rothstein, 2009).

Amino acids are one of the main components of root exudates, are omnipresent in the soil environment at low concentrations, and might therefore represent important triggers of plant responses to changing N availability in soil. Indeed, it was demonstrated that amino acids are the main indicator of the N status of plants, which is important for the regulation of plant N uptake (Paľove-Balang and Mistrík, 2002; Nacry et al., 2013; Forde, 2014; Kellermeier et al., 2014; Gent and Forde, 2017). For example, it was found that amino acid export from the leaf to the phloem depends on the N level belowground (Caputo and Barneix, 1997). Also, in a split-plot experiment, N-deprived roots received significantly lower amino acid concentrations with altered composition from the phloem compared to N-supplied roots, which had similar amino acid composition in the phloem flow compared to the control (Tillard et al., 1998). Furthermore, amino acids represent a potential source of N for plants (Forsum et al., 2008; Jämtgård et al., 2008; Näsholm et al., 2009; Inselsbacher and Näsholm, 2012), and recent studies have demonstrated that amino acids

play an important role in shaping root system architecture and nutrient foraging. For example, plants shut down nitrate uptake when amino acids are present in the growth medium at relatively high concentrations (Padgett and Leonard, 1996; Aslam et al., 2001; Henry and Jefferies, 2003; Dluzniewska et al., 2006). More specifically, many amino acids can induce repression of NRT2.1 gene expression, which is an important transporter and sensor of nitrate (Nazoa et al., 2003). On the other hand, NO_3^- was shown to have no effect on the root uptake of the amino acid glycine (Gioseffi et al., 2012).

Among the 20 proteinogenic amino acids, the amino acid L-glutamate has been proven to cause the most intense responses in root system architecture in *Arabidopsis thaliana* (Forde, 2014). However, many other amino acids can cause similar responses in root system architecture. It has been suggested that it is not a single amino acid, but their overall concentration regulates these cell responses (Padgett and Leonard, 1996; Aslam et al., 2001). Glutamate acts in a way similar to auxin (indole-3-acetic acid, which is known to influence root system architecture and many other aspects of plant biology). These compounds, added exogenously to plant cells, elicit rapid membrane depolarization and a transient increase in $[Ca^{2+}]_{cytosol}$ (Zimmermann et al., 1999; Dennison and Spalding, 2000; Ni et al., 2016). Therefore, glutamate could create an electrical signal similar to what is observed in synaptic transmission processes in mammals (Baluška and Mancuso, 2013). While auxin can cause responses in roots at very low concentrations, the glutamate response requires higher concentrations of about 10^{-5} M compared to 10^{-11} M of auxin (Evans et al., 1994). The difference between the two molecules may lay in the fact that glutamate fulfills the dual role of primary metabolite and signal molecule, and physiological concentrations have to be maintained for metabolic activity in cells (Forde and Lea, 2007). Glutamate is also one of the most abundant amino acids in soils in the pool of dissolved organic N (Paynel et al., 2001). While in soil solution, glutamate concentrations are lower than 10 μM (Friedel and Scheller, 2002; Jones et al., 2005), around the root tip and in areas close to decomposing organic residues they are expected to be several-fold higher (Walch-Liu et al., 2006b). In agar plate experiments, locally high glutamate concentrations slowed primary root growth and encouraged root branching behind the primary root tip (Walch-Liu et al., 2006a). It has been hypothesized that this localized increase in root branching at the root tip would lead to increased precision of root placement within an organic N-rich patch (Walch-Liu et al., 2006a; Forde and Lea, 2007), which would represent a foraging response particularly important in low-fertility soils of temperate regions where rates of N mineralization may be low (Schimel and Bennett, 2004; Rothstein, 2009; Forde, 2014). Indeed, glutamate possesses all the characteristics to make it an important signaling molecule. First, plants possess effective mechanisms for glutamate re-absorption. Six members of the Arabidopsis AAP family (AAP1–AAP6) have been shown to catalyze the low affinity root uptake of a broad range of amino acids, including glutamate (Fischer et al., 2002), and the LHT1 gene appears to encode a high-affinity glutamate influx system (Hirner et al., 2006). Also, a ubiquitous family of receptors, termed glutamate receptor-like genes (GLR) (Teardo et al., 2011; Tapken et al., 2013; Vincill et al., 2013), are involved in amino acid sensing throughout the whole plant (Forde, 2014). The 20 GLR genes in *Arabidopsis* are differentially expressed in the plant at least at the mRNA level, and in roots, all 20 have been found to be expressed (Chiu et al., 2002; Roy et al., 2008). Studies on GLR knockout mutants have shown that in rice, the OsGLR3.1 gene positively regulates cell proliferation in the root apical meristem (Li et al., 2006). A knockout mutation of AtGLR3.2 and AtGLR3.4 genes affected lateral root primordia, suggesting a possible negative regulation of lateral root initiation by GLR (Vincill et al., 2013). Interestingly, expression analysis of the AtGLR3.2 and AtGLR3.4 proteins revealed that in the root they are primarily targeted to the phloem, particularly to the distal parts of mature phloem cells, in the vicinity of the sieve plates (Vincill et al., 2013). At least some members of the GLR receptor family that are expressed in roots are now known to act as amino-acid-gated Ca^{2+} channels with broad ligand specificity (Vincill et al., 2012). Moreover, we mentioned that amino acid loading into the phloem depends on the plant N level (Caputo and Barneix, 1997), and glutamate is commonly found in phloem sap. Thus, it was hypothesized that glutamate sent from shoots could be the signal to communicate plant N status to the roots (Forde and Lea, 2007). Therefore, given that glutamate can be sensed in the root tip phloem (Vincill et al., 2013) and translated into a signal affecting the root system architecture (Walch-Liu et al., 2006a; Forde and Lea, 2007), any change in influx or efflux of glutamate at the root tip will likely affect root development (**Figure 3**). While this highlights the specificity in the glutamate response, other amino acids have been shown to trigger changes in root system architecture, such as D-serine (Forsum, 2016). Also, most of the studies were carried out on *Arabidopsis*, while other plant species have shown different responses to glutamate (Domínguez-May et al., 2013; Kan et al., 2017). Our understanding of the effects of different amino acids on root system architecture and the mechanisms underlying different plant responses to glutamate therefore remain incomplete.

In low fertility soils where amino acids are the dominant form of N (Rothstein, 2009), they may represent a major driver of root nutrient foraging strategies. However, in high fertility soils, inorganic forms of N dominate and it is unclear what role amino acids may play in nutrient foraging under such conditions. It was shown that exudation rates of sugars, amino acids (glycine), organic acids, and phenolics increased with inorganic N addition rates increasing from 0 to 160 mg N L^{-1} in hydroponics (Zhu et al., 2016). Uptake of different N forms by plant roots can also affect root exudation patterns as, for example, plant ammonium nutrition strongly promotes sugar exudation compared to nitrate-grown plants and switching plants from ammonium to nitrate nutrition in hydroponics rapidly downregulated sugar efflux by 30-fold (Mahmood et al., 2002). Therefore, plant N nutrition, either in organic or in inorganic

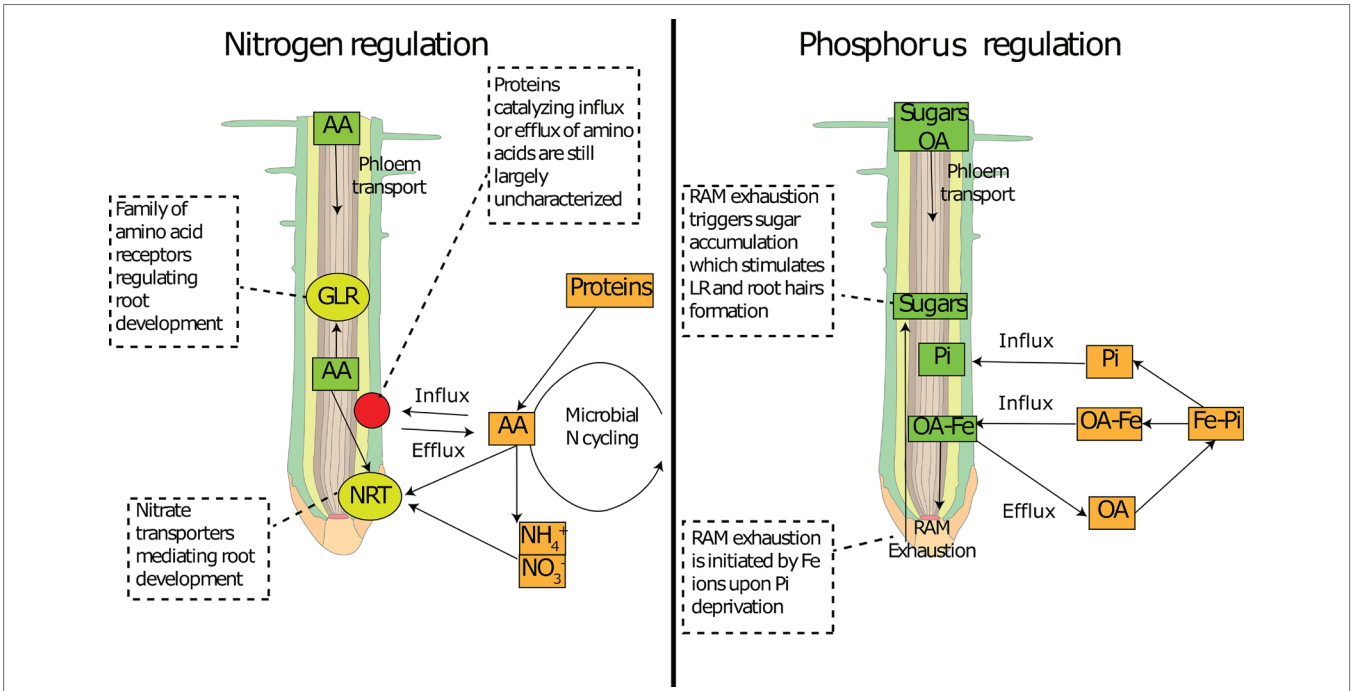

FIGURE 3 | Involvement of common metabolites in nutrient sensing at the root tip. Schematic representation of how common primary metabolites allows nutrient sensing at the root tip for nitrogen (left panel) and phosphorus (right panel). Amino acid concentration can be sensed by specific receptors (GLR) and can interfere with N transporter expression (NRT). Amino acid concentration inside the root tip depends on the delivery from the phloem and on root exudation, the latter of which depends on concentration gradients mediated by soil micro-organisms. Organic acids can deliver Fe to the root tip, which activates the RAM exhaustion and temporarily increases sugar concentrations. Sugars can be sensed at the root tip and activate changes in root architecture. AA: amino acids; OA: organic acids; Pi: inorganic phosphorus; RAM: root apical meristem; NRT: nitrate transporters; GLR: glutamate-like receptors.

form, by having a strong effect on root exudation patterns might interact with expression of N uptake carriers and root system architecture in a way that is currently difficult to predict.

The Role of Organic Acids and Sugars in P Acquisition Strategies

Root responses to P appear to play a major role in root system architecture compared to other nutrients (Kellermeier et al., 2014). Phosphorus deficiency causes drastic changes in root system architecture, generally by increasing the number of root hairs and lateral roots to increase the root surface area and thereby acquisition of P, which has very limited mobility in soil (Nadira et al., 2016). For example, many plants growing in extreme P limited environments have developed specialized root structures to release higher amounts of organic acids: the cluster roots or proteoid roots (Shane and Lambers, 2005; Lambers et al., 2006). Interestingly, the release of organic acids from cluster roots of Proteaceae and Fabaceae and also from roots of other plants is associated with young parts of the root system, such as the root apex (Shane and Lambers, 2005; Ryan et al., 2014). Rates of citrate efflux are the highest during the photoperiod, and no correlation with the activity of enzymes involved in citrate biosynthesis in roots was found (Watt and Evans, 1999). A primary requirement to initiate the root response is to establish root contact with areas of very low P. Contact of the root tip with a low-P_i medium results in the arrest of primary root growth, including reduced cell elongation, cell division, and meristematic activity, regardless of shoot P_i status (Chevalier et al., 2003; Ticconi and Abel, 2004; Svistoonoff et al., 2007). A recent study using mutants lacking a root cap revealed that while the root cap is responsible for about 20% of total P absorption in *Arabidopsis*, it is not involved in adaptations of root system architecture (Kanno et al., 2016). An important mechanism necessary for the root architecture response to P deficiency was found to be root exudation of malate (Mora-Macías et al., 2017). Indeed organic acids such as malate and citrate are important compounds exuded to mobilize inorganic P in soils (Carvalhais et al., 2011; Krishnapriya and Pandey, 2016; Lyu et al., 2016; Giles et al., 2017), solubilizing P bound to iron or aluminum (hydr)oxides (Otani et al., 1996). It was recently discovered that in response to abiotic stress, plant can control malate efflux anions channel (ALMT) which is regulated by anions and gamma-aminobutyric acid (GABA) at the root tip (Ramesh et al., 2015). The anion channels ALMT allow the diffusion of malate along their concentration gradients outside root cells (Gilliham and Tyerman, 2016). In addition, Mora-Macías et al. (2017) found that malate exudation is involved in the signaling of P deficiency. Malate is required for the accumulation of Fe in the apoplast of meristematic cells, triggering the differentiation of meristematic cells in response to Pi deprivation. This activates the root apical meristem exhaustion process, consisting in the loss of meristematic potential and arrest of cell proliferation, ultimately leading to

the inhibition of primary root growth and consequently lateral root proliferation. It was also shown that mutants that do not show this response to low P can restore the same P-limitation phenotype by exogenous application of malate in a concentration-dependent manner (Mora-Macías et al., 2017).

Application of exogenous carbohydrates can also initiate the same response (Karthikeyan et al., 2007), albeit with no effect on primary root growth (Hammond and White, 2011). This is interesting as sugars have been shown to be a crucial player in the root response to P-deficiency (Liu et al., 2005; Liu and Vance, 2010; Rouached et al., 2010) and are usually sensed intracellularly (Rolland et al., 2006). The external application implies either that roots can sense external sugar concentrations or that external gradients of organic molecules such as sugars affect internal concentrations either through secondary active uptake or by affecting exudation and efflux rates (by limiting their diffusion to the soil environment). The precise pathways through which sugars can activate the P starvation response is as yet unknown, although several pathways for sugar signaling at the whole plant level have been demonstrated where protein kinases are central in coordinating several of these responses (Hanson and Smeekens, 2009).

When local soil P_i concentrations are low, if malate efflux and re-uptake of Fe-malate are necessary to cause the arrest of meristematic activity in primary roots (Mora-Macías et al., 2017), we speculate that it is this response that triggers sugar accumulation (**Figure 3**). During root apical meristem exhaustion, meristematic cells undergo disruption of symplastic connections (probably due to callose deposition) and cell differentiation (Shishkova et al., 2008; Ogden et al., 2018), changes that would lead to decreased root exudation. Therefore, if sugar transport to the root tip is maintained and meristematic activity is curtailed (decreased loss through root exudation), it would cause a transient increase in sugar concentrations, which represents a potential signal molecule for root architecture. Sugar accumulation is often found in roots in response to P deficiency (Hammond and White, 2011), and the above proposed mechanism would also explain the effect of exogenous applications of sugars on root system architecture. This is mostly related to responses to local P deficiency, while systemic signaling of P homeostasis is likely to include more complex coordinated processes.

Role of Primary Metabolite Exudation in Nutrient Foraging and Plant-Microbe Interactions

A growing number of studies show that the root tip functions as control center for sensing external nutrient concentrations and translating this into an alteration of root system architecture (Desnos, 2008; Baluška et al., 2010; Péret et al., 2011; Baluška and Mancuso, 2013). The root tip is also the hot spot of root exudation, where amino acids, organic acids, and sugars represent the major chemical classes exuded. Each of these compounds can be sensed in the root by different mechanisms, and all have effects on the root system architecture in a concentration dependent manner, as described above (see **Figure 3**). In order to increase the cellular concentration in the root tip, changes need to occur either at the source level (phloem loading and transport) or at the sink level (phloem unloading, metabolism, exudation, and microbial consumption). These changes depend on the nutritional status of the plant and the soil environment. Therefore, the flow of root exudates could represent a key determinate of root growth and development, by affecting temporary concentrations of organic solutes at the root tip. Even though we know a great deal about the concentrations of solutes in whole roots, our knowledge of the spatial and temporal dynamics of root organic solutes, especially at the root tip, is highly limited.

More recent studies have appointed the transition zone (**Figure 1**) as an area acting as the command center for root responses to the environment (Baluška et al., 2010; Baluška and Mancuso, 2013). Baluška and Mancuso (2013) showed that cells in the transition zone are highly active in terms of cytoskeletal rearrangements, endocytosis and endocytic vesicle recycling, as well as in electrical activities. In addition, we previously highlighted that two members of the GLR family are now known to be preferentially expressed in the root tip phloem where they have a role in regulating lateral root initiation (Vincill et al., 2013) and where they may affect root growth *via* electrical signals modulating phloem loading or transport (Baluška and Mancuso, 2013). This indicates that the root exudation process takes place in a highly restricted root area to translate environmental cues into signals for root system development. It is therefore tempting to speculate that any changes in relative concentration gradients of metabolites at the root tip caused by changes of either influx (phloem) and/or efflux (exudates) will signal the transition zone, which could then act as a command center for root growth and architecture.

Soil micro-organisms also add a great complexity to our understanding of the involvement of primary metabolites in plant nutrient foraging. Indeed, micro-organisms quickly consume these compounds, making it practically impossible to collect pure root exudates in real soil environments (Oburger and Jones, 2018). Soil microbes can also affect the root exudation process. We previously highlighted that soil microbes can release secondary compounds to stimulate root amino acid exudation (Phillips et al., 2004), while specific soil microbes were shown to have the ability to modify the metabolite composition of the whole plant (Curzi et al., 2008; Fernandez et al., 2012). This highlights a bi-directional influence between roots and their rhizosphere microbial communities. At the same time, changes in the temporal concentration of primary metabolites at the root tip can affect root system architecture, as discussed above. Therefore, plant strategies for nutrient foraging may be strongly affected by the plant-associated microbial population (Pii et al., 2015a; Alegria Terrazas et al., 2016). Indeed, root-microbe interactions have been shown to affect whole plant growth, particularly *via* effects of rhizosphere microbes on root system architecture and consequent effects on plant aboveground performance (Verbon and Liberman, 2016). In recent years, many studies have discovered plant systemic regulation networks of nutrient sensing that involves cross communications between the below and aboveground

part of the plant (Reid et al., 2011a,b; Ohkubo et al., 2017; Tsikou et al., 2018). Therefore, plant-microbe interactions at the root level may exert stronger effects than we think on the whole plant and on nutrient cycling. A recent study demonstrated that root exudation is linked as a functional trait to nutritional strategies (exploitative vs. conservative) of plants (Guyonnet et al., 2018), mostly explained by links to root traits (Guyonnet et al., 2018; Herz et al., 2018). Because a different rhizosphere microbiome develops depending on soil and plant type (Berg and Smalla, 2009), the specific plant-soil feedback can be variable. Yet, it is undeniable that the interplays between plant and soil microbes can shape an ecosystem because of the strong interactions between plant nutritional strategy (and therefore its root exudates) and the soil microbes (Teste et al., 2017).

IMPLICATIONS AT THE ECOSYSTEM SCALE

Decomposition of Organic Matter and CO_2 Emissions

Terrestrial belowground C allocation represents an important process linking plant C fixation to soil C losses, exercising a strong control on soil respiration (Mencuccini and Hölttä, 2010), and structuring the soil microbial community (Eisenhauer et al., 2017), leading to enhanced or reduced soil organic matter decomposition (Kuzyakov, 2010). Many studies have shown that the "autotrophic" component of soil respiration (including roots, associated mycorrhizal fungi, and rhizosphere microbes dependent on recently plant-fixed C) accounts for a significant fraction of soil CO_2 efflux (Högberg et al., 2001; Scott-Denton et al., 2006; Bahn et al., 2008; Burri et al., 2014). Therefore, understanding how plants exude C and control belowground C fluxes in response to the environment is pivotal. Furthermore, root exudates as an input of labile C substrate can stimulate the decomposition of the more stable soil organic matter pool (Kuzyakov, 2010). This process is termed "rhizosphere priming" and depends among other factors on the amount and chemical composition of labile substrates added to the soils relative to the active microbial biomass (Kuzyakov and Blagodatskaya, 2015). Different organic compounds have been shown to cause different degrees of priming (Hamer and Marschner, 2005), highlighting the complexity of this process. It has recently been proposed that the priming effect responds to the relative availability of N and P, following contrasting results from two experimental grassland studies (Dijkstra et al., 2013). The authors argued that two opposing mechanisms operate when N or P becomes limiting to plants. Soil N is mostly present as high-molecular-weight organic material, while P can be present in both forms, organic and inorganic P. Priming the decomposition of organic matter could therefore be beneficial for plants mining for N (Meier et al., 2017). Instead the release of P can follow different pathways, such as hydrolysis of organic P compounds by extracellular enzymes or Pi desorption/dissolution through enhanced exudation of organic acids, both of which do not necessarily involve carbon release due to SOM decomposition. Our explanation of root exudate responses to nutrient limitation could further support the hypothesis put forward by Dijkstra et al. (2013). Indeed, when P is limiting and meristematic activity stops, this will curtail the exudation of C-rich metabolites (such as sugars) over time that act as a labile source of C to micro-organisms, consequently decreasing the rhizosphere priming effect. On the other hand, under N limiting conditions, low concentrations of organic nitrogen outside the root cells may cause a stronger concentration gradient and increase the flux of exudates to the rhizosphere microbial community, eventually causing an enhanced rhizosphere priming effect. In contrast, roots reaching organic-rich or nutrient-rich patches with high microbial depolymerization activity will encounter enhanced amino acid concentrations, effectively downregulating the efflux of amino acids and eventually other compounds (because of the slowdown of the meristematic activity and therefore regulating sink activity; see Section 3.1) and reducing the rhizosphere priming effect. Therefore, further investigations into the relationship between soil nutrient availability, plant nutrient status, and root exudation will greatly help to predict the consequences for SOC turnover. Indeed, a recent study has shown for the first time that plant nutrient strategy is tightly linked to exudation of primary metabolites, which have significant correlations with soil denitrification (Guyonnet et al., 2017). Specifically, targeted investigations are needed on the effect of biological processes (source-sink activity, efflux carrier expression, etc.) and environmental stresses on the flux of solutes from the roots under realistic conditions, with a great challenge posed by the overwhelming difficulty in collecting representative root exudate samples (Oburger and Jones, 2018).

Plant Community Composition, Plant Productivity, and Agricultural Production

Plant community composition responds to environmental stresses and to competition for available resources, either aboveground (e.g., light) or belowground (e.g., nutrients and water). Root exudates, nutrient availability, and soil microbial communities form a close interaction network, simultaneously affecting plant growth and competition (Pierik et al., 2013). While many specific compounds in root exudates playing a role in plant community composition have been characterized, such as allelopathic compounds (e.g., sorgoleone in *Sorghum bicolor*) (Bertin et al., 2003), the multitude of compounds exuded by roots poses a challenge in understanding the mechanisms of plant-plant interactions and to decipher those compounds that play a major role. Understanding whether specific root exudates or a combination of them are involved in plant recognition remains a challenge. Therefore, it also remains unresolved whether root exudation of primary metabolites plays an important role in plant-plant interactions as we suggested for nutrient sensing and signaling. A few studies have demonstrated that the concentration of specific root exudates is an important trigger in self-recognition and recognition of other plants (Caffaro et al., 2011). Indeed accumulation of "own" compounds secreted by the same species inhibited root growth (Falik et al., 2005; Semchenko et al., 2007) and played a role in self-recognition and neighbor-recognition

(Caffaro et al., 2011, 2013). It was also shown that responses to nutrients can become dominant compared to avoidance of neighboring plants, and that plants integrate signals from both nutrients and competitors (Cahill et al., 2010). Therefore, the ultimate response of plants to their neighbors depends on the complex interplay of mechanisms that integrate numerous environmental cues in which root exudates are undoubtedly involved. Recent studies have shown how plant-soil feedbacks, mostly determined by the relationship between the plant and the soil microbial community, can determine plant performance and community structure (Kardol et al., 2007; Reinhart, 2012; Ma et al., 2017; Van Nuland et al., 2017; Bukowski et al., 2018; Eppinga et al., 2018; Hu et al., 2018; Wubs and Bezemer, 2018). Indeed, in recent experiments, it was shown that effects on plant performance by soil microbiota through plant-soil feedbacks were dependent on the plant nutrient strategy and soil nutrient conditions (Png et al., 2019; Teste et al., 2017). More specifically, Teste et al. (2017) revealed that these nutritional strategy-dependent feedbacks were the key in maintaining plant functional and taxonomic diversity in Mediterranean-climate shrublands. These results are extremely important and highlight our need to understand how plant nutrient strategies affect root exudation patterns and how this can elicit feedback on plant community assembly.

Understanding the role of root exudates in plant recognition and competition is likely to have significant impacts on agricultural productivity. Modern agriculture calls for sustainable systems that can maintain productivity while reducing inputs and losses and increasing the biodiversity of agro-ecosystems (Foley et al., 2011). Highly successful results were obtained with intercropping systems, where two or more crop species were grown together to maximize light and resource use while reducing susceptibility to pests, an approach that could represent a highly valuable tool for increasing the sustainability of food production (Brooker et al., 2015; Mariotte et al., 2018). In this context, understanding belowground interactions determining competition and facilitation and nutrient foraging strategies is essential (Giles et al., 2017). For example, it was shown that root exudates of maize promoted N_2 fixation of faba bean, whereas root exudates of barley and wheat did not (Li et al., 2016). Indeed, in agro-ecosystems, the natural complexity can be reduced, as plant community composition, nutrient, and water regimes can all be manipulated. By reducing the complexity of plant-plant and plant-microbe interactions, it might become easier to successfully apply fundamental research to agricultural systems. However, more studies need to specifically address the role of root exudates in nutrient foraging and plant recognition in order to understand the mechanisms involved and successfully develop combinations of plant species and soil microbes that improve the sustainability of food production.

SUMMARY

In this manuscript, we synthesized recent advances in biology to explain and propose a mechanism by which root exudation of primary metabolites is controlled, and how this process can affect plant nutrient acquisition strategies and root system architecture. We propose two concepts to build a mechanistic understanding of how root exudation can affect plant nutrition:

1. *Root exudation of primary metabolites is driven by facilitated diffusion but plants and microbes can control the root exudation process by modifying concentration gradients depending on their nutritional status*:
   Root exudation occurs mainly at the root meristematic apex, where fluxes of metabolites into the soil are the highest, due to the lack of root endodermis differentiation. Concentration gradients are fundamental in driving root exudation as most of the primary metabolites efflux from root cells through membrane transporters that facilitate diffusion. Soil microbes actively consume root exudates and keep concentrations of the respective substance low in the soil environment and at the same time can stimulate specific root exudation patterns. Plants, on the other side, can control concentration gradients by different mechanisms: they can adjust the supply rate through phloem loading and transport (source activity) or modify phloem unloading and sink activity, including the inhibition of root meristematic activity or up/downregulation of efflux transporters. The functioning of efflux carriers can also be controlled by rapid post-translational mechanisms (e.g., phosphorylation), which suggest that a fast control of root exudation is possible. The exudation flux ultimately will reflect the nutritional status and strategy of the plant or of the micro-organisms (soil environment). While plant source-sink dynamics are increasingly recognized as being fundamental to understanding C allocation and nutrient uptake, we support the idea that plant-associated micro-organisms affect plant carbon allocation by affecting concentration gradients that drive root exudation (Farrar and Jones, 2000; Savage et al., 2016). Hence, we introduce a novel conceptual framework for the control of root exudation that considers source-sink dynamics of plants and micro-organisms together as an integrated system.
2. *Changes in the concentration of primary metabolites at the root tip are sensed by the plant and signals are translated to modify root system architecture*:
   We present multiple examples of how important root metabolite concentrations can be increased or decreased inside the root tip. Specifically, regulation of efflux transporter expression in roots, root exudate re-uptake, phloem loading, and modulation of meristematic activity are major mechanisms that integrate the root exudation process with the soil environment surrounding the root tips. Modulating this flux can change the temporal concentrations of solutes inside the root tip, which elicits responses in root system architecture to modulate root growth to environmental cues. Indeed, the three chemical groups mentioned above (sugars, amino acids and organic acids), comprising a vast proportion of the root exudates, can all be sensed in different ways and induce a range of responses in the root system architecture from lateral root formation to root meristem exhaustion, depending on the plant and soil nutritional status. Soil microbes can create specific patterns of metabolite concentrations around the root tip by preferentially consuming some metabolites

and by stimulating plant exudation. Therefore, soil microbes can exert a strong control on plant nutrient sensing.

This proposed framework has strong repercussions on the understanding of ecosystem functioning (**Figure 4**). Indeed, plant belowground C allocation and root exudation in response to environmental changes has attracted much interest, especially on the implications for soil C sequestration and losses. Yet, a conclusive mechanistic explanation of the underlying processes has remained elusive. In comparison to fertilization, little research has targeted the manipulation of plant carbon transport and sensing of organic molecules for improving agricultural productivity (Tegeder and Masclaux-Daubresse, 2018), even though a decrease in fertilization and an increase in agricultural sustainability is called for. Studies on plant-microbe interactions are currently increasing, and it will be pivotal to understand the links between primary metabolite exudation and soil micro-organisms. Indeed, exudation of primary metabolites has strong effects on SOM decomposition by soil microbes, and primary metabolite exudation patterns are linked to plant nutrient strategies, which through plant-soil feedback mechanisms can determine an ecosystem performance. Also how mycorrhizal association affects root exudation and the processes influenced thereby is still largely unknown, largely due to having a majority of studies being performed with the non-mycorrhizal

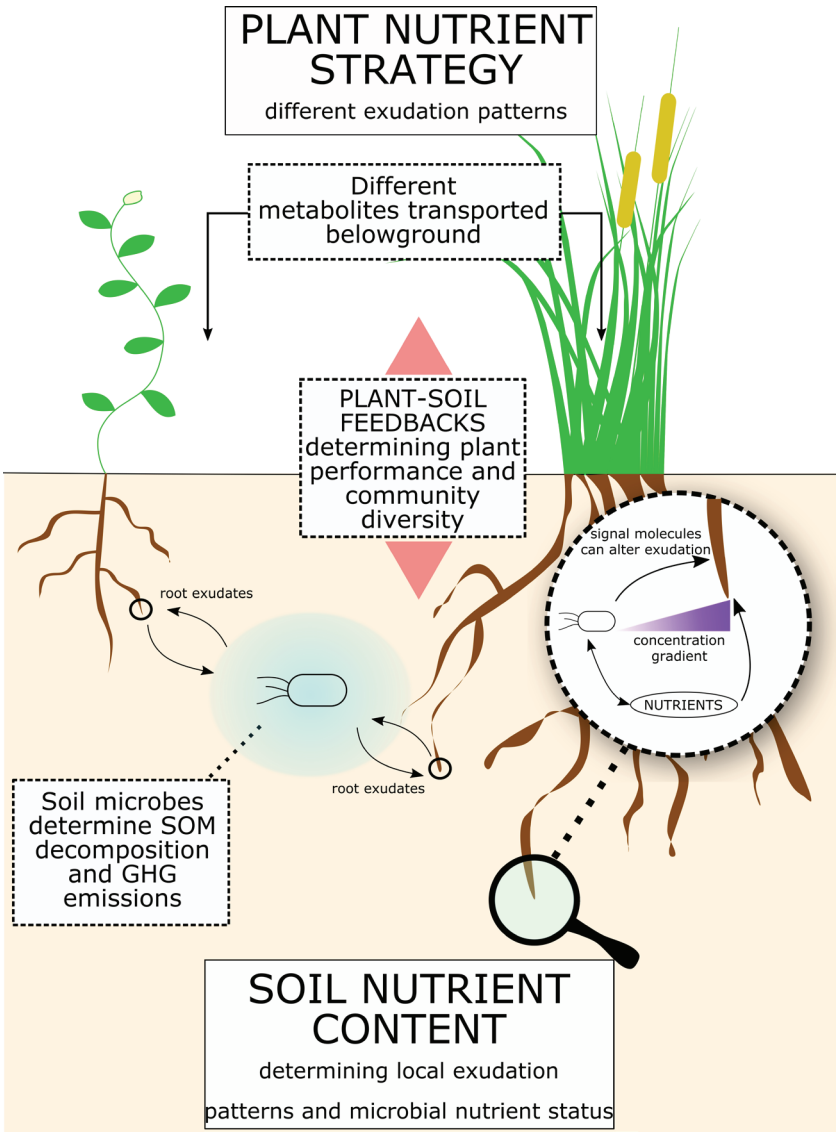

FIGURE 4 | Root exudates link soil nutrients to plant nutrient strategy. Figure illustrates a summary of the concepts proposed for the role of root exudates in plant-microbe interactions and consequences for ecosystems. Plant nutrient strategy determines different exudation patterns, while the soil physical and nutrient composition determines the microbial community and its nutrient demand. Root exudation is a flux with a bi-directional influence between plant and soil microbes. Indeed, while plants can regulate root exudation, soil micro-organism can enhance exudation rates and release molecules that affect root exudation patterns. Ultimately, root exudation has a significant effect on SOM decomposition and greenhouse gases (GHGs) release from soil. Also, plant-soil feedbacks can significantly affect plant performance and plant community composition.

plant *Arabidopsis*, leaving uncertainties on their potential use in agriculture (Thirkell et al., 2017). Despite the undeniable importance of nutrient uptake transporters, we here suggest that exudation of primary metabolites and plant-microbe interactions plays a pivotal role in nutrient uptake and plant community dynamics and that their mechanistic understanding will be crucial in building more nutrient-efficient agro-ecosystems.

AUTHOR CONTRIBUTIONS

AC conceived and designed the manuscript structure. AC, WW, and CK collected references and wrote the manuscript with substantial contributions from AM and AR.

FUNDING

This study was funded, in part, by the Austrian Science Fund (FWF; project n. P 28572 and P 30339-B29). AM is a recipient of funding from the Australian Research Council Legumes for Sustainable Agriculture Industrial Transformation Hub (IH140100013) and an Australian Research Council Future Fellowship (FT120100200).

ACKNOWLEDGMENTS

We thank Dr. Feike Dijkstra (The University of Sydney) for the helpful discussion and constructive comments to the manuscript.

REFERENCES

Ahmed, M. A., Passioura, J., and Carminati, A. (2018). Hydraulic processes in roots and the rhizosphere pertinent to increasing yield of water-limited grain crops: a critical review. *J. Exp. Bot.* 69, 3255–3265. doi: 10.1093/jxb/ery183

Alegria Terrazas, R., Giles, C., Paterson, E., Robertson-Albertyn, S., Cesco, S., Mimmo, T., et al. (2016). "Chapter one: Plant–microbiota interactions as a driver of the mineral turnover in the rhizosphere," in *Advances in applied microbiology*. eds. Sariaslani S., and Gadd G. M. (Cambridge, Massachusetts, USA: Academic Press), 1–67.

Aslam, M., Travis, R. L., and Rains, D. W. (2001). Differential effect of amino acids on nitrate uptake and reduction systems in barley roots. *Plant Sci.* 160, 219–228. doi: 10.1016/S0168-9452(00)00391-5

Badri, D. V., Loyola-Vargas, V. M., Du, J., Stermitz, F. R., Broeckling, C. D., Iglesias-Andreu, L., et al. (2008). Transcriptome analysis of Arabidopsis roots treated with signaling compounds: a focus on signal transduction, metabolic regulation and secretion. *New Phytol.* 179, 209–223. doi: 10.1111/j.1469-8137.2008.02458.x

Badri, D. V., Quintana, N., El Kassis, E. G., Kim, H. K., Choi, Y. H., Sugiyama, A., et al. (2009). An ABC transporter mutation alters root exudation of phytochemicals that provoke an overhaul of natural soil microbiota. *Plant Physiol.* 151, 2006–2017. doi: 10.1104/pp.109.147462

Badri, D. V., and Vivanco, J. M. (2009). Regulation and function of root exudates. *Plant Cell Environ.* 32, 666–681. doi: 10.1111/j.1365-3040.2009.01926.x

Bahn, M., Rodeghiero, M., Anderson-Dunn, M., Dore, S., Gimeno, C., Drösler, M., et al. (2008). Soil respiration in European grasslands in relation to climate and assimilate supply. *Ecosystems* 11, 1352–1367. doi: 10.1007/s10021-008-9198-0

Baluška, F., and Mancuso, S. (2013). Root apex transition zone as oscillatory zone. *Front. Plant Sci.* 4, 354. doi: 10.3389/fpls.2013.00354

Baluška, F., Mancuso, S., Volkmann, D., and Barlow, P. W. (2010). Root apex transition zone: a signalling–response nexus in the root. *Trends Plant Sci.* 15, 402–408. doi: 10.1016/j.tplants.2010.04.007

Berg, G., and Smalla, K. (2009). Plant species and soil type cooperatively shape the structure and function of microbial communities in the rhizosphere. *FEMS Microbiol. Ecol.* 68, 1–13. doi: 10.1111/j.1574-6941.2009.00654.x

Bertin, C., Yang, X., and Weston, L. A. (2003). The role of root exudates and allelochemicals in the rhizosphere. *Plant Soil* 256, 67–83. doi: 10.1023/A:1026290508166

Besnard, J., Pratelli, R., Zhao, C., Sonawala, U., Collakova, E., Pilot, G., et al. (2016). UMAMIT14 is an amino acid exporter involved in phloem unloading in Arabidopsis roots. *J. Exp. Bot.* 67, 6385–6397. doi: 10.1093/jxb/erw412

Bharadwaj, D. P., Alström, S., and Lundquist, P.-O. (2012). Interactions among *Glomus irregulare*, arbuscular mycorrhizal spore-associated bacteria, and plant pathogens under in vitro conditions. *Mycorrhiza* 22, 437–447. doi: 10.1007/s00572-011-0418-7

Biondini, M., Klein, d. A., and Redente, e. F. (1988). Carbon and nitrogen losses through root exudation by *Agropyron cristatum*, *A smithii* and *Bouteloua gracilis*. *Soil Biol. Biochem.* 20, 477–482. doi: 10.1016/0038-0717(88)90061-2

Bonfante, P., and Requena, N. (2011). Dating in the dark: how roots respond to fungal signals to establish arbuscular mycorrhizal symbiosis. *Curr. Opin. Plant Biol.* 14, 451–457. doi: 10.1016/j.pbi.2011.03.014

Brooker, R. W., Bennett, A. E., Cong, W. -F., Daniell, T. J., George, T. S., Hallett, P. D., et al. (2015). Improving intercropping: a synthesis of research in agronomy, plant physiology and ecology. *New Phytol.* 206, 107–117. doi: 10.1111/nph.13132

Brundrett, M. C. (2009). Mycorrhizal associations and other means of nutrition of vascular plants: understanding the global diversity of host plants by resolving conflicting information and developing reliable means of diagnosis. *Plant Soil* 320, 37–77. doi: 10.1007/s11104-008-9877-9

Bukowski, A. R., Schittko, C., and Petermann, J. S. (2018). The strength of negative plant-soil feedback increases from the intraspecific to the interspecific and the functional group level. *Ecol. Evol.* 8, 2280–2289. doi: 10.1002/ece3.3755

Burri, S., Sturm, P., Prechsl, U. E., Knohl, A., and Buchmann, N. (2014). The impact of extreme summer drought on the short-term carbon coupling of photosynthesis to soil CO_2 efflux in a temperate grassland. *Biogeosciences* 11, 961–975. doi: 10.5194/bg-11-961-2014

Caffaro, M. M., Vivanco, J. M., Boem, F. H. G., and Rubio, G. (2011). The effect of root exudates on root architecture in *Arabidopsis thaliana*. *Plant Growth Regul.* 64, 241–249. doi: 10.1007/s10725-011-9564-3

Caffaro, M. M., Vivanco, J. M., Botto, J., and Rubio, G. (2013). Root architecture of *Arabidopsis* is affected by competition with neighbouring plants. *Plant Growth Regul.* 70, 141–147. doi: 10.1007/s10725-013-9786-7

Cahill, J. F., McNickle, G. G., Haag, J. J., Lamb, E. G., Nyanumba, S. M., and St. Clair, C. C. (2010). Plants integrate information about nutrients and neighbors. *Science* 328, 1657–1657. doi: 10.1126/science.1189736

Caputo, C., and Barneix, A. J. (1997). Export of amino acids to the phloem in relation to N supply in wheat. *Physiol. Plant.* 101, 853–860. doi: 10.1111/j.1399-3054.1997.tb01073.x

Carvalhais, L. C., Dennis, P. G., Fedoseyenko, D., Hajirezaei, M. R., Borriss, R., and von Wiren, N. (2011). Root exudation of sugars, amino acids, and organic acids by maize as affected by nitrogen, phosphorus, potassium, and iron deficiency. *J. Plant Nutr. Soil Sci.* 174, 3–11. doi: 10.1002/jpln.201000085

Chen, H. -Y., Huh, J. -H., Yu, Y. -C., Ho, L. -H., Chen, L. -Q., Tholl, D., et al. (2015). The Arabidopsis vacuolar sugar transporter SWEET2 limits carbon sequestration from roots and restricts Pythium infection. *Plant J.* 83, 1046–1058. doi: 10.1111/tpj.12948

Cheng, L., Booker, F. L., Tu, C., Burkey, K. O., Zhou, L., Shew, H. D., et al. (2012). Arbuscular mycorrhizal fungi increase organic carbon decomposition under elevated CO_2. *Science* 337, 1084–1087. doi: 10.1126/science.1224304

Cheng, L., Zhu, J., Chen, G., Zheng, X., Oh, N. -H., Rufty, T. W., et al. (2010). Atmospheric CO_2 enrichment facilitates cation release from soil. *Ecol. Lett.* 13, 284–291. doi: 10.1111/j.1461-0248.2009.01421.x

Chevalier, F., Pata, M., Nacry, P., Doumas, P., and Rossignol, M. (2003). Effects of phosphate availability on the root system architecture: large-scale analysis of the natural variation between Arabidopsis accessions. *Plant Cell Environ.* 26, 1839–1850. doi: 10.1046/j.1365-3040.2003.01100.x

Chiu, J. C., Brenner, E. D., DeSalle, R., Nitabach, M. N., Holmes, T. C., and Coruzzi, G. M. (2002). Phylogenetic and expression analysis of the glutamate-receptor-like gene family in *Arabidopsis thaliana*. *Mol. Biol. Evol.* 19, 1066–1082. doi: 10.1093/oxfordjournals.molbev.a004165

Curzi, M. J., Ribaudo, C. M., Trinchero, G. D., Curá, J. A., and Pagano, E. A. (2008). Changes in the content of organic and amino acids and ethylene production of rice plants in response to the inoculation with *Herbaspirillum seropedicae*. *J. Plant Interact.* 3, 163–173. doi: 10.1080/17429140802255167

Dakora, F. D., and Phillips, D. A. (2002). Root exudates as mediators of mineral acquisition in low-nutrient environments. *Plant Soil* 245, 35–47. doi: 10.1023/a:1020809400075

Darwent, M. J., Paterson, E., McDonald, A. J. S., and Tomos, A. D. (2003). Biosensor reporting of root exudation from *Hordeum vulgare* in relation to shoot nitrate concentration. *J. Exp. Bot.* 54, 325–334. doi: 10.1093/jxb/erg017

De Schepper, V., De Swaef, T., Bauweraerts, I., and Steppe, K. (2013). Phloem transport: a review of mechanisms and controls. *J. Exp. Bot.* 64, 4839–4850. doi: 10.1093/jxb/ert302

Dennison, K. L., and Spalding, E. P. (2000). Glutamate-gated calcium fluxes in Arabidopsis. *Plant Physiol.* 124, 1511–1514. doi: 10.1104/pp.124.4.1511

Depuydt, S. (2014). Arguments for and against self and non-self root recognition in plants. *Front. Plant Sci.* 5:614 doi: 10.3389/fpls.2014.00614

Desnos, T. (2008). Root branching responses to phosphate and nitrate. *Curr. Opin. Plant Biol.* 11, 82–87. doi: 10.1016/j.pbi.2007.10.003

Dijkstra, F. A., Carrillo, Y., Pendall, E., and Morgan, J. A. (2013). Rhizosphere priming: a nutrient perspective. *Front. Microbiol.* 4:216. doi: 10.3389/fmicb.2013.00216

Dinkeloo, K., Boyd, S., and Pilot, G. (2017). Update on amino acid transporter functions and on possible amino acid sensing mechanisms in plants. *Semin. Cell Dev. Biol.* 74, 105–113. doi: 10.1016/j.semcdb.2017.07.010

Dluzniewska, P., Gessler, A., Kopriva, S., Strnad, M., NovÁK, O., Dietrich, H., et al. (2006). Exogenous supply of glutamine and active cytokinin to the roots reduces NO_3–uptake rates in poplar. *Plant Cell Environ.* 29, 1284–1297. doi: 10.1111/j.1365-3040.2006.01507.x

Doan, T. H., Doan, T. A., Kangas, M. J., Ernest, A. E., Tran, D., Wilson, C. L., et al. (2017). A low-cost imaging method for the temporal and spatial colorimetric detection of free amines on maize root surfaces. *Front. Plant Sci.* 8:1513. doi: 10.3389/fpls.2017.01513

Domínguez-May, Á. V., Carrillo-Pech, M., Barredo-Pool, F. A., Martínez-Estévez, M., Us-Camas, R. Y., Moreno-Valenzuela, O. A., et al. (2013). A novel effect for glycine on root system growth of habanero pepper. *J. Am. Soc. Hortic. Sci.* 138, 433–442. doi: 10.21273/JASHS.138.6.433

Drigo, B., Pijl, A. S., Duyts, H., Kielak, A. M., Gamper, H. A., Houtekamer, M. J., et al. (2010). Shifting carbon flow from roots into associated microbial communities in response to elevated atmospheric CO_2. *Proc. Natl. Acad. Sci.* 107, 10938–10942. doi: 10.1073/pnas.0912421107

Eisenhauer, N., Lanoue, A., Strecker, T., Scheu, S., Steinauer, K., Thakur, M. P., et al. (2017). Root biomass and exudates link plant diversity with soil bacterial and fungal biomass. *Sci. Rep.* 7:44641 doi: 10.1038/srep44641

el Zahar Haichar, F., Santaella, C., Heulin, T., and Achouak, W. (2014). Root exudates mediated interactions belowground. *Soil Biol. Biochem.* 77, 69–80. doi: 10.1016/j.soilbio.2014.06.017

Eppinga, M. B., Baudena, M., Johnson, D. J., Jiang, J., Mack, K. M. L., Strand, A. E., et al. (2018). Frequency-dependent feedback constrains plant community coexistence. *Nat. Ecol. Evol.* 2, 1403–1407. doi: 10.1038/s41559-018-0622-3

Evans, M. L., Ishikawa, H., and Estelle, M. A. (1994). Responses of Arabidopsis roots to auxin studied with high temporal resolution: comparison of wild type and auxin-response mutants. *Planta* 194, 215–222. doi: 10.1007/bf00196390

Falik, O., Reides, P., Gersani, M., and Novoplansky, A. (2005). Root navigation by self inhibition. *Plant Cell Environ.* 28, 562–569. doi: 10.1111/j.1365-3040.2005.01304.x

Farrar, J. F., and Jones, D. L. (2000). The control of carbon acquisition by roots. *New Phytol.* 147, 43–53. doi: 10.1046/j.1469-8137.2000.00688.x

Fatichi, S., Leuzinger, S., and Körner, C. (2014). Moving beyond photosynthesis: from carbon source to sink-driven vegetation modeling. *New Phytol.* 201, 1086–1095. doi: 10.1111/nph.12614

Fernandez, O., Theocharis, A., Bordiec, S., Feil, R., Jacquens, L., Clément, C., et al. (2012). Burkholderia phytofirmans PsJN acclimates grapevine to cold by modulating carbohydrate metabolism. *Mol. Plant-Microbe Interact.* 25, 496–504. doi: 10.1094/MPMI-09-11-0245

Fischer, W.-N., Loo, D. D. F., Koch, W., Ludewig, U., Boorer, K. J., Tegeder, M., et al. (2002). Low and high affinity amino acid H+−cotransporters for cellular import of neutral and charged amino acids. *Plant J.* 29, 717–731. doi: 10.1046/j.1365-313X.2002.01248.x

Foley, J. A., Ramankutty, N., Brauman, K. A., Cassidy, E. S., Gerber, J. S., Johnston, M., et al. (2011). Solutions for a cultivated planet. *Nature* 478, 337–342. doi: 10.1038/nature10452

Forde, B. G. (2014). Nitrogen signalling pathways shaping root system architecture: an update. *Current opinion in plant biology* 21, 30–36.

Forde, B. G., and Lea, P. J. (2007). Glutamate in plants: metabolism, regulation, and signalling. *J. Exp. Bot.* 58, 2339–2358. doi: 10.1093/jxb/erm121

Forsum, O. (2016). *On plant responses to D-amino acids.* (Doctoral dissertation). Retrieved from: https://pub.epsilon.slu.se/12997/

Forsum, O., Svennerstam, H., Ganeteg, U., and Näsholm, T. (2008). Capacities and constraints of amino acid utilization in Arabidopsis. *New Phytol.* 179, 1058–1069. doi: 10.1111/j.1469-8137.2008.02546.x

Friedel, J. K., and Scheller, E. (2002). Composition of hydrolysable amino acids in soil organic matter and soil microbial biomass. *Soil Biol. Biochem.* 34, 315–325. doi: 10.1016/S0038-0717(01)00185-7

Fusconi, A. (2014). Regulation of root morphogenesis in arbuscular mycorrhizae: what role do fungal exudates, phosphate, sugars and hormones play in lateral root formation? *Ann. Bot.* 113, 19–33. doi: 10.1093/aob/mct258

Gent, L., and Forde, B. G. (2017). How do plants sense their nitrogen status? *J. Exp. Bot.* 68, 2531–2539. doi: 10.1093/jxb/erx013

Giehl, R. F. H., and von Wirén, N. (2014). Root nutrient foraging. *Plant Physiol.* 166, 509–517. doi: 10.1104/pp.114.245225

Giles, C. D., Brown, L. K., Adu, M. O., Mezeli, M. M., Sandral, G. A., Simpson, R. J., et al. (2017). Response-based selection of barley cultivars and legume species for complementarity: root morphology and exudation in relation to nutrient source. *Plant Sci.* 255, 12–28. doi: 10.1016/j.plantsci.2016.11.002

Gill, A. L., and Finzi, A. C. (2016). Belowground carbon flux links biogeochemical cycles and resource-use efficiency at the global scale. *Ecol. Lett.* 19, 1419–1428. doi: 10.1111/ele.12690

Gilliham, M., and Tyerman, S. D. (2016). Linking metabolism to membrane signaling: the GABA-Malate connection. *Trends Plant Sci.* 21, 295–301. doi: 10.1016/j.tplants.2015.11.011

Gioseffi, E., de Neergaard, A., and Schjoerring, J. K. (2012). Interactions between uptake of amino acids and inorganic nitrogen in wheat plants. *Biogeosciences* 9, 1509–1518. doi: 10.5194/bg-9-1509-2012

Godt, D., and Roitsch, T. (2006). The developmental and organ specific expression of sucrose cleaving enzymes in sugar beet suggests a transition between apoplasmic and symplasmic phloem unloading in the tap roots. *Plant Physiol. Biochem.* 44, 656-665. doi: 10.1016/j.plaphy.2006.09.019

Gorka, S., Dietrich, M., Mayerhofer, W., Gabriel, R., Wiesenbauer, J., Martin, V., et al. (2019). Rapid transfer of plant photosynthates to soil bacteria via ectomycorrhizal hyphae and its interaction with nitrogen availability. *Front. Microbiol.* 10. doi: 10.3389/fmicb.2019.00168

Grimoldi, A. A., Kavanová, M., Lattanzi, F. A., Schäufele, R., and Schnyder, H. (2006). Arbuscular mycorrhizal colonization on carbon economy in perennial ryegrass: quantification by $13CO_2/12CO_2$ steady-state labelling and gas exchange. *New Phytol.* 172, 544–553. doi: 10.1111/j.1469-8137.2006.01853.x

Groleau-Renaud, V., Plantureux, S., Tubeileh, A., and Guckert, A. (2000). Influence of microflora and composition of root bathing solution on root exudation of maize plants. *J. Plant Nutr.* 23, 1283–1301. doi: 10.1080/01904160009382100

Gutjahr, C., and Parniske, M. (2013). Cell and developmental biology of arbuscular mycorrhiza symbiosis. *Annu. Rev. Cell Dev. Biol.* 29, 593–617. doi: 10.1146/annurev-cellbio-101512-122413

Guyonnet, J. P., Cantarel, A. A. M., Simon, L., and Haichar, F. e. Z. (2018). Root exudation rate as functional trait involved in plant nutrient-use strategy classification. *Ecol. Evol.* 8, 8573–8581. doi: 10.1002/ece3.4383

Guyonnet, J. P., Vautrin, F., Meiffren, G., Labois, C., Cantarel, A. A. M., Michalet, S., et al. (2017). The effects of plant nutritional strategy on soil microbial denitrification activity through rhizosphere primary metabolites. *FEMS Microbiol. Ecol.* 93:fix022 doi: 10.1093/femsec/fix022

Hamer, U., and Marschner, B. (2005). Priming effects in different soil types induced by fructose, alanine, oxalic acid and catechol additions. *Soil Biol. Biochem.* 37, 445–454. doi: 10.1016/j.soilbio.2004.07.037

Hammond, J. P., and White, P. J. (2011). Sugar signaling in root responses to low phosphorus availability. *Plant Physiol.* 156, 1033–1040. doi: 10.1104/pp.111.175380

Hanson, J., and Smeekens, S. (2009). Sugar perception and signaling—an update. *Curr. Opin. Plant Biol.* 12, 562–567. doi: 10.1016/j.pbi.2009.07.014

Häusler, R. E., Ludewig, F., and Krueger, S. (2014). Amino acids – a life between metabolism and signaling *Plant Sci.* 229, 225–237. doi: 10.1016/j.plantsci.2014.09.011

Hawes, M., Allen, C., Turgeon, B. G., Curlango-Rivera, G., Minh Tran, T., Huskey, D. A., et al. (2016). Root border cells and their role in plant defense. *Annu. Rev. Phytopathol.* 54, 143–161. doi: 10.1146/annurev-phyto-080615-100140

Hawes, M. C., Bengough, G., Cassab, G., and Ponce, G. (2002). Root caps and rhizosphere. *J. Plant Growth Regul.* 21, 352–367. doi: 10.1007/s00344-002-0035-y

Henry, H. A. L., and Jefferies, R. L. (2003). Interactions in the uptake of amino acids, ammonium and nitrate ions in the Arctic salt-marsh grass, *Puccinellia phryganodes*. *Plant Cell Environ.* 26, 419–428. doi: 10.1046/j.1365-3040.2003.00973.x

Herz, K., Dietz, S., Gorzolka, K., Haider, S., Jandt, U., Scheel, D., et al. (2018). Linking root exudates to functional plant traits. *PLoS One* 13:e0204128. doi: 10.1371/journal.pone.0204128

Hirner, A., Ladwig, F., Stransky, H., Okumoto, S., Keinath, M., Harms, A., et al. (2006). Arabidopsis LHT1 is a high-affinity transporter for cellular amino acid uptake in both root epidermis and leaf mesophyll. *Plant Cell* 18, 1931–1946. doi: 10.1105/tpc.106.041012

Högberg, P., Nordgren, A., Buchmann, N., Taylor, A. F. S., Ekblad, A., Högberg, M. N., et al. (2001). Large-scale forest girdling shows that current photosynthesis drives soil respiration. *Nature* 411, 789. doi: 10.1038/35081058

Hu, L., Robert, C. A. M., Cadot, S., Zhang, X., Ye, M., Li, B., et al. (2018). Root exudate metabolites drive plant-soil feedbacks on growth and defense by shaping the rhizosphere microbiota. *Nat. Commun.* 9:2738. doi: 10.1038/s41467-018-05122-7

Inselsbacher, E., and Näsholm, T. (2012). The below-ground perspective of forest plants: soil provides mainly organic nitrogen for plants and mycorrhizal fungi. *New Phytol.* 195, 329–334. doi: 10.1111/j.1469-8137.2012.04169.x

Jaeger, C. H., Lindow, S. E., Miller, W., Clark, E., and Firestone, M. K. (1999). Mapping of sugar and amino acid availability in soil around roots with bacterial sensors of sucrose and tryptophan. *Appl. Environ. Microbiol.* 65, 2685–2690.

Jämtgård, S., Näsholm, T., and Huss-Danell, K. (2008). Characteristics of amino acid uptake in barley. *Plant Soil* 302, 221–231. doi: 10.1007/s11104-007-9473-4

Jansa, J., Bukovská, P., and Gryndler, M. (2013). Mycorrhizal hyphae as ecological niche for highly specialized hypersymbionts or just soil free-riders? *Front. Plant Sci.* 4:134 doi: 10.3389/fpls.2013.00134

Johnson, N. C., Wilson, G. W. T., Wilson, J. A., Miller, R. M., and Bowker, M. A. (2015). Mycorrhizal phenotypes and the law of the minimum. *New Phytol.* 205, 1473–1484. doi: 10.1111/nph.13172

Jones, D., and Darrah, P. (1993). Re-sorption of organic compounds by roots of Zea mays L. and its consequences in the rhizosphere. *Plant Soil* 153, 47–59. doi: 10.1007/BF00010543

Jones, D. L., Nguyen, C., and Finlay, R. D. (2009). Carbon flow in the rhizosphere: carbon trading at the soil-root interface. *Plant Soil* 321, 5–33. doi: 10.1007/s11104-009-9925-0

Jones, D. L., Shannon, D., Junvee-Fortune, T., and Farrar, J. F. (2005). Plant capture of free amino acids is maximized under high soil amino acid concentrations. *Soil Biol. Biochem.* 37, 179–181. doi: 10.1016/j.soilbio.2004.07.021

Kaiser, C., Kilburn, M. R., Clode, P. L., Fuchslueger, L., Koranda, M., Cliff, J. B., et al. (2015). Exploring the transfer of recent plant photosynthates to soil microbes: mycorrhizal pathway vs direct root exudation. *New Phytol.* 205, 1537–1551. doi: 10.1111/nph.13138

Kan, C.-C., Chung, T.-Y., Wu, H.-Y., Juo, Y.-A., and Hsieh, M.-H. (2017). Exogenous glutamate rapidly induces the expression of genes involved in metabolism and defense responses in rice roots. *BMC Genomics* 18:186. doi: 10.1186/s12864-017-3588-7

Kanno, S., Arrighi, J.-F., Chiarenza, S., Bayle, V., Berthomé, R., Péret, B., et al. (2016). A novel role for the root cap in phosphate uptake and homeostasis. *elife* 5:e14577. doi: 10.7554/eLife.14577

Kardol, P., Cornips, N. J., van Kempen, M. M. L., Bakx-Schotman, J. M. T., and van der Putten, W. H. (2007). Microbe-mediated plant-soil feedback causes historical contingency effects in plant community assembly. *Ecol. Monogr.* 77, 147–162. doi: 10.1890/06-0502

Karthikeyan, A. S., Varadarajan, D. K., Jain, A., Held, M. A., Carpita, N. C., and Raghothama, K. G. (2007). Phosphate starvation responses are mediated by sugar signaling in Arabidopsis. *Planta* 225, 907–918. doi: 10.1007/s00425-006-0408-8

Kellermeier, F., Armengaud, P., Seditas, T. J., Danku, J., Salt, D. E., and Amtmann, A. (2014). Analysis of the root system architecture of Arabidopsis provides a quantitative readout of crosstalk between nutritional signals. *Plant Cell* 26, 1480–1496. doi: 10.1105/tpc.113.122101

Khan, M. A., Gemenet, D. C., and Villordon, A. (2016). Root system architecture and abiotic stress tolerance: current knowledge in root and tuber crops. *Front. Plant Sci.* 7:1584. doi: 10.3389/fpls.2016.01584

Knoblauch, M., Knoblauch, J., Mullendore, D. L., Savage, J. A., Babst, B. A., Beecher, S. D., et al. (2016). Testing the Münch hypothesis of long distance phloem transport in plants. *elife* 5:e15341. doi: 10.7554/eLife.15341

Kochian, L. V., Pineros, M. A., and Hoekenga, O. A. (2005). "The physiology, genetics and molecular biology of plant aluminum resistance and toxicity" in *Root physiology: from gene to function*. (New York City, USA: Springer), 175–195.

Körner, C. (2015). Paradigm shift in plant growth control. *Curr. Opin. Plant Biol.* 25, 107–114. doi: 10.1016/j.pbi.2015.05.003

Kramer, E. M., Frazer, N. L., and Baskin, T. I. (2007). Measurement of diffusion within the cell wall in living roots of *Arabidopsis thaliana*. *J. Exp. Bot.* 58, 3005–3015. doi: 10.1093/jxb/erm155

Krishnapriya, V., and Pandey, R. (2016). Root exudation index: screening organic acid exudation and phosphorus acquisition efficiency in soybean genotypes. *Crop Pasture Sci.* 67, 1096–1109. doi: 10.1071/cp15329

Kuzyakov, Y. (2010). Priming effects: interactions between living and dead organic matter. *Soil Biol. Biochem.* 42, 1363–1371. doi: 10.1016/j.soilbio.2010.04.003

Kuzyakov, Y., and Blagodatskaya, E. (2015). Microbial hotspots and hot moments in soil: concept and review. *Soil Biol. Biochem.* 83, 184–199. doi: 10.1016/j.soilbio.2015.01.025

Kuzyakov, Y., Raskatov, A., and Kaupenjohann, M. (2003). Turnover and distribution of root exudates of Zea mays. *Plant Soil* 254, 317–327. doi: 10.1023/a:1025515708093

Lambers, H., Shane, M. W., Cramer, M. D., Pearse, S. J., and Veneklaas, E. J. (2006). Root structure and functioning for efficient acquisition of phosphorus: matching morphological and physiological traits. *Ann. Bot.* 98, 693–713. doi: 10.1093/aob/mcl114

Ledo, A., Paul, K. I., Burslem, D. F. R. P., Ewel, J. J., Barton, C., Battaglia, M., et al. (2018). Tree size and climatic water deficit control root to shoot ratio in individual trees globally. *New Phytol.* 217, 8–11. doi: 10.1111/nph.14863

Li, B., Li, Y.-Y., Wu, H.-M., Zhang, F.-F., Li, C.-J., Li, X.-X., et al. (2016). Root exudates drive interspecific facilitation by enhancing nodulation and N(2) fixation. *Proc. Natl. Acad. Sci. USA* 113, 6496–6501. doi: 10.1073/pnas.1523580113

Li, J., Zhu, S., Song, X., Shen, Y., Chen, H., Yu, J., et al. (2006). A rice glutamate receptor-like gene is critical for the division and survival of individual cells in the root apical meristem. *Plant Cell* 18, 340–349. doi: 10.1105/tpc.105.037713

Liese, R., Lübbe, T., Albers, N. W., and Meier, I. C. (2018). The mycorrhizal type governs root exudation and nitrogen uptake of temperate tree species. *Tree Physiol.* 38, 83–95. doi: 10.1093/treephys/tpx131

Liu, J., Samac, D. A., Bucciarelli, B., Allan, D. L., and Vance, C. P. (2005). Signaling of phosphorus deficiency-induced gene expression in white lupin requires sugar and phloem transport. *Plant J.* 41, 257–268. doi: 10.1111/j.1365-313X.2004.02289.x

Liu, J., and Vance, C. P. (2010). Crucial roles of sucrose and microRNA399 in systemic signaling of P deficiency: a tale of two team players? *Plant Signal. Behav.* 5, 1556–1560. doi: 10.4161/psb.5.12.13293

López-Bucio, J., Cruz-Ramırez, A., and Herrera-Estrella, L. (2003). The role of nutrient availability in regulating root architecture. *Curr. Opin. Plant Biol.* 6, 280–287. doi: 10.1016/S1369-5266(03)00035-9

Lucas García, J., Barbas, C., Probanza, A., Barrientos, M., and Gutierrez Mañero, F. (2001). Low molecular weight organic acids and fatty acids in root exudates of two Lupinus cultivars at flowering and fruiting stages. *Phytochem. Anal.* 12, 305–311.

Lynch, J. (1995). Root architecture and plant productivity. *Plant Physiol.* 109:7. doi: 10.1104/pp.109.1.7

Lyu, Y., Tang, H. L., Li, H. G., Zhang, F. S., Rengel, Z., Whalley, W. R., et al. (2016). Major crop species show differential balance between root morphological and physiological responses to variable phosphorus supply. *Front. Plant Sci.* 7:1939. doi: 10.3389/fpls.2016.01939

Ma, H.-K., Pineda, A., van der Wurff, A. W. G., Raaijmakers, C., and Bezemer, T. M. (2017). Plant-soil feedback effects on growth, defense and susceptibility to a soil-borne disease in a cut flower crop: species and functional group effects. *Front. Plant Sci.* 8, 2127–2127. doi: 10.3389/fpls.2017.02127

Ma, J. F., Ryan, P. R., and Delhaize, E. (2001). Aluminium tolerance in plants and the complexing role of organic acids. *Trends Plant Sci.* 6, 273–278. doi: 10.1016/S1360-1385(01)01961-6

Mahmood, T., Woitke, M., Gimmler, H., and Kaiser, W. M. (2002). Sugar exudation by roots of kallar grass [*Leptochloa fusca* (L.) Kunth] is strongly affected by the nitrogen source. *Planta* 214, 887–894. doi: 10.1007/s00425-001-0697-x

Manck-Götzenberger, J., and Requena, N. (2016). Arbuscular mycorrhiza symbiosis induces a major transcriptional reprogramming of the potato SWEET sugar transporter family. *Front. Plant Sci.* 7:487. doi: 10.3389/fpls.2016.00487

Mariotte, P., Mehrabi, Z., Bezemer, T. M., De Deyn, G. B., Kulmatiski, A., Drigo, B., et al. (2018). Plant-soil feedback: bridging natural and agricultural sciences. *Trends Ecol. Evol.* 33, 129–142. doi: 10.1016/j.tree.2017.11.005

Martin, F. M., Uroz, S., and Barker, D. G. (2017). Ancestral alliances: plant mutualistic symbioses with fungi and bacteria. *Science* 356:eaad4501. doi: 10.1126/science.aad4501

McCormack, M. L., Dickie, I. A., Eissenstat, D. M., Fahey, T. J., Fernandez, C. W., Guo, D., et al. (2015). Redefining fine roots improves understanding of below-ground contributions to terrestrial biosphere processes. *New Phytol.* 207, 505–518. doi: 10.1111/nph.13363

McCully, M. E., and Canny, M. J. (1985). Localisation of translocated 14C in roots and root exudates of field-grown maize. *Physiol. Plant.* 65, 380–392. doi: 10.1111/j.1399-3054.1985.tb08661.x

Meharg, A., and Killham, K. (1995). Loss of exudates from the roots of perennial ryegrass inoculated with a range of micro-organisms. *Plant Soil* 170, 345–349. doi: 10.1007/BF00010488

Meier, I. C., Finzi, A. C., and Phillips, R. P. (2017). Root exudates increase N availability by stimulating microbial turnover of fast-cycling N pools. *Soil Biol. Biochem.* 106, 119–128. doi: 10.1016/j.soilbio.2016.12.004

Meier, I. C., Pritchard, S. G., Brzostek, E. R., McCormack, M. L., and Phillips, R. P. (2015). The rhizosphere and hyphosphere differ in their impacts on carbon and nitrogen cycling in forests exposed to elevated CO_2. *New Phytol.* 205, 1164–1174. doi: 10.1111/nph.13122

Mencuccini, M., and Hölttä, T. (2010). The significance of phloem transport for the speed with which canopy photosynthesis and belowground respiration are linked. *New Phytol.* 185, 189–203. doi: 10.1111/j.1469-8137.2009.03050.x

Meyer, S., De Angeli, A., Fernie, A. R., and Martinoia, E. (2010). Intra- and extra-cellular excretion of carboxylates. *Trends Plant Sci.* 15, 40–47. doi: 10.1016/j.tplants.2009.10.002

Moe, L. A. (2013). Amino acids in the rhizosphere: from plants to microbes. *Am. J. Bot.* 100, 1692–1705. doi: 10.3732/ajb.1300033

Mommer, L., Kirkegaard, J., and van Ruijven, J. (2016). Root-root interactions: towards a rhizosphere framework. *Trends Plant Sci.* 21, 209–217. doi: 10.1016/j.tplants.2016.01.009

Mora-Macias, J., Ojeda-Rivera, J. O., Gutierrez-Alanis, D., Yong-Villalobos, L., Oropeza-Aburto, A., Raya-Gonzalez, J., et al. (2017). Malate-dependent Fe accumulation is a critical checkpoint in the root developmental response to low phosphate. *Proc. Natl. Acad. Sci. USA* 114, E3563–E3572. doi: 10.1073/pnas.1701952114

Mora-Macías, J., Ojeda-Rivera, J. O., Gutiérrez-Alanís, D., Yong-Villalobos, L., Oropeza-Aburto, A., Raya-González, J., et al. (2017). Malate-dependent Fe accumulation is a critical checkpoint in the root developmental response to low phosphate. *Proc. Natl. Acad. Sci.* 114, E3563–E3572. doi: 10.1073/pnas.1701952114

Münch, E. (1930). *Die stoffbewegungen in der Pflanze*. Jena: Carl Fischer.

Nacry, P., Bouguyon, E., and Gojon, A. (2013). Nitrogen acquisition by roots: physiological and developmental mechanisms ensuring plant adaptation to a fluctuating resource. *Plant Soil* 370, 1–29. doi: 10.1007/s11104-013-1645-9

Nadira, U. A., Ahmed, I. M., Wu, F., and Zhang, G. (2016). The regulation of root growth in response to phosphorus deficiency mediated by phytohormones in a Tibetan wild barley accession. *Acta Physiol. Plant.* 38, 105. doi: 10.1007/s11738-016-2124-8

Naseer, S., Lee, Y., Lapierre, C., Franke, R., Nawrath, C., and Geldner, N. (2012). Casparian strip diffusion barrier in Arabidopsis is made of a lignin polymer without suberin. *Proc. Natl. Acad. Sci.* 109, 10101–10106. doi: 10.1073/pnas.1205726109

Näsholm, T., Kielland, K., and Ganeteg, U. (2009). Uptake of organic nitrogen by plants. *New Phytol.* 182, 31–48. doi: 10.1111/j.1469-8137.2008.02751.x

Nazoa, P., Vidmar, J. J., Tranbarger, T. J., Mouline, K., Damiani, I., Tillard, P., et al. (2003). Regulation of the nitrate transporter gene AtNRT2.1 in Arabidopsis thaliana: responses to nitrate, amino acids and developmental stage. *Plant Mol. Biol.* 52, 689–703. doi: 10.1023/a:1024899808018

Nehls, U. (2008). Mastering ectomycorrhizal symbiosis: the impact of carbohydrates. *J. Exp. Bot.* 59, 1097–1108. doi: 10.1093/jxb/erm334

Ni, J., Yu, Z., Du, G., Zhang, Y., Taylor, J. L., Shen, C., et al. (2016). Heterologous expression and functional analysis of rice glutamate receptor-like family indicates its role in glutamate triggered calcium flux in rice roots. *Rice* 9, 9. doi: 10.1186/s12284-016-0081-x

Oburger, E., and Jones, D. L. (2018). Sampling root exudates – mission impossible? *Rhizosphere* 6, 116–133. doi: 10.1016/j.rhisph.2018.06.004

Ogden, M., Hoefgen, R., Roessner, U., Persson, S., and Khan, G. (2018). Feeding the walls: how does nutrient availability regulate cell wall composition? *Int. J. Mol. Sci.* 19:2691. doi: 10.3390/ijms19092691

Ohkubo, Y., Tanaka, M., Tabata, R., Ogawa-Ohnishi, M., and Matsubayashi, Y. (2017). Shoot-to-root mobile polypeptides involved in systemic regulation of nitrogen acquisition. *Nat. Plants.* 3, 17029. doi: 10.1038/nplants.2017.29

Okumoto, S., and Pilot, G. (2011). Amino acid export in plants: a missing link in nitrogen cycling. *Mol. Plant* 4, 453–463. doi: 10.1093/mp/ssr003

Ortíz-Castro, R., Contreras-Cornejo, H. A., Macías-Rodríguez, L., and López-Bucio, J. (2009). The role of microbial signals in plant growth and development. *Plant Signal. Behav.* 4, 701–712.

Otani, T., Ae, N., and Tanaka, H. (1996). Phosphorus (P) uptake mechanisms of crops grown in soils with low P status. II. Significance of organic acids in root exudates of pigeonpea. *Soil Sci. Plant Nutr.* 42, 553–560. doi: 10.1080/00380768.1996.10416324

Padgett, P. E., and Leonard, R. T. (1996). Free amino acid levels and the regulation of nitrate uptake in maize cell suspension cultures. *J. Exp. Bot.* 47, 871–883. doi: 10.1093/jxb/47.7.871

Pal'ove-Balang, P., and Mistrík, I. (2002). Control of nitrate uptake by phloem-translocated glutamine in *Zea mays* L. seedlings. *Plant Biol.* 4, 440–445. doi: 10.1055/s-2002-34123

Parniske, M. (2008). Arbuscular mycorrhiza: the mother of plant root endosymbioses. *Nat. Rev. Microbiol.* 6, 763. doi: 10.1038/nrmicro1987

Paterson, E., Sim, A., Davidson, J., and Daniell, T. J. (2016). Arbuscular mycorrhizal hyphae promote priming of native soil organic matter mineralisation. *Plant Soil* 408, 243–254. doi: 10.1007/s11104-016-2928-8

Paynel, F., Murray, P. J., and Bernard Cliquet, J. (2001). Root exudates: a pathway for short-term N transfer from clover and ryegrass. *Plant Soil* 229, 235–243. doi: 10.1023/a:1004877214831

Péret, B., Clément, M., Nussaume, L., and Desnos, T. (2011). Root developmental adaptation to phosphate starvation: better safe than sorry. *Trends Plant Sci.* 16, 442–450. doi: 10.1016/j.tplants.2011.05.006

Phillips, D. A., Fox, T. C., King, M. D., Bhuvaneswari, T. V., and Teuber, L. R. (2004). Microbial products trigger amino acid exudation from plant roots. *Plant Physiol.* 136, 2887–2894. doi: 10.1104/pp.104.044222

Pierik, R., Mommer, L., and Voesenek, L. A. C. J. (2013). Molecular mechanisms of plant competition: neighbour detection and response strategies. *Funct. Ecol.* 27, 841–853. doi: 10.1111/1365-2435.12010

Pii, Y., Mimmo, T., Tomasi, N., Terzano, R., Cesco, S., and Crecchio, C. (2015a). Microbial interactions in the rhizosphere: beneficial influences of plant growth-promoting rhizobacteria on nutrient acquisition process. A review. *Biol. Fertil. Soils* 51, 403–415. doi: 10.1007/s00374-015-0996-1

Pii, Y., Penn, A., Terzano, R., Crecchio, C., Mimmo, T., and Cesco, S. (2015b). Plant-microorganism-soil interactions influence the Fe availability in the rhizosphere of cucumber plants. *Plant Physiol. Biochem.* 87, 45–52. doi: 10.1016/j.plaphy.2014.12.014

Png, G. K., Lambers, H., Kardol, P., Turner, B. L., Wardle, D. A., and Laliberté, E. (2019). Biotic and abiotic plant–soil feedback depends on nitrogen-acquisition strategy and shifts during long-term ecosystem development. *Journal of Ecology* 107, 142–153. doi: 10.1111/1365-2745.13048

Pratelli, R., Voll, L. M., Horst, R. J., Frommer, W. B., and Pilot, G. (2010). Stimulation of nonselective amino acid export by glutamine dumper proteins. *Plant Physiol.* 152, 762–773. doi: 10.1104/pp.109.151746

Prikryl, Z., and Vancura, V. (1980). Root exudates of plants. 6. Wheat root exudation as dependent on growth concentration gradient of exudates and the presence of bacteria. *Plant Soil* 57, 69–83.

Ramesh, S. A., Tyerman, S. D., Xu, B., Bose, J., Kaur, S., Conn, V., et al. (2015). GABA signalling modulates plant growth by directly regulating the activity of plant-specific anion transporters. *Nat. Commun.* 6:7879. doi: 10.1038/ncomms8879

Reid, D. E., Ferguson, B. J., and Gresshoff, P. M. (2011a). Inoculation- and nitrate-induced CLE peptides of soybean control NARK-dependent nodule formation. *Mol. Plant-Microbe Interact.* 24, 606–618. doi: 10.1094/mpmi-09-10-0207

Reid, D. E., Ferguson, B. J., Hayashi, S., Lin, Y. -H., and Gresshoff, P. M. (2011b). Molecular mechanisms controlling legume autoregulation of nodulation. *Ann. Bot.* 108, 789–795. doi: 10.1093/aob/mcr205

Reinhart, K. O. (2012). The organization of plant communities: negative plant-soil feedbacks and semiarid grasslands. *Ecology* 93, 2377–2385. doi: 10.1890/12-0486.1

Rolland, F., Baena-Gonzalez, E., and Sheen, J. (2006). Sugar sensing and signaling in plants: conserved and novel mechanisms. *Annu. Rev. Plant Biol.* 57, 675–709. doi: 10.1146/annurev.arplant.57.032905.105441

Ross-Elliott, T. J., Jensen, K. H., Haaning, K. S., Wager, B. M., Knoblauch, J., Howell, A. H., et al. (2017). Phloem unloading in Arabidopsis roots is convective and regulated by the phloem-pole pericycle. *elife* 6:e24125. doi: 10.7554/eLife.24125

Rothstein, D. E. (2009). Soil amino-acid availability across a temperate-forest fertility gradient. *Biogeochemistry* 92, 201–215. doi: 10.1007/s10533-009-9284-1

Rouached, H., Arpat, A. B., and Poirier, Y. (2010). Regulation of phosphate starvation responses in plants: signaling players and cross-talks. *Mol. Plant* 3, 288–299. doi: 10.1093/mp/ssp120

Roy, S. J., Gilliham, M., Berger, B., Essah, P. A., Cheffings, C., Miller, A. J., et al. (2008). Investigating glutamate receptor-like gene co-expression in *Arabidopsis thaliana*. *Plant Cell Environ.* 31, 861–871. doi: 10.1111/j.1365-3040.2008.01801.x

Rutschow, H. L., Baskin, T. I., and Kramer, E. M. (2011). Regulation of solute flux through plasmodesmata in the root meristem. *Plant Physiol.* 155, 1817–1826. doi: 10.1104/pp.110.168187

Ryan, P. R., James, R. A., Weligama, C., Delhaize, E., Rattey, A., Lewis, D. C., et al. (2014). Can citrate efflux from roots improve phosphorus uptake by plants? Testing the hypothesis with near-isogenic lines of wheat. *Physiol. Plant.* 151, 230–242. doi: 10.1111/ppl.12150

Sasse, J., Martinoia, E., and Northen, T. (2018). Feed your friends: do plant exudates shape the root microbiome? *Trends Plant Sci.* 23, 25–41. doi: 10.1016/j.tplants.2017.09.003

Savage, J. A., Clearwater, M. J., Haines, D. F., Klein, T., Mencuccini, M., Sevanto, S., et al. (2016). Allocation, stress tolerance and carbon transport in plants: how does phloem physiology affect plant ecology? *Plant Cell Environ.* 39, 709–725. doi: 10.1111/pce.12602

Schimel, J. P., and Bennett, J. (2004). Nitrogen mineralization: challenges of a changing paradigm. *Ecology* 85, 591–602. doi: 10.1890/03-8002

Schmidt, H., Nunan, N., Höck, A., Eickhorst, T., Kaiser, C., Woebken, D., et al. (2018). Recognizing patterns: spatial analysis of observed microbial colonization on root surfaces. *Front. Environ. Sci.* 6:61. doi: 10.3389/fenvs.2018.00061

Scott-Denton, L. E., Rosenstiel, T. N., and Monson, R. K. (2006). Differential controls by climate and substrate over the heterotrophic and rhizospheric components of soil respiration. *Glob. Chang. Biol.* 12, 205–216. doi: 10.1111/j.1365-2486.2005.01064.x

Semchenko, M., Hutchings, M. J., and John, E. A. (2007). Challenging the tragedy of the commons in root competition: confounding effects of neighbour presence and substrate volume. *J. Ecol.* 95, 252–260. doi: 10.1111/j.1365-2745.2007.01210.x

Shane, M. W., and Lambers, H. (2005). Cluster roots: a curiosity in context. *Plant Soil* 274, 101–125. doi: 10.1007/s11104-004-2725-7

Shi, S., Richardson, A. E., O'Callaghan, M., DeAngelis, K. M., Jones, E. E., Stewart, A., et al. (2011). Effects of selected root exudate components on soil bacterial communities. *FEMS Microbiol. Ecol.* 77, 600–610. doi: 10.1111/j.1574-6941.2011.01150.x

Shishkova, S., Rost, T. L., and Dubrovsky, J. G. (2008). Determinate root growth and meristem maintenance in angiosperms. *Ann. Bot.* 101, 319–340. doi: 10.1093/aob/mcm251

Smith, S. E., and Read, D. J. (2008). *Mycorrhizal symbiosis*. Amsterdam: Academic Press.

Smith, S. E., and Smith, F. A. (2011). Roles of arbuscular mycorrhizas in plant nutrition and growth: new paradigms from cellular to ecosystem scales. *Annu. Rev. Plant Biol.* 62, 227–250. doi: 10.1146/annurev-arplant-042110-103846

Somssich, M., Khan, G. A., and Persson, S. (2016). Cell wall heterogeneity in root development of arabidopsis. *Front. Plant Sci.* 7:1242. doi: 10.3389/fpls.2016.01242

Steinauer, K., Chatzinotas, A., and Eisenhauer, N. (2016). Root exudate cocktails: the link between plant diversity and soil microorganisms? *Ecol. Evol.* 6, 7387–7396. doi: 10.1002/ece3.2454

Ström, L., Owen, A. G., Godbold, D. L., and Jones, D. L. (2002). Organic acid mediated P mobilization in the rhizosphere and uptake by maize roots. *Soil Biol. Biochem.* 34, 703–710. doi: 10.1016/S0038-0717(01)00235-8

Sun, C.-H., Yu, J.-Q., and Hu, D. -G. (2017). Nitrate: a crucial signal during lateral roots development. *Front. Plant Sci.* 8, 485. doi: 10.3389/fpls.2017.00485

Svistoonoff, S., Creff, A., Reymond, M., Sigoillot-Claude, C., Ricaud, L., Blanchet, A., et al. (2007). Root tip contact with low-phosphate media reprograms plant root architecture. *Nat. Genet.* 39, 792–796. http://www.nature.com/ng/journal/v39/n6/suppinfo/ng2041_S1.html

Tapken, D., Anschutz, U., Liu, L. H., Huelsken, T., Seebohm, G., Becker, D., et al. (2013). A plant homolog of animal glutamate receptors is an ion channel gated by multiple hydrophobic amino acids. *Sci. Signal.* 6:279, ra47. doi: 10.1126/scisignal.2003762

Teardo, E., Formentin, E., Segalla, A., Giacometti, G. M., Marin, O., Zanetti, M., et al. (2011). Dual localization of plant glutamate receptor AtGLR3.4 to plastids and plasmamembrane. *Biochim. Biophys. Acta* 1807 359–367. doi: 10.1016/j.bbabio.2010.11.008

Tegeder, M., and Masclaux-Daubresse, C. (2018). Source and sink mechanisms of nitrogen transport and use. *New Phytol.* 217, 35–53. doi: 10.1111/nph.14876

Teste, F. P., Kardol, P., Turner, B. L., Wardle, D. A., Zemunik, G., Renton, M., et al. (2017). Plant-soil feedback and the maintenance of diversity in Mediterranean-climate shrublands. *Science* 355, 173–176. doi: 10.1126/science.aai8291

Thirkell, T. J., Charters, M. D., Elliott, A. J., Sait, S. M., and Field, K. J. (2017). Are mycorrhizal fungi our sustainable saviours? Considerations for achieving food security. *J. Ecol.* 105, 921–929. doi: 10.1111/1365-2745.12788

Ticconi, C. A., and Abel, S. (2004). Short on phosphate: plant surveillance and countermeasures. *Trends Plant Sci.* 9, 548–555. doi: 10.1016/j.tplants.2004.09.003

Tillard, P., Passama, L., and Gojon, A. (1998). Are phloem amino acids involved in the shoot to root control of NO^{-3} uptake in *Ricinus communis* plants? *J. Exp. Bot.* 49, 1371–1379. doi: 10.1093/jxb/49.325.1371

Toljander, J. F., Lindahl, B. D., Paul, L. R., Elfstrand, M., and Finlay, R. D. (2007). Influence of arbuscular mycorrhizal mycelial exudates on soil bacterial growth and community structure. *FEMS Microbiol. Ecol.* 61, 295–304. doi: 10.1111/j.1574-6941.2007.00337.x

Tsikou, D., Yan, Z., Holt, D. B., Abel, N. B., Reid, D. E., Madsen, L. H., et al. (2018). Systemic control of legume susceptibility to rhizobial infection by a mobile microRNA. *Science* 362, 233–236. doi: 10.1126/science.aat6907

Valentinuzzi, F., Cesco, S., Tomasi, N., and Mimmo, T. (2015). Influence of different trap solutions on the determination of root exudates in *Lupinus albus* L. *Biol. Fertil. Soils* 51, 757–765. doi: 10.1007/s00374-015-1015-2

Van Der Heijden, M. G., Martin, F. M., Selosse, M. A., and Sanders, I. R. (2015). Mycorrhizal ecology and evolution: the past, the present, and the future. *New Phytol.* 205, 1406–1423. doi: 10.1111/nph.13288

Van Nuland, M. E., Bailey, J. K., and Schweitzer, J. A. (2017). Divergent plant-soil feedbacks could alter future elevation ranges and ecosystem dynamics. *Nat. Ecol. Evol.* 1, 0150. doi: 10.1038/s41559-017-0150

Verbon, E. H., and Liberman, L. M. (2016). Beneficial microbes affect endogenous mechanisms controlling root development. *Trends Plant Sci.* 21, 218–229. doi: 10.1016/j.tplants.2016.01.013

Vidal, A., Hirte, J., Bender, S. F., Mayer, J., Gattinger, A., Höschen, C., et al. (2018). Linking 3D soil structure and plant-microbe-soil carbon transfer in the rhizosphere. *Front. Environ. Sci.* 6:9. doi: 10.3389/fenvs.2018.00009

Vincill, E. D., Bieck, A. M., and Spalding, E. P. (2012). Ca^{2+} conduction by an amino acid-gated ion channel related to glutamate receptors. *Plant Physiol.* 159, 40–46. doi: 10.1104/pp.112.197509

Vincill, E. D., Clarin, A. E., Molenda, J. N., and Spalding, E. P. (2013). Interacting glutamate receptor-like proteins in phloem regulate lateral root initiation in Arabidopsis. *Plant Cell* 25, 1304–1313. doi: 10.1105/tpc.113.110668

Vranova, V., Rejsek, K., Skene, K. R., Janous, D., and Formanek, P. (2013). Methods of collection of plant root exudates in relation to plant metabolism and purpose: a review. *J. Plant Nutr. Soil Sci.* 176, 175–199. doi: 10.1002/jpln.201000360

Walch-Liu, P., Liu, L.-H., Remans, T., Tester, M., and Forde, B. G. (2006a). Evidence that l-glutamate can act as an exogenous signal to modulate root growth and branching in *Arabidopsis thaliana*. *Plant Cell Physiol.* 47, 1045–1057. doi: 10.1093/pcp/pcj075

Walch-Liu, P. I. A., Ivanov, I. I., Filleur, S., Gan, Y., Remans, T., and Forde, B. G. (2006b). Nitrogen regulation of root branching. *Ann. Bot.* 97, 875–881. doi: 10.1093/aob/mcj601

Warren, C. R. (2015). Wheat roots efflux a diverse array of organic N compounds and are highly proficient at their recapture. *Plant Soil* 397, 147–162. doi: 10.1007/s11104-015-2612-4

Warren, C. R. (2016). Simultaneous efflux and uptake of metabolites by roots of wheat. *Plant Soil* 406, 359–374. doi: 10.1007/s11104-016-2892-3

Watt, M., and Evans, J. R. (1999). Linking development and determinacy with organic acid efflux from proteoid roots of white lupin grown with low phosphorus and ambient or elevated atmospheric CO_2 concentration. *Plant Physiol.* 120, 705–716. doi: 10.1104/pp.120.3.705

Watt, M., Hugenholtz, P., White, R., and Vinall, K. (2006). Numbers and locations of native bacteria on field-grown wheat roots quantified by fluorescence in situ hybridization (FISH). *Environ. Microbiol.* 8, 871–884. doi: 10.1111/j.1462-2920.2005.00973.x

Williams, L. E., Lemoine, R., and Sauer, N. (2000). Sugar transporters in higher plants – a diversity of roles and complex regulation. *Trends Plant Sci.* 5, 283–290. doi: 10.1016/S1360-1385(00)01681-2

Wubs, E. R. J., and Bezemer, T. M. (2018). Plant community evenness responds to spatial plant-soil feedback heterogeneity primarily through the diversity of soil conditioning. *Funct. Ecol.* 32, 509–521. doi: 10.1111/1365-2435.13017

Yang, H., Bogner, M., Stierhof, Y. -D., and Ludewig, U. (2010). H^+-independent glutamine transport in plant root tips. *PLoS One* 5:e8917. doi: 10.1371/journal.pone.0008917

Yang, N. J., and Hinner, M. J. (2015). Getting across the cell membrane: an overview for small molecules, peptides, and proteins. *Methods Mol. Biol.* 1266, 29–53. doi: 10.1007/978-1-4939-2272-7_3

Yin, H., Li, Y., Xiao, J., Xu, Z., Cheng, X., and Liu, Q. (2013). Enhanced root exudation stimulates soil nitrogen transformations in a subalpine coniferous forest under experimental warming. *Glob. Chang. Biol.* 19, 2158–2167. doi: 10.1111/gcb.12161

Zhang, L., Feng, G., and Declerck, S. (2018). Signal beyond nutrient, fructose, exuded by an arbuscular mycorrhizal fungus triggers phytate mineralization by a phosphate solubilizing bacterium. *ISME J.* 12, 2339–2351. doi: 10.1038/s41396-018-0171-4

Zhu, S., Vivanco, J. M., and Manter, D. K. (2016). Nitrogen fertilizer rate affects root exudation, the rhizosphere microbiome and nitrogen-use-efficiency of maize. *Appl. Soil Ecol.* 107(Suppl. C), 324–333. doi: 10.1016/j.apsoil.2016.07.009

Zimmermann, S., Ehrhardt, T., Plesch, G., and Müller-Röber, B. (1999). Ion channels in plant signaling. *Cell. Mol. Life Sci.* 55, 183–203. doi: 10.1007/s000180050284

Conflict of Interest Statement: The authors declare that the research was conducted in the absence of any commercial or financial relationships that could be construed as a potential conflict of interest.

frontiers in Plant Science

CORRECTION
published: 09 April 2019
doi: 10.3389/fpls.2019.00420

Corrigendum: Root Exudation of Primary Metabolites: Mechanisms and Their Roles in Plant Responses to Environmental Stimuli

Alberto Canarini[1]*, *Christina Kaiser*[1], *Andrew Merchant*[2], *Andreas Richter*[1] and *Wolfgang Wanek*[1]

[1] Terrestrial Ecosystem Research, Department of Microbiology and Ecosystem Science, Research Network 'Chemistry Meets Microbiology', University of Vienna, Vienna, Austria, [2] Faculty of Science, Sydney Institute of Agriculture, The University of Sydney, Sydney, NSW, Australia

OPEN ACCESS

Edited and reviewed by:
Davide Bulgarelli,
University of Dundee, United Kingdom

***Correspondence:**
Alberto Canarini
alberto.canarini@univie.ac.at

Specialty section:
This article was submitted to Plant Microbe Interactions, a section of the journal Frontiers in Plant Science

Received: 05 March 2019
Accepted: 19 March 2019
Published: 09 April 2019

Citation:
Canarini A, Kaiser C, Merchant A, Richter A and Wanek W (2019) Corrigendum: Root Exudation of Primary Metabolites: Mechanisms and Their Roles in Plant Responses to Environmental Stimuli. Front. Plant Sci. 10:420. doi: 10.3389/fpls.2019.00420

Keywords: root exudates, soil micro-organisms, root architecture, nutrient sensing, priming effect, mycorrhiza

A Corrigendum on

Root Exudation of Primary Metabolites: Mechanisms and Their Roles in Plant Responses to Environmental Stimuli

by Canarini, A., Kaiser, C., Merchant, A., Richter, A., and Wanek, W. (2019). Front. Plant Sci. 10:157. doi: 10.3389/fpls.2019.00157

In the original article, there was a mistake in **Figure 1** as published. The group of cells highlighted in red (in the upper part of the figure) are named "meristem," while it should more specifically refer to the "quiescent center." The corrected **Figure 1** appears below.

The authors apologize for this error and state that this does not change the scientific conclusions of the article in any way. The original article has been updated.

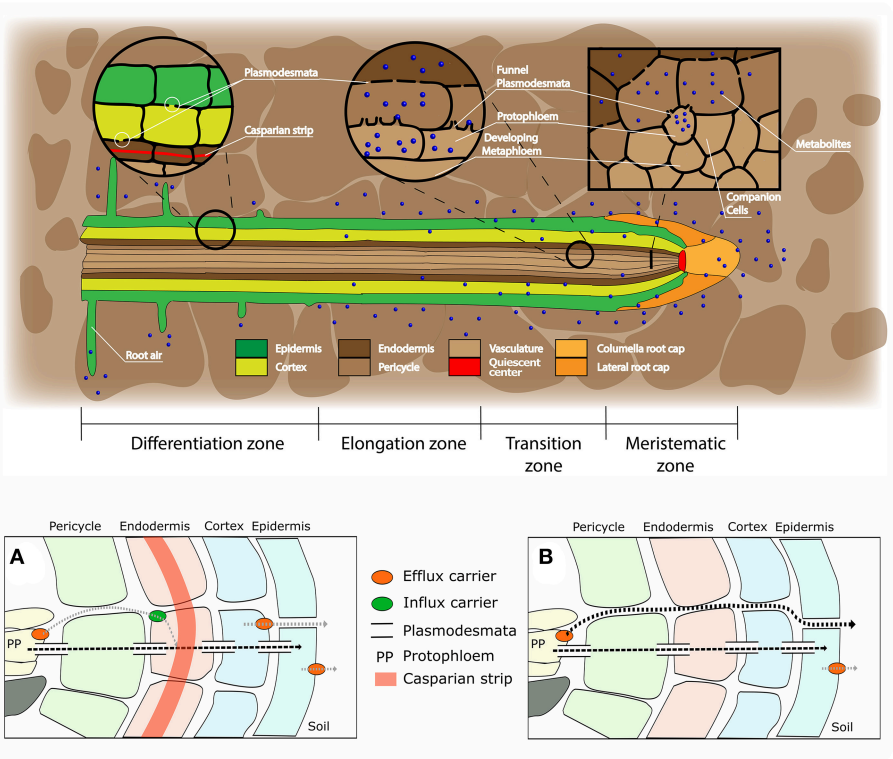

FIGURE 1 | Root structure and areas of root exudation. The upper figure represents the longitudinal section of a root. Tissues are indicated in different colors for the different zones of the root (listed at the bottom). The two circles focus on two distinct zones, a differentiated vs. an undifferentiated area, to show the presence of a Casparian strip and low abundance of plasmodesmata in the differentiated area (left circle), and the presence of funnel plasmodesmata in the undifferentiated area (right circle). The square represents a cross section close to the meristematic area where root exudation is the highest. The lower figures represent a schematic representation of solute movement sites from phloem unloading to the soil environment, either in the differentiation zone **(A)** or in the undifferentiated root tip **(B)**. **(A)** Solutes move both through the symplastic and apoplastic pathways, but then they are re-uptaken into the cytoplasm as the Casparian strip limits the apoplastic pathway. Only the cortex and epidermis are responsible for the flux of metabolites into the apoplast and consecutively into the soil (root exudation). Cortex and epidermis represents the major control point for root exudation. **(B)** At the phloem unloading site, both symplastic and apoplastic pathways are used. Because of the lack of a Casparian strip solutes can move out of the root (root exudation) through both the apoplastic and the symplastic pathway.

frontiers in Environmental Science

ORIGINAL RESEARCH
published: 27 November 2018
doi: 10.3389/fenvs.2018.00140

Root Exudates Induce Soil Macroaggregation Facilitated by Fungi in Subsoil

Vera L. Baumert[1], Nadezda A. Vasilyeva[2], Artem A. Vladimirov[2,3], Ina C. Meier[4], Ingrid Kögel-Knabner[1,5] and Carsten W. Mueller[1]*

[1] Chair of Soil Science, Technical University of Munich, Freising, Germany, [2] Interdisciplinary Laboratory for Mathematical Modeling of Soil Systems, V.V. Dokuchaev Soil Science Institute, Moscow, Russia, [3] Bogoliubov Laboratory of Theoretical Physics, Joint Institute for Nuclear Research, Dubna, Russia, [4] Plant Ecology, Albrecht-von-Haller Institute for Plant Sciences, University of Göttingen, Göttingen, Germany, [5] Institute for Advanced Study, Technical University of Munich, Garching, Germany

Subsoils are known to harbor large amounts of soil organic carbon (SOC) and may represent key global carbon (C) sinks given appropriate management. Although rhizodeposition is a major input pathway of organic matter to subsoils, little knowledge exists on C dynamics, particularly stabilization mechanisms, such as soil aggregation, in the rhizosphere of different soil depths. The aim of this study was to investigate the influence of natural and elevated root exudation on C allocation and aggregation in the topsoil and subsoil of a mature European beech (*Fagus sylvatica* L.) forest. We experimentally added model root exudates to soil at two different concentrations using artificial roots and analyzed how these affect SOC, nitrogen, microbial community composition, and size distribution of water-stable aggregates. Based on the experimental data, a mathematical model was developed to describe the spatial distribution of the formation of soil aggregates and their binding strength. Our results demonstrate that greater exudate additions affect the microbial community composition in favor of fungi which promote the formation of macroaggregates. This effect was most pronounced in the C-poor subsoil, where macroaggregation increased by 86% and SOC content by 10%. Our modeling exercise reproduced the observed increase in subsoil SOC at high exudate additions. We conclude that elevated root exudation has the potential to increase biotic macroaggregation and thus the C sink strength in the rhizosphere of forest subsoils.

Keywords: soil organic carbon, soil depth, rhizosphere, aggregate fractionation, artificial roots, microbial community composition, aggregation model

OPEN ACCESS

Edited by:
Hannes Schmidt, Universität Wien, Austria

Reviewed by:
Paul Hallett, University of Aberdeen, United Kingdom
Lukas Van Zwieten, New South Wales Department of Primary Industries, Australia

****Correspondence:***
Vera L. Baumert
vera.baumert@wzw.tum.de

Specialty section:
This article was submitted to Soil Processes, a section of the journal Frontiers in Environmental Science

Received: *03 September 2018*
Accepted: *02 November 2018*
Published: *27 November 2018*

Citation:
Baumert VL, Vasilyeva NA, Vladimirov AA, Meier IC, Kögel-Knabner I and Mueller CW (2018) Root Exudates Induce Soil Macroaggregation Facilitated by Fungi in Subsoil. Front. Environ. Sci. 6:140. doi: 10.3389/fenvs.2018.00140

INTRODUCTION

Soils represent the largest terrestrial organic carbon (OC) pool, thus, an increase in soil OC (SOC) stocks via improved management practices has the potential to mitigate global climate change (Jobbágy and Jackson, 2000; Lal et al., 2011; Powlson et al., 2011; Stockmann et al., 2013; Lal, 2016; Minasny et al., 2017). However, most studies on the carbon (C) sink strength of soils have focused on C dynamics in topsoils only. These usually harbor high OC concentrations, but are often very shallow, particularly in forest soils. In contrast, subsoils are characterized by low OC concentrations

and a large volume. As a consequence of this large volume, subsoils store up to 70% of the global SOC stocks (Batjes, 1996; Jobbágy and Jackson, 2000).

Compared with the topsoil, the input of fresh organic matter (OM) is scarce and more heterogeneous in deeper soil layers (Chabbi et al., 2009). A major input pathway of OC to subsoils is plant roots, which provide OM in the form of rhizodeposits such as dead root cells, soluble root exudates, sloughed-off cells, or mucilage (Rasse et al., 2005; Jones et al., 2009; Rumpel et al., 2012). These root-derived compounds trigger the development of a narrow zone around the roots, which is influenced by their activity and considered as a hotspot of biological, chemical, and physical activities in soils, i.e., the rhizosphere (Hinsinger et al., 2009). Rhizodeposits and especially soluble root exudates represent an easily available C source for soil microbes (van Hees et al., 2005) and have frequently been observed to alter the native C mineralization rates of inherent SOC (Huo et al., 2017), a process widely referred to as the priming effect (Kuzyakov, 2010; Dijkstra et al., 2013). This effect can be either positive or negative (i.e., accelerated or reduced decomposition of inherent SOM), and several studies have found that its magnitude may vary among soil types, soil depths (Paterson and Sim, 2013), and exudate addition rates (Blagodatskaya and Kuzyakov, 2008).

Plant roots and rhizodeposits as well as microorganisms in the rhizosphere promote soil aggregation (Amézketa, 1999) and thereby the occlusion of OM which is an important mechanism of C stabilization (Blanco-Canqui and Lal, 2004; von Lützow et al., 2006). In this regard, plant roots and fungi are of special importance for the formation of macroaggregates (>250 μm) (Tisdall and Oades, 1982; Chantigny et al., 1997; Helfrich et al., 2008), whereas polysaccharides exuded by roots or microbes and OM in general may be relevant gluing agents for the formation of microaggregates (Amézketa, 1999; Totsche et al., 2018). Because soil aggregation is strongly influenced by biotic processes, it has long been considered less relevant in deeper, less biologically active soil horizons (Lorenz and Lal, 2005; von Lützow et al., 2006). Recently, evidence is growing that it is of similar importance for the stabilization of SOM in topsoils and subsoils (Rasmussen et al., 2005; Moni et al., 2010; Sanaullah et al., 2010; Rumpel et al., 2012). Because roots have been shown to play a significant role in the input and dynamics of OC in subsoils (Angst et al., 2016; Heinze et al., 2018), the question remains to what extent soluble root exudates drive the C allocation and soil aggregation in subsoil vs. topsoils.

By applying artificial root exudate mixtures as a surrogate for soluble rhizodeposits, their effects on soil processes can be examined. Most of the previous studies applying root exudates have focused mainly on biological parameters, such as soil respiration and microbial community structure and activity (Marx et al., 2010; Drake et al., 2013; Luo et al., 2014), and not on soil aggregation. Moreover, only few studies have investigated the effects of labile C additions to different soil depths so far, and if so, they were restricted to the determination of priming effects. Although the observed responses varied from an increased (Karhu et al., 2016) to a decreased (de Graaff et al., 2014) or even absent (Salomé et al., 2010) relative priming effect in deeper soil layers as compared with the topsoil, they agreed that subsoils appear to react differently to labile C additions than topsoils.

Currently, much uncertainty still exists regarding the mechanisms underlying SOM dynamics and rhizosphere processes in subsoils. In particular, their role as a source or sink of CO_2 facing climate change and the mechanisms by which C is stored and protected in subsoils are largely unexplored (Rumpel and Kögel-Knabner, 2011). Knowledge regarding these processes, particularly including the influence on aggregation as a way to stabilize SOC, is urgently needed to improve the modeling of SOC cycling and to assess the role of subsoils in soil C dynamics.

For the study and prediction of SOC dynamics, mathematical models that are based on processes involved in C cycling are of high importance (Campbell and Paustian, 2015). Although it is known that aggregation plays an important role in SOC stabilization, it is rarely considered in current soil biogeochemical models (Abramoff et al., 2017). Abramoff et al. (2017) recently made an attempt to include C storage within aggregates in their conceptual model, but concluded that the lack of robust data on aggregate turnover made soil aggregation the model's most uncertain component. Mathematical models that simulate the process of soil aggregation itself and could be implemented in general SOM models are especially scarce to date. Albalasmeh and Ghezzehei (2014) modeled soil structure development under consideration of root exudation and soil moisture, but did not consider soil microbes nor link aggregation to SOC storage. Several studies modeled soil aggregate formation based on the conceptual model that macroaggregates form around particulate OM and release microaggregates upon disruption (Oades, 1984): Segoli et al. (2013) thereby accounted for the effects of microbial activity on macroaggregate formation and integrated it in SOM dynamics, while Stamati et al. (2013) linked aggregate turnover with different conceptual SOC pools, among them microbial biomass. Still, there is a lack of modeling approaches addressing soil aggregation processes in the rhizosphere as a protection mechanism for SOC. Especially the effect of soil moisture on microbial abundance and the influence of both parameters on soil structure formation needs to be further addressed (Crawford et al., 2012; Vasilyeva et al., 2016; Banwart et al., 2017).

In the present study, we combined experimental approaches and mathematical modeling in order to investigate the effect of artificial root exudates on SOC content, and aggregate formation under consideration of the microbial community structure in topsoil and subsoil. To do so, we inserted artificial roots (Kuzyakov et al., 2006; Keiluweit et al., 2015; Meier et al., 2017) in microcosms repacked with soil material from different depths and used them to inject root exudates. Varying addition rates of labile C have been found to affect the decomposition of inherent SOM (Blagodatskaya and Kuzyakov, 2008) as well as activities of enzymes that degrade fast-cycling nitrogen (N) pools nonlinearly (Meier et al., 2017). Thus, we aimed to assess the effect of different quantities of exudate amendments. One of our exudate addition treatments simulated natural C concentrations of root exudation in temperate acidic beech forests (Meier, personal communication), whereas the other one was an experimentally increased exudate concentration that has been applied in several

similar experiments (Keiluweit et al., 2015; Meier et al., 2017). The aggregate formation model presented in this study uses a novel approach by modeling spatial gradients of microbial abundance, moisture, and gluing agents around the exuding root. This defines patterns of binding strength between soil particles and finally simulates aggregate size distribution.

In our laboratory experiment, we are not aiming at completely simulating natural conditions such as subsoil specific temperature and aeration or mycorrhizal symbiosis. Despite these limitations, our well-defined model system enabled us to experimentally simulate the local formation of rhizosphere properties under controlled conditions and to study the processes involved. Based on these experimentally measured variables, we propose a new approach to model aggregate formation driven by microbial SOM transformations and soil moisture due to the release of varying rates of soluble root exudates within the rhizosphere.

MATERIALS AND METHODS

Study Site and Soil Sampling

Soil samples were taken in March 2017 in an even aged forest dominated by European beech (*Fagus sylvatica* L.) near Rüdershausen, Lower Saxony, Germany (51° 34′ 51.52″ N, 10° 14′ 43.03″ O). The study site is located at 200 m a.s.l., and is characterized by a mean annual temperature of 9.2°C and mean annual precipitation of 650 mm (Deutscher Wetterdienst, Station Goettingen). The soil developed on quaternary loess deposits was classified as a Haplic Cambisol (IUSS Working Group WRB, 2015) (Ol/Ah/Bw/Bwg1/Bwg2). The soil material used for the laboratory incubation was sampled from one soil profile at two horizons: the uppermost mineral horizon (Ah, 0–5 cm) is subsequently referred to as topsoil, and the Bwg1 horizon (33–50 cm) is referred to as subsoil. After sieving of the soil materials <2 mm, the remaining root and litter fragments were removed manually by picking with tweezers. Until the start of the incubation experiment, the soils were stored field-moist at 4°C. **Table 1** lists soil texture and other basic soil properties of the top and subsoil materials used for the incubation experiment.

TABLE 1 | Basic soil properties of the soil material used for incubation (before incubation).

	Topsoil	Subsoil
OC (mg g^{-1})	33.31	3.26
N (mg g^{-1})	2.31	0.41
C/N ratio	14.44	7.97
TEXTURE (%)		
Medium and coarse sand (>250 μm)	0.7	0.4
Fine sand (>53 μm)	9.2	6.0
Silt (53–2 μm)	64.0	67.2
Clay (<2 μm)	26.2	26.4
Total PLFA content (nmol g^{-1})	133.7	4.4
$F:B_{PLFA}$	0.4	0.3
Total AS content (μg AS C g^{-1} SOC)	26.2	46.1
$F:B_{AS}$	1.7	2.3
AGGREGATE SIZE CLASS DISTRIBUTION (%)		
>250 μm	52	24
250–53 μm	36	58
53–20 μm	9	13
<20 μm	4	4
OC (mg g^{-1})		
>250 μm	41.9	4.5
250–53 μm	28.9	3.1
53–20 μm	14.1	2.6
<20 μm	16.1	6.6
DOC	0.6	0.5
N (mg g^{-1})		
>250 μm	2.7	0.4
250–53 μm	2.0	0.4
53–20 μm	1.1	0.3
<20 μm	1.6	0.8
dNt	0.1	0.1
C/N		
>250 μm	15.5	11.3
250–53 μm	14.5	7.8
53–20 μm	12.8	8.7
<20 μm	10.1	8.3
DOM	4.6	9.0

Experimental Setup

Square Petri dishes prepared with a cut-out for the artificial root and aeration holes were used as microcosms. They were packed with soil at field bulk density (1.06 g cm^{-3} for topsoil and 1.40 g cm^{-3} for subsoil) and 60% water holding capacity (WHC). Rhizon soil moisture samplers (Rhizosphere Research Products, Wageningen, Netherlands) were completely inserted in the center of the microcosm during the packing process to ensure tight soil contact. Rhizon samplers are microporous capillaries (9.3 cm length, 2.5 mm outer diameter, mean pore size of 0.15 μm), which served as artificial roots (**Figure S1**). The tubing of the Rhizon sampler was sealed using a back-pressure valve (Infuvalve®, BBraun, Melsungen, Germany) to prevent air from entering the system.

After a preincubation period of 7 days, the artificial roots were supplied with 0.5 ml of model exudate solution twice per day over the course of 30 days at 20°C (at atmospheric oxygen levels). The artificial exudate solution contained 60% acetic acid, 35% glucose, and 5% serine. These compounds were selected based on the reported exudate chemistry of trees (Smith, 1970, 1976; Shen et al., 1996), and the specific contents correspond to the relative proportions of organic acids, simple sugars, and amino acids, respectively, as exuded by mature trees (Smith, 1976). The respective concentrations of the exudate solutions for the treatments were set to 0, 6, and 180 μg C cm^{-2} root surface d^{-1} and are subsequently referred to as "water control," "moderate," and "high." The water control samples received only deionized water, whereas the moderate treatment represents realistic C-based exudation rates for European beech trees (Brzostek et al., 2012; Tückmantel et al., 2017). The amount used in the high treatment was

chosen with reference to previous experiments with artificial root exudates that used such high concentrations (Keiluweit et al., 2015; Meier et al., 2017). The solutions were injected manually with a syringe, having a syringe filter attached for sterile filtration (0.22 μm) (**Figure S1**). Fresh exudate solutions were prepared weekly and stored at 4°C. Each treatment was run in four replicates. During the incubation period, soil moisture content was regularly checked and maintained at 60% WHC by adding small amounts of deionized water through the aeration holes of the microcosms. The addition rate of 1 ml exudate solution per day and microcosm almost equaled the daily amount of evaporation so that nearly no additional water had to be provided to the microcosms in order to hold constant moisture.

After an incubation period of 30 days, soil within a radius of 6 mm around the artificial roots which was assumed to be directly influenced by the exudate solution (Drake et al., 2013), was sampled as the artificial rhizosphere (subsequently referred to as rhizosphere) and the remaining material (>6 mm from the Rhizon sampler) as the bulk soil. Normalized to the mass of the rhizosphere soil, moderate exudate additions amounted to 2.8 and 2.1 μg C $g^{-}1$ dry soil d^{-1} and those of the high treatment to 83.9 and 63.7 μg C $g^{-}1$ dry soil d^{-1} in topsoil and subsoil, respectively. Aliquots of the sampled soil material were stored air-dried and freeze-dried, respectively, for subsequent analyses.

Phospholipid Fatty Acid Analysis

Phospholipid fatty acids (PLFA) were extracted following the method described by Frostegård et al. (1991) with modifications by Kramer et al. (2013). Approximately 2 g of topsoil and 7 g of subsoil (freeze-dried aliquot) were treated with Bligh & Dyer solution [methanol, chloroform, citrate buffer (pH = 4), 2:1:0.8, v/v/v] to extract the lipids. The PLFA fraction was separated by solid phase extraction on silica columns (0.5 g SiOH, Chromabond®, Macherey-Nagel, Düren, Germany) and transformed into fatty acid methyl esters (FAMEs) by alkaline methanolysis. The dried extracts were dissolved in isooctane and determined using a Trace 1300 gas chromatograph (Thermo Fisher Scientific, Waltham, MA, USA) with flame ionization detection (GC-FID) using a ZB-5HT fused silica capillary column (60 m, 0.25 I.D., 0.25 μm film thickness; Phenomenex Ltd., Aschaffenburg, Germany). The PLFA concentrations were quantified relative to non-adecanoic acid methyl ester (19:0) as internal standard and subsequently normalized to the mean long-term results of a standard soil that was extracted parallel in order to level differences between single extractions.

The PLFAs were categorized into groups indicative of bacteria (i15:0, a15:0, i16:0, i17:0, cy17:0, cy19:0, 15:0, 16:1n7, and 17:0) and fungi (18:2n6 and 18:1n9). Although it is also present in bacteria and plants in minor contents, 18:1n9 has been shown to be a reliable indicator for fungi in forest soils (Kaiser et al., 2010; Frostegård et al., 2011). All the above mentioned fatty acids together with 14:0, 16:0, 18:1n9, 18:1n9t, 18:0, and 20:0 were used for the calculation of total microbial PLFAs. The total microbial PLFA content is used as an indicator for changes in microbial biomass (Frostegård et al., 1991; Bailey et al., 2002). Several other PLFAs were detected in the samples, which could be of microbial origin as well. However, only PLFA peaks that were identified unambiguously via mass spectrometry in pre-experiments were selected as biomarkers. Therefore, PLFA extracts from test samples as well as qualitative standard mixtures (37-Component FAME Mix and Bacterial Acid Methyl Esters Mix; Supelco, Bellefonte, PA, USA) were measured on a Trace GC Ultra coupled to an ISQ mass spectrometer (Thermo Fisher Scientific) using the same capillary column and temperature program that was used for GC-FID analysis. A PLFA-based fungal-to-bacterial-ratio ($F:B_{PLFA}$) was calculated from the PLFA contents of the fungal PLFA and total bacterial PLFAs.

Amino Sugar Analysis

The amino sugars (AS) glucosamine (GluN), mannosamine (ManN), galactosamine (GalN), and muramic acid (MurA) were extracted from rhizosphere and bulk soil samples according to Zhang and Amelung (1996). Freeze-dried aliquots of the samples were ground and hydrolyzed with 6 M HCl at 105°C for 8 h. Subsequently, the extracts were filtered and neutralized to separate impurities by precipitation and derivatized to form aldonitrile acetates. The dried extracts were redissolved in ethyl acetate:hexane (1:1; v/v) before measurement on a Trace 1300 gas chromatograph (Thermo Fisher Scientific) equipped with a ZB-5HT fused silica capillary column (60 m, 0.25 I.D., 0.25 μm film thickness; Phenomenex LTD, Aschaffenburg, Germany) and a flame ionization detector. The internal standard myoinositol was used as a reference to quantify AS concentrations.

The total AS content was calculated per sample as the sum of the four AS. Following Van Groenigen et al. (2007), the bacterial- and fungal-derived AS C was calculated and used to obtain an estimate of the AS-based fungal-to-bacterial ratio ($F:B_{AS}$).

Aggregate Fractionation

The rhizosphere and bulk soil samples were fractionated by wet sieving, yielding different size classes of water-stable aggregates (Puget et al., 1999). Therefore, 5 g of air-dried sample material was rewetted in deionized water for 30 min, transferred to a sieve tower (250, 53, and 20 μm stainless steel sieves, 100 mm diameter), and placed in a beaker with deionized water. The sieve tower was moved up and down through a vertical distance of 2 cm at 30 cycles per minute for 5 min. The single fractions were washed from the sieves and freeze-dried. Fractions <20 μm that remained in the beaker were filtered at 0.45 μm in a pressure filtration unit, washed off from the filter, and freeze-dried as well. This method resulted in the following four aggregate fractions: >250 μm (macroaggregates), 250–53, 53–20, and <20 μm. The average recovery rate of the aggregate fractionation procedure was 98.8% of the initial soil mass for samples from either depth. Additionally, the filtrate was analyzed for dissolved OC (DOC) and dissolved total N (dNt) on a total C analyzer coupled to a total bound N (TN_b) module (DIMATOC 2000 and DIMA-N; Dimatec Analysentechnik GmbH, Essen, Germany).

Carbon and Nitrogen Measurements

C and nitrogen (N) contents of the rhizosphere and the bulk soil, and the aggregate size fractions, were analyzed by dry combustion using an elemental analyzer (Eurovector, Milan, Italy). AR, bulk soil, and fractions >53 μm were finely ground in a ball mill before

the analysis. All measurements were performed in duplicate. Because the soils did not contain carbonates, total C contents were considered to be equal to OC contents.

Mathematical Modeling

The introduced model comprisesof two parts: The first one is a biochemical cycle that describes exudate diffusion in water, followed by local OM transformations, microbial growth, and turnover, resulting in the formation of gluing agents that provide a mechanism of aggregation (**Figure 1**). Spatial patterns of these model variables are generated up to a distance of 12 mm from the artificial root. The second part is an aggregation model that describes how the distribution of water-stable aggregate size classes is obtained from the spatial patterns of gluing agents and fungi. All model parameter estimates are listed in **Table 2**.

Modeling of Rhizosphere Patterns

The evolution of spatial patterns of the biochemical cycle (**Figure 1**) was modeled by a system of partial differential equations solved in 2D using cylindrical coordinates (Equation 1). The model variables are: bacterial biomass (B), root exudates (E), gluing agents (G), fungal biomass (F), and SOM (S). All concentrations in the model are expressed in g C cm^{-3} soil using soil bulk densities. Water saturation (θ) affects all rates of biological processes by a moisture factor $W = \theta - \theta_0$, where θ_0 is the minimal saturation for biological processes.

$$\frac{\partial \mathbf{u}}{\partial t} = \frac{1}{r}\frac{\partial}{\partial r}(r\mathbf{D}(u)\frac{\partial \mathbf{u}}{\partial r}) + \frac{\partial}{\partial z}(\mathbf{D}(\mathbf{u})\frac{\partial \mathbf{u}}{\partial z}) + \boldsymbol{\phi}(\mathbf{u}), \quad (1)$$

where $\mathbf{u}(r,z) \equiv (B,F,E,G,S,\theta)$ is the vector of volumetric concentrations of the state variables of the system measured in $[g\ cm^{-3}]$ and $\boldsymbol{\phi}(\mathbf{u})$ is the reaction part and defined as:

$$\phi_B = (T_{EB} + T_{GB})(1 - B/m_1) - r_B B, \quad (2)$$
$$\phi_F = (T_{EF} + T_{GF})(1 - F/m_1) - r_F F, \quad (3)$$
$$\phi_E = -T_{EB} - T_{EF}, \quad (4)$$
$$\phi_G = -T_{GB} - T_{GF} + T_{SG} + r_B B/2 + r_F F/2, \quad (5)$$
$$\phi_S = -T_{SG}, \quad (6)$$
$$\phi_\theta = -d_\theta \theta, \quad (7)$$

where T_{ij} denotes the C transfer rate from pool i to pool j, and d_θ is a constant evaporation rate fitted under the assumption that average moisture was kept constant during the incubation experiment. The decline in carbon use efficiency (CUE) with growing biomass is introduced by m_1 which reflects the environmental capacity for microbes. At this maximum of microbial biomass, microbes are supposed to stop growth but continue respiration and thus reach minimal CUE.

Carbon transfer rates describe the bacterial and fungal growth on root exudates (T_{EB}, T_{EF}) and gluing agents (T_{GB}, T_{GF}) and enzymatic (proportional to B and F) as well as abiotic breakdown of SOM into the pool of gluing agents (T_{SG}) according to the model scheme shown in **Figure 1**:

$$T_{EB} = k_1 EBW, \quad (8)$$
$$T_{EF} = k_3 EFW, \quad (9)$$
$$T_{GB} = k_2 GBW(1 - B/m_1), \quad (10)$$
$$T_{GF} = k_4 GFW(1 - F/m_1), \quad (11)$$
$$T_{SG} = k_S(B + F + k_{S0})SW, \quad (12)$$

where k_1, k_2, k_3, and k_4 are substrate consumption rates by microbes.

Considering community-level regulated processes that are introduced using density-dependence (Georgiou et al., 2017), we formulate a gradual change in substrate preference in favor of root exudates, which are assumed to be the more easily degradable substrate. In the model we expect that the concentration of organic gluing agents increases with the C concentration of the added exudates. Because, the production is expected to increase due to higher microbial biomass and subsequent enzymatic breakdown of SOM, the consumption is expected to decrease due to microbial substrate preference at high biomass. The latter is described by the factors $(1 - B/m_1)$ and $(1 - F/m_1)$ and introduces the possibility of both positive and negative priming effects (Kuzyakov et al., 2000). The transformation of SOM to gluing agents (T_{SG}) is controlled by the enzymatic breakdown rate k_S and the abiotic breakdown rate k_{S0}. Microbial decay rates (r_B and r_F) are also assumed to be density-dependent (Georgiou et al., 2017), slowing down to dormant biomass threshold m_0 at low biomass and increasing until m_1 at high biomass.

$$r_B = k_{rb}\theta(1 - m_0/B)/(1 - B/m_1) \quad (13)$$
$$r_F = k_{rf}\theta(1 - m_0/F)/(1 - F/m_1), \quad (14)$$

where k_{rb} and k_{rf} are the decay constants for bacteria and fungi, correspondingly.

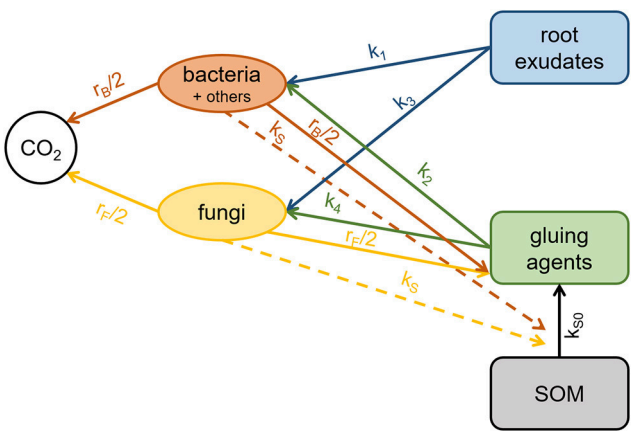

FIGURE 1 | Scheme of the biochemical cycle underlying the mathematical model, where solid arrows represent C transfer rates and dashed arrows catalytic effects.

TABLE 2 | Model parameter estimates.

Parameter	Description	Topsoil	Subsoil
θ_0	Minimal saturation for biological processes	0.2	0.2
d_θ	Constant evaporation rate	9 × 10–5 s–1	9 × 10–5 s–1
D_E	Diffusion constant of root exudates	5.33×10^{-7} mm^2 s^{-1}	5.33×10^{-7} mm^2 s^{-1}
D_θ	Diffusion constant of water	1.07×10^{-6} mm^2 s^{-1}	1.07×10^{-6} mm^2 s^{-1}
k_1	Substrate consumption rate	0.047 s^{-1}	0.037 s^{-1}
k_2	Substrate consumption rate	0.021 s^{-1}	0.018 s^{-1}
k_3	Substrate consumption rate	0.0504 s^{-1}	0.0055 s^{-1}
k_4	Substrate consumption rate	0.0035 s^{-1}	0.0030 s^{-1}
k_S	Enzymatic breakdown rate	7.02×10^{-5} s^{-1}	3.13×10^{-5} s^{-1}
k_{S0}	Abiotic breakdown rate	1.26×10^{-4} g g^{-1}	0
k_{rb}	Decay constant bacteria	3.5×10^{-7} s^{-1}	8.4×10^{-7} s^{-1}
k_{rf}	Decay constant fungi	5.6×10^{-7} s^{-1}	8.4×10^{-7} s^{-1}
m_0	Dormant biomass threshold	3.2×10^{-5} g g^{-1}	2.2×10^{-6} g g^{-1}
m_1	Maximum biomass	6.4×10^{-4} g g^{-1}	4.5×10^{-5} g g^{-1}
p_0	Mean disruptive force	10.2 mm^{-1}	11.8 mm^{-1}
v_1	Coefficient of gluing agents effect on binding strength	578 cm^3 g^{-1}	820 cm^3 g^{-1}
v_2	Coefficient of fungi effect on binding strength	2.89×10^3 cm^3 g^{-1}	4.1×10^3 cm^3 g^{-1}
θ_a	Coefficient of moisture effect on binding strength	0.5	2.8

The moisture-dependent diffusion of water and exudate was calculated as

$$\mathbf{D}(\mathbf{u}) = \mathbf{D}_0(\mathbf{u})\left(0.75 + \theta^2\right), \tag{15}$$

where $\mathbf{D}_0$ is a vector of diffusion constants. Cylindrical model parameters correspond to the experimental setup geometry and include the root radius ($r_0 = 1.25$ mm), microcosm width ($r_1 = 13.25$ mm), and microcosm height ($z_1 = 93$ mm). Thus, model boundary conditions comprise no fluxes through the upper and lower surfaces of the sample cylinder, no fluxes through the side cylindric surface, and no fluxes from the root surface, except for exudate and water, which have a constant value at the root surface:

$$\frac{\partial \mathbf{u}}{\partial z} = 0|_{z=0, z=z_1} \tag{16}$$

$$\frac{\partial \mathbf{u}}{\partial r} = 0|_{r=r_1} \tag{17}$$

$$\frac{\partial B}{\partial r} = \frac{\partial F}{\partial r} = \frac{\partial G}{\partial r} = \frac{\partial S}{\partial r} = 0|_{r=r_0} \tag{18}$$

$$E = E_0|_{r=r_0} \tag{19}$$

$$\theta = 1|_{r=r_0} \tag{20}$$

The initial conditions for all state variables were set uniform, with values taken from measurements of the soil samples before incubation. Microbial biomass was converted from total microbial PLFA content as follows: 1 nmol microbial PLFAs = 3.2 μg microbial biomass C (Willers et al., 2015).

Aggregation Model

An energy-based approach is applied to obtain aggregate size distribution from the modeled rhizosphere pattern. We adopt the assumption that the energy required for aggregate formation is proportional to the newly formed surface (Rittinger's law). Soil binding strength at each point in space is defined as the energy required to create a unit of new surface (v). It depends on the concentration of gluing agents and fungal biomass:

$$v = (1 + v_1 G + v_2 F) \times \frac{1 + \theta_a}{\theta + \theta_a} \tag{21}$$

The unit of soil binding strength is expressed relative to the minumum binding strength ($v = 1$) which is given when no gluing agents or fungi are present and the soil is fully water saturated ($G = 0$, $F = 0$, $\theta = 1$). From the spatial pattern of soil binding strength we obtain the distribution of aggregate size classes by applying disrupting force p_d (energy per unit volume). An aggregate of a certain radius is stable against disrupting force if the energy needed to form an aggregate surface (vr^2) is greater or equal to the energy applied to the aggregate volume ($r^3 p_d$). This results in a larger aggregate radius with larger binding strength and smaller disrupting force ($r = v/p_d$). We assume that p_d is distributed according to truncated normal probability ($p_d > 0$) with a mean value p_0 and a standard deviation $\sigma = 0.5\ p_0$, where p_0 is estimated from fitting procedure.

Parameter Estimates

The model parameters of the biochemical submodel were estimated by fitting the modeled total microbial biomass, fungal biomass, total OC content, and the relative distribution of aggregate size classes at the end of the incubation period to measured ones using the Nelder-Mead optimization method (Nelder and Mead, 1965). We calculated integrals I^{ijk} of the

model state variables B, F, and S over the sample volume:

$$I^{ijk} = \int_{a_k}^{b_k} u_{ij}\, r\, dr, \quad (22)$$

where u_{ij} is the simulation result for variable $i \in$ (B, F, S) and treatment j, whereas k is either rhizosphere (RS in the equation) or bulk soil (BS in the equation) with $a_{RS} = r_0$, $b_{RS} = r_0 + 6$, $a_{BS} = r_0 + 6$, $b_{BS} = r_1$.

In total, for the three variables, three exudate addition treatments and two sampling regions (rhizosphere and bulk soil), 18 data points were obtained for topsoil and 18 for the subsoil. Topsoil and subsoil parameters were fitted independently.

The objective function for minimization is a sum of logarithmic residuals squared of the abovementioned integrals:

$$\sum_{i,j,k} [\log(I^{ijk}_{exp}) - \log(I^{ijk}_{model})]^2 \quad (23)$$

The parameters for aggregation were estimated with a similar procedure according to Equations (22) and (23), where index i corresponds to aggregate size fraction instead of state variable, giving also 18 points of aggregate size distributions for each subsoil and topsoil. We modeled fractions 53–20 and <20 μm as one aggregate size fraction, due to the small share of material in the aggregate size class <20 μm.

Statistical Analysis

All statistical analyses were performed using SPSS Statistics 24 (IBM, Armonk, NY, USA). All variables were tested for normality using the Shapiro–Wilk test and for homogeneity of variance using Levene's test. Treatment means were tested for significant differences within the soil region (rhizosphere and bulk soil) and depth using analysis of variance (ANOVA) followed by Tukey's *post-hoc* test or the non-parametric Kruskal–Wallis test followed by the Wilcoxon test, depending on whether the assumption of normality and homogeneity of variance were met. The differences between soil regions were tested using paired *t*-test. We refer to a *p*-value $\leq$0.05 as statistically significant. To estimate the exudate addition treatment strength in comparison to the water control samples, standardized effect sizes were calculated as bias-corrected Hedges' g* values (Hedges and Olkin, 1985):

$$g = \frac{x_t - x_c}{\sqrt{\frac{(n_t-1)\bullet s_t^2 + (n_c-1)\bullet s_c^2}{n_t+n_c-2}}}$$

$$g^* = g \bullet \left(1 - \frac{3}{4\,(n_t + n_c) - 9}\right)$$

According to Cohen (1988), the effect sizes are classified as small (<0.2), medium (<0.5), and large (>0.8).

RESULTS

Basic Soil Properties

The soil material before incubation varied considerably between topsoil and subsoil (**Table 1**). The OC content of the topsoil amounted to 33.3 mg g^{-1}, whereas it was only 3.3 mg g^{-1} in the subsoil. The C/N ratio decreased by almost 50% from 14 to 8 with soil depth. In contrast, soil texture was similar at the two soil depths. Microbial residues as determined by the AS content strongly increased with depth from 26 to 46 μg AS C g^{-1} SOC when standardized to SOC content. The aggregate size class distribution varied between soil depths. In the topsoil, the relative abundance of the water-stable aggregate size fractions decreased with aggregate size. Macroaggregates >250 μm thereby comprised the largest fraction, which accounted for ~50% of the topsoil mass. In the subsoil, macroaggregates made up only 25% of the soil mass, whereas the large microaggregate fraction (250–53 μm) clearly dominated with a contribution of more than 50%. The OC and N contents of the aggregates decreased with size for the aggregate fractions from >250 to 53–20 μm and then increased again in the aggregate fraction <20 μm. Although this pattern was observed in soils sampled from either depth, macroaggregates had by far the highest OC concentrations of the topsoil aggregates (42 mg g^{-1}), whereas the fraction <20 μm was the one with the highest OC concentrations in the subsoil (6.6 mg g^{-1}). The C/N ratio was generally lower in the subsoil aggregate fractions than in the topsoil aggregate fractions and was particularly low in DOM (6 and 5 for topsoil and subsoil, respectively) (**Table 1**).

Comparing the soil before incubation with the water control samples, it can be seen that incubation slightly decreased OC contents in soils from both depths (**Tables 1**, **3**). In addition, the total PLFA content as a measure of microbial biomass decreased during the incubation from 134 nmol g^{-1} before incubation to 98 nmol g^{-1} for the water control in the topsoil and from 4.4 to 3.7 nmol g^{-1} in the subsoil (**Table 1**; **Figure 3A**).

Organic Carbon and Total Nitrogen Contents

Within the topsoil rhizosphere, the addition of exudate solutions did not induce statistically significant effects regarding OC and N contents compared with the water control (32.98 mg OC g^{-1} and 3.21 mg N g^{-1}). However, the OC and N contents both slightly decreased after moderate exudate additions (32.37 mg OC g^{-1} and 3.13 mg N g^{-1}), which was reflected by a strong negative effect size (−1.6) and resulted in a significant difference from high exudate additions (33.22 mg OC g^{-1} and 3.52 mg N g^{-1}, $p = 0.034$). In the subsoil rhizosphere, high exudate additions led to significantly increased OC and N contents, with a high positive effect size (+4.6) for subsoil OC contents. Moderate exudate additions had a strong negative effect size (−2.7) for subsoil OC contents (**Table 3**; **Figure 2**). The C/N ratio significantly widened from 7.9 in the water control to 8.3 with high treatment (**Table 3**).

Bulk soil showed no treatment response over soils sampled from either depth. It did, however, partly differ from the rhizosphere: In the topsoil water control, OC and N contents were significantly higher in the rhizosphere than in the bulk soil. In both topsoil and subsoil, high exudate additions led to increased OC and N concentrations in the rhizosphere compared with the bulk soil, being significant in the subsoil. Furthermore, in the subsoil samples treated with moderate exudate additions,

TABLE 3 | Organic carbon (OC) and nitrogen (N) contents and the C/N ratio.

		Topsoil			Subsoil		
		Water control	**Moderate**	**High**	**Water control**	**Moderate**	**High**
OC content (mg g^{-1})	Rhizosphere	^{ab}**32.98 (0.40)**	^{a}32.37 (0.23)	^{b}33.22 (0.51)	^{a}3.21 (0.02)	^{a}3.13 (0.03)	^{b}**3.52 (0.08)**
	Bulk soil	**32.01 (0.43)**	32.77 (0.61)	32.96 (1.03)	3.21 (0.14)	3.14 (0.06)	**3.20 (0.05)**
N content (mg g^{-1})	Rhizosphere	^{ab}**2.29 (0.01)**	^{a}2.25 (0.03)	^{b}2.33 (0.04)	^{a}0.41 (0.00)	^{a}0.40 (0.00)	^{b}**0.42 (0.01)**
	Bulk soil	**2.23 (0.02)**	2.28 (0.04)	2.28 (0.11)	0.40 (0.01)	0.39 (0.01)	**0.39 (0.00)**
C:N ratio	Rhizosphere	14.42 (0.18)	14.41 (0.15)	14.25 (0.11)	^{a}7.92 (0.04)	^{a}**7.81 (0.07)**	^{b}8.34 (0.12)
	Bulk soil	14.33 (0.12)	14.37 (0.16)	14.44 (0.47)	8.05 (0.30)	**7.97 (0.13)**	8.17 (0.09)

Standard deviations from the mean are given in brackets. Different letters indicate statistically significant differences between the treatments within one soil depth. Bold pairs of values indicate statistically significant differences between the rhizosphere and bulk soil within one soil depth and treatment ($p < 0.05$).

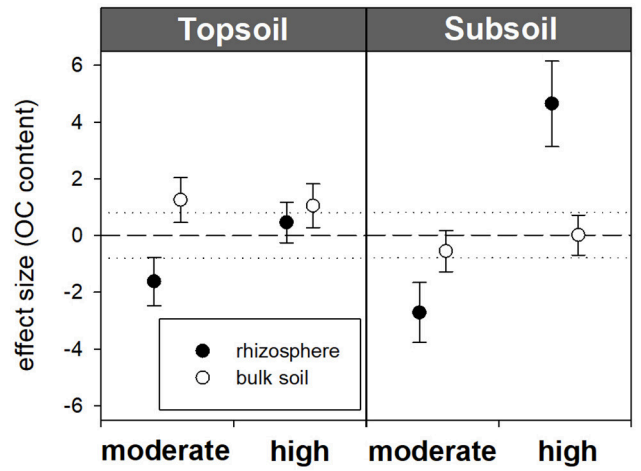

FIGURE 2 | Standardized effect sizes for total OC contents. Hedges' g* of the exudate addition treatments compared to the water control. Bars indicate the standard error of the effect size estimate. Dotted lines mark thresholds of −0.8 and 0.8 below or above which, respectively, effect sizes are considered as high.

the C/N ratio was lower in the rhizosphere than in the bulk soil (**Table 3**).

Microbial Biomarkers

The AS contents of the samples did not respond to the exudate additions, neither when standardized to soil DW, nor to soil OC content. The same holds true for the F:B_{AS} ratio (**Table S1**).

Contrary to the AS data, PLFA analysis revealed a pronounced effect of artificial exudate additions on microbial community composition as well as microbial biomass (indicated by the total microbial PLFA content). The total microbial PLFA content in the topsoil rhizosphere tended to increase in the high exudate addition treatment (124.6 nmol g^{-1}) compared with the water control (98.1 nmol g^{-1}, $p < 0.1$). This was accompanied by a high effect size of +1.8. In the subsoil rhizosphere, a high positive effect size was observed for moderate exudate supply. Although this effect was not statistically significant, the total microbial PLFA content increased from 3.7 nmol g^{-1} in the water control to 5.1 nmol g^{-1} in the moderate treatment. The high exudate addition treatment strongly increased total microbial PLFA content in the subsoil rhizosphere by more than 300% to 11.2 nmol g^{-1} (**Figures 3A**, **4A**).

High exudate additions significantly increased the total microbial PLFA content in the rhizosphere as compared with the bulk soil in soils sampled from either depth. The same holds true for the moderately treated samples in the subsoil (**Figure 3A**).

For the topsoil as well as the subsoil, high exudate supply led to a significant increase in F:B_{PLFA} ratio compared with the water control and the moderate treatment. It increased from 0.4 to 0.7 (effect size +2.0) in the topsoil and from 0.3 to 2.5 (effect size +4.7) in the subsoil in the water control and high exudate addition treatment samples, respectively. The latter, extreme effect was also visible in the bulk soil, where it increased F:B_{PLFA} from 0.3 to 0.7 and produced a high effect size of +4.96 (**Figures 3B**, **4B**).

Compared with the respective bulk soil, F:B_{PLFA} was significantly higher in the rhizosphere of the subsoil samples receiving moderate treatment and in the rhizosphere of both topsoil and subsoil samples receiving the high treatment (**Figure 3B**).

Aggregate Size Classes

The relative distribution of aggregate size classes in the topsoil rhizosphere did not show statistically significant responses to the two exudate addition treatments. However, high exudate supply tended to induce the formation of macroaggregates as their relative abundance increased from 51% in the water control to 57% in the high exudate addition treatment ($p = 0.07$, effect size +3.4). In contrast, moderate exudate supply negatively affected macroaggregation (effect size −0.97) (**Figures 5**, **6**). This caused significant differences between the moderate and the high exudate addition treatments for all aggregate fractions >20 µm (**Figure 5**). In the subsoil rhizosphere, the distribution of aggregate size classes was strongly affected by high exudate addition treatment: the macroaggregate abundance increased by 89% compared with the water control (effect size +6.6). This effect was accompanied by a decrease in all microaggregate fractions, but mostly the aggregates 250–53 µm in size (**Figure 5**).

In the bulk topsoil, the aggregate size distribution differed significantly from that of both the soil before incubation and the rhizosphere (**Table 1**; **Figure 5**). In comparison to the rhizosphere, the relative abundance of macroaggregates in the

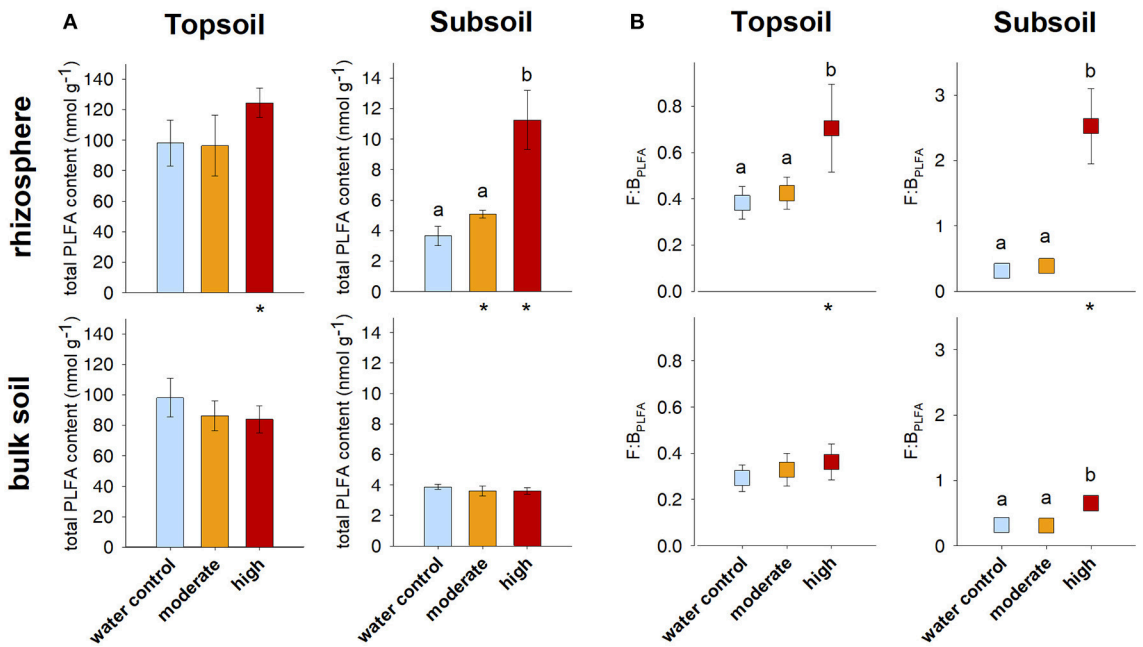

FIGURE 3 | (A) Total microbial PLFA content and **(B)** fungal-to-bacterial ratio based on PLFA analysis ($F:B_{PLFA}$). Bars represent standard deviation from the mean (SD). Different letters indicate statistically significant differences between the treatments within one soil region and depth ($p < 0.05$), asterisks indicate statistically significant differences between the soil regions rhizosphere and bulk soil within one soil depth and treatment.

bulk soil was significantly enhanced by ∼25% over all treatments. This was accompanied by a decrease in large microaggregates (250–53 μm) in all treatments as well as a decrease in smaller microaggregates in the moderately treated samples.

In the subsoil, the above mentioned strong effect of the high exudate additions in the rhizosphere also led to significant differences with respect to the bulk soil in all aggregate size classes >20 μm for this treatment. Furthermore, macroaggregates increased and large microaggregates (250–53 μm) decreased in the bulk soil of the water control compared with the respective rhizosphere (**Figure 5**). In addition to these differences between the bulk soil and the rhizosphere, there occurred a significant treatment effect within the bulk topsoil: The samples treated with moderate exudate additions showed higher macroaggregation and correspondingly lower relative proportion of free microaggregation than the water control and the highexudate addition treatment (**Figure 5**).

The relative contributions of the individual water-stable aggregate size classes to total OC contents were mainly governed by the mass distribution of the aggregate size classes themselves (**Figure S2**). Moderate exudate additions significantly increased the share of water-stable aggregate size classes on total OC in the subsoil rhizosphere (**Figure S2**, **Table S2**) as well as the total amount of DOC (**Table S3**).

Modeled Soil Aggregation

The modeled average microbial biomass, fungal biomass, OC concentration, and distribution of water-stable aggregate size classes fit well with the experimental data, as shown in 1:1 plots (**Figure S3**). The spatially explicit model demonstrates that soluble root exudates influence soil up to a distance of 6 mm around the artificial root, which affirms the choice of rhizosphere boundary in the incubation experiment (**Figure 7**).

The model parameter estimates reveal SOM to be more stable against biotic and abiotic breakdown in the subsoil (lower coefficient k_S and zero k_{S0}) and to have a lower capacity for microbial growth (lower m_0 and m_1), and overall slower biochemical processes (k_1 – k_4; **Table 2**). This may reflect either differences in chemical composition or spatial restrictions for enzymatic breakdown and substrate consumption at lower SOC concentrations in the subsoil. In contrast, the production of gluing agents by lysis (k_r) is greater in the subsoil than in the topsoil. The lower θ_a in the topsoil compared with the subsoil (**Table 2**) indicates that moisture has a more negative effect on the binding strength in the topsoil.

Total microbial as well as fungal biomass showed similar patterns with distance from the root. After moderate and high exudate additions, biomass was predicted to strongly increase in the rhizosphere at both soil depths. In the topsoil, this effect reached out only 1–2 mm, whereas in the subsoil, it influenced a larger area of soil (3–6 mm distance from the root; **Figures 7A,B**). The model results of organic gluing agent concentrations also showed an increase relative to exudate addition rate in soils sampled from either depth. Again, a smaller soil volume was affected in the topsoil than in the subsoil. The amount of gluing agents in the water control was slightly decreased in close proximity to the root (**Figure 7C**). The modeled total

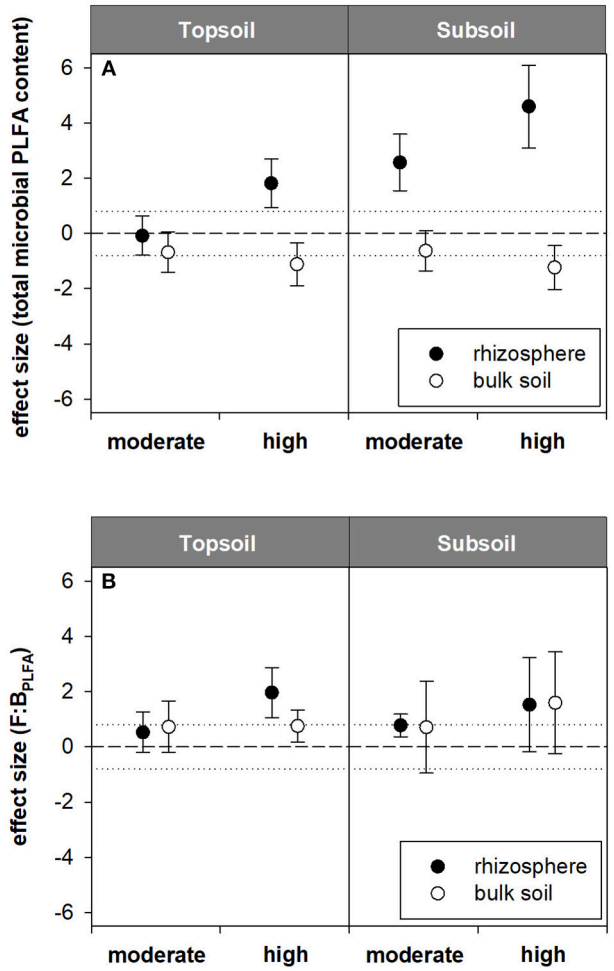

FIGURE 4 | Standardized effect sizes for **(A)** total microbial PLFA content and **(B)** F:B_{PLFA} ratio. Hedges' g* of the exudate addition treatments compared to the water control. Bars indicate the standard error of the effect size estimate. Dotted lines mark thresholds of −0.8 and 0.8 below or above which, respectively, effect sizes are considered as high.

OC content increased with exudate additions in the subsoil. In the topsoil, however, a divergent effect was predicted by the model: Moderate exudate additions decreased total OC content, whereas the high exudate addition treatment was predicted to induce a strong but spatially limited increase in total OC content (**Figure 7D**). Modeled soil moisture formed a negative gradient with distance from the root (**Figure 7E**). This, together with the spatial patterns of the abundance of fungi and gluing agents, resulted in the soil binding strength responsible for the formation of water-stable aggregates (**Figure 7F**). The soil binding strength profile for the topsoil water control reveals that the binding strength increases with distance from the artificial root, leading to higher aggregation in the bulk soil. For the exudate addition treatments in turn, binding strength was the highest in close proximity to the root and decreased toward the bulk soil. Topsoil binding strength profiles were overall similar to those of the subsoil. However, the profiles of the exudate amended soils showed minima at 1–2 mm distance from the root (**Figure 7F**).

DISCUSSION

Accelerated Macroaggregation With the Addition of Labile C

Our study clearly demonstrates that artificially high doses of root exudates induce strong positive effects on soil structure, which are accompanied by a change in microbial community composition. High exudate treatment strongly increased macroaggregation compared with the water control and the moderate treatment in the subsoil rhizosphere. In the topsoil rhizosphere, a similar trend was observed (**Figures 5**, **6**). Furthermore, high exudate treatment induced strong fungal growth, as indicated by the significant increase in F:B_{PLFA} in samples from both soil depths. In the C-poor subsoil, this effect was more pronounced, which even extended to the bulk soil region (**Figures 3B**, **4B**) and was also visually evident as fungal mycelium in the soil around the artificial roots of some samples at harvest. This observation is in contrast with the modeling data where no influence of root exudates beyond a distance of 6 mm from the root surface was predicted. However, fungal biomass in the subsoil was affected over a larger distance from the root than that in the topsoil (**Figure 7B**). Fungi have been found to utilize rhizodeposits more intensely than bacteria (Butler et al., 2003). Consequently, high addition rates of root exudates favor a shift in the microbial community composition toward higher relative abundance of fungi (Griffiths et al., 1998). It is well-documented that fungi are important agents in the formation of macroaggregates (Amézketa, 1999; Helfrich et al., 2008; Lehmann et al., 2017). We assume that the significantly increased fungal biomass due to high exudate additions led to enhanced subsoil macroaggregation in our study. The concomitant significant decrease in free aggregates 250–53 μm in size points toward the formation of macroaggregates particularly out of big microaggregates (**Figure 5**) and thus supports the aggregate hierarchy model, a conceptual framework that hypothesizes that microaggregates are glued together by temporary binding agents, such as roots and hyphae (Tisdall and Oades, 1982; Oades and Waters, 1991). The absence of any trend with respect to the amount of AS (**Table S1**) is in strong contrast to the distinct response of PLFA contents to the artificial exudate additions. Amino sugars are promising indicators when it comes to integrating long-term changes in microbial community structure, but may not be suitable for analyzing the effects of a relatively short incubation experiment, such as ours (Glaser et al., 2004).

Mechanisms of Macroaggregation in Topsoil and Subsoil

It is often observed that most of the SOC in subsoils is stored in clay- and silt-sized mineral fractions (Angst et al., 2018) via the formation of organomineral associations. Therefore, the occlusion of SOM within aggregates has long been a rather disregarded mechanism for C storage in deep soil layers (Lorenz

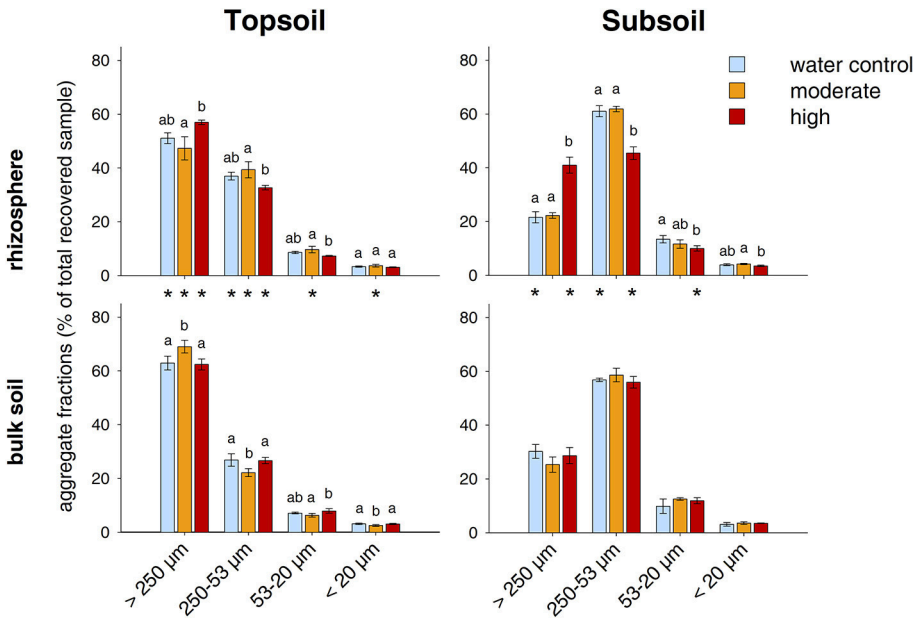

FIGURE 5 | Distribution of water-stable aggregate size classes. Bars represent standard deviation from the mean (SD). Different letters indicate statistically significant differences between the treatments within one soil region and depth ($p < 0.05$), asterisks indicate statistically significant differences between the soil regions rhizosphere and bulk soil within one soil depth and treatment.

and Lal, 2005; von Lützow et al., 2006). The soil studied here was well aggregated in samples from both soil depths: although the soil had a silty loam texture with more than 90 % primary particles <53 µm (**Table 1**), the particles <53 µm obtained by aggregate fractionation amounted to <20% of the soil mass in both depths and contained approximately only 10 and 30% of the total SOC in topsoil and subsoil, respectively (**Figure 5**; **Figure S2**). Aggregation is known to greatly increase the persistence of SOM via occlusion, thus providing physical protection from decomposition (Dungait et al., 2012), and it has been shown that this is also the case in C-poor subsoils (Rasmussen et al., 2005; Schrumpf et al., 2013). Our findings show that the effects of high exudate C addition rates were much more pronounced in the subsoil than in the topsoil presumably because the C-rich topsoils are already well aggregated due to the high amount of SOM and organic gluing agents. The modeled coefficients of the effect of gluing agents and fungi on binding strength (v_1, v_2) furthermore revealed that their influence on aggregation is stronger in subsoils than in topsoils. In the topsoil, water-stable macroaggregates made up more than 50% of the soil mass before incubation and also stored most of the OC. In contrast, the subsoil was characterized by substantially less macroaggregation because it comprised 60% large microaggregates (250–53 µm). In soils sampled from either depth, macroaggregates showed higher OC contents than the microaggregates they were composed of (**Table 1**). This reveals that for the formation of macroaggregates, OC is needed, presumably in the form of OM as binding agents (Tisdall and Oades, 1982). It has been speculated that the mechanisms of aggregation in topsoils and subsoils are different and that in subsoils physical processes may be more important than biological processes (Lorenz and Lal, 2005; von Lützow et al., 2006; Rumpel and Kögel-Knabner, 2011). Based on our results, we assume that biologically-induced macroaggregation in subsoils may be limited by the scarce and heterogeneous input of OM. We prove that the addition of OM at high rates may boost biotic macroaggregation by the growth of fungi and strongly alter subsoil structure within relatively short time scales. The high positive effect sizes for total PLFA content as well as $F:B_{PLFA}$ after the moderate exudation treatment indicate that similar processes might be triggered by moderate rates of root exudates in the long term (**Figure 4**). Thus, the deficiency of OC appears to be causative for the limitation of biotic macroaggregation in the subsoil and can be alleviated by the addition of OM, such as soluble root exudates. The high experimental exudate additions in our study exceed naturally occurring C input by root exudates, yet rhizodeposition may increase under rising CO_2 concentrations (Phillips et al., 2006; Keidel et al., 2018). Our study indicates that deep soil layers containing less (macro)aggregates may harbor a higher potential for further aggregation and thereby C stabilization than topsoils if supplied with additional OM.

Bulk topsoil exhibited a significantly higher relative abundance of macroaggregates than the rhizosphere (**Figure 5**). Because neither OC content nor $F:B_{AS}$ ratio in the bulk topsoil was elevated in comparison to the rhizosphere, this enhanced macroaggregation did not appear to be induced by the addition of SOM or the growth of fungi. Thus, we presume that macroaggregation in the bulk topsoil occurred in response to abiotic causes. The aggregation model confirmed this hypothesis, because the differences in aggregation between the rhizosphere

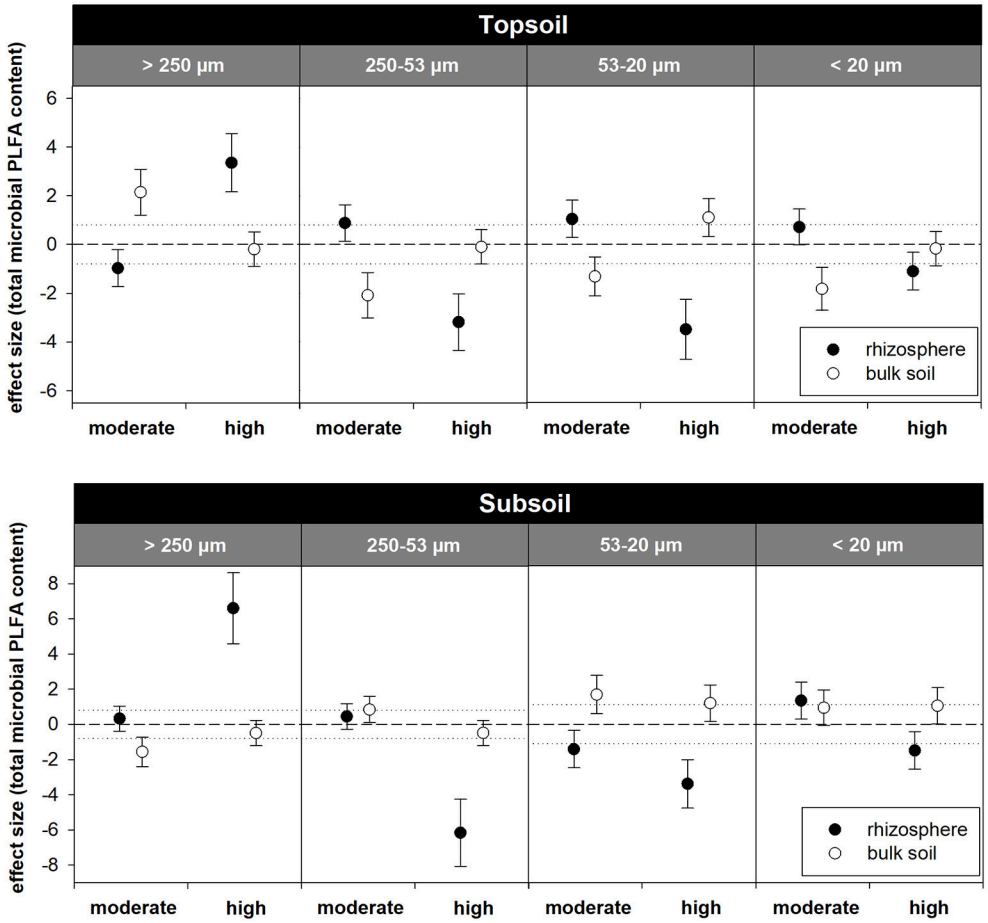

FIGURE 6 | Standardized effect sizes for the distribution of water-stable aggregate size classes. Hedges' g* of the exudate addition treatments compared to the water control. Bars indicate the standard error of the effect size estimate. Dotted lines mark thresholds of −0.8 and 0.8 below or above which, respectively, effect sizes are considered as high.

and bulk soil samples can be described well via a moisture factor. Soil moisture is assumed to affect aggregation by slaking and by its influence on SOM decomposition rates and thereby the microbial decay of gluing agents. Although we did not measure soil moisture within the individual sampling regions, we assume drier conditions in the bulk soil compared with the rhizosphere, which presumably favored the development of stable aggregates (Caron et al., 1992). The hypothesis of higher amounts of water within the rhizosphere is in accordance with the findings of Carminati et al. (2010).

Importance of the Choice of Exudate Addition Rates

Moderate exudate additions induced a trend of decreased OC content in samples from both soil depths (**Table 3**; **Figure 2**), significantly increased DOM abundance in the subsoil rhizosphere (**Tables S2, S3**; **Figure S2**), and negatively affected macroaggregation in the topsoil rhizosphere (**Figure 5**). Although we did not measure soil respiration to determine the possible priming effects in our study, these findings may indicate the occurrence of such an effect and hence the decomposition of native SOM in response to the addition of moderate exudate concentration. Root exudation by tree seedlings (with rates similar to that of our moderate treatment) was found to strongly enhance SOM decomposition and N mineralization (Bengtson et al., 2012). It is hypothesized that the relatively low amounts of labile C stimulate the synthesis of enzymes that decompose SOM (Bengtson et al., 2012), possibly to mine for nutrients (Dijkstra et al., 2013). This corroborates the findings of a study applying artificial root exudates over a range of concentrations, which found that the activity of enzymes that degrade fast-cycling N compounds was generally increased by artificial root exudates within the upper 10 cm of the soil (Meier et al., 2017). Surprisingly, in unfertilized soils, the most pronounced effect was triggered by the lowest exudate addition rate, which resembles our moderate treatment. Tian et al. (2016) found SOM within macroaggregates to be less protected against decomposition induced by glucose addition than that associated with microaggregates. Thus, OM acting as a gluing agent of macroaggregates appears to be prone

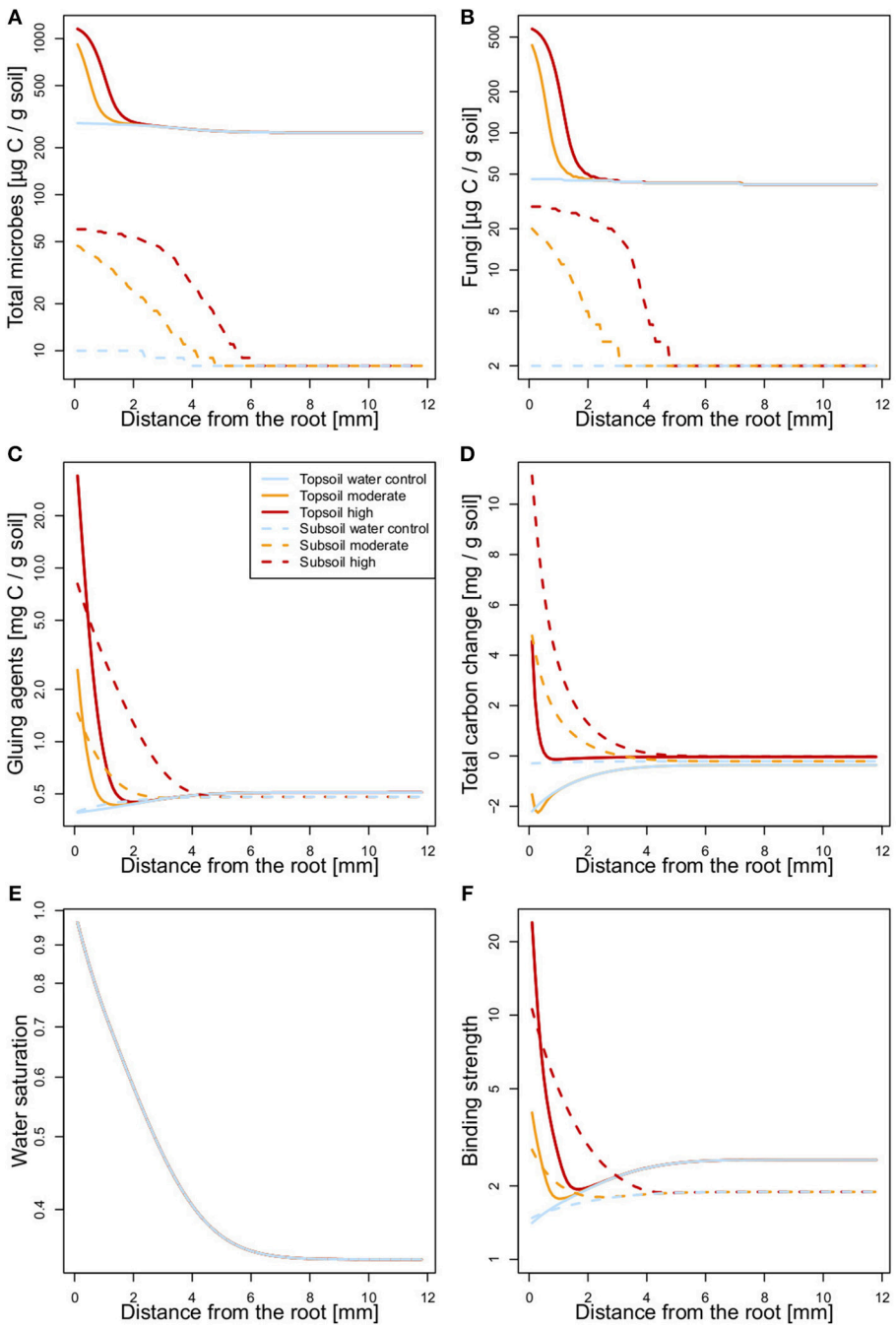

FIGURE 7 | State variables [**(A)** total microbial biomass, **(B)** fungal biomass, **(C)** concentration of gluing agents, **(D)** change in total OC, **(E)** water saturation], and **(F)** binding strength as functions of distance from the artificial root at the end of incubation. For total carbon change in case of the high exudate addition treatment the scale is multiplied by a factor of 0.1.

to enhanced degradation after the moderate addition of root exudates, explaining the tendency toward disaggregation and breakup into smaller microaggregates in the topsoil (**Figure 5**). The model results confirm the observed decline in total OC due to moderate exudate addition treatment in the topsoil rhizosphere. In the subsoil rhizosphere, however, the model predicts an increase in total OC after moderate exudate additions. This indicates a higher potential for the accumulation of SOC due to the addition of root exudates in deeper soil layers than in the topsoil.

In contrast, as discussed above, the high exudate addition treatment strongly enhanced macroaggregation in the subsoil

rhizosphere (**Figure 5**) and tended to do so in the topsoil (**Figure 6**). Furthermore, it strongly increased the OC and N concentrations of the rhizosphere in the subsoil (**Table 3**), indicating that the addition of such high amounts of labile C saturates the system. When exposed to very high C addition rates, soil microbes might preferentially utilize this abundant and easily available substrate (negative priming effect) instead of undertaking the above mentioned metabolic effort to decompose native SOM (Blagodatskaya and Kuzyakov, 2008; Bengtson et al., 2012; Wang et al., 2015). The high exudate addition treatment did not lead to increased amounts of DOM (**Tables S2, S3**; **Figure S2**), which proves that even these high concentrations were either sorbed to soil minerals or taken up by microbes to a large extent instead of remaining in a free state.

Microbial biomass (total microbial PLFA content) did not increase in response to the moderate treatment in the topsoil (**Figure 3A**). This confirms the observations of Drake et al. (2013) for exudates at similar concentrations. After high exudate additions, total PLFA content increased in soils sampled from either depth (**Figures 3A**, **4A**). Priming effects after high additions of labile C are often accompanied by increases in microbial biomass (Huo et al., 2017), whereas trace amounts of substrates presumably only activate microorganisms (shift from dormant to active), thereby accelerating their metabolism but not inducing microbial growth, a mechanism referred to as the "triggering effect" (De Nobili et al., 2001; Mondini et al., 2006).

Our model scheme includes measured microbial pools as well as mechanisms necessary to describe change in substrate preference, which are both required to model priming effects (Georgiou et al., 2015). The predicted decline in topsoil OC content in response to moderate exudate additions indicates a positive priming or triggering effect. In contrast, SOC accumulation at high exudate additions may be the result of a negative priming effect, although experiments including isotopic labeling would be needed for proof.

Thus, both the experimental and modeled data suggest that different addition rates of root exudates induce opposing effects. This is in line with a meta-analysis by Blagodatskaya and Kuzyakov (2008), who found the relationship between substrate addition rate and priming to be nonlinear: The authors reported that low concentrations of labile C additions induced a linear increase in primed CO_2-C efflux in agriculturally managed topsoils, whereas it decreased exponentially and eventually even became negative for high C addition rates. Hence, the choice of application rates in artificial root experiments is crucial regarding their interpretation and explanatory power. In previous artificial root exudate studies, addition rates were often not clearly attributable to natural root exudation rates or concentrations and possibly were chosen deliberately higher to certainly trigger measurable effects (Traoré et al., 2000; Keiluweit et al., 2015; Steinauer et al., 2016). We recommend for future studies to apply a range of exudate addition rates, including those representing natural soluble root exudation. That way, valuable and applicable knowledge on the effects of soluble root exudates on C dynamics can be gathered.

CONCLUSION

This study provides evidence that biotic aggregation in subsoils is promoted by increased provision of easily available OM in the rhizosphere. Our experimental data show that sufficient amendment with soluble root exudates induces biotic macroaggregation and C storage in subsoil horizons. This reveals a high potential for C sequestration via the physical protection of SOM in subsoils.

Furthermore, our study demonstrates that the impact of soluble root exudates on SOC storage and structural development differs substantially between the topsoil and subsoil. These effects tend to be divergent for different concentrations of exudates potentially due to the occurrence of positive and negative priming effects.

The proposed model of biochemical and biophysical processes involved in rhizosphere aggregation predicts the existence of different gradients with distance from the root and suggests future developments for the experimental design with spatial explicit measurements of moisture, bulk density, and aeration to simulate differences in conditions with depth.

For future studies, we recommend to test our results in different soil types by applying a range of exudate addition rates, including those representing natural soluble root exudation.

AUTHOR CONTRIBUTIONS

VB, IK-K, and CM designed the experiment. VB conducted the laboratory analyses, evaluated the experimental data, and wrote the manuscript. CM supervised the analyses. NV and AV performed mathematical modeling and drafted the paragraphs on modeling for the manuscript. IM provided data concerning the natural rates of root exudation. VB, NV, AV, IM, IK-K, and CM discussed the results, commented on the manuscript, and revised it for publication.

FUNDING

This work was financially supported by the Deutsche Forschungsgemeinschaft (German Research Foundation, DFG) and was conducted within the project Rhizosphere as driver of subsoil organic matter distribution and composition (MU 3021/4-2) in the frame of the DFG research unit FOR1806 The forgotten part of carbon cycling: Soil organic matter storage and turnover in subsoils (SUBSOM). Soil aggregate modeling was funded by the Russian Foundation for Basic Research (grant no. 16-04-01624, Dynamic modeling of formation mechanisms for soil profile aggregate structure).

ACKNOWLEDGMENTS

The authors would like to thank Dr. Stefanie Schulz and Gudrun Hufnagel for performing DOC and dNt measurements; Karolin Müller, Sebastian Preußer, and Sabine Rudolph for providing assistance with PLFA extraction; Stefanie Mayer for her help in texture analysis; and Timo Tückmantel for sharing

information regarding natural exudation rates in European beech forests. We appreciate the help of Bärbel Angres, Maria Greiner, Stefanie Scheidel and several student assistants in maintaining the incubation experiment and performing analyses in the laboratory.

SUPPLEMENTARY MATERIAL

The Supplementary Material for this article can be found online at: https://www.frontiersin.org/articles/10.3389/fenvs.2018.00140/full#supplementary-material

REFERENCES

Abramoff, R., Xu, X., Hartman, M., O'Brien, S., Feng, W., Davidson, E., et al. (2017). The Millennial model: in search of measurable pools and transformations for modeling soil carbon in the new century. *Biogeochemistry* 137, 51–71. doi: 10.1007/s10533-017-0409-7

Albalasmeh, A. A., and Ghezzehei, T. A. (2014). Interplay between soil drying and root exudation in rhizosheath development. *Plant Soil* 374, 739–751. doi: 10.1007/s11104-013-1910-y

Amézketa, E. (1999). Soil aggregate stability: a review. *J. Sustain. Agric.* 14, 83–151. doi: 10.1300/J064v14n02_08

Angst, G., Kögel-Knabner, I., Kirfel, K., Hertel, D., and Mueller, C. W. (2016). Spatial distribution and chemical composition of soil organic matter fractions in rhizosphere and non-rhizosphere soil under European beech (*Fagus sylvatica* L.). *Geoderma* 264, 179–187. doi: 10.1016/j.geoderma.2015.10.016

Angst, G., Messinger, J., Greiner, M., Häusler, W., Hertel, D., Kirfel, K., et al. (2018). Soil organic carbon stocks in topsoil and subsoil controlled by parent material, carbon input in the rhizosphere, and microbial-derived compounds. *Soil Biol. Biochem.* 122, 19–30. doi: 10.1016/j.soilbio.2018.03.026

Bailey, V. L., Peacock, A. D., Smith, J. L., and Bolton, H. (2002). Relationships between soil microbial biomass determined by chloroform fumigation–extraction, substrate-induced respiration, and phospholipid fatty acid analysis. *Soil Biol. Biochem.* 34, 1385–1389. doi: 10.1016/S0038-0717(02)00070-6

Banwart, S. A., Bernasconi, S. M., Blum, W. E. H., de Souza, D. M., Chabaux, F., Duffy, C., et al. (2017). Soil functions in Earth's Critical Zone: key results and conclusions. *Adv. Agron.* 142, 1–27. doi: 10.1016/bs.agron.2016.11.001

Batjes, N. H. (1996). Total carbon and nitrogen in the soils of the world. *Eur. J. Soil Sci.* 47, 151–163. doi: 10.1111/j.1365-2389.1996.tb01386.x

Bengtson, P., Barker, J., and Grayston, S. J. (2012). Evidence of a strong coupling between root exudation, C and N availability, and stimulated SOM decomposition caused by rhizosphere priming effects. *Ecol. Evol.* 2, 1843–1852. doi: 10.1002/ece3.311

Blagodatskaya, E., and Kuzyakov, Y. (2008). Mechanisms of real and apparent priming effects and their dependence on soil microbial biomass and community structure: critical review. *Biol. Fertil. Soils* 45, 115–131. doi: 10.1007/s00374-008-0334-y

Blanco-Canqui, H., and Lal, R. (2004). Mechanisms of carbon sequestration in soil aggregates. *CRC. Crit. Rev. Plant Sci.* 23, 481–504. doi: 10.1080/07352680490886842

Brzostek, E. R., Greco, A., Drake, J. E., and Finzi, A. C. (2012). Root carbon inputs to the rhizosphere stimulate extracellular enzyme activity and increase nitrogen availability in temperate forest soils. *Biogeochemistry* 115, 65–76. doi: 10.1007/s10533-012-9818-9

Butler, J. L., Williams, M. A., Bottomley, P. J., and Myrold, D. D. (2003). Microbial community dynamics associated with rhizosphere carbon flow. *Appl. Environ. Microbiol.* 69, 6793–6800. doi: 10.1128/AEM.69.11.6793-6800.2003

Campbell, E. E., and Paustian, K. (2015). Current developments in soil organic matter modeling and the expansion of model applications: a review. *Environ. Res. Lett.* 10, 123004–123004. doi: 10.1088/1748-9326/10/12/123004

Carminati, A., Moradi, A. B., Vetterlein, D., Vontobel, P., Lehmann, E., Weller, U., et al. (2010). Dynamics of soil water content in the rhizosphere. *Plant Soil* 332, 163–176. doi: 10.1007/s11104-010-0283-8

Caron, J., Kay, B. D., and Stone, J. A. (1992). Improvement of structural stability of a clay loam with drying. *Soil Sci. Soc. Am. J.* 56, 1583–1590. doi: 10.2136/sssaj1992.03615995005600050041x

Chabbi, A., Kögel-Knabner, I., and Rumpel, C. (2009). Stabilised carbon in subsoil horizons is located in spatially distinct parts of the soil profile. *Soil Biol. Biochem.* 41, 256–261. doi: 10.1016/j.soilbio.2008.10.033

Chantigny, M. H., Angers, D. A., Prévost, D., Vézina, L.-P., and Chalifour, F.-P. (1997). Soil aggregation and fungal and bacterial biomass under annual and perennial cropping systems. *Soil Sci. Soc. Am. J.* 61:262. doi: 10.2136/sssaj1997.03615995006100010037x

Cohen, J. (1988). *Statistical Power Analysis for the Behavioral Sciences*. New York, NY: Routledge.

Crawford, J. W., Deacon, L., Grinev, D., Harris, J. A., Ritz, K., Singh, B. K., et al. (2012). Microbial diversity affects self-organization of the soil–microbe system with consequences for function. *J. R. Soc. Interface* 9, 1302–1310. doi: 10.1098/rsif.2011.0679

de Graaff, M.-A., Jastrow, J. D., Gillette, S., Johns, A., and Wullschleger, S. D. (2014). Differential priming of soil carbon driven by soil depth and root impacts on carbon availability. *Soil Biol. Biochem.* 69, 147–156. doi: 10.1016/j.soilbio.2013.10.047

De Nobili, M., Contin, M., Mondini, C., and Brookes, P. C. (2001). Soil microbial biomass is triggered into activity by trace amounts of substrate. *Soil Biol. Biochem.* 33, 1163–1170. doi: 10.1016/S0038-0717(01)00020-7

Dijkstra, F. A., Carrillo, Y., Pendall, E., and Morgan, J. A. (2013). Rhizosphere priming: a nutrient perspective. *Front. Microbiol.* 4:8. doi: 10.3389/fmicb.2013.00216

Drake, J. E., Darby, B. A., Giasson, M. A., Kramer, M. A., Phillips, R. P., and Finzi, A. C. (2013). Stoichiometry constrains microbial response to root exudation- insights from a model and a field experiment in a temperate forest. *Biogeosciences* 10, 821–838. doi: 10.5194/bg-10-821-2013

Dungait, J. A. J., Hopkins, D. W., Gregory, A. S., and Whitmore, A. P. (2012). Soil organic matter turnover is governed by accessibility not recalcitrance. *Glob. Chang. Biol.* 18, 1781–1796. doi: 10.1111/j.1365-2486.2012.02665.x

Frostegård, Å., Tunlid, A., and Bååth, E. (1991). Microbial biomass measured as total lipid phosphate in soils of different organic content. *J. Microbiol. Methods* 14, 151–163. doi: 10.1016/0167-7012(91)90018-L

Frostegård, Å., Tunlid, A., and Bååth, E. (2011). Use and misuse of PLFA measurements in soils. *Soil Biol. Biochem.* 43, 1621–1625. doi: 10.1016/j.soilbio.2010.11.021

Georgiou, K., Abramoff, R. Z., Harte, J., Riley, W. J., and Torn, M. S. (2017). Microbial community-level regulation explains soil carbon responses to long-term litter manipulations. *Nat. Commun.* 8:1223. doi: 10.1038/s41467-017-01116-z

Georgiou, K., Koven, C. D., Riley, W. J., and Torn, M. S. (2015). Toward improved model structures for analyzing priming: potential pitfalls of using bulk turnover time. *Glob. Chang. Biol.* 21, 4298–4302. doi: 10.1111/gcb.13039

Glaser, B., Turrión, M. A.-B., and Alef, K. (2004). Amino sugars and muramic acid—biomarkers for soil microbial community structure analysis. *Soil Biol. Biochem.* 36, 399–407. doi: 10.1016/j.soilbio.2003.10.013

Griffiths, B. S., Ritz, K., Ebblewhite, N., and Dobson, G. (1998). Soil microbial community structure: effects of substrate loading rates. *Soil Biol. Biochem.* 31, 145–153. doi: 10.1016/S0038-0717(98)00117-5

Hedges, L. V., and Olkin, I. (1985). *Statistical Methods for Meta-Analysis*. San Diego, CA: Academic Press.

Heinze, S., Ludwig, B., Piepho, H.-P., Mikutta, R., Don, A., Wordell-Dietrich, P., et al. (2018). Factors controlling the variability of organic matter in the top- and subsoil of a sandy Dystric Cambisol under beech forest. *Geoderma* 311, 37–44. doi: 10.1016/j.geoderma.2017.09.028

Helfrich, M., Ludwig, B., Potthoff, M., and Flessa, H. (2008). Effect of litter quality and soil fungi on macroaggregate dynamics and associated partitioning of litter carbon and nitrogen. *Soil Biol. Biochem.* 40, 1823–1835. doi: 10.1016/j.soilbio.2008.03.006

Hinsinger, P., Bengough, A. G., Vetterlein, D., and Young, I. M. (2009). Rhizosphere: biophysics, biogeochemistry and ecological relevance. *Plant Soil* 321, 117–152. doi: 10.1007/s11104-008-9885-9

Huo, C., Luo, Y., and Cheng, W. (2017). Rhizosphere priming effect: a meta-analysis. *Soil Biol. Biochem.* 111, 78–84. doi: 10.1016/j.soilbio.2017.04.003

IUSS Working Group (2015). *Worl Reference Base for Soil Resources 2014, Update 2015 International Soil Classification System for Naming Soils and Creating Legends for Soil Maps*. World Soil Resources Report No. 106. Rome: FAO.

Jobbágy, E. G., and Jackson, R. B. (2000). The vertical distribution of soil organic carbon and its relation to climate and vegetation. *Ecol. Appl.* 10, 423–436. doi: 10.1890/1051-0761(2000)010[0423:TVDOSO]2.0.CO;2

Jones, D. L., Nguyen, C., and Finlay, R. D. (2009). Carbon flow in the rhizosphere: carbon trading at the soil–root interface. *Plant Soil* 321, 5–33. doi: 10.1007/s11104-009-9925-0

Kaiser, C., Frank, A., Wild, B., Koranda, M., and Richter, A. (2010). Negligible contribution from roots to soil-borne phospholipid fatty acid fungal biomarkers 18:2omega6,9 and 18:1omega9. *Soil Biol. Biochem.* 42, 1650–1652. doi: 10.1016/j.soilbio.2010.05.019

Karhu, K., Hilasvuori, E., Fritze, H., Biasi, C., Nykänen, H., Liski, J., et al. (2016). Priming effect increases with depth in a boreal forest soil. *Soil Biol. Biochem.* 99, 104–107. doi: 10.1016/j.soilbio.2016.05.001

Keidel, L., Lenhart, K., Moser, G., and Müller, C. (2018). Depth-dependent response of soil aggregates and soil organic carbon content to long-term elevated CO 2 in a temperate grassland soil. *Soil Biol. Biochem.* 123, 145–154. doi: 10.1016/j.soilbio.2018.05.005

Keiluweit, M., Bougoure, J. J., Nico, P. S., Pett-Ridge, J., Weber, P. K., and Kleber, M. (2015). Mineral protection of soil carbon counteracted by root exudates. *Nat. Clim. Chang.* 5, 588–595. doi: 10.1038/nclimate2580

Kramer, S., Marhan, S., Haslwimmer, H., Ruess, L., and Kandeler, E. (2013). Temporal variation in surface and subsoil abundance and function of the soil microbial community in an arable soil. *Soil Biol. Biochem.* 61, 76–85. doi: 10.1016/j.soilbio.2013.02.006

Kuzyakov, Y. (2010). Priming effects: interactions between living and dead organic matter. *Soil Biol. Biochem.* 42, 1363–1371. doi: 10.1016/j.soilbio.2010.04.003

Kuzyakov, Y., Friedel, J. K., and Stahr, K. (2000). Review of mechanisms and quantification of priming effects. *Soil Biol. Biochem.* 32, 1485–1498. doi: 10.1016/S0038-0717(00)00084-5

Kuzyakov, Y., Hill, P. W., and Jones, D. L. (2006). Root exudate components change litter decomposition in a simulated rhizosphere depending on temperature. *Plant Soil* 290, 293–305. doi: 10.1007/s11104-006-9162-8

Lal, R. (2016). Beyond COP 21: potential and challenges of the "4 per Thousand" initiative. *J. Soil Water Conserv.* 71, 20A−25A. doi: 10.2489/jswc.71.1.20A

Lal, R., Delgado, J. A., Groffman, P. M., Millar, N., Dell, C., and Rotz, A. (2011). Management to mitigate and adapt to climate change. *J. Soil Water Conserv.* 66, 276–285. doi: 10.2489/jswc.66.4.276

Lehmann, A., Zheng, W., and Rillig, M. C. (2017). Soil biota contributions to soil aggregation. *Nat. Ecol. Evol.* 1, 1828–1835. doi: 10.1038/s41559-017-0344-y

Lorenz, K., and Lal, R. (2005). The depth distribution of soil organic carbon in relation to land use and management and the potential of carbon sequestration in subsoil horizons. *Adv. Agron.* 88, 35–66. doi: 10.1016/S0065-2113(05)88002-2

Luo, Y., Zhao, X., Andrén, O., Zhu, Y., and Huang, W. (2014). Artificial root exudates and soil organic carbon mineralization in a degraded sandy grassland in northern China. *J. Arid Land* 6, 423–431. doi: 10.1007/s40333-014-0063-z

Marx, M., Buegger, F., Gattinger, A., Zsolnay, Á., and Charles Munch, J. (2010). Determination of the fate of regularly applied13C-labeled-artificial-exudates C in two agricultural soils. *J. Plant Nutr. Soil Sci.* 173, 80–87. doi: 10.1002/jpln.200800104

Meier, I. C., Finzi, A. C., and Phillips, R. P. (2017). Root exudates increase N availability by stimulating microbial turnover of fast-cycling N pools. *Soil Biol. Biochem.* 106, 119–128. doi: 10.1016/j.soilbio.2016.12.004

Minasny, B., Malone, B. P., McBratney, A. B., Angers, D. A., Arrouays, D., Chambers, A., et al. (2017). Soil carbon 4 per mille. *Geoderma* 292, 59–86. doi: 10.1016/j.geoderma.2017.01.002

Mondini, C., Cayuela, M. L., Sanchez-Monedero, M. A., Roig, A., and Brookes, P. C. (2006). Soil microbial biomass activation by trace amounts of readily available substrate. *Biol. Fertil. Soils* 42, 542–549. doi: 10.1007/s00374-005-0049-2

Moni, C., Rumpel, C., Virto, I., Chabbi, A., and Chenu, C. (2010). Relative importance of sorption versus aggregation for organic matter storage in subsoil horizons of two contrasting soils. *Eur. J. Soil Sci.* 61, 958–969. doi: 10.1111/j.1365-2389.2010.01307.x

Nelder, J. A., and Mead, R. (1965). A simplex method for function minimization. *Comput. J.* 7, 308–313. doi: 10.1093/comjnl/7.4.308

Oades, J. M. (1984). Soil organic matter and structural stability: mechanisms and implications for management. *Plant Soil* 76, 319–337. doi: 10.1007/BF02205590

Oades, J. M., and Waters, A. G. (1991). Aggregate hierarchy in soils. *Austr. J. Soil Res.* 29:815. doi: 10.1071/SR9910815

Paterson, E., and Sim, A. (2013). Soil-specific response functions of organic matter mineralization to the availability of labile carbon. *Glob. Chang. Biol.* 19, 1562–1571. doi: 10.1111/gcb.12140

Phillips, D. A., Fox, T. C., and Six, J. (2006). Root exudation (net efflux of amino acids) may increase rhizodeposition under elevated CO2. *Glob. Chang. Biol.* 12, 561–567. doi: 10.1111/j.1365-2486.2006.01100.x

Powlson, D. S., Whitmore, A. P., and Goulding, K. W. T. (2011). Soil carbon sequestration to mitigate climate change: a critical re-examination to identify the true and the false. *Eur. J. Soil Sci.* 62, 42–55. doi: 10.1111/j.1365-2389.2010.01342.x

Puget, P., Angers, D. A., and Chenu, C. (1999). Nature of carbohydrates associated with water-stable aggregates of two cultivated soils. *Soil Biol. Biochem.* 31, 55–63. doi: 10.1016/S0038-0717(98)00103-5

Rasmussen, C., Torn, M. S., and Southard, R. J. (2005). Mineral assemblage and aggregates control carbon dynamics in a california conifer forest. *Soil Sci. Soc. Am. J.* 69:6. doi: 10.2136/sssaj2005.0040

Rasse, D. P., Rumpel, C., and Dignac, M.-F. (2005). Is soil carbon mostly root carbon? Mechanisms for a specific stabilisation. *Plant Soil* 269, 341–356. doi: 10.1007/s11104-004-0907-y

Rumpel, C., Chabbi, A., and Marschner, B. (2012). "Carbon storage and sequestration in subsoil horizons: knowledge, gaps and potentials," in *Recarbonization of the Biosphere,* eds R. Lal, K. Lorenz, R. Hüttl, B. Schneider, and J. von Braun (Dordrecht: Springer).

Rumpel, C., and Kögel-Knabner, I. (2011). Deep soil organic matter—a key but poorly understood component of terrestrial C cycle. *Plant Soil* 338, 143–158. doi: 10.1007/s11104-010-0391-5

Salomé, C., Nunan, N., Pouteau, V., Lerch, T. Z., and Chenu, C. (2010). Carbon dynamics in topsoil and in subsoil may be controlled by different regulatory mechanisms. *Glob. Chang. Biol.* 16, 416–426. doi: 10.1111/j.1365-2486.2009.01884.x

Sanaullah, M., Chabbi, A., Leifeld, J., Bardoux, G., Billou, D., and Rumpel, C. (2010). Decomposition and stabilization of root litter in top- and subsoil horizons: what is the difference? *Plant Soil* 338, 127–141. doi: 10.1007/s11104-010-0554-4

Schrumpf, M., Kaiser, K., Guggenberger, G., Persson, T., Kögel-Knabner, I., and Schulze, E. D. (2013). Storage and stability of organic carbon in soils as related to depth, occlusion within aggregates, and attachment to minerals. *Biogeosciences* 10, 1675–1691. doi: 10.5194/bg-10-1675-2013

Segoli, M., De Gryze, S., Dou, F., Lee, J., Post, W. M., Denef, K., et al. (2013). AggModel: a soil organic matter model with measurable pools for use in incubation studies. *Ecol. Modell.* 263, 1–9. doi: 10.1016/j.ecolmodel.2013.04.010

Shen, Y., Ström, L., Jönsson, J.-Å., and Tyler, G. (1996). Low-molecular organic acids in the rhizosphere soil solution of beech forest (*Fagus sylvatica* L.) cambisols determined by ion chromatography using supported liquid membrane enrichment technique. *Soil Biol. Biochem.* 28, 1163–1169. doi: 10.1016/0038-0717(96)00119-8

Smith, W. H. (1970). Root exudates of seedling and mature sugar maple. *Phytopathology* 60, 701–703. doi: 10.1094/Phyto-60-701

Smith, W. H. (1976). Character and significance of forest tree root exudates. *Ecology* 57, 324–331. doi: 10.2307/1934820

Stamati, F. E., Nikolaidis, N. P., Banwart, S., and Blum, W. E. H. (2013). A coupled carbon, aggregation, and structure turnover (CAST) model for topsoils. *Geoderma* 211–212, 51–64. doi: 10.1016/j.geoderma.2013.06.014

Steinauer, K., Chatzinotas, A., and Eisenhauer, N. (2016). Root exudate cocktails: the link between plant diversity and soil microorganisms? *Ecol. Evol.* 6, 7387–7396. doi: 10.1002/ece3.2454

Stockmann, U., Adams, M. A., Crawford, J. W., Field, D. J., Henakaarchchi, N., Jenkins, M., et al. (2013). The knowns, known unknowns and unknowns of sequestration of soil organic carbon. *Agric. Ecosyst. Environ.* 164, 80–99. doi: 10.1016/j.agee.2012.10.001

Tian, J., Pausch, J., Yu, G., Blagodatskaya, E., and Kuzyakov, Y. (2016). Aggregate size and glucose level affect priming sources: a three-source-partitioning study. *Soil Biol. Biochem.* 97, 199–210. doi: 10.1016/j.soilbio.2016.03.013

Tisdall, J. M., and Oades, J. M. (1982). Organic matter and water-stable aggregates in soils. *J. Soil Sci.* 33, 141–163. doi: 10.1111/j.1365-2389.1982.tb01755.x

Totsche, K. U., Amelung, W., Gerzabek, M. H., Guggenberger, G., Klumpp, E., Knief, C., et al. (2018). Microaggregates in soils. *J. Plant Nutr. Soil Sci.* 181, 104–136. doi: 10.1002/jpln.201600451

Traoré, O., Groleau-Renaud, V., Plantureux, S., Tubeileh, A., and Boeuf-Tremblay, V. (2000). Effect of root mucilage and modelled root exudates on soil structure. *Eur. J. Soil Sci.* 51, 575–581. doi: 10.1046/j.1365-2389.2000.00348.x

Tückmantel, T., Leuschner, C., Preusser, S., Kandeler, E., Angst, G., Mueller, C. W., et al. (2017). Root exudation patterns in a beech forest: dependence on soil depth, root morphology, and environment. *Soil Biol. Biochem.* 107, 188–197. doi: 10.1016/j.soilbio.2017.01.006

Van Groenigen, K.-J., Six, J., Harris, D., and Van Kessel, C. (2007). Elevated CO2 does not favor a fungal decomposition pathway. *Soil Biol. Biochem.* 39, 2168–2172. doi: 10.1016/j.soilbio.2007.03.009

van Hees, P. A. W., Jones, D. L., Finlay, R., Godbold, D. L., and Lundström, U. S. (2005). The carbon we do not see—the impact of low molecular weight compounds on carbon dynamics and respiration in forest soils: a review. *Soil Biol. Biochem.* 37, 1–13. doi: 10.1016/j.soilbio.2004.06.010

Vasilyeva, N. A., Ingtem, J. G., and Silaev, D. A. (2016). Nonlinear dynamical model of microorganism growth in soil. *Comput. Math. Model.* 27, 172–180. doi: 10.1007/s10598-016-9312-7

von Lützow, M., Kogel-Knabner, I., Ekschmitt, K., Matzner, E., Guggenberger, G., Marschner, B., et al. (2006). Stabilization of organic matter in temperate soils: mechanisms and their relevance under different soil conditions - a review. *Eur. J. Soil Sci.* 57, 426–445. doi: 10.1111/j.1365-2389.2006.00809.x

Wang, H., Xu, W., Hu, G., Dai, W., Jiang, P., and Bai, E. (2015). The priming effect of soluble carbon inputs in organic and mineral soils from a temperate forest. *Oecologia* 178, 1239–1250. doi: 10.1007/s00442-015-3290-x

Willers, C., Jansen van Rensburg, P. J., and Claassens, S. (2015). Phospholipid fatty acid profiling of microbial communities–a review of interpretations and recent applications. *J. Appl. Microbiol.* 119, 1207–1218. doi: 10.1111/jam.12902

Zhang, X., and Amelung, W. (1996). Gas chromatographic determination of muramic acid, glucosamine, mannosamine, and galactosamine in soils. *Soil Biol. Biochem.* 28, 1201–1206. doi: 10.1016/0038-0717(96)00117-4

Conflict of Interest Statement: The authors declare that the research was conducted in the absence of any commercial or financial relationships that could be construed as a potential conflict of interest.

frontiers in Environmental Science

ORIGINAL RESEARCH
published: 16 October 2018
doi: 10.3389/fenvs.2018.00117

Interactions of Mycorrhiza and Protists in the Rhizosphere Systemically Alter Microbial Community Composition, Plant Shoot-to-Root Ratio and Within-Root System Nitrogen Allocation

Gunnar Jakob Henkes[1], *Ellen Kandeler*[2], *Sven Marhan*[2], *Stefan Scheu*[1,3,4] *and Michael Bonkowski*[1,5,6]*

[1] Department of Biology, Institute of Zoology, Technical University Darmstadt, Darmstadt, Germany, [2] Institute of Soil Science and Land Evaluation, Department Soil Biology, University of Hohenheim, Stuttgart, Germany, [3] J.F. Blumenbach Institute of Zoology and Anthropology, Department of Animal Ecology, University of Göttingen, Göttingen, Germany, [4] Centre of Biodiversity and Sustainable Land Use, University of Göttingen, Göttingen, Germany, [5] Department of Biology, Institute of Zoology, Terrestrial Ecology, University of Cologne, Köln, Germany, [6] Cluster of Excellence on Plant Sciences (CEPLAS), Cologne, Germany

OPEN ACCESS

Edited by:
Caroline Gutjahr,
Technische Universität München,
Germany

Reviewed by:
Karin E. Groten,
Max-Planck-Institut für chemische Ökologie, Germany
Philipp Franken,
Leibniz-Institut für Gemüse- und Zierpflanzenbau (IGZ), Germany

***Correspondence:**
Michael Bonkowski
m.bonkowski@uni-koeln.de

Specialty section:
This article was submitted to Soil Processes, a section of the journal Frontiers in Environmental Science

Received: 31 May 2018
Accepted: 20 September 2018
Published: 16 October 2018

Citation:
Henkes GJ, Kandeler E, Marhan S, Scheu S and Bonkowski M (2018) Interactions of Mycorrhiza and Protists in the Rhizosphere Systemically Alter Microbial Community Composition, Plant Shoot-to-Root Ratio and Within-Root System Nitrogen Allocation. Front. Environ. Sci. 6:117. doi: 10.3389/fenvs.2018.00117

Arbuscular mycorrhizal fungi (AMF) are important symbionts for plant nutrient uptake, but their exact role in plant nitrogen (N) nutrition is unclear. Protists on the other hand play an acknowledged role in plant N acquisition, and there is increasing evidence for a close interaction with AMF. In a split root set up, we investigated the distinct roles of mycorrhiza (*Rhizophagus irregularis*), protists (*Acanthamoeba castellanii*), and their interaction on plant N uptake, within-root system allocation patterns, and shoot-to-root ratio of winter wheat. In addition, we applied a quantitative metabolomics approach to characterize associated changes in soil microbial communities by microbial phospholipid fatty acid (PLFA) analysis from rhizosphere soil. AMF markedly altered plant shoot-to-root allometry by reducing root biomass of wheat, and mycorrhiza partly took over root system functioning. Protists promoted shoot and root growth, and improved plant N uptake by the release of N from consumed bacterial biomass, a mechanism known as microbial loop. The shoot system however responded little to these alterations of the root system and of the rhizosphere community composition, indicating that the plants optimized shoot growth despite varying investment into roots. Mycorrhiza reduced root biomass and plant N, especially in the combined treatments with protists by changing within root system allocation of N and root biomass. These systemic effects on root allocation pattern suggest that mycorrhiza also gained control over N provided by protist grazers. Protists and mycorrhiza altered rhizosphere bacterial communities in contrasting but consistent ways as shown by quantitative shifts in microbial PLFA profiles. Remarkably, the changes in bacterial community composition were systemically conveyed within the root system to the split-root chamber where the symbionts were lacking. Accordingly the synergistic effects of protists and mycorrhiza indicated systemic effects on nutrient- and on root-allocation within root systems as an emergent property

that could not be predicted from single treatments with mycorrhiza or protists alone. The tight plant and microbial feed backs uncovered in this study have far reaching implications for understanding the assembly of plant microbiomes, and testify central roles of both protists and mycorrhizas in the assembly process.

Keywords: arbuscular mycorrhiza, wheat, nitrogen, amoebae, protists, microbial loop, shoot-to-root allocation, spit-root experiment

INTRODUCTION

Frameworks on shoot-to-root allometry of plants are based on models of competition between shoots and roots for plant carbohydrates and nutrients (Bloom et al., 1985; Van Noordwijk and De Willigen, 1987; Ericsson, 1995). Recently, models on resource stoichiometry (Johnson, 2010) and microbial markets (Werner et al., 2014; Revillini et al., 2016) have been applied to plant-symbiont interactions, but these approaches have not been rigorously tested on the individual plant level. In particular root traits have been considered to be determined by plant physiology and genetic disposition (Hoad et al., 2001; Wasson et al., 2012) or by external factors, such as different forms of nutrients (López-Bucio et al., 2003; Tian et al., 2014). On the other hand an abundant literature exists on influence of soil microorganisms affecting the root architecture of plants.

In the past decade much has been learned about how free-living rhizosphere microorganisms shape plant traits (Friesen et al., 2011; Lau and Lennon, 2012). Arbuscular mycorrhizal fungi (AMF) are among the most important mutualists improving nutrient acquisition of plants (Smith and Read, 2008; Bonfante and Genre, 2010). This is well confirmed for plant phosphorus uptake (Sanders and Tinker, 1971; Olsson et al., 2010; Smith F. A. and Smith, 2011), but the role of AMF in plant nitrogen (N) uptake is controversial (Smith S. E. and Smith, 2011; Veresoglou et al., 2012a). Although AMF hyphae have been shown to preferentially colonize N-containing organic patches in soil (Bukovská et al., 2016) and can aid in plant N-uptake (Hodge et al., 2001), they also function as N sink (Hodge and Fitter, 2010). Moreover, AMF lack the enzymatic machinery for N mineralization (Smith S. E. and Smith, 2011) and hence rely on other microorganisms for the supply of mineral N (Herman et al., 2012; Koller et al., 2013a).

Protists are ubiquitous predators of soil bacteria in the plant rhizosphere and release considerable amounts of N from consumed bacterial prey (Kuikman et al., 1991), a mechanism described as "microbial loop" (Clarholm, 1985; Bonkowski, 2004). While it has been shown that bacteria suppress AMF colonization of roots when competing for N (Leigh et al., 2011; Hodge and Storer, 2014), protist predation shifts nutrient competition in favor of the mycorrhizal symbiont since AMF hyphae effectively take up the N released by protist predators (Herdler et al., 2008; Koller et al., 2013b; Bukovská et al., 2018).

There is also potential conflict between AMF and protists in respect to the allocation of plant C in the rhizosphere. AMF act as strong sink for host plant C (Gange and Ayres, 1999; Klironomos, 2003; Lerat et al., 2003) and generally lead to reduced root growth (Veresoglou et al., 2012b). AMF also reduce the concentration of carbohydrates in root exudates (Graham et al., 1981; Ryan et al., 2012), resulting in reduced substrate supply to free-living rhizosphere bacteria and their consumers. Acanthamoebae have been found to stimulate lateral root branching and root growth, thereby likely enhancing root exudation and triggering a positive feedback in the rhizosphere microbial food web (Bonkowski and Brandt, 2002; Kreuzer et al., 2006; Krome et al., 2009, 2010; Bonkowski and Clarholm, 2012). These effects are reminiscent of the stimulation of root growth by plant growth promoting rhizobacteria (Bonkowski and Brandt, 2002; Bonkowski, 2004). In accordance with this view, changes in the rhizosphere bacterial community due to protist predation are non-random (Kreuzer et al., 2006; Jousset et al., 2008, 2009; Rosenberg et al., 2009), but also AMF have been reported to affect rhizosphere bacterial communities in specific ways (Marschner and Baumann, 2003; Rillig et al., 2006; Scheublin et al., 2010; Nuccio et al., 2013; Bukovská et al., 2016), suggesting additive effects on bacterial community assembly.

Here we investigated the specific roles of AMF and protists in determining nutrient fluxes in the rhizosphere. Further, we explore the interaction of AMF and protists as major rhizosphere symbionts and their effects on rhizosphere bacterial communities. A split root experiment was established to investigate systemic effects, and the role of the plant in mediating AMF and protist interactions. Rhizosphere nutrient fluxes were quantified by measuring plant biomass and nutrient concentrations in roots and shoots. Changes in the microbial community composition and activity were measured using phospholipid fatty acid (PLFA) profiles and microbial respiration.

The following hypotheses were tested:

1) From the perspective of the plant mycorrhiza and protists appear complementary. Mycorrhizal hyphae take over root system functions by capturing and transporting nutrients to the plant, while protists increase nutrient availability by mineralizing nutrients locked in bacterial biomass.
2) Both, mycorrhiza and protists alter the structure of the bacterial community in the rhizosphere with mycorrhiza increasing and protists decreasing bacterial biomass.

MATERIALS AND METHODS

Soil

A clay loess soil was taken from a meadow ("Molino-Arrhenatheretea") on a basalt outcropping near Darmstadt, Germany. The soil was sampled from 5 to 20 cm depth and sieved

(5 mm) to remove roots and stones. The soil was autoclaved (121°C, 110 kPa, 30 min). The soil $pH_{(KCl)}$ was 6.9 and the C:N ratio 18 (16 mg g^{-1} C and 0.9 mg g^{-1} N).

Plants

Winter wheat (*Triticum aestivum* L. var. Naxos) seeds were sterilized according to Hensel et al. (1990), by subsequent treatment with 96% ethanol (2 min), and 5% NaOCl (5 min) under vacuum in a desiccator. After rinsing with distilled water the seeds were germinated in 100 µl Neff's Modified Amoeba Saline (NMAS; Page, 1976) in individual wells of 96 well microtitre plates (Greiner, Solingen Germany) in darkness at 20°C. After 4 days, sterile seedlings were transferred on sterile 1% Agar containing nutrient broth (NB; Merck, Darmstadt, Germany) and NMAS (at 1:9 v:v; NB-NMAS) in a Petri dish and stored in a climate chamber (20°C, 70% relative humidity, 14/10 h light/ dark cycle). A total of 25 sterile wheat seedlings of 8 cm shoot length and multiple secondary roots of over 5 cm length were selected for the experiment.

Microbial Inocula

The autoclaved soil was immediately inoculated with a bacterial filtrate from meadow rhizosphere soil to re-establish a diverse bacterial community. The protist-free bacterial filtrate was obtained by suspending 50 g fresh meadow soil (Biology Campus, TU Darmstadt) in 200 ml sterile tap water and filtering it through paper filters (Schleicher & Schuell, Dassel, Germany) and subsequent 5.0 and 1.2 µm Isopore filters (Millipore, Schwalbach, Germany). The filtrate was incubated at 15°C for 7 days and controlled daily for protist contaminations.

Acanthamoeba castelanii Neff, a ubiquitous naked amoeba in soils was used as model protist (Fiore-Donno et al., 2016). *Acanthamoeba castelanii* was isolated from a beechforest soil and kept in NB-NMAS at 5°C on native soil bacteria as food (Bonkowski and Brandt, 2002). The amoebae were separated from the bacteria using repeated centrifugation (1 min, 1,000 rpm) and washing with NB-NMAS (Herdler et al., 2008). The resulting protists suspension was used to inoculate the protist treatments (0.5 ml per chamber). The supernatant containing bacteria from the amoeba culture was filtered (3 µm, Millipore Corporation, Bedford MA, USA) to obtain a protist-free mock community and to inoculate all non-protist treatments.

An AMF *in vitro* culture of *Rhizophagus irregularis* (previously *Glomus intraradices*; Stockinger et al., 2009) was sourced from the Mycothèque de l'Université Catholique de Louvain (MUCL, Belgium) and used as a mycorrhizal inoculum (Bonkowski, 2018).

Split Root Containers

Split root containers were constructed out of PVC with inner dimensions of 8 × 7.5 × 2 cm of each root compartment (**Figure 1**). The front and back walls were transparent, allowing for monitoring root growth and soil moisture. The containers were divided into equally dimensioned right and left chambers. The only connection point between the two chambers was a groove introduced at the top of the split root container to house the plant's root crown. The plant groove and the mating faces

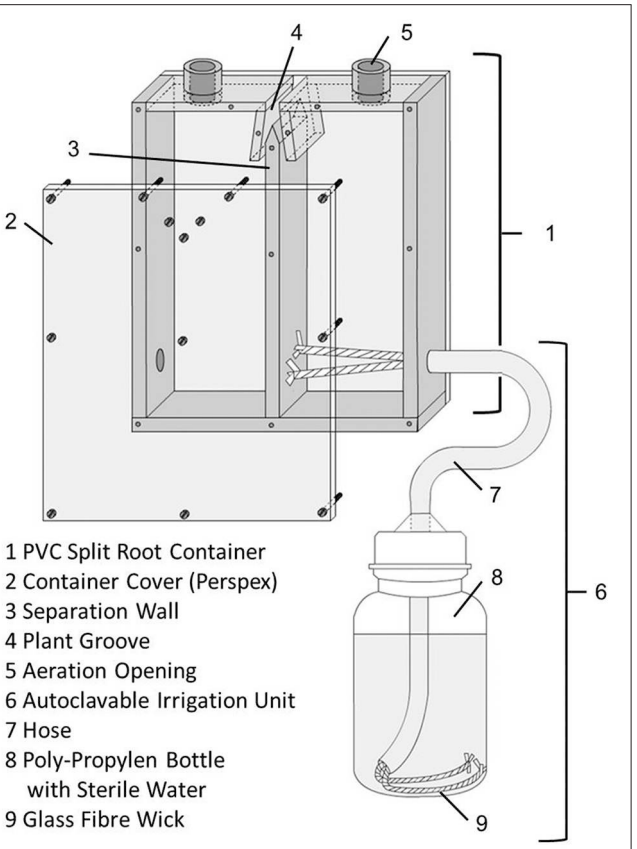

FIGURE 1 | Technical sketch of the split root container, outer dimensions were 18.0 × 15.6 × 2.6 cm. Irrigation system only shown for the right chamber.

of the chamber walls were coated with high viscosity silicone paste (Baysilone, Bayer, Leverkusen, Germany) to completely isolate each soil chamber, and the walls were secured at multiple points with screws. The top of each chamber contained a 10 mm diameter aeration opening. Each chamber was watered in an automatic way using a glass fiber capillary wick (Ortmann, Hilden, Germany) housed in a PE hose fed into through the bottom of the chamber, leading into a 250 ml PP wide neck bottle. This enabled the individual plant roots to adjust their water uptake according to demand. This is crucial in the early growth phase, as water demand of individual root systems in a split root chamber cannot be exactly determined by weighing and external watering.

The containers were sterilized in 70% ethanol and the irrigation systems were autoclaved at 121°C and 110 kPa for 30 min prior to construction. Each chamber was filled with soil corresponding to 200 g dry weight. A seedling was set into the plant groove and its roots were equally separated into both root chambers. A 1 cm^2 piece of agar containing spores and hyphae of *R. irregularis* was applied to the roots in chambers designated for mycorrhiza. Each chamber was inoculated with 1 ml bacterial suspension. Chambers designated for protists were inoculated with 1 ml amoeba suspension, all other chambers received 1 ml NB-NMAS containing the mock community from

amoeba cultures. The aeration openings were closed by sterile cotton plugs to protect the soil from airborne contamination. After inoculation, the chambers were wrapped in aluminum foil to prevent light exposure of soil and roots.

Experimental Design

The experiment was set up in a two-factorial design with the factors protists (*A. castelanii*) and mycorrhiza (*R. irregularis*). Five treatments and treatment combinations were set up, each with five replicates: (1) control (0-0) with only bacterial inoculum in both chambers of the split-root container, (2) protists (0-P) as 0-0, but inoculated additionally with *A. castellanii* in one chamber, (3) mycorrhiza (0-M) as 0-0, but inoculated additionally with *R. irregularis* in one chamber, (4) as 0-0, but protists and mycorrhiza (0-PM) inoculated together in one chamber, (5) protists and mycorrhiza inoculated on separate chambers (P-M), i.e., one chamber containing protists and the other mycorrhiza. The split root containers were arranged in a randomized complete block design with five containers of each treatment in each of five blocks, which were clockwise rotated every 3 days. During these rotations the poly-propylen water suppply bottles (**Figure 1**) were weighed to check for water loss. These measurements allowed calculating the water use of each plant.

The experiment was run for 65 days in a climate chamber at 20 $\pm$ 2°C and a relative humidity of 70%. The climate chamber was illuminated with HI-R lights (Osram, Munich Germany) with 350 μmol m^{-2} s^{-1} and a 14/10 h day/night cycle. After 4 weeks, plant water requirements exceeded the capacity of the capillary wicks, and root chambers were irrigated through the aeration openings with equal volumes of supplementary sterile distilled water every 3 days to adjust for weight lost.

Measurements After Destructive Sampling of the Experiment

Plant roots were carefully picked and sieved from the soil, and the collected roots from both chambers were washed separately and dried, along with the shoots, at 60°C for 72 h, then weighed to obtain dry weight biomass. The dried shoots were blender homogenized (Krups; Solingen, Germany). One gram of shoot material and 1 g of root material taken from the center of the root sample of each root halve was pulverized in a ball mill (MM 200 Retsch, Haan, Germany), and its C and N concentration measured using an elemental analyser (Na1500; Carlo Erba; Milan, Italy). In addition, 200 mg of the milled shoots and roots were dissolved in 2 ml 65% nitric acid and digested using a closed vessel microwave digester (Agazzi and Pirola, 2000). The concentrations of P, Mn, Mg, Ca, K, Al, Na, Fe, and S were determined using Inductive Coupled Plasma—Atom Emission Spectral analysis (ICP-AES, Thermo Scientific iCAP6500).

Microbial Parameters

Soil remaining after the collection of roots was sieved (2 mm), and a sample corresponding to 2 g dry weight was brought to a moisture content of 30% with distilled water. The O_2 consumption rate of this soil was measured every hour over 48 h using a respirometer (Scheu, 1992). Microbial basal respiration (μl O_2 g^{-1} h^{-1}) was measured over 24 h. Microbial biomass (C_{mic}; μg C g^{-1} dw) was measured by substrate-induced respiration (SIR; Anderson and Domsch, 1978) after adding glucose (8 mg g^{-1} dry wt soil), and calculated according to Beck et al. (1997). Microbial specific respiration was calculated as the quotient of basal respiration and microbial biomass.

Nutrient limitation of the microbial community was investigated by adding N [as $NH_4NO_{3(aq)}$] and P [as $KH_2PO_{4(aq)}$] along with C [as glucose$_{(aq)}$; 8 mg g^{-1} dry wt] at a C:N:P mass ratio of 10:2:1 (Anderson and Domsch, 1980) and measuring the slope of the corresponding microbial growth curve (log transformed) using the O_2 microcompensation system (Griffiths et al., 2001).

Protist density (**Figure S2**) was determined by the Most Probable Number technique (MPN; Darbyshire et al., 1974). Five g fresh weight soil from different locations of each chamber were suspended in 20 ml NMAS by shaking (100 rpm, 20 min). Four replicated 100 μl aliquots suspension per sample were 3-fold diluted in NB-NMAS in 96-well microtiter plates and incubated in darkness at 20°C. Wells were checked daily for amoebae, flagellates and ciliates over a period of 10 days using an inverse microscope (100 −400x; Fluovert FU, Leitz; Marburg, Germany).

Soil PLFA Analysis

A quantitative metabolomics approach was used to characterize shifts in microbial communities. The phospholipid fatty acids (PLFAs) composing the membrane lipids of the microorganisms in soil were quantitatively extracted from 1 g soil following Frostegård et al. (1991) with Bligh/Dyer solution [chloroform, methanol, citrate buffer (pH = 4; 1:2:0.8; v/v/v)] and the solution passed through silica acid columns (0.5 g silicic acid, 3 ml; Varian Medical Systems, Palo Alto, California).

PLFAs were transformed into fatty acid methyl esters (FAMEs) by mild alkaline methanolysis as described in Frostegård et al. (1991). The FAMEs were measured using an AutoSystem XL gas chromatograph (Perkin-Elmer Corporation, Norwalk, CT, USA). GC settings were as in Kramer et al. (2013). Identification of FAMEs was based on their retention time assessed with a FAME and a bacterial acid methyl ester mix standard (Sigma-Aldrich, St. Louis, USA). An internal FAME standard (Sigma-Aldrich, St. Louis, USA) added to the samples before methanolysis was used for quantification.

FAMEs were identified by GC-MS using a HP 5890 Series II Plus coupled with a 5972 mass selective detector (Hewlett Packard/Agilent, Waldbronn, Germany) equipped with a DB-5MS column. GC-MS settings were as in Kramer et al. (2013). A mass range of *m/z* 50–450 was monitored. The branched fatty acids i15:0, a15:0, i16:0, and i17:0 were considered as Gram positive and the cy17:0 and cy19:0 as Gram negative bacterial markers (Zelles, 1999). The following PLFAs were used to infer microbial community structure: 14:0, i15:0, a15:0, 15:0, i16:0, 16:1ω7, 16:0, i17:0, cy17:0, 17:0, 18:2ω6, 18:2ω6t/18:1ω9/18:3ω3, 18:1ω7/18:1ω9t, 18:0, cy19:0 (Frostegård and Bååth, 1996; Zelles, 1999). Since the PLFA 16:1ω5, often being used as mycorrhizal marker in environmental studies, can be found in both bacteria and mycorrhiza (see Ngosong et al., 2012) it was discarded from

the analysis. Likewise, unsaturated C20 PLFAs occur in a wide range of eukaryotes (Ruess and Chamberlain, 2010) and were discarded from the analyses.

Statistical Analysis

The data were analyzed by a two factorial (protists and mycorrhiza) general linear model (GLM) with *a priori* singular contrasts. Shoot and root data were analyzed separately. In the first step, treatments with protists (0-P) and mycorrhiza (0-M) alone were compared to the control (0-0). Subsequently, the shoot and root data of the combined treatments (0-PM, P-M) were compared to those of treatments with mycorrhiza alone (0-M) and protists alone (0-P). Roots in the split-root containers had a "treated" and a "non-treated" chamber, except in P-M where both root chambers were differently treated. The split-root set up therefore allowed to compare the "treated" chambers *between* treatments; and further to analyze systemic effects of the "treated" root section on the "non-treated" root section by comparing root chambers *within* treatments. In the 0-0 treatment one root chamber of each replicate was *a priori* randomly assigned as control. For between-treatment comparisons, the root chambers treated with protists (0-P) or mycorrhiza (0-M) were compared to the control chamber of the 0-0 treatment, and to the chamber treated with protists and mycorrhiza (0-PM). In the P-M treatment, where protists and mycorrhiza were spatially separated, the protist-inoculated chamber was compared to the protist treated chamber of 0-P, while the mycorrhiza-inoculated chamber was compared to the mycorrhiza treated chamber of 0-M. Statistically significant contrasts between "treated" root chambers are indicated by horizontal bars in figures. Subsequently, systemic effects of the "treated" root section vs. the "non-treated" root section *within* treatments, and between both treated chambers of the P-M treatment were analyzed by one-way analysis of variance (ANOVA). Data were analyzed using SAS V8.2 software (SAS Institute; Cary, North Carolina, USA). Discriminant function analysis (DFA) was used to inspect the overall structure of the PLFA profiles in order to differentiate the effects of different treatments on soil bacteria. Through subsequent correlation of single fatty acids with both major axes of the DFA, we investigated which fatty acids were responsible for the discrimination of samples. DFA was carried out in R version 3.3.3, using the packages MASS (Venables and Ripley, 2002), and ggplot2 (Wickham, 2016) for plotting.

RESULTS

Plant Biomass

Plant shoot-to-root allometry and within-root system allometry between both split-root chambers provides information on potential competition between shoots and roots and between roots and microbes for carbohydrates and nutrients. Average total biomass of shoots and roots in the control treatment (0-0) was 4.93 ± 0.7 and 6.14 ± 2.3 g dry wt, respectively. Presence of protists (0-P) caused a significant increase in total plant biomass by 24% as compared to the control (**Figure 2A**; **Table 1**). Protists also tended to increase shoot biomass (+22%). Mycorrhiza in contrast had no effect on shoot biomass but significantly increased the shoot-to-root ratio (+74%), due to (in trend) reduced total root biomass [−37%, 0-0 vs. 0-M, $F_{(1,23)} = 3.15$; $p = 0.089$; **Figure 2A**]. Root biomass of the mycorrhiza chamber in the 0-M treatment appeared particularly low, but the reduction was not statistically significant due to high variation in the non-inoculated root compartment [$F_{(1,6)} = 3.60$; $p = 0.107$]. Total root biomass was also reduced when both mycorrhiza and protists were combined (0-PM, P-M; **Table 1**). Total root biomass decreased as compared to 0-P by −34 and −31% in the 0-PM and P-M treatments, and resulted in an increased shoot-to-root ratio by 38 and 40% in the 0-PM and P-M treatments, respectively (**Figure 2A**; **Table 1**).

Protists mitigated some of the mycorrhiza induced reductions of root systems, resulting in a 2.57-fold increase of root biomass in the mycorrhiza chamber of the P-M treatment as compared to the mycorrhiza chamber of the 0-M treatment [$F_{(1,23)} = 5.69$; $p = 0.026$]. This was because root biomass in the mycorrhiza chamber of the P-M treatment was 2-fold higher than that in the neighboring protist chamber, albeit with marginal significance [$F_{(1,8)} = 4.42$; $p = 0.069$]. The complementarity of protists in combination with mycorrhiza was further supported by measurements of plant water uptake, which was significantly higher in 0-PM ($p < 0.001$) and P-M ($p = 0.018$) treatments compared to the 0-M treatment (**Figure S2**, **Table S2**).

Nutrients

Differences in plant nutrient uptake between control (0-0) and microbial treatments reveal either mutualistic, neutral or parasitic relationships in symbioses. Comparing differently inoculated root chambers can reveal competition or synergism between different microorganism groups. Mycorrhiza and protists altered root N mass in opposite directions, with protists increasing and mycorrhiza reducing it; and the negative mycorrhiza effect continued to dominate in 0-PM and P-M treatments. In the 0-P treatment, root N mass of the protist chamber increased by 52% as compared to the control [0-0; $F_{(1,23)} = 4.32$; $p = 0.049$], but this effect was local and increased total root N mass (+30%) and total plant N mass (+22%) only with marginal significance (**Figure 2B**; **Table 2**).

In the mycorrhiza chamber of the 0-M treatment, the root N mass decreased by 66% as compared to the control [0-0; $F_{(1,23)} = 6.05$; $p = 0.022$]. This led to a 58% reduction in total root N mass, while total plant N mass was only reduced by 32% (**Figure 2B**; **Table 2**). The nitrogen reduction in the mycorrhiza chamber of the 0-M treatment led to a 2.72-fold increase in the shoot-to-root N mass ratio as compared to the control (0-0) as shoot N was not affected (**Table 2**). The negative effect of mycorrhiza on plant N mass prevailed in the presence of protists (0-PM, P-M), and was also reflected in root N concentrations (**Figure S3**, **Table S2**). Root N concentration in the mycorrhiza + protist chamber of the 0-PM treatment (0.60 mg g^{-1}) was significantly reduced as compared to the protist chamber of the 0-P treatment [1.02 mg g^{-1}; $F_{(1,23)} = 41.3$; $p < 0.001$; **Figure S3**]. This reduced both, total root N mass and total plant N mass by 56% in 0-P vs. 0-PM treatments (**Table 2**). In a similar way total root N mass was reduced in the P-M as compared to the 0-P treatment by 77%. These nitrogen reductions in roots led to

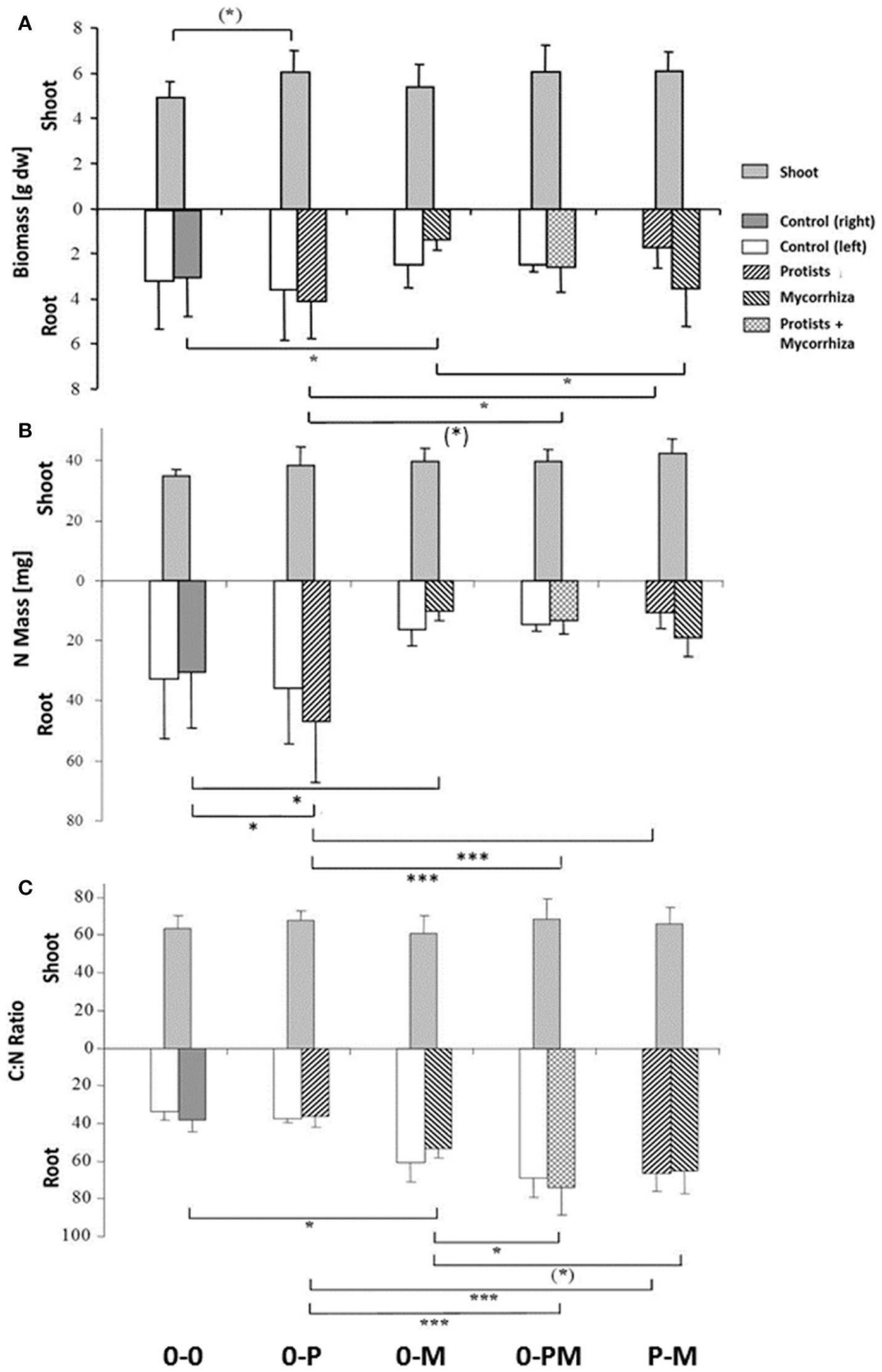

FIGURE 2 | Biomass **(A)** total N mass (mg) **(B)** and C:N mass ratio **(C)** of shoots and of roots of *Triticum aestivum* in both root chambers of control plants (0-0), plants treated with protists in the right root chamber (0-P), or treated with mycorrhiza in the right root chamber (0-M), or treated with protists and mycorrhiza together in the right root chamber (0-PM), or where the left and right root chambers were separately treated with protists and mycorrhiza (P-M). Means and standard deviation; horizontal lines denote significant contrasts with $^{(*)}p < 0.1$, $^{*}p < 0.05$, $^{***}p < 0.001$.

2.57 and 2.58-fold enhanced shoot-to-root N mass ratios in 0-PM and P-M treatments as compared to the control, respectively (**Figure 2B**, **Table 2**). Interestingly, the root N concentration of the protist + mycorrhiza chamber in the 0-PM treatment was also significantly reduced as compared to the mycorrhiza chamber of the 0-M treatment [from 0.75 to 0.60 mg g^{-1}; $F_{(1,23)} = 4.57$; $p = 0.043$], suggesting N uptake by mycorrhiza in PM (**Figure S3**). Unexpectedly, total mass of root N in the

TABLE 1 | *F*- and *p*-values of GLM contrasts showing treatment effects on total plant biomass, shoot biomass, biomass of the total root system, and shoot-to-root ratio of *Triticum aestivum*.

Comparison	Total biomass		Shoot biomass		Total root biomass		Shoot-to-root ratio	
	$F_{(1,19)}$	*P*	$F_{(1,19)}$	*P*	$F_{(1,19)}$	*P*	$F_{(4,19)}$	*P*
0-0 vs. 0-P	**4.46**	**0.049**	*3.53*	*0.077*	1.99	0.174	0.67	0.424
0-0 vs. 0-M	1.76	0.201	0.77	0.391	*3.69*	*0.070*	**11.65**	**0.003**
0-M vs. 0-PM	2.00	0.175	1.05	0.320	1.06	0.316	0.82	0.378
0-M vs. P-M	2.46	0.135	0.96	0.340	1.50	0.235	2.08	0.167
0-P vs. 0-PM	*4.08*	*0.058*	0.02	0.836	**5.56**	**0.029**	**29.35**	**<0.001**
0-P vs. P-M	*3.45*	*0.080*	0.01	0.919	**4.62**	**0.045**	**35.89**	**<0.001**

Treatments: control plants (0-0), root chambers treated with protists (0-P), with mycorrhiza (0-M), with protists and mycorrhiza together (0-PM), or where the left and right root chambers were separately treated with protists and mycorrhiza (P-M). Nominator and denominator degrees of freedom in brackets. Significant effects p< 0.05 in bold; p< 0.1 in italics.

TABLE 2 | *F*- and *P*-values of GLM contrasts showing treatment effects on total shoot N mass, total root N mass, total plant N mass, and shoot-to-root N mass ratio of *Triticum aestivum*.

Comparison	Shoot N mass		Total root system N mass		Total plant N mass		Shoot-to-root N mass	
	$F_{(1,19)}$	*P*	$F_{(1,19)}$	*P*	$F_{(1,19)}$	*P*	$F_{(4,19)}$	*P*
0-0 vs. 0-P	1.29	0.270	*3.20*	*0.090*	*4.22*	*0.055*	0.15	0.705
0-0 vs. 0-M	2.65	0.119	**10.27**	**<0.005**	**7.70**	**0.012**	**16.41**	**<0.001**
0-M vs. 0-PM	0.01	0.926	0.01	0.915	0.01	0.909	0.01	0.907
0-M vs. P-M	0.82	0.377	0.08	0.785	0.29	0.599	0.01	0.928
0-P vs. 0-PM	0.24	0.628	**25.72**	**<0.001**	**23.87**	**<0.001**	**20.76**	**<0.001**
0-P vs. P-M	2.41	0.137	**23.94**	**<0.001**	**19.72**	**<0.001**	**21.03**	**<0.001**

Treatments: control plants (0-0), root halves treated with protists (0-P), with mycorrhiza (0-M), with protists and mycorrhiza together (0-PM), or where the left and right root compartments were separately treated with protists and mycorrhiza (P-M). Nominator and denominator degrees of freedom in brackets. Significant effects p < 0.05 in bold; p< 0.1 in italics.

P-M treatment was almost 2-fold reduced in the protist chamber (10.6 mg N) as compared to the mycorrhiza chamber [19.2 mg N; $F_{(1,8)} = 5.57$; $p = 0.046$; **Figure 2B**].

Root P mass in the 0-M treatment was reduced by 64% as compared to the control [0-0; $F_{(1,23)} = 6.96$; $p = 0.015$], resulting in a 55% reduction in total root P mass (**Figure 3**, **Table 3**), but a 3.7-fold increase in the shoot-to-root P mass ratio. Although root P mass was not affected in the 0-P treatment (**Table 3**), root P levels were diluted by an increased root biomass, with root P concentration in the protist chamber of the 0-P treatment being only 0.10 mg g^{-1} as compared to the control (0-0) with 0.14 mg g^{-1} [$F_{(1,23)} = 4.73$; $p = 0.041$; **Figure S4**].

Root P mass in the protist chamber of the P-M treatment was reduced by 54% as compared to the 0-P treatment [**Figure 3**; $F_{(1,23)} = 5.27$; $p = 0.031$], but in the mycorrhiza chamber of the P-M treatment root P mass was more than 2.5-fold higher than in the 0-M treatment [$F_{(1,23)} = 5.04$; $p = 0.035$]. Comparing both split-root chambers in the P-M treatment, root P mass almost doubled (x 1.91) in the mycorrhiza vs. the protist chamber [$F_{(1,8)} = 5.61$, $p = 0.045$], indicating compensation of P deficiency by mycorrhiza since total root P and total plant P mass were not significantly affected (**Figure 3**; **Table 3**; **Table S3**). Only in the 0-PM treatment total root P and whole plant P tended to be reduced by 37 and 16% in 0-PM vs. 0-P, respectively, although with marginal significance (**Figure 3**; **Table 3**). This was because root P mass in the mycorrhiza + protist chamber of the 0-PM treatment tended to be 42% lower as compared to the protist chamber in the 0-P treatment [**Figure 3**; $F_{(1,23)} = 3.17$; $p = 0.088$]. Thus, mycorrhiza appeared to reduce the P gain of plants in direct contact with protists (0-PM), but significantly shifted within-root system allocation of P to the mycorrhiza chamber in P-M.

Plant C:N Ratio

The C:N ratio reflects a critical balance of carbohydrate gain (by photosynthesis) and/or investment (e.g., in root symbionts) relative to plant nutrient uptake. Mycorrhiza increased the root C:N ratio across treatments (**Figure 2C**). The root C:N ratio in the mycorrhiza chamber of the 0-M treatment (53) was significantly higher as compared to the control (0-0) at 38 [$F_{(1,23)} = 5.16$; $p = 0.033$]. Interestingly, the effect of mycorrhiza on root nutrient status was systemic, reflected in comparably high root C:N ratios of 61 and 53 in the bacteria only vs. mycorrhiza chambers of the 0-M treatment, respectively [$F_{(1,6)} = 1{,}74$, $p = 0.24$]. Accordingly, total plant C:N ratio was higher in the 0-M treatment (60) than in the control (46; **Table 4**). Thus, mycorrhiza strongly reduced root N levels relative to C, but the shoot C:N ratio remained constant.

Mycorrhiza effects also dominated the root C:N ratio in the presence of protists, reflected by root C:N ratios of 74 and 66 in the protist chambers of 0-PM and P-M as compared to the 0-P (37) treatment [**Figure 2C**; 0-P vs. 0-PM: $F_{(1,23)} = 37.14$; $p <$

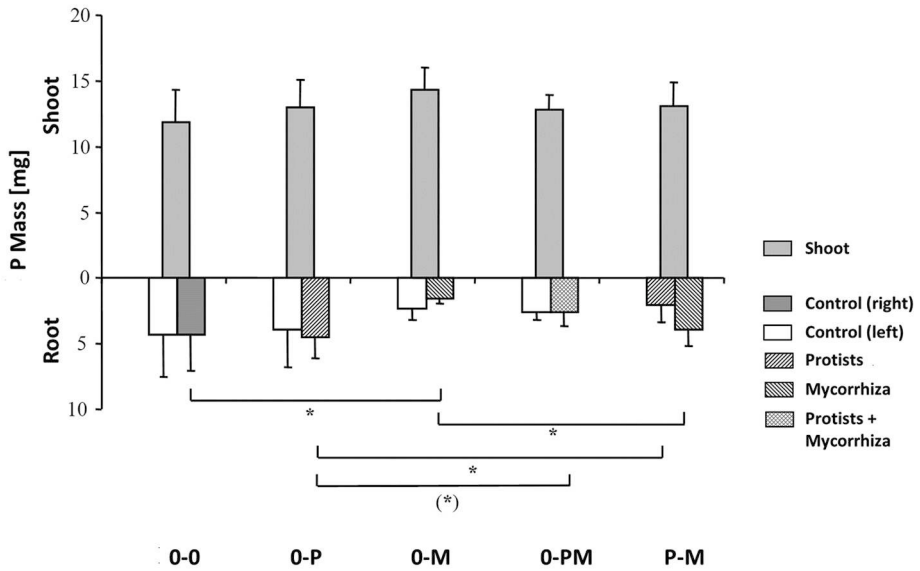

FIGURE 3 | Total P mass (mg) of shoots and of roots in both root chambers in control plants (0-0), plants treated with protists in the right root chamber (0-P), or treated with mycorrhiza in the right root chamber (0-M), or treated with protists and mycorrhiza together in the right root chamber (0-PM), or where the left and right root chambers were separately treated with protists and mycorrhiza (P-M). Means and standard deviation; horizontal lines denote significant contrasts with $^{(*)}p < 0.1$, $^{*}p < 0.05$.

TABLE 3 | *F*- and *P*-values of GLM contrasts showing treatment effects on the total shoot P mass, total root P mass, total plant P mass, and shoot-to-root P mass of *Triticum aestivum*.

Comparison	Shoot P mass		Total root system P mass		Total plant P mass		Shoot-to-root P mass	
	$F_{(1,19)}$	*P*	$F_{(1,19)}$	*P*	$F_{(1,19)}$	*P*	$F_{(4,19)}$	*P*
0-0 vs. 0-P	0.71	0.410	0.02	0.878	0.20	0.663	0.01	0.937
0-0 vs. 0-M	0.30	0.587	**9.21**	**0.007**	1.90	0.186	**5.50**	**0.031**
0-M vs. 0-PM	1.61	0.219	0.79	0.385	0.00	0.950	1.84	0.192
0-M vs. P-M	1.73	0.204	1.84	0.192	0.26	6.150	*3.68*	*0.072*
0-P vs. 0-PM	0.01	0.935	3.96	0.062	3.56	0.076	1.14	0.299
0-P vs. P-M	0.00	0.975	2.32	0.145	1.72	0.207	0.26	0.618

Treatments: control plants (0-0), root halves treated with protists (0-P), with mycorrhiza (0-M), with protists and mycorrhiza together (0-PM), or where the left and right root compartments were separately treated with protists and mycorrhiza (P-M). Nominator and denominator degrees of freedom in brackets. Significant effects $p < 0.05$ in bold; $p < 0.1$ in italics.

0.001; 0-P vs. P-M: $F_{(1,23)} = 23.40$; $p < 0.001$]. At the whole plant level the C:N ratio increased from 46 in the 0-P treatment to 70 and 66 in the 0-PM and P-M treatments, respectively (**Table 4**).

The N sink effect of the combined treatments with mycorrhiza and protists was also enhanced in comparison to the 0-M treatment. The root C:N ratio was particularly enhanced in the protist + mycorrhiza chamber of the 0-PM treatment (74) as compared to the mycorrhiza chamber of the 0-M treatment [53; $F_{(1,23)} = 10.41$; $p = 0.004$], and also tended to be higher in the mycorrhiza chamber of the P-M treatment [65; $F_{(1,23)} = 3.49$; $p = 0.075$].

Microbial Biomass and Nutrient Limitation of Microbial Growth

Microbial biomass in this experimental set up was almost exclusively bacterial biomass. Its measurements may allow to detect differences in biomass pools (e.g., by protist grazing), C release (basal respiration), and microbial C turnover (specific respiration). Microbial biomass in the protist chamber of the 0-P treatment tended to be reduced by 9% as compared to the control (0-0), although the effect was only marginally significant [$F_{(1,21)} = 3.07$; $p = 0.09$]. There were no treatment effects on microbial basal respiration and specific respiration (data not shown).

Steeper slopes of microbial growth after nutrient addition reflect limitation of microbes and of plant growth by this particular nutrient. Slopes of microbial growth after CN addition were 30-fold higher than slopes of microbial growth after CP addition [$F_{(1,91)} = 692.6$, $p < 0.001$], showing a strong N limitation of microbial growth in our experimental soil. Compared to the 0-P treatment, microbial growth increased by 34% after CN addition in the protist chamber of the 0-PM

TABLE 4 | *F*- and *P*-values of GLM contrasts showing treatment effects on the C:N ratio of *Triticum aestivum* shoots, the total root system, and of whole plants.

Comparison	Shoot C:N ratio		Total root system C:N ratio		Total plant C:N ratio	
	$F_{(1,19)}$	*P*	$F_{(1,19)}$	*P*	$F_{(1,19)}$	*P*
0-0 vs. 0-P	0.63	0.4380	0.05	*0.8260*	*0.06*	0.8160
0-0 vs. 0-M	0.21	0.6550	**25.35**	**0.0001**	**8.37**	**0.0097**
0-M vs. 0-PM	1.92	0.1820	**9.05**	**0.0070**	**4.76**	**0.0426**
0-M vs. P-M	0.81	0.3810	2.82	0.1090	2.05	0.1690
0-P vs. 0-PM	0.04	0.8470	**69.03**	**0.0001**	**26.74**	**0.0001**
0-P vs. P-M	0.10	0.7510	**47.59**	**0.0001**	**19.12**	**0.0004**

Treatments: control plants (0-0), root halves treated with protists (0-P), with mycorrhiza (0-M), with protists and mycorrhiza together (0-PM), or where the left and right root compartments were separately treated with protists and mycorrhiza, respectively (P-M). Nominator and denominator degrees of freedom in brackets. Significant effects $p < 0.05$ in bold; $p < 0.1$ in italics.

treatment [$F_{(6,22)} = 5.16$, $p = 0.034$], indicating a much stronger N-limitation in PM as compared to P. Also compared to the 0-M treatment, there was a tendency of increased growth after CN addition (+26%) in the protist + mycorrhiza chamber of the 0-PM treatment [$F_{(6,22)} = 3.88$, $p = 0.062$], suggesting an even stronger N-limitation in PM as compared to M. There were no treatment effects on microbial growth after CP addition (data not shown).

PLFA Profiles

Since PLFA profiles reflect the composition of microbial membrane lipids they are highly sensitive to detect changes in microbial community composition. DFA clearly separated the PLFA profiles of the 0-0, 0-M, and 0-P treatments (**Figure 4**); mycorrhiza and in particular protists led to strong and contrasting shifts in microbial PLFA patterns as compared to the control. The first axis of the DFA represented 77.1% of the variation and correlated closely with short chain branched fatty acids typical for Gram positive bacteria (i15:0, a15:0, 15:0, i16:0; **Table S1**). It clearly separated the 0-P treatment from the 0-M and 0-0 treatments, with the PLFA patterns of the combined treatments with mycorrhiza and protists (0-PM and P-M) being more similar to the 0-P treatment. The second axis represented 12.2% of the variation and clearly separated 0-P and 0-M treatments from the control (0-0) and the combined treatments (0-PM, P-M). The second axis correlated with fatty acids typical for Gram negative bacteria (cy19:0; **Table S1**).

Notably, as indicated by DFA, bacterial communities between different root chambers within the same treatment did not differ significantly except for the protist and mycorrhiza chambers of the P-M treatment ($p < 0.05$; **Figure 4**). The protist chamber contained fewer fatty acids typical for Gram positive bacteria than the chamber without protists. Specifically, these fatty acids were significantly reduced in the 0-P as compared to the control (0-0) treatment, and both combined treatments had significantly lower levels of these fatty acids than the MYC treatment (**Figure 5**).

Treatment Performance

In the 15 root chambers treated with *A. castelanii,* the amoebae reached densities of 16,700 (0-P, protist treated chamber), 14,400 (0-PM, protist+mycorrhiza treated chamber) and 10,200 ind. g^{-1} dw soil (P-M, protist treated chamber; **Figure S1**). One replicate of the 0-M treatment was discarded from the statistical analyses as it was contaminated by protists.

Unfortunately, the determination of root colonization by mycorrhiza failed because the roots disintegrated after boiling in KOH. However, mycorrhiza in this experiment is a treatment factor and not treated as a continuous variable. The clear treatment effects by mycorrhiza on plant performance leave no doubt that mycorrhization was successful.

DISCUSSION

We hypothesized that both, mycorrhiza and protists, would show complementary functions for plant growth, comparable to findings from tripartite symbioses between rhizobia, mycorrhiza and their host plants (Kafle et al., 2018). As expected, mycorrhiza and protists, when inoculated separately, had opposite effects on plant N limitation with fundamental consequences for plant stoichiometry and shoot-to-root allometry. High shoot biomass relative to roots is an important plant trait in modern wheat cultivars (Siddique et al., 1990; Slafer and Araus, 2007). Conform to earlier studies (Veresoglou et al., 2012b) and our hypothesis, mycorrhiza increased plant shoot-to-root biomass ratio and shoot-to-root N mass ratio almost 3-fold, and shoot-to-root P mass ratio almost 4-fold. In part this was due to reducing root biomass (−38%), root N mass (−58%), and P mass (−55%), however, shoot biomass was not significantly affected by mycorrhiza. Split root experiments with barley already described *R. irregularis* as a strong C-sink for its plant hosts (Lerat et al., 2003). The strong reduction of root biomass, despite unchanged shoot biomass of wheat indicates that mycorrrhiza indeed partly replaced root system function as hypothesized. It seems that plants preferently invested in the shoot system even though root biomass and root nutrient levels were strongly reduced by mycorrhiza.

We further hypothesized that mycorrhiza would increase the P content of their plant hosts, but complemented by protist grazers of bacteria (Trap et al., 2016), we expected mycorrhiza to capture and transport N released by protist predation to the plant (Koller et al., 2013b; Trap et al., 2016). Mycorrhiza did

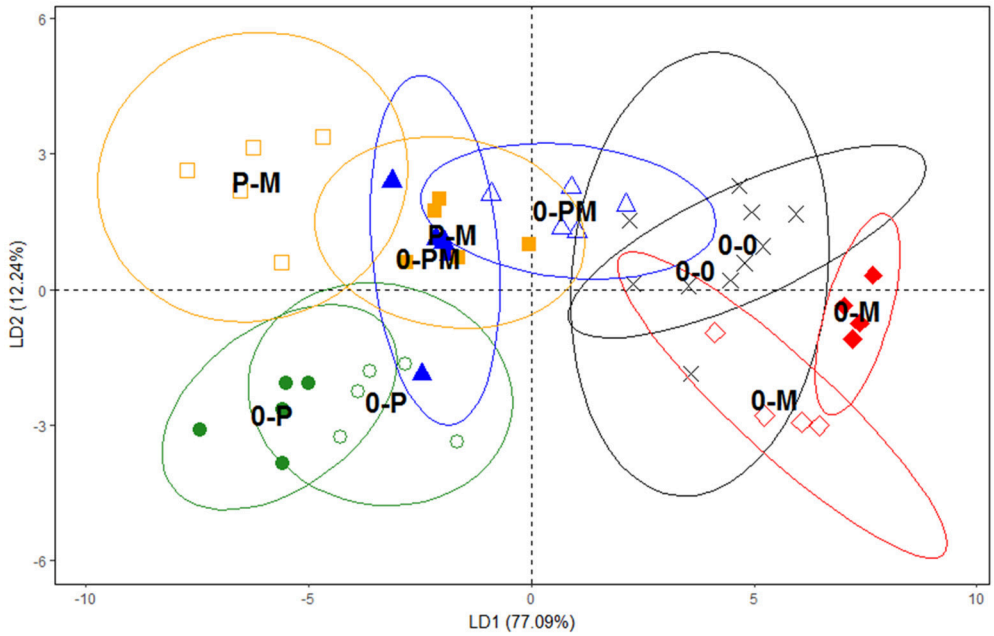

FIGURE 4 | Separation of microbial communities according to PLFA groupings using a discriminant function analysis (DFA). Control plants (0-0, **x**), plants treated with protists (0-P treated chamber •, non-treated chamber ○), with mycorrhiza (0-M treated chamber ♦, non-treated chamber ◊), with both protists and mycorrhiza together (0-PM, treated chamber ▲, non-treated chamber Δ), or where the left and right root chambers were separately treated with protists and mycorrhiza (P-M, protists □, mycorrhiza ■). Ellipses represent confidence ranges of 95%. Variation explained by axes 1 and 2 in parentheses.

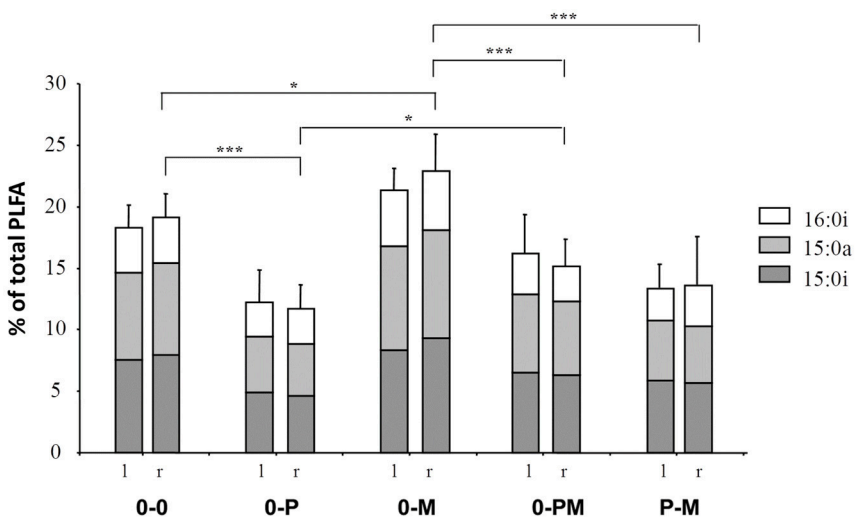

FIGURE 5 | Influence of treatments on the levels of fatty acids (% of total) typical of Gram positive bacteria (15:0i, 15:0a, and 16:0i) in the left (l) and right (r) root compartment, respectively. Treatments: control plants (0-0), plants treated with protists in the right root chamber (0-P), or treated with mycorrhiza in the right root chamber (0-M), or treated with protists and mycorrhiza together in the right root chamber (0-PM), or where the left and right root chambers were separately treated with protists and mycorrhiza (P-M). Mean and standard deviation; $^{*}p < 0.05$, $^{***}p < 0.001$.

not increase plant P uptake, but despite reduced root biomass, mycorrhiza infection kept whole plant P uptake constant. Interestingly, mycorrhiza caused a translocation of P from roots to shoots. This was confirmed by the lower N:P ratio of shoots, the strongly reduced mass of P in roots, but unaltered total mass of plant P in the 0-M treatment. It has been argued that replacement of root system function by mycorrhiza might be more economic to plants than investment into own roots (Fitter, 1991; Hodge, 2004). The reduction of root biomass indeed indicates a replacement of root system function by mycorrhiza, but at the same time mycorrhiza caused a severe reduction of total plant N (−32%). The reduced plant N levels show that

a replacement of roots by mycorrhiza was not beneficial to the plants at N-limiting conditions. Rather, the results suggest that the plants partly lost control over root system function—a symbiont strategy to make itself indispensable according to microbial market theory (Werner et al., 2014). Likely the fungus diverted N for its own investment, e.g., into chitin polymers, for the establishment of an extraradical hyphal network (Herdler et al., 2008; Hodge and Fitter, 2010).

In contrast to AMF, protists are known to increase N availability to plants by releasing significant amounts of NH_4^+ from consumed microbial biomass, a mechanism known as microbial loop (Clarholm, 1985; Bonkowski and Clarholm, 2012). Such changes in nitrogen form can feed back on mycorrhizal development (Giovannetti et al., 2017; Bukovská et al., 2018; Mollavali et al., 2018). Corresponding to the N-limiting experimental conditions, the increase in total plant N uptake (+22%) in the 0-P treatment corresponded to a 24% increased plant biomass as compared to the control (0-0). However, the protist effect on plant N nutrition was mainly due to a local increase in N contents in the protist chamber of the 0-P treatment (+52%). Further, contrasting the effect of mycorrhiza, protists did not change the shoot-to-root biomass ratio, suggesting that they stimulated above- and belowground growth in a balanced way.

In soils mycorrhiza and protists always co-occur and therefore their individual effect on plants is difficult to study. By manipulating them independently from each other, our split root design not only allowed deeper insight into their individual effect but also their interactions. The positive influence of AMF on plant growth primarily manifests as an improvement of P status against a background of P limitation (Nagy et al., 2009; Smith F. A. and Smith, 2011). Thus, from the plant's perspective, mycorrhiza, and protists seem complementary by respectively improving its P and N status. According to the functional equilibrium model (Mooney, 1972; Johnson et al., 2003), plants should allocate more biomass to those specific structures and rhizosphere symbionts that best garner the limiting resource (Revillini et al., 2016). Assuming that plants are under full control of the mycorrhiza symbiosis (Smith S. E. and Smith, 2011), plants would gain most benefit by investing in the protist rather than the mycorrhizal partner under N limiting conditions, as shown by increased plant biomass in the 0-P treatment. Recent studies indicated that *R. irregularis* is unable to compete for N mineralized by bacteria, but effectively captures N released from consumed microbial biomass by protist grazers (Koller et al., 2013a,b). Here we showed that AMF, although specialized for efficient P foraging, also gain control over N. It has been widely speculated why AMF hyphae proliferate in organic patches, despite being unable of a direct uptake of organic N (Hodge and Storer, 2014). The significantly stronger microbial N limitation in the mycorrhiza + protist chamber of the 0-PM treatment as compared to the protist chamber of the 0-P treatment indicates that mycorrhiza efficiently captured N mobilized by protists (Herdler et al., 2008; Koller et al., 2013b). This finding positions mycorrhiza as a critical player in the microbial loop (Bukovská et al., 2018).

However, plants did not benefit from the interaction between protists and mycorrhiza as indicated by the absence of plant growth promotion as compared to the 0-P treatment, and the widest C:N ratio of shoots and roots in the 0-PM as compared to all other treatments. Evidently the N released by protists was not delivered to the plant host, since plant N contents in the 0-PM and P-M treatments were as low as in the 0-M treatment. The mycorrhiza effects on plants clearly dominated in the combined treatments with mycorrhiza and protists (0-PM, P-M), suggesting that mycorrhiza, at least in part, took over control of the interactions—a crucial prerequisite for the equitable exchange of resources in mutualisms (Werner et al., 2014).

Remarkably, allocation of resources into roots considerably changed in the P-M treatment where protists and mycorrhiza were spatially separated. According to the 0-P and 0-M treatments one would expect a narrow C:N ratio and increased root growth in presence of protists, and a wide C:N ratio and reduced root growth in presence of mycorrhiza. Strikingly, the opposite pattern was found. Protists generally had a positive effect on root proliferation as observed here in the 0-P treatment and earlier (Bonkowski, 2004; Krome et al., 2010), but the AM fungus is a strong C sink and likely thereby root allocation was translocated to the mycorrhiza chamber in the P-M treatment. In addition, mycorrhiza altered N allocation within roots in a systemic way. Root system architecture is highly sensitive to different forms of nutrients, particularly N (Tian et al., 2014). Mycorrhiza generally reduced root N mass and root concentration of N, but in the 0-M treatment root N mass was also reduced in the non-mycorrhiza chamber of the split-root containers. This was reversed in the P-M treatment, where the doubling of N uptake in the mycorrhiza chamber as compared to the protist compartment suggests that N taken up by roots in the protist chamber was subsequently translocated to the mycorrhiza chamber. Taken together, the provisioning of roots by N through the microbial loop in the protist chamber was coupled with a systemic shift of N allocation to mycorrhiza in P-M. At the same time, also root proliferation shifted to the mycorrhiza chamber, potentially resulting from of a systemic protist effect on root growth. The combination of these effects caused the observed wide C:N ratio of roots in the protist chamber and the shift of root allocation within root systems in the P-M treatment. Importantly, the synergistic effects of protists and mycorrhiza in the P-M treatment could not have been predicted from the individual effects of protists and mycorrhiza in the 0-P and 0-M treatments. Rather, the interactions suggest that mycorrhiza as the root-infecting symbiont at least in part took over control of the tripartite interaction for diverting resources to its own benefit.

Mycorrhiza and Protists as Drivers of Rhizosphere Microbial Community Composition

In recent years much has been learned how plants shape their root-associated soil and its inhabiting microorganisms (Berg and Smalla, 2009; Hartmann et al., 2009). It is assumed that soil type and rhizodeposits act as environmental filters for the enrichment of specific microorganisms (Bais et al., 2006; Bulgarelli et al., 2012; Schreiter et al., 2014), while host genotype–dependent

fine tuning at the rhizoplane further selects for specific root-associated microbial consortia (Edwards et al., 2015; van der Heijden and Schlaeppi, 2015). Our results partly challenge this plant-centered view of community assembly, because the unique PLFA groupings in the 0-P and 0-M treatments as compared to the control (0-0) suggest fundamentally different effects of protist grazers and mycorrhiza on bacterial community assembly in the wheat rhizosphere. Also previous studies support this rhizosphere symbiont view of structuring rhizosphere microbial communities by documenting that both protists through top-down control (Kreuzer et al., 2006; Rosenberg et al., 2009) and AMF through bottom-up modifications of resources alter bacterial communities in the rhizosphere (Marschner and Baumann, 2003; Rillig et al., 2006; Bukovská et al., 2016; Rodríguez-Caballero et al., 2017). Since protist grazing is highly selective, preferential grazing together with competitive shifts in bacterial community composition are likely responsible for changes in root-associated bacterial communities (Jousset et al., 2008; Jousset, 2012; Flues et al., 2017). The shifts in PLFA pattern by mycorrhiza and protists support our general hypothesis on differences in bacterial community composition. However, the fact that the non-treated chambers of the split root containers displayed the same PLFA patterns as the treated chambers indicates that the effects of protists and mycorrhiza were communicated by the roots to the chamber not colonized by these symbionts. This supports the view that root symbionts exert systemic effects on rhizosphere community assembly (Marschner and Baumann, 2003; Marschner and Timonen, 2005; Veresoglou et al., 2012a) and that this also applies to the studied protists. Interestingly, microbial communities in the mycorrhiza chamber of the P-M and 0-M treatments were most different, indicating that in addition to mycorrhiza, protists may have altered microbial community assembly in the myco-rhizosphere in a systemic way (Bukovská et al., 2018). Implications of systemic root-responses to protists and mycorrhiza would be far reaching, indicating an adjustment of the root response via changing the quantity and quality of root exudates (Benizri et al., 2002, 2007; Jones et al., 2004). Such responses however, need to be confirmed in subsequent studies by gene expression studies of roots and their metabolites.

The strong effect of protists on the rhizosphere microbial community was unexpected considering the dominance of mycorrhiza on shoot-to-root allometry and plant nutrient uptake. The discovery that the genome of *A. castellanii* harbors genes for auxin biosynthesis as well as for free-auxin deactivation via formation of IAA conjugates led Clarke et al. (2013) to suggest that *A. castellanii* directly manipulates the root architecture of plants. Certainly, more research on how protist-root and protist-mycorrhiza interactions alter root allometry, and the assembly and functioning of the plant microbiome is needed. Split-root experiments as used in the present study provide an essential tool to uncover systemic root responses and their modulation by rhizosphere symbionts (Bonkowski, 2018).

CONCLUSIONS

Results of the present study provide compelling evidence for a tight functional coupling of the microbial loop and nutrient foraging by AMF. Mycorrhiza markedly altered plant shoot-to-root allometry by reducing root biomass of wheat, and it partly took over root system functioning. Notably, the shoot system responded little to alterations in the root system and rhizosphere community composition, indicating that the plants optimized shoot growth despite varying investment into roots. Protists increased plant growth and N uptake via the microbial loop, but this effect vanished in combined treatments with mycorrhiza, suggesting that mycorrhiza gained control over N provided by protist grazers. Combined effects of protists and mycorrhiza revealed systemic effects on within root system biomass allocation and root N allocation of winter wheat, and on rhizosphere microorganisms. Structuring rhizosphere communities by plants (roots) and root allocation thereby represent emergent properties that could not be predicted from individual treatments with mycorrhiza or protists alone. Notably, protists and mycorrhiza altered rhizosphere microbial communities in contrasting ways and these changes were systemically conveyed to the root side where the symbionts were lacking. The tight plant and microbial feed backs have far reaching implications for understanding the assembly of plant microbiomes, and testify central roles of both protists and mycorrhizas in the assembly process.

AUTHOR CONTRIBUTIONS

MB and SS conceived and designed the experiment. GH and MB designed the split root containers. GH performed the experiment and measurements after harvest, except the PLFA analyses that were carried out by SM and EK. Statistical analyses were performed by GH and MB drafted the manuscript. All co-authors contributed to the interpretation of the data and significantly improved the manuscript by critical revisions.

ACKNOWLEDGMENTS

The authors thank Garvin Schulz for his help with the DFA analysis, Heather Hillers for revising an earlier version of the manuscript and two reviewers for their helpful comments. The study received funding from the European Union Marie Curie BIORHIZ Research Network.

SUPPLEMENTARY MATERIAL

The Supplementary Material for this article can be found online at: https://www.frontiersin.org/articles/10.3389/fenvs.2018.00117/full#supplementary-material

Figure S1 | Numbers of amoebae in soil (ind. g^{-1} soil dry wt) of protist-inoculated root-chambers at the end of the experiment. No protists were detected in non-inoculated chambers, except in one replicate of the 0-M treatment, which was excluded from all analyses. Differences between treatments were not statistically significant.

Figure S2 | Cumulative average requirements of water (g) of plants in split-root microcosms until 32 days after the set up of the experiment, measured by weighing the water supply bottles attached to each microcosm. Treatments: control plants (0-0), plants treated with protists in one root chamber (0-P), or treated with mycorrhiza in one root chamber (0-M), or treated with protists and mycorrhiza together in one root chamber (0-PM), or where the root chambers were separately treated with protists and mycorrhiza (P-M).

Figure S3 | Concentration of N (%) in shoots and in roots of both root chambers in control plants (0-0), plants treated with protists in the right root chamber (0-P), or treated with mycorrhiza in the right root chamber (0-M), or treated with protists and mycorrhiza together in the right root chamber (0-PM), or where the left and right root chambers were separately treated with protists and mycorrhiza (P-M). Means and standard deviation; horizontal lines denote significant contrasts with $^{(*)}p < 0.1$, $^{*}p < 0.05$, $^{***}p < 0.001$.

Figure S4 | Concentration of P (%) in shoots and in roots of both root chambers in control plants (0-0), plants treated with protists in the right root chamber (0-P), or treated with mycorrhiza in the right root chamber (0-M), or treated with protists and mycorrhiza together in the right root chamber (0-PM), or where the left and right root chambers were separately treated with protists and mycorrhiza (P-M). Means and standard deviation; horizontal lines denote significant contrasts with $^{(*)}p < 0.1$, $^{*}p < 0.05$.

Table S1 | Correlation of single PLFAs with the major axes of the DFA (**Figure 4**). Significant correlations ($p < 0.05$) are shown in bold.

Table S2 | *F*- and *P*-values of GLM contrasts showing treatment effects on N concentration (%) of shoots, N (%) of the treated root chambers inoculated with protists or/and mycorrhiza, N (%) of the whole root system, N (%) of the whole plants, and treatment effects on the total use of water of *Triticum aestivum.* Treatments: control plants (0-0), root halves treated with protists (0-P), with mycorrhiza (0-M), with protists and mycorrhiza together (0-PM), or where the left and right root compartments were separately treated with protists and mycorrhiza (P-M). Nominator and denominator degrees of freedom in brackets. Significant effects $p < 0.05$ in bold; $p < 0.1$ in italics.

Table S3 | *F*- and *P*-values of GLM contrasts showing treatment effects on P concentration (%) of shoots, P (%) of the treated root chambers inoculated with protists or/and mycorrhiza, P (%) of the whole root system, P (%) of the whole *Triticum aestivum* plants. Treatments: control plants (0-0), root halves treated with protists (0-P), with mycorrhiza (0-M), with protists and mycorrhiza together (0-PM), or where the left and right root compartments were separately treated with protists and mycorrhiza (P-M). Nominator and denominator degrees of freedom in brackets. Significant effects $p < 0.05$ in bold; $p < 0.1$ in italics.

REFERENCES

Agazzi, A., and Pirola, C. (2000). Fundamentals, methods and future trends of environmental microwave sample preparation. *Microchem. J.* 67, 337–341. doi: 10.1016/S0026-265X(00)00085-0

Anderson, J. P. E., and Domsch, K. H. (1978). A physiological method for the quantitative measurement of microbial biomass in soils. *Soil Biol. Biochem.* 10, 215–221. doi: 10.1016/0038-0717(78)90099-8

Anderson, J. P. E., and Domsch, K. H. (1980). Quantities of plant nutrients in the microbial biomass of selected soils. *Soil Sci.* 130, 211–216. doi: 10.1097/00010694-198010000-00008

Bais, H., Weir, T., Perry, L., Gilroy, S., and Vivanco, J. (2006). The role of root exudates in rhizosphere interactions with plants and other organisms. *Annu. Rev. Plant Biol.* 57, 233–266. doi: 10.1146/annurev.arplant.57.032905.105159

Beck, T., Joergensen, R. G., Kandeler, E., Makeschin, F., Nuss, E., Oberholzer, H. R., et al. (1997). An inter-laboratory comparison of ten different ways of measuring soil microbial biomass C. *Soil Biol. Biochem.* 29, 1023–1032. doi: 10.1016/S0038-0717(97)00030-8

Benizri, E., Dedourge, O., Dibattista-Leboeuf, C., Piutti, S., Nguyen, C., and Guckert, A. (2002). Effect of maize rhizodeposits on soil microbial community structure. *Appl. Soil Ecol.* 21, 261–265. doi: 10.1016/S0929-1393(02)00094-X

Benizri, E., Nguyen, C., Piutti, S., Slezack-Deschaumes, S., and Philippot, L. (2007). Additions of maize root mucilage to soil changed the structure of the bacterial community. *Soil Biol. Biochem.* 39, 1230–1233. doi: 10.1016/j.soilbio.2006.12.026

Berg, G., and Smalla, K. (2009). Plant species and soil type cooperatively shape the structure and function of microbial communities in the rhizosphere. *FEMS Microbiol. Ecol.* 68, 1–13. doi: 10.1111/j.1574-6941.2009.00654.x

Bloom, A. J., Chapin, F. S. III. and Mooney, H. A. (1985). Resource limitation in plants-an economic analogy. *Annu. Rev. Ecol. Syst.* 16, 363–392. doi: 10.1146/annurev.es.16.110185.002051

Bonfante, P., and Genre, A. (2010). Mechanisms underlying beneficial plant-fungus interactions in mycorrhizal symbiosis. *Nat. Commun.* 1:48. doi: 10.1038/ncomms1046

Bonkowski, M. (2004). Protozoa and plant growth: the microbial loop in soil revisited. *N. Phytol.* 162, 617–631. doi: 10.1111/j.1469-8137.2004.01066.x

Bonkowski, M. (2018). "Microcosm approaches to investigate multitrophic interactions between bacteria, protists, symbiotic fungi and their host plants," in *Methods in Rhizosphere Biology Research,* eds D. Reinhard and A. K. Sharma (Singapore: Springer), 80–100.

Bonkowski, M., and Brandt, F. (2002). Do soil protozoa enhance plant growth by hormonal effects? *Soil Biol. Biochem.* 34, 1709–1715. doi: 10.1016/S0038-0717(02)00157-8

Bonkowski, M., and Clarholm, M. (2012). Stimulation of plant growth through interactions of bacteria and protozoa: testing the auxillary microbial loop hypothesis. *Acta Protozool.* 51, 237–247. doi: 10.4467/16890027AP.12.019.0765

Bukovská, P., Bonkowski, M., Konvalinková, T., Beskid, O., Hujslová, M., Püschel, D., et al. (2018). Utilization of organic nitrogen by arbuscular mycorrhizal fungi—is there a specific role for protists and ammonia oxidizers? *Mycorrhiza* 28, 269–283. doi: 10.1007/s00572-018-0825-0

Bukovská, P., Gryndler, M., Gryndlerová, H., Püschel, D., and Jansa, J. (2016). Organic nitrogen-driven stimulation of arbuscular mycorrhizal fungal hyphae correlates with abundance of ammonia oxidizers. *Front. Microbiol.* 7:711. doi: 10.3389/fmicb.2016.00711

Bulgarelli, D., Rott, M., Schlaeppi, K., Ver Loren van Themaat, E., Ahmadinejad, N., Assenza, F., et al. (2012). Revealing structure and assembly cues for *Arabidopsis* root-inhabiting bacterial microbiota. *Nature* 488, 91–95. doi: 10.1038/nature11336

Clarholm, M. (1985). Interactions of bacteria, protozoa and plants leading to mineralization of soil nitrogen. *Soil Biol. Biochem.* 17, 181–187. doi: 10.1016/0038-0717(85)90113-0

Clarke, M., Lohan, A., Liu, B., Lagkouvardos, I., Roy, S., Zafar, N., et al. (2013). Genome of *Acanthamoeba castellanii* highlights extensive lateral gene transfer and early evolution of tyrosine kinase signaling. *Genome Biol.* 14:R11. doi: 10.1186/gb-2013-14-2-r11

Darbyshire, J. F., Wheatley, R. E., Greaves, M. P., and Inkson, R. H. E. (1974). A rapid micromethod for estimating bacterial and protozoan populations in soil. *Reviev d'Ecologie et Biologie du Sol* 11, 465–475.

Edwards, J., Johnson, C., Santos-Medellin, C., Lurie, E., Podishetty, N. K., Bhatnagar, S., et al. (2015). Structure, variation, and assembly of the root-associated microbiomes of rice. *Proc. Natl. Acad. Sci. U.S.A.* 112, 911–920. doi: 10.1073/pnas.1414592112

Ericsson, T. (1995). Growth and shoot-root ratio of seedlings in relation to nutrient availability. *Plant Soil* 168, 205–214. doi: 10.1007/BF00029330

Fiore-Donno, A. M., Weinert, J., Wubet, T., and Bonkowski, M. (2016). Metacommunity analysis of amoeboid protists in grassland soils. *Sci. Rep.* 6:19068. doi: 10.1038/srep19068

Fitter, A. (1991). Costs and benefits of mycorrhizas: implications for functioning under natural conditions. *Cell. Molecul. Life Sci.* 47, 350–355. doi: 10.1007/BF01972076

Flues, S., Bass, D., and Bonkowski, M. (2017). Grazing of Cercomonads (Protists: *Rhizaria*: *Cercozoa*) structures bacterial phyllosphere communities and function. *Environ. Microbiol.* 19, 3297–3309. doi: 10.1111/1462-2920.13824

Friesen, M. L., Porter, S. S., Stark, S. C., von Wettberg, E. J., Sachs, J. L., and Martinez-Romero, E. (2011). Microbially mediated plant functional traits. *Annu. Rev. Ecol. Evol. Syst.* 42, 23–46. doi: 10.1146/annurev-ecolsys-102710-145039

Frostegård, Å., and Bååth, E. (1996). The use of phospholipid fatty acid analysis to estimate bacterial and fungal biomass in soil. *Biol. Fertil. Soils* 22, 59–65. doi: 10.1007/BF00384433

Frostegård, Å., Tunlid, A., and Bååth, E. (1991). Microbial biomass measured as total lipid phosphate in soils of different organic content. *J. Microbiol. Methods* 14, 151–163. doi: 10.1016/0167-7012(91)90018-L

Gange, A., and Ayres, R. (1999). On the relation between arbuscular mycorrhizal colonization and plant 'benefit'. *Oikos* 87, 615–621. doi: 10.2307/3546829

Giovannetti, M., Volpe, V., Salvioli, A., and Bonfante, P. (2017). "Fungal and plant tools for the uptake of nutrients in arbuscular mycorrhizas: a molecular view," in *Mycorrhizal Mediation of Soil*, eds N. C. Johnson, C. Gehring, and J. Jansa (Amsterdam: Elsevier), 107–128.

Graham, J. H., Leonard, R. T., and Menge, J. A. (1981). Membrane-mediated decrease in root exudation responsible for phorphorus inhibition of vesicular-arbuscular mycorrhiza formation. *Plant Physiol.* 68, 548–552. doi: 10.1104/pp.68.3.548

Griffiths, B. S., Bonkowski, M., Roy, J., and Ritz, K. (2001). Functional stability, substrate utilisation and biological indicators of soils following environmental impacts. *Appl. Soil Ecol.* 16, 49–61. doi: 10.1016/S0929-1393(00)00081-0

Hartmann, A., Schmid, M., van Tuinen, D., and Berg, G. (2009). Plant-driven selection of microbes. *Plant Soil* 321, 235–257. doi: 10.1007/s11104-008-9814-y

Hensel, M., Bieleit, G., Meyer, R., and Jagnow, G. (1990). A reliable method for the selection of axenic seedlings. *Biol. Fertil. Soils* 9, 281–282. doi: 10.1007/BF00336240

Herdler, S., Kreuzer, K., Scheu, S., and Bonkowski, M. (2008). Interactions between arbuscular mycorrhizal fungi (*Glomus intraradices*, *Glomeromycota*) and amoebae (*Acanthamoeba castellanii*, Protozoa) in the rhizosphere of rice (*Oryza sativa*). *Soil Biol. Biochem.* 40, 660–668. doi: 10.1016/j.soilbio.2007.09.026

Herman, D. J., Firestone, M. K., Nuccio, E., and Hodge, A. (2012). Interactions between an arbuscular mycorrhizal fungus and a soil microbial community mediating litter decomposition. *FEMS Microbiol. Ecol.* 80, 236–247. doi: 10.1111/j.1574-6941.2011.01292.x

Hoad, S., Russell, G., Lucas, M., and Bingham, I. (2001). The management of wheat, barley, and oat root systems. *Adv. Agron.* 74, 193–246. doi: 10.1016/S0065-2113(01)74034-5

Hodge, A. (2004). The plastic plant: root responses to heterogeneous supplies of nutrients. *N. Phytol.* 162, 9–24. doi: 10.1111/j.1469-8137.2004.01015.x

Hodge, A., Campbell, C., and Fitter, A. (2001). An arbuscular mycorrhizal fungus accelerates decomposition and acquires nitrogen directly from organic material. *Nature* 413, 297–299. doi: 10.1038/35095041

Hodge, A., and Fitter, A. H. (2010). Substantial nitrogen acquisition by arbuscular mycorrhizal fungi from organic material has implications for N cycling. *Proc. Natl. Acad. Sci. U.S.A.* 107, 13754–13759. doi: 10.1073/pnas.1005874107

Hodge, A., and Storer, K. (2014). Arbuscular mycorrhiza and nitrogen: implications for individual plants through to ecosystems. *Plant Soil* 386, 1–19. doi: 10.1007/s11104-014-2162-1

Johnson, N. C. (2010). Resource stoichiometry elucidates the structure and function of arbuscular mycorrhizas across scales. *N. Phytol.* 185, 631–647. doi: 10.1111/j.1469-8137.2009.03110.x

Johnson, N. C., Rowland, D. L., Corkidi, L., Egerton-Warburton, L. M., and Allen, E. B. (2003). Nitrogen enrichment alters mycorrhizal allocation at five mesic to semiarid grasslands. *Ecology* 84, 1895–1908. doi: 10.1890/0012-9658(2003)084[1895:NEAMAA]2.0.CO;2

Jones, D., Hodge, A., and Kuzyakov, Y. (2004). Plant and mycorrhizal regulation of rhizodeposition. *N. Phytol.* 163, 459–480. doi: 10.1111/j.1469-8137.2004.01130.x

Jousset, A. (2012). Ecological and evolutive implications of bacterial defences against predators. *Environ. Microbiol.* 14, 1830–1843. doi: 10.1111/j.1462-2920.2011.02627.x

Jousset, A., Rochat, L., Péchy-Tarr, M., Keel, C., Scheu, S., and Bonkowski, M. (2009). Predators promote defence of rhizosphere bacterial populations by selective feeding on non-toxic cheaters. *ISME J.* 3, 666–674. doi: 10.1038/ismej.2009.26

Jousset, A., Scheu, S., and Bonkowski, M. (2008). Secondary metabolite production facilitates establishment of rhizobacteria by reducing both protozoan predation and the competitive effects of indigenous bacteria. *Funct. Ecol.* 22, 714–719. doi: 10.1111/j.1365-2435.2008.01411.x

Kafle, A., Garcia, K., Wang, X., Pfeffer, P. E., Strahan, G. D., and Bücking, H. (2018). Nutrient demand and fungal access to resources control the carbon allocation to the symbiotic partners in tripartite interactions of *Medicago truncatula*. *Plant Cell Environ.* doi: 10.1111/pce.13359. [Epub ahead of print].

Klironomos, J. N. (2003). Variation in plant response to native and exotic arbuscular mycorrhizal fungi. *Ecology* 84, 2292–2301. doi: 10.1890/02-0413

Koller, R., Rodriguez, A., Robin, C., Scheu, S., and Bonkowski, M. (2013a). Protozoa enhance foraging efficiency of arbuscular mycorrhizal fungi for mineral nitrogen from organic matter in soil to the benefit of host plants. *N. Phytol.* 199, 203–211. doi: 10.1111/nph.12249

Koller, R., Scheu, S., Bonkowski, M., and Robin, C. (2013b). Protozoa stimulate N uptake and growth of arbuscular mycorrhizal plants. *Soil Biol. Biochem.* 65, 204–210. doi: 10.1016/j.soilbio.2013.05.020

Kramer, S., Marhan, S., Haslwimmer, H., Ruess, L., and Kandeler, E. (2013). Temporal variation in surface and subsoil abundance and function of the soil microbial community in an arable soil. *Soil Biol. Biochem.* 61, 76–85. doi: 10.1016/j.soilbio.2013.02.006

Kreuzer, K., Adamczyk, J., Iijima, M., Wagner, M., Scheu, S., and Bonkowski, M. (2006). Grazing of a common species of soil *protozoa* (*Acanthamoeba castellanii*) affects rhizosphere bacterial community composition and root architecture of rice (*Oryza sativa L.*). *Soil Biol. Biochem.* 38, 1665–1672. doi: 10.1016/j.soilbio.2005.11.027

Krome, K., Rosenberg, K., Bonkowski, M., and Scheu, S. (2009). Grazing of protozoa on rhizosphere bacteria alters growth and reproduction of *Arabidopsis thaliana*. *Soil Biol. Biochem.* 41, 1866–1873. doi: 10.1016/j.soilbio.2009.06.008

Krome, K., Rosenberg, K., Dickler, C., Kreuzer, K., Ludwig-Müller, J., Ullrich-Eberius, C., et al. (2010). Soil bacteria and protozoa affect root branching via effects on the auxin and cytokinin balance in plants. *Plant Soil* 328, 191–201. doi: 10.1007/s11104-009-0101-3

Kuikman, P. J., Jansen, A. G., and van Veen, J. A. (1991). 15N-nitrogen mineralization from bacteria by protozoan grazing at different soil moisture regimes. *Soil Biol. Biochem.* 23, 193–200. doi: 10.1016/0038-0717(91)90134-6

Lau, J. A., and Lennon, J. T. (2012). Rapid responses of soil microorganisms improve plant fitness in novel environments. *Proc. Natl. Acad. Sci. U.S.A.* 109, 14058–14062. doi: 10.1073/pnas.1202319109

Leigh, J., Fitter, A. H., and Hodge, A. (2011). Growth and symbiotic effectiveness of an arbuscular mycorrhizal fungus in organic matter in competition with soil bacteria. *FEMS Microbiol. Ecol.* 76, 428–438. doi: 10.1111/j.1574-6941.2011.01066.x

Lerat, S., Lapointe, L., Gutjahr, S., and Y. P., Vierheilig, H. (2003). Carbon partitioning in a split-root system of arbuscular mycorrhizal plants is fungal and plant species dependent. *N. Phytol.* 157, 589–595. doi: 10.1046/j.1469-8137.2003.00691.x

López-Bucio, J., Cruz-Ramírez, A., and Herrera-Estrella, L. (2003). The role of nutrient availability in regulating root architecture. *Curr. Opin. Plant Biol.* 6, 280–287. doi: 10.1016/S1369-5266(03)00035-9

Marschner, P., and Baumann, K. (2003). Changes in bacterial community structure induced by mycorrhizal colonisation in split-root maize. *Plant Soil* 251, 279–289. doi: 10.1023/A:1023034825871

Marschner, P., and Timonen, S. (2005). Interactions between plant species and mycorrhizal colonization on the bacterial community composition in the rhizosphere. *Appl. Soil Ecol.* 28, 23–36. doi: 10.1016/j.apsoil.2004.06.007

Mollavali, M., Perner, H., Rohn, S., Riehle, P., Hanschen, F. S., and Schwarz, D. (2018). Nitrogen form and mycorrhizal inoculation amount and timing affect flavonol biosynthesis in onion (*Allium cepa L.*). *Mycorrhiza* 28, 59–70. doi: 10.1007/s00572-017-0799-3

Mooney, H. A. (1972). The carbon balance of plants. *Annu. Rev. Ecol. Syst.* 3, 315–346. doi: 10.1146/annurev.es.03.110172.001531

Nagy, R., Drissner, D., Amrhein, N., Jakobsen, I., and Bucher, M. (2009). Mycorrhizal phosphate uptake pathway in tomato is phosphorus-repressible and transcriptionally regulated. *N. Phytol.* 181, 950–959. doi: 10.1111/j.1469-8137.2008.02721.x

Ngosong, C., Gabriel, E., and Ruess, L. (2012). Use of the signature fatty acid 16:1ω5 as a tool to determine the distribution of arbuscular mycorrhizal fungi in soil. *J. Lipids* 2012:236807. doi: 10.1155/2012/236807

Nuccio, E. E., Hodge, A., Pett-Ridge, J., Herman, D. J., Weber, P. K., and Firestone, M. K. (2013). An arbuscular mycorrhizal fungus significantly modifies the soil bacterial community and nitrogen cycling during litter decomposition. *Environ. Microbiol.* 15, 1870–1881. doi: 10.1111/1462-2920.12081

Olsson, P. A., Rahm, J., and Aliasgharzad, N. (2010). Carbon dynamics in mycorrhizal symbioses is linked to carbon costs and phosphorus benefits. *FEMS Microbiol. Ecol.* 72, 123–131. doi: 10.1111/j.1574-6941.2009.00833.x

Page, F. C. (1976). *An Illustrated Key to Freshwater and Soil Amoebae.* Vol. 34. Ambleside: Freshwater Biological Association, 11.

Revillini, D., Gehring, C. A., Johnson, N. C., and Bailey, J. (2016). The role of locally adapted mycorrhizas and rhizobacteria in plant-soil feedback systems. *Funct. Ecol.* 30, 1086–1098. doi: 10.1111/1365-2435.12668

Rillig, M. C., Mummey, D. L., Ramsey, P. W., Klironomos, J. N., and Gannon, J. E. (2006). Phylogeny of arbuscular mycorrhizal fungi predicts community composition of symbiosis-associated bacteria. *FEMS Microbiol. Ecol.* 57, 389–395. doi: 10.1111/j.1574-6941.2006.00129.x

Rodríguez-Caballero, G., Caravaca, F., Fernández-González, A. J., Alguacil, M. M., Fernández-López, M., and Roldán, A. (2017). Arbuscular mycorrhizal fungi inoculation mediated changes in rhizosphere bacterial community structure while promoting revegetation in a semiarid ecosystem. *Sci. Total Environ.* 584–585, 838–848. doi: 10.1016/j.scitotenv.2017.01.128

Rosenberg, K., Bertaux, J., Krome, K., Hartmann, A., Scheu, S., and Bonkowski, M. (2009). Soil amoebae rapidly change bacterial community composition in the rhizosphere of *Arabidopsis thaliana*. *ISME J.* 3, 675–684. doi: 10.1038/ismej.2009.11

Ruess, L., and Chamberlain, P. M. (2010). The fat that matters: soil food web analysis using fatty acids and their carbon stable isotope signature. *Soil Biol. Biochem.* 42, 1898–1910. doi: 10.1016/j.soilbio.2010.07.020

Ryan, M. H., Tibbett, M., Edmonds-Tibbett, T., Suriyagoda, L. D., Lambers, H., Cawthray, G. R., et al. (2012). Carbon trading for phosphorus gain: the balance between rhizosphere carboxylates and arbuscular mycorrhizal symbiosis in plant phosphorus acquisition. *Plant Cell Environ.* 35, 2170–2180. doi: 10.1111/j.1365-3040.2012.02547.x

Sanders, F. E., and Tinker, P. B. (1971). Mechanism of absorption of phosphate from soil by Endogone mycorrhizas. *Nature* 233, 278–279. doi: 10.1038/233278c0

Scheu, S. (1992). Automated measurement of the respiratory response of soil microcompartments: active microbial biomass in earthworm faeces. *Soil Biol. Biochem.* 24, 1113–1118. doi: 10.1016/0038-0717(92)90061-2

Scheublin, T. R., Sanders, I. R., Keel, C., and van der Meer, J. R. (2010). Characterisation of microbial communities colonising the hyphal surfaces of arbuscular mycorrhizal fungi. *ISME J.* 4, 752–763. doi: 10.1038/ismej.2010.5

Schreiter, S., Sandmann, M., Smalla, K., and Grosch, R. (2014). Soil type dependent rhizosphere competence and biocontrol of two bacterial inoculant strains and their effects on the rhizosphere microbial community of field-grown lettuce. *PLoS ONE* 9:e103726. doi: 10.1371%2Fjournal.pone.0103726

Siddique, K., Belford, R., and Tennant, D. (1990). Root: shoot ratios of old and modern, tall and semi-dwarf wheats in a Mediterranean environment. *Plant Soil* 121, 89–98. doi: 10.1007/BF00013101

Slafer, G., and Araus, J. (2007). "Physiological traits for improving wheat yield under a wide range of conditions," in *Scale and Complexity in Plant Systems Research: Gene-Plant-Crop Relations,* eds J. H. J. Spiertz, P. C. Struik, H. H. van Laar (Heidelberg: Springer), 145–154.

Smith, F. A., and Smith, S. E. (2011). What is the significance of the arbuscular mycorrhizal colonisation of many economically important crop plants? *Plant Soil* 348, 63–79. doi: 10.1007/s11104-011-0865-0

Smith, S. E., and Read, D. (2008). *The Symbionts Forming Arbuscular Mycorrhizas. Mycorrhizal Symbiosis 3rd Edn.* London: Academic Press, 13–41.

Smith, S. E., and Smith, F. A. (2011). Roles of arbuscular mycorrhizas in plant nutrition and growth: new paradigms from cellular to ecosystem scales. *Annu. Rev. Plant Biol.* 62, 227–250. doi: 10.1146/annurev-arplant-042110-103846

Stockinger, H., Walker, C., and Schüßler, A. (2009). 'Glomus intraradices DAOM197198', a model fungus in arbuscular mycorrhiza research, is not Glomus intraradices. *N. Phytol.* 183, 1176–1187. doi: 10.1111/j.1469-8137.2009.02874.x

Tian, H., De Smet, I., and Ding, Z. (2014). Shaping a root system: regulating lateral versus primary root growth. *Trends Plant Sci.* 19, 426–431. doi: 10.1016/j.tplants.2014.01.007

Trap, J., Bonkowski, M., Plassard, C., Villenave, C., and Blanchart, E. (2016). Ecological importance of soil bacterivores for ecosystem functions. *Plant Soil* 398, 1–24. doi: 10.1007/s11104-015-2671-6

van der Heijden, M. G., and Schlaeppi, K. (2015). Root surface as a frontier for plant microbiome research. *Proc. Natl. Acad. Sci. U.S.A.* 112, 2299–2300. doi: 10.1073/pnas.1500709112

Van Noordwijk, M., and De Willigen, P. (1987). Agricultural concepts of roots: from morphogenetic to functional equilibrium between root and shoot growth. *Neth. J. Agricul. Sci.* 35, 487–496.

Venables, W. N., and Ripley, B. D. (2002). *Modern Applied Statistics with S.* New York, NY: Springer. doi: 10.1007/978-0-387-21706-2

Veresoglou, S. D., Chen, B., and Rillig, M. C. (2012a). Arbuscular mycorrhiza and soil nitrogen cycling. *Soil Biol. Biochem.* 46, 53–62. doi: 10.1016/j.soilbio.2011.11.018

Veresoglou, S. D., Menexes, G., and Rillig, M. C. (2012b). Do arbuscular mycorrhizal fungi affect the allometric partition of host plant biomass to shoots and roots? A meta-analysis of studies from 1990 to 2010. *Mycorrhiza* 22, 227–235. doi: 10.1007/s00572-011-0398-7

Wasson, A. P., Richards, R. A., Chatrath, R., Misra, S. C., Prasad, S. V., Rebetzke, G. J., et al. (2012). Traits and selection strategies to improve root systems and water uptake in water-limited wheat crops. *J. Exp. Bot.* 63, 3485–3498. doi: 10.1093/jxb/ers111

Werner, G. D., Strassmann, J. E., Ivens, A. B., Engelmoer, D. J., Verbruggen, E., Queller, D. C., et al. (2014). Evolution of microbial markets. *Proc. Natl. Acad. Sci. U.S.A.* 111, 1237–1244. doi: 10.1073/pnas.1315980111

Wickham, H. (2016). *Ggplot2: Elegant Graphics for Data Analysis*. New York, NY: Springer-Verlag.

Zelles, L. (1999). Fatty acid patterns of phospholipids and lipopolysaccharides in the characterisation of microbial communities in soil: a review. *Biol. Fertil. Soils* 29, 111–129. doi: 10.1007/s003740050533

Conflict of Interest Statement: The authors declare that the research was conducted in the absence of any commercial or financial relationships that could be construed as a potential conflict of interest.

frontiers in Environmental Science

REVIEW
published: 09 January 2019
doi: 10.3389/fenvs.2018.00159

Dynamic Phosphate Uptake in Arbuscular Mycorrhizal Roots Under Field Conditions

*Yoshihiro Kobae**

Laboratory of Crop Nutrition, Department of Sustainable Agriculture, Rakuno Gakuen University, Ebetsu, Japan

Many crops are colonized with arbuscular mycorrhizal fungi (AMF), which can efficiently absorb nutrients such as phosphate from the soil. The utilization of mycorrhizal symbioses is one of the most promising options for developing resource-saving and sustainable agricultural systems. Most laboratory studies have illustrated the roles of AM symbiosis by inoculating plants with limited AMF isolates. In the field, however, the roots of crops are co-colonized with multiple AMF species, which are difficult to separate and identify and may have different abilities regarding phosphate uptake. In addition, it is difficult to understand which AMF are functional due to the dynamics of AMF colonization processes and the largely unknown genomic structure. This review summarizes key discoveries supporting the importance of the dynamics of AM colonization and genomic structure, which potentially influence the characteristics of AM phosphate uptake. Moreover, this review aims to identify the research direction necessary to obtain a better understanding of the phosphate uptake systems of crops in the field.

Keywords: arbuscular mycorrhizal fungi (AMF), colonization dynamics, indigenous AMF, infection unit, phosphate uptake

OPEN ACCESS

Edited by:
Caroline Gutjahr,
Technische Universität München,
Germany

Reviewed by:
Natacha Bodenhausen,
Research Institute of Organic Agriculture, Switzerland
Marcel Bucher,
Universität zu Köln, Germany

***Correspondence:**
Yoshihiro Kobae
kobae@rakuno.ac.jp

Specialty section:
This article was submitted to Soil Processes, a section of the journal Frontiers in Environmental Science

Received: *08 May 2018*
Accepted: *18 December 2018*
Published: *09 January 2019*

Citation:
Kobae Y (2019) Dynamic Phosphate Uptake in Arbuscular Mycorrhizal Roots Under Field Conditions. Front. Environ. Sci. 6:159. doi: 10.3389/fenvs.2018.00159

INTRODUCTION

To grow large amounts of crop biomass agricultural fields need to be fertilized because otherwise soils inevitably will become depleted of nutrients. However, excessive use of chemical fertilizer induces environmental pollution and promotes the depletion of natural resources (Fan et al., 2011). The nutrient uptake system of crops includes not only their unique transport system on the root epidermis but also a transport system mediated by specific soil microorganisms. However, the nutrient cycling arising in plant-microbial interaction is highly dynamic and complex associated with soil types, environmental changes, crop species, and cultivation management (Jacoby et al., 2017). Accordingly, a better understanding of the nutrient uptake system of crops in the field could help establish a resource saving and sustainable agricultural system.

Regarding the mobility of the inorganic nutrients that are essential for plants, that of phosphate in the soil is generally low and its absorption leads to the formation of depletion zones around the roots and rapidly limits its further uptake (Schachtman et al., 1998). Therefore, plants often suffer from phosphorus deficiency (Vance, 2001). To overcome this problem, plants have developed a wide array of phosphate uptake strategies, including biotic interactions with diverse soil microorganisms (Sharma et al., 2013). Among these interactions, symbiosis with arbuscular mycorrhizal fungi (AMF) in the roots is an ancient and ubiquitous relationship that began over 400 million years ago (Remy et al., 1994; Fonseca and Berbara, 2008). This symbiosis is observed

in many economically important crops such as soybean, wheat, and corn. AMF hyphae growing outside roots allow plants to access phosphate further away from the root surface (Smith et al., 2011).

There are numerous AMF propagules in soil (e.g., spores, hyphae, and root remnants), and crop roots are commonly mycorrhizal (Sanders et al., 1996). As there are few soils with a complete absence of AMF in nature, the importance of mycorrhizal functioning (e.g., phosphate uptake) in crops is hardly noticeable (i.e., there is no mock control). Even if the plants are inoculated with AMF in the field, indigenous AMF in the soil are highly adapted to the local biotic and abiotic conditions and resistant to competition from novel AMF species (Hart et al., 2017). In fact, few studies have demonstrated the effectiveness of AMF inoculation under field conditions (Rodriguez and Sanders, 2015). Accordingly, to evaluate the ability of phosphate uptake by mycorrhizas, laboratory-scale pot-culture experiments involving the inoculation of a plant with one or more AMF isolates under AMF-free soil conditions have been conducted (Tawaraya, 2003; Deguchi et al., 2012). These studies clearly established that AMF mediate the phosphate uptake of plants and, in many cases, improve the nutrition and the productivity (Bucher, 2007).

Pot experiments with different AMF inoculations have shown that the level of plant phosphorus are different; thus the ability of mycorrhizal phosphate uptake may differ among AMF species (Smith and Smith, 2011; Walder and van der Heijden, 2015). At the same time, it has been established that mycorrhization is strongly suppressed under a high concentration of phosphate in soil (Baylis, 1967; Mosse, 1973), but the degree of this may differ among AMF and plant species (Johnson, 1993; Van Geel et al., 2016). Observations of mycorrhization processes at the cellular level revealed that AMF intracellular colonization was essentially transient, basically not synchronized among colonized cells, but roots stably interact with AMF (Gutjahr and Parniske, 2017), suggesting the dynamic nature of mycorrhization processes (i.e., physiologically/functionally active and inactive colonization can co-exist in the roots). It has been recently reported that the hyphal structure of AMF and fine root endophytes (*Glomus tenue*) in the roots rapidly changes over the course of a growing season associated with plant phenology and seasonal changes in the environment (Bueno de Mesquita et al., 2018). Accordingly, it is expected that the ability and stability of mycorrhizal phosphate uptake of crops under field conditions will change depending on several biotic and abiotic factors, although many of which are not experimentally validated. To utilize AM symbiosis to improve crop phosphorus nutrition, it is important to increase our basic knowledge of the colonization dynamics and the growth conditions under which the mycorrhizas express phosphate uptake activity associated with their symbiotic behavior.

This article reviews recent findings about phosphate uptake during mycorrhizal symbiosis from the perspective of AMF's highly dynamic colonization processes at the cellular level and the coexistence of genetically different AMF. Accordingly, this review attempts to bridge the gap between laboratory-level and field-level knowledge of the phosphate uptake mechanisms of mycorrhizal roots.

CHALLENGES: DYNAMICS IN MYCORRHIZAL PHOSPHATE UPTAKE

Mycorrhizal Phosphate Uptake Pathway

A specific morphological feature of AM symbiosis is the penetration of AMF into root cortical cells and the development of a highly branched hyphal structure called an arbuscule (Bonfante-Fasolo, 1984). Although AMF colonize inside root cells, they are not completely taken up as plant organelles because they are surrounded by periarbuscular membranes connected to the plasma membrane of plant cells (Harrison and Ivanov, 2017), indicating that AMF are localized outside the cells. As arbuscules are formed, the expression of host phosphate transporter genes is induced, which promotes phosphate uptake from the arbuscules (Pumplin et al., 2012). The expressed protein is specifically localized on the periarbuscular membrane (Harrison et al., 2002; **Figure 1**). In mutant plants carrying a deficient allele of these symbiotic phosphate transporter genes, an abnormally early degradation of the arbuscules along with reduction in the total phosphate uptake is observed (Javot et al., 2007; Yang et al., 2012; Willmann et al., 2013). This suggests a pivotal role of the phosphate transport system in the establishment of mycorrhizal roots. Besides the upregulation of the expression of symbiotic phosphate transporter genes and establishment of the "mycorrhizal pathway" of the phosphate uptake system in mycorrhizal plants, the expression of some phosphate transporter genes that are probably involved in the epidermal "direct pathway" of phosphate uptake is downregulated (Grunwald et al., 2009; Tamura et al., 2012; Yang et al., 2012). Accordingly, phosphate uptake can be dominated by the mycorrhizal pathway (Smith and Smith, 2011). Thus, the contribution of the direct pathway and the mycorrhizal pathway is not simply additive. More efforts are needed to investigate the mechanism that balances the contribution of these two pathways (Sawers et al., 2010; Smith and Smith, 2011; Chu et al., 2013; Facelli et al., 2014).

Benefits of AM symbiosis may not be provided without carbon cost (Sawers et al., 2017). The host plants must supply carbohydrates and lipids to AMF to support their growth (Rich et al., 2017; Roth and Paszkowski, 2017; Keymer and Gutjahr, 2018; Lanfranco et al., 2018), thereby maintaining a balance with the cost for the other metabolism. Recent studies have shown that the balance is influenced by plant genetic factors. A panel of 30 maize varieties was inoculated with *Rhizophagus irregularis*, a commonly used model AMF (Sawers et al., 2017). The levels of mycorrhizal phosphate uptake, plant and AMF biomass, and the accumulation of maize phosphate transporter gene transcripts varied among the maize varieties. An increase in biomass caused by mycorrhizal symbiosis is positively correlated with the level of mycorrhizal phosphate uptake and the amount of extraradical hyphae at least in the maize and *R. irregularis* interaction (Sawers et al., 2017). Additionally, the ionome of the same 30 maize varieties used in Sawers et al. (2017) revealed variety-specific responses to the colonization of *Funneliformis mosseae* in the concentration of some metal elements (Ramírez-Flores et al., 2017). These data clearly indicate that host genetic factors influence fungal growth strategy and have a great impact on

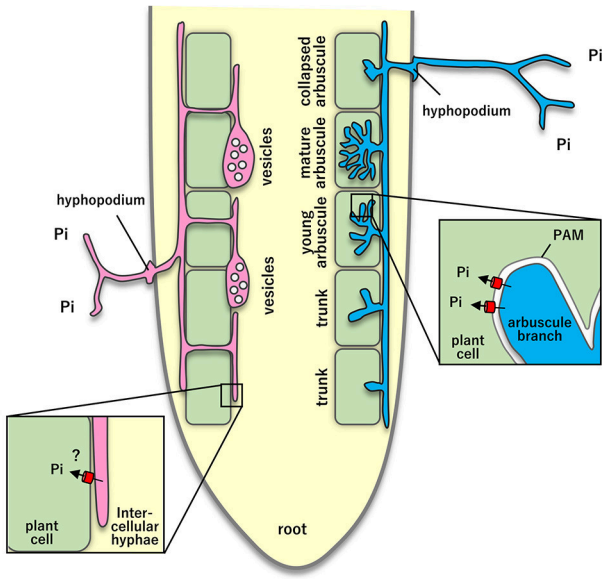

FIGURE 1 | Lifecycle of intraradical colonization and the expression of phosphate transporter in arbuscular mycorrhizal symbiosis. A colonized region derived from one AMF hypha is called "infection unit." Hyphae penetrate root epidermis and extends into the intercellular space (*Arum*-type) or intracellularly (*Paris*-type; not shown) in cortical cells. In these processes, arbuscules that are involved in nutrient exchange are formed in cortical cells in order from the initial penetration site (hyphopodium). Therefore, the arbuscules that are closest to the penetration site are the oldest, and the arbuscule close to the tip of the growing hyphae is the newest. Since the arbuscules have short lifespan (1–2 days), they collapse in order from the oldest one. Arbuscules are surrounded by plant membrane (periarbuscular membrane). Plant phosphate transporter proteins are localized on this membrane and are responsible for the uptake of phosphate from the arbuscules. In the senescent colonization stages of infection unit, vesicles and intercellular hyphae are often observed. The role of these intraradical AMF structures is still unclear.

plant mycorrhiza-mediated mineral nutrition (Sawers et al., 2017).

A shift from the wild to cultivated species (domestication) may have decreased the ability of plants to positively respond to AMF (Lehmann et al., 2012; Sawers et al., 2018). Intensive breeding for high-input farming systems (i.e., intensive chemical fertilization) may have reduced the capacity of crops to gain maximum benefits from AM symbiosis. A recent study has investigated the response of 27 crop varieties compared with that of their wild progenitors to AM symbiosis (Martín-Robles et al., 2018). Among these varieties, the comparison of a subset of 14 pairs of wild and domesticated species revealed that the growth response of domesticated species to AM symbiosis was significantly reduced at high inorganic phosphate levels in the domesticated counterparts compared with that in their wild progenitors (Martín-Robles et al., 2018). This indicates the possibility that AM-independent nutrition and growth system of domesticated plants are related to high phosphate fertilization (Lanfranco et al., 2018).

High phosphate conditions significantly decrease the level of AMF colonization (Nagy et al., 2009; Balzergue et al., 2010; Breuillin et al., 2010). A recent study has shown that the supply of exogenous phosphate leads to a rapid (<5 h) suppression in arbuscule development and temporarily inhibits the growth of intraradical colonization (Kobae et al., 2016). Although transcriptomic analyses have failed to find any clear defense response of petunia plants during phosphate inhibition (Breuillin et al., 2010), recent QTL analyses using 94 bread wheat genotypes for root length colonization by a mixed inoculum of three AMF species have revealed at least two genetic loci related to defense and cell wall metabolism (Lehnert et al., 2017). It is hypothesized that defense mechanisms participate in limiting AMF colonization in plants cultivated in phosphorus-sufficient condition (Lehnert et al., 2017). One can speculate that a resistance mechanism to fungi has been selected in domesticated plants under high-input agriculture that led to a decrease of the activity or the contribution of mycorrhizal phosphate uptake pathway. However, based on the detected QTL, it is still unclear whether these genetic loci are functionally associated with mycorrhizal phosphate uptake (Lehnert et al., 2017). In the future, QTL mapping and further functional analyses such as RNAseq are needed to obtain more detailed information about the AM colonization of domesticated plants.

These recent studies have shown that crop varieties are one of the important biotic factors affecting the outcome of the inoculation of certain AMF strains. This suggests a difficulty of the utilization of AMF in agriculture, where crop varieties to be grown is determined depending on the local environment and economy and the AMF type in the soil is unclear. This does not mean that AMF function can be neglected. Most of the domesticated AMF-host crop species are inevitably colonized by native AMF community, where the effects of each colonization can be positive, neutral and negative (Johnson et al., 1997; Jones and Smith, 2004). The direct and mycorrhizal phosphate-uptake pathway may be inadequately balanced in wheat and barley, leading to negative mycorrhizal responses (Smith and Smith, 2011). This is explained as due to a reduced direct phosphate uptake by colonization of AMF; however, mycorrhizal phosphate uptake inadequately compensates for direct phosphate uptake, although further analysis is needed. As mentioned previously, mutation of mycorrhizal phosphate transporter in the plant causes an inhibitory effect on AMF colonization (Javot et al., 2007; Yang et al., 2012; Willmann et al., 2013). A possible explanation for these observations is that the plant can assess the costs and the benefits (e.g., the favorable balance of phosphate-carbon exchange) in the interaction, and inhibits AM colonization if the balance is unfavorable (Nouri et al., 2014). Further analysis is needed whether such a balancing mechanism is conserved in domesticated plants.

High-input agriculture may have influenced not only plant traits but also AMF traits. For example, frequent soil disturbance (e.g., tillage) may act as a selection pressure for rapidly colonizing fungi, causing them to efficiently regenerate hyphal networks after disturbance and produce abundant spores (Niwa et al., 2018). These AMF traits possibly influence field crop nutrition. In future, it will be important to determine whether an adequate

balance exists between the direct and mycorrhizal phosphate-uptake pathway in field crops. For this, mycorrhizal phosphate uptake-defective mutant and wild-type plant pairs will be used to investigate the molecular mechanisms underlying the balance of direct/mycorrhizal phosphate uptake using radiolabeled phosphate (e.g., ^{32}P; Jakobsen et al., 2001; Smith et al., 2004; Yang et al., 2012; Willmann et al., 2013) as a tracer using the soil of conventional agriculture (Rillig et al., 2008; Watts-Williams SJ Cavagnaro, 2015). The balance of mycorrhizal/direct phosphate uptake associated with indigenous AMF species also remains to be investigated.

A Mosaic of AMF Is Responsible for Phosphate Uptake

Inoculation of AMF can have a significant effect on plant phosphate uptake; however, there are many cases in which the phosphate uptake in inoculated plants does not increase compared with that of uninoculated plants (Tawaraya, 2003; Smith and Read, 2008). One reason for this is the potentially different level of mycorrhizal phosphate uptake among the types of AMF (Munkvold et al., 2004). Supporting this, the inoculation of *Medicago sativa* with more than 30 AMF types revealed that the performance of phosphate uptake differs markedly among AMF types (Mensah et al., 2015). In the field, roots are generally co-colonized with multiple AMF types (Kivlin et al., 2011). Strict host specificity, as found in plant–pathogenic fungi interaction, has not been recognized for the colonization of AMF except in mycoheterotrophic species (Redecker et al., 2003; Smith and Read, 2008). Accordingly, multiple AMF can co-colonize, overlap of individual AMF colonization in the roots and multiple AMF species have been detected in only a 1-cm-long root fragment (van Tuinen et al., 1998). Therefore, the ability of mycorrhizal roots to perform phosphate uptake in the field is assumed to be a mosaic of the different abilities of diverse AMF (Jansa et al., 2008); alternatively, only a portion of the AMF colonizing roots may temporarily contribute to phosphate uptake in response to specific environmental conditions (Compant et al., 2010).

As mycorrhizal phosphate uptake under the field condition may be achieved by the contribution of diverse AMF species colonizing the roots, it is crucially important to delimit species of AMF to obtain biological information about the mycorrhizas. To determine the biological type, the species of AMF should be generalized and described with "common language" (Öpik and Davison, 2016) to delimit and identify the AMF species among different studies. Unless AMF species in different fields are successfully delimited and classified with universal criteria, determining their phenotypes (e.g., phosphate uptake ability) in roots in a specific field will not be meaningful (Rosendahl, 2008).

Unfortunately, the morphology of intraradical mycelia is hardly distinguishable among the different AMF types, and different AMF physically overlap in the roots (Smith and Read, 2008); accordingly, the morphological identification of AMF species in mycorrhizal roots in the field is impossible. However, the advent of high-throughput sequencing methodologies has made it possible to characterize the co-colonization of genetically diverse AMF in roots in the field (Öpik et al., 2009). A total of 288 AMF species have been described (mostly delimited by their spore morphology), ∼60% of which have undergone sequencing of their nuclear ribosomal markers: small subunit (SSU) rRNA gene, ITS region, and large subunit (LSU) rRNA gene (Öpik and Davison, 2016). However, information about AMF assemblages obtained from DNA-based approaches can vary depending on the sample type, marker properties, sequencing approach, and choices made during bioinformatic analyses (Öpik et al., 2013; Hart et al., 2015; Varela-Cervero et al., 2015). The taxonomic resolution with at least SSU sequences, used in a well-maintained reference database for AMF (Öpik and Davison, 2016), is thought to be similar (i.e., at least at the genera level but not at the species or finer clade) to that of morphological delimitation (Davison et al., 2015). Importantly, however, the longer-read-length PacBio sequencing of the *R. irregularis* genome suggested the presence of intra-isolate variation in the rRNA genes (Maeda et al., 2018). Whether this variation is commonly observed in AMF and its biological effects are unclear; however, the finding suggests the need to re-evaluate the resolution power of commonly used DNA-based delimitation of AMF species. More importantly, most AMF in roots are thought to be unculturable or have not yet been cultured (Ohsowski et al., 2014). Fine endophyte, previously known as *Glomus tenue*, has been difficult to culture for a long time (Walker et al., 2018) but was proven not to be Glomus but was instead reclassified as Mucoromycotina (Orchard et al., 2017). Owing to the lack of reference nucleotide sequences of most AMF colonizing field roots and the current technical limitation in the robust delimitation of AMF species, we may have overlooked endemic cryptic AMF species in roots in the field (Rosendahl, 2008). The difficulties associated with defining AMF species have been reviewed in several review articles (Hibbett et al., 2016; Öpik and Davison, 2016; Sanders and Rodriguez, 2016; Selosse et al., 2016) and have recently been discussed in a workshop at the International Conference on Mycorrhiza (Bruns et al., 2017).

The Nucleotide Sequence Does Not Necessarily Reflect the Functionality

Despite the difficulty in the taxonomic characterization of AMF, high-throughput sequencing techniques can provide a comprehensive information of AMF genes in the roots. As information about the existence of AMF in roots accrues, questions related to the functional properties of individual AMF are receiving increasing attention (Lekberg and Koide, 2014; Öpik and Davison, 2016). A recently established approach designed for single-cell genomics and transcriptomics enables more high-throughput simultaneous analysis of many AMF species to discover the potential of the expression of their specific functions. Spore-based RNA sequencings were successfully applied to obtain transcript datasets from several AMF taxa, including genetically obscure genera such as *Paraglomus*, *Ambispora,* and *Diversispora* (Beaudet et al., 2018), highlighting their reproduction process, translation, amino acid metabolism, or energy production (Beaudet et al., 2018). However, not only quantitative evaluation of the "existence" of AMF nucleotide sequences but also evaluation of the hidden "dynamics" of the

function in the mosaic of AMF might be necessary to accurately track the functionality of mycorrhizal roots (van der Heijden and Scheublin, 2007). This is because AMF colonization in roots has a short life cycle and some AMF may actively colonize while others may be inactive at a certain time point. Supporting this, not all intraradical mycelia derived from one hyphal colonization (infection unit) containing fine-branched arbuscules in roots grown in field soils are metabolically active (Kobae et al., 2017). Under specific environmental conditions, certain AMF may be deeply involved in host phosphate nutrition compared with others due to differing life cycles and biological characteristics. Thus, a list of AMF at a single time point can comprise the colonization of different contribution levels.

Detailed morphological studies of mycorrhization processes have suggested that arbuscule formation is basically transient (Gutjahr and Parniske, 2017), at least in the earliest developmental stages of mycorrhization (Kobae and Fujiwara, 2014). AMF hyphae penetrating root epidermal cells extend several millimeters in a longitudinal direction inside the root (Smith and Read, 2008). The extending intercellular hyphae successively form arbuscules inside cortical cells (Sanders and Sheikh, 1983). The lifespan of mature arbuscules that are accompanied by the expression of plant phosphate transporters is only a few days, which is followed by their immediate collapse (Kobae and Hata, 2010). Accordingly, the lifespan of active infection unit is probably within 1 week, at least in rice seedlings (Kobae and Fujiwara, 2014). It should be noted that some AMF species tend to produce vesicles in root areas with many senescent arbuscules (Kobae et al., 2016). Although the precise biological roles of vesicles remain unclear (Smith and Read, 2008), the protoplasm of vesicles contains nuclei, glycogen granules, small vacuoles, and lipid droplets (Bonfante-Fasolo, 1984). Given that the number of vesicles often increases in old or dead roots (Bonfante-Fasolo, 1984), vesicles are thought to be resting organs (Smith and Read, 2008). Moreover, roots are often colonized with intercellular hyphae without arbuscules (**Figure 1**). The role of intercellular hyphae and their lifespan are unknown (Smith and Read, 2008). As total phosphate uptake is largely reduced in plants with mutation of symbiotic phosphate transporter genes, intracellular colonization (arbuscule formation) most likely make a major contribution to mycorrhizal phosphate uptake, at least under laboratory conditions, with model plants and model AMF interaction. However, the life cycle and the functionalities of intraradical mycelia of native AMF have not been characterized.

To date, the cycle of intracellular colonization has rarely been taken into consideration when assessing the functionality of AMF via nucleotide information (genome and transcriptome) on the AMF that colonize roots, which includes both the active state and the inactive state of colonization. Because the colonization cycle is basically regulated in a cell-autonomous manner (Bucher et al., 2014), the functions of the mosaic of AMF in roots may not be synchronized. High-resolution analysis of the colonization process of individual AMF as well as their phosphate uptake ability will be necessary to obtain a better understanding of the mechanism of phosphate uptake by the mosaic of AMF. To this end, a new technique that enables tracking the dynamics of individual AMF colonization should be applied. This possibility will be mentioned in the last section.

Role of Bacteria in Phosphate Uptake by AMF

AMF can only utilize soluble inorganic phosphate. The majority of soil phosphate is present in an insoluble form because of immobilization and precipitation with other soil minerals and is, thus, poorly available for the plant. Phosphate solubilizing bacteria (PSB) are present in most soils and can potentially improve phosphate availability to the plant by solubilizing organic and inorganic phosphorus (Chen et al., 2006). Further, it has been shown *in vitro* that PSB solubilize phosphate via phosphatases, by lowering the soil pH and/or by chelating phosphate from soil minerals, such as iron and aluminum in acidic soils and calcium in alkaline soils, aided by organic acids (Rodriguez and Fraga, 1999; Browne et al., 2009). Recent studies have shown that the interaction of AMF with PSB in mycorrhizosphere also influences the mycorrhizal phosphate uptake. Ordoñez et al. (2016) investigated the influence of inoculation of *Pseudomonas* spp., which solubilizes tri-calcium phosphate *in vitro*, on AMF growth, root colonization, and plant phosphate uptake and revealed that AMF did not aid plant phosphate uptake in the presence of insoluble phosphate (rock phosphate) as the only phosphorus source, whereas PSB inoculation significantly aided the phosphate uptake. Interestingly, PSB inoculation strongly affected the growth of intra- and extra-radical hyphae of AMF (Ordoñez et al., 2016; Battini et al., 2017). Specifically, PSB enhanced metabolically active mycorrhizal colonization, measured as percentage root length colonized by AMF stained for phosphatase activity, even in unsterilized soil containing a native AMF and microbial communities (Ordoñez et al., 2016). Importantly, the *in vitro* ability of PSB in solubilizing insoluble phosphate was not a predictor of strains that result in improved phosphate acquisition by roots (Ordoñez et al., 2016). The strong effect exerted by PSB on the level of AMF colonization did not translate into obvious patterns of increased phosphate acquisition by plants, which was consistent with earlier findings (Smith et al., 2011). It is likely that AMF and PSB synergistically interact. However, such a biotic interaction under field conditions may be highly dynamic and complex (Ordoñez et al., 2016), and may include members of putative helper/antagonistic bacteria for AMF (Frey-Klett et al., 2007; Battini et al., 2017; Svenningsen et al., 2018).

One of the difficulties in the accurate detection of the occurrence of synergistic effects is deciphering the mechanistic basis of cooperative interaction. PSB involved in the solubilization of organic phosphates have been detected on the surface of AMF hyphae (Feng et al., 2002; Zhang et al., 2014). They thrive in close vicinity of AMF extraradical hyphae and intimately cooperate with AMF by providing inorganic minerals (e.g., phosphate) released from organic matter decomposition in exchange for carbon exuded by the hyphae (Zhang et al., 2016). Zhang et al. (2018) have reported the mechanism underlying the cooperative interaction of phosphate–carbon exchanges between *R. irregularis* and *Rahnella aquatilis* at the transcriptional level

and demonstrated that fructose, glucose, and trehalose were exuded by the AMF hyphae. The transcript levels of fructose transporter and phosphatase genes of *R. aquatilis* increased 1 h after the presence of AMF hyphae. Treatment with 20 μM fructose but not glucose (the approximate concentration detected in hyphal exudates) induced the expression of *R. aquatilis* phosphatase genes, indicating that the uptake of fructose by *R. aquatilis* triggered the expression of phosphatase-encoding genes. They also demonstrated that acid and alkaline phosphatase activities in the culture medium increased in the presence of AMF hyphae, which then enhanced the solubilization of phytate phosphate. Finally, the transcript levels of the AMF phosphate transporter gene was increased in the presence of *R. aquatilis*. Given that bacteria can selectively use substrates from a mixture of different carbon sources (Görke and Stülke, 2008), the type of carbon exudates from AMF hyphae can change bacterial communities in the mycorrhizosphere (Zhang et al., 2018). In future, it will be important to study whether specific AMF families are associated with similar PSB communities or whether a change in PSB community can occur even in single AMF through various developmental stages of the host plant. In addition, the phosphate uptake, translocation, and export processes of AMF are important (Ezawa and Saito, 2018). The first identification of AMF phosphate transporter gene was reported in 1995 (Harrison and van Buuren, 1995). To date, several phosphate transporter genes have been isolated from AMF isolates and demonstrated that many of them expressed in both extraradical hyphae and intraradical hyphae, suggesting that they are involved in phosphate uptake from the soil, phosphate reabsorption from the periarbuscular space (Benedetto et al., 2005; Balestrini et al., 2007; Fiorilli et al., 2013) and phosphorus signal transduction (Xie et al., 2016). Molecular basis of these processes may be elucidated in model AMF using new genetic manipulation techniques (e.g., host-induced gene silencing, virus-induced gene silencing, and spray-induced gene silencing; Helber et al., 2011; Kikuchi et al., 2016; Xie et al., 2016; Wang and Jin, 2017). It is interesting to study whether the phosphate transport system of a model AMF is conserved in colonization of native AMF. A better understanding of phosphate homeostasis and translocation process of native AMF will further improve understanding regarding the function of the AMF–PSB interaction.

Environmental Factors Influence Colonization Dynamics

Among the environmental factors that influence the colonization of AMF in roots, the most intensely investigated is the level of phosphorus in the soil. It is well known that the AMF colonization level is remarkably decreased by the intense application of phosphorus fertilizer (Baylis, 1967; Mosse, 1973); this phenomenon is called "phosphate inhibition" (Graham et al., 1981). Rice seedlings that express the symbiotic phosphate transporter GFP (green fluorescent protein) fusion protein were infected with *R. irregularis*, treated with phosphate, and the colonization dynamics was examined by live imaging (Kobae et al., 2016). Mature arbuscules with fine branches were found to be resistant to phosphate treatment and their lifespan did not change compared with that of the control. However, the development of young arbuscules with insufficient branching was found to be severely suppressed in a short period, and the development of infection units was also suppressed. Eventually, overall mycorrhization temporarily stopped after the phosphate treatment, but the formation of a new infection unit began at least 2 days after treatment. Therefore, the functionality of AMF in roots is dynamically regulated according to phosphate availability in the soil. Importantly, phosphate inhibition induces the formation of vesicles of *R. irregularis* in rice roots by 1 day after phosphate treatment (Kobae et al., 2016), suggesting the resting state of intraradical colonization during phosphate inhibition. Moreover, the arbuscule/vesicle ratio varies depending on the AMF species even within the same subgenus Glomus Ab (Kiers et al., 2011); the genera *Gigaspora* and *Scutellospora* do not form intraradical vesicles (Smith and Read, 2008), suggesting the interspecific and intraspecific differences of resource hoarding strategies such as the morphological changes in high phosphate condition. Thus, the physiological status of intraradical colonization for individual AMF types and root cells along with the state of environmental factors (e.g., phosphate availability) should be clarified and taken into consideration when we assess the phosphate uptake of the mycorrhizas based on the nucleotide data from high-throughput sequencing studies.

PERSPECTIVE: HOW DO WE KNOW ABOUT DYNAMIC MYCORRHIZAL PHOSPHATE UPTAKE?

Genetic Variability of AMF

Our current knowledge about mycorrhizal phosphate uptake has largely been obtained through laboratory studies conducted on culturable AMF isolates, and we have a limited understanding of how diverse AMF members cooperatively or competitively influence phosphate uptake in the field (Burleigh et al., 2002; Engelmoer et al., 2014; van der Heijden et al., 2017). At present, high-throughput sequencing studies can produce metagenomic data for all AMF species in field samples. The drop in sequencing costs and the advances in informatics offer new opportunities for the reconstruction of individual microbial genomes (Parks et al., 2017), which may enable us to understand the genomic structures (e.g., genetic variations that can exist among nuclei or rRNA genes) of individual AMF and to more robustly define the species of AMF.

It is still unclear whether the genome of an individual AMF is stable. In other words, the definition of the species concept of AMF is enigmatic (Bruns et al., 2017). Early studies suggested that the AMF genomic structure is highly heterogeneous; in other words, their coenocytic mycelia and spores contain a mixture of thousands of genetically different nuclei, so they might be heterokaryons (Sanders and Croll, 2010). This is supported by the observation that, in laboratory *in vitro* studies, anastomosis (hyphal fusion) can occur between genetically different AMF types, suggesting the potential for genetic variability of AMF (Chagnon, 2014; Novais et al., 2017). However, in the fungal

genetic system, the somatic incompatibility system usually triggers programmed cell death because nonself hyphal fusion is a risky endeavor that can rapidly disrupt cellular homeostasis (Strom and Bushley, 2016).

Recent advances in the genomic study of model AMF culture lines have suggested that these lines have a little genetic heterogeneity and the presence of sex genes (Tisserant et al., 2013; Lin et al., 2014; Ropars et al., 2016; Tang et al., 2016). This may lead to the acceptance of concepts of biological species (De Queiroz, 2005) in AMF as well as in many other organisms and to prediction of the phenotypic similarity within the same AMF species. Moreover, finding of the presence of intra-isolate heterologous rRNA genes may solve the problem of the complex genomic organization of AMF (Maeda et al., 2018). In addition, it is observed that isolates of the same AMF species undergo anastomosis and exchange nuclei (Croll et al., 2009; Sbrana et al., 2018). Based on the genome sequences of five *R. irregularis* isolates, it is also expected that they may undergo karyogamy, and eventually recombine through meiosis or parasexuality (Chen et al., 2018; Mathieu et al., 2018). More interestingly, *Burkholderia* endobacteria has a role in the reproductive biology of this host *Rhizopus microsporus* (Mucoromycotina) (Partida-Martinez et al., 2007; Torres-Cortés et al., 2015; Mondo et al., 2017). AMF also have the propensity to host diverse endobacteria (Bianciotto et al., 2003; Naito et al., 2017), suggesting the intriguing theoretical scenario that AMF endobactirea influence the genetic dynamics (Pawlowska et al., 2018). Accordingly, although many investigation is needed, in contrast to previous situation where there was little information underlying genetic heterogeneity, the genetics of model AMF may be easier to understand than previously thought, and the genetic control and utilization of the specific functional traits of AMF in the field may become possible. However, some researchers still suggest that natural AMF may have genetic heterogeneity (Sanders and Croll, 2010; Bruns et al., 2017). In fact, sister spores generated from the anastomosis between different AMF isolates were shown to have different influences on the growth of the host plants (Croll et al., 2009; Angelard et al., 2010). Study of the genetics of AMF is still in its infancy. It is thus still unclear whether the situation described in laboratory-cultured lines can be generalized in AMF including unknown natural species.

In the field, mycorrhizae of conspecific AMF are thought to be connected with common mycorrhizal networks (CMNs; Bücking et al., 2016). A CMN shares cellular constituents including nucleus, organelles, viruses, and endobacteria in the same cytoplasm of coenocytic mycelia (Jany and Pawlowska, 2010). If it is true that the genotype and phenotype of AMF mycelia can change rapidly in response to environmental changes (e.g., host plant; Angelard et al., 2014), it is reasonable to think that some portion of CMN terminal branches may change their genetic and functional traits by encountering different biotic (host species, microbiome) and abiotic (nutrient status, cultivation management, soil properties) stimuli during their colonization process. In this case, CMN may not be genetically homogeneous and may be heterogeneous over time, suggesting the potential impact of genetic variation from the perspective of long-term and field-level cultivation (Vályi et al., 2016). To obtain a better understanding of AMF genetic variability under field conditions, continuous observation of the genomic structure of AMF at a fixed point in soil will be important. Especially, it will be important to investigate whether and how crop species, crop rotation, field management, and fertilization affect the genomes and the functionality of individual AMF.

Colonization Dynamics

Arbuscules are thought to be the parts essential for phosphate uptake because symbiotic phosphate transporter proteins are specifically expressed and localized in arbuscule-containing cells and their mutation causes a reduction of mycorrhizal phosphate uptake ability (Gutjahr and Parniske, 2017). However, most of our understanding of the phosphate uptake at arbuscules is based on recent studies analyzing the associations between model plant species and culturable AMF. Because all unculturable AMF that colonize roots grown under field conditions have not been experimentally characterized, there is the unsatisfactory situation that the phosphate uptake of field mycorrhizas can only be interpreted with the current knowledge of AM symbiosis. Recent studies on the lifecycle of intracellular colonization and its dynamic environmental responses (e.g., phosphate inhibition, vesicle formation) suggest that the colonization dynamics may affect the phosphate uptake ability of mycorrhizal roots. However, it is unclear whether such colonization dynamics observed in model systems is a general phenomenon in AMF in the field. For example, some AMF extend intercellular hyphae during the development of an infection unit (*Arum* type) and others extend their intraradical hyphae by penetrating root cortical cells (*Paris* type; Smith and Read, 2008). The former type is probably able to rapidly withdraw from plant cells after the collapse of arbuscule branches Kobae and Hata, 2010, but it is unknown whether the latter's intracellular hyphal coil (Dickson et al., 2007) can withdraw from plant cells. Are there differences in the strategy of nutrient exchange between these groups? Since the biology and even the colonization processes of culturable AMF have yet to be fully characterized, the characteristics of field AMF, which are not cultured, are completely unknown.

To date, few groups have conducted colonization dynamics-based functional studies. This is probably because we still do not have suitable molecular or histological tools to detect and analyze the lifecycle of colonization. Interestingly, Floss et al. (2017) recently demonstrated that a transcription factor of *Medicago truncatula*, MYB1, is a central regulator of arbuscule degeneration. MYB1 regulates the expression of a number of genes encoding digesting hydrolytic enzymes such as chitinase, lipase, and proteases, which are likely candidate markers, using it simultaneously with a symbiotic phosphate transporter, precisely reflecting the lifecycle of colonization. Next, it will be important to investigate the colonization dynamics of unculturable AMF colonizing field roots using new molecular markers or techniques.

As mentioned above, mycorrhizae can be regarded as a mosaic of diverse AMF individuals in symbiosis with the root. Because the individual AMF in the roots are the pieces of the puzzle of the functionality of field mycorrhizae, the need

to explore the functioning of AMF *in situ* and at the single-cell level has been pointed out (Limpens and Geurts, 2014; Öpik and Davison, 2016; Taylor et al., 2017; van der Heijden et al., 2017). In particular, genetic and functional analyses of infection units in roots grown in the field might be a major frontier for understanding the biology of field AMF and their functionality. Recently, a new technique for elucidating the rRNA gene information of metabolically active infection units has been reported (Kobae et al., 2016). Root segments (<3 mm) of rice containing an active infection unit were dissected and squashed, large subunit rRNA genes were amplified using fungal universal primers and the sequences were directly determined by Sanger sequencing. By combining this method with the latest single-cell-level, ultra-low input micro-transcriptome analysis (Beaudet et al., 2018) coupled with the reconstruction of genomes of each infection unit, we should be able to increase our basic knowledge of the genetics of AMF, mycorrhization processes by tracing specific AMF (Schlaeppi et al., 2016), and the expression of functionality. In this approach, fluorescent marker plants (e.g., phosphate transporter-GFP rice; Kobae and Hata, 2010) would be feasible for efficiently detecting the functional colonization.

On the other hand, AMF functioning may be influenced by interacting microorganisms (e.g., PSB). These interactions will be partly characterized by the studies of molecular dialogues with fungal/bacterial effectors (Sedzielewska Toro, 2016; Kamel et al., 2017), plant hormones (Sawers et al., 2018), expression of nutrient transporters and metabolic crosstalk among symbionts (Lanfranco et al., 2018). As mentioned above, mycorrhizal phosphate uptake in the field is assumed to be driven by the mosaic of different AMF. The combined investigation of colonization dynamics and high-resolution functional cross-talk among symbionts presents a logical next step for the better understanding of the mechanism of mycorrhizal phosphate uptake.

CONCLUSION

In field, the roots of crops are co-colonized with multiple AMF species, which are difficult to separate and identify. The ability of mycorrhizal roots to perform phosphate uptake in the field is assumed to be a mosaic of the different abilities of diverse AMF. However, the biology of uncultured AMF in the field is hardly understood. Given advances in high-throughput sequencing technologies, such complex phosphate uptake systems under field conditions are the new frontier in mycorrhizal research and are crucial for managing the phosphate nutrition of crops. To this end, the understanding of the dynamics of colonization and the genetics of field AMF coupled with their functionality will be important. Many economically important crops (e.g., maize, soybean, wheat, and barley) are commonly mycorrhizal and their nutrition is influenced by the biology of AMF. Accordingly, a better understanding of the mineral nutrient uptake systems of crop mycorrhizas in the field could help establish a resource-saving and sustainable agricultural system.

AUTHOR CONTRIBUTIONS

The author confirms being the sole contributor of this work and has approved it for publication.

FUNDING

This work was supported partly by ACCEL from the Japan Science and Technology Agency (grant number JPMJAC1403).

REFERENCES

Angelard, C., Colard, A., Niculita-Hirzel, H., Croll, D., and Sanders, I. R. (2010). Segregation in a mycorrhizal fungus alters rice growth and symbiosis-specific gene transcription. Curr. *Biol*. 20, 1216–1221. doi: 10.1016/j.cub.2010.05.031

Angelard, C., Tanner, C. J., Fontanillas, P., Niculita-Hirzel, H., Masclaux, F., and Sanders, I. R. (2014). Rapid genotypic change and plasticity in arbuscular mycorrhizal fungi is caused by a host shift and enhanced by segregation. *ISME J*. 8, 284–294. doi: 10.1038/ismej.2013.154

Balestrini, R., Gómez-Ariza, J., Lanfranco, L., and Bonfante, P. (2007). Laser microdissection reveals that transcripts for five plant and one fungal phosphate transporter genes are contemporaneously present in arbusculated cells. *Mol. Plant Microbe Interact*. 20, 1055–1062. doi: 10.1094/MPMI-20-9-1055

Balzergue, C., Puech-Pagès, V., Bécard, G., and Rochange, S. F. (2010). The regulation of arbuscular mycorrhizal symbiosis by phosphate in pea involves early and systemic signalling events. *J. Exp. Bot*. 62, 1049–1060. doi: 10.1093/jxb/erq335

Battini, F., Grønlund, M., Agnolucci, M., Giovannetti, M., and Jakobsen, I. (2017). Facilitation of phosphorus uptake in maize plants by mycorrhizosphere bacteria. *Sci. Rep*. 7:4686. doi: 10.1038/s41598-017-04959-0

Baylis, G. T. S. (1967). Experiments on the ecological significance of phycomycetous mycorrhizas. *New Phytol*. 66, 231–243. doi: 10.1111/j.1469-8137.1967.tb06001.x

Beaudet, D., Chen, E. C. H., Mathieu, S., Yildirir, G., Ndikumana, S., Dalpé Y., et al. (2018). Ultra-low input transcriptomics reveal the spore functional content and phylogenetic affiliations of poorly studied arbuscular mycorrhizal fungi. *DNA Res*. 25, 217–227. doi: 10.1093/dnares/dsx051

Benedetto, A., Magurno, F., Bonfante, P., and Lanfranco, L. (2005). Expression profiles of a phosphate transporter gene (GmosPT) from the endomycorrhizal fungus Glomus mosseae. *Mycorrhiza* 15, 620–627. doi: 10.1007/s00572-005-0006-9

Bianciotto, V., Lumini, E., Bonfante, P., and Vandamme, P. (2003). 'Candidatus Glomeribacter gigasporarum' gen. nov., sp nov., an endosymbiont of arbuscular mycorrhizal fungi. *Int. J. Syst. Evol. Microbiol*. 53, 121–124. doi: 10.1099/ijs.0.02382-0

Bonfante-Fasolo, P. (1984). "Anatomy and morphology of VA mycorrhizae," in *VA Mycorrhizas,* eds C. L. Powell and D. J. Bagyaraj (Boca Raton, FL: CRC Press), 5–33.

Breuillin, F., Schramm, J., Hajirezaei, M., Ahkami, A., Favre, P., Druege, U., et al. (2010). Phosphate systemically inhibits development of arbuscular mycorrhiza in Petunia hybrida and represses genes involved in mycorrhizal functioning. *Plant J*. 64, 1002–1017. doi: 10.1111/j.1365-313X.2010.04385.x

Browne, P., Rice, O., Miller, S. H., Burke, J., Dowling, D. V., Morrissey, J. P., et al. (2009). Superior inorganic phosphate solubilization is linked to phylogeny within the *Pseudomonas* fluorescens complex. *Appl. Soil Ecol*. 43, 131–138. doi: 10.1016/j.apsoil.2009.06.010

Bruns, T. D., Corradi, N., Redecker, D., and Taylor, J. W., Öpik, M. (2017). Glomeromycotina: what is a species and why should we care? *New Phytol*. 220, 963–967. doi: 10.1111/nph.14913

Bucher, M. (2007). Functional biology of plant phosphate uptake at root and mycorrhiza interfaces. *New Phytol.* 173, 11–26 doi: 10.1111/j.1469-8137.2006.01935.x

Bucher, M., Hause, B., Krajinski, F., and Küster, H. (2014). Through the doors of perception to function in arbuscular mycorrhizal symbioses. *New Phytol.* 204, 833–840. doi: 10.1111/nph.12862

Bücking, H., Mensah, J. A., and Fellbaum, C. R. (2016). Common mycorrhizal networks and their effect on the bargaining power of the fungal partner in the arbuscular mycorrhizal symbiosis. *Commun. Integr. Biol.* 9:e1107684. doi: 10.1080/19420889.2015.1107684

Bueno de Mesquita, C. P., Martinez Del Río, C. M., Suding, K. N., and Schmidt, S. K. (2018). Rapid temporal changes in root colonization by arbuscular mycorrhizal fungi and fine root endophytes, not dark septate endophytes, track plant activity and environment in an alpine ecosystem. *Mycorrhiza* 28, 717–726. doi: 10.1007/s00572-018-0863-7

Burleigh, S. H., Cavagnaro, T., and Jakobsen, I. (2002). Functional diversity of arbuscular mycorrhizas extends to the expression of plant genes involved in P nutrition. *J. Exp. Bot.* 53, 1593–1601. doi: 10.1093/jxb/erf013

Chagnon, P. L. (2014). Ecological and evolutionary implications of hyphal anastomosis in arbuscular mycorrhizal fungi. *FEMS Microbiol. Ecol.* 88, 437–444. doi: 10.1111/1574-6941.12321

Chen, E. C. H., Morin, E., Beaudet, D., Noel, J., Yildirir, G., Ndikumana, S., et al. (2018). High intraspecifc genome diversity in the model arbuscular mycorrhizal symbiont Rhizophagus irregularis. *New Phytol.* 220, 1161–1171. doi: 10.1111/nph.14989

Chen, Y. P., Rekha, P. D., Arun, A. B., Shen, F. T., Lai, W. A., and Young, C. C. (2006). Phosphate solubilizing bacteria from subtropical soil and their tricalcium phosphate solubilizing abilities. *Appl. Soil Ecol.* 34, 33–41. doi: 10.1016/j.apsoil.2005.12.002

Chu, Q., Wang, X., Yang, Y., Chen, F., Zhang, F., and Feng, G. (2013). Mycorrhizal responsiveness of maize (Zea mays L.) genotypes as related to releasing date and available P content in soil. *Mycorrhiza* 23, 497–505. doi: 10.1007/s00572-013-0492-0

Compant, S., van der Heijden, M. G., and Sessitsch, A. (2010). Climate change effects on beneficial plant-microorganism interactions. *FEMS Microbiol. Ecol.* 73, 197–214. doi: 10.1111/j.1574-6941.2010.00900.x

Croll, D., Giovannetti, M., Koch, A. M., Sbrana, C., Ehinger, M., Lammers, P. J., et al. (2009). Nonself vegetative fusion and genetic exchange in the arbuscular mycorrhizal fungus Glomus intraradices. *New Phytol.* 181, 924–937. doi: 10.1111/j.1469-8137.2008.02726.x

Davison, J., Moora, M., Öpik, M., Adholeya, A., and Ainsaar, L., Bâ, A. et al. (2015). Global assessment of arbuscular mycorrhizal fungus diversity reveals very low endemism. *Science* 349, 970–973. doi: 10.1126/science.aab1161

de Queiroz, K. (2005). Ernst Mayr and the modern concept of species. *Proc. Natl. Acad. Sci. U.S.A.* 102, 6600–6607. doi: 10.1073/pnas.0502030102

Deguchi, S., Uozumi, S., Touno, E., Kaneko, M., and Tawaraya, K. (2012). Arbuscular mycorrhizal colonization increases phosphorus uptake and growth of corn in a white clover living mulch system. *Soil Sci. Plant Nutr.* 58, 169–172. doi: 10.1080/00380768.2012.662697

Dickson, S., Smith, F. A., and Smith, S. E. (2007). Structural differences in arbuscular mycorrhizal symbioses: more than 100 years after Gallaud, where next? *Mycorrhiza* 17, 375–393. doi: 10.1007/s00572-007-0130-9

Engelmoer, D. J., Behm, J. E., and Toby Kiers, E. (2014). Intense competition between arbuscular mycorrhizal mutualists in an in vitro root microbiome negatively affects total fungal abundance. *Mol. Ecol.* 23, 1584–1593. doi: 10.1111/mec.12451

Ezawa, T., and Saito, K. (2018). How do arbuscular mycorrhizal fungi handle phosphate? New insight into fine-tuning of phosphate metabolism. *New Phytol.* 220, 1116–1121. doi: 10. 1111/nph.15187

Facelli, E., Duan, T., Smith, S. E., Christophersen, H. M., Facelli, J. M., and Smith, F. A. (2014). Opening the black box: outcomes of interactions between arbuscular mycorrhizal (AM) and non-host genotypes of Medicago depend on fungal identity, interplay between P uptake pathways and external P supply. *Plant Cell. Environ.* 37, 1382–1392. doi: 10.1111/pce.12237

Fan, M., Shen, J., Yuan, L., Jiang, R., Chen, X., Davies, W. J., et al. (2011). Improving crop productivity and resource use efficiency to ensure food security and environmental quality in China. *J Exp. Bot.* 63, 13–24. doi: 10.1093/jxb/err248

Feng, G., Su, Y. B., Li, X. L., Wang, H., Zhang, F. S., Tang, C. X., et al. (2002). Histochemical visualization of phosphatase released by arbuscular mycorrhizal fungi in soil. *J. Plant Nutr.* 25, 969–980. doi: 10.1081/PLN-120003932

Fiorilli, V., Lanfranco, L., and Bonfante, P. (2013). The expression of GintPT, the phosphate transporter of Rhizophagus irregularis, depends on the symbiotic status and phosphate availability. *Planta* 237, 1267–1277. doi: 10.1007/s00425-013-1842-z

Floss, D. S., Gomez, S. K., Park, H. J., MacLean, A. M., Müller, L. M., Bhattarai, K. K., et al. (2017). A transcriptional program for arbuscule degeneration during AM symbiosis is regulated by MYB1. *Curr. Biol.* 27, 1206–1212. doi: 10.1016/j.cub.2017.03.003

Fonseca, H. M., and Berbara, R. L. (2008). Does Lunularia cruciata form symbiotic relationships with either Glomus proliferum or G. *Intraradices? Mycol. Res.* 112, 1063–1068. doi: 10.1016/j.mycres.2008.03.008

Frey-Klett, P., Garbaye, J. A., and Tarkka, M. (2007). The mycorrhiza helper bacteria revisited. *New Phytol.* 176, 22–36. doi: 10.1111/j.1469-8137.2007.02191.x

Görke, B., and Stülke, J. (2008). Carbon catabolite repression in bacteria: many ways to make the most out of nutrients. *Nat Rev Microbiol.* 6:613. doi: 10.1038/nrmicro1932

Graham, J. H., Leonard, R. T., and Menge, J. A. (1981). Membrane-mediated decrease in root exudation responsible for phorphorus inhibition of vesicular arbuscular mycorrhiza formation. *Plant Physiol.* 68, 548–552. doi: 10.1104/pp.68.3.548

Grunwald, U., Guo, W., Fischer, K., Isayenkov, S., Ludwig-Müller, J., Hause, B., et al. (2009). Overlapping expression patterns and differential transcript levels of phosphate transporter genes in arbuscular mycorrhizal, Pi-fertilised and phytohormone-treated Medicago truncatula roots. *Planta* 229, 1023–1034. doi: 10.1007/s00425-008-0877-z

Gutjahr, C., and Parniske, M. (2017). Control of partner lifetime in a plant-fungus relationship. *Curr. Biol.* 27, R420–R423. doi: 10.1016/j.cub.2017.04.020

Harrison, M. J., Dewbre, G. R., and Liu, J. (2002). A phosphate transporter from Medicago truncatula involved in the acquisition of phosphate released by arbuscular mycorrhizal fungi. *Plant Cell* 14, 2413–2429. doi: 10.1105/tpc.004861

Harrison, M. J., and Ivanov, S. (2017). Exocytosis for endosymbiosis: membrane trafficking pathways for development of symbiotic membrane compartments. *Curr. Opin. Plant Biol.* 38, 101–108. doi: 10.1016/j.pbi.2017.04.019

Harrison, M. J., and van Buuren, M. L. (1995). A phosphate transporter from the mycorrhizal fungus Glomus versiforme. *Nature* 378, 626–629. doi: 10.1038/378626a0

Hart, M. M., Aleklett, K., Chagnon, P. L., Egan, C., Ghignone, S., Helgason, T., et al. (2015). Navigating the labyrinth: a guide to sequence-based, community ecology of arbuscular mycorrhizal fungi. *New Phytol.* 207, 235–247. doi: 10.1111/nph.13340

Hart, M. M., Antunes, P. M., Chaudhary, V. B., and Abbott, L. K. (2017). Fungal inoculants in the field: is the reward greater than the risk? *Funct. Ecol.* 32, 126–135. doi: 10.1111/1365-2435.12976

Helber, N., Wippel, K., Sauer, N., Schaarschmidt, S., Hause, B., and Requena, N. (2011). A versatile monosaccharide transporter that operates in the arbuscular mycorrhizal fungus Glomus sp. is crucial for the symbiotic relationship with plants. *Plant Cell* 23, 3812–3823. doi: 10.1105/tpc.111.089813

Hibbett, D., Abarenkov, K., Kõljalg, U., Öpik, M., and Chai, B., Cole J et al (2016). Sequence-based classification and identification of Fungi. *Mycologia* 108, 1049–1068. doi: 10.3852/16-130

Jacoby, R., Peukert, M., Succurro, A., Koprivova, A., and Kopriva, S. (2017). The role of soil microorganisms in plant mineral nutrition—current knowledge and future directions. *Front. Plant Sci.* 8:1617. doi: 10.3389/fpls.2017.01617

Jakobsen, I., Gazey, C., and Abbott, L. K. (2001). Phosphate transport by communities of arbuscular mycorrhizal fungi in intact soil cores. *New Phytol.* 149, 95–103. doi: 10.1046/j.1469-8137.2001.00006.x

Jansa, J., Smith, F. A., and Smith, S. E. (2008). Are there benefits of simultaneous root colonization by different arbuscular mycorrhizal fungi? *New Phytol.* 177, 779–789. doi: 10.1111/j.1469-8137.2007.02294.x

Jany, J. L., and Pawlowska, T. E. (2010). Multinucleate spores contribute to evolutionary longevity of asexual Glomeromycota. *Am. Nat.* 175, 424–435. doi: 10.1086/650725

Javot, H., Pumplin, N., and Harrison, M. J. (2007). Phosphate in the arbuscular mycorrhizal symbiosis: transport properties and regulatory roles. *Plant Cell Environ*. 30, 310–322. doi: 10.1111/j.1365-3040.2006.01617.x

Johnson, N. C. (1993). Can fertilization of soil select less mutualistic mycorrhizae? *Ecol. Appl*. 3, 749–757. doi: 10.2307/1942106

Johnson, N. C., Graham, J. H., and Smith, F. A. (1997). Functioning of mycorrhizal associations along the mutualism-parasitism continuum. *New Phytol*. 135, 575–586. doi: 10.1046/j.1469-8137.1997.00729.x

Jones, M. D., and Smith, S. E. (2004). Exploring functional definitions of mycorrhizas: are mycorrhizas always mutualisms? *Can. J. Bot*. 82, 1089–1109. doi: 10.1139/b04-110

Kamel, L., Tang, N., Malbreil, M., San Clemente, H., Le Marquer, M., Roux, C., et al. (2017). The comparison of expressed candidate secreted proteins from two arbuscular mycorrhizal fungi unravels common and specific molecular tools to invade different host plants. *Front. Plant Sci*. 8:124. doi: 10.3389/fpls.2017.00124

Keymer, A., and Gutjahr, C. (2018). Cross-kingdom lipid transfer in arbuscular mycorrhiza symbiosis and beyond. *Curr. Opin. Plant Biol*. 44, 137–144. doi: 10.1016/j.pbi.2018.04.005

Kiers, E. T., Duhamel, M., Beesetty, Y., Mensah, J. A., Franken, O., Verbruggen, E., et al. (2011). Reciprocal rewards stabilize cooperation in the mycorrhizal symbiosis. *Science* 333, 880–882. doi: 10.1126/science.1208473

Kikuchi, Y., Hijikata, N., Ohtomo, R., Handa, Y., Kawaguchi, M., Saito, K., et al. (2016). Aquaporin-mediated long-distance polyphosphate translocation directed towards the host in arbuscular mycorrhizal symbiosis: application of virus-induced gene silencing. *New Phytol*. 211, 1202–1208. doi: 10.1111/nph.14016

Kivlin, S. N., Hawkes, C. V., and Treseder, K. K. (2011). Global diversity and distribution of arbuscular mycorrhizal fungi. *Soil. Biol. Biochem*. 43, 2294–2303. doi: 10.1016/j.soilbio.2011.07.012

Kobae, Y., and Fujiwara, T. (2014). Earliest colonization events of Rhizophagus irregularis in rice roots occur preferentially in previously uncolonized cells. *Plant Cell Physiol*. 55, 1497–1510. doi: 10.1093/pcp/pcu081

Kobae, Y., and Hata, S. (2010). Dynamics of periarbuscular membranes visualized with a fluorescent phosphate transporter in arbuscular mycorrhizal roots of rice. *Plant Cell Physiol*. 51, 341–353. doi: 10.1093/pcp/pcq013

Kobae, Y., Ohmori, Y., Saito, C., Yano, K., Ohtomo, R., and Fujiwara, T. (2016). Phosphate treatment strongly inhibits new arbuscule development but not the maintenance of arbuscule in mycorrhizal rice roots. *Plant Physiol*. 171, 566–579. doi: 10.1104/pp.16.00127

Kobae, Y., Ohtomo, R., Oka, N., and Morimoto, S. (2017). A simple model system for identifying arbuscular mycorrhizal fungal taxa that actively colonize rice roots grown in field soil. *Soil Sci. Plant Nutr*. 63, 29–36. doi: 10.1080/00380768.2016.1277156

Lanfranco, L., Fiorilli, V., and Gutjahr, C. (2018). Partner communication and role of nutrients in the arbuscular mycorrhizal symbiosis. *New Phytol*. 220, 1031–1046. doi: 10.1111/nph.15230.

Lehmann, A., Barto, E. K., Powell, J. R., and Rillig, M. C. (2012). Mycorrhizal responsiveness trends in annual crop plants and their wild relatives – a meta-analysis on studies from 1981 to 2010. *Plant Soil* 355, 231–250. doi: 10.1007/s11104-011-1095-1

Lehnert, H., Serfling, A., Enders, M., Friedt, W., and Ordon, F. (2017). Genetics of mycorrhizal symbiosis in winter wheat (Triticum aestivum). *New Phytol*. 215, 779–791. doi: 10.1111/nph.14595

Lekberg, Y., and Koide, R. T. (2014). Integrating physiological, community and evolutionary perspectives of the arbuscular mycorrhizal symbiosis. *Botany* 92, 241–251. doi: 10.1139/cjb-2013-0182

Limpens, E., and Geurts, R. (2014). Plant-driven genome selection of arbuscular mycorrhizal fungi. *Mol. Plant Pathol*. 15, 531–534. doi: 10.1111/mpp.12149

Lin, K., Limpens, E., Zhang, Z., Ivanov, S., Saunders, D. G., Mu, D., et al. (2014). Single nucleus genome sequencing reveals high similarity among nuclei of an endomycorrhizal fungus. *PLoS Genet*. 10:e1004078. doi: 10.1371/journal.pgen.1004078

Maeda, T., Kobayashi, Y., Kameoka, H., Okuma, N., Takeda, N., Yamaguchi, K., et al. (2018). Evidence of non-tandemly repeated rDNAs and their intragenomic heterogeneity in Rhizophagus irregularis. *Commun. Biol*. 1:87. doi: 10.1038/s42003-018-0094-7

Martín-Robles, N., Lehmann, A., Seco, E., Aroca, R., Rillig, M. C., and Milla, R. (2018). Impacts of domestication on the arbuscular mycorrhizal symbiosis of 27 crop species. *New Phytol*. 218, 322–334. doi: 10.1111/nph.14962

Mathieu, S., Cusant, L., Roux, C., and Corradi, N. (2018). Arbuscular mycorrhizal fungi: intraspecific diversity and pangenomes. *New Phytol*. 220, 1129–1134. doi: 10.1111/nph.15275

Mensah, J. A., Koch, A. M., Antunes, P. M., Hart, M. M., Kiers, E. T., and Bücking, H. (2015). High functional diversity within arbuscular mycorrhizal fungal species is associated with differences in phosphate and nitrogen uptake and fungal phosphate metabolism. *Mycorrhiza* 25, 533–546. doi: 10.1007/s00572-015-0631-x

Mondo, S. J., Lastovetsky, O. A., Gaspar, M. L., Schwardt, N. H., Barber, C. C., Riley, R., et al. (2017). Bacterial endosymbionts influence host sexuality and reveal reproductive genes of early divergent fungi. *Nat. Commun*. 8:1843. doi: 10.1038/s41467-017-02052-8

Mosse, B. (1973). Plant growth responses to vesicular-arbuscular mycorrhiza IV. in soil given additional phosphate. *New Phytol*. 72, 127–136. doi: 10.1111/j.1469-8137.1973.tb02017.x

Munkvold, L., Kjøller, R., Vestberg, M., Rosendahl, S., and Jakobsen, I. (2004). High functional diversity within species of arbuscular mycorrhizal fungi. *New Phytol*. 164, 357–364. doi: 10.1111/j.1469-8137.2004.01169.x

Nagy, R., Drissner, D., Amrhein, N., Jakobsen, I., and Bucher, M. (2009). Mycorrhizal phosphate uptake pathway in tomato is phosphorus-repressible and transcriptionally regulated. *New Phytol*. 181, 950–959. doi: 10.1111/j.1469-8137.2008.02721.x

Naito, M., Desirò, A., González, J. B., Tao, G., Morton, J. B., Bonfante, P., et al. (2017). 'Candidatus Moeniiplasma glomeromycotorum', an endobacterium of arbuscular mycorrhizal fungi. *Int. J. Syst. Evol. Microbiol*. 67, 1177–1184. doi: 10.1099/ijsem.0.001785

Niwa, R., Koyama, T., Sato, T., Adachi, K., Tawaraya, K., Sato, S., et al. (2018). Dissection of niche competition between introduced and indigenous arbuscular mycorrhizal fungi with respect to soybean yield responses. *Sci. Rep*. 8:7419. doi: 10.1038/s41598-018-25701-4

Nouri, E., Breuillin-Sessoms, F., Feller, U., and Reinhardt, D. (2014). Phosphorus and nitrogen regulate arbuscular mycorrhizal symbiosis in Petunia hybrida. *PLoS ONE* 9:e90841. doi: 10.1371/journal.pone.0090841

Novais, C. B. D., Pepe, A., Siqueira, J. O., Giovannetti, M., and Sbrana, C. (2017). Compatibility and incompatibility in hyphal anastomosis of arbuscular mycorrhizal fungi. *Sci. Agricola* 74, 411–416. doi: 10.1590/1678-992x-2016-0243

Ohsowski, B. M., Zaitsoff, P. D., and Opik, M., Hart, M. M. (2014). Where the wild things are: looking for uncultured Glomeromycota. *New Phytol*. 204, 171–179. doi: 10.1111/nph.12894

Öpik, M., Davison, J. (2016). Uniting species- and community-oriented approaches to understand arbuscular mycorrhizal fungal diversity. *Fungal Ecol*. 24, 106–113. doi: 10.1016/j.funeco.2016.07.005

Öpik, M., Davison, J., and Moora, M., Zobel, M. (2013). DNA-based detection and identification of Glomeromycota: the virtual taxonomy of environmental sequences. *Botany* 92, 135–147. doi: 10.1139/cjb-2013-0110

Opik, M., Metsis, M., Daniell, T. J., and Zobel, M., Moora, M. (2009). Large-scale parallel 454 sequencing reveals host ecological group specificity of arbuscular mycorrhizal fungi in a boreonemoral forest. *New Phytol*. 184, 424–437. doi: 10.1111/j.1469-8137.2009.02920.x

Orchard, S., Standish, R. J., Dickie, I. A., Renton, M., Walker, C., Moot, D., et al. (2017). Fine root endophytes under scrutiny: a review of the literature on arbuscule-producing fungi recently suggested to belong to the Mucoromycotina. *Mycorrhiza* 27, 619–638. doi: 10.1007/s00572-017-0782-z

Ordoñez, Y. M., Fernandez, B. R., Lara, L. S., Rodriguez, A., Uribe-Vélez, D., and Sanders, I. R. (2016). Bacteria with phosphate solubilizing capacity alter mycorrhizal fungal growth both inside and outside the root and in the presence of native microbial communities. *PLoS ONE* 11:e0154438. doi: 10.1371/journal.pone.0154438

Parks, D. H., Rinke, C., Chuvochina, M., Chaumeil, P. A., Woodcroft, B. J., Evans, P. N., et al. (2017). Recovery of nearly 8,000 metagenome-assembled genomes substantially expands the tree of life. *Nat. Microb*. 2:1533. doi: 10.1038/s41564-017-0012-7

Partida-Martinez, L. P., Monajembashi, S., Greulich, K. O., and Hertweck, C. (2007). Endosymbiont-dependent host reproduction maintains bacterial-fungal mutualism. *Curr. Biol.* 17, 773–777. doi: 10.1016/j.cub.2007.03.039

Pawlowska, T. E., Gaspar, M. L., Lastovetsky, O. A., Mondo, S. J., Real-Ramirez, I., Shakya, E., et al. (2018). Biology of fungi and their bacterial endosymbionts. *Annu. Rev. Phytopathol.* 56, 289–309. doi: 10.1146/annurev-phyto-080417-045914

Pumplin, N., Zhang, X., Noar, R. D., and Harrison, M. J. (2012). Polar localization of a symbiosis-specific phosphate transporter is mediated by a transient reorientation of secretion. *Proc. Natl. Acad. Sci. U.S.A.* 109, E665–E672. doi: 10.1073/pnas.1110215109

Ramírez-Flores, M. R., Rellán-Álvarez, R., Wozniak, B., Gebreselassie, M. N., Jakobsen, I., Olalde-Portugal, V., et al. (2017). Co-ordinated changes in the accumulation of metal ions in maize (Zea mays ssp. *mays L.)* in response to inoculation with the arbuscular mycorrhizal fungus Funneliformis mosseae. *Plant Cell Physiol.* 58, 1689–1699. doi: 10.1093/pcp/pcx100

Redecker, D., Hijri, I., and Wiemken, A. (2003). Molecular identification of arbuscular mycorrhizal fungi in roots: perspectives and problems. *Folia Geobot.* 38, 113–124. doi: 10.1007/BF02803144

Remy, W., Taylor, T. N., Hass, H., and Kerp, H. (1994). Four-hundred-million year-old vesicular-arbuscular mycorrhizae. *Proc. Natl. Acad. Sci. U.S.A.* 91, 11841–11843. doi: 10.1073/pnas.91.25.11841

Rich, M. K., Nouri, E., Courty, P. E., and Reinhardt, D. (2017). Diet of arbuscular mycorrhizal fungi: bread and butter? *Trends Plant Sci.* 22, 652–660. doi: 10.1016/j.tplants.2017.05.008

Rillig, M. C., Ramsey, P. W., Gannon, J. E., Mummey, D. L., Gadkar, V., and Kapulnik, Y. (2008). Suitability of mycorrhiza-defective mutant/wildtype plant pairs (*Solanum lycopersicum* L. cv Micro-Tom) to address questions in mycorrhizal soil ecology. *Plant Soil* 308, 267–275. doi: 10.1007/s11104-008-9629-x

Rodriguez, A., and Sanders, I. R. (2015). The role of community and population ecology in applying mycorrhizal fungi for improved food security. *ISME J.* 9, 1053–1061. doi: 10.1038/ismej.2014.207

Rodríguez, H., and Fraga, R. (1999). Phosphate solubilizing bacteria and their role in plant growth promotion. *Biotechnol. Adv.* 17, 319–339. doi: 10.1016/S0734-9750(99)00014-2

Ropars, J., Toro, K. S., Noel, J., Pelin, A., Charron, P., Farinelli, L., et al. (2016). Evidence for the sexual origin of heterokaryosis in arbuscular mycorrhizal fungi. *Nat. Microbiol.* 1:16033. doi: 10.1038/nmicrobiol.2016.33

Rosendahl, S. (2008). Communities, populations and individuals of arbuscular mycorrhizal fungi. *New Phytol.* 178, 253–266. doi: 10.1111/j.1469-8137.2008.02378.x

Roth, R., and Paszkowski, U. (2017). Plant carbon nourishment of arbuscular mycorrhizal fungi. *Curr. Opin. Plant Biol.* 39, 50–56. doi: 10.1016/j.pbi.2017.05.008

Sanders, F. E., and Sheikh, N. A. (1983). The development of vesicular-arbuscular mycorrhizal infection in plant root system. *Plant Soil* 71, 223–246. doi: 10.1007/BF02182658

Sanders, I. R., Clapp, J. P., and Wiemken, A. (1996). The genetic diversity of arbuscular mycorrhizal fungi in natural ecosystems—a key to understanding the ecology and functioning of the mycorrhizal symbiosis. *New Phytol.* 133, 123–134. doi: 10.1111/j.1469-8137.1996.tb04348.x

Sanders, I. R., and Croll, D. (2010). Arbuscular mycorrhiza: the challenge to understand the genetics of the fungal partner. *Annu. Rev. Genet.* 44, 271–292. doi: 10.1146/annurev-genet-102108-134239

Sanders, I. R., and Rodriguez, A. (2016). Aligning molecular studies of mycorrhizal fungal diversity with ecologically important levels of diversity in ecosystems. *ISME J.* 10, 2780–2786. doi: 10.1038/ismej.2016.73

Sawers, R. J., Gebreselassie, M. N., Janos, D. P., and Paszkowski, U. (2010). Characterizing variation in mycorrhiza effect among diverse plant varieties. *Theor. Appl. Genet.* 120, 1029–1039. doi: 10.1007/s00122-009-1231-y

Sawers, R. J., Svane, S. F., Quan, C., Grønlund, M., Wozniak, B., Gebreselassie, M. N., et al. (2017). Phosphorus acquisition efficiency in arbuscular mycorrhizal maize is correlated with the abundance of root-external hyphae and the accumulation of transcripts encoding PHT1 phosphate transporters. *New Phytol.* 214, 632–643. doi: 10.1111/nph.14403

Sawers, R. J. H., Ramírez-Flores, M. R., Olalde-Portugal, V., and Paszkowski, U. (2018). The impact of domestication and crop improvement on arbuscular mycorrhizal symbiosis in cereals: insights from genetics and genomics. *New Phytol.* 220, 1135–1140. doi: 10.1111/nph.15152.

Sbrana, C., Strani, P., Pepe, A., de Novais, C. B., and Giovannetti, M. (2018). Divergence of Funneliformis mosseae populations over 20 years of laboratory cultivation, as revealed by vegetative incompatibility and molecular analysis. *Mycorrhiza* 28, 329–341. doi: 10.1007/s00572-018-0830-3

Schachtman, D. P., Reid, R. J., and Ayling, S. M. (1998). Phosphorus uptake by plants: from soil to cell. *Plant Physiol.* 116, 447–453. doi: 10.1104/pp.116.2.447

Schlaeppi, K., Bender, S. F., Mascher, F., Russo, G., Patrignani, A., Camenzind, T., et al. (2016). High-resolution community profiling of arbuscular mycorrhizal fungi. *New Phytol.* 212, 780–791. doi: 10.1111/nph.14070

Sedzielewska Toro, K. and Brachmann, A. (2016). The effector candidate repertoire of the arbuscular mycorrhizal fungus Rhizophagus clarus. *BMC Genomics* 17:101. doi: 10.1186/s12864-016-2422-y

Selosse, M. A., Vincenot, L., and Öpik, M. (2016). Data processing can mask biology: towards better reporting of fungal barcoding data? *New Phytol.* 210, 1159–1164. doi: 10.1111/nph.13851

Sharma, S. B., Sayyed, R. Z., Trivedi, M. H., and Gobi, T. A. (2013). Phosphate solubilizing microbes: sustainable approach for managing phosphorus deficiency in agricultural soils. *SpringerPlus* 2:587. doi: 10.1186/2193-1801-2-587

Smith, S. E., Jakobsen, I., Grønlund, M., and Smith, F. A. (2011). Roles of arbuscular mycorrhizas in plant phosphorus nutrition: interactions between pathways of phosphorus uptake in arbuscular mycorrhizal roots have important implications for understanding and manipulating plant phosphorus acquisition. *Plant Physiol.* 156, 1050–1057. doi: 10.1104/pp.111.174581

Smith, S. E., and Read, D. J. (2008). *Mycorrhizal Symbiosis. 3rd ed*. London: Academic Press Ltd.

Smith, S. E., and Smith, F. A. (2011). Roles of arbuscular mycorrhizas in plant nutrition and growth: new paradigms from cellular to ecosystem scales. *Annu. Rev. Plant Biol.* 62, 227–250. doi: 10.1146/annurev-arplant-042110-103846

Smith, S. E., Smith, F. A., and Jakobsen, I. (2004). Functional diversity in arbuscular mycorrhizal (AM) symbioses: the contribution of the mycorrhizal P uptake pathway is not correlated with mycorrhizal responses in growth or total P uptake. *New Phytol.* 162, 511–524. doi: 10.1111/j.1469-8137.2004.01039.x

Strom, N. B., and Bushley, K. E. (2016). Two genomes are better than one: history, genetics, and biotechnological applications of fungal heterokaryons. *Fungal Biol. Biotechnol.* 3:4. doi: 10.1186/s40694-016-0022-x

Svenningsen, N. B., Watts-Williams, S. J., Joner, E. J., Battini, F., Efthymiou, A., Cruz-Paredes, C., et al. (2018). Suppression of the activity of arbuscular mycorrhizal fungi by the soil microbiota. *ISME J.* 12, 1296–1307. doi: 10.1038/s41396-018-0059-3

Tamura, Y., Kobae, Y., Mizuno, T., and Hata, S. (2012). Identification and expression analysis of arbuscular mycorrhiza-inducible phosphate transporter genes of soybean. *Biosci. Biotechnol. Biochem.* 76, 309–313. doi: 10.1271/bbb.110684

Tang, N., San Clemente, H., Roy, S., Bécard, G., Zhao, B., and Roux, C. (2016). A survey of the gene repertoire of Gigaspora rosea unravels conserved features among Glomeromycota for obligate biotrophy. *Front. Microbiol.* 7:233. doi: 10.3389/fmicb.2016.00233

Tawaraya, K. (2003). Arbuscular mycorrhizal dependency of different plant species and cultivars. *Soil Sci. Plant Nutr.* 49, 655–668. doi: 10.1080/00380768.2003.10410323

Taylor, J. D., and Helgason, T., Öpik, M. (2017). "Molecular community ecology of arbuscular mycorrhizal fungi," in *The Fungal Community: Its Organization and Role in the Ecosystem,* eds J. Dighton, J. White, and P. Oudemans (Florida, FL: CRC Press), 3–26. doi: 10.1079/9781845930622.0000

Tisserant, E., Malbreil, M., Kuo, A., Kohler, A., Symeonidi, A., Balestrini, R., et al. (2013). Genome of an arbuscular mycorrhizal fungus provides insight into the oldest plant symbiosis. 2013: genome of an arbuscular mycorrhizal fungus provides insight into the oldest plant symbiosis. *Proc. Natl. Acad. Sci. U.S.A.* 111, 562–563. doi: 10.1073/pnas.1313452110

Torres-Cortés, G., Ghignone, S., Bonfante, P., and Schüßler, A. (2015). Mosaic genome of endobacteria in arbuscular mycorrhizal fungi: Transkingdom gene transfer in an ancient mycoplasma-fungus association. *Proc. Natl. Acad. Sci. U.S.A.* 112, 7785–7790. doi: 10.1073/pnas.1501540112

Vályi, K., Mardhiah, U., Rillig, M. C., and Hempel, S. (2016). Community assembly and coexistence in communities of arbuscular mycorrhizal fungi. *ISME J.* 10, 2341–2351. doi: 10.1038/ismej.2016.46

van der Heijden, M. G., and Scheublin, T. R. (2007). Functional traits in mycorrhizal ecology: their use for predicting the impact of arbuscular mycorrhizal fungal communities on plant growth and ecosystem functioning. *New Phytol.* 174, 244–250. doi: 10.1111/j.1469-8137.2007.02041.x

van der Heijden, M. G. A., Dombrowski, N., and Schlaeppi, K. (2017). Continuum of root–fungal symbioses for plant nutrition. *Proc. Natl. Acad. Sci. U.S.A.* 114, 11574–11576. doi: 10.1073/pnas.1716329114

Van Geel, M., De Beenhouwer, M., Ceulemans, T., Caes, K., Ceustermans, A., Bylemans, D., et al. (2016). Application of slow-release phosphorus fertilizers increases arbuscular mycorrhizal fungal diversity in the roots of apple trees. *Plant Soil* 402, 291–301. doi: 10.1007/s11104-015-2777-x

van Tuinen, D., Jacquot, E., Zhao, B., Gollotte, A., and Gianinazzi-Pearson, V. (1998). Characterization of root colonization profiles by a microcosm community of arbuscular mycorrhizal fungi using 25S rDNA-targeted nested PCR. *Mol. Ecol.* 7, 879–887. doi: 10.1046/j.1365-294x.1998.00410.x

Vance, C. P. (2001). Symbiotic nitrogen fixation and phosphorus acquisition. *Plant nutrition in a world of declining renewable resources. Plant Physiol.* 127, 390–397. doi: 10.1104/pp.010331

Varela-Cervero, S., Vasar, M., Davison, J., Barea, J. M., and Öpik, M., Azcón-Aguilar, C. (2015). The composition of arbuscular mycorrhizal fungal communities differs among the roots, spores and extraradical mycelia associated with five Mediterranean plant species. *Environ. Microb.* 17, 2882–2895. doi: 10.1111/1462-2920.12810

Walder, F., and van der Heijden, M. G. (2015). Regulation of resource exchange in the arbuscular mycorrhizal symbiosis. *Nat. Plants* 1:15159. doi: 10.1038/nplants.2015.159

Walker, C., Gollotte, A., and Redecker, D. (2018). A new genus, Planticonsortium (Mucoromycotina), and new combination (P. tenue), for the fine root endophyte, Glomus tenue (basionym Rhizophagus tenuis). *Mycorrhiza* 28, 213–219. doi: 10.1007/s00572-017-0815-7

Wang, M., and Jin, H. (2017). Spray-induced gene silencing: a powerful innovative strategy for crop protection. *Trends Microbiol.* 25, 4–6. doi: 10.1016/j.tim.2016.11.011

Watts-Williams SJ Cavagnaro, T. R. (2015). Using mycorrhiza-defective mutant genotypes of non-legume plant species to study the formation and functioning of arbuscular mycorrhiza: a review. *Mycorrhiza* 25, 587–597. doi: 10.1007/s00572-015-0639-2

Willmann, M., Gerlach, N., Buer, B., Polatajko, A., and Nagy, R., Koebke, E. et al. (2013). Mycorrhizal phosphate uptake pathway in maize: vital for growth and cob development on nutrient poor agricultural and greenhouse soils. *Front. Plant Sci.* 4:533. doi: 10.3389/fpls.2013.00533

Xie, X., Lin, H., Peng, X., Xu, C., Sun, Z., Jiang, K., et al. (2016). Arbuscular mycorrhizal symbiosis requires a phosphate transceptor in the Gigaspora margarita fungal symbiont. *Mol. Plant* 9, 1583–1608. doi: 10.1016/j.molp.2016.08.011

Yang, S. Y., Grønlund, M., Jakobsen, I., Grotemeyer, M. S., Rentsch, D., Miyao, A., et al. (2012). Nonredundant regulation of rice arbuscular mycorrhizal symbiosis by two members of the PHOSPHATE TRANSPORTER1 gene family. *Plant Cell* 24, 4236–4251. doi: 10.1105/tpc.112.104901

Zhang, L., Fan, J., Ding, X., He, X., Zhang, F., and Feng, G. (2014). Hyphosphere interactions between an arbuscular mycorrhizal fungus and a phosphate solubilizing bacterium promote phytate mineralization in soil. *Soil Biol Biochem.* 74, 177–183. doi: 10.1016/j.soilbio.2014.03.004

Zhang, L., Feng, G., and Declerck, S. (2018). Signal beyond nutrient, fructose, exuded by an arbuscular mycorrhizal fungus triggers phytate mineralization by a phosphate solubilizing bacterium. *ISME J.* 12, 2339–2351. doi: 10.1038/s41396-018-0171-4

Zhang, L., Xu, M., Liu, Y., Zhang, F., Hodge, A., and Feng, G. (2016). Carbon and phosphorus exchange may enable cooperation between an arbuscular mycorrhizal fungus and a phosphate-solubilizing bacterium. *New Phytol.* 210, 1022–1032. doi: 10.1111/nph.13838

Conflict of Interest Statement: The author declares that the research was conducted in the absence of any commercial or financial relationships that could be construed as a potential conflict of interest.

frontiers in Environmental Science

ORIGINAL RESEARCH
published: 07 March 2019
doi: 10.3389/fenvs.2019.00026

Carbon Investment Required for the Mobilization of Inorganic and Organic Phosphorus Bound to Goethite by an Arbuscular Mycorrhiza (*Solanum lycopersicum x Rhizophagus irregularis*)

Alberto Andrino[1], *Jens Boy*[1]*, *Robert Mikutta*[2], *Leopold Sauheitl*[1] and *Georg Guggenberger*[1]

[1] Institute of Soil Science, Leibniz Universität Hannover, Hannover, Germany, [2] Soil Science and Soil Protection, Martin Luther University Halle-Wittenberg, Halle, Germany

OPEN ACCESS

Edited by:
Carsten W. Mueller,
Technische Universität München,
Germany

Reviewed by:
Luis Carlos Colocho Hurtarte,
Technische Universität München,
Germany
Alix Vidal,
Technische Universität München,
Germany
Marie Spohn,
University of Bayreuth, Germany

***Correspondence:**
Jens Boy
boy@ifbk.uni-hannover.de

Specialty section:
This article was submitted to Soil Processes, a section of the journal Frontiers in Environmental Science

Received: 31 August 2018
Accepted: 13 February 2019
Published: 07 March 2019

Citation:
Andrino A, Boy J, Mikutta R, Sauheitl L and Guggenberger G (2019) Carbon Investment Required for the Mobilization of Inorganic and Organic Phosphorus Bound to Goethite by an Arbuscular Mycorrhiza (Solanum lycopersicum x Rhizophagus irregularis). Front. Environ. Sci. 7:26. doi: 10.3389/fenvs.2019.00026

Nutrient supply in phosphorus (P)-limited ecosystems, with most P being associated with secondary minerals, has to rely on efficient nutrient allocation strategies, such as those involving mycorrhizal symbioses. Yet, little is known about the extent of photo-assimilate transfer to the fungal partner, who in turn mobilizes mineral-bound P sources required by the plant. This study aims to explore the carbon (C)–P trade between an arbuscular mycorrhizal (AM) plant and its ability to incorporate P from differently accessible P sources. We compared P uptake rates of AM plants for orthophosphate (OP) and phytic acid (PA), applied to mesocosms in either dissolved form or bound to goethite (α-FeOOH). The design of the mesocosms allowed the plant to only access the P in the fungal compartment via the AM hyphae. We hypothesized the AM plant to invest more C into the symbiosis, if P is present in the less accessible form. To estimate the C budget of the symbiosis, we determined total organic carbon (OC), 16:1ω5c phospholipid fatty acid (PLFA; AM fungi extraradical mycelium), 16:1ω5c neutral lipid fatty acid (NLFA; AM fungi energy storage), and CO_2 cumulative respiration in the fungal compartment. A ratio to the total C translocated into the fungal compartment (OC+CO_2-C cumulative respiration) and the P incorporated into the AM plant (Total C/P) was calculated to estimate the C investment made by the AM plant into its symbiotic partner. AM plants incorporated P derived from all four P sources exclusively via the mycorrhizal pathway in different amounts and kinetics. The Total C/P ratio was significantly larger for those AM plants accessing the goethite-bound P compounds. They also transferred significantly larger amounts of PLFA and NLFA to their fungal partner, both indicating a larger plant C investment per P taken up. Our data provide first evidence about the ability of an AM plant to incorporate P from an organic source bound to a secondary mineral. The different C investments of AM plants into P allocation from variably available sources suggests a broad nexus between P mining strategies, resource partitioning in soil, and the amounts of C accumulated in terrestrial soils.

Keywords: goethite, organic phosphorus, inorganic phosphorus, arbuscular mycorrhiza, carbon-phosphorus trading, PLFA 16:1ω5c, NLFA 16:1ω5c

INTRODUCTION

Phosphorus (P) is an essential element for plant growth and productivity. While excessive utilization of P as fertilizer has led to widespread eutrophication of inland and coastal waters (Rowe et al., 2016), its deficiency is still a major constraint to agricultural productivity, affecting an estimated area of >20 million km^2 worldwide (Oberson et al., 2001). This is especially true for tropical soils where secondary minerals immobilize P to a large extent. In 2014, phosphate rocks were included in the list of the 20 critical raw materials of the European Commission (George et al., 2016), suggesting that this finite resource could be exhausted within this century (Gilbert, 2009). Consequently, all plant strategies which increase P uptake and improve its use-efficiency will be increasingly valuable to prevent P loss to adjacent ecosystems and lower the need of P fertilizers (Smith and Smith, 2011).

Plants can only take up P as free phosphate anions, either as $H_2PO_4^-$ or as HPO_4^{2-} (Becquer et al., 2014). Phosphate concentrations in soil solutions span from 1 to 10 μM, being about 1,000-fold smaller than cellular contents in plants, thus are often insufficient for optimal growth (Smith and Smith, 2012). Soil P occurs in forms of varying accessibility to plants with >90% of it being bound in plant-inaccessible forms (Mengel and Kirkby, 2001). Phosphorus occurs either as inorganic phosphates, primarily in associations with Ca, Fe, and Al, or in organic forms. Organic P constitutes 20–80% of total soil P and includes phosphomonoesters such as inositol phosphates (IP), phosphodiesters as ribonucleic acid, deoxyribonucleic acid, lipoteichoic acid, phospholipid fatty acids, and organic polyphosphates, e.g., adenosine triphosphates. The most prevalent phosphomonoester is myo-IP6, which contains six phosphate groups bound to cyclohexane and has nine stereoisomers. The myo-IP6 stereoisomer or phytic acid (PA) is the most common form of inositol phosphates and represents >50% of the organic P in soils (Ognalaga et al., 1994; Nash et al., 2014).

Phosphorus deficiency of plants is caused by strong adsorption of inorganic and organic P to Al and Fe hydroxides and oxides (summarized as "oxides"), making large proportions of total P unavailable to plants (Osorio and Habte, 2001; Javaid, 2009). The specific adsorption and high affinity to soil oxides is greater for the organic P forms (He and Zhu, 1998). As compared to inorganic P forms, the dynamics of organic P species in soils are much less investigated. This is surprising since this fraction is highly relevant to the supply of P to crops in deeply weathered soils like Oxisols (Rodrigues et al., 2016). To overcome soil P limitation, plants developed different strategies to acquire P from soil solution. One strategy is to increase the exchange-surface of the root–soil interface; another strategy lies in solubilizing complexed P by root exudates, such as low-molecular-weight organic acids and phosphatases. The most widespread strategy nevertheless is to rely on symbiotic associations with mycorrhizal fungi and P-solubilizing or organic P-mineralizing bacteria (Richardson et al., 2009; Giles et al., 2012).

In P-deficient environments, e.g., Spodosols, Ultisols, or Oxisols (Yang et al., 2013), selection pressure commonly results in the proliferation of free-living microorganisms and symbiotic associations with mycorrhizal fungi which have the potential to mobilize and mineralize unavailable organic P (Nash et al., 2014). Most terrestrial plants form symbioses with one or more kinds of mycorrhizal fungi. About 80% of plant species are associated with arbuscular mycorrhizal fungi (AMF) (Cairney, 2000; Smith et al., 2008; Johnson, 2010), which enhance the plant's access to limiting belowground resources (Read, 1991).

Plants that establish symbiosis with an AMF can acquire part or almost all of the phosphorus for their metabolic activities, over this pathway (Javot et al., 2007; Willis et al., 2013; Lambers et al., 2015). As they are able to mine soils for P, research on P release rates from secondary minerals is important to improve models on plant nutrient cycling by AMF (Cardoso et al., 2006). Though some studies have shown that mycorrhizal and non-mycorrhizal plants seem to use the same labile P sources (Bolan et al., 1984; García, 2000; Frossard et al., 2011), others demonstrated that mycorrhizal plants obtain P from usually unavailable sources of organic and inorganic P (Rychter et al., 2016). In addition, Bolan et al. (1987) proposed that AMF may cleave the bond between Fe and P and thus release P, but they did not depict the underlying mechanisms.

Turner (2008) suggested that the different soil P species constitute a gradient of biological availability based on the plant's investment to access the phosphate. For example, phytate, being most resistant to hydrolysis, is hypothesized as the metabolically most expensive P source. This makes necessary to understand if there exists a C-P trading in arbuscular mycorrhizal symbiosis.

In return for providing almost all P needed by the AM plant, the fungus receives up to 20% of net plant photosynthates under ambient atmospheric CO_2 (Pfeffer et al., 2004). The C assimilates are transported mainly as lipid droplets and glycogen to the AM fungal hyphae (Bago et al., 2002). Recently, three publications have shown that AMF do not have the capacity to produce fatty acids completely on their own (Bravo et al., 2017; Keymer et al., 2017; Luginbuehl et al., 2017). Instead, AMF were found completely depending on plant-derived fatty acids. These studies suggest a model in which a chain length of 16 carbons (C16) b-monoacylglycerol molecules are transported from the root cell through the periarbuscular membrane to the fungus. Fatty acids of chain lengths up to C16 are needed, because the fungus apparently lacks genes encoding multi-domain cytosolic fatty acid synthase subunits. This makes fatty acids a major good of trade between plant and fungus in AM.

To compare the true costs of incorporating different P forms into the plant by the AMF pathway requires the quantification of the C fluxes. The development of AM itself already presents a complex series of trade-offs between the C cost of the fungus and the benefits of enhanced nutrient supply to the plant (Cavagnaro et al., 2008). Quantification of the fluxes in mycorrhiza is one of the most important, yet little explored tasks of mycorrhizal physiology and ecology. In order to identify the behavior of AM in mobilizing P from differently accessible P forms, we carried out a mesocosm experiment under controlled conditions. Our work aimed at (i) clarifying whether the AM plant can take up P from less accessible sources and (ii) to determine whether there exists a trading between C and P over the AM. We hypothesize that

less accessible P sources cause larger photoassimilate investments by the plant partner, resulting in differing kinetics of the AMF providing P to the host plant.

MATERIALS AND METHODS

Plant Growth and Mycorrhization

We selected the AM mycorrhizal association between *Solanum lycopersicum* L. (var. Moneymaker) x *Rhizophagus irregularis* (DAOM 197198) for our experiment. The association has been previously investigated to elucidate processes related with the nutritional benefits offered by the AMF to the tomato plant (Nagy et al., 2005; Schaarschmidt et al., 2006; Giovannetti et al., 2012). The reason for using the AMF *R. irregularis* is due to its global distribution and adaptation to intensive agricultural practices. This ubiquitous occurrence indicates that *R. irregularis* is compatible with a wide range of soil conditions like pH (5.6–8.0), P availability (0.3–18.8 mg/kg), sand content (17.5–57.0%), and C content (1.0–10.5%) (Köhl et al., 2016). *Rhizophagus irregularis* DAOM 197198 (syn: *Glomus irregulare*) recently reassigned from *Glomus intraradices* Schenck and Smith (Krüger et al., 2012) was used as the mycorrhizal inoculum. It consisted of 0.4 g of spores, hyphae, and root fragments from a *Sorghum bicolor* trap plant culture (Brundrett, 1996). Seeds of *Solanum lycopersicum* L. var. Moneymaker (Volmary GmbH) were surface sterilized with 5% H_2O_2 for 10 min and washed three times with sterile distilled water. Seeds were germinated on petri dishes for 3 days at 27°C. Moneymaker germinated seeds were sowed on 75 ml pots QP96 (HerkuPlast Kubern GmbH) containing the AM inoculum and 70 ml autoclaved acid washed quartz sand, which has been successfully used as plant and fungal growth substrate before (Johansen et al., 1996; Olsson and Johansen, 2000). Allowing the AM mycelium to grow from a colonized root into purified quartz sand, a relatively pure mycelium could be extracted and used for our studies. Mycorrhized and non-mycorrhized control tomato plants were grown in a greenhouse (16/8 light/dark, 24/20°C light/dark, 50–60% relative humidity, photon flux density of 175–230 μmol/m/s). Seedlings were watered every day with 10 ml deionized water and were fertilized with 5 ml low P (0.32 mM) Long Ashton nutrient solution pH 6.5 (Hewitt, 1966) on alternate days. The complete root system of 10 individuals was processed to test for the presence of arbuscular mycorrhiza in the roots of 4 week old plants before transplanting. A root subsample was digested with 10% KOH (35 min, 95°C) and stained using the ink and vinegar staining technique for AMF (Vierheilig et al., 1998b). Stained root fragments were mounted on glass slides and observed at 400× magnification using an Olympus BH2 microscope (Olympus Optical Company Ltd, Tokyo, Japan), to determine the mycorrhizal status using the methodology from McGonigle et al. (1990), before the plants were transplanted to the mesocosms.

Mesocosm Experiment

Each mesocosms consisted of a plant compartment connected to a fungal compartment in which only the mycelium was able to develop and access the different P sources due to two barriers (**Figure 1**). Each mesocosms was fabricated from a Nalgene® 250 ml square polypropylene bottle cut at 45° angle. The threaded section of the bottle was glued with Pattex ® hot glue on the side with the largest surface of the bottle base. A second Nalgene®100 ml square polypropylene bottle was cut into two sections, one as irrigation compartment (30 ml) and the second as support for the mesocosms. Through a 3 mm diameter perforation at the base of the plant compartment, a 3 mm diameter fiberglass wick (Ortmann Kapillarbewässerung, Vlotho, Germany) was passed through, leaving 5 cm of the wick inside the irrigation compartment, where twice a week 10 ml deionized water were applied (**Supplementary Figure 1**). The wick irrigation system operates in a closed cycle, without runoff and covers maximum water requirements of the plant (Son et al., 2006; Kuntz, 2013). At the plant compartment side a polyamide mesh with a pore size of 20 μm and 30 mm side (Franz Eckert GmbH) separated mycorrhizal roots and mycelium (Watkins et al., 1996; Fitter et al., 1998). The second barrier was a 25 mm diameter polytetrafluoroethylene membrane with a pore size of 5–10 μm (Pieper Filter GmbH). The second membrane allowed the AM hyphae to cross but prevented mass flow and diffusion of ions into the plant compartment (Mäder et al., 1993, 2000; Vierheilig et al., 1998a). Hence, P sources were exclusively accessible to the plant by the hyphae. There were no other P sources present in the system as the cultivation substrate in the plant compartment consisted of acid washed quartz sand (1–2 mm) free of nutrients (data not shown). Four-week-old mycorrhized and non-mycorrhized seedlings were transplanted into each mesoscosm and placed in a glasshouse under controlled climatic conditions (24/20°C light/dark; photoperiod 16/8 h light/dark; 50–60% relative humidity; photon flux density of 175–230 μmol/m^2/s).

Once a week all mesocosms were rotated to achieve homogeneous growth conditions and were fertilized twice a week on top of the plant substrate with 5 ml no-P Long Ashton nutrient solution at pH 6.5 (Hewitt, 1966). The P sources offered in the fungal compartment, including the control treatments, are summarized in **Table 1**. The 55 ml volume of the fungal compartment was amended by a total P amount of 30 mg and water volume was adjusted to field capacity. The water volume at the fungal compartment was determined with a time-domain reflectometry probe Trime Pico connected to a Trime-FM version P2 (Imko Micromodultechnik GmbH, Ettlingen, Germany). The treatments containing quartz sand as a substrate (60 g) in the fungal compartment exhibited 19% water volume while the ones containing goethite (24.3 g) exhibited 41% water volume. The water volume was checked once a week and amended with autoclaved MilliQ water to field capacity. A nylon black cloth with a 1 mm pore was placed on the mouth of the fungal compartment to prevent algae growth, water evaporation and to facilitate gas diffusion to the outside of the fungal compartment (**Supplementary Figure 1**).

The P uptake and C investment was tracked for 91 days. The first harvest point was on the day of transplanting (day 0) to determine the P stocks of the plants ($n = 5$), followed by another six sampling points at days 7, 21, 35, 49, 77, and 91. In each of the six harvest points, three biological replicates of each treatment were processed.

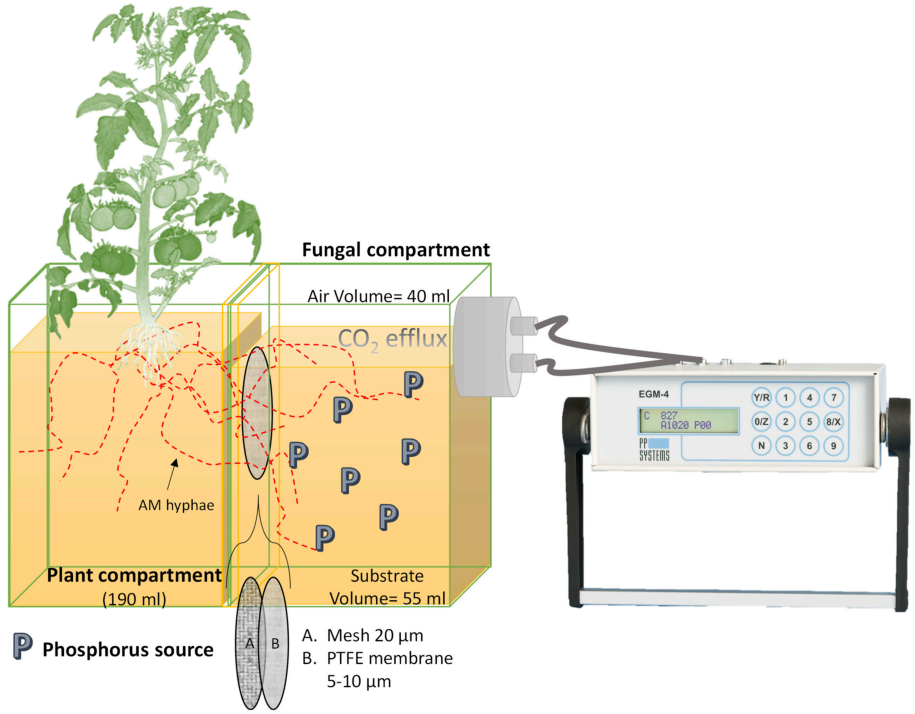

FIGURE 1 | Mesocosm design. The mesocosms is made of a plant compartment (PC) linked to a fungal compartment (FC). Only the AMF is able to access the P sources located in the FC. In between both compartments, two membranes prevent roots from entering the FC, a 20-µm polyamide mesh and a polytetrafluoroethylene (PTFE) membrane with a pore size of 5–10 µm. The PTFE membrane does not allow mass flow and diffusion of ions to the PC. The FC is connected to the CO_2 measuring device (EGM-4) allowing its assembly every time a measurement is made.

TABLE 1 | Description of the treatments tested by the time course experiment.

Treatment	Treatment code	Fungal compartment (Total volume: 55 ml)	P content (mg)
Mycorrhizal plant without P	M+	Acid washed quartz sand (Awqs) (60 g) + MilliQ water (16 ml)	0
Non mycorrhizal plant without P	M-	Awqs (60 g) + MilliQ water (16 ml)	
Mycorrhizal plant with goethite	GOE	Goethite (24.3 g) + MilliQ water (28 ml)	
Mycorrhizal plant with orthophosphate bound to goethite (1.24 mg P/g)	GOE-OP	GOE-OP (24.3 g) + MilliQ water (28 ml)	30
Mycorrhizal plant with phytic acid bound to goethite (1.79 mg P/g)	GOE-PA	GOE-PA (16.7 g) + Goethite (7.6 g) + MilliQ water (28 ml)	
Mycorrhizal plant with orthophosphate (KH_2PO_4)	OP	Awqs (60 g) + MilliQ water (16 ml P solution)	
Mycorrhizal plant with phytic acid ($C_6H_{18}O_{24}P_6$)	PA	Awqs (60 g) + MilliQ water (16 ml P solution)	

Preparation of Phosphorus Sources and Phosphorus Desorption

Each P source was placed inside the fungal compartment as explained in **Table 1**. The orthophosphate (OP) source was added as KH_2PO_4 (Sigma Aldrich, Taufkirchen, Germany) and the organic P source was added as phytic acid (PA) sodium salt hydrate (Sigma Aldrich). Two adsorption complexes were produced using the OP and the PA bound to goethite. The adsorption complexes were prepared equilibrating the P compounds with goethite (Bayferrox 920 Z). First, 50 g of goethite were equilibrated for 16 h in 250 ml MilliQ H_2O adjusted to pH 4. Then, 250 ml MilliQ H_2O containing either 17 g KH_2PO_4 or 0.7191 g $C_6H_{18}O_{24}P_6$ were added to the goethite suspension and equilibrated for 48 h on an overhead shaker. The goethite-P suspensions were centrifuged (3,000 × *g*, 15 min) and the pellets were subsequently washed with MilliQ H_2O until the electric conductivity was <40 µS/cm. The resulting goethite-P associations were shock-frozen in liquid N_2, and freeze-dried. The OP and PA bound to the goethite adsorption complexes was determined in triplicate by hydrolysing 5 mg of the goethite-P associations in concentrated HNO_3 and subsequent measurement of P contents by ICP-MS Agilent 7500C (Agilent Technologies Ireland Ltd., Cork, Ireland). The adsorption complexes contained 1.24 mg P/g in case of GOE-OP and 1.79 mg P/g for GOE-PA, respectively. A second analysis on the adsorption complexes was carried out to determine the

amount of desorbable P, by shaking 1.0 g of each goethite-P association ($n = 3$) in 30 ml of MilliQ water for 24 h on an overhead shaker. The centrifuged supernatant (3,000 × *g*, 15 min) was filtered through a 0.45 μm syringe filter (PVDF) and 1 ml was mixed with 1 ml 30% HNO_3 and the mixture was filled up to 10 ml with MilliQ water and P content was then measured by ICP-MS.

Plant and Fungal Phosphorus Contents

At each harvest point, shoots and roots were air dried (70°C, 48 h), weighed and ball milled. Plant samples were incinerated at 480°C for 8 h, digested with 1 ml 30% HNO_3, filtered and analyzed by ICP-MS. The P stocks were determined for the whole plant. The amount of total P incorporated by the AM plant over time was calculated as the difference of the P stock at each harvest point and the P stock initially present in the transplanted plant on day 0 (determined from five subsamples). The separation of hyphae/spores took place on day 91 following a modified method of Brundrett (1996). First, 4 g of goethite-P associations (GOE-OP, GOE-PA) or 10 g of sand (OP, PA) were sampled from each fungal compartment in 50 ml Falcon test tubes. Tubes were then filled with a fixative solution (0.9 g/l NaCl plus 3% glutaraldehyde), equilibrated for 2 h on an overhead shaker, and then centrifuged (3,000 × *g*, 15 min). The supernatant was filtered through a polyethersulfone 0.45 μm filter (Supor® PES membrane disc filters, Pall Life Sciences, Hampshire, UK), using a vacuum pump system. Pellets were re-suspended in a 50% sucrose solution by vigorously shaking plus an equilibration step (1 h) on an overhead shaker. The samples were then centrifuged for 15 min at 3,000 × *g* to facilitate the separation of hyphae and spores in the glucose density gradient. Immediately after centrifugation, hyphae and spores in the sucrose supernatant were poured onto the same polyethersulfone 0.45 μm filter and carefully washed with MilliQ H_2O to remove the sucrose and the fixative solution. This step was repeated three times per sample. After rinsing the hyphae and spores, the filters were placed in petri dishes. The hyphae/spores were collected under a stereomicroscope with a glass pipette and deposited in 2 ml Eppendorf tubes. The fungal material was air-dried at 50°C for 96 h. The P content (P mg /hyphae mg) was determined for an aliquot of fungal material. Samples were incinerated at 480°C for 8 h, digested with 1 ml 30% HNO_3, filtered, and analyzed by ICP-MS. Additionally, the P stock incorporated into the plant tissues at day 91 was calculated as the percentage of the initial total 30 mg P offered at the fungal compartment, for each P source.

Organic Carbon and Carbon Dioxide Production at the Fungal Compartment

At each harvest point, 2 g from each fungal compartment were air-dried (70°C, 48 h), weighed, and ball milled. The C content of these samples was measured using an Elementar vario MICRO cube C/N analyzer (Elementar GmbH, Hanau, Germany). For the calculation of the C stock in the fungal compartment, it was multiplied the C content (mg/g), determined at the analyzer, by the total weight of substrate in the fungal compartment reported in **Table 1**. As there was no inorganic C in the fungal compartment, all C measured in the fungal compartment was considered as organic carbon (OC).

The CO_2 efflux (mmol CO_2 m^2 h^{-1}) was measured in the fungal compartment twice a week using an EGM-4 infrared gas analyzer (PP-systems, Hitchin, UK), a close dynamic system (Vermue et al., 2008). At each measuring point, the black cloth was removed, the airtight lid was placed in the mouth of the fungal compartment and the inlet and outlet tubes were connected to the EGM-4 (**Supplementary Figure 1**). CO_2 efflux was automatically calculated for a headspace volume of 40 ml and an exposed area of 0.0012 m^2 of the fungal compartment. The CO_2 content was measured every 4.8 s and the CO_2 flux was measured for at least 3 min or until a good quadratic fit was obtained. Cumulative CO_2 production was calculated in mg by interpolation using a cubic spline function (Gentsch et al., 2018) for each fungal compartment.

At each time point, the Total C/P ratio was used to evaluate and estimate the investment made by the AM plant into its symbiotic partner at the fungal compartment per plant P incorporated (Equation 1), since all the C measured at the fungal compartment, in the form of total OC and cumulative CO_2-C will be exclusively carried by the AMF.

$$\text{Total C/P} = \frac{(\text{OC (mg)} + \text{cumulative } CO_2 - \text{C (mg)})}{\text{P incorporated } \left(\text{total mg per plant}\right)} \quad (1)$$

Where OC is the total C (mg) per fungal compartment; cumulative CO_2-C is the total C present in the cumulative respired CO_2 (mg) at the fungal compartment.

Fatty Acid Analysis and *R. irregularis* Biomass Estimation

Using a chloroform-methanol-citrate buffer (1:2:0.8 v/v/v), lipids were extracted twice from 16 g of fungal compartments containing quartz sand or 8 g for the ones with goethite. Thereafter, extracts were fractionated by solid phase extraction with activated Silica gel (Sigma Aldrich, pore size 60 Å, 70–230 mesh) into neutral lipid fatty acids (NLFA), glycolipids, and phospholipid fatty acids (PLFA) by elution with 5 ml of chloroform, 20 ml of acetone, and 20 ml of methanol, respectively. The PLFA and NLFA samples were subjected to mild alkaline methanolysis, which transformed the neutral lipids and the phospholipids into free fatty acid methyl esters, as outlined in Frostegård et al. (1991) with modifications by Bischoff et al. (2016). The methyl esters were then separated by gas chromatography using an Agilent 7890A GC system (Agilent Technologies Ireland Ltd., Cork, Ireland) equipped with a 60 m Zebron capillary GC column (0.25 mm diameter and 0.25 μm film thickness; Phenomenex, Torrance, California, USA) and quantified with a flame ionization detector, using He as carrier gas. Glyceryl tridodecanoate (25 μg) and nonadecanoic acid (25 μg) were used as internal standards during the extraction and tridecanoic acid methyl ester (15 μg) was added to each sample and standard before analysis as a recovery standard. Identification of the fatty acids was achieved by use of the relative retention times, in comparison to that of the internal

standard using the GC ChemStation (B.03.02.341) software (Agilent Technologies Ireland Ltd., Cork, Ireland).

The AMF *R. irregularis* DAOM 197198 model organism (Daubois et al., 2016) has a fatty acid composition ranging from C16:0 to C22:2 with 16:1ω5 as major fatty acid (Aarle and Olsson, 2003; Calonne et al., 2010; Wewer et al., 2014). The PLFA 16:1ω5c can be used for evaluating the amount of extraradical mycelia of AMF, making it a good predictor for the amount of C allocated to AMF (Olsson and Johansen, 2000; Aarle and Olsson, 2003; Marschner, 2007). In addition, the NLFA 16:1ω5c is considered a good predictor on energy storage by the fungus (Bååth, 2003). NLFA are stored in intraradical vesicles, spores, extraradical mycelium and make up a large proportion of the AM fungal biomass. They are metabolized in the mycelium through the glyoxalate cycle, and might provide the major fungal energy source as respiratory substrate (Olsson and Wilhelmsson, 2000; Aarle and Olsson, 2003; Olsson and Johnson, 2005). Therefore, PLFA and NLFA 16:1ω5c were analyzed to assess the biomass and energy storage of AMF in the fungal compartment, respectively (Johansen et al., 1996; Olsson et al., 1997, 2002; Larsen et al., 1998; Stumpe et al., 2005). Ratios of 16:1ω5c PLFA to plant P uptake (Equation 3) and NLFA to plant P uptake (Equation 4), were used to estimate the investment made by the tomato plants into their fungal partner in either biomass or energy storage to obtain P from each source, respectively. The NLFA 16:1ω5c/PLFA 16:1ω5c ratio (Equation 5) was calculated as an index for the growth strategy of *R. irregularis* (Green et al., 1999; Rinnan and Bååth, 2009). For each P source, the mean NLFA 16:1ω5c/PLFA 16:1ω5c ratio was calculated for sampling points belonging to the periods where no P incorporation was detected in the AM plant tissue as well as for those where we detected P in the AM plant.

$$\frac{\text{PLFA } 16:1\omega5c}{\text{P}} = \frac{\text{PLFA } 16:1\omega5c \text{ (total ug at the fungal compartment)}}{\text{P incorporated (total mg per plant)}} \quad (2)$$

$$\frac{\text{NLFA } 16:1\omega5c}{\text{P}} = \frac{\text{NLFA } 16:1\omega5c \text{ (total ug at the fungal compartment)}}{\text{P incorporated (total mg per plant)}} \quad (3)$$

$$\frac{\text{NLFA}}{\text{PLFA}} = \frac{\text{NLFA } 16:1\omega5c \text{ (total ug at the fungal compartment)}}{\text{PLFA } 16:1\omega5c \text{ (total ug at the fungal compartment)}} \quad (4)$$

A high NLFA 16:1ω5c/PLFA 16:1ω5c ratio indicates preferential C allocation to storage products in form of neutral lipids. Moreover, the ratio identifies the origin of the 16:1ω5c fatty acid. At NLFA 16:1ω5c/PLFA 16:1ω5c>1, the majority of this fatty acid is considered to originate from AM fungi and not from bacteria (Olsson, 1999; Hammer et al., 2011a; Vestberg et al., 2012; Cozzolino et al., 2016). To estimate the amount of AMF grown in the fungal compartment, we used a conversion factor of 1.2 nmol PLFA 16:1ω5c per mg dry hyphae (Olsson and Johansen, 2000; Olsson and Wilhelmsson, 2000; van Diepen et al., 2010). The estimated total AM biomass was used together with the fungal P content to infer the P stock incorporated by the AMF. Furthermore, we calculated the percentage of the initial total 30 mg P offered at the fungal compartment incorporated into the AMF biomass at day 91, for each P source.

Data Analysis

The normality of the data was verified with the Shapiro-Wilk's test and homogeneity of variances using the Levene's test. One-way ANOVA analysis of the variance and the Tukey *post-hoc* test (**Supplementary Tables 1–6**) were employed to test for differences of mean values ($P < 0.05$) of measured variables between the treatment groups, presented by the different P sources offered in the fungal compartment. Data analysis was performed using SPSS v.24 for Windows (IBM Corporation, 2016).

RESULTS

Phosphorus derived from each offered source was incorporated by the AM tomato plants, while none of the controls (GOE, M+, and M−; **Table 1**) showed P incorporation (**Figure 2**). Those AM plants which had access to OP incorporated the highest amount of P, followed by PA, GOE-OP, and GOE-PA. The first P incorporation was detected at day 49 in case of the treatments offering OP and PA and at day 77 in case of GOE-OP and GOE-PA as P sources. At day 91, AM plants reached the maximum P incorporation, with P taken up in the following order: OP (30.4% of the initially added P) > PA (10.4%) > GOE-OP (5.9%) > GOE-PA (2.1%) (**Figure 3**).

AM plants with access to OP had significantly larger P contents in their hyphae and spores, followed by plants supplied with GOE-OP and PA. The GOE-PA and M+ (day 0) treatments exhibited significantly smaller P contents in the AMF (**Figure 4**). Although the hyphal content of P was significantly larger for the fungal compartment containing OP, the total amount of P accumulated in the hyphae was smaller, as there was significantly less AMF biomass. On average, the extraradical hyphae accumulated less P in the fungal compartment containing OP (0.03 mg P; 0.1%) and PA (0.015 mg P; 0.05%) as compared to the goethite-bound forms GOE-OP (2.39 mg P; 8%), and P for

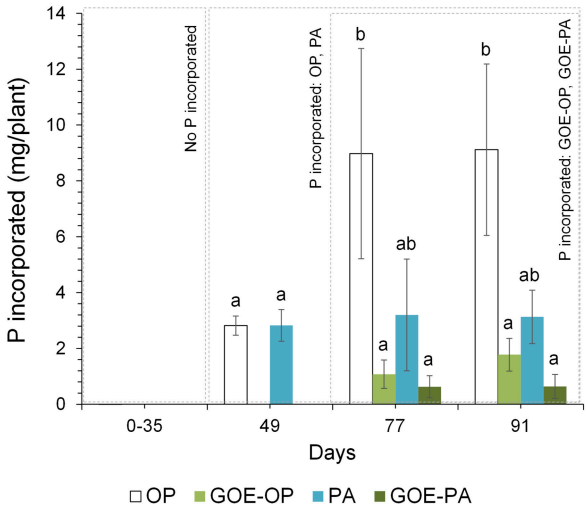

FIGURE 2 | Total P (mg) incorporated by the AM tomato plant from the different P sources over 91 days. Each bar indicates the mean of three biological replicates and error bars are standard error. Within each P source and day, treatments with significant differences are labeled with different letters ($p < 0.05$) as result of a one-way ANOVA.

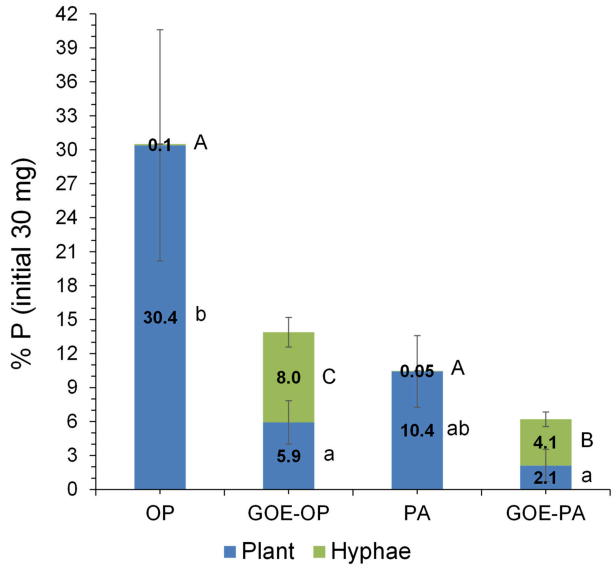

FIGURE 3 | P stocks compartmentalized into plant tissues and external hyphae at day 91 (percentage of the initial total 30 mg P offered at the fungal compartment). Bars indicate the mean of three biological replicates and error bars are standard error. Within each P source and plant/hyphae, treatments with significant differences ($P < 0.05$) are labeled with different lowercase letters for P% Plant stock and capital letters for P% hyphae stock lowercase as result of a one-way ANOVA.

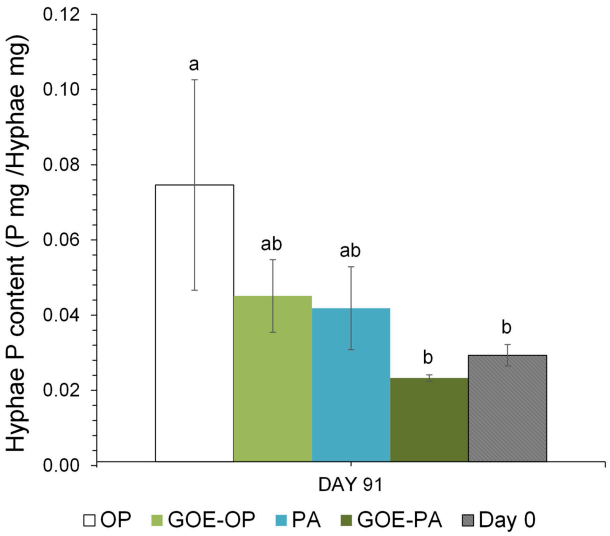

FIGURE 4 | Total P content in the hyphae (P mg/Hyphae mg) grown at the fungal compartment for the different P sources on day 91, when the maximum P mobilization was achieved in the four treatments. Each bar indicates the mean of three biological replicates and error bars are standard error. Within each P source, treatments with significant differences are labeled with different letters ($P < 0.05$) as result of a one-way ANOVA.

GOE-PA (1.22 mg P; 4.1%) (**Figure 3**). When these P amounts are summed up to the P incorporated by the plant, *R. irregularis* mobilized 9.15 mg P (30.5% of the initially added P) from the OP, followed by GOE-OP (4.17 mg P; 13.9%), PA (3.14 mg P; 10.5%), and GOE-PA (1.86 mg P; 6.2%) (**Figure 3**). Compared to that, P desorption from the goethite in water was 7.4% for GOE-OP and 1.2% for GOE-PA. These proportions corresponded to P amounts of 2.2 ± 0.25 mg in the GOE-OP treatment and 0.35 ± 0.008 mg P in the GOE-PA treatment, which likely were mobilized by desorption processes. Hence, the difference between the P incorporated in the plant tissues/AM mycelium and the P desorbed in water of the goethite-bound P sources, resulted in a net P mobilization from the goethite complexes by the AMF between 5% (GOE-PA) and 6.5% (GOE-OP) of the initially added P.

Organic C contents (mg/g fungal compartment) show that the M- control treatment did not accumulate any C throughout the experiment. From day 7 to day 91, fungal compartments containing OP, PA and M+ control showed significantly smaller accumulation of OC compared to GOE-OP, GOE-PA, and GOE control. From day 7 to 77, the fungal compartment containing PA showed significantly larger OC contents than those with OP and control without P (M+) (**Figure 5A**). The same occurred for fungal compartments containing GOE-PA as compared to those with GOE-OP and GOE control (**Figure 5A**).

In case of cumulative CO_2 production (mg/g fungal compartment), the M- treatment, without mycorrhiza and without P, showed significantly smaller production than any other treatment (**Figure 5B**). Fungal compartments containing OP, PA and the M+ control showed significantly smaller cumulative CO_2 production from day 7 to 91 as compared to the production of GOE-OP, GOE-PA, and the GOE control. The cumulative CO_2 production showed no significant difference between those containing OP, PA and the M+ control. Throughout the experiment, the GOE control showed significantly larger cumulative CO_2 production values than any other treatment.

At days 77 and 91, when AM plants reached their maximum P incorporation, the Total C/P was significantly higher for those AM plants that had access to GOE-OP, GOE-PA, and PA, as compared to OP (**Figure 6**). The P incorporated from GOE-OP showed larger PLFA 16:1ω5c/P ratios than the OP and PA treatments at days 77 and 91, while for GOE-PA this ratio was larger than for OP and PA at day 91 only (**Figure 7A**). The NLFA 16:1ω5c/P was significantly larger for both P sources bound to goethite in comparison to OP and PA (**Figure 7B**). For all P sources, the NLFA 16:1ω5c/PLFA 16:1ω5c ratio was above one, meaning that the PLFA and NLFA originated largely from AM fungi (**Figure 7C**). The NLFA 16:1ω5c/PLFA 16:1ω5c ratios increased for all AM plants accessing a P source in the fungal compartment during the period of P incorporation. The NLFA 16:1ω5c/PLFA 16:1ω5c ratio showed always significant larger values for the treatment offering GOE-OP as P source.

DISCUSSION

Phosphorus Plant Uptake From Different Sources

We tested the role of AMF in taking up P from four different sources having a different accessibility. For this, a mesocosm was designed where exclusively the AM hyphae were involved in plant

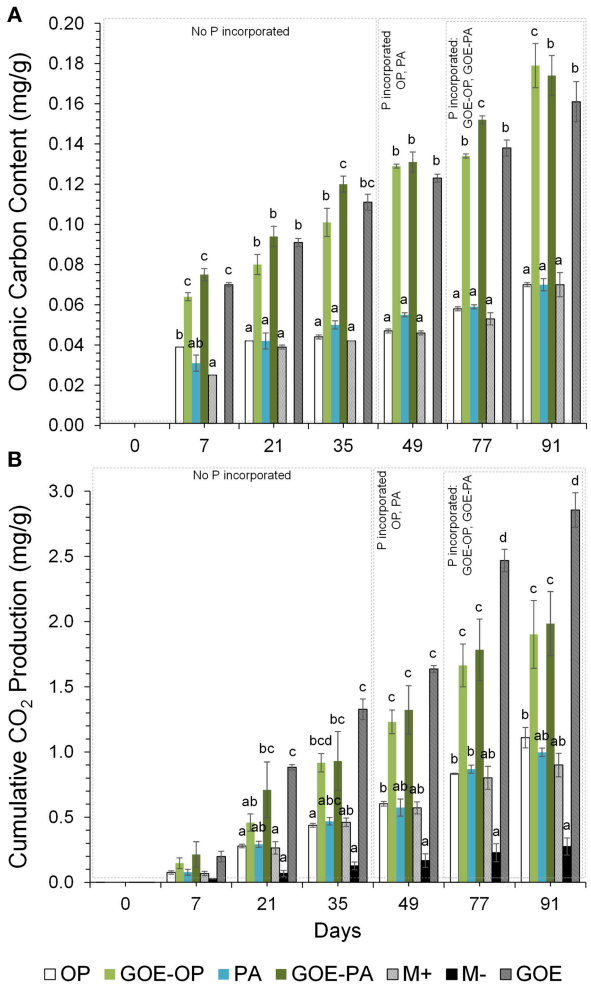

FIGURE 5 | (A) Organic carbon content (mg/g fungal compartment). Each bar indicates the mean of three biological replicates and error bars are standard error. **(B)** Cumulative CO_2 production (mg/g fungal compartment). The bars show the mean of three biological replicates and error bars are standard error. Within each P source and day, treatments with significant differences are labeled with different letters ($P < 0.05$) as result of a one-way ANOVA.

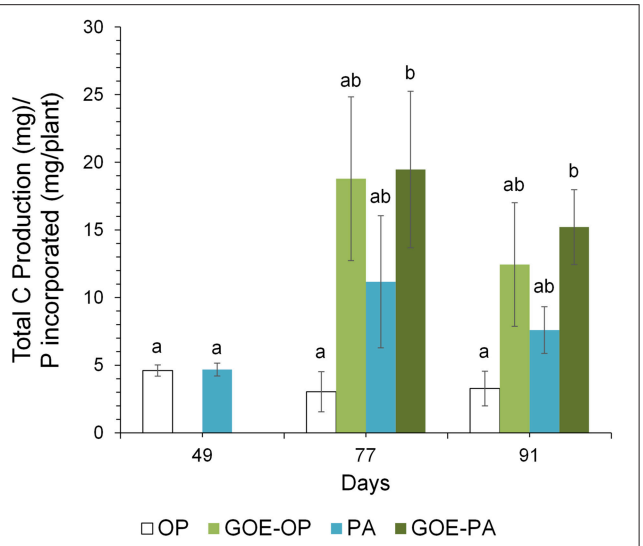

FIGURE 6 | Mean values and standard errors ($n = 3$) of the total C/P ratio. Within each P source and day, treatments with significant differences are labeled with different letters ($P < 0.05$) as result of a one-way ANOVA.

P acquisition. Our results indicate that all AM plants colonized with *R. irregularis* incorporated P derived from inorganic (OP) or organic (PA) sources, no matter if added either in their free form or bound to goethite. Phosphorus from the different P forms was taken up in different amounts and kinetics via the mycorrhizal pathway. In contrast to other studies where roots and hyphae are only separated by a 20 μm nylon mesh (Argüello et al., 2016; Jakobsen et al., 2016; Zhang et al., 2016; Sawers et al., 2017), the hydrophobic polytetrafluoroethylene membrane used in our mesocosms avoided not only the direct P uptake by roots, but also the influence of root exudates and the diffusive transport from the fungal compartment to plant compartment, as well as the P absorption by the roots. This membrane type has been successfully used in other studies investigating on nitrogen transfer by AMF (Mäder et al., 1993, 2000; Frey et al., 1998), but not for P nutrition via the mycorrhizal pathway. The hydrophobic and selective nature of this barrier, however, is of paramount importance for separating the effects of the root and the fungus and quantifying the nutrient fluxes. These first results do thus not only give evidence of the importance for mycorrhiza in the uptake of P but also proof the advantage of hydrophobic polytetrafluoroethylene membranes (**Figure 1**).

Plant P incorporation appeared quickest in OP and PA treatments, followed 1 month later by the P forms bound to goethite. In addition, P from the freely accessible forms of OP and PA was incorporated to a greater extent (**Figure 2**). The faster plant P uptake in case of OP can be explained by the fact that an AM plant can absorb OP directly via the mycorrhizal pathway (Smith et al., 2003). Usually most of the studies on plant nutrition only consider inorganic phosphate—but not the organic P fraction—as biologically available, even though organic P represents the major part of the total soil P (Turner, 2008). To be available for the plant, PA has to be hydrolyzed first by phytases, a group of phosphatases, which are either of plant or microbial origin (Li et al., 1997; Baldwin et al., 2001, 2008; Javaid, 2009). In our study we did not measure enzymatic activities, but it has been demonstrated that *R. irregularis* DAOM 197198 is able to secrete acid phosphatase, which contributes to the mineralization of P-bearing organic compounds in soil and thus increases the concentration of available inorganic P (Tisserant et al., 2012). Tarafdar and Marschner (1994a,b) reported the mobilization of organic P sources for plant P uptake by exudation of fungal acid phosphatase in an experiment using *Glomus mosseae*. Accumulating evidence suggests that *Rhizophagus* species can hydrolyze organic P forms and the resultant inorganic P can be taken up and transported to host roots (Joner et al., 2000; Koide and Kabir, 2000; Sato et al., 2015). Utilization of organic P is thus assumed to contribute in a comparable manner to AM plant P nutrition as inorganic P (Feng

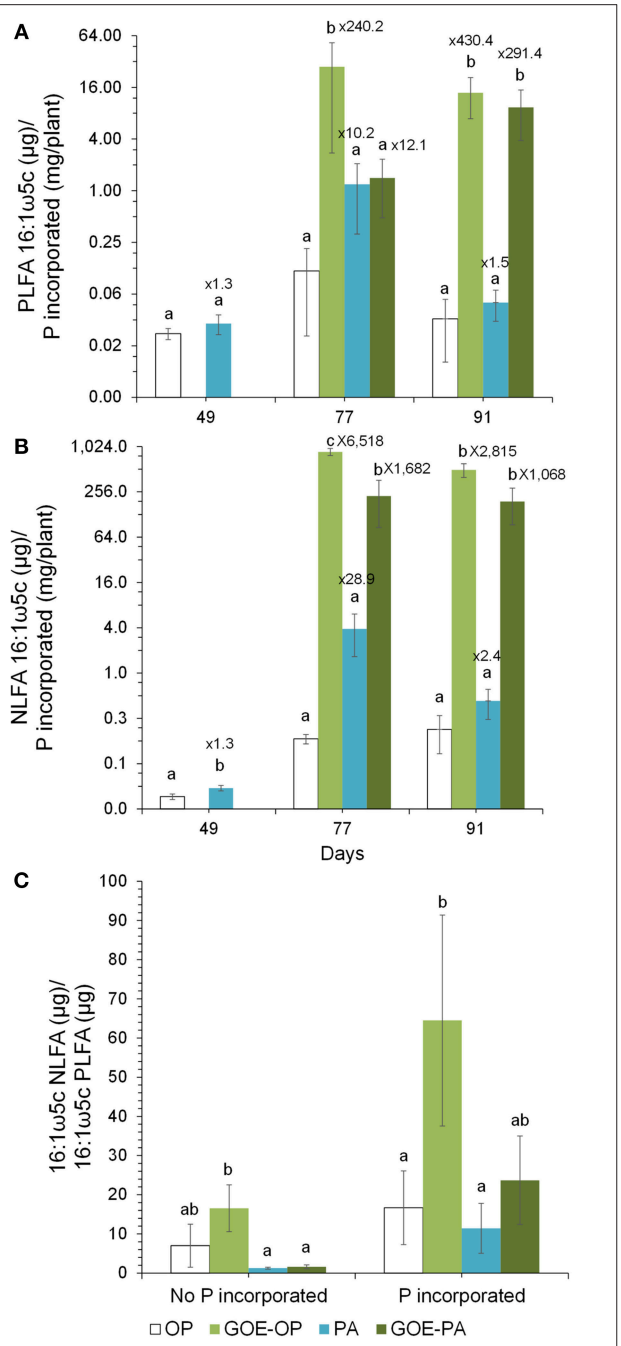

FIGURE 7 | Ratios of PLFA 16:1ω5c to P incorporated within the tomato plant **(A)** and ratio of NLFA16:1ω5c to P incorporated within the tomato plant **(B)** from the different P sources along the time course experiment. Shown are mean values and standard errors ($n = 3$). Within each P source and day, treatments with significant differences are labeled with different letters ($P < 0.05$) as result of a one-way ANOVA. The numbers on top of each bar represent a multiplication factor compared to the P source with the lower ratio value. In all cases, the P source with the lowest ratios was OP. **(C)** Ratio of NLFA 16:1ω5c to PLFA 16:1ω5c. Shown are the mean values and standard errors of the NLFA 16:1ω5c/PLFA 16:1ω5c ratio for the sampling points belonging to the periods where no P incorporation was detected in the AM plant tissue as well as for those where we detected P in the AM plant. Within each P source, treatments with significant differences are labeled with different letters ($P < 0.05$) as result of a one-way ANOVA.

et al., 2003), as we did not find significant differences among the amount of P mobilized from OP and PA.

We also did not find differences in the amount of P incorporated into the plant between the treatments offering GOE-OP and GOE-PA as P sources. Phosphorus from both P-goethite associations was incorporated by the mycorrhizal plant on average less and also later than free OP. Concerning OP, our results support earlier conclusions by Parfitt (1979), who provided the only available study addressing the mobilization of OP adsorbed to goethite. They showed that *Lolium perenne* mycorrhized with *Glomus tenuis* desorbed phosphate from goethite after 55 days. However, in this experiment there was no physical separation between the plant and hyphae. For that reason, Parfitt's results should be interpreted with caution, as desorption may be partially caused by the acidification of the rhizosphere mediated by root exudates containing an excess of protons, and not exclusively by the AMF (Hinsinger and Gilkes, 1996). To our knowledge, this is the first experiment proving that an AM plant incorporated P from PA bound to a secondary mineral. Noteworthy, the amounts of mobilized P were larger than the portion of most weakly sorbed PA, as determined in the separate desorption experiment. This finding suggests that AMF play an active role in the mobilization of mineral-bound P. A possible mechanism used by AMF to desorb P from the surface of the goethite is through the release of exudates containing organic acids, as observed by Tawaraya et al. (2006). The delay to incorporate P from GOE-OP and GOE-PA associations may be due to two reasons: firstly, both P forms had to be desorbed from the goethite by means of organic acids; with the P diffusion being likely impaired in the goethite substrate. Secondly, in contrast to the desorbed OP, the released PA had still to be hydrolyzed through the action of phosphatases.

AMF not only supplied P to the plant, but also accumulated it into the hyphae grown in the fungal compartment. On the one hand, the P contents in the AM hyphae were larger for the treatments offering free P forms OP and PA, followed by those treatments offering GOE-OP and GOE-PA as P sources (**Figure 4**). On the other hand, the P stocks in the fungal biomass for OP and PA were significantly smaller than those determined in GOE-OP and GOE-PA (**Figure 3**). Thus, the P from the goethite-bound forms was evenly distributed between the fungus and the plant, while the non-bound forms were preferably incorporated into the plant. Our results point to a smaller P content inside the hyphae growing in the fungal compartments with the lees P accessible sources, GOE-OP and GOE-PA. This result would be in accordance with the observations made by Ezawa et al. (2002), who found that the P content in the hyphae appears to respond flexibly to P availability in the environment, varying its internal content proportionally.

Rhizophagus irregularis did not transfer all of the mobilized P from the goethite sources to the plant but stored it within its hyphae, as a potential strategy of the fungus to accumulate P under deficient conditions to keep a well-balanced homeostasis (Solaiman et al., 1999). Another possible interpretation of the P accumulation within the hyphae/spores in a broader sense, could be significant from the perspective of the AM plant in the common mycorrhizal network, where accumulated P indicates a

likely support for the growth of a new mycelium and maybe even act as an "entrance fee" for a new colonization (Olsson et al., 2008; Hammer et al., 2011b). Likewise, this accumulation of P would not be a futile waste of energy, due to the fact that P storage within microbial biomass may account for 1–10% (10–100 kg of P/ha) of the total soil P (Richardson, 2001) and may become available to plants once the microbes die (Deubel and Merbach, 2005).

Carbon and Phosphorus Trading

No OC was detected in the fungal compartment for M- control treatment, while treatments containing PA and goethite-P associations showed larger OC contents as compared to those fungal compartments for OP and control M+ (**Figure 5A**). AMF tends to develop more readily under nutrient-poor conditions than under nutrient-rich or heavily P-fertilized conditions (Bryla and Eissenstat, 2005; Olsson et al., 2010), as would be the case for those fungal compartments where there was GOE, PA and sources of goethite-P. Before any P was incorporated between days 0 and 35, the GOE-OP, GOE-PA and GOE treatments exhibited significantly higher OC contents. The data suggests that OC increased more rapidly in those fungal compartments containing goethite compared to fungal compartments with OP or PA. Supposedly, this is due to a greater investment of photoassimilates via the AMF to mobilize less accessible forms before and during the P acquisition. The organic substances exuded by the AMF may be also well stabilized against fast microbial decomposition, as goethite effectively binds organic molecules via ligand exchange below its point of zero charge (Kaiser and Guggenberger, 2007).

Along with the larger OC contents in the fungal compartment of the AM plants, we detected a larger CO_2 production at all sampling points in any of the AM plant treatments, especially those where goethite was present, as for the M- treatment (**Figure 5B**). The total CO_2 production might have been a bit overestimated as we also measured a small CO_2 production in the M- treatment, which was likely caused by gas permeability of the two membranes between the plant and the fungal compartment. We also cannot exclude the presence of root CO_2 production in treatments with AM plants. However, similar mesocosm systems were used to indirectly estimate CO_2 production of extraradical mycelium (Heinemeyer et al., 2006; Nottingham et al., 2010; Karasawa et al., 2012), and different calculations were applied to estimate the contribution of AM extraradical mycelium, such as the difference in total CO_2 emission between AM and non-AM fungal compartments (Karasawa et al., 2012). We did not indirectly estimate the CO_2 production of the extraradical mycelium as a variable soil nutrient availability is known to demand different amounts of root and respiratory energy (Atkin et al., 2009). In line with Atkin et al. (2009), we could show that AM tomato plants were associated with larger CO_2 rates in the fungal compartment compared with M- plants and increased soil CO_2 release. The nature of the respired CO_2 at the fungal compartment, is the sum of the autotrophic and the heterotrophic respirations. The autotrophic respiration comprises the fraction derived from current photosynthates (Olsson et al., 2005). In our case includes the respiration by mycorrhizal fungi, and likely other microorganisms using C that has been recently fixed by plant photosynthesis, since we inoculated the plants with *R. irregularis* carrying the microorganisms naturally associated with its hyphosphere. The heterotrophic respiration is due to the decomposition of OC (Kuzyakov and Gavrichkova, 2010) made up mostly of dead hyphae and bacteria, mediated by the microbes present at the fungal compartment. Taking together the results of OC content and CO_2 production in the fungal compartment, we can assume that treatments containing less accessible phosphorus sources showed higher C investments into autotrophic and heterotrophic metabolic processes, before and during the incorporation of P in the AM plant. Consequently, the Total C/P ratio was significantly larger in those fungal compartments containing free PA and both P sources bound to goethite (**Figure 6**). The total C as the sum of total OC and cumulative CO_2 accounted for most of the C exclusively carried by the AMF into the fungal compartment. The results point to a greater investment of plant photoassimilates compared to the free OP treatment and controls. Similarly, a more active metabolism for the less accessible P sources was indicated by a larger CO_2 production for the same amount of P mobilized from PA, GOE-OP and GOE-PA compared to OP. Respiratory energy is required by the microbiont for constructing new intraradical and extraradical fungal tissue (including reproductive structures), for maintenance and repair of existing fungal tissue and for cellular processes in the fungal tissue associated with the absorption and transfer of nutrients to the host (Bryla and Eissenstat, 2005). The photoassimilate investment into respiration (fast) or structural (slow) C pools in soil has been reported frequently before (Zhu and Miller, 2003), but was not related to a direct nutrient allocation mechanism as in our case. Staddon et al. (2003) suggested AM hyphae do not contribute substantially to C sequestration in soil. In contrast, our results point toward larger C sequestration rates and metabolic activity in the less accessible sources, being consistent with the general line of argumentation of Turner (2008). This energy investment into fungal compartments with less accessible P sources, taken together with more structural C contents found in the respective compartments clearly show that AM fungi are able to adjust to the requirements imposed by a given nutrient source.

Growth of *R. irregularis* Under Variable Phosphorus Availability

The PLFA 16:1ω5c /P and NLFA 16:1ω5c/P showed a significant larger amount of both fatty acids accumulated into the fungal compartment relative to P uptake, in those fungal compartments containing GOE-OP and GOE-PA compared to OP and PA (**Figures 7A,B**). The fungal lipids extracted from the fungal compartment indicate a different growth strategy to mobilize P from the goethite-bound compounds compared to the free forms. The AMF grown in those fungal compartment containing GOE-OP and PA accumulated two and three orders of magnitude more PLFA and NLFA, respectively, compared to OP and PA. This observation confirms a larger C investment in energy storage and mycelium per unit of P incorporated into the AM plant. *Rhizophagus irregularis* grown in the fungal compartment

containing GOE-OP accumulated significant more NLFA, as indicated by the ratio NLFA 16:1ω5c/PLFA 16:1ω5c, meaning that the AMF stored energy in the form of neutral lipids before and during the P mobilization, compared to GOE-PA and the free P forms (**Figure 7C**). One potential explanation for the more pronounced development of fungal infrastructure in the presence of P forms bound to goethite is the need to establish a sufficient extraradical hyphae of *R. irregularis* to mobilize and transport P more efficiently to the plant (Abbott and Robson, 1982; Joner et al., 2000; Smith et al., 2003). According to Bryla and Eissenstat (2005), mycorrhizas tend to be favored under nutrient-poor conditions, as in case of the goethite-P treatments. The reduced hyphal growth in both fungal compartment containing OP and PA with a high P content indicate that the roots may reduce the C flux to the fungus under larger P availability (Olsson et al., 1997, 2002). It has been suggested that a reduced carbohydrate allocation would be a regulatory saving mechanism by the plant host where there is an excess of phosphate ion (Torres de los Santos et al., 2016; Konvalinková et al., 2017). Bååth (2003) showed the NLFA 16:1ω5c/PLFA 16:1ω5c is a good indicator to express preferential C allocation to storage products, when comparing different nutritional scenarios. Our results corroborate this observation and suggest that the preferential energy storage in the form of neutral lipid could be used to support the extensive growth of *R. irregularis* mycelium in the goethite systems.

The plant is often considered as being in control of the symbiosis, and this "phytocentric" view is supported by the idea that AM symbiosis is a strategy that could be suppressed by the plants at sufficient P supply. But in natural ecosystems, instead of luxurious P availability, suppression of AM colonization by the plant is not the normal situation (Smith and Smith, 2012), as plants have evolved diverse adaptations to acquire different forms of soil P (Ceulemans et al., 2017). Hammer et al. (2011b) suggest a fungal control mechanism of the P transfer to the plant, and that the C-P exchange between the symbionts is closely linked. Our results, showing a different content and partitioning of C into NLFA and PLFA 16:1ω5c for those *R. irregularis* grown in treatments with mineral-bound P sources, corroborate that point. This more "mycocentric" view of symbiosis explains the evolutionarily stable mutualistic relationship between these symbionts. If AMF are able to reduce the delivery of P to plants with a limited supply of C (Kiers et al., 2011), they possess an important function to actively increase their fitness by choosing the best plant partner, which in turn could increase selection pressure on the plant species within a community (Hammer et al., 2011b). Under our experimental conditions, where the tomato plants could only acquire the P through the AMF, we observed different trading costs between C for P, distinct P acquisition strategies resulting in differing C costs for the AM plant. Our results show that the mobilization of a certain P source by a plant, comes at differing photoassimilatory costs and, by this, necessarily changes the functional trait of this plant. Thus, we propose this mechanism as a potential driver of nutritional partitioning in plant communities, as described by e.g., Turner (2008).

CONCLUDING REMARKS

Our study provided evidence that AM plants are able to mobilize P sources differing in their accessibility. This mobilization happened exclusively via the mycorrhizal pathway at contrasting kinetics and accumulation rates, and was driven by the amount of photoassimilates needed for the mobilization of the P sources. The mobilized P was redistributed between fungus and plant in differing amounts, which again was influenced by the P species. Both P sources adsorbed to goethite (GOE-OP, GOE-PA) facilitated a greater investment of the AM plant into the production of fungal vegetative structures than in case of the free OP and PA. Larger contents of PLFA 16:1ω5c and NLFA 16:1ω5c were observed especially in systems with goethite-associated P, suggesting the accumulation of significantly larger amounts of extraradical hyphae. Further, the lipid accumulation in form of PLFA 16:1ω5c and NLFA 16:1ω5c suggests different growth strategies to mobilize P from the goethite-bound compounds. This is also mirrored by the larger C investment per P incorporated, as compared to OP and PA. Our data also suggest that the C investment by mycorrhized plants into P acquisition from differently available P sources has a direct effect on the amount of C accumulating in soils.

AUTHOR CONTRIBUTIONS

JB, GG, AA, and RM designed the experiment. AA prepared the plant and fungal material. AA conducted the experiment and analyzed the data. JB, LS, GG, and RM supervised the research. AA wrote the paper with contributions from JB, GG, LS, and RM.

FUNDING

We want to thank the German Federal Ministry of Education and Research for the funding of this project in the framework of the DFG-RTG 1798 Signaling at the Plant-Soil Interface as well as the DFG priority program SPP 1685 Forest Strategies for limited Phosphorus Resources. The publication of this article was funded by the Open Access fund of Leibniz Universität Hannover.

ACKNOWLEDGMENTS

We are thankful for the great help and guidance received by Silke Bokeloh, Elke Eichmann-Prusch, Ulrike Pieper, Heike Steffen, and Michael Klatt.

SUPPLEMENTARY MATERIAL

The Supplementary Material for this article can be found online at: https://www.frontiersin.org/articles/10.3389/fenvs.2019.00026/full#supplementary-material

REFERENCES

Aarle, I. M. V., and Olsson, P. A. (2003). fungal lipid accumulation and development of mycelial structures by two arbuscular mycorrhizal fungi fungal lipid accumulation and development of mycelial structures by two arbuscular mycorrhizal fungi. *Appl. Environ. Microbiol.* 69, 6762–6767. doi: 10.1128/AEM.69.11.6762-6767.2003

Abbott, L. K., and Robson, A. D. (1982). The role of vesicular arbuscular mycorrhizal fungi in agriculture and the selection of fungi for inoculation. *Aust. J. Agric. Res.* 33, 389–408. doi: 10.1071/AR9820389

Argüello, A., O'Brien, M. J., van der Heijden, M. G. A., Wiemken, A., Schmid, B., and Niklaus, P. A. (2016). Options of partners improve carbon for phosphorus trade in the arbuscular mycorrhizal mutualism. *Ecol. Lett.* 19, 648–656. doi: 10.1111/ele.12601

Atkin, O. K., Sherlock, D., Fitter, A. H., Jarvis, S., Hughes, J. K., Campbell, C., et al. (2009). Temperature dependence of respiration in roots colonized by arbuscular mycorrhizal fungi. *New Phytol.* 182, 188–199. doi: 10.1111/j.1469-8137.2008.02727.x

Bååth, E. (2003). The use of neutral lipid fatty acids to indicate the physiological conditions of soil fungi. *Microb. Ecol.* 45, 373–383. doi: 10.1007/s00248-003-2002-y

Bago, B., Zipfel, W., Williams, R. M., Jun, J., Arreola, R., Lammers, P. J., et al. (2002). Translocation and utilization of fungal storage lipid in the arbuscular mycorrhizal symbiosis. *Plant Physiol.* 128, 108–124. doi: 10.1104/pp.010466

Baldwin, J. C., Karthikeyan, A. S., Cao, A., and Raghothama, K. G. (2008). Biochemical and molecular analysis of LePS2;1: a phosphate starvation induced protein phosphatase gene from tomato. *Planta* 228, 273–280. doi: 10.1007/s00425-008-0736-y

Baldwin, J. C., Karthikeyan, A. S., and Raghothama, K. G. (2001). LEPS2, a phosphorus starvation-induced novel acid phosphatase from tomato. *Plant Physiol.* 125, 728–737. doi: 10.1104/pp.125.2.728

Becquer, A., Trap, J., Irshad, U., Ali, M. A., and Claude, P. (2014). From soil to plant, the journey of P through trophic relationships and ectomycorrhizal association. *Front. Plant Sci.* 5:548. doi: 10.3389/fpls.2014.00548

Bischoff, N., Mikutta, R., Shibistova, O., Puzanov, A., Reichert, E., Silanteva, M., et al. (2016). Land-use change under different climatic conditions: consequences for organic matter and microbial communities in Siberian steppe soils. *Agric. Ecosyst. Environ.* 235, 253–264. doi: 10.1016/j.agee.2016.10.022

Bolan, N. S., Robson, A. D., and Barrow, N. J. (1987). Effects of vesicular-arbuscular mycorrhiza on the availability of iron phosphates to plants. *Plant Soil* 99, 401–410. doi: 10.1007/BF02370885

Bolan, N. S. S., Robson, A. D. D., Barrow, N. J. J., and Aylmore, L. A. G. A. G. (1984). Specific activity of phosphorus in mycorrhizal and non-mycorrhizal plants in relation to the availability of phosphorus to plants. *Soil Biol. Biochem.* 16, 299–304. doi: 10.1016/0038-0717(84)90023-3

Bravo, A., Brands, M., Wewer, V., Dörmann, P., and Harrison, M. J. (2017). Arbuscular mycorrhiza-specific enzymes FatM and RAM2 fine-tune lipid biosynthesis to promote development of arbuscular mycorrhiza. *New Phytol.* 214, 1631–1645. doi: 10.1111/nph.14533

Brundrett, M. (1996). *Working With Mycorrhizas in Forestry and Agriculture*. Canberra: Australian Centre for International Agricultural Research.

Bryla, D. R., and Eissenstat, D. M. (2005). "Respiratory costs of Mycorrhizal Associations," in *Plant Respiration*, eds H. Lambers and M. Ribas-Carbo (Berlin; Dordrecht: Springer-Verlag), 207–219.

Cairney, J. W. G. (2000). Evolution of mycorrhiza systems. *Naturwissenschaften* 87, 467–475. doi: 10.1007/s001140050762

Calonne, M., Fontaine, J., Debiane, D., Laruelle, F., Grandmougin-ferjani, A., and Sahraoui, A. L. (2010). "Propiconazole toxicity on the non-target organism, the arbuscular Mycorrhizal fungus, Glomus irregulare," in *Fungicides*, ed O. Carisse (InTech), 325–346. doi: 10.5772/10482

Cardoso, I. M., Boddington, C. L., Janssen, B. H., Oenema, O., and Kuyper, T. W. (2006). Differential access to phosphorus pools of an oxisol by mycorrhizal and nonmycorrhizal maize. *Commun. Soil Sci. Plant Anal.* 37, 1537–1551. doi: 10.1080/00103620600710074

Cavagnaro, T. R., Langley, A. J., Jackson, L. E., Smukler, S. M., and Koch, G. W. (2008). Growth, nutrition, and soil respiration of a mycorrhiza-defective tomato mutant and its mycorrhizal wild-type progenitor. *Funct. Plant Biol.* 35:228. doi: 10.1071/FP07281

Ceulemans, T., Bodé, S., Bollyn, J., Harpole, S., Coorevits, K., Peeters, G., et al. (2017). Phosphorus resource partitioning shapes phosphorus acquisition and plant species abundance in grasslands. *Nat. Plants* 3:16224. doi: 10.1038/nplants.2016.224

Cozzolino, V., Di Meo, V., Monda, H., Spaccini, R., and Piccolo, A. (2016). The molecular characteristics of compost affect plant growth, arbuscular mycorrhizal fungi, and soil microbial community composition. *Biol. Fertil. Soils* 52, 15–29. doi: 10.1007/s00374-015-1046-8

Daubois, L., Beaudet, D., Hijri, M., and De La Providencia, I. (2016). Independent mitochondrial and nuclear exchanges arising in Rhizophagus irregularis crossed-isolates support the presence of a mitochondrial segregation mechanism Ecological and evolutionary microbiology. *BMC Microbiol.* 16:11. doi: 10.1186/s12866-016-0627-5

Deubel, A., and Merbach, W. (2005). "Influence of microorganisms on phosphorus bioavailability in soils," in *Microorganisms in Soils: Roles in Genesis and Functions*, Vol 3, eds A. Varma and F. Buscot (Berlin; Heidelberg: Springer-Verlag), 177–191.

Ezawa, T., Smith, S. E., and Smith, F. A. P. (2002). P metabolism and transport in AM fungi. *Plant Soil* 244, 221–230. doi: 10.1023/A:1020258325010

Feng, G., Song, Y. C., Li, X. L., and Christie, P. (2003). Contribution of arbuscular mycorrhizal fungi to utilization of organic sources of phosphorus by red clover in a calcareous soil. *Appl. Soil Ecol.* 22, 139–148. doi: 10.1016/S0929-1393(02)00133-6

Fitter, A. H., Graves, J. D., Watkins, N. K., Robinson, D., and Scrimgeour, C. (1998). Carbon transfer between plants and its control in networks of arbuscular mycorrhizas. *Funct. Ecol.* 12, 406–412. doi: 10.1046/j.1365-2435.1998.00206.x

Frey, B., Brunner, I., Christie, P., Wiemken, A., and Mäder, P. (1998). "The use of Polytetrafluoroethylene (PTFE) hydrophobic membranes to study transport of 15N by Mycorrhizal Hyphae," in *Mycorrhiza Manual*, ed A. Varma (Berlin: Springer), 151–158.

Frossard, E., Achat, D. L., Bernasconi, S. M., Bünemann, E. K., Fardeau, J.-C., Jansa, J., et al. (2011). "The use of tracers to investigate phosphate cycling in soil-plant systems," in *Phosphorus in Action. Soil Biology,* Vol 26, eds E. Bünemann, A. Oberson, and E. Frossard (Berlin; Heidelberg: Springer), 59–91.

Frostegård, Å., Tunlid, A., and Bååth, E. (1991). Microbial biomass measured as total lipid phosphate in soils of different organic content. *J. Microbiol. Methods* 14, 151–163. doi: 10.1016/0167-7012(91)90018-L

García, G. H. G. C. A. (2000). Behaviour of arbuscular-mycorrhizal fungi on *Vigna luteola* growth and its effect on the exchangeable (32 P) phosphorus of soil. *Biol. Fertil. Soils* 31, 232–236. doi: 10.1007/s003740050650

Gentsch, N., Wild, B., Mikutta, R., Capek, P., Diáková, K., Schrumpf, M., et al. (2018). Temperature response of permafrost soil carbon is attenuated by mineral protection. *Glob. Chang. Biol.* 24, 3401–3415. doi: 10.1111/gcb.14316

George, T. S., Hinsinger, P., and Turner, B. L. (2016). Phosphorus in soils and plants: facing phosphorus scarcity. *Plant Soil* 401, 1–6. doi: 10.1007/s11104-016-2846-9

Gilbert, N. (2009). Environment: the disappearing nutrient. *Nature* 461, 716–718. doi: 10.1038/461716a

Giles, C. D., Richardson, A. E., Druschel, G. K., and Hill, J. E. (2012). Organic anion-driven solubilization of precipitated and sorbed phytate improves hydrolysis by phytases and bioavailability to *Nicotiana tabacum*. *Soil Sci.* 177, 591–598. doi: 10.1097/SS.0b013e318272f83f

Giovannetti, M., Avio, L., Barale, R., Ceccarelli, N., Cristofani, R., Iezzi, A., et al. (2012). Nutraceutical value and safety of tomato fruits produced by mycorrhizal plants. *Br. J. Nutr.* 107, 242–251. doi: 10.1017/S000711451100290X

Green, H., Larsen, J., Olsson, P. A., Jensen, D. F., and Jakobsen, I. (1999). Suppression of the biocontrol agent *Trichoderma harzianum* by mycelium of the arbuscular mycorrhizal fungus Glomus intraradices in root-free soil. *Appl. Environ. Microbiol.* 65, 1428–1434.

Hammer, E. C., Nasr, H., Pallon, J., Olsson, P. A., and Wallander, H. (2011a). Elemental composition of arbuscular mycorrhizal fungi at high salinity. *Mycorrhiza* 21, 117–129. doi: 10.1007/s00572-010-0316-4

Hammer, E. C., Pallon, J., Wallander, H., and Olsson, P. A. (2011b). Tit for tat? a mycorrhizal fungus accumulates phosphorus under

low plant carbon availability. *FEMS Microbiol. Ecol.* 76, 236–244. doi: 10.1111/j.1574-6941.2011.01043.x

He, Z., and Zhu, J. U. N. (1998). Microbial utilization and transformation of phosphate adsorbed by variable charge minerals. *Soil Biol. Biochem.* 30, 917–923. doi: 10.1016/S0038-0717(97)00188-0

Heinemeyer, A., Ineson, P., Ostle, N., and Fitter, A. H. (2006). Respiration of the external mycelium in the arbuscular mycorrhizal symbiosis shows strong dependence on recent photosynthates and acclimation to temperature. *New Phytol.* 171, 159–170. doi: 10.1111/j.1469-8137.2006.01730.x

Hewitt, E. J. (1966). *Sand and Water Culture Methods Used in the Study of Plant Nutrition*. Kent: University of Bristol Agricultural and Horticultural Research Station, Bristol.

Hinsinger, P., and Gilkes, R. J. (1996). Mobilization of phosphate from phosphate rock and alumina-sorbed phosphate by the roots of ryegrass and clover as related to rhizosphere pH. *Eur. J. Soil Sci.* 47, 533–544. doi: 10.1111/j.1365-2389.1996.tb01853.x

IBM Corporation (2016). *IBM SPSS Statistics for Windows*. Version 24.0.2016.

Jakobsen, I., Smith, S. E., Smith, F. A., Watts-Williams, S. J., Clausen, S. S., and Grønlund, M. (2016). Plant growth responses to elevated atmospheric CO 2 are increased by phosphorus sufficiency but not by arbuscular mycorrhizas. *J. Exp. Bot.* 67, 6173–6186. doi: 10.1093/jxb/erw383

Javaid, A. (2009). Arbuscular mycorrhizal mediated nutrition in plants. *J. Plant Nutr.* 32, 1595–1618. doi: 10.1080/01904160903150875

Javot, H., Pumplin, N., and Harrison, M. J. (2007). Phosphate in the arbuscular mycorrhizal symbiosis: transport properties and regulatory roles. *Plant Cell Environ.* 30, 310–322. doi: 10.1111/j.1365-3040.2006.01617.x

Johansen, A., Finlay, R. D., and Olsson, P. A. (1996). Nitrogen metabolism of external hyphae of the arbuscular mycorrhizal fungus Glomus intraradices. *New Phytol.* 133, 705–712. doi: 10.1111/j.1469-8137.1996.tb01939.x

Johnson, N. C. (2010). Resource stoichiometry elucidates the structure and function of arbuscular mycorrhizas across scales. *New Phytol.* 185, 631–647. doi: 10.1111/j.1469-8137.2009.03110.x

Joner, E. J., Ravnskov, S., and Jakobsen, I. (2000). Arbuscular mycorrhizal phosphate transport under monoxenic conditions using radio-labelled inorganic and organic phosphate. *Biotechnol. Lett.* 22, 1705–1708. doi: 10.1023/A:1005684031296

Kaiser, K., and Guggenberger, G. (2007). Sorptive stabilization of organic matter by microporous goethite: sorption into small pores vs. surface complexation. *Eur. J. Soil Sci.* 58, 45–59. doi: 10.1111/j.1365-2389.2006.00799.x

Karasawa, T., Hodge, A., and Fitter, A. H. (2012). Growth, respiration and nutrient acquisition by the arbuscular mycorrhizal fungus Glomus mosseae and its host plant *Plantago lanceolata* in cooled soil. *Plant Cell Environ.* 35, 819–828. doi: 10.1111/j.1365-3040.2011.02455.x

Keymer, A., Pimprikar, P., Wewer, V., Huber, C., Brands, M., Bucerius, S. L., et al. (2017). Lipid transfer from plants to arbuscular mycorrhiza fungi. *Elife* 6:e29107. doi: 10.7554/eLife.29107

Kiers, E. T., Duhamel, M., Beesetty, Y., Mensah, J. A., Franken, O., Verbruggen, E., et al. (2011). Reciprocal rewards stabilize cooperation in the mycorrhizal symbiosis. *Science* 333, 880–882. doi: 10.1126/science.1208473

Köhl, L., Lukasiewicz, C. E., and Van der Heijden, M. G. A. (2016). Establishment and effectiveness of inoculated arbuscular mycorrhizal fungi in agricultural soils. *Plant Cell Environ.* 39, 136–146. doi: 10.1111/pce.12600

Koide, R. T., and Kabir, Z. (2000). Extraradical hyphae of the mycorrhizal fungus Glomus intraradices can hydrolyse inorganic phosphate. *New Phytol.* 148, 511–517. doi: 10.1046/j.1469-8137.2000.00776.x

Konvalinková, T., Püschel, D., Rezáčová, V., Gryndlerová, H., and Jansa, J. (2017). Carbon flow from plant to arbuscular mycorrhizal fungi is reduced under phosphorus fertilization. *Plant Soil* 419, 1–15. doi: 10.1007/s11104-017-3350-6

Krüger, M., Krüger, C., Walker, C., Stockinger, H., Schüßler, A., Krüger, M., et al. (2012). Phylogenetic reference data for systematics and phylotaxonomy of arbuscular mycorrhizal fungi from phylum to species level. *New Phytol.* 193, 970–984. doi: 10.1111/j.1469-8137.2011.03962.x

Kuntz, L. B. (2013). *Wick Irrigation Systems for Subsistence Farming*. Available online at: https://dspace.mit.edu/handle/1721.1/83726 (Accessed Oct 21, 2018).

Kuzyakov, Y., and Gavrichkova, O. (2010). Time lag between photosynthesis and carbon dioxide efflux from soil: a review of mechanisms and controls. *Glob. Chang. Biol.* 16, 3386–3406. doi: 10.1111/j.1365-2486.2010.02179.x

Lambers, H., Martinoia, E., and Renton, M. (2015). Plant adaptations to severely phosphorus-impoverished soils. *Curr. Opin. Plant Biol.* 25, 23–31. doi: 10.1016/j.pbi.2015.04.002

Larsen, J., Olsson, P. A., and Jakobsen, I. (1998). The use of fatty acid signatures to study mycelial interactions between the arbuscular mycorrhizal fungus Glomus intraradices and the saprotrophic fungus *Fusarium culmorum* in root-free soil. *Mycol. Res.* 102, 1491–1496. doi: 10.1017/S0953756298006558

Li, M., Osaki, M., Honma, M., and Tadano, T. (1997). Purification and characterization of phytase induced in tomato roots under phosphorus-deficient conditions. *Soil Sci. Plant Nutr.* 43, 179–190. doi: 10.1080/00380768.1997.10414726

Luginbuehl, L. H., Menard, G. N., Kurup, S., Van Erp, H., Radhakrishnan, G. V., Breakspear, A., et al. (2017). Fatty acids in arbuscular mycorrhizal fungi are synthesized by the host plant. *Science* 356, 1175–1178. doi: 10.1126/science.aan0081

Mäder, P., Vierheilig, H., Alt, M., and Wiemken, A. (1993). Boundaries between soil compartments formed by microporous hydrophobic membranes (GORE-TEXR) can be crossed by vesicular-arbuscular mycorrizal fungi but not by ions in the soil solution. *Plant Soil* 152, 201–206. doi: 10.1007/BF00029089

Mäder, P., Vierheilig, H., Streitwolf-Engel, R., Boller, T., Frey, B., Christie, P., et al. (2000). Transport of 15N from a soil compartment separated by a polytetrafluoroethylene membrane to plant roots via the hyphae of arbuscular mycorrhizal fungi. *New Phytol.* 146, 155–161. doi: 10.1046/j.1469-8137.2000.00615.x

Marschner, P. (2007). "Soil microbial community structure and function assessed by FAME, PLFA and DGGE — advantages and limitations," in *Advanced Techniques in Soil Microbiology*, eds A. Varma and R. Oelmüller (Berlin: Springer), 181–200.

McGonigle, T. P., Miller, M. H., Evans, D. G., Fairchild, G. L., and Swan, J. A. (1990). A new method which gives an objective measure of colonization of roots by vesicular- arbuscular mycorrhizal fungi. *New Phytol.* 115, 495–501. doi: 10.1111/j.1469-8137.1990.tb00476.x

Mengel, K., and Kirkby, E. A. (2001). "Phosphorus," in *Principles of Plant Nutrition*, eds. K. Mengel, E. A. Kirkby, H. Kosegarten, and T. Appel (Dordrecht: Springer), 453–479. doi: 10.1007/978-94-010-1009-2

Nagy, R., Karandashov, V., Chague, V., Kalinkevich, K., Tamasloukht, M., Xu, G., et al. (2005). The characterization of novel mycorrhiza-specific phosphate transporters from and *Solanum tuberosum* uncovers functional redundancy in symbiotic phosphate transport in solanaceous species. *Plant J.* 42, 236–250. doi: 10.1111/j.1365-313X.2005.02364.x

Nash, D. M., Haygarth, P. M., Turner, B. L., Condron, L. M., McDowell, R. W., Richardson, A. E., et al. (2014). Using organic phosphorus to sustain pasture productivity: a perspective. *Geoderma* 221–222, 11–19. doi: 10.1016/j.geoderma.2013.12.004

Nottingham, A. T., Turner, B. L., Winter, K., van der Heijden, M. G. A., and Tanner, E. V. J. (2010). Arbuscular mycorrhizal mycelial respiration in a moist tropical forest. *New Phytol.* 186, 957–967. doi: 10.1111/j.1469-8137.2010.03226.x

Oberson, A., Friesen, D. K., Rao, I. M., Bühler, S., Frossard, E., Buhler, S., et al. (2001). Phosphorus transformations in an oxisol under contrasting land-use systems: the role of the soil microbial biomass. *Plant Soil* 237, 197–210. doi: 10.1023/A:1013301716913

Ognalaga, M., Frossard, E., and Thomas, F. (1994). Glucose-1-phosphate and myo-inositol hexaphosphate adsorption mechanisms on goethite. *Soil Sci. Soc. Am. J.* 58, 332–337. doi: 10.2136/sssaj1994.03615995005800020011x

Olsson, P., Linder, S., Giesler, R., and Högberg, P. (2005). Fertilization of boreal forest reduces both autotrophic and heterotrophic soil respiration. *Glob. Chang. Biol.* 11, 1745–1753. doi: 10.1111/j.1365-2486.2005.001033.x

Olsson, P. A. (1999). Signature fatty acids provide tools for determination of the distribution and interactions of mycorrhizal fungi in soil. *FEMS Microbiol. Ecol.* 29, 303–310. doi: 10.1111/j.1574-6941.1999.tb00621.x

Olsson, P. A., Bååth, E., and Jakobsen, I. (1997). Phosphorus effects on the mycelium and storage structures of an arbuscular mycorrhizal fungus as studied in the soil and roots by analysis of fatty acid signatures. *Appl. Environ. Microbiol.* 63, 3531–3538.

Olsson, P. A., Hammer, E. C., Wallander, H., and Pallon, J. (2008). Phosphorus availability influences elemental uptake in the mycorrhizal fungus Glomus intraradices, as revealed by particle-induced X-ray emission analysis. *Appl. Environ. Microbiol.* 74, 4144–4148. doi: 10.1128/AEM.00376-08

Olsson, P. A., and Johansen, A. (2000). Lipid and fatty acid composition of hyphae and spores of arbuscular mycorrhizal fungi at different growth stages. *Mycol. Res.* 104, 429–434. doi: 10.1017/S0953756299001410

Olsson, P. A., and Johnson, N. C. (2005). Tracking carbon from the atmosphere to the rhizosphere. *Ecol. Lett.* 8, 1264–1270. doi: 10.1111/j.1461-0248.2005.00831.x

Olsson, P. A., Rahm, J., and Aliasgharzad, N. (2010). Carbon dynamics in mycorrhizal symbioses is linked to carbon costs and phosphorus benefits. *FEMS Microbiol. Ecol.* 72, 125–131. doi: 10.1111/j.1574-6941.2009.00833.x

Olsson, P. A., van Aarle, I. M., Allaway, W. G., Ashford, A. E. A. E., and Rouhier, H. (2002). Phosphorus effects on metabolic processes in monoxenic arbuscular mycorrhiza cultures. *Plant Physiol.* 130, 1162–1171. doi: 10.1104/pp.009639

Olsson, P. A., and Wilhelmsson, P. (2000). The growth of external AM fungal mycelium in sand dunes and in experimental systems. *Plant Soil* 226, 161–169. doi: 10.1023/A:1026565314345

Osorio, N. W., and Habte, M. (2001). Synergistic influence of an arbuscular mycorrhizal fungus and a P solubilizing fungus on growth and P uptake of *Leucaena leucocephala* in an Oxisol. *Arid L. Res. Manag.* 15, 263–274. doi: 10.1080/15324980152119810

Parfitt, R. L. (1979). The availability of P from phosphate-goethite bridging complexes. desorption and uptake by ryegrass. *Plant Soil* 53, 55–65. doi: 10.1007/BF02181879

Pfeffer, P. E., Douds, D. D., Bücking, H., Schwartz, D. P., and Shachar-Hill, Y. (2004). The fungus does not transfer carbon to or between roots in an arbuscular mycorrhizal symbiosis. *New Phytol.* 163, 617–627. doi: 10.1111/j.1469-8137.2004.01152.x

Read, D. J. (1991). "Mycorrhizas in ecosystems - Nature's response to the 'Law of the minimum,'" in *Frontiers in Mycology*, ed D. L. Hawksworth (Regensburg: CAB International), 101–130.

Richardson, A. E. (2001). Prospects for using soil microorganisms to improve the acquisition of phosphorus by plants. *Aust. J. Plant Physiol.* 28, 897–906. doi: 10.1071/PP01093

Richardson, A. E., Hocking, P. J., Simpson, R. J., and George, T. S. (2009). Plant mechanisms to optimise access to soil phosphorus. *Crop Pasture Sci.* 60, 124–143. doi: 10.1071/CP07125

Rinnan, R., and Bååth, E. (2009). Differential utilization of carbon substrates by bacteria and fungi in tundra soil. *Appl. Environ. Microbiol.* 75, 3611–3620. doi: 10.1128/AEM.02865-08

Rodrigues, M., Pavinato, P. S., Withers, P. J. A., Teles, A. P. B., and Herrera, W. F. B. (2016). Legacy phosphorus and no tillage agriculture in tropical oxisols of the Brazilian savanna. *Sci. Total Environ.* 542, 1050–1061. doi: 10.1016/j.scitotenv.2015.08.118

Rowe, H., Withers, P. J. A., Baas, P., Chan, N. I., Doody, D., Holiman, J., et al. (2016). Integrating legacy soil phosphorus into sustainable nutrient management strategies for future food, bioenergy and water security. *Nutr. Cycl. Agroecosyst.* 104, 393–412. doi: 10.1007/s10705-015-9726-1

Rychter, A., Rao, I., and Cardoso, J. (2016). "Role of phosphorus in photosynthetic carbon assimilation and partitioning," in *Handbook of Photosynthesis*, ed M. Pessarakli, 603–625.

Sato, T., Ezawa, T., Cheng, W., and Tawaraya, K. (2015). Release of acid phosphatase from extraradical hyphae of arbuscular mycorrhizal fungus rhizophagus clarus. *Soil Sci. Plant Nutr.* 61, 269–274. doi: 10.1080/00380768.2014.993298

Sawers, R. J. H., Svane, S. F., Quan, C., Grønlund, M., Wozniak, B., Gebreselassie, M. N., et al. (2017). Phosphorus acquisition efficiency in arbuscular mycorrhizal maize is correlated with the abundance of root-external hyphae and the accumulation of transcripts encoding PHT1 phosphate transporters. *New Phytol.* 214, 632–643. doi: 10.1111/nph.14403

Schaarschmidt, S., Roitsch, T., and Hause, B. (2006). Arbuscular mycorrhiza induces gene expression of the apoplastic invertase LIN6 in tomato (*Lycopersicon esculentum*) roots. *J. Exp. Bot.* 57, 4015–4023. doi: 10.1093/jxb/erl172

Smith, F. A., and Smith, S. E. (2011). What is the significance of the arbuscular mycorrhizal colonisation of many economically important crop plants? *Plant Soil* 348, 63–79. doi: 10.1007/s11104-011-0865-0

Smith, S. E., Read, D. J., Kiers, E. T., Duhamel, M., Beesetty, Y., et al. (2008). "The symbionts forming VA mycorrhizas," in *Mycorrhizal Symbiosis*, eds S. E. Smith and D. J. Read (New York, NY: Academic Press), 11–I. doi: 10.1016/b978-012652840-4/50002-4

Smith, S. E., and Smith, F. A. (2012). Fresh perspectives on the roles of arbuscular mycorrhizal fungi in plant nutrition and growth. *Mycologia* 104, 1–13. doi: 10.3852/11-229

Smith, S. E., Smith, F. A., and Jakobsen, I. (2003). Mycorrhizal fungi can dominate phosphate supply to plants irrespective of growth responses. *Plant Physiol.* 133, 16–20. doi: 10.1104/pp.103.024380

Solaiman, M. Z., Ezawa, T., Kojima, T., and Saito, M. (1999). Polyphosphates in intraradical and extraradical hyphae of an arbuscular mycorrhizal fungus, Gigaspora margarita. *Appl. Environ. Microbiol.* 65, 5604–5606.

Son, J. E., Oh, M. M., Lu, Y. J., Kim, K. S., and Giacomelli, G. A. (2006). Nutrient-flow wick culture system for potted plant production: system characteristics and plant growth. *Sci. Hortic.* 107, 392–398. doi: 10.1016/j.scienta.2005.11.001

Staddon, P. L., Ramsey, C. B., Ostle, N., Ineson, P., and Fitter, A. H. (2003). Rapid turnover of hyphae of mycorrhizal fungi determined by AMS microanalysis of 14C. *Science* 300, 1138–1140. doi: 10.1126/science.1084269

Stumpe, M., Carsjens, J.-G. G., Stenzel, I., Göbel, C., Lang, I., Pawlowski, K., et al. (2005). Lipid metabolism in arbuscular mycorrhizal roots of *Medicago truncatula*. *Phytochemistry* 66, 781–791. doi: 10.1016/j.phytochem.2005.01.020

Tarafdar, J. C., and Marschner, H. (1994a). Efficiency of VAM hyphae in utilisation of organic phosphorus by wheat plants. *Soil Sci. Plant Nutr.* 40, 593–600. doi: 10.1080/00380768.1994.10414298

Tarafdar, J. C., and Marschner, H. (1994b). Phosphatase activity in the rhizosphere and hyphosphere of VA mycorrhizal wheat supplied with inorganic and organic phosphorus. *Soil Biol. Biochem.* 26, 387–395. doi: 10.1016/0038-0717(94)90288-7

Tawaraya, K., Naito, M., and Wagatsuma, T. (2006). Solubilization of insoluble inorganic phosphate by hyphal exudates of arbuscular mycorrhizal fungi. *J. Plant Nutr.* 29, 657–665. doi: 10.1080/01904160600564428

Tisserant, E., Kohler, A., Dozolme-Seddas, P., Balestrini, R., Benabdellah, K., Colard, A., et al. (2012). The transcriptome of the arbuscular mycorrhizal fungus Glomus intraradices (DAOM 197198) reveals functional tradeoffs in an obligate symbiont. *New Phytol.* 193, 755–769. doi: 10.1111/j.1469-8137.2011.03948.x

Torres de los Santos, R., Molinero Rosales, N., Ocampo, J. A., and García-Garrido, J. M. (2016). Ethylene alleviates the suppressive effect of phosphate on arbuscular mycorrhiza formation. *J. Plant Growth Regul.* 35, 611–617. doi: 10.1007/s00344-015-9570-1

Turner, B. L. (2008). Resource partitioning for soil phosphorus: a hypothesis. *J. Ecol.* 96, 698–702. doi: 10.1111/j.1365-2745.2008.01384.x

van Diepen, L. T. A., Lilleskov, E. A., Pregitzer, K. S., and Miller, R. M. (2010). Simulated nitrogen deposition causes a decline of intra- and extraradical abundance of arbuscular mycorrhizal fungi and changes in microbial community structure in northern hardwood forests. *Ecosystems* 13, 683–695. doi: 10.1007/s10021-010-9347-0

Vermue, E., Elbers, J., and Hoosbeek, M. (2008). *A Comparative Field Study of Four Soil Respiration Systems*. Available online at: http://edepot.wur.nl/120659 (Accessed Oct 25, 2018).

Vestberg, M., Palojarvi, A., Pitkanen, T., Kaipainen, S., Puolakka, E., and Keskitalo, M. (2012). Neutral lipid fatty acid analysis is a sensitive marker for quantitative estimation of arbuscular mycorrhizal fungi in agricultural soil with crops of different mycrotrophy. *Agric. Food Sci.* 21, 12–27. doi: 10.23986/afsci.4996

Vierheilig, H., Alt-Hug, M., Engel-Streitwolf, R., Mäder, P., and Wiemken, A. (1998a). Studies on the attractional effect of root exudates on hyphal growth of an arbuscular mycorrhizal fungus in a soil compartment-membrane system. *Plant Soil* 203, 137–144. doi: 10.1023/A:1004329919005

Vierheilig, H., Coughlan, A. P., Wyss, U., and Piché, Y. (1998b). Ink and vinegar, a simple staining technique for arbuscular-mycorrhizal fungi. *Appl. Environ. Microbiol.* 64, 5004–5007.

Watkins, N. K., Fitter, A. H., Graves, J. D., and Robinson, D. (1996). Carbon transfer between C3 and C4 plants linked by a common mycorrhizal network, quantified using stable carbon isotopes. *Soil Biol. Biochem.* 28, 471–477. doi: 10.1016/0038-0717(95)00189-1

Wewer, V., Brands, M., and Dörmann, P. (2014). Fatty acid synthesis and lipid metabolism in the obligate biotrophic fungus *Rhizophagus irregularis* during mycorrhization of Lotus japonicus. *Plant J.* 79, 398–412. doi: 10.1111/tpj.12566

Willis, A., Rodrigues, B. F., and Harris, P. J. C. (2013). The ecology of arbuscular mycorrhizal fungi. *Crit. Rev. Plant Sci.* 32, 1–20. doi: 10.1080/07352689.2012.683375

Yang, X., Post, W. M., Thornton, P. E., and Jain, A. (2013). The distribution of soil phosphorus for global biogeochemical modeling. *Biogeosciences* 10, 2525–2537. doi: 10.5194/bg-10-2525-2013

Zhang, L., Xu, M., Liu, Y., Zhang, F., Hodge, A., and Feng, G. (2016). Carbon and phosphorus exchange may enable cooperation between an arbuscular mycorrhizal fungus and a phosphate-solubilizing bacterium. *New Phytol.* 210, 1022–1032. doi: 10.1111/nph.13838

Zhu, Y. G., and Miller, R. M. (2003). Carbon cycling by arbuscular mycorrhizal fungi in soil-plant systems. *Trends Plant Sci.* 8, 407–409. doi: 10.1016/S1360-1385(03)00184-5

Conflict of Interest Statement: The authors declare that the research was conducted in the absence of any commercial or financial relationships that could be construed as a potential conflict of interest.

frontiers in Microbiology

ORIGINAL RESEARCH
published: 27 November 2018
doi: 10.3389/fmicb.2018.02862

Soil Matrix Determines the Outcome of Interaction Between Mycorrhizal Symbiosis and Biochar for *Andropogon gerardii* Growth and Nutrition

*Zahra Paymaneh[1,2], Milan Gryndler[2,3], Tereza Konvalinková[2], Oldřich Benada[4], Jan Borovička[5], Petra Bukovská[2], David Püschel[2,6], Veronika Řezáčová[2], Mehdi Sarcheshmehpour[1] and Jan Jansa[2]**

[1] Department of Soil Science, Faculty of Agriculture, Shahid Bahonar University of Kerman, Kerman, Iran, [2] Laboratory of Fungal Biology, Institute of Microbiology, Czech Academy of Sciences, Prague, Czechia, [3] Faculty of Science, Jan Evangelista Purkyně University in Ústí nad Labem, Ústí nad Labem, Czechia, [4] Laboratory of Molecular Structure Characterization, Institute of Microbiology, Czech Academy of Sciences, Prague, Czechia, [5] Institute of Geology, Czech Academy of Sciences, Prague, Czechia, [6] Institute of Botany, Czech Academy of Sciences, Průhonice, Czechia

OPEN ACCESS

Edited by:
Caroline Gutjahr,
Technische Universität München,
Germany

Reviewed by:
Katie Field,
University of Leeds, United Kingdom
Raffaella Balestrini,
Consiglio Nazionale delle Ricerche
(CNR), Italy

***Correspondence:**
Jan Jansa
jansa@biomed.cas.cz

Specialty section:
This article was submitted to
Terrestrial Microbiology,
a section of the journal
Frontiers in Microbiology

Received: 31 July 2018
Accepted: 06 November 2018
Published: 27 November 2018

Citation:
Paymaneh Z, Gryndler M,
Konvalinková T, Benada O,
Borovička J, Bukovská P, Püschel D,
Řezáčová V, Sarcheshmehpour M and
Jansa J (2018) Soil Matrix Determines
the Outcome of Interaction Between
Mycorrhizal Symbiosis and Biochar
for Andropogon gerardii Growth
and Nutrition.
Front. Microbiol. 9:2862.
doi: 10.3389/fmicb.2018.02862

Biochar has been heralded as a multipurpose soil amendment to sustainably increase soil fertility and crop yields, affect soil hydraulic properties, reduce nutrient losses, and sequester carbon. Some of the most spectacular results of biochar (and organic nutrient) inputs are the *terra preta* soils in the Amazon, dark anthropogenic soils with extremely high fertility sustained over centuries. Such soil improvements have been particularly difficult to achieve on a short run, leading to speculations that biochar may need to age (weather) in soil to show its best. Further, interaction of biochar with arbuscular mycorrhizal fungi (AMF), important root symbionts of a great majority of terrestrial plants including most agricultural crops, remains little explored. To study the effect of aged biochar on highly mycotrophic *Andropogon gerardii* plants and their associated AMF, we made use of softwood biochar, collected from a historic charcoal burning site. This biochar (either untreated or chemically activated, the latter serving as a proxy for freshly prepared biochar) was added into two agricultural soils (acid or alkaline), and compared to soils without biochar. These treatments were further crossed with inoculation with a synthetic AMF community to address possible interactions between biochar and the AMF. Biochar application was generally detrimental for growth and mineral nutrition of our experimental plants, but had no effect on the extent of their root colonized by the AMF, nor did it affect composition of their root-borne AMF communities. In contrast, biochar affected development of two out of five AMF (*Claroideoglomus* and *Funneliformis*) in the soil. Establishment of symbiosis with AMF largely mitigated biochar-induced suppression of plant growth and mineral nutrition, mainly by improving plant acquisition of phosphorus. Both mycorrhizal and non-mycorrhizal plants grew well in the acid soil without biochar application, whereas non-mycorrhizal plants remained

stunted in the alkaline soils under all situations (with or without biochar). These different and strong effects indicate that response of plants to biochar application are largely dependent on soil matrix and also on microbes such as AMF, and call for further research to enable qualified predictions of the effects of different biochar applications on field-grown crops and soil processes.

Keywords: arbuscular mycorrhizal fungi, community, historic biochar, mycorrhizal response, nitrogen, phosphorus

INTRODUCTION

Biochar (*sensu lato*, including charcoal and activated biochar) is a solid product of exposure of any organic (carbonaceous) materials such as plant biomass (be it wood, grass biomass or straw) or different kinds of organic waste matter to heat under total or partial absence of oxygen (Hagemann et al., 2018). It is formed either during wildfires or intentionally produced to obtain charcoal/biochar to be used as a fuel or for industrial application (e.g., sorbent) or for soil amendments. It contains highly condensed carbon (C) and by-products of the charring process such as bio-oils and tars, including polycyclic aromatic hydrocarbons (PAHs, which are particularly abundant in fresh biochar, Zhu et al., 2017 and references therein). Application of biochar to soils has previously been proposed to substantially and sustainably increase soil fertility, water holding capacity, and also to sequester C as a mitigation measure to offset anthropogenic CO_2 emissions (Atkinson et al., 2010; Roberts et al., 2010). These suggestions originate from existence of *terra preta* soils in the Amazon and elsewhere in the tropics, where generally unfertile, highly weathered and mostly acid soils have historically been managed by biochar and organic nutrient additions to improve crop nutrition and yields (Glaser and Birk, 2012; Mao et al., 2012). Proposed mechanisms of such soil improvements were enhanced nutrient, mainly nitrogen (N) and phosphorus (P) availabilities, and limitation of nutrient (particularly N) losses to the environment, remediation of pH extremes (particularly the low pH of some of the tropical soils), reducing toxicity of metals (such as aluminum and manganese) and improving cation exchange capacity of the soils (Schulz and Glaser, 2012; Alling et al., 2014; Gul and Whalen, 2016). Further, biochar amendments can improve water holding capacity in sandy soils and aeration in heavy clays through affecting soil porosity (Mickan et al., 2016; Koide, 2017). In contrast to tropical soils, where biochar applications sometimes lead to truly spectacular effects, applications of biochar to temperate soils has generally caused much weaker effects on plants and on the soil quality (Borchard et al., 2012; Jeffery et al., 2017; Koide, 2017). Previously, this has partly been attributed to the fact that biochar was applied fresh in most studies with temperate soils. And it has also been suggested that greatest benefits would only be achieved when biochar slowly weathers and interacts with minerals in the soil over large temporal scales (Atkinson et al., 2010; Borchard et al., 2012; Ren et al., 2018). Such long-term phenomena are, however, very difficult to study directly. Further, it has been proposed that only certain types of biochar could effectively ameliorate certain soil properties such as pH extremes, textural limitations and bioavailability of toxic metals, depending on the biochar feedstock and also on the charring conditions such as temperature and oxygen availability (Jeffery et al., 2011; Kloss et al., 2012; Butnan et al., 2015). In consequence, the type of biochar and also its application rates may need to be finely tuned up for each recipient soil/ecosystem, so as to fit the plant, environment, nutrient inputs and forms, as well as abiotic and biotic soil conditions (Lehmann et al., 2011; Shen et al., 2016; Luo et al., 2017). Particularly, the interactions of biochar with soil microbes including the arbuscular mycorrhizal fungi (AMF) received relatively little experimental attention so far, although evidence for such interactions is currently mounting from different experimental systems (Mickan et al., 2016; Luo et al., 2017; Ohsowski et al., 2018). For example, the ratio between AMF and saprotrophic soil fungal abundances in soil increased due to high rates (30 and 50 tons ha^{-1}) of field biochar application and the saprotrophic fungal to bacterial abundance ratio increased in the 50 tons biochar ha^{-1} treatment in northwest China (Luo et al., 2017). Recent meta-analysis synthesizing effects of biochar on soil microbial communities (Zhang et al., 2018) largely confirmed that biochar soil amendments generally increased soil fungal to bacterial biomass ratios, ratios of Gram-positive to Gram-negative bacteria, as well as total microbial biomass and activity. Biochar also significantly modulated dynamics of ammonia oxidizers in soil, increased their abundance and caused shift in their community composition (promoting diversity of ammonia oxidizing bacteria in contrast to ammonia oxidizing archaea, Song et al., 2014). Different mechanisms behind these effects were suggested such as promotion of soil aggregate formation due to significant inputs of labile C and N with biochar application (particularly of the low-temperature pyrolyzed biochar), shifting soil pH (low-temperature pyrolysis yields biochar with lower pH than higher pyrolysis temperatures), inputs of toxic/signaling compounds with biochar such as PAHs and flavonoids, which could directly affect soil microbes, and also modulating soil properties such as cation exchange capacity and water availability and formation of organo-mineral layers over time (Zhang et al., 2018 and references therein). Biochar has also been proposed to protect beneficial soil microbes (particularly the bacteria) from their predators by providing refugia of appropriate sizes (Lehmann et al., 2011).

Particularly important could be the effects of biochar on the AMF because of their tight functional linkages to the plants. The AMF establish symbiotic relationship with roots of more than a half of extant plant species including many important

crop and grassland species. This symbiosis is responsible for up to 100% of phosphorus (P) uptake of the mycorrhizal plants and also for a significant share of nitrogen (N) uptake by the plants, particularly from the organic N sources (Hodge et al., 2001; Smith et al., 2004; van der Heijden et al., 2008; Hodge and Storer, 2015). It has been reported that AMF hyphae could penetrate biochar particles and gain P that has transiently been adsorbed onto their surfaces (Hammer et al., 2014). Further, biochar amendment to soil exposed to drought promoted the growth of AMF extraradical hyphae in such soils as compared to unamended soil (Mickan et al., 2016). Analysis of microbial communities in African Dark Earths indicated absence of a strong effect of biochar on indigenous AMF (while reporting significantly higher fungal to bacterial ratio) in spite of elevated mineral fertility of such soils as compared to unamended soils (Camenzind et al., 2018). This absence of strong effect of biochar on mycorrhizal abundance is also consistent with the message conveyed from earlier meta-analysis by Biederman and Harpole (2013). However, biochar could still indirectly affect the AMF community and its functioning through changing abiotic soil properties such as pH (Hazard et al., 2013; Jansa et al., 2014), modulating the composition and activity of microbial communities in soil (Luo et al., 2017), and/or affecting biological soil processes such as nitrification (Schulz and Glaser, 2012; Prommer et al., 2014; Gul and Whalen, 2016) – because these processes could importantly feed back on the AMF functioning (e.g., Cheng et al., 2012; Bukovská et al., 2018).

The aim of this study was thus to address interactions between biochar and mycorrhiza with respect to growth and mineral (P and N) nutrition of a highly mycotrophic host plant *Andropogon gerardii* (Püschel et al., 2016; Bukovská et al., 2018), in two different temperate agricultural soils – one developed on a granitic moraine (acid), and the other derived from calcareous river sediments (alkaline). Instead of using freshly prepared biochar, we used historic biochar that has been "composted" for a number of decades in a forest soil, so as to better mimic processes that would only establish after some time from biochar addition to the soil. We used this biochar either untreated or activated through autoclaving and treating it with hydrogen peroxide. The latter treatment has been included as a proxy for freshly prepared biochar, where the biochar active surfaces and pores are typically devoid of microbes or products of their activity and usually show different physico-chemical properties (e.g., greater cation sorption capacity) than aged biochar (Zhu et al., 2017 and references therein). We expected additive and positive effects of both biochar and mycorrhiza on plant P nutrition (in agreement with previous studies, Hammer et al., 2015; Liu et al., 2018). Further, we also expected negative interactions between N nutrition of plants and biochar amendment, based on current literature demonstrating slowing down some pathways involved in soil N cycling due to biochar application (Prommer et al., 2014). To address this latter point, we provided isotopically (^{15}N-) labeled organic N source in a spatially discrete soil patch beyond direct reach of the roots but accessible to AMF hyphae (similarly as in Řezáčová et al., 2018), and measured N transfer to plants by using ^{15}N-isotopic analyses of the plant tissues. Besides, we also addressed whether soil properties and/or biochar amendment affected composition of synthetic AMF communities, by using previously developed quantitative real-time PCR protocol (Thonar et al., 2012).

MATERIALS AND METHODS

Experimental Design

The experiment included all combinations of the three following factor levels: (1) Soil (either acid or alkaline), (2) Mycorrhizal inoculation (with or without an infective AMF community), and (3) Amendment with biochar (none, native historic biochar, or the same biochar activated by autoclaving and hydrogen peroxide). The experiment was carried out in 1-l pots under glasshouse conditions in a completely randomized design with five replicate pots per each of the 12 treatments (i.e., 60 pots altogether).

Pot Experiment Setup

The pots were filled with soil mixed or not with biochar (3.6% by weight, 200 g in total of 5,500 g soil prepared per each treatment) and the mycorrhizal inoculum, alive or autoclaved (9.1% by weight, 500 g in total of 5,500 g soil prepared per each treatment). Further, each pot was supplied with a small root-free patch [a plastic tube with a diameter of 3.6 cm and 3 cm long, covered at both openings with a hydrophilic 40-μm root exclusion mesh manufactured from polyamide (Silk & Progress, Brněnec, Czechia)]. The mesh excluded roots, but allowed most microbes including fungi as well as aqueous solutions to move through the pores. The root-free patches were buried at a depth of 6 cm below surface before sowing the plants. The patches were filled with 41 g the same material as the rest of each of the pots, and supplemented with organic N source (^{15}N-labeled clover biomass, described in Bukovská et al., 2018; 205 mg per patch, i.e., 0.5% enrichment by weight). Microbial wash from a previous pot cultures grown under the same conditions as the pots used for production of mycorrhizal inoculum but lacking any AMF propagules (i.e., non-mycorrhizal inoculum pots, also called mock inoculum) was added to all pots to equalize composition of microbial communities at the beginning of the experiment (Gryndler et al., 2018). To this end, potting substrate from the non-mycorrhizal inoculum pots was mixed with water in proportion 1:10 (*w:v*) and filtered through 40-μm analytical sieve. This suspension was then added and mixed to all soils at a rate of 200 ml per 5,500 g of soil (i.e., 3.6% *v:w*).

Biochar

The native softwood biochar was obtained from a place where charcoal was historically produced for industry applications (glassworks) using large charcoal piles, and was at least 70 years old, deposited under forest litter, overgrown by trees (**Figure 1**), and sparsely colonized by fungal hyphae (**Figure 1**). It was collected in large pieces (2–7 cm in diameter), broken to small particles by a hammer and sieved through a 2-mm sieve. It was used either untreated (unsterile, native) or activated in two steps: (1) Autoclaving at 121°C for 30 min, cooled down and incubated at room temperature for 7 days. (2) Subjected to oxidation by

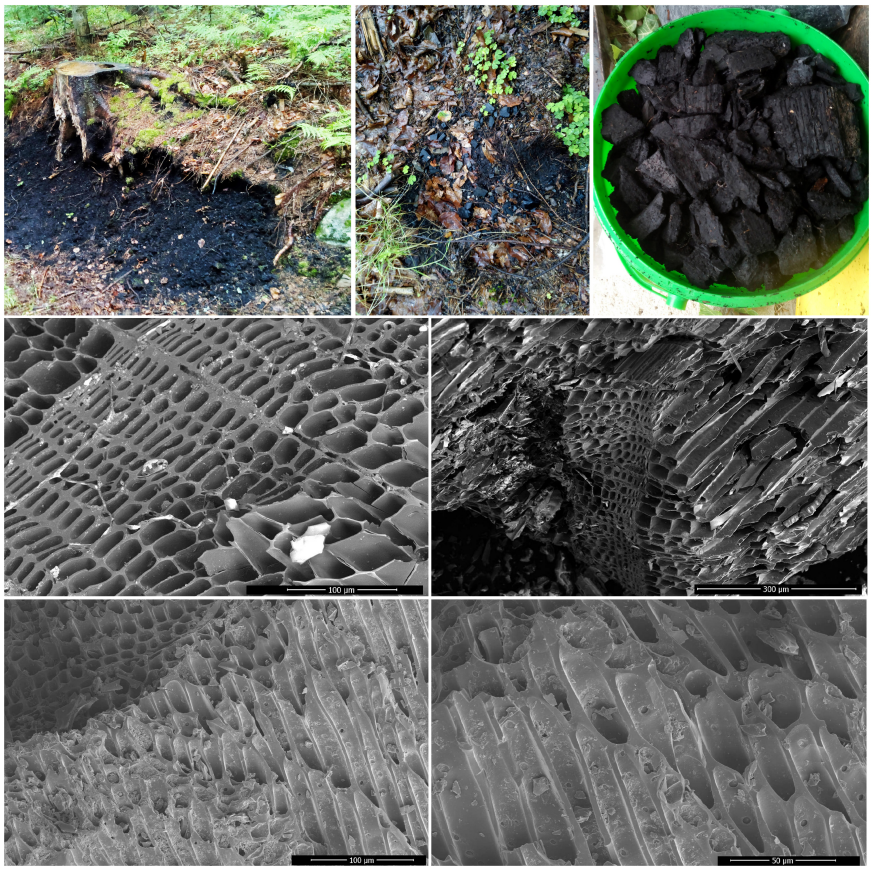

FIGURE 1 | Remnants of a historic charcoal pile under a tree stump and a photo of charcoal fragments recovered from that site (upper row). Scanning electron microphotographs of the biochar recovered from the historic charcoal burning site (native biochar, middle row) and of the biochar activated by autoclaving and hydrogen peroxide treatment (bottom row).

10% H_2O_2 (3 l of such hydrogen peroxide solution added to 1 kg of the biochar). After 30 min from addition of the peroxide, the temperature of the slurry raised to +80°C, at which point we added 3 l of distilled water and cooled the slurry in snow (0°C). The solution was then separated from the biochar by filtration through glass fiber paper. Initial eluent was black–brown. The biochar was then thoroughly washed with 1 l of distilled water three times until the eluent was only slightly colored, and dried in the oven at 65°C for 2 days, yielding about 840 g of dry activated biochar (starting with 1 kg of native biochar).

Soils, Plants, and the Glasshouse

Two kinds of soil were used in the experiment described here: Acid soil was collected from Tänikon, Switzerland (pH = 6.5, for further details please see **Table 1** and Jansa et al., 2003), while alkaline soil was collected in Litoměřice, Czechia (pH = 7.8, for further details please see **Table 1** and Řezáčová et al., 2016). Both soils were air-dried at room temperature and sieved (<8 mm), homogenized and sterilized by gamma-irradiation (min 25 kGy) 3 months prior to the pot experiment described here. The pots were sown with *Andropogon gerardii* (30 seeds per pot) provided by Jelitto Staudensamen GmbH (Schwarmstedt, Germany), and the plants were grown in experimental glasshouse of the Institute of Microbiology in Prague under supplemental lighting providing a minimum of 150 µmol m^{-2} s^{-1} photosynthetically active radiation over a 14 h photoperiod. Temperature in the glasshouse fluctuated between 20°C and 30°C during the experiment, with some few warmer episodes (see temperature log in the **Supplementary Table S1**). Pots were watered daily with deionized water to maintain approximately 80% water holding capacity of the soils. No fertilization was provided with the irrigation water throughout the experiment. Yellow charts were installed around the pots to catch adult sciarid flies (*Bradysia paupera*) throughout the cultivation, and, additionally, a pyrethroid insecticide (Karate, Syngenta) was sprayed twice to all pots throughout the cultivation. A few pots, which had most of the plants dead due to the activity of the flies, were re-sown with 30 seeds of *Andropogon gerardii* during the first 3 weeks of the experiment. The duration of the cultivation was 65 days altogether.

Mycorrhizal Fungi

Synthetic community of five monospecific AMF isolates originally obtained from a single field site in Switzerland

TABLE 1 | Chemical properties of the differently amended soils and the biochars before cultivation of the plants.

Material	Amendment	pH	P total [1] (mg/kg)	P water extractable [2] (mg/kg)	P immediately available [3] (mg/kg)	C (%)	N (%)
Acid soil	None	6.53	614	4.31	2.45	1.99	0.11
Acid soil	Active biochar	6.49	579	1.57	2.14	3.76	0.14
Acid soil	Native biochar	6.84	772	1.35	1.64	3.58	0.14
Alkaline soil	None	7.80	658	4.14	2.45	0.79	0.08
Alkaline soil	Active biochar	7.13	539	4.17	0.72	2.77	0.13
Alkaline soil	Native biochar	7.08	588	3.22	0.46	3.86	0.18
Biochar active		3.46	133	38.8	38.1	51.2	0.30
Biochar native		4.36	80.8	6.86	3.97	57.0	0.31

Phosphorus (P) concentrations were analyzed spectrophotometrically at 610 nm according to Ohno and Zibilske (1991), and the concentrations of total organic carbon (C) and total organic nitrogen (N) were measured using Flash 2000 elemental analyzer (Thermo Fisher Scientific). Average values out of two technical replicates each are shown. [1] P concentration in the soils/biochar measured after incineration of the samples at 550°C for 12 h and extraction of the ashes with concentrated (65%) and hot (200°C) HNO_3. [2] P concentration in the soils/biochar measured in water extracts (1:10, w:v) after shaking for 18 h and filtration through 0.22 μm membrane filter. [3] Concentration of instantaneously available P in the samples (exchangeable within 1 min of isotopic exchange), assessed by the Isotope Exchange Kinetics method and carried out according to Frossard and Sinaj (1998).

(Jansa et al., 2002) was used to inoculate the soils. The AMF isolates originated from the same field site from which the acid soil was collected for the experiment described here. The AMF inocula were produced in open pot cultures with leek (*Allium porrum* L.) as a host plant for more than 2 years prior to setting up the pot experiment described here. Pots for production of the AMF inocula were filled with substrate composed of 10% (by volume) of sterilized soil, 45% autoclaved sand and 45% autoclaved zeolite[1] (1–2.5 mm grain size). For inoculum production of *Gigaspora* and *Racocetra*, we used substrate mixture containing the acid soil described above, and for production of *Funneliformis*, *Claroideoglomus*, and *Rhizophagus*, we used substrate with the alkaline soil (see above). Spore density in the inoculum production pots ranged from about 5 spores per gram for *Racocetra* to more than 250 spores per gram for *Rhizophagus*. Based on this rough estimate of infective propagule density and previous experience on competition between the AMF isolates (Thonar et al., 2014), we mixed the different monospecific inocula as follows: *Racocetra pellucida* BEG[2] 153–1,800 g, *Gigaspora margarita* BEG 152–1,800 g, *Claroideoglomus claroideum* BEG 155–1,800 g, *Rhizophagus irregularis* BEG 158–900 g, and *Funneliformis mosseae* BEG 161–300 g. Half of the mix (3.3 kg) was autoclaved at 121°C for 30 min to create non-mycorrhizal inoculum, whereas the other half (3.3 kg) was used alive as mycorrhizal inoculum. One hundred grams of the inocula (either autoclaved or not, containing the substrate from previous pot cultures, fragments of leek roots from the previous pot culture, cut to <1 cm length, AMF spores and hyphae as well as other microbes) were administered to each pot.

Plant, Soil, and AMF Analyses

Upon harvest, the shoots of the plants were cut at the substrate level, weighed fresh, dried at 65°C for 72 h and then, their dry weights were recorded. The roots were shaken off loosely adhering soil, cleaned under tap water, blotted against paper towel and fresh weight of the entire root system per pot was recorded. Thereafter, roots from each pot were cut to approximately 1-cm long fragments, mixed and a part of the roots (between 0.2 and 4 g fresh weight, exact values recorded) taken for staining and microscopy assessment of root colonization by AMF structures. The remaining roots were weighed fresh once again, then dried at 65°C for 72 h and dry weights recorded. Dried root and shoot samples were then pulverized using an oscillatory ball mill (MM200, Retsch, Haan, Germany). In those samples, concentration and isotopic composition of N were assessed using elemental analyzer (Flash EA 2000) coupled with an isotope-ratio mass-spectrometer (Delta V Advantage, Thermo Fisher Scientific, Waltham, MA, United States). The concentration of P in the biomass samples was assessed by malachite green method (Ohno and Zibilske, 1991), following incineration of the samples at 550°C as described previously (Slavíková et al., 2017). DNA from the roots was extracted using the glassmilk method (Gryndler et al., 2014), employing the internal DNA standard to check for presence of PCR inhibitors and to estimate DNA losses during the extraction (Thonar et al., 2012). DNA extraction from the soil samples (separately for the rooted soil and for the root-free patch) was carried out using the NucleoSpin® Soil DNA extraction kit (Macherey-Nagel, Düren, Germany), employing SL1 lysis buffer and extraction enhancer SX, according to manufacturer's recommendations. Taxon-specific primers and hydrolysis (TaqMan) probes targeting taxon-specific sequence motifs in the nuclear large ribosomal subunit RNA gene were used to quantify the abundance of the five AMF species administered with the AMF inoculum, in the roots of the experimental plants as well as in the soil samples. The analyses were carried out according to the quantitative real-time PCR protocol and cycling conditions described previously (Thonar et al., 2012), using StepOnePlus real-time cycler (Applied Biosystems), 20 μl reaction format (including 2 μl DNA template), Soil Biodyne chemistry (5x HOT FIREPol® Probe qPCR Mix Plus with ROX) and amplicons of large ribosomal subunit RNA gene of the respective AMF taxa to calibrate the analyses. Primers and TaqMan probes were synthesized and HPLC purified in Generi Biotech (Hradec Králové, Czechia).

[1] www.zeopol.com

[2] The International Bank for the Glomeromycota, www.i-beg.eu.

Roots for microscopy assessment of the colonization by the different AMF structures were processed as described previously (Püschel et al., 2016). Briefly, the samples were stored temporarily in 50% ethanol and then stained using the modified method of Koske and Gemma (1989): The roots were first macerated in 10% KOH (60 min at 90°C, followed by 25 min at room temperature), then washed with tap water, neutralized in 2% lactic acid (30 min at 90°C), and stained with 0.05% Trypan blue in LG (lactic acid–glycerol–water, 1:1:1, v:v:v) for 30 min at 90°C followed by overnight incubation in LG at room temperature. The next day, the roots were washed with tap water and further stored in LG. Colonization of the roots by AMF was quantified under a dissecting microscope at 100× magnification following the method of McGonigle et al. (1990). One hundred root intersections were observed per root sample through the eyepiece grid while recording separately the occurrence of AM fungal hyphae, arbuscules, and vesicles in each root intersection.

All different soils amended or not with the different biochars, and the biochars themselves, were analyzed for their physico-chemical properties. Specifically, we measured pH in 1:2.5 (*w:v*) slurry, and the total and water-extractable P concentrations as well as immediately plant-available P concentrations as per the isotope exchange kinetics (Frossard and Sinaj, 1998). For total P concentration assessment, soil samples (0.5 g) were first incinerated at 550°C for 12 h, extracted with 1 ml boiling HNO_3, made up to 50 ml with ultrapure water, and the P concentrations in the extracts was measured with malachite green method (Ohno and Zibilske, 1991). Water-extractable P concentrations in the soils were assessed in samples shaken with water (1:10, *w:v*) for 18 h, filtered through 0.22-μm membrane filter and the P concentrations measured with the malachite green method as above. The C and N concentrations in the soils and the isotopic composition of these two elements were assessed using elemental analyzer coupled with isotope ratio mass spectrometer as above. Acidic soil extracts used previously for estimation of total P were subsequently used for quantification of concentrations of selected metals and potentially toxic trace elements by either inductively coupled plasma sector field mass spectrometry (ICPSFMS, Element 2, Thermo Fisher Scientific, United States) or inductively coupled plasma optical emission spectrometry (ICPOES, Agilent 5100 SVDV, United States) as appropriate (see **Supplementary Table S1** for details).

Calculations and Statistics

Total dry weight of roots per pot was calculated from the ratio of dry-to-fresh weight of the root aliquot subjected to drying × fresh weight of the entire root system in the respective pot. The P and N contents of the plants were calculated from the concentrations of the respective elements in shoot and root biomass and the biomass of the shoots and roots in the individual pots, respectively, and then summed together. Mycorrhizal growth, P uptake, and N uptake responses for the pots inoculated with living AMF inoculum were calculated as natural logarithm of a ratio of plant biomass, P or N content of the plants, respectively, in the individual pots inoculated with living AMF inoculum, and the average of the respective non-mycorrhizal control treatment. Measured abundances of the different AMF taxa in the root and soil samples (gene copies per unit weight of the samples) were corrected for recovery of the internal DNA standard per each individual sample as described previously (Thonar et al., 2012). Preferential allocation of the biomass of each AMF taxon to the root-free compartment (RFC) amended with organic N source as compared to the rooted soil was calculated for each pot as follows:

$$\textit{Hyphal allocation index} = \ln\left(\frac{\textit{abundance of AMF taxon in RFC} + 1}{\textit{abundance of AMF taxon in rooted soil} + 1}\right),$$

where both of the abundances are given as gene copies of the nuclear large ribosomal subunit of the specific AMF taxon per gram of the respective soil sample.

Rates of transfer of ^{15}N from organic fertilizer to the plant were calculated as described previously (Bukovská et al., 2018). The data were analyzed using one-, two-, and three-way analyses of variance (ANOVA). Significant deviation of the hyphal allocation index from zero was tested by using one-sample *t*-test. Meeting assumptions of the different ANOVA analyses were confirmed by visual inspection of the residual plots. No data transformations were needed in order to fulfill the ANOVA assumptions for data analysis. Tukey's honestly significant different tests were used to separate means at $p < 0.05$ level following significant ANOVA. The stats were calculated in Statgraphics Plus for Windows v. 3.1.

RESULTS

Biochar and Soil Properties

Both native and active biochars showed low pH values between 3.5 and 4.5, high total C concentrations, comparable total organic N and low total P concentrations relative to the soils, and very different P availabilities, with immediately available P concentrations being about 10-fold higher for the active as compared to the native (untreated) biochar (**Table 1**). Biochar addition to the two experimental soils has not markedly changed total P concentrations in those soils, but decreased P availability particularly in the acid soil, and the pH of the alkaline soil, besides markedly increasing C concentration of the soils (**Table 1**).

Plant Growth and Nutrition

Comprehensive statistics of the effects of soil matrix, inoculation with AMF, and the addition of different biochars (and of the interactions between those experimental factors) on plant biomass production and plant mineral nutrition is given in **Tables 2**, **3**. Due to generally strong effect of soil matrix on plant growth and mineral nutrition, and also due to multiple significant interactions between the soil and the other experimental factors, we describe the results of plant biomass production and mineral nutrient (P and N) uptake separately for the acid and alkaline soils below.

Both the biomass production as well as uptake of P and N by the plants were strongly suppressed by biochar addition in the ***acid soil***, particularly in absence of living AMF (see **Figure 2** for graphs and **Figure 3** for photos). Noteworthy, the

TABLE 2 | Results of three-way analyses of variance of plant-related parameters, showing *F*-values and associated *p*-value ranges (ns $p \geq 0.05$, * $0.05 > p \geq 0.01$, ** $0.01 > p \geq 0.001$, *** $0.001 > p$) for individual experimental factors and their combinations (conc., concentration).

Parameter	Soil (A)	Mycorrhiza (B)	Biochar (C)	A × B	A × C	B × C	A × B × C
DW plants[1]	136.2***	60.9***	103.0***	6.2*	67.3***	3.4*	16.2***
P content plants[2]	99.0***	119.1***	100.8***	4.2*	43.5***	0.9 ns	17.5***
N content plants[3]	141.0***	98.6***	82.5***	3.2 ns	48.0***	2.4 ns	9.2***
P conc.[4] shoots	1.3 ns	211.8***	15.7***	9.4**	1.4 ns	6.1**	11.2***
P conc.[4] roots	0.03 ns	434.8***	23.0***	16.2***	2.9 ns	3.1 ns	9.8***
N conc.[5] shoots	1.7 ns	4.6*	2.4 ns	0.6 ns	22.6***	4.5*	17.9***
N conc.[5] roots	0.2 ns	0.03 ns	9.5***	0.2 ns	21.8***	0.1 ns	9.2***
^{15}N transport from RFC to plant[6]	9.2**	129.8***	47.6***	7.7**	15.1***	0.5 ns	2.9 ns

[1] Dry weight (DW) of plants, roots and shoots combined, g/pot.[2] Amount of phosphorus (P) contained in the plant biomass, roots and shoots combined, mg/pot.[3] Amount of nitrogen (N) contained in the plant biomass, roots and shoots combined, mg/pot.[4] Concentration of phosphorus (P) in the shoots or roots, mg/g.[5] Concentration of nitrogen (N) in the shoots or roots, mg/g.[6] Transfer of ^{15}N isotope from the organic amendment placed in the root-free compartment (RFC) to the plant biomass (% of added ^{15}N).

TABLE 3 | Results of two-way analyses of variance of mycorrhiza-related parameters, showing *F*-values and associated *p*-value ranges (ns $p \geq 0.05$, * $0.05 > p \geq 0.01$,*** $0.001 > p$) for individual experimental factors and their combination.

Parameter	Soil (A)	Biochar (B)	A × B
Mycorrhizal growth response	50.5***	12.3***	31.2***
Mycorrhizal P uptake response	93.4***	40.1***	61.3***
Mycorrhizal N uptake response	63.7***	19.8***	17.4***
H%[1]	2.5 ns	0.6 ns	0.3 ns
A%[2]	0.6 ns	1.9 ns	0.1 ns
V%[3]	0.2 ns	0.4 ns	0.4 ns
Claroideoglomus abundance (roots)[4]	7.4*	1.5 ns	1.5 ns
Rhizophagus abundance (roots)[4]	0.8 ns	0.4 ns	0.3 ns
Funneliformis abundance (roots)[4]	0.2 ns	0.3 ns	1.0 ns
Racocetra abundance (roots)[4]		n.a. – no positive detection	
Gigaspora abundance (roots)[4]	1.3 ns	1.3 ns	1.3 ns
Claroideoglomus abundance (soil)[4]	8.5**	2.0 ns	3.7*
Rhizophagus abundance (soil)[4]	0.6 ns	0.8 ns	0.1 ns
Funneliformis abundance (soil)[4]	6.3*	2.1 ns	2.3 ns
Racocetra abundance (soil)[4]	2.2 ns	1.2 ns	1.2 ns
Gigaspora abundance (soil)[4]	2.8 ns	1.2 ns	1.1 ns
Claroideoglomus abundance (RFC)[4]	7.6*	3.1 ns	3.5*
Rhizophagus abundance (RFC)[4]	3.7 ns	0.5 ns	1.9 ns
Funneliformis abundance (RFC)[4]	0.5 ns	5.6**	0.0 ns
Racocetra abundance (RFC)[4]	0.6 ns	0.9 ns	0.3 ns
Gigaspora abundance (RFC)[4]	0.1 ns	1.1 ns	1.6 ns

Only mycorrhizal pots (i.e., the pots inoculated with living AMF inoculum) have been considered for the analyses presented above.[1] Fraction of root length colonized by mycorrhizal hyphae (% root length).[2] Fraction of root length colonized by arbuscules (% root length).[3] Fraction of root length colonized by vesicles (% root length).[4] Abundance of Claroideoglomus claroideum/Rhizophagus irregularis/Funneliformis mosseae/Racocetra pellucida/Gigaspora margarita in roots/rooted soil (soil)/root-free compartment (RFC), as assessed by quantitative real-time PCR (qPCR) using previously described primers and TaqMan probes (Thonar et al., 2012).

production of biomass as well as uptake of both P and N by the non-mycorrhizal plants was always lower with the native as compared to active biochar ($p < 0.05$ in all three cases). This biochar-induced suppression was to a great extent (although not fully) mitigated by AMF inoculation of the acid soil, with the differences between the native and active biochar treatments vanishing for the mycorrhizal plants (**Figure 2**). This pattern of effects resulted in the mycorrhizal growth- and nutrient uptake-responses in the acid soil being highest for the native biochar treatment, intermediate for the active biochar treatment and none (to slightly negative, $p = 0.04$ for a *t*-test addressing the difference of mycorrhizal growth response from zero) for the plants growing in acid soil without any biochar addition (**Figure 4**).

Growth and nutrition of the experimental plants in the ***alkaline soil*** was mainly affected by AMF inoculation. Non-mycorrhizal plants were generally stunted in alkaline soil amended or not with the different biochars, with no significant differences between the different biochar treatments (**Figure 2**, see also **Figure 3** for photos). When mycorrhizal, the plants

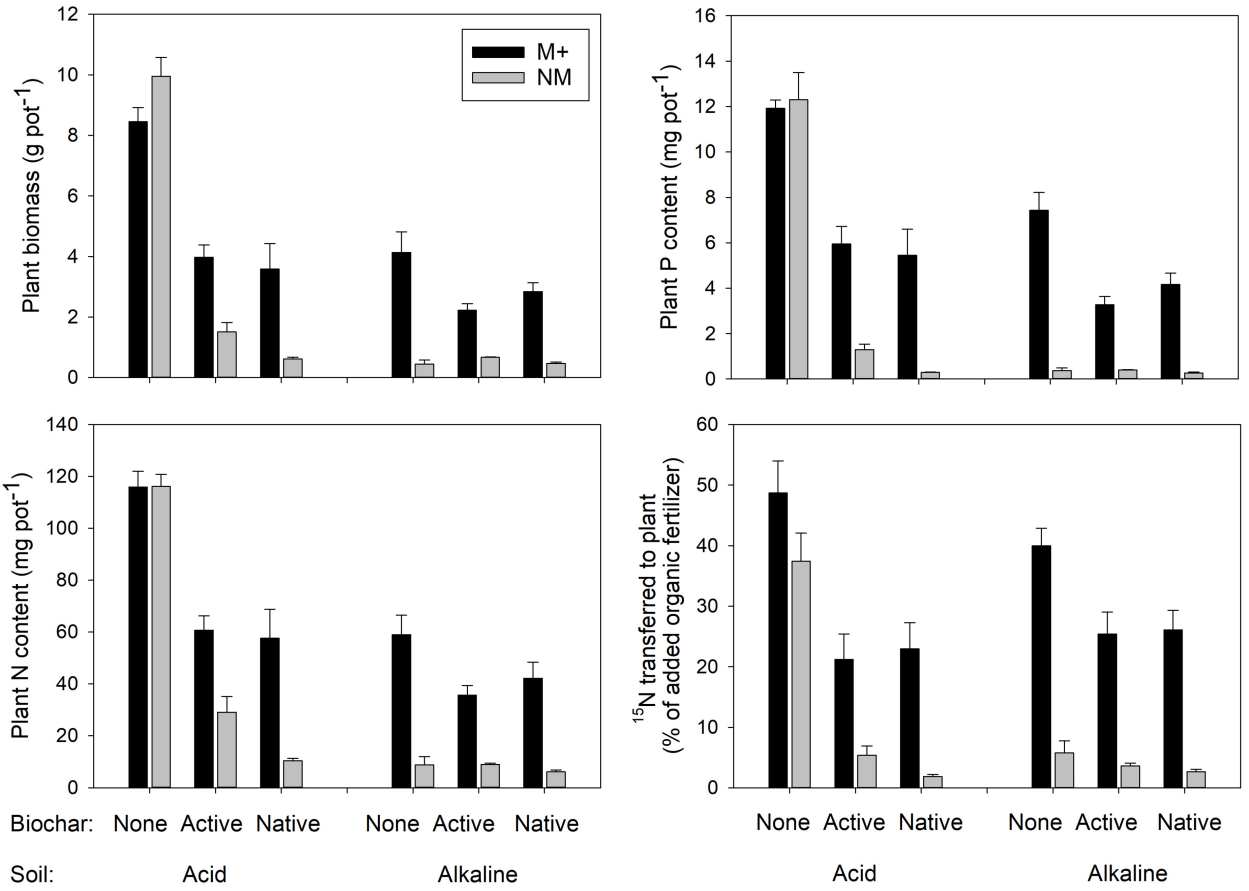

FIGURE 2 | Biomass, phosphorus (P), and nitrogen (N) contents of the *Andropogon gerardii* plants and the rates of transfer of ^{15}N-labeled N from the organic fertilizer (plant litter) provided in a root-free compartment to the plants. Plants were grown in either of two different soils amended or not with differently treated biochar. Black bars stand for mycorrhizal (M+) plants, gray bars for the non-mycorrhizal (NM) control treatment. Mean values +SE of means are shown (n = 5).

produced the largest biomass in and took the highest amounts of N and P from alkaline soil without biochar addition, whereas addition of the soil with active biochar always resulted in poorer performance (be it growth or mineral nutrition) of the plants as compared to those growing in absence of any biochar ($p < 0.05$ for all three cases). This resulted in the mycorrhizal growth- and nutrient uptake-responses being high and not significantly different from each other for plants growing in soil without biochar or with native biochar, whereas the responses were always smaller for the active biochar treatment in the alkaline soil (**Figure 4**).

Transfer of ^{15}N From Organic Fertilizer to Plants

Transfer of ^{15}N from the organic fertilizer administered within the RFC to the plant was affected mainly by the inoculation with AMF, with only a minor contribution of the other experimental factors (**Table 2**). Mycorrhizal plants showed systematically higher rates of ^{15}N uptake from the organic fertilizer as compared to the non-mycorrhizal plants (**Figure 2** and **Table 2** for the stats). The second most influential factor affecting ^{15}N uptake by plants from the organic fertilizer was biochar addition. Plants growing in soils without biochar addition showed generally higher rates of ^{15}N transfer than those growing in soils added with one or the other biochar (**Figure 2**). There was also a significant effect of soil, as well as interactions of soil × mycorrhizal inoculation and soil × biochar amendment, but the share of explained variability due to these other factors or their interactions was much smaller than the variability explained by the first two single factors and thus the interactions are not further elaborated here (but see **Table 2** for the complete stats).

Mycorrhizal Colonization of Roots and Soils

The extent of root length colonized by mycorrhizal fungi was not affected in the plants provided with the living AMF inoculum by any of the experimental factors for either of the individual structures recorded microscopically (grand mean ± SE across all mycorrhizal plants: hyphae 34.8 ± 2.9 %, arbuscules 20.4 ± 2.0%, and vesicles 3.3 ± 0.8%, see **Table 3** for the stats). No AMF structures were observed in the roots of plants inoculated with autoclaved AMF inoculum (see data in **Supplementary**

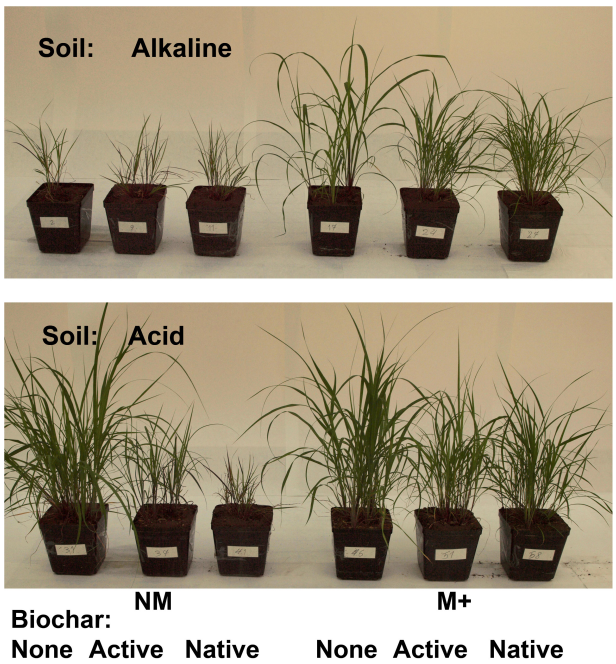

FIGURE 3 | Appearance of the pots and plants shortly before harvest. The photo show mycorrhizal (M+) and non-mycorrhizal (NM) treatments in two different soils, added or not with native or active biochar.

Table S1). Abundances of individual AMF taxa in the roots of plants provided with the living AMF inoculum was not affected by any of the experimental factor except *Claroideoglomus* sp., which was significantly less abundant in the roots of plants growing in alkaline as compared to the acid soil (**Figure 5** and **Table 3**). *Racocetra* was not detected in any root sample, and only trace amounts of *Gigaspora* were detected in the roots from two pots inoculated with the living AMF inoculum and filled with acid soil not amended with any biochar (see **Supplementary Table S1** for details).

Systematically higher abundances of *Claroideoglomus* and *Funneliformis* were recorded in the acid as compared to the alkaline soil (**Figure 5** and **Table 3**). The abundance of *Claroideoglomus* in the rooted soil was further modulated by biochar addition so that the native biochar amendment stimulated ($p < 0.05$) its abundance in alkaline as compared to biochar-free alkaline soil, whereas its abundance tended ($p < 0.1$) to be lower in biochar-amended acid soils than in the acid soil without biochar, resulting in significant interaction between the two (i.e., soil and biochar) experimental factors (**Table 3**). A similar response pattern for *Claroideoglomus* abundance was also observed in the soil collected from the RFC (**Table 3** and **Figure 5**). In the RFC, we also observed a strong and systematic suppression of *Funneliformis* development by both biochar amendments, regardless of the soil matrix (**Table 3**), with the values in biochar-amended RFC reaching only about one third of the values observed in the biochar-free soils (see **Figure 5** and **Supplementary Table S1** for details).

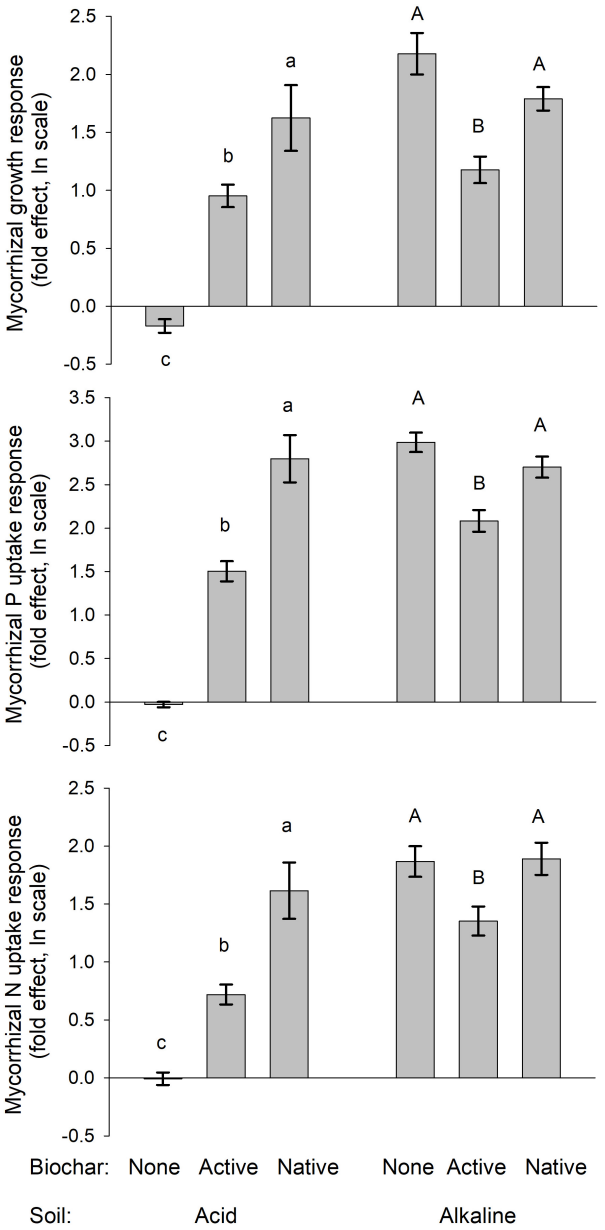

FIGURE 4 | Mycorrhizal growth-, P uptake-, and N uptake-responses of the mycorrhizal plants grown in different soils and amended or not with differently treated biochar. Mean values ± SE of means are shown ($n = 5$). Different lowercase letters indicate statistically significantly different treatments within the acid soil treatment group, whereas different uppercase letters indicate different treatments within the alkaline soil treatment group.

For the three dominant AMF taxa (i.e., *Funneliformis*, *Rhizophagus*, and *Claroideoglomus*), we observed significantly greater hyphal allocation to the organic N-amended RFC than to the rooted soil compartment ($p < 0.05$ in all three cases), whereas no preferential hyphal allocation to the RFC was observed for *Gigaspora* or *Racocetra* (see **Supplementary Table S1** for data, analyses not shown). Besides, preferential hyphal allocation to the RFC was greater in alkaline soil than in the acid soil for

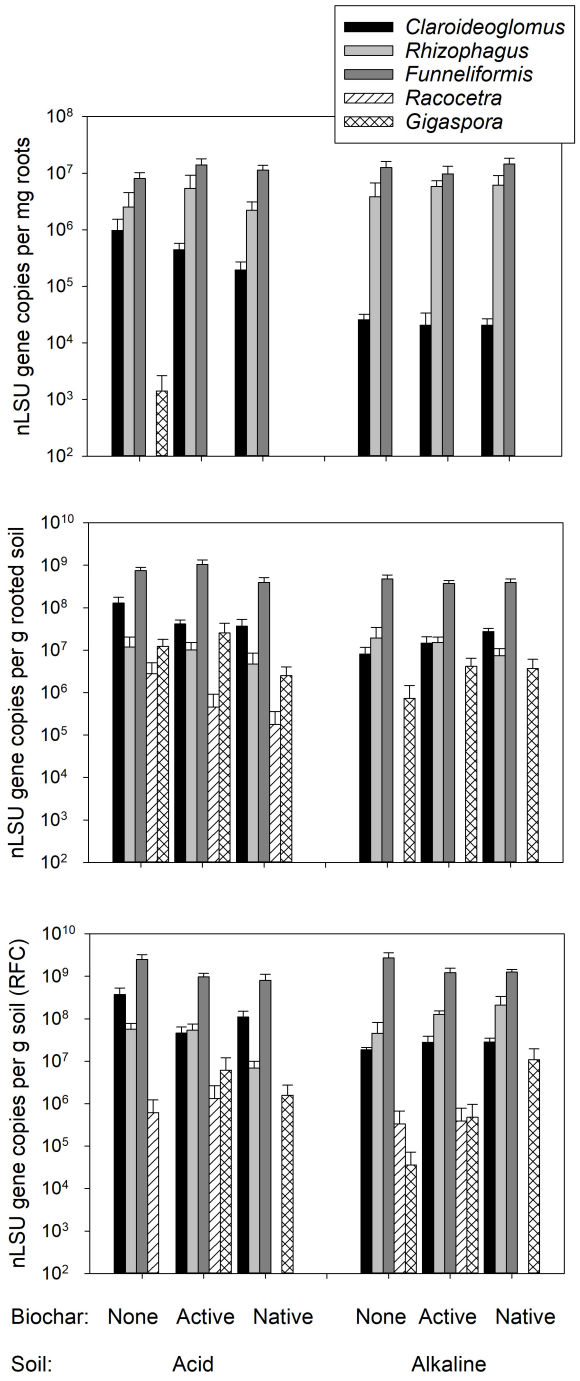

FIGURE 5 | Abundance of the different arbuscular mycorrhizal fungal (AMF) taxa in the roots of plants inoculated with living mycorrhizal inoculum, rooted soil and the root free compartment (RFC), as assessed by quantitative real-time PCR targeting taxon-specific motifs in the nuclear large ribosomal subunit (nLSU) RNA gene. Mean values +SE of means are shown on a logarithmic scale (n = 5).

Funneliformis ($p < 0.05$). Hyphal allocation to the RFC was never affected by any biochar application for any of the AMF taxa included in this study (analyses not shown).

DISCUSSION

Establishment of arbuscular mycorrhizal symbiosis was obviously very important for *Andropogon* growth and nutrition in the alkaline soil (see also previous research: Bukovská et al., 2018; Gryndler et al., 2018), whereas the performance of the experimental plants in the acid soil (without biochar) was not significantly improved by the AMF inoculation (**Figure 2**). Addition of biochar to either of the soils was generally suppressing plant growth and nutrition as compared to the respective soil treatments without biochar. In the acid soil, mycorrhizal symbiosis significantly (though not fully) counteracted biochar-induced growth and nutrient uptake suppressions. In the alkaline soil, the growth of non-mycorrhizal plants was so stunted that no detrimental effects of biochar (as compared to the treatment without biochar) were detectable in the non-mycorrhizal control treatment. Yet, the mycorrhizal plants growing in biochar-amended alkaline soil grew smaller and took up less nutrients than those growing in the soil without biochar, indicating negative effect of biochar on our experimental plants, which obviously could not fully be restored by the symbiosis with the AMF. Interestingly, the active biochar caused systematically lower mycorrhizal growth and nutritional responses than the native biochar in both of the soils included in this study (**Figure 4**). These results were surprising and partly cross to our expectations of neutral to positive effects of biochar on plant growth and/or mineral nutrition, in concert with the earlier literature reports (Jeffery et al., 2011; Spokas et al., 2012; Biederman and Harpole, 2013). Further, we expected synergistic and positive effects of both biochar and AMF on the plants, whereas the actual outcome of the interaction turned to be very much dependent on the soil matrix. Our results indicate that biochar either directly intoxicated the plants and/or interfered with their nutrient uptake or that it caused changes in the soil microbiome with detrimental consequences for the plant nutrition and/or growth. These different scenarios and the fact that the detrimental effect of biochar could at least partly be counteracted by the AMF, deserve specific attention here.

Possible Biochar Phytotoxicity

Freshly prepared biochar could be toxic to the plants due to presence of a variety of tars and oily substances including PAHs (Dutta et al., 2017; Liu et al., 2017; Zhu et al., 2017, and references therein). By using aged biochar that spent decades in the forest soil prior to the experiment described here, being exposed to temperature fluctuations, biological activity and percolating rainwater throughout the years, we expected to eliminate presence of such toxic and partly volatile compounds in our experiment – although, admittedly, we did not measure presence of such compounds directly nor did we carry out any standardized toxicity biotest with our biochars. Still another option would be that the biochar could have, over the years, absorbed significant amounts of toxic elements or other environmental pollutants. Then the biochars could poison our experimental plants in the pots. However, given no elevated toxic element concentrations in our biochars were detected

(see **Supplementary Table S1** for data), and also because we did not observe any specific toxicity symptoms such as leaf discolorations or stripes (personal observations), direct toxicity of the biochars to our experimental plants is rather an unlikely scenario.

Biochar Interference With Plant Nutrition

Untreated historic biochar applied to acid soil decreased the growth and N uptake of non-mycorrhizal *Andropogon* plants more than 10-fold. Furthermore, the P uptake of the non-mycorrhizal plants decreased more than 30-fold due to application of the untreated biochar into acid soil, whereas the negative effects of active biochar on non-mycorrhizal plants in the acid soil were much less prominent (**Figure 2**). We interpret this as extraordinary capacity of the untreated historic biochar to decrease P availability in the acid soil (although the measured decrease in immediately available P pool due to untreated biochar application to acid soil was "only" up to sixfold, **Table 1**). Mycorrhizal plants in both acid and alkaline soils were suppressed by about 50% in their growth and mineral (P and N) nutrition as compared to the mycorrhizal plants in the respective soils without biochar (**Figure 2**). In alkaline soils, the suppression of plant growth and mineral uptake tended to be greater in soils added with active as compared to untreated biochar. This may be a result of higher P availability in the soil due to application of active as compared to untreated biochar (**Table 1** and **Figure 3**), in line with resource stoichiometry framework (Johnson et al., 2010, 2015) which predicts that increasing P availability in soil loosens tight mutualism between the plant and the AMF. The plants, in consequence, become more reliant on the direct (root) P uptake pathway upon active as compared to untreated biochar application, which may however not be able to fully compensate for particularly effective P acquisition via the indirect (mycorrhizal) P uptake pathway (see Smith and Smith, 2012, for further discussion).

Collectively, the above results indicate that growth of the plants in our experimental system was primarily limited by P availability in the differently treated soils. This is because both P concentrations (**Figure 6**) and also P contents of plants (**Figure 2**) were usually dramatically increased by presence of AMF, whereas biochar generally caused a decrease in both P concentrations and P contents of the plants (consistent with its effect on decreasing available P in soil, see **Table 1** for P availability data and **Table 2** for the plant experiment stats). The effects of experimental treatments on N concentration in the plants (that would be suggestive of N limitation) have been much milder as compared to the effects on P concentrations/contents (**Figure 6** and **Table 2**). Importantly, the N:P ratio sharply increased with decreasing plant biomass, being around 10 for large plants (3 g total dry biomass per pot and higher) and rocketing up to 90 for the smallest plants (see **Supplementary Table S1** for data). This further suggests that it was the P, and not the N, which was the primary limitation of the growth, and also explains why mycorrhiza was such a prominent factor of plant growth/nutrition in our experimental system – because of its well-recognized role in plant P nutrition, namely supplying P from soil to the host plant via the mycorrhizal (indirect) P uptake pathway (Smith et al., 2004; Johnson et al., 2015). Such a pathway is highly effective under low P availability in soil, but may become an energetic burden for the plant under high P availabilities, resulting in down-regulation of the mycorrhizal colonization of roots and also in declining mycorrhizal benefits upon elevated P concentration in soil (Konvalinková et al., 2017 and references therein).

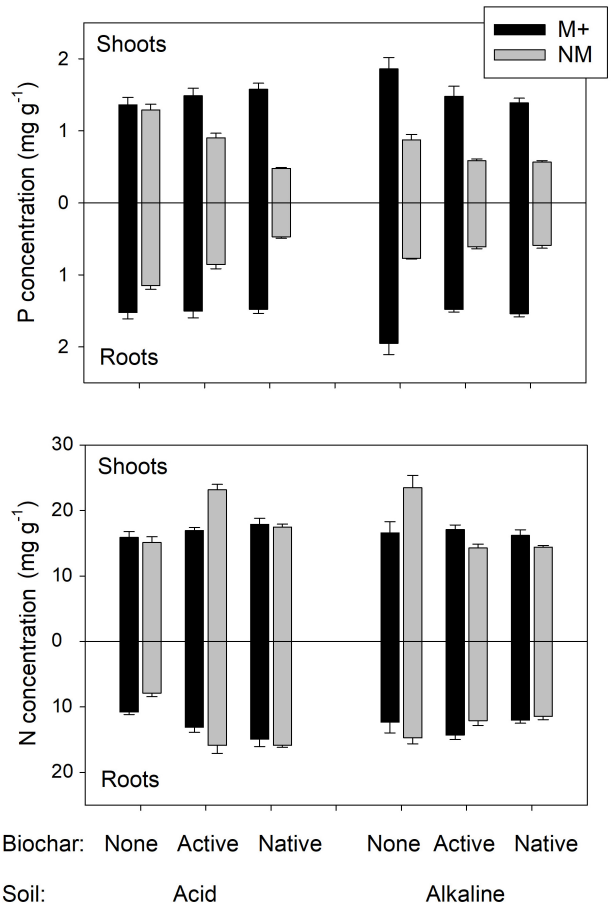

FIGURE 6 | Phosphorus (P) and nitrogen (N) concentrations in shoots and roots of experimental plants. Plants were grown in either of two different soils amended or not with differently treated biochar. Black bars stand for mycorrhizal (M+) plants, gray bars for the non-mycorrhizal (NM) control treatment. Mean values +SE of means are shown (n = 5).

There are several possible options to explain how biochar does lower the P availability in the soil – both for the roots and also for the AMF hyphae. This could be achieved either directly, e.g., by adsorbing orthophosphate onto inner surfaces of biochar particles (see **Figure 1** for photos) that could not easily be accessed by roots and/or the hyphae due to small pore sizes. Further, it could promote soil aggregation and/or stabilize Al/Fe/Ca complexes that could either irreversibly bind inorganic orthophosphate or make it spatially inaccessible to (hidden from) the roots and/or hyphae (Dai et al., 2017; Zhang et al., 2017; Borno et al., 2018). Biochar could also bind/inactivate root or hyphal exudates such as organic acid responsible for increasing

P availability in the immediate vicinity of the roots/hyphae (Lehmann et al., 2011; Spokas et al., 2011; Ameloot et al., 2013; Sun et al., 2016; Koide, 2017). The biochar could, in addition, also suppress microbial nutrient cycling (Prommer et al., 2014) which could have consequences for both P and N availabilities to the roots and/or to the AMF hyphae. Still another scenario would be that some microbes would directly feed on the biochar C (Zhu et al., 2017), and in consequence immobilizing inorganic nutrients such as P and/or N from the soil solution in their biomass – such a scenario is however rather unlikely for aged biochar that has previously been exposed to microbial degradation for a couple of decades such as in our case.

Whereas mycorrhizal symbiosis certainly has improved P nutrition of our plants (see above), it also seems to have positively affected plant N acquisition from organic N source labeled with ^{15}N and supplied in the RFC. Noteworthy, the ^{15}N transfer from the organic fertilizer to the plants correlated significantly with size of the plants (R^2 = 68.9%, $p < 0.001$). This may mean, on one hand, that ^{15}N was taken up mainly passively with the water mass flow (which would be much higher for larger than for smaller plants) or that it was taken up actively to AMF hyphae and then transported to the plants, because mycorrhizal plants were generally larger that their non-mycorrhizal counterparts, particularly in the biochar-amended soils. This latter notion is indirectly supported by the fact that the ratio of the amount of ^{15}N transferred from the RFC to the plants was nearly twice as high for mycorrhizal as compared to the non-mycorrhizal plants (t-test $p = 0.024$) growing in acid soil without biochar (size of the plants in those two treatments was namely well comparable, **Figure 2**). This is also consistent with previous literature providing experimental evidence for active N transport from soil to plant via AMF hyphae (Mäder et al., 2000; Hodge et al., 2001; Hodge and Fitter, 2010; Bukovská et al., 2018). What needs further research, however, is whether and how the AMF promoted organic N mineralization. There is quite some controversy on this topic in the literature; an obvious problem being the fact that AMF are thought to be completely dependent on other microbes to release mineral N from organic N sources. However, some other reports also show that AMF may also suppress microbial activity in the soil through effectively mining the mineral N and P from the soil solution, or through direct or indirect allelopathy (Herman et al., 2012; Nuccio et al., 2013; Gui et al., 2017; Bukovská et al., 2018; Koide and Fernandez, 2018). Further research in this direction is thus certainly warranted.

Possible Changes of Soil Microbiome Due to Biochar Application

Biochar application can exert significant changes on soil microbial communities (Zhu et al., 2017; Zhang et al., 2018). Theoretically, biochar could stimulate specific plant-pathogenic microorganisms that would negatively affect *Andropogon* performance in our pot experiment and this apparent negative effect could be counteracted by the AMF because the AMF have previously been reported to play a role in plant tolerance to pathogens (e.g., Newsham et al., 1995). The native biochar could also carry with it some living microorganisms that could affect the plants/AMF in the pots – whereas the active charcoal is unlikely to cause any significant biological inputs, in contrast. However, thorough investigation of the microbial (e.g., prokaryotic) communities in the different soil treatment was beyond the scope of the research described here. Therefore, it remains a speculation whether native biochar introduced any specific plant pathogens to our experimental system or whether the biochar amendment to our pots consistently stimulated any pathogenic microbes from the pool of microbes already present in the pots.

Our analyses concentrated on the abundance of AMF taxa inoculated into the pots and on possible AMF inputs (contaminations) with the untreated biochar, recovered from the forest floor. And there we saw surprisingly little effect of the biochar on both the extent of root colonization by the inoculant AMF (**Table 3**) and the abundance of the individual AMF taxa in the roots and in the soil (**Table 3** and **Figure 5**). These results are in line with the field observations showing no major effect of biochar on AMF (e.g., Camenzind et al., 2018). Besides, we obtained no evidence for any significant AMF load with the native biochar as the plants growing in soil with untreated biochar and not inoculated with living AMF all remained non-mycorrhizal (see **Supplementary Table S1** for data).

Whereas there was no strong effect of biochar on most of the AMF taxa and the extent of root colonization by AMF structures in our pots experiment, both *Claroideoglomus* and *Funneliformis* showed some preference for the acid soil, which was actually their home environment – possibly because of the soil pH (Jansa et al., 2014). This latter notion is further supported by the fact that *Claroideoglomus* was differentially affected by biochar application into the different soils, co-incident with pH shifts induced by the biochar application (compare **Table 1** and **Figure 5**). The reason why preferential hyphal allocation of *Funneliformis* to RFC was greater in alkaline than in the acid soil remains unclear, however – the hyphae could be attracted either by free N or other cues, but we have no unequivocal mechanistic explanation for the observed effect at this stage of research.

A notable and unique observation was that biochar specifically and systematically suppressed hyphal development of *Funneliformis* in the RFC, though not necessarily in the rooted soil (**Figure 5**). This may have something to do with biochar changing porosity of the soils as it has previously been shown that AMF hyphal growth could indeed be affected by soil porosity (Drew et al., 2003; Martin et al., 2012). Why *Funneliformis* and not the other AMF taxa reacted to biochar remains unclear, though. Another explanation is that the combination of biochar with organic fertilizer in the RFC was a particularly unsuitable environment for *Funneliformis* (but see above for the discussion on the differential hyphal allocation of *Funneliformis* to RFC in the different soils). Since we did not include RFC without organic fertilizers nor we did compensate for N inputs in the rooted soil, elucidating possible specific interactions between *Funneliformis* hyphal networks, organic N fertilizer and biochar additions, and distance from the roots, would require lot of additional research efforts.

Caveats

There were a few uncontrolled factors in our experiment that could have partly biased the results and/or their interpretation:

First, all pots were sprayed with an insecticide in order to prevent uncontrolled damage of the plants by insects. Whereas spraying all pots (and not just their selection) hopefully eliminated a systematic bias of any of the experimental factors tested here, pesticide inputs could have stimulated or suppressed the AMF, for example. This was not tested here for obvious reasons (because it would require a whole new experiment and selective application of the pesticide on some pots and not on others). Yet the insecticides are usually exerting only a mild effect on the AMF, in contrast to herbicides or fungicides (Jansa et al., 2006).

Second, autoclaving of mycorrhizal inoculum for addition into the non-mycorrhizal control treatment could have affected nutrient (e.g., P) availability or other physico-chemical soil properties as reported before (e.g., Mahmood et al., 2014, and multiple references therein). Yet the mycorrhizal inoculum only contained 10% (by volume) of soil, the rest being intact carriers (zeolite and sand), so the effects on nutrient availability in the entire pot (containing about 1 kg of γ-rays sterilized soil each) amended with as little as 10 g autoclaved soil (and some organic matter including leek roots from the previous pot cultures) was likely negligible. Since the soil for filling the pots was not autoclaved but only γ-rays sterilized (well in advance of the experiment setup), the bias due to soil sterilization should not invalidate the results of our study (although, admittedly, it could have affected them to some limited extent).

Third, we did not compensate for differential porosity and/or volume of biochar-added soils in the biochar-unamended treatments. Given the rates of biochar amendments in our experiment were rather high and the density of the biochar being generally very low compared to soils, this is an issue that should be paid particular attention to in the future (see also Koide, 2017, for extensive discussion on this topic).

Fourth, we only used AMF originally isolated from the acid soil, so they were, strictly speaking, non-native to the alkaline soil. This could have explained some of the soil effects on the abundance of the individual AMF taxa (see above), although at least three of the AMF strains were previously cultured ("trained") in a mixture of the alkaline soil included in this study, zeolite and sand (to produce the AMF inoculum). Admittedly, it would be interesting to directly scrutinize whether soil origin of the AMF isolates had any systematic effect on the interactions of AMF with the biochar, although this would require a whole research program to be thoroughly addressed. Particularly, the AMF native to the alkaline soil included in our study are not yet available in pure cultures for conducting pot experiments such as described in this study.

Fifth, organic fertilizer labeled with ^{15}N was provided in a root-inaccessible nutrient enriched patch, with the nutrient inputs not compensated for in the entire volume of the pot. This is a specific situation, which is justified to test localized response of AMF hyphae to elevated organic nutrient inputs (e.g., Hodge et al., 2001; Bukovská et al., 2016, 2018), although different research questions would have required differently designed experimental setup.

CONCLUSION AND OUTLOOK

Here, we observed strong and negative effects of aged biochar (either untreated or chemically activated) on the growth and nutrition of *Andropogon gerardii* plants in two different soils, and partial remediation of the negative effect of biochar on the plants by inoculation with synthetic AMF communities. Biochar did not strongly affect the composition of the AMF communities nor did it affect the extent of root colonization by AMF structures, although we noted some negative effect of biochar on spatial spread of soil hyphae of *Funneliformis mosseae*. We interpret our results mainly as biochar interfering with root P uptake from soil (most likely by decreasing P bioavailability in soil directly through sorption of free orthophosphate ions from soil solution or occluding soil sorption sites, responsible for exchange of P ions between soil solid phase and soil solution). This is supported by the fact that all poorly growing non-mycorrhizal plants (i.e., all those in alkaline soil and those growing in acid soil added with native biochar) invariably showed symptoms of P deficiency such as violet coloration of leaves (**Figure 3**). Because the AMF provide an alternative P uptake pathway to the direct (root) uptake pathway (e.g., Smith and Smith, 2012), which was likely more effective than the root uptake pathway in biochar-amended soils, the AMF could partly remediate the biochar-induced suppression of plant P nutrition and growth. Our research described here is limited only to one plant species (notably, a non-native plant species to Europe, and the experiment conducted with two European soils), on which biochar application obviously had a strongly negative impact in terms of growth and mineral nutrition. Additional experiments with other plant species, other soils and other biochars and their application rates will thus be needed to allow generalizations (or not) of the results of biochar application and mycorrhizal symbiosis interactions reported here. Particular attention should then be paid to separation of physico-chemical and biological mechanisms by combining sterilization/microbial inoculation treatments and isotopic labeling to directly trace nutrient (and possibly also C) flows in the experimental system. Further, it needs more dynamic (time-series) studies and also testing different biochar amendments in combination with organic nutrient sources as they are thought to interactively affect plant and crop performance in the field soils (Atkinson et al., 2010; Song et al., 2014; Butnan et al., 2015; Ohsowski et al., 2018).

AUTHOR CONTRIBUTIONS

ZP conceived and conducted the experiments and carried out the qPCR analyses on root DNA samples. MG helped with biochar activation and analyses. TK helped with the harvest and manuscript revisions. OB conducted electron microscopy and EDS microanalyses of biochar samples. JB conducted the metal and trace element analyses of soil and biochar. PB provided the ^{15}N-labeled organic fertilizer and helped with the pot experiment harvest and qPCR analyses. DP prepared the soils, helped with the harvest

and contributed to revisions of the manuscript. VŘ helped with the harvest and revised the manuscript. MS helped to designing the experiments and data interpretation. JJ helped to designing the experiments and wrote first draft of the manuscript. All authors contributed to revisions and approved the final version of the manuscript.

FUNDING

This research was supported by Czech Science Foundation (projects 15-05466S and 18-04892S), and by Long-Term Research Development Programs RVO 61348971, RVO 67985939, and RVO 67985831. The authors also gratefully acknowledge access to the electron microscopy facility, supported by project LO1509 of the Ministry of Education, Youth and Sports of the Czech Republic.

ACKNOWLEDGMENTS

Hana Gryndlerová, Eva Rydlová, and Zuzana Čermáková are gratefully acknowledged for their extraordinarily careful support with microscopic, chemical, isotopic and molecular analyses. Constructive criticism by two reviewers led to multiple improvements of the manuscript for which the authors are very grateful.

SUPPLEMENTARY MATERIAL

The Supplementary Material for this article can be found online at: https://www.frontiersin.org/articles/10.3389/fmicb.2018.02862/full#supplementary-material

TABLE S1 | Original (raw) experimental data and datalogger records of the glasshouse condition.

REFERENCES

Alling, V., Hale, S. E., Martinsen, V., Mulder, J., Smebye, A., Breedveld, G. D., et al. (2014). The role of biochar in retaining nutrients in amended tropical soils. *J. Plant Nutr. Soil Sci.* 177, 671–680. doi: 10.1002/jpln.201400109

Ameloot, N., Graber, E. R., Verheijen, F. G. A., and De Neve, S. (2013). Interactions between biochar stability and soil organisms: review and research needs. *Eur. J. Soil Sci.* 64, 379–390. doi: 10.1111/ejss.12064

Atkinson, C. J., Fitzgerald, J. D., and Hipps, N. A. (2010). Potential mechanisms for achieving agricultural benefits from biochar application to temperate soils: a review. *Plant Soil* 337, 1–18. doi: 10.1007/s11104-010-0464-5

Biederman, L. A., and Harpole, W. S. (2013). Biochar and its effects on plant productivity and nutrient cycling: a meta-analysis. *Glob. Chang. Biol. Bioenergy* 5, 202–214. doi: 10.1111/gcbb.12037

Borchard, N., Wolf, A., Laabs, V., Aeckersberg, R., Scherer, H. W., Moeller, A., et al. (2012). Physical activation of biochar and its meaning for soil fertility and nutrient leaching - a greenhouse experiment. *Soil Use Manag.* 28, 177–184. doi: 10.1111/j.1475-2743.2012.00407.x

Borno, M. L., Muller-Stover, D. S., and Liu, F. L. (2018). Contrasting effects of biochar on phosphorus dynamics and bioavailability in different soil types. *Sci. Total Environ.* 627, 963–974. doi: 10.1016/j.scitotenv.2018.01.283

Bukovská, P., Bonkowski, M., Konvalinková, T., Beskid, O., Hujslová, M., Püschel, D., et al. (2018). Utilization of organic nitrogen by arbuscular mycorrhizal fungi-is there a specific role for protists and ammonia oxidizers? *Mycorrhiza* 28, 269–283. doi: 10.1007/s00572-018-0825-0

Bukovská, P., Gryndler, M., Gryndlerová, H., Püschel, D., and Jansa, J. (2016). Organic nitrogen-driven stimulation of arbuscular mycorrhizal fungal hyphae correlates with abundance of ammonia oxidizers. *Front. Microbiol.* 7:711. doi: 10.3389/fmicb.2016.00711

Butnan, S., Deenik, J. L., Toomsan, B., Antal, M. J., and Vityakon, P. (2015). Biochar characteristics and application rates affecting corn growth and properties of soils contrasting in texture and mineralogy. *Geoderma* 237, 105–116. doi: 10.1016/j.geoderma.2014.08.010

Camenzind, T., Hammer, E. C., Lehmann, J., Solomon, D., Horn, S., Rillig, M. C., et al. (2018). Arbuscular mycorrhizal fungal and soil microbial communities in African Dark Earths. *FEMS Microbiol. Ecol.* 94:fiy033. doi: 10.1093/femsec/fiy033

Cheng, L., Booker, F. L., Tu, C., Burkey, K. O., Zhou, L. S., Shew, H. D., et al. (2012). Arbuscular mycorrhizal fungi increase organic carbon decomposition under elevated CO_2. *Science* 337, 1084–1087. doi: 10.1126/science.1224304

Dai, L. C., Tan, F. R., Li, H., Zhu, N. M., He, M. X., Zhu, Q. L., et al. (2017). Calcium-rich biochar from the pyrolysis of crab shell for phosphorus removal. *J. Environ. Manage.* 198, 70–74. doi: 10.1016/j.jenvman.2017.04.057

Drew, E. A., Murray, R. S., Smith, S. E., and Jakobsen, I. (2003). Beyond the rhizosphere: growth and function of arbuscular mycorrhizal external hyphae in sands of varying pore sizes. *Plant Soil* 251, 105–114. doi: 10.1023/A:1022932414788

Dutta, T., Kwon, E., Bhattacharya, S. S., Jeon, B. H., Deep, A., Uchimiya, M., et al. (2017). Polycyclic aromatic hydrocarbons and volatile organic compounds in biochar and biochar-amended soil: a review. *Glob. Chang. Biol. Bioenergy* 9, 990–1004. doi: 10.1111/gcbb.12363

Frossard, E., and Sinaj, S. (1998). The isotope exchange kinetic technique: a method to describe the availability of inorganic nutrients. Applications to K, P, S and Zn. *Isotopes Environ. Health Stud.* 34, 61–77.

Glaser, B., and Birk, J. J. (2012). State of the scientific knowledge on properties and genesis of anthropogenic dark earths in central Amazonia (terra preta de Indio). *Geochim. Cosmochim. Acta* 82, 39–51. doi: 10.1016/j.gca.2010.11.029

Gryndler, M., Černá, L., Bukovská, P., Hršelová, H., and Jansa, J. (2014). *Tuber aestivum* association with non-host roots. *Mycorrhiza* 24, 603–610. doi: 10.1007/s00572-014-0580-9

Gryndler, M., Šmilauer, P., Püschel, D., Bukovská, P., Hršelová, H., Hujslová, M., et al. (2018). Appropriate nonmycorrhizal controls in arbuscular mycorrhiza research: a microbiome perspective. *Mycorrhiza* 28, 435–450. doi: 10.1007/s00572-018-0844-x

Gui, H., Hyde, K., Xu, J. C., and Mortimer, P. (2017). Arbuscular mycorrhiza enhance the rate of litter decomposition while inhibiting soil microbial community development. *Sci. Rep.* 7:45947. doi: 10.1038/srep45947

Gul, S., and Whalen, J. K. (2016). Biochemical cycling of nitrogen and phosphorus in biochar-amended soils. *Soil Biol. Biochem.* 103, 1–15. doi: 10.1016/j.soilbio.2016.08.001

Hagemann, N., Spokas, K., Schmidt, H. P., Kägi, R., Böhler, M. A., and Bucheli, T. D. (2018). Activated carbon, biochar and charcoal: linkages and synergies across pyrogenic carbon's ABCs. *Water* 10:182. doi: 10.3390/w10020182

Hammer, E. C., Balogh-Brunstad, Z., Jakobsen, I., Olsson, P. A., Stipp, S. L. S., and Rillig, M. C. (2014). A mycorrhizal fungus grows on biochar and captures phosphorus from its surfaces. *Soil Biol. Biochem.* 77, 252–260. doi: 10.1016/j.soilbio.2014.06.012

Hammer, E. C., Forstreuter, M., Rillig, M. C., and Kohler, J. (2015). Biochar increases arbuscular mycorrhizal plant growth enhancement and ameliorates salinity stress. *Appl. Soil Ecol.* 96, 114–121. doi: 10.1016/j.apsoil.2015.07.014

Hazard, C., Gosling, P., Van Der Gast, C. J., Mitchell, D. T., Doohan, F. M., and Bending, G. D. (2013). The role of local environment and geographical distance in determining community composition of arbuscular mycorrhizal fungi at the landscape scale. *ISME J.* 7, 498–508. doi: 10.1038/ismej.2012.127

Herman, D. J., Firestone, M. K., Nuccio, E., and Hodge, A. (2012). Interactions between an arbuscular mycorrhizal fungus and a soil microbial community mediating litter decomposition. *FEMS Microbiol. Ecol.* 80, 236–247. doi: 10.1111/j.1574-6941.2011.01292.x

Hodge, A., Campbell, C. D., and Fitter, A. H. (2001). An arbuscular mycorrhizal fungus accelerates decomposition and acquires nitrogen directly from organic material. *Nature* 413, 297–299. doi: 10.1038/35095041

Hodge, A., and Fitter, A. H. (2010). Substantial nitrogen acquisition by arbuscular mycorrhizal fungi from organic material has implications for N cycling. *Proc. Natl. Acad. Sci. U.S.A.* 107, 13754–13759. doi: 10.1073/pnas.1005874107

Hodge, A., and Storer, K. (2015). Arbuscular mycorrhiza and nitrogen: implications for individual plants through to ecosystems. *Plant Soil* 386, 1–19. doi: 10.1007/s11104-014-2162-1

Jansa, J., Erb, A., Oberholzer, H. R., Smilauer, P., and Egli, S. (2014). Soil and geography are more important determinants of indigenous arbuscular mycorrhizal communities than management practices in Swiss agricultural soils. *Mol. Ecol.* 23, 2118–2135. doi: 10.1111/mec.12706

Jansa, J., Mozafar, A., Anken, T., Ruh, R., Sanders, I. R., and Frossard, E. (2002). Diversity and structure of AMF communities as affected by tillage in a temperate soil. *Mycorrhiza* 12, 225–234. doi: 10.1007/s00572-002-0163-z

Jansa, J., Mozafar, A., Kuhn, G., Anken, T., Ruh, R., Sanders, I. R., et al. (2003). Soil tillage affects the community structure of mycorrhizal fungi in maize roots. *Ecol. Appl.* 13, 1164–1176. doi: 10.1007/s12275-015-5108-2

Jansa, J., Wiemken, A., and Frossard, E. (2006). "The effects of agricultural practices on arbuscular mycorrhizal fungi," in *Function of Soils for Human Societies and the Environment*, eds E. Frossard, W. E. H. Blum, and B. P. Warkentin (London: Geological Society), 89–115.

Jeffery, S., Abalos, D., Prodana, M., Bastos, A. C., Van Groenigen, J. W., Hungate, B. A., et al. (2017). Biochar boosts tropical but not temperate crop yields. *Environ. Res. Lett.* 12:053001. doi: 10.1088/1748-9326/aa67bd

Jeffery, S., Verheijen, F. G. A., Van Der Velde, M., and Bastos, A. C. (2011). A quantitative review of the effects of biochar application to soils on crop productivity using meta-analysis. *Agric. Ecosyst. Environ.* 144, 175–187. doi: 10.1016/j.agee.2011.08.015

Johnson, N. C., Wilson, G. W. T., Bowker, M. A., Wilson, J. A., and Miller, R. M. (2010). Resource limitation is a driver of local adaptation in mycorrhizal symbioses. *Proc. Natl. Acad. Sci. U.S.A.* 107, 2093–2098. doi: 10.1073/pnas.0906710107

Johnson, N. C., Wilson, G. W. T., Wilson, J. A., Miller, R. M., and Bowker, M. A. (2015). Mycorrhizal phenotypes and the law of the minimum. *New Phytol.* 205, 1473–1484. doi: 10.1111/nph.13172

Kloss, S., Zehetner, F., Dellantonio, A., Hamid, R., Ottner, F., Liedtke, V., et al. (2012). Characterization of slow pyrolysis biochars: effects of feedstocks and pyrolysis temperature on biochar properties. *J. Environ. Qual.* 41, 990–1000. doi: 10.2134/jeq2011.0070

Koide, R. T. (2017). "Biochar-arbuscular mycorrhiza interaction in temperate soils," in *Mycorrhizal Mediation of Soil: Fertility, Structure, and Carbon Storage*, eds N. C. Johnson, C. Gehring, and J. Jansa (Amsterdam: Elsevier), 461–477. doi: 10.1016/b978-0-12-804312-7.00025-5

Koide, R. T., and Fernandez, C. W. (2018). The continuing relevance of "older" mycorrhiza literature: insights from the work of John Laker Harley (1911-1990). *Mycorrhiza* 28, 577–586. doi: 10.1007/s00572-018-0854-8

Konvalinková, T., Püschel, D., Řezáčová, V., Gryndlerová, H., and Jansa, J. (2017). Carbon flow from plant to arbuscular mycorrhizal fungi is reduced under phosphorus fertilization. *Plant Soil* 419, 319–333. doi: 10.1007/s11104-017-3350-6

Koske, R. E., and Gemma, J. N. (1989). A modified procedure for staining roots to detect VA mycorrhizas. *Mycol. Res.* 92, 486–505. doi: 10.1016/S0953-7562(89)80195-9

Lehmann, J., Rillig, M. C., Thies, J., Masiello, C. A., Hockaday, W. C., and Crowley, D. (2011). Biochar effects on soil biota - a review. *Soil Biol. Biochem.* 43, 1812–1836. doi: 10.1016/j.soilbio.2011.04.022

Liu, C., Liu, F., Ravnskov, S., Rubaek, G. H., Sun, Z., and Andersen, M. N. (2017). Impact of wood biochar and its interactions with mycorrhizal fungi, phosphorus fertilization and irrigation strategies on potato growth. *J. Agron. Crop Sci.* 203, 131–145. doi: 10.1111/jac.12185

Liu, L., Li, J. W., Yue, F. X., Yan, X. W., Wang, F. Y., Bloszies, S., et al. (2018). Effects of arbuscular mycorrhizal inoculation and biochar amendment on maize growth, cadmium uptake and soil cadmium speciation in Cd-contaminated soil. *Chemosphere* 194, 495–503. doi: 10.1016/j.chemosphere.2017.12.025

Luo, S. S., Wang, S. J., Tian, L., Li, S. Q., Li, X. J., Shen, Y. F., et al. (2017). Long-term biochar application influences soil microbial community and its potential roles in semiarid farmland. *Appl. Soil Ecol.* 117, 10–15. doi: 10.1016/j.apsoil.2017.04.024

Mäder, P., Vierheilig, H., Streitwolf-Engel, R., Boller, T., Frey, B., Christie, P., et al. (2000). Transport of ^{15}N from a soil compartment separated by a polytetrafluoroethylene membrane to plant roots via the hyphae of arbuscular mycorrhizal fungi. *New Phytol.* 146, 155–161. doi: 10.1046/j.1469-8137.2000.00615.x

Mahmood, T., Mehnaz, S., Fleischmann, F., Ali, R., Hashmi, Z. H., and Iqbal, Z. (2014). Soil sterilization effects on root growth and formation of rhizosheaths in wheat seedlings. *Pedobiologia* 57, 123–130. doi: 10.1016/j.pedobi.2013.12.005

Mao, J. D., Johnson, R. L., Lehmann, J., Olk, D. C., Neves, E. G., Thompson, M. L., et al. (2012). Abundant and stable char residues in soils: implications for soil fertility and carbon sequestration. *Environ. Sci. Technol.* 46, 9571–9576. doi: 10.1021/es301107c

Martin, S. L., Mooney, S. J., Dickinson, M. J., and West, H. M. (2012). The effects of simultaneous root colonisation by three *Glomus* species on soil pore characteristics. *Soil Biol. Biochem.* 49, 167–173. doi: 10.1016/j.soilbio.2012.02.036

McGonigle, T. P., Miller, M. H., Evans, D. G., Fairchild, G. L., and Swan, J. A. (1990). A new method which gives an objective measure of colonization of roots by vesicular arbuscular mycorrhizal fungi. *New Phytol.* 115, 495–501. doi: 10.1111/j.1469-8137.1990.tb00476.x

Mickan, B. S., Abbott, L. K., Stefanova, K., and Solaiman, Z. M. (2016). Interactions between biochar and mycorrhizal fungi in a water-stressed agricultural soil. *Mycorrhiza* 26, 565–574. doi: 10.1007/s00572-016-0693-4

Newsham, K. K., Fitter, A. H., and Watkinson, A. R. (1995). Multi-functionality and biodiversity in arbuscular mycorrhizas. *Trends Ecol. Evol.* 10, 407–411. doi: 10.1016/S0169-5347(00)89157-0

Nuccio, E. E., Hodge, A., Pett-Ridge, J., Herman, D. J., Weber, P. K., and Firestone, M. K. (2013). An arbuscular mycorrhizal fungus significantly modifies the soil bacterial community and nitrogen cycling during litter decomposition. *Environ. Microbiol.* 15, 1870–1881. doi: 10.1111/1462-2920.12081

Ohno, T., and Zibilske, L. M. (1991). Determination of low concentrations of phosphorus in soil extracts using malachite green. *Soil Sci. Soc. Am. J.* 55, 892–895. doi: 10.2136/sssaj1991.03615995005500030046x

Ohsowski, B. M., Dunfield, K., Klironomos, J. N., and Hart, M. M. (2018). Plant response to biochar, compost, and mycorrhizal fungal amendments in post-mine sandpits. *Restor. Ecol.* 26, 63–72. doi: 10.1111/rec.12528

Prommer, J., Wanek, W., Hofhansl, F., Trojan, D., Offre, P., Urich, T., et al. (2014). Biochar delerates soil organic nitrogen cycling but stimulates soil nitrification in a temperate arable field trial. *PLoS One* 9:e86388. doi: 10.1371/journal.pone.0086388

Püschel, D., Janoušková, M., Hujslová, M., Slavíková, R., Gryndlerová, H., and Jansa, J. (2016). Plant-fungus competition for nitrogen erases mycorrhizal growth benefits of *Andropogon gerardii* under limited nitrogen supply. *Ecol. Evol.* 6, 4332–4346. doi: 10.1002/ece3.2207

Ren, X. H., Wang, F., Zhang, P., Guo, J. K., and Sun, H. W. (2018). Aging effect of minerals on biochar properties and sorption capacities for atrazine and phenanthrene. *Chemosphere* 206, 51–58. doi: 10.1016/j.chemosphere.2018.04.125

Řezáčová, V., Gryndler, M., Bukovská, P., Šmilauer, P., and Jansa, J. (2016). Molecular community analysis of arbuscular mycorrhizal fungi - Contributions of PCR primer and host plant selectivity to the detected community profiles. *Pedobiologia* 59, 179–187. doi: 10.1016/j.pedobi.2016.04.002

Řezáčová, V., Zemková, L., Beskid, O., Püschel, D., Konvalinková, T., Hujslová, M., et al. (2018). Little cross-feeding of the mycorrhizal networks shared between C_3-*Panicum bisulcatum* and C_4-*Panicum maximum* under different temperature regimes. *Front. Plant Sci.* 9:449. doi: 10.3389/fpls.2018.00449

Roberts, K. G., Gloy, B. A., Joseph, S., Scott, N. R., and Lehmann, J. (2010). Life cycle assessment of biochar systems: estimating the energetic, economic, and climate change potential. *Environ. Sci. Technol.* 44, 827–833. doi: 10.1021/es902266r

Schulz, H., and Glaser, B. (2012). Effects of biochar compared to organic and inorganic fertilizers on soil quality and plant growth in a greenhouse experiment. *J. Plant Nutr. Soil Sci.* 175, 410–422. doi: 10.1002/jpln.201100143

Shen, Q., Hedley, M., Arbestain, M. C., and Kirschbaum, M. U. F. (2016). Can biochar increase the bioavailability of phosphorus? *J. Soil Sci. Plant Nutr.* 16, 268–286. doi: 10.4067/S0718-95162016005000022

Slavíková, R., Püschel, D., Janoušková, M., Hujslová, M., Konvalinková, T., Gryndlerová, H., et al. (2017). Monitoring CO_2 emissions to gain a dynamic view of carbon allocation to arbuscular mycorrhizal fungi. *Mycorrhiza* 27, 35–51. doi: 10.1007/s00572-016-0731-2

Smith, S. E., and Smith, F. A. (2012). Fresh perspectives on the roles of arbuscular mycorrhizal fungi in plant nutrition and growth. *Mycologia* 104, 1–13. doi: 10.3852/11-229

Smith, S. E., Smith, F. A., and Jakobsen, I. (2004). Functional diversity in arbuscular mycorrhizal (AM) symbioses: the contribution of the mycorrhizal P uptake pathway is not correlated with mycorrhizal responses in growth or total P uptake. *New Phytol.* 162, 511–524. doi: 10.1111/j.1469-8137.2004.01039.x

Song, Y. J., Zhang, X. L., Ma, B., Chang, S. X., and Gong, J. (2014). Biochar addition affected the dynamics of ammonia oxidizers and nitrification in microcosms of a coastal alkaline soil. *Biol. Fertil. Soils* 50, 321–332. doi: 10.1007/s00374-013-0857-8

Spokas, K. A., Cantrell, K. B., Novak, J. M., Archer, D. W., Ippolito, J. A., Collins, H. P., et al. (2012). Biochar: a synthesis of its agronomic impact beyond carbon sequestration. *J. Environ. Qual.* 41, 973–989. doi: 10.2134/jeq2011.0069

Spokas, K. A., Novak, J. M., Stewart, C. E., Cantrell, K. B., Uchimiya, M., Dusaire, M. G., et al. (2011). Qualitative analysis of volatile organic compounds on biochar. *Chemosphere* 85, 869–882. doi: 10.1016/j.chemosphere.2011.06.108

Sun, B. B., Lian, F., Bao, Q. L., Liu, Z. Q., Song, Z. G., and Zhu, L. Y. (2016). Impact of low molecular weight organic acids (LMWOAs) on biochar micropores and sorption properties for sulfamethoxazole. *Environ. Pollut.* 214, 142–148. doi: 10.1016/j.envpol.2016.04.017

Thonar, C., Erb, A., and Jansa, J. (2012). Real-time PCR to quantify composition of arbuscular mycorrhizal fungal communitiesumarker design, verification, calibration and field validation. *Mol. Ecol. Res.* 12, 219–232. doi: 10.1111/j.1755-0998.2011.03086.x

Thonar, C., Frossard, E., Šmilauer, P., and Jansa, J. (2014). Competition and facilitation in synthetic communities of arbuscular mycorrhizal fungi. *Mol. Ecol.* 23, 733–746. doi: 10.1111/mec.12625

van der Heijden, M. G. A., Bardgett, R. D., and Van Straalen, N. M. (2008). The unseen majority: soil microbes as drivers of plant diversity and productivity in terrestrial ecosystems. *Ecol. Lett.* 11, 296–310. doi: 10.1111/j.1461-0248.2007.01139.x

Zhang, H., Voroney, R. P., and Price, G. W. (2017). Effects of temperature and activation on biochar chemical properties and their impact on ammonium, nitrate, and phosphate sorption. *J. Environ. Qual.* 46, 889–896. doi: 10.2134/jeq2017.02.0043

Zhang, L. Y., Jing, Y. M., Xiang, Y. Z., Zhang, R. D., and Lu, H. B. (2018). Responses of soil microbial community structure changes and activities to biochar addition: a meta-analysis. *Sci. Total Environ.* 643, 926–935. doi: 10.1016/j.scitotenv.2018.06.231

Zhu, X. M., Chen, B. L., Zhu, L. Z., and Xing, B. S. (2017). Effects and mechanisms of biochar-microbe interactions in soil improvement and pollution remediation: a review. *Environ. Pollut.* 227, 98–115. doi: 10.1016/j.envpol.2017.04.032

Conflict of Interest Statement: The authors declare that the research was conducted in the absence of any commercial or financial relationships that could be construed as a potential conflict of interest.

frontiers in Microbiology

ORIGINAL RESEARCH
published: 13 August 2018
doi: 10.3389/fmicb.2018.01847

Fungi Indirectly Affect Plant Root Architecture by Modulating Soil Volatile Organic Compounds

*Denis Schenkel[1,2], Jose G. Maciá-Vicente[2,3], Alexander Bissell[1] and Richard Splivallo[1,2]**

[1] Institute for Molecular Biosciences, Goethe University Frankfurt, Frankfurt, Germany, [2] Integrative Fungal Research Cluster, Frankfurt, Germany, [3] Institute of Ecology, Evolution and Diversity, Goethe University Frankfurt, Frankfurt, Germany

The plant-growth modulating effect of microbial volatile organic compounds (VOCs) has been demonstrated repeatedly. This has most often been performed by exposing plants to VOC released by microbes grown on nutrient rich media. Here, we used soil instead to grow fungi of the *Fusarium* genus and investigate how VOCs emitted by this system influenced the development of *Arabidopsis* plants. The volatile profiles of *Fusarium* strains grown in soil and malt extract were also compared. Our results demonstrate that distinct volatile signatures can be attributed to different *Fusarium* genetic clades but also highlight a major influence of the growth medium on volatile emission. Furthermore, all soil-grown *Fusarium* isolates increased primary root length in *Arabidopsis* by decreasing VOC concentrations in soil. This result represents a major paradigm shift in plant-microbe interactions since growth modulating effects have been attributed so far to the emission and not the consumption of volatile signals.

Keywords: *Fusarium*, *Arabidopsis*, volatile organic compounds, plant-microbe interactions, soil VOCs

OPEN ACCESS

Edited by:
Caroline Gutjahr, Technische Universität München, Germany

Reviewed by:
Ruth Lydia Schmidt, University of Quebec, Canada
Martin Heil, Centro de Investigación y de Estudios Avanzados del Instituto Politécnico Nacional (CINVESTAV-IPN), Mexico

***Correspondence:**
Richard Splivallo
richard.splivallo@a3.epfl.ch

Specialty section:
This article was submitted to Plant Microbe Interactions, a section of the journal Frontiers in Microbiology

Received: *16 May 2018*
Accepted: *24 July 2018*
Published: *13 August 2018*

Citation:
Schenkel D, Maciá-Vicente JG, Bissell A and Splivallo R (2018) Fungi Indirectly Affect Plant Root Architecture by Modulating Soil Volatile Organic Compounds. Front. Microbiol. 9:1847. doi: 10.3389/fmicb.2018.01847

INTRODUCTION

Volatile organic compounds (VOCs), small molecules with low boiling point and high vapor pressure, include numerous signals involved in plant-microbial interactions (Junker and Tholl, 2013; Schulz-Bohm et al., 2017). To date, a few thousands VOCs have been described in flowering plants (Knudsen et al., 2006) and microbes (Lemfack et al., 2018). These VOCs predominantly include terpenoids, phenylpropanoids/benzenoids, fatty acids, and amino acid derivatives (Dudareva et al., 2013). By contrast to their well-established functions aboveground (Šimpraga et al., 2016), the role of VOCs released belowground has only started to emerge recently.

Rhizosphere microbes might regulate plant growth by emitting VOCs as demonstrated by *Bacillus* bacteria (Ryu et al., 2003; Zhang et al., 2007) that promote plant growth through the release of 2,3-butanediol and acetoin (Ryu et al., 2003). Similar growth promotion in *Arabidopsis* was reported for *Trichoderma viride* fungi with growth regulators putatively identified as isobutyl alcohol, isopentyl alcohol and 3-methylbutanal (Hung et al., 2013). VOCs emitted by the fungal root pathogen *Rhizoctonia solani* have also been shown to increase shoot and root biomass in *Arabidopsis* and at the same time compromising resistance to above-ground herbivory (Cordovez et al., 2017). Microbial VOCs might also inhibit plant growth and affect root development as documented for bacteria (Wenke et al., 2012) and mycorrhizal fungi (Splivallo et al., 2007; Ditengou et al., 2015). These examples illustrate the seemingly wide-spread ability of rhizospheric microbes to regulate plant development through VOCs.

Regulation of plant growth by secondary metabolites occurs in a concentration-dependent manner, with promotion typically reported at low concentrations and inhibition at higher concentrations as demonstrated for benzaldehyde derivatives (Choi et al., 2016). Bioactive concentrations mimic hormonal levels as shown for some VOCs (i.e., 13-tetradecadien-1-ol, 3-hydroxy-2-butanone, 2,3-butanediol) that promote plant growth in the ng-μg range for microbes grown on non-soil matrices (Ryu et al., 2003; Zou et al., 2010; Blom et al., 2011; Park et al., 2015). As most media used in previous studies are rich in terms of nutrients, it might be more challenging for organisms growing on soil to produce secondary metabolites. In bulk soil and the rhizosphere, bioactivity will eventually depend on the half-life of specific signaling molecules as well as the ability of the emitter to sustain stable VOCs concentrations over longer periods of time.

In terms of phylogeny, the ability to regulate plant-growth via VOCs seems widespread among diverse microbial species (Sánchez-López et al., 2016) and microbial VOCs might act by modulating the auxin and the cytokinine signaling pathways of plants (Ryu et al., 2003; Zhang et al., 2007; Bitas et al., 2015; Sánchez-López et al., 2016). Volatile signals of *Trichoderma* fungi have been shown to increase the uptake of iron in roots of *Arabidopsis* and tomato, resulting in the priming of jasmonic acid signaling pathway in plant shoots (Martínez-Medina et al., 2017). It has also been suggested that microbes occupying particular niches (i.e., rhizosphere) or having specific lifestyles (ectomycorrhizal, pathogenic or saprophytic) might produce distinct ecologically relevant VOCs (Müller et al., 2013; Schenkel et al., 2015). If confirmed, this hypothesis might corroborate the importance of specific VOCs in plant/microbial interactions.

The influence of microbial VOCs on plant growth has been tested in various static and flow-through systems where plants and microbes are physically separated but exchanged VOCs via a common headspace (Kai et al., 2016). Static systems such as a split Petri dish have been widely used, with plants in one compartment and microbes in a second compartment (Blom et al., 2011; Kai et al., 2016; Lazazzara et al., 2017). One shortcoming of the static systems described previously is that they used artificial (nutrient rich) media to grow microbes. VOCs profiles emitted by microbes grown on nutrient rich media might drastically differ from those emitted under more natural conditions (i.e., with microbes grown on soil), which might in turn affect plant phenotype. Thus growth conditions should be carefully selected when investigating potential ecologically relevant signaling compounds. Another shortcoming of static systems is that they are prone to the artificial accumulation of humidity (Tholl and Röse, 2006; Kai et al., 2016) and CO_2 (Kai and Piechulla, 2009) that must to be controlled for unbiased results (Piechulla and Schnitzler, 2016). Ultimately, bioactive VOCs must be identified and quantified, and their plant growth regulation ability should be demonstrated with pure compounds in concentrations similar to the ones observed in the assays with plants.

The first aim of our study was to investigate the influence of growth medium (a nutrient rich medium versus soil) on the emission of fungal volatiles. The second aim was to test the outcome of VOC-mediated interactions between plants and soil-grown fungi. For this purpose, we employed *Arabidopsis thaliana* as a model plant and different species belonging to the *Fusarium* genus. This genus comprises globally distributed ascomycete fungi of the Hypocreales order (Karim et al., 2016) that range in lifestyle from plant pathogens and saprophytes (Karim et al., 2016) to symptomless endophytes (Maciá-Vicente et al., 2008; Glynou et al., 2016). Members of the *Fusarium* genus cannot be strictly classified as saprophytes or pathogen since their lifestyle is highly dependent on the colonized host plant and possibly other environmental conditions (Kia et al., 2017; Lofgren et al., 2018). Previous work on *F. oxysporum* grown on nutrient rich media highlighted its ability to alter plant growth via the emission of VOCs (Bitas et al., 2015). In contrast to the latter study, soil was employed here as substrate for fungal growth. Additionally, further species of the same genus were tested to understand whether general patterns of VOC-mediated growth regulation could be inferred from phylogenetic data.

MATERIALS AND METHODS

Identification of Fungal Strains

Twenty-eight fungal strains, including twenty-seven *Fusarium* (Hypocreales) and one unclassified Helotiales strains were used in this study. All strains were isolated as endophytes from the roots of two species of the Brassicaceae family, *Microthlaspi perfoliatum* and *Microthlaspi erraticum* originating from several locations in Europe and Turkey (Glynou et al., 2016) (**Table 1**).

The strains, characterized earlier (Glynou et al., 2016) by internal transcribed spacer (ITS) sequencing, were further characterized here through sequencing of the transcription elongation factor 1-α gene (*tef1*-α), which provides a better species resolution for *Fusarium* spp. than the ITS (O'Donnell et al., 2015). Using primers ef1/ef2 and PCR conditions reported earlier (Geiser et al., 2004), the partial *tef1*-α gene was amplified from fungal DNA (Glynou et al., 2016). The resulting amplicons were purified and sequenced by GATC Biotech AG (Konstanz, Germany). The quality-filtered sequences were first manually compared against the FUSARIUM-ID database (Geiser et al., 2004) using BLAST (Altschul et al., 1990). Then a maximum-likelihood (ML) phylogenetic tree was built alongside sequences from reference strains. To do this, all the strains' *tef1*-α sequences were compared using BLAST against the full NCBI GenBank database and against subsets of it containing only sequences from vouchered strains or species type specimens. A maximum of ten BLAST best hit sequences were retrieved from each dataset and aligned with the query sequences applying the G-INS-I algorithm of MAFFT v7.123b (Katoh and Standley, 2013). The alignment was trimmed with Gblocks v0.91b (Castresana, 2000) and then a ML tree was constructed with the program RAxML v8.0.0 (Stamatakis, 2014), using a GTRGAMMA model of nucleotide substitution and rate heterogeneity and 1,000 bootstraps. Another ML tree was likewise built using only the strain sequences, to compare

the phylogenetic relationships among strains with their VOC production profiles.

Experimental Design and Preparation of Fungal Inocula

Fungal strains, maintained on corn meal agar (CMA, Sigma-Aldrich, St. Louis, MO, United States) at room temperature, were used in a series of experiments aimed at characterizing VOC profiles and VOC mediated interactions of fungi and plants (see **Figure 1** for an overview of the experimental design).

Fungal inocula for VOC profiling and bioassays were prepared by growing each strain for 16 days in 100 ml Erlenmeyer flasks containing 30 ml of 15 gl^{-1} malt extract broth, pH 7.0 (Becton, Dickinson and Company, Heidelberg, Germany) at 24°C (step 1, **Figure 1**). Resulting fungal VOC profiles were characterized by gas chromatography/mass spectroscopy (GC/MS) (step 2, **Figure 1** and "VOC profiling" hereafter) while the remaining fungal biomass was used to test the effect of VOCs emitted by selected *Fusarium* and the Helotiales strains on the model plant *Arabidopsis thaliana* ecotype Col-0 (*Arabidopsis* onward; step 3, **Figure 1**). These assays were also employed to profile the VOCs emitted by *Fusarium* grown in soil (step 4, **Figure 1**). Details about each experimental step is given hereafter.

VOC Profiling

Volatile organic compound profiling was performed in 20 ml solid-phase micro extraction (SPME) vials for fungal cultures or soil samples. Specifically, samples in malt extract contained either pelleted fungal biomass (1.25 g harvested after centrifugation at 12,000 $\times$ *g* for 10 min) or culture medium without fungal inoculum (1.00 $\pm$ 0.05 ml). Alternatively, samples contained 1.50 $\pm$ 0.05 g of soil either inoculated with *Fusarium* or without fungus (control), taken directly at the end of the bioassays from the plate harboring soil (refer to "Bioassays with plants and fungi grown in soil").

Solid-phase micro extraction vials, sealed with a silicon/polytetrafluoroethylene septum, were incubated at 60°C for 20 min prior to VOC sampling. VOCs from the head-space were subsequently extracted for 15 min at 60°C using a Divinylbenzene/Carboxen/Polydimethylsiloxane

TABLE 1 | *Fusarium* and Helotiales strains used in this study.

Strain number	Species	Country	NCBI GenBank ITS accession	NCBI GenBank *tef1*-α accession	Experiment*
P1006	*F. equiseti*	Turkey	KT268325	MH093655	VOC_{ME}
P1007	*F. acuminatum*	Turkey	KT268326	MH093656	VOC_{ME}
P1013	*F. redolens*	Turkey	KT268332	MH093657	VOC_{ME}
P1065	*F. acuminatum*	Turkey	KT268384	MH093658	$VOC_{ME\ +SOIL}$ / Bioassay
P1076	*F. equiseti*	Turkey	KT268395	MH093659	VOC_{ME}
P1078	*F. acuminatum*	Turkey	KT268397	MH093660	VOC_{ME}
P1112	*F. acuminatum*	France	KT268430	MH093661	VOC_{ME}
P1141	*F. oxysporum*	France	KT268459	MG570086	$VOC_{ME\ +SOIL}$ / Bioassay
P1143	*F. oxysporum*	France	KT268461	MH093662	VOC_{ME}
P1144	*F. oxysporum*	France	KT268462	MH093663	VOC_{ME}
P1185	*F. oxysporum*	Croatia	KT268501	MH093664	$VOC_{ME\ +SOIL}$ / Bioassay
P1286	*F. oxysporum*	Spain	KT268581	MH093665	$VOC_{ME\ +SOIL}$ / Bioassay
P1304	*F. acuminatum*	Spain	KT268599	MG570084	VOC_{ME}
P1388	*F. flocciferum*	Spain	KT268683	MH093666	VOC_{ME}
P1431	*F. acuminatum*	Spain	KT268725	MH093667	$VOC_{ME\ +SOIL}$ / Bioassay
P1473	*F. tricinctum*	Croatia	KT268767	MH093668	VOC_{ME}
P1520	*F. tricinctum*	Croatia	KT268725	MH093669	$VOC_{ME\ +SOIL}$ / Bioassay
P1546	*F. equiseti*	Croatia	KT268840	MH093670	VOC_{ME}
P1547	*F. tricinctum*	Croatia	KT268841	MH093671	VOC_{ME}
P2134	*F. culmorum*	France	KT269397	MH093672	VOC_{ME}
P2186	*F. redolens*	Greece	KT269449	MH093673	$VOC_{ME\ +SOIL}$ / Bioassay
P2190	*F. flocciferum*	Greece	KT269453	MG570085	VOC_{ME}
P2191	*F. torulosum*	Greece	KT269454	MH093674	VOC_{ME}
P2194	*F. equiseti*	Greece	KT269457	MH093675	VOC_{ME}
P2195	*F. oxysporum*	Greece	KT269458	MH093676	VOC_{ME}
P6053	*F. acuminatum*	Spain	KT270246	MH093677	VOC_{ME}
P6075	*F. oxysporum*	France	KT270268	MH093678	VOC_{ME}
P1176	Unclassified Helotiales	Croatia	KT268493	Not available	Bioassay

**The experiment column indicates whether a fungal strain was used for VOC profiling on malt extract (VOC_{ME}), VOC profiling on soil (VOC_{SOIL}), or for testing VOC-mediated interactions with Arabidopsis (Bioassay).*

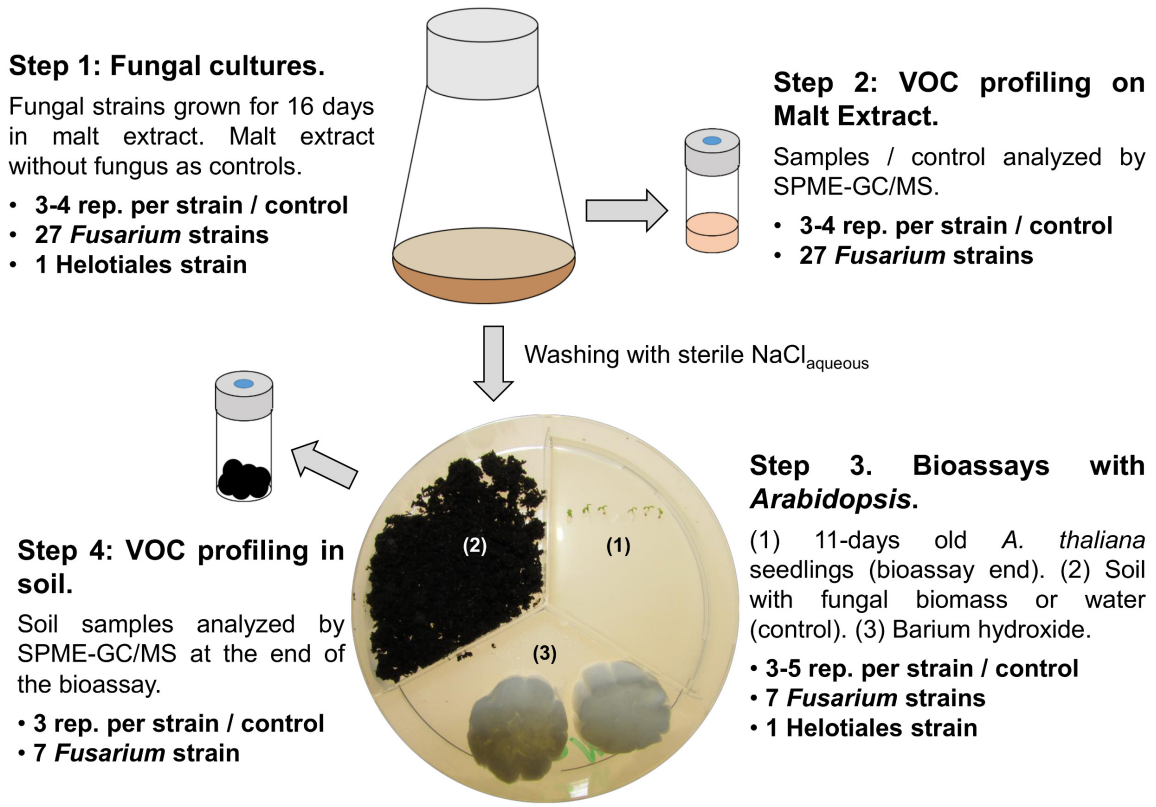

FIGURE 1 | Experimental design. The figure illustrates the four experimental steps as well as the specific fungal strains and numbers of replicates used for each experiment. Step 1: Fungal strains were grown in liquid medium; sterile medium was used as control. Step 2: Fungi were harvested by centrifugation, one part of the mycelium or control medium was analyzed by GC/MS, one part was used to inoculate sterilized soil for the bioassays (step 3). Bioassay setup: six seeds of *A. thaliana* were grown exposed to VOCs released from the soil compartment. Plant morphology was determined at the end of the experiment and soil samples were analyzed by GC/MS (step 4).

SPME fiber (DVB/CARB/PDMS) pre-conditioned following the manufacturer's instructions (Sigma-Aldrich, Munich, Germany). Empty vials were regularly included in between runs to check for carry-over and at the beginning of each run to generate a blank. GC/MS analysis was performed on an Agilent 7890B GC coupled to an Agilent 5977B MSD (Agilent, Waldbronn, Germany). VOCs were desorbed from the SPME fiber at 250°C (GC inlet temperature) in splitless mode and were separated on an HP-5ms Ultra Inert capillary column (30 m × 0.25 mm with 0.25 μm coating) using the following program: 40°C for 5 min, ramp 3°C min^{-1} until 160°C, ramp 50°C min^{-1} until 260°C, hold 260°C for 6 min. Helium was used as a carrier gas (1.2 ml min^{-1}). The MS scan range was 50–350 atomic mass units and ionization was performed at 70 eV. An EI 350 XTR was used as MS source. Source temperature was 230°C, MS quad temperature 150°C.

Chromatograms derived from the GC/MS analysis of fungal cultures and soil samples were aligned with the TagFinder 4.1 software (Luedemann et al., 2008) using parameters described earlier (Sherif et al., 2016), with the exception of the threshold which was set to 500. This resulted in a data matrix comprised of TAGs equivalent to single m/z values within a specific time range [(m/z, RT range)]. TAGs (made of one or more VOCs) present in empty SPME vials were subtracted from the data (3× blank removal). The data were normalized by dividing specific TAGs in each sample by the sum of all TAGs in that sample. This procedure is equivalent to normalizing the peak areas of single VOCs to the Total Ion Current (TIC).

Volatile organic compounds in TAGs of interest were either tentatively identified by comparison of their mass spectra to the ones found in the NIST Mass Spectral Search Program 2.0 (National Institute of Standards and Technology, Gaithersburg, MD, United States) or fully identified based on MS spectra, Kovats retention indices (n-alkane) and injection of an authentic standard. Specific VOCs that were fully identified were purchased from Sigma-Aldrich and Merck (Darmstadt, Germany), including (CAS number in parenthesis): furfural (98-01-1), 4-heptanone (123-19-3), 5-methyl-3-heptanone (541-85-5), benzaldehyde (100-52-7), 5-methyl-2-furancarboxaldehyde (620-02-0), 3-octanone (106-68-3), octanal (124-13-0), 2-ethyl-1-hexanol (104-76-7), benzeneacetaldehyde (122-78-1), nonanal (124-19-6), camphor (76-22-2), 1,2-dimethoxy-benzene (91-16-7) and decanal (112-31-2).

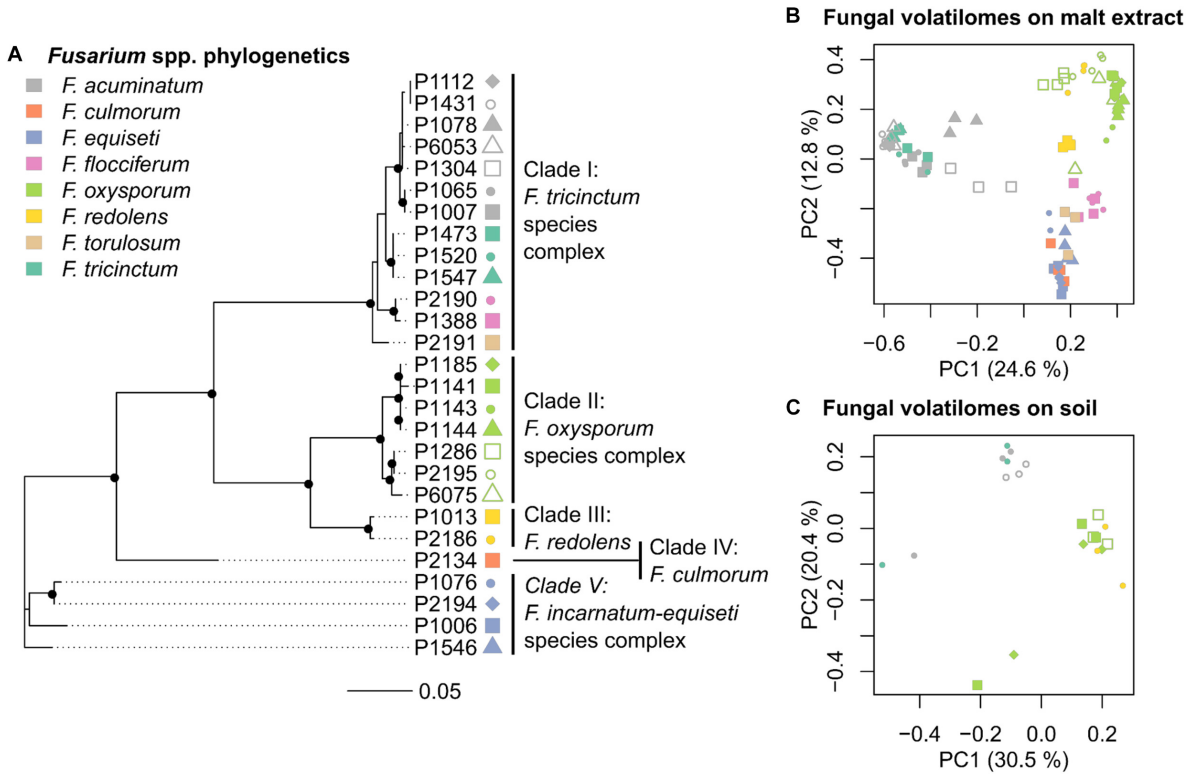

FIGURE 2 | Phylogeny and volatilome of *Fusarium* spp. **(A)** Phylogenetic tree of 27 Fusarium strains based on partial *tef-1α* sequences (**Table 1**). Black dots in the tree nodes indicate bootstrap values ≥70% based on 1,000 replicates. **(B)** Principle Coordinate Analysis (PCoA) based on the VOC profiles of 27 *Fusarium* strains grown in malt extract (n = 3–4 replicates per strain) **(C)** PCoA based on the *VOC* profiles of 7 Fusarium strains grown in soil (n = 3 replicates per strain). Each point in PCoAs correspond to an independently measured volatile profile, with point color indicating the species (see color key), and different point types within each clade denoting different strains. Both PCoAs highlight that differences in *VOC* profiles among strains correspond by large to genotypic differences.

Quantification of VOCs Emitted From Soil

The concentration of seven VOCs (namely benzaldehyde, decanal, 5-methyl-2-furancarboxaldehyde, furfural, 5-methyl-3-heptanone, 2-ethyl-1-hexanol, nonanal) were quantified in soil by standard addition. These seven compounds were selected based on a linear model suggesting that they might be responsible for the root shortening of *Arabidopsis* observed in non-inoculated soil (see for details "*Fusarium* spp. decrease the emission of soil VOCs in the results section). For this purpose, water was first added to dried soil to adjust water content to the one determined at the end of the bioassays with *Arabidopsis*. The resulting sample (1.50 g wet soil = 0.26 g soil + 1.24 g water) was placed into a 20 ml SPME vial, and spiked either with 20 µl pure dichloromethane, or 20 µl dichloromethane with varying concentrations of single VOCs. Quantification was obtained by calculating the x-intercept of the resulting linear calibration curves.

Bioassays With Plants and Fungi Grown in Soil

Bioassays in tripartite Petri dishes (Greiner Bio One, Frickenhausen, Germany) were used to test the influence of fungi on root development. The partitioning in the Petri dishes ensured that interactions among organisms were strictly mediated by VOCs (see the illustration in **Figure 1**). The setup was based on Kai and Piechulla (2009), reviewed in Piechulla and Schnitzler (2016) and Kai et al. (2016). One compartment of each plate contained sterile soil inoculated with a single fungal strain (or non-inoculated as control). A sterile cotton piece with barium hydroxide (3 ml of a 25.7 g l^{-1} BaOH aqueous solution) was placed in another compartment to mitigate CO_2 buildup (Piechulla and Schnitzler, 2016), and the third compartment harbored six seeds of *Arabidopsis*.

The plant compartment of the tripartite plates was filled with half strength Murashige and Skoog basal medium with 15 g l^{-1} sucrose (M9274, Sigma) and 1.5% agar (w/v). The *Arabidopsis* seeds were surface-sterilized for 2 min with 70% ethanol (v/v) followed by 20 min in a 1% sodium hypochlorite ($NaHClO_3$) solution in water (v/v) and rinsed three times with sterile water. Seeds on Murashige and Skoog medium were stratified for 2 days at 4°C prior to the bioassays. Thereafter, the remaining Petri dish compartments were completed with barium hydroxide and soil/fungal biomass. Specifically, twice autoclaved commercial soil (Vermehrungssubstrat C200, Stender AG, Schermbeck) (4 g) was added to one compartment of the Petri dish.

To test the effect of fungal volatiles on early plant development, mycelium pre-grown for 16 days of one of seven selected *Fusarium* strains was placed on soil in the remaining compartment (**Figure 1**). These seven strains were selected from the three genetic clades I, II, and III (**Figure 2A**) based on the similarities and differences observed on their VOC profiles on malt extract (**Figure 2B**). To evaluate specificity of effects observed, one Helotiales strain was included in the bioassay. Fungal biomass (**Figure 1**, step 1 and **Table 1**) was homogenized for 1 min with a blender (IKA T18 digital Ultra-Turrax IKA-Werke GMBH, Staufen, Germany), washed twice with 0.85% (w/v) $NaCl_{aq}$ to remove traces of malt extract, and pelleted by centrifugation at 12,000 × *g* for 10 min. A wet fungal biomass of 50.0 ± 0.5 mg was transferred to fresh tubes and resuspended in 1 ml 0.85% (w/v) $NaCl_{aq}$. These were homogenously distributed on the soil surface (**Figure 1**, Step 3). The same volume of 0.85% (w/v) $NaCl_{aq}$ without fungus was used for control Petri dishes.

Plates, sealed with Parafilm, were incubated in an upright position in a growth chamber (Binder KBW 400, Tuttlingen, Germany) for 11 days (23°C, a 16 h photo period, 8,140 lux). Plates were digitalized at the end of the assays with a flat-bed scanner and leaf size and primary root length were measured with the ImageJ (v1.51q) software (Schneider et al., 2012). Secondary root branching was determined under a stereomicroscope (Leica MZ16, Leica Microsystems, Wetzlar, Germany).

Bioassays With Plants and Synthetic VOCs

Bioassays with mixtures of seven synthetic VOCs were performed similarly to the ones with soil, except that soil was replaced with a piece of sterile cotton harboring mixtures of synthetic VOCs in 20 µl dichloromethane. The mixture of compounds tested in these assays were benzaldehyde, decanal, 5-methyl-2-furancarboxaldehyde, furfural, 5-methyl-3-heptanone, 2-ethyl-1-hexanol, and nonanal. Specific mixtures contained 0.00015, 0.15, 1.5, 10, 20, and 100 µg of each volatile compound in 20 µl dichloromethane. Quantities were selected to reflect the concentrations of single VOCs determined in soil (**Table 2**). These mixtures were added to the Petri dish at the beginning of the bioassay and once again after 6 days. Control Petri dishes were prepared with 2× 20 µl dichloromethane similarly added at the start of the assay and on day six. Plant morphology was evaluated as in the earlier assays after eleven days of exposure to VOCs.

Statistical Analysis

Statistical tests were conducted at several stages using Past 3.04 (Hammer et al., 2001) or R version 3.4.3 (R Core Team, 2017) and packages within. Nonparametric Kruskal-Wallis tests were performed in Past to identify VOCs (TAGs) which concentrations significantly differed among samples and to assess differences in plant morphology (*Arabidopsis* primary root length, leaf size and root branching) resulting from different treatments. Correlation of VOCs and *Arabidopsis* primary root length was tested via a linear model with Past. Boxplots of primary root length were generated with R, as well as phylogenetic trees (using the package "ape" 5.0 (Paradis et al., 2004)) and Principle Coordinate analyses (PCoAs) (using the package "vegan" 2.4-5 (Oksanen et al., 2017)). For PCoAs all VOC matrices were square root transformed. Details about statistics and number of replicates are given in figure legends.

RESULTS

Fungal VOC Profiles Depend Both on Genotype and Culture Media

The first objective was to genetically characterize fungal isolates to relate genotypic diversity to variability in VOC profiles. Partial sequencing of the *tef1*-α gene indicates that the twenty-seven *Fusarium* strains used in this study belong to five genetic clades (**Figure 2** and **Supplementary Figure S1** for a phylogenetic tree including reference strains). These clades harbor members of several *Fusarium* species complexes, namely *F. tricinctum* (clade I - *F. tricinctum*, *F. acuminatum*, *F. flocciferum* and *F. torulosum*), *F. oxysporum* (clade II), *F. redolens* (clade III), *F. culmorum* (clade IV) and *F. incarnatum-equiseti* (clade V) (**Figure 2A**).

Volatile organic compounds profiles were generated by SPME-GC/MS for all 27 *Fusarium* strains on malt extract and for seven selected strains grown in soil (**Table 1**). Chromatograms were processed with the Tagfinder software (Luedemann et al., 2008) for alignment. Multivariate analysis was applied to normalized VOC profiles after removal of the signal emitted by the respective control samples (either pure malt extract or non-inoculated soil). A PCoA plot showing all replicates ($n \geq 3$) per strains illustrates that the VOC profiles of the 27 *Fusarium* strains on malt extract varied by large in accordance to genetic identity (**Figure 2B**). Those strains formed three major clusters. The first cluster included several strains from the *F. tricinctum* species complex, the second cluster all strains of the *F. oxysporum* and *F. redolens* complex and the third complex all remaining strains, including *F. torulosum* and *F. flocciferum* from the *F. tricinctum* complex. Given the axes displayed, 37.4% of total variation could be explained by the model displayed in **Figure 2B**. The same conclusion, that volatilomes depend on genetic identities, can be reached for strains grown in soil (**Figure 2C**). Strains from the *F. tricinctum* species complex were separated from *F. oxysporum* and *F. redolens* strains. Explained variation of the model was 50.9% in **Figure 2C**. Overall this confirms that, regardless of the medium used for fungal growth, species identity has the biggest impact on the VOC profiles of *Fusarium* strains.

Fusarium Strains Increase Primary Root Length in *Arabidopsis* Seedlings

Since genetically distinct *Fusarium* strains differed in their VOC profiles, we hypothesized that these differences might also affect plant growth in specific ways (i.e., stimulation in some cases and inhibition in others). Hence, the influence of selected soil-grown *Fusarium* strains on plant development was tested in a system

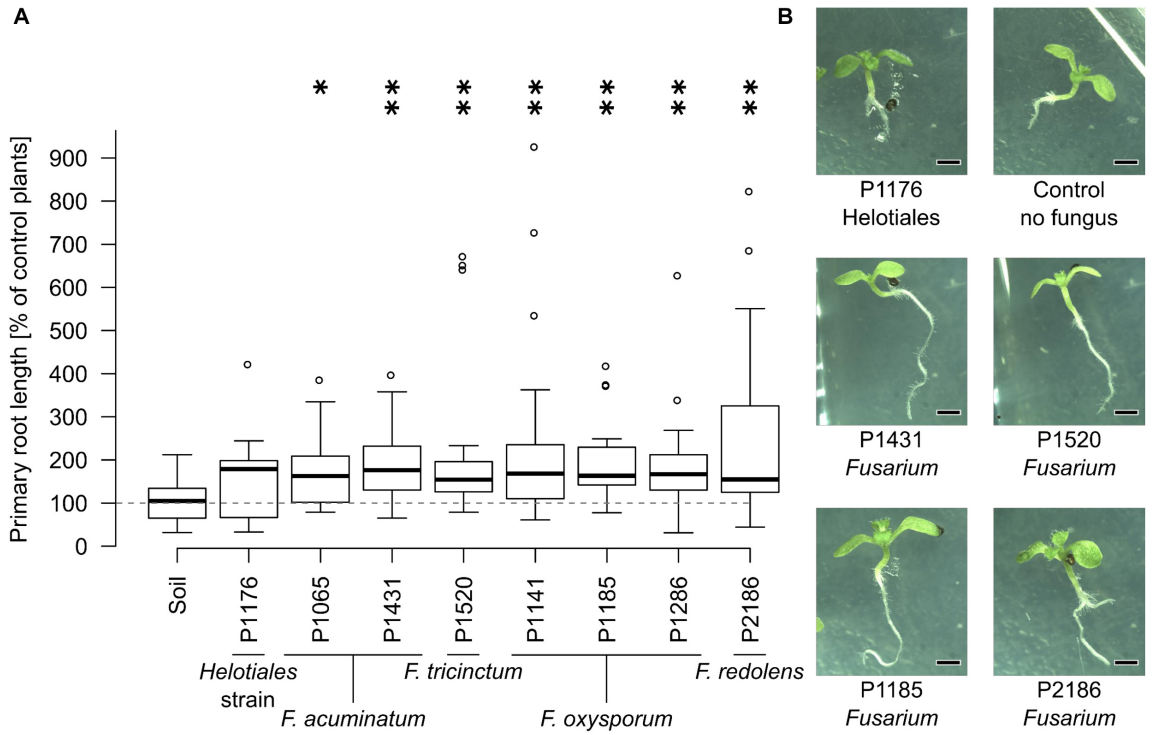

FIGURE 3 | The presence of *Fusarium* increases *Arabidopsis* primary root length. Bioassays were conducted as described in **Figure 1**. **(A)** All soil-grown *Fusarium* strains but not the Helotiales one significantly increased primary root length compared to control seedlings (exposed to soil VOCs only) (Kruskal-Wallis test, *indicates a p-value of $\leq$0.05, **$\leq$ 0.01, n = 14 to 20 seedlings pooled from 3 to 5 Petri dishes). **(B)** Representative 11 days old seedlings grown with or without fungi (scale bar = 1 mm).

which prevents physical contact between the test fungus and plant but allows indirect interactions through VOCs (**Figure 1**). The effect of seven *Fusarium* strains and one unclassified Helotiales strain on *Arabidopsis* development (primary root length, root branching and leaf size) was recorded and compared to control seedlings grown in the presence of soil only (no fungus).

Due to high variability between time independent replicates, primary root length and leaf surface area were normalized to control plants (not exposed to fungi). Similarly, root branching was normalized to primary root length. Most fungal strains strongly influenced primary root growth but no significant differences were detected in terms of leaf surface area or root branching (**Supplementary Figure S2**). Specifically, seedlings grown in the presence of all *Fusarium* strains had significantly longer roots than control plants, while the Helotiales strain did not affect primary root development (**Figure 3**). Overall this indicates that all *Fusarium* strains tested had the ability to increase primary root growth. In contrast, the unidentified Helotiales strain did not.

Fusarium spp. Decrease the Emission of Soil VOCs

Given the primary root growth stimulation observed with all *Fusarium* strains, we aimed at indentifying the VOC(s) responsible for this effect. VOC profiles of soil-grown *Fusarium* were compared to the one of non-inoculated soil (samples were taken at the end of the biossays documented in **Figure 3**). Chromatograms for soil-grown strains and non-inoculated soil are visible in **Figure 4** (GC/MS data files are available as **Supplementary Data Sheet S3**). Specifically, VOC(s) (TAGs) whose concentration significantly differed among strains and non-inoculated soil were identified by a Kruskal-Wallis test ($p < 0.05$). The resulting data matrix was used to generate a PCoA ordination showing that the VOC profile of non-inoculated soil drastically differed from that of soil inoculated with *Fusarium* (**Figure 5A**). The model overall explained 51% of the data varability. The PCoA scores of individual TAGs (**Figure 5B**) highlight that specific VOCs were responsible for the differences between non-inoculated soil and *Fusarium* inoculated soil seen in **Figure 5A**. TAGs representing VOCs identified by authentic standards are indicatied as red numbered dots in **Figure 5B**.

A heatmap was constructed to vizualize how the concentration of 14 VOCs that could be identified differed among treatments (**Figure 5C**). The corresponding heatmap with an extra 33 unidentified compounds in shown in **Supplementary Figure S5** and corresponding mass spectras can be obtained from GC/MS data files available as **Supplementary Data Sheet S3**. It shows that the concentrations of these VOCs significantly differed between *Fusarium*-inoculated and non-inoculated soil, in most cases due to a reduction of the concentration of numerous VOCs in respect to non-inoculated soil. By contrast, only 3-octanone was absent

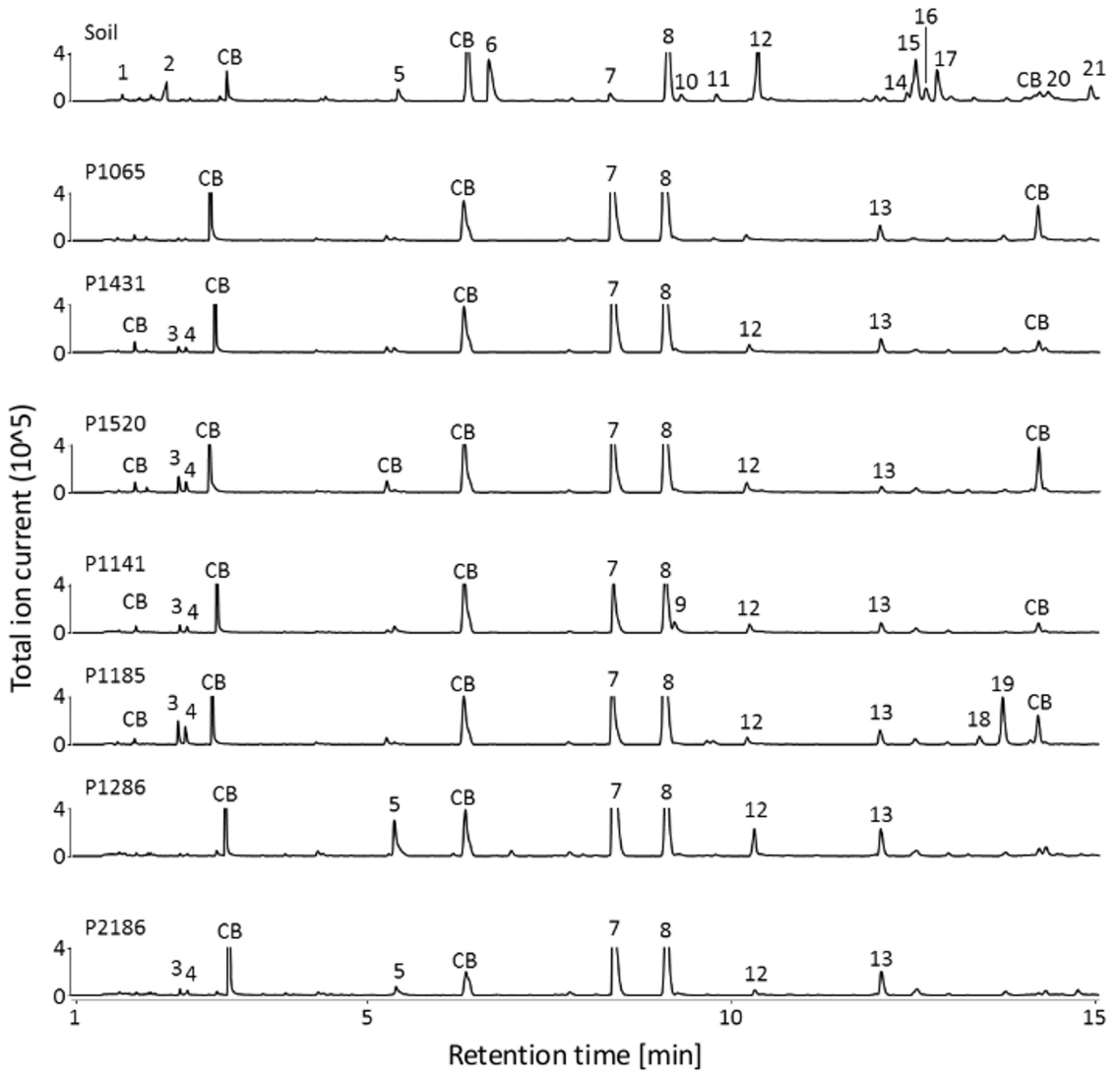

FIGURE 4 | VOCs detected in non-inoculated and *Fusarium*-inoculated soil samples. GC/MS chromatograms (TIC) illustrating the volatile profiles of non-inoculated soil samples and of *Fusarium* inoculated soil samples. *Fusarium* strains overall decreased the number of VOCs detected in the chromatograms compared to non-inoculated soil. CB: column bleed (siloxane derivatives), 1: unidentified, 2: unidentified, 3: 3-methylbutanal, 4: 2-methylbutanal, 5: hexanal, 6: 3-furancarbaldehyde, 7: 4-heptanone*, 8: styrene, 9: 4-heptanol, 10: 2-heptanone, 11: heptanal, 12: methyl-(Z)-N-hydroxybenzenecarboximidate, 13: 7-ethyl-4-nonanone, 14: 2-ethylhexanal, 15: benzaldehyde*, 16: unidentified, 17: 5-methyl-2-furancarboxaldehyde*, 18: unidentified, 19: 1-octen-3-ol, 20: unidentified, 21: octanal*. * Fully identified compounds (based on authentic standard, Kovats-retention indices, mass fragmentation), all other compounds were tentatively identified based on Kovats-retention indices and mass fragmentation).

from non-inoculated soil but present only in two *Fusarium* treatments (**Figure 5C**). Overall this indicates that *Fusarium* spp. have the ability to drastically reduce the concentration of soil VOCs.

To pinpoint VOCs that might be responsible for the root length stimulation described herewith, a linear model was used to test for significant correlations among the concentrations of specific VOCs and primary root length. Seven VOCs, with maximal concentrations in non-inoculated soil, were significantly and negatively correlated to primary root length (**Figure 5C**) and might thus explain root length stimulation observed in the presence of *Fusarium*.

Mixtures of Synthetic VOCs Decrease Primary Root Length at Concentrations Comparable to Those Emitted by Soil

The linear model of **Figure 5C** suggests that, among identified VOC, seven might be specifically responsible for the primary root length stimulation observed with *Fusarium* (**Figure 3**). The concentrations of these VOCs were quantified from soil by standard addition and ranged at the end of the bioassays from 26 ng g^{-1} to 16 $\mu g\ g^{-1}$ soil (wet weight) (**Table 2**).

Bioassays with *Arabidopsis* were subsequently performed using mixtures of the former seven VOCs dissolved in

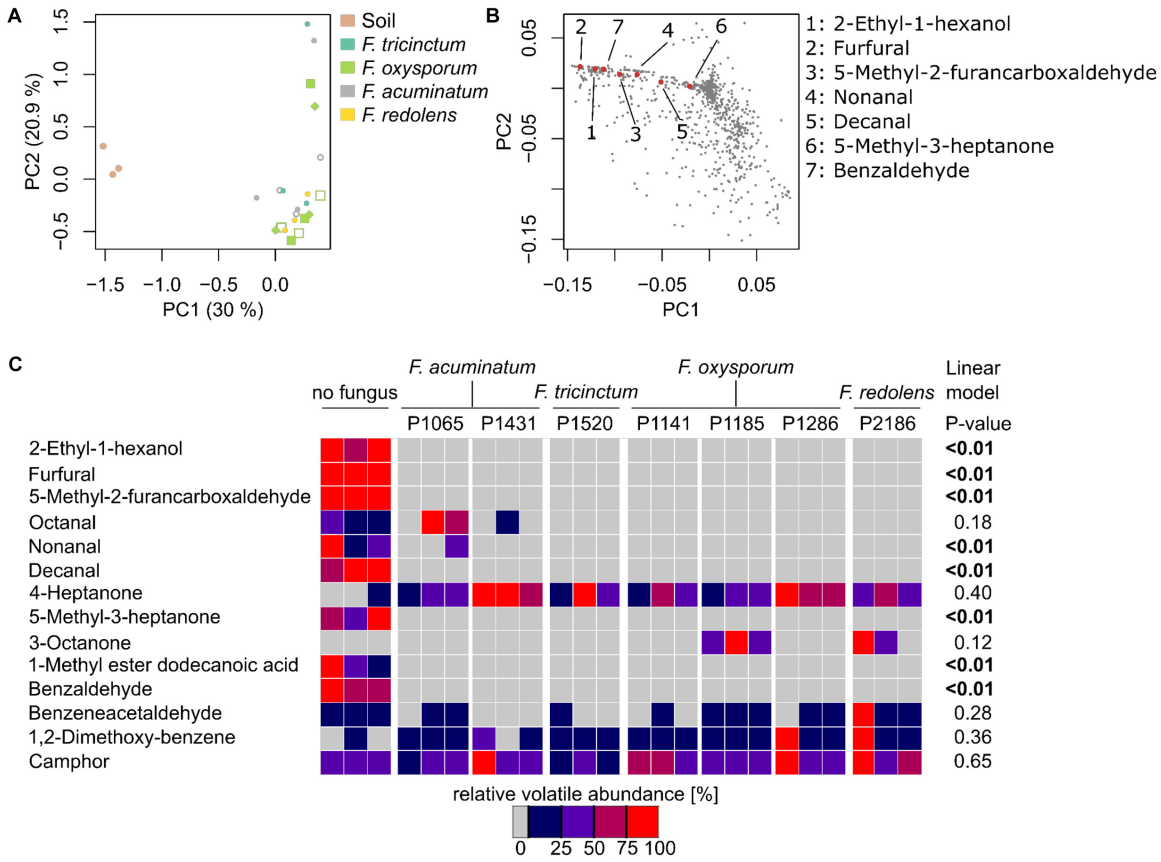

FIGURE 5 | *Fusarium* spp. reduces the emission of soil VOCs. **(A)** Principle Coordinate Analysis ordination (PCoA) based on VOCs emitted by non-inoculated soil and *Fusarium*-inoculated soil samples highlights major differences among non-inoculated and *Fusarium*-inoculated soil (n = 3 replicates per strain). **(B)** PCoA illustrating the distribution of TAGs (VOCs) across samples, showing those responsible of the differences observed in (a). Red, numbered dots correspond to identified VOCs. **(C)** Heatmap illustrating the concentration of 14 identified VOCs in n = 3 replicates (**Supplementary Figure S5** includes unidentified VOCs as well) and highlighting that non-inoculated soil tends to have a higher concentration of VOCs compared to *Fusarium*-inoculated soil. *P*-values reported on the right side of the heatmap correspond to significant negative correlations among VOC concentration and primary root length (reported in **Figure 3**) obtained through a linear model.

dichloromethane at varying concentrations. Since all those VOCs were emitted by sterilized and non-inoculated soil, a piece of cotton was used in compartment 2 (**Figure 1**) of the bioassay instead of soil. This mixture of VOCs significantly inhibited growth of primary roots at quantities corresponding to 10–20 μg and fully blocked germination from 100 μg onward (**Figure 6**). Overall this demonstrates that a mixture of synthetic soil VOCs effectively decreased primary root length at concentrations comparable to those emitted by soil.

TABLE 2 | Quantity of selected VOCs in soil at the end of the bioassays.

VOCs	CAS number	R^2 linear fit for calibration curve	Concentrations in soil [μg^{-1} soil (wet weight)]
2-Ethyl-1-hexanol	104-76-7	0.95	$25.91 * 10^{-3}$
Furfural	98-01-1	0.99	15.64
5-Methyl-2-furancarboxaldehyde	620-02-0	0.98	16.19
Nonanal	124-19-6	0.99	1.01
Decanal	112-31-2	0.85	2.16
Benzaldehyde	100-52-7	1.00	1.11
5-Methyl-3-heptanone	541-85-5	0.99	0.10–0.16

DISCUSSION

Here we investigated the variability in the VOC profiles of various *Fusarium* fungal species and demonstrated that microbial genetic background and media composition influenced volatile profiles. VOC fingerprints were generated on malt extract for all isolates and on soil for representative members of dominant *Fusarium* clades (**Figure 2**). Medium composition and species identity impacted *Fusarium* VOC emission (**Supplementary Figure S3**), which is in line with previous results illustrating that biotic and abiotic factors can greatly impact secondary metabolism (Blom et al., 2011; Brakhage and Schroeckh, 2011; Schenkel et al., 2015; Schmidt et al., 2016; Lazazzara et al., 2017). Specifically, emission

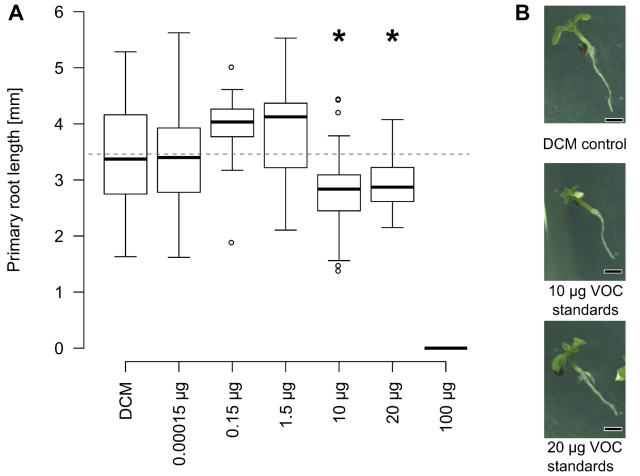

FIGURE 6 | Effect of VOC standards identified in soil on root growth. **(A)** *Arabidopsis* plants were grown on tripartite plates, as described in **Figure 1**. Instead of soil, the second compartment harbored cotton with mixtures of 2-ethyl-1-hexanol, furfural, 5-methyl-2-furancarboxaldehyde, nonanal, decanal, 5-methyl-3-heptanone and benzaldehyde in dichloromethane. Primary root length was mostly unaffected by low concentration, significantly smaller between 10 and 20 µg than plants exposed to dichloromethane without additional VOCs. Germination was fully suppressed at 100 µg (*$p \leq 0.05$, Kruskal Wallis, n = 15–45 seedlings pooled from 6 to 15 Petri dishes). **(B)** Speciemen of 11-days old *Arabidopsis* plants exposed to different volatile blends at the end of the experiment (scale bar = 1 mm).

of fungal VOCs might for instance depend on the age/growth stage of mycelium (Naznin et al., 2013; Lee et al., 2015). The influence of growth medium on secondary metabolism can be attributed to the direct availability of precursors in the growth medium or the modulating effects of specific metabolites on secondary metabolism (Zain et al., 2011). Whereas malt extract is a sugar-rich medium (Balcerek et al., 2016), soil is nutrient poor and rich in amino acids and lipids (Pétriacq et al., 2017). These dissimilarities might explain the drastic differences in VOC profiles observed here for the same species grown on soil or malt extract (**Figures 2B**, **5A**, **Supplementary Figures S3**, **S4**). Furthermore, the fact that soil contains a large pool of uncharacterized metabolites (Pétriacq et al., 2017) might explain why the structure of numerous VOCs could not be elucidated based on existing mass spectral databases. VOCs emitted by soil indeed depend on a plethora of variables including environmental and soil physico-chemical factors (Insam and Seewald, 2010). Elucidating the structure of novel soil VOCs and understanding how they are formed will be a challenge for future studies.

Bioassays investigating VOC-based interactions between soil-grown *Fusarium* and *Arabidopsis* highlighted the ability of the *Fusarium* genus to increase primary root length. This growth promoting effect was not observed for the unidentified Helotiales strain, suggesting a high impact of genetic background. It has been hypothesized that fungi with different lifestyles (i.e., pathogens, saprophytes, symbiotic) might emit different volatiles (Müller et al., 2013; Schenkel et al., 2015), which could in turn partially explain plant phenotype. The dataset presented here is however not optimal to validate this hypothesis, first because the Helotiales strain used here has not been fully characterized and, second because numerous *Fusarium* isolates can switch their lifestyle depending on plant hosts and environmental conditions (Kia et al., 2017; Lofgren et al., 2018). Thus, attributing a strict pathogenic/saprotrophic/endophytic lifestyle to these strains would be difficult and likely misleading.

Volatile organic compound-based root length stimulation comparable to the one reported here (i.e., 49–126% increase compared to control plants) have been described by others (Bitas et al., 2015; Ditengou et al., 2015). By contrast to primary root length, leaf area and root branching of the 11-days-old seedlings were not significantly affected by the presence of *Fusarium* strains in this study. This is in opposition with earlier results that reported increased leaf size and root branching in *Arabidopsis* seedlings of comparable age along with primary root length stimulation (Ryu et al., 2003; Splivallo et al., 2009; Bitas et al., 2015; Ditengou et al., 2015). This might indicate that under our experimental conditions, *Fusarium* specifically stimulated primary root length or that root branching and leaf surface would only have been affected at a later plant developmental stage. The root length shortening observed with *Arabidopsis* could be attributed to seven VOCs that showed bioactivity from 70 µg (a mixture of 10 µg each) up. This is comparable to quantities of bioactive VOCs reported by others (Ryu et al., 2003; Zou et al., 2010; Blom et al., 2011; Park et al., 2015). Additionally, one of the bioactive VOC tested here (2-ethyl-1-hexanol) is phytotoxic to ornamental plants (Hörmann et al., 2018). Demonstrating whether similar effects occur under field conditions will be a challenge that will require to carefully take soil parameters as well as source and sink mechanisms under consideration.

Lastly, our results indicate that *Fusarium* has the capacity to decrease soil VOCs. The mechanism behind this phenomenon is elusive, yet the ability of microbes to consume VOCs has been occasionally described. For instance, microbial communities are able to degrade VOCs in soil including benzene and toluene under aerobic conditions (Yoshikawa et al., 2017). Tracer experiments with radioactive carbon revealed that the labelled monoterpene geraniol was metabolized by unidentified soil/rhisophere microbes and transformed into another monoterpene (limonene) (Owen et al., 2007). Mono- and sesquiterpenes can also serve as carbon source to rhizobacteria (Best et al., 1987; Kleinheinz et al., 1999; Del Giudice et al., 2008; Schulz-Bohm et al., 2015, 2017). It has also been suggested that VOCs might act as carbon source for fungal growth on carbon-poor substrate (Cale et al., 2016). Besides being metabolized or transformed, soil VOCs might also be adsorbed to fungal hyphae. Demonstrating the exact mechanism that leads to the decrease of specific VOCs by *Fusarium* will require combining labeling experiments to metabolomics in order to understand the fate of specific VOCs.

Overall our results constitute an important paradigm shift in plant-microbial interactions since they suggest that microbes shall not only be considered as the possible emitter of bioactive VOCs, but also as a possible sink. Shedding light

on the implications of VOC degradation by microbes will require understanding their breakdown mechanisms which remains elusive. Nevertheless, this finding might have important implications in plant-microbial interactions and suggest that considering the soil volatilome might help to predict plant productivity.

AUTHOR CONTRIBUTIONS

RS and DS designed all the experiments. DS performed all the experiments with input from AB for the bioassays on soil. JM-V provided plant and fungal material and contributed to fungal characterization. DS, RS, and JM-V analyzed the data and wrote the manuscript.

FUNDING

We thankfully acknowledge the LOEWE research program of the government of Hesse, Germany, in the framework of the Integrative Fungal Research Cluster (IPF) for funding and access to the fungal collection.

SUPPLEMENTARY MATERIAL

The Supplementary Material for this article can be found online at: https://www.frontiersin.org/articles/10.3389/fmicb.2018.01847/full#supplementary-material

FIGURE S1 | Phylogenetic tree of *Fusarium* strains used in this study and reference strains. Phylogenetic tree of 27 *Fusarium* strains (**Table 1**) and reference strains [FUSARIUM-ID database (Geiser et al., 2004)] based on *tef-1α* sequences. Numbers at nodes indicates bootstrap values (1,000 replications).

FIGURE S2 | The presence of *Fusarium* does not affect *Arabidopsis* root branching or leaf surface area. Bioassays were conducted as described in **Figure 1**. No significant differences in leaf surface area or root branching (number of secondary roots) were observed between *Arabidopsis* seedlings exposed to VOCs from non-inoculated soil or *Fusarium* or Helotiales-inoculated soil (statistics: Kruskal-Wallis test, $p \leq 0.05$).

FIGURE S3 | Comparison the effect of substrate on the VOC profile of *Fusarium*. Cluster analysis of the VOC profile of seven *Fusarium* strains grown either on malt extract (3–4 replicates per strain) or soil (3 replicates per strain). A representative VOC profile for each strain was generated by considering only TAGs (VOCs) which consistently appeared in all replicates, and these representative profiles were used to compute the dendrogram presented here. Signal present in the respective controls (i.e., soil or pure malt extract) was removed. TAGs transformed into binary data (i.e., presence–absence) were used to generate a cluster tree using Jaccard similarity index. • represent nodes with ≥70% (1,000 bootstraps).

FIGURE S4 | VOC profiles of *Fusarium* strain P1065 on malt extract and soil. The two upper chromatograms represent the VOC profile of strain P1065 on malt extract and the profile of the control (malt extract without fungus), whereas the two lower chromatograms illustrate the VOC emitted by the same fungus on soil (or the soil control). These results exemplify the influence of the medium (malt extract versus soil) on microbial VOC emission. VOCs were identified or tentatively identified as: (1) 1-hexanol; (2) 4-heptanone; (3) styrene; (4) 7-ethyl-4-noanone; (5) benzaldehyde; (6) 1,3,5-trimethylbenzene; (7) 5-methyl-2-furancarboxaldehyde; (8) 1-heptanol.

FIGURE S5 | VOC profiles of soil samples at the end of the bioassay. Heatmap illustrating the concentration of 14 identified VOCs and 33 not identified VOCs in $n = 3$ replicates per fungal strain and highlighting that non-inoculated soil tends to have a higher concentration of VOCs compared to *Fusarium*-inoculated soil.

DATA SHEET S3 | GC/MS data for non-inoculated and *Fusarium* inoculated soil.

REFERENCES

Altschul, S. F., Gish, W., Miller, W., Myers, E. W., and Lipman, D. J. (1990). Basic local alignment search tool. *J. Mol. Biol.* 215, 403–410. doi: 10.1016/S0022-2836(05)80360-2

Balcerek, M., Pielech-Przybylska, K., Strąk, E., Patelski, P., and Dziekońska, U. (2016). Comparison of fermentation results and quality of the agricultural distillates obtained by application of commercial amylolytic preparations and cereal malts. *Eur. Food Res. Technol.* 242, 321–335. doi: 10.1007/s00217-015-2542-7

Best, D. J., Floyd, N. C., Magalhaes, A., Burfield, A., and Rhodes, P. M. (1987). Initial enzymatic steps in the degradation of alpha-pinene by *Pseudomonas fluorescens* Ncimb 11671. *Biocatalysis* 1, 147–159. doi: 10.3109/10242428709040139

Bitas, V., McCartney, N., Li, N., Demers, J., Kim, J.-E., Kim, H.-S., et al. (2015). *Fusarium oxysporum* volatiles enhance plant growth via affecting auxin transport and signaling. *Front. Microbiol.* 6:1248. doi: 10.3389/fmicb.2015.01248

Blom, D., Fabbri, C., Connor, E. C., Schiestl, F. P., Klauser, D. R., Boller, T., et al. (2011). Production of plant growth modulating volatiles is widespread among rhizosphere bacteria and strongly depends on culture conditions: volatile-mediated impact of bacteria on *Arabidopsis thaliana*. *Environ. Microbiol.* 13, 3047–3058. doi: 10.1111/j.1462-2920.2011.02582.x

Brakhage, A. A., and Schroeckh, V. (2011). Fungal secondary metabolites – strategies to activate silent gene clusters. *Fungal Genet. Biol.* 48, 15–22. doi: 10.1016/j.fgb.2010.04.004

Cale, J. A., Collignon, R. M., Klutsch, J. G., Kanekar, S. S., Hussain, A., and Erbilgin, N. (2016). Fungal volatiles can act as carbon sources and semiochemicals to mediate interspecific interactions amongbark beetle-associated fungal symbionts. *PLoS One* 11:e0162197. doi: 10.1371/journal.pone.0162197

Castresana, J. (2000). Selection of conserved blocks from multiple alignments for their use in phylogenetic analysis. *Mol. Biol. Evol.* 17, 540–552. doi: 10.1093/oxfordjournals.molbev.a026334

Choi, G.-H., Ro, J.-H., Park, B.-J., Lee, D.-Y., Cheong, M.-S., Lee, D.-Y., et al. (2016). Benzaldehyde as a new class plant growth regulator on *Brassica campestris*. *J. Appl. Biol. Chem.* 59, 159–164. doi: 10.3839/jabc.2016.029

Cordovez, V., Mommer, L., Moisan, K., Lucas-Barbosa, D., Pierik, R., Mumm, R., et al. (2017). Plant phenotypic and transcriptional changes induced by volatiles from the fungal root pathogen *Rhizoctonia solani*. *Front. Plant Sci.* 8:1262. doi: 10.3389/fpls.2017.01262

R Core Team (2017). *R: A Language and Environment for Statistical Computing*. Vienna: R Foundation for Statistical Computing.

Del Giudice, L., Massardo, D. R., Pontieri, P., Bertea, C. M., Mombello, D., Carata, E., et al. (2008). The microbial community of Vetiver root and its involvement into essential oil biogenesis: vetiver root bacteria and essential oil biogenesis. *Environ. Microbiol.* 10, 2824–2841. doi: 10.1111/j.1462-2920.2008.01703.x

Ditengou, F. A., Müller, A., Rosenkranz, M., Felten, J., Lasok, H., van Doorn, M. M., et al. (2015). Volatile signalling by sesquiterpenes from ectomycorrhizal fungi reprogrammes root architecture. *Nat. Commun.* 6:6279. doi: 10.1038/ncomms7279

Dudareva, N., Klempien, A., Muhlemann, J. K., and Kaplan, I. (2013). Biosynthesis, function and metabolic engineering of plant volatile organic compounds. *New Phytol.* 198, 16–32. doi: 10.1111/nph.12145

Geiser, D. M., del Mar Jiménez-Gasco, M., Kang, S., Makalowska, I., Veeraraghavan, N., Ward, T. J., et al. (2004). FUSARIUM-ID v. 1.0: a DNA

sequence database for identifying *Fusarium*. *Eur. J. Plant Pathol.* 110, 473–479. doi: 10.1023/B:EJPP.0000032386.75915.a0

Glynou, K., Ali, T., Buch, A.-K., Haghi Kia, S., Ploch, S., Xia, X., et al. (2016). The local environment determines the assembly of root endophytic fungi at a continental scale. *Environ. Microbiol.* 18, 2418–2434. doi: 10.1111/1462-2920.13112

Hammer, Ø, David, A., Harper, T., and Ryan, P. D. (2001). Past: paleontological statistics software package for education and data analysis. *Palaeontol. Electron.* 4, 1–9.

Hörmann, V., Brenske, K.-R., and Ulrichs, C. (2018). Assessment of filtration efficiency and physiological responses of selected plant species to indoor air pollutants (toluene and 2-ethylhexanol) under chamber conditions. *Environ. Sci. Pollut. Res.* 25, 447–458. doi: 10.1007/s11356-017-0453-9

Hung, R., Lee, S., and Bennett, J. W. (2013). *Arabidopsis thaliana* as a model system for testing the effect of *Trichoderma* volatile organic compounds. *Fungal Ecol.* 6, 19–26. doi: 10.1016/j.funeco.2012.09.005

Insam, H., and Seewald, M. S. A. (2010). Volatile organic compounds (VOCs) in soils. *Biol. Fertil. Soils* 46, 199–213. doi: 10.1007/s00374-010-0442-3

Junker, R. R., and Tholl, D. (2013). Volatile organic compound mediated interactions at the plant-microbe interface. *J. Chem. Ecol.* 39, 810–825. doi: 10.1007/s10886-013-0325-9

Kai, M., Effmert, U., and Piechulla, B. (2016). Bacterial-plant-interactions: approaches to unravel the biological function of bacterial volatiles in the rhizosphere. *Front. Microbiol.* 7:108. doi: 10.3389/fmicb.2016.00108

Kai, M., and Piechulla, B. (2009). Plant growth promotion due to rhizobacterial volatiles–an effect of CO2? *FEBS Lett.* 583, 3473–3477. doi: 10.1016/j.febslet.2009.09.053

Karim, N. F. A., Mohd, M., Nor, N. M. I. M., and Zakaria, L. (2016). Saprophytic and potentially pathogenic *Fusarium* species from peat soil in Perak and Pahang. *Trop. Life Sci. Res.* 27, 1–20.

Katoh, K., and Standley, D. M. (2013). MAFFT multiple sequence alignment software version 7: improvements in performance and usability. *Mol. Biol. Evol.* 30, 772–780. doi: 10.1093/molbev/mst010

Kia, S. H., Glynou, K., Nau, T., Thines, M., Piepenbring, M., and Maciá-Vicente, J. G. (2017). Influence of phylogenetic conservatism and trait convergence on the interactions between fungal root endophytes and plants. *ISME J.* 11, 777–790. doi: 10.1038/ismej.2016.140

Kleinheinz, G. T., Bagley, S. T., John, W. P. S., Rughani, J. R., and McGinnis, G. D. (1999). Characterization of alpha-pinene-degrading microorganisms and application to a bench-scale biofiltration system for VOC degradation. *Arch. Environ. Contam. Toxicol.* 37, 151–157. doi: 10.1007/s002449900500

Knudsen, J. T., Eriksson, R., Gershenzon, J., and Ståhl, B. (2006). Diversity and distribution of floral scent. *Bot. Rev.* 72, 1–120.

Lazazzara, V., Perazzolli, M., Pertot, I., Biasioli, F., Puopolo, G., and Cappellin, L. (2017). Growth media affect the volatilome and antimicrobial activity against *Phytophthora infestans* in four *Lysobacter* type strains. *Microbiol. Res.* 201, 52–62. doi: 10.1016/j.micres.2017.04.015

Lee, S., Hung, R., Yap, M., and Bennett, J. W. (2015). Age matters: the effects of volatile organic compounds emitted by *Trichoderma atroviride* on plant growth. *Arch. Microbiol.* 197, 723–727. doi: 10.1007/s00203-015-1104-5

Lemfack, M. C., Gohlke, B.-O., Toguem, S. M. T., Preissner, S., Piechulla, B., and Preissner, R. (2018). mVOC 2.0: a database of microbial volatiles. *Nucleic Acids Res.* 46, D1261–D1265. doi: 10.1093/nar/gkx1016

Lofgren, L. A., LeBlanc, N. R., Certano, A. K., Nachtigall, J., LaBine, K. M., Riddle, J., et al. (2018). *Fusarium graminearum*: pathogen or endophyte of North American grasses? *New Phytol.* 217, 1203–1212. doi: 10.1111/nph.14894

Luedemann, A., Strassburg, K., Erban, A., and Kopka, J. (2008). TagFinder for the quantitative analysis of gas chromatography–mass spectrometry (GC-MS)-based metabolite profiling experiments. *Bioinformatics* 24, 732–737. doi: 10.1093/bioinformatics/btn023

Maciá-Vicente, J. G., Jansson, H.-B., Abdullah, S. K., Descals, E., Salinas, J., and Lopez-Llorca, L. V. (2008). Fungal root endophytes from natural vegetation in Mediterranean environments with special reference to *Fusarium* spp. *FEMS Microbiol. Ecol.* 64, 90–105. doi: 10.1111/j.1574-6941.2007.00443.x

Martínez-Medina, A., Van Wees, S. C. M., and Pieterse, C. M. J. (2017). Airborne signals from Trichoderma fungi stimulate iron uptake responses in roots resulting in priming of jasmonic acid-dependent defences in shoots of *Arabidopsis thaliana* and *Solanum lycopersicum*: fungal volatiles trigger iron uptake responses and ISR. *Plant Cell Environ.* 40, 2691–2705. doi: 10.1111/pce.13016

Müller, A., Faubert, P., Hagen, M., Zu Castell, W., Polle, A., Schnitzler, J.-P., et al. (2013). Volatile profiles of fungi–Chemotyping of species and ecological functions. *Fungal Genet. Biol.* 54, 25–33. doi: 10.1016/j.fgb.2013.02.005

Naznin, H. A., Kimura, M., Miyazawa, M., and Hyakumachi, M. (2013). Analysis of volatile organic compounds emitted by plant growth-promoting fungus *Phoma* sp. GS8-3 for growth promotion effects on Tobacco. *Microbes Environ.* 28, 42–49. doi: 10.1264/jsme2.ME12085

O'Donnell, K., Ward, T. J., Robert, V. A. R. G., Crous, P. W., Geiser, D. M., and Kang, S. (2015). DNA sequence-based identification of *Fusarium*: current status and future directions. *Phytoparasitica* 43, 583–595. doi: 10.1007/s12600-015-0484-z

Oksanen, J., Blanchet, F. G., Michael, F., Kindt, R., Legendre, P., McGlinn, D., et al. (2017). *Vegan: Community Ecology Package. R Package Version 2.4–5*.

Owen, S. M., Clark, S., Pompe, M., and Semple, K. T. (2007). Biogenic volatile organic compounds as potential carbon sources for microbial communities in soil from the rhizosphere of *Populus tremula*. *FEMS Microbiol. Lett.* 268, 34–39. doi: 10.1111/j.1574-6968.2006.00602.x

Paradis, E., Claude, J., and Strimmer, K. (2004). APE: analyses of phylogenetics and evolution in R language. *Bioinforma. Oxf. Engl.* 20, 289–290.

Park, Y.-S., Dutta, S., Ann, M., Raaijmakers, J. M., and Park, K. (2015). Promotion of plant growth by *Pseudomonas fluorescens* strain SS101 via novel volatile organic compounds. *Biochem. Biophys. Res. Commun.* 461, 361–365. doi: 10.1016/j.bbrc.2015.04.039

Pétriacq, P., Williams, A., Cotton, A., McFarlane, A. E., Rolfe, S. A., and Ton, J. (2017). Metabolite profiling of non-sterile rhizosphere soil. *Plant J.* 92, 147–162. doi: 10.1111/tpj.13639

Piechulla, B., and Schnitzler, J.-P. (2016). Circumvent CO2 effects in volatile-based microbe–plant interactions. *Trends Plant Sci.* 21, 541–543. doi: 10.1016/j.tplants.2016.05.001

Ryu, C.-M., Farag, M. A., Hu, C.-H., Reddy, M. S., Wei, H.-X., Pare, P. W., et al. (2003). Bacterial volatiles promote growth in *Arabidopsis*. *Proc. Natl. Acad. Sci. U.S.A.* 100, 4927–4932. doi: 10.1073/pnas.0730845100

Sánchez-López, ÁM., Baslam, M., De Diego, N., Muñoz, F. J., Bahaji, A., Almagro, G., et al. (2016). Volatile compounds emitted by diverse phytopathogenic microorganisms promote plant growth and flowering through cytokinin action: VCs from microbial phytopathogens promote growth. *Plant Cell Environ.* 39, 2592–2608. doi: 10.1111/pce.12759

Schenkel, D., Lemfack, M. C., Piechulla, B., and Splivallo, R. (2015). A meta-analysis approach for assessing the diversity and specificity of belowground root and microbial volatiles. *Front. Plant Sci.* 6:707. doi: 10.3389/fpls.2015.00707

Schmidt, R., Etalo, D. W., de Jager, V., Gerards, S., Zweers, H., de Boer, W., et al. (2016). Microbial small talk: volatiles in fungal–bacterial interactions. *Front. Microbiol.* 6:1495. doi: 10.3389/fmicb.2015.01495

Schneider, C. A., Rasband, W. S., and Eliceiri, K. W. (2012). NIH Image to ImageJ: 25 years of image analysis. *Nat. Methods* 9, 671–675. doi: 10.1038/nmeth.2089

Schulz-Bohm, K., Martín-Sánchez, L., and Garbeva, P. (2017). Microbial Volatiles: small molecules with an important role in intra- and inter-kingdom interactions. *Front. Microbiol.* 8:2484. doi: 10.3389/fmicb.2017.02484

Schulz-Bohm, K., Zweers, H., de Boer, W., and Garbeva, P. (2015). A fragrant neighborhood: volatile mediated bacterial interactions in soil. *Front. Microbiol.* 6:1212. doi: 10.3389/fmicb.2015.01212

Sherif, M., Becker, E.-M., Herrfurth, C., Feussner, I., Karlovsky, P., and Splivallo, R. (2016). Volatiles emitted from maize ears simultaneously infected with two *Fusarium* species mirror the most competitive fungal pathogen. *Front. Plant Sci.* 7:1460. doi: 10.3389/fpls.2016.01460

Šimpraga, M., Takabayashi, J., and Holopainen, J. K. (2016). Language of plants: Where is the word? Language of plants. *J. Integr. Plant Biol.* 58, 343–349. doi: 10.1111/jipb.12447

Splivallo, R., Fischer, U., Gobel, C., Feussner, I., and Karlovsky, P. (2009). Truffles regulate plant root morphogenesis via the production of auxin and ethylene. *Plant Physiol.* 150, 2018–2029. doi: 10.1104/pp.109.141325

Splivallo, R., Novero, M., Bertea, C. M., Bossi, S., and Bonfante, P. (2007). Truffle volatiles inhibit growth and induce an oxidative burst in *Arabidopsis thaliana*. *New Phytol.* 175, 417–424. doi: 10.1111/j.1469-8137.2007.02141.x

Stamatakis, A. (2014). RAxML version 8: a tool for phylogenetic analysis and post-analysis of large phylogenies. *Bioinformatics* 30, 1312–1313. doi: 10.1093/bioinformatics/btu033

Tholl, D., and Röse, U. (2006). "Detection and identification of floral scent compounds," in *Biology of Floral Scent*, eds E. Pichersky and N. Dudareva (Boca Raton, FL: CRC Press), 3–25. doi: 10.1201/9781420004007.sec1

Wenke, K., Wanke, D., Kilian, J., Berendzen, K., Harter, K., and Piechulla, B. (2012). Volatiles of two growth-inhibiting rhizobacteria commonly engage AtWRKY18 function: bacterial volatiles: a new form of stress elicitor. *Plant J.* 70, 445–459. doi: 10.1111/j.1365-313X.2011.04891.x

Yoshikawa, M., Zhang, M., Kurisu, F., and Toyota, K. (2017). Bacterial degraders of coexisting dichloromethane, benzene, and toluene, identified by stable-isotope probing. *Water Air Soil Pollut.* 228:418. doi: 10.1007/s11270-017-3604-1

Zain, M. E., El-Sheikh, H. H., Soliman, H. G., and Khalil, A. M. (2011). Effect of certain chemical compounds on secondary metabolites of *Penicillium janthinellum* and *P. duclauxii*. *J. Saudi Chem. Soc.* 15, 239–246. doi: 10.1016/j.jscs.2010.09.004

Zhang, H., Kim, M.-S., Krishnamachari, V., Payton, P., Sun, Y., Grimson, M., et al. (2007). Rhizobacterial volatile emissions regulate auxin homeostasis and cell expansion in *Arabidopsis*. *Planta* 226, 839–851. doi: 10.1007/s00425-007-0530-2

Zou, C., Li, Z., and Yu, D. (2010). Bacillus megaterium strain XTBG34 promotes plant growth by producing 2-pentylfuran. *J. Microbiol.* 48, 460–466. doi: 10.1007/s12275-010-0068-z

Conflict of Interest Statement: The authors declare that the research was conducted in the absence of any commercial or financial relationships that could be construed as a potential conflict of interest.

frontiers in Plant Science

MINI REVIEW
published: 19 December 2018
doi: 10.3389/fpls.2018.01896

The Role of Host Genetic Signatures on Root–Microbe Interactions in the Rhizosphere and Endosphere

Peng Yu and Frank Hochholdinger**

Institute of Crop Science and Resource Conservation, Crop Functional Genomics, University of Bonn, Bonn, Germany

Microbiomes inhabiting plants are crucial for plant productivity and well-being. A plethora of interactions between roots, microbiomes, and soil shapes the self-organization of the microbial community associated with the root system. The rhizosphere (i.e., the soil close to the root surface) and endosphere (i.e., all inner root tissues) are critical interfaces for the exchange of resources between roots and the soil environment. In recent years, next-generation sequencing technologies have enabled systemic studies of root-associated microbiomes in the endosphere and interactions between roots and microbes at the root-soil interfaces. Genetic factors such as species and genotype of host plants are the driving force of microbial community differentiation and composition. In this mini-review, we will survey the role of these factors on plant–microbe interactions by highlighting the results of next-generation genomic and transcriptomic studies in the rhizosphere and endosphere of land plants. Moreover, environmental factors such as geography and soil type shape the microbiome. Relationships between the root-associated microbiome, architectural variations and functional switches within the root system determine the health and fitness of the whole plant system. A detailed understanding of plant–microbe interactions is of fundamental agricultural importance and significance for crop improvement by plant breeding.

Keywords: endosphere, interaction, microbial diversity, rhizosphere, root

OPEN ACCESS

Edited by:
Caroline Gutjahr,
Technische Universität München, Germany

Reviewed by:
Gregor Langen,
Universität zu Köln, Germany
Pierre-Marc Delaux,
UMR5546 Laboratoire de Recherche en Sciences Vegetales (LRSV), France

****Correspondence:***
Peng Yu
yupeng@uni-bonn.de
Frank Hochholdinger
hochholdinger@uni-bonn.de

Specialty section:
This article was submitted to Plant Microbe Interactions, a section of the journal Frontiers in Plant Science

Received: *01 July 2018*
Accepted: *06 December 2018*
Published: *19 December 2018*

Citation:
Yu P and Hochholdinger F (2018) The Role of Host Genetic Signatures on Root–Microbe Interactions in the Rhizosphere and Endosphere. Front. Plant Sci. 9:1896. doi: 10.3389/fpls.2018.01896

INTRODUCTION

In vascular plants, the root system is the main interface for interactions with the soil microbiome. Roots influence biological activity and diversity of microbes in the soil by secreting organic substances including amino acids, carbohydrates and organic acids as well as by depositing root cap border cells and polysaccharide mucilage to soil environments (Marschner, 1995). Thus, root systems provide nutrient-rich niches for microbes. The interactions of roots and microbes are also enhanced by the highly active uptake of water and soluble molecules by roots and by transporting them to the energy delivering green part of plants. Soil provides a vital habitat for microorganisms (Marschner, 1995). Genomic studies have indicated that the soil type has in general a stronger influence on the composition of the plant root microbiome in both the rhizosphere and the endosphere than the plant species (Bulgarelli et al., 2012; Peiffer et al., 2013; Schreiter et al., 2014). However, under identical soil conditions, the plant genotype drives the diversity of root microbial community structure and function, thus demonstrating that plants are able to filter their root microbiomes in a defined environment (Reinhold-Hurek and Hurek, 2011). Different plant

species even genotypes within a species have shown distinct metabolic activities thus producing different types and amounts of organic compounds. Early studies have demonstrated that microbial communities of root systems varied between different plant genera (Smalla et al., 2001) and species (Tan et al., 2011). For instance, highly diverged angiosperm species vary with respect to bacterial diversity and composition in both the rhizosphere and endosphere (Fitzpatrick et al., 2018). In addition, the composition of root microbiomes can be divergent at the level of subspecies, as shown from different cultivars of potato (Sessitsch et al., 2002; Andreote et al., 2010) and rice (Hardoim et al., 2011). Comparative genomic analyses of microbial communities in the endosphere and rhizosphere, require suitable methods to efficiently separate these compartments along the complex morphological and anatomical structure of the root system (Reinhold-Hurek et al., 2015).

Recent studies have applied high-throughput DNA sequencing to study the composition and organization of different plant microbiomes (16S rRNA gene based community profiling), including both dicot (Bulgarelli et al., 2012; Lundberg et al., 2012; Schlaeppi et al., 2014) and monocot (Knief et al., 2012; Peiffer et al., 2013; Edwards et al., 2015; Walters et al., 2018) species. This mini review will highlight recent progress in deciphering the influence of the genetic background of host plants on the microbial diversity and composition in the rhizosphere and endosphere of the root system.

COMMUNITY PROFILING OF HOST–MICROBE INTERACTION IN THE RHIZOSPHERE

The rhizosphere is the narrow soil zone directly surrounding the root system, which is highly modulated by the root system (Marschner, 1995). Roots release low-molecular-weight exudates, which decompose very quickly. Those exudates attract soil microorganisms into the rhizosphere where they multiply and enrich by several orders of magnitude compared to bulk soil (Sasse et al., 2017). Attracted microorganisms strongly influence plant nutrition by mineralizing organic nutrients and transformation of inorganic nutrients (Marschner, 1995). Moreover, host–microbe interaction studies have revealed that plants are able to recruit beneficial microbes to increase microbial activity and reduce pathogen attacks to maintain plant health in the rhizosphere (Berendsen et al., 2012). Recent surveys have revealed that different plant species can shape their rhizosphere microbiome, as shown from the host specific microbial communities grown under identical soil condition (Ofek-Lalzar et al., 2014). Rhizosphere microbiome composition has been suggested to be controlled by root exudate composition (Badri et al., 2009; Lakshmanan et al., 2012; Carvalhais et al., 2013; Lebeis et al., 2015). Particular plant species and even specific cultivars shape the composition of the rhizosphere microbiome (Peiffer et al., 2013; Turner et al., 2013; Ofek-Lalzar et al., 2014).

Human selection during domestication has significant reduced the genetic diversity of modern crop species in comparison to their progenitors (Doebley et al., 2006). Recent work has emphasized that domestication strongly shaped microbial diversity in the rhizosphere (Pérez-Jaramillo et al., 2016; Schmidt et al., 2016). Domesticated barley (*Hordeum vulgare*) shows a distinct microbiome compared to its wild progenitor with respect to function (Bulgarelli et al., 2015). Some of the genes affecting host–microbe interactions in domesticated barley show evidence of positive selection (Bulgarelli et al., 2015). Moreover, the maize progenitor teosinte shows significantly higher bacterial abundance and diversity in the rhizosphere compared to modern maize sweet corn and popcorn inbred lines (Szoboszlay et al., 2015). Nevertheless, a significant fraction of endophytic bacterial diversity observed in teosinte is conserved in modern hybrid maize (Johnston-Monje and Raizada, 2011; Johnston-Monje et al., 2014). In vegetable species as for instance beet and lettuce, rhizosphere bacterial community composition of wild ancestors is different from their corresponding modern varieties (Zachow et al., 2014; Cardinale et al., 2015). Similarly, genetically divergent wild and modern bean genotypes display distinct bacterial communities (Pérez-Jaramillo et al., 2017). Interestingly, recent findings indicate that fungal communities are stronger influenced by host genotypes than by bacterial communities in the rhizosphere during sunflower domestication and breeding (Leff et al., 2017). These results indicate that microbial composition and diversity in the rhizosphere co-evolved with host domestication and modern breeding but that it is also dependent on their own genetic and genomic identity in plants.

High-yielding maize hybrids display a significantly higher bacterial abundance and more elite probiotic rhizospheric strains with higher productivity of 2,4-diacetylphloroglucinol and superior root-colonization ability in the rhizosphere than their parental inbred lines (Picard and Bosco, 2006). It has been suggested that this is due to more secretion of exudates relative to their parental inbred lines (Picard et al., 2004, 2008; Picard and Bosco, 2005, 2006). Specifically, the antibiotic 2,4-diacetylphloroglucinol produced by probiotic rhizobacteria has been shown growth-promoting properties and inhibition of phytopathogenic bacteria and fungi in crops (Haas and Keel, 2003; Vacheron et al., 2013). In rice, enrichment of a particular group of *Alphaproteobacteria* and *Ascomycota* has been shown in hybrid cultivars in comparison to conventional cultivars (Hussain et al., 2011). These results suggest that hybrids display beneficial plant–microbe interactions that might be related to heterosis i.e., the superior vigor of these plants. Thus, it would be interesting to compare additional hybrids to survey how heterosis affects the root microbiome.

COMMUNITY PROFILING OF HOST–MICROBE INTERACTION IN THE ENDOSPHERE

The endosphere, which comprises all inner root tissues is inhabited by microbes (Reinhold-Hurek et al., 2015). Function

and composition of microbial communities are very different between the rhizosphere and the endosphere. These observations indicate that the endosphere of plants has the potential to attract or filter the microbes inhabiting the rhizosphere (Edwards et al., 2015; Naylor et al., 2017). Microbial communities inhabiting the root endosphere also engage in symbiosis, which is defined as close and long-term biological interaction between two different biological organisms with their host. Endophytic communities of the root system are distinct assemblies and not mere subsets of the microbial communities in the rhizosphere (Gottel et al., 2011). Microbes have been successfully isolated from the endosphere by sonication in Arabidopsis (Bulgarelli et al., 2012; Lundberg et al., 2012). Recent experiments have demonstrated that the host genotypes have relatively little effects on the composition of bacteria in the endosphere of the Arabidopsis root (Bulgarelli et al., 2012; Lundberg et al., 2012). A study in rice has demonstrated that spatially separated parts of the endosphere harbor distinct and overlapping bacterial communities, which are affected by the genotype of the host plant (Edwards et al., 2015). These findings indicate that microbiomes are selected distinctively by the root interior and the rhizosphere in response to multiple signals from the plant. A systemic investigation of cereals suggests that bacterial communities of the host root endosphere correlate with host phylogenetic distance (Naylor et al., 2017). These findings highlight that the composition and diversity of microbial communities in the endosphere depend on specific species and genotypes under a certain geographical condition during the evolutionary history.

It has been shown that beneficial association between host and plant growth promoting rhizobacteria is an inherited trait in the endosphere of tomato plants (Smith et al., 1999). Moreover, it has been demonstrated that hybrids tend to enrich more phylogenetic subgroups of arbuscular mycorrhizal fungi in comparison to their parental inbred lines in the endosphere (Picard et al., 2008). In addition, arbuscular mycorrhizal colonization between inbred lines varies with diverse geographic origin and year of release in maize (An et al., 2010). Finally, modern maize hybrids have a substantially higher colonization rate with arbuscular mycorrhizal fungi than their parental inbred lines or landraces (An et al., 2010). These results substantiate the notion that modern breeding lead to beneficial association between maize and arbuscular mycorrhizal fungi in the endosphere.

In contrast to the model plant Arabidopsis and most dicot plant species, cereal plants display distinct root types including seminal roots and postembryonic shoot-borne crown and brace roots, which show diverse anatomical structures and transcriptomic signatures during development (Hochholdinger et al., 2018). Moreover, lateral roots contribute substantially to the overall surface for water and nutrient uptake in maize (Yu et al., 2016). Recent observations have demonstrated that distinct functional and metabolic characteristics of different root types significantly influence root-inhabiting microbiomes in both maize and Brachypodium (Kawasaki et al., 2016; Yu et al., 2018). These results highlight, that microbiomes diverge even between distinct regions of the root system (Yu et al., 2018). Moreover, some earlier studies have shown that metabolic and genetic fingerprinting along the root are highly diversified for different plant species (Yang and Crowley, 2000; Baudoin et al., 2002). This results in distinct microbial signatures along the different root zones (Kawasaki et al., 2016). These discoveries demonstrate that distinct root microbiomes of specific root types will be averaged out by studying the microbial community structure in a whole root system (Kawasaki et al., 2016). Therefore, it will be necessary to compare root type-specific microbial communities between dicot and monocot species. This will provide an evolutionary perspective to the understanding of how developmental characteristics affect the microbiome in the endosphere and rhizosphere.

CONCLUSION AND PERSPECTIVES

Microbial diversity of the rhizosphere and endosphere is regulated by physical and chemical characteristics of the rhizosphere. These are partly determined by the species and genotype of the host root. Nevertheless, it is still unclear whether the phylogenetic distance between genotypes is correlated with the microbial community composition in the rhizosphere (Bouffaud et al., 2012, 2014; Peiffer et al., 2013; Schlaeppi et al., 2014). Differences in microbial community composition might only be observed between genotypes which display large genetic distances. For example, domesticated genotypes usually display distinct microbiome compositions in comparison with their wild progenitor (Schmidt et al., 2016). Similarly, genetically diverse modern inbred lines also display largely distinct microbiomes (Peiffer et al., 2013; Walters et al., 2018). Another instrumental factor determining the divergence of microbiome composition between different genotypes within a species is the sampling strategy to harvest the rhizosphere and endosphere. Many rhizosphere sampling strategies are likely not reproducible enough because of their low resolution. Recent studies in maize and Brachypodium indicate, that different root types harbor different microbial communities (Kawasaki et al., 2016; Yu et al., 2018), indicating microbiome variations even in the same organ of a single plant. Longitudinal separation of developmentally diverse root zones (root tip, elongation zone, differentiation zone and maturation zone) in single root types will be beneficial to comprehensively detect the development-dependent microbial gradients of host–microbe interaction. In addition, fine-scale isolation of rhizosphere and endosphere by laser capture microdissection in combination with next-generation sequencing would be an important tool to systemically target the direct interaction between plants and microbes at the cellular level.

AUTHOR CONTRIBUTIONS

Both PY and FH contributed to the writing of this mini review.

FUNDING

FH was supported by DFG grant nos. HO2249/9-3, HO2249/12-1 and within the Priority Program (SPP2089) "Rhizosphere Spatiotemporal Organisation – a Key to Rhizosphere Functions" by grant HO2249/17-1. Funding by the Bundesministerium für Bildung und Forschung (BMBF) was provided by grant no. 031 B195C. PY's work on maize roots was funded by DFG grant no. YU 272/1-1.

REFERENCES

An, G. H., Kobayashi, S., Enoki, H., Sonobe, K., Muraki, M., Karasawa, T., et al. (2010). How does arbuscular mycorrhizal colonization vary with host plant genotype? An example based on maize (*Zea mays*) germplasms. *Plant Soil* 327, 441–453. doi: 10.1007/s11104-009-0073-3

Andreote, F. D., Rocha, U. N., Araujo, W. L., Azevedo, J. L., and van Overbeek, L. S. (2010). Effect of bacterial inoculation, plant genotype and developmental stage on root-associated and endophytic bacterial communities in potato (*Solanum tuberosum*). *Antonie Van Leeuwenhoek* 97, 389–399. doi: 10.1007/s10482-010-9421-9

Badri, D. V., Quintana, N., El Kassis, E. G., Kim, H. K., Choi, Y. H., Sugiyama, A., et al. (2009). An ABC transporter mutation alters root exudation of phytochemicals that provoke an overhaul of natural soil microbiota. *Plant Physiol.* 151, 2006–2017. doi: 10.1104/pp.109.147462

Baudoin, E., Benizri, E., and Guckert, A. (2002). Impact of growth stage on the bacterial community structure along maize roots, as determined by metabolic and genetic fingerprinting. *Appl. Soil Ecol.* 19, 135–145. doi: 10.1016/S0929-1393(01)00185-8

Berendsen, R. L., Pieterse, C. M., and Bakker, P. A. (2012). The rhizosphere microbiome and plant health. *Trends Plant Sci.* 17, 478–486. doi: 10.1016/j.tplants.2012.04.001

Bouffaud, M. L., Kyselková, M., Gouesnard, B., Grundmann, G., Muller, D., and Moënne-Loccoz, Y. V. A. N. (2012). Is diversification history of maize influencing selection of soil bacteria by roots? *Mol. Ecol.* 21, 195–206. doi: 10.1111/j.1365-294X.2011.05359.x

Bouffaud, M. L., Poirier, M. A., Muller, D., and Moënne-Loccoz, Y. (2014). Root microbiome relates to plant host evolution in maize and other Poaceae. *Environ. Microbiol.* 16, 2804–2814. doi: 10.1111/1462-2920.12442

Bulgarelli, D., Garrido-Oter, R., Münch, P. C., Weiman, A., Dröge, J., Pan, Y., et al. (2015). Structure and function of the bacterial root microbiota in wild and domesticated barley. *Cell Host Microbe* 17, 392–403. doi: 10.1016/j.chom.2015.01.011

Bulgarelli, D., Rott, M., Schlaeppi, K., Ver Loren van Themaat, E., Ahmadinejad, N., et al. (2012). Revealing structure and assembly cues for Arabidopsis root-inhabiting bacterial microbiota. *Nature* 488, 91–95. doi: 10.1038/nature11336

Cardinale, M., Grube, M., Erlacher, A., Quehenberger, J., and Berg, G. (2015). Bacterial networks and co-occurrence relationships in the lettuce root microbiota. *Environ. Microbiol.* 17, 239–252. doi: 10.1111/1462-2920.12686

Carvalhais, L. C., Dennis, P. G., Fan, B., Fedoseyenko, D., Kierul, K., Becker, A., et al. (2013). Linking plant nutritional status to plant-microbe interactions. *PLoS One* 8:e68555. doi: 10.1371/journal.pone.0068555

Doebley, J. F., Gaut, B. S., and Smith, B. D. (2006). The molecular genetics of crop domestication. *Cell* 127, 1309–1321. doi: 10.1016/j.cell.2006.12.006

Edwards, J., Johnson, C., Santos-Medellín, C., Lurie, E., Podishetty, N. K., Bhatnagar, S., et al. (2015). Structure, variation, and assembly of the root-associated microbiomes of rice. *Proc. Natl. Acad. Sci. U.S.A.* 112, 911–920. doi: 10.1073/pnas.1414592112

Fitzpatrick, C. R., Copeland, J., Wang, P. W., Guttman, D. S., Kotanen, P. M., and Johnson, M. T. (2018). Assembly and ecological function of the root microbiome across angiosperm plant species. *Proc. Natl. Acad. Sci. U.S.A.* 115, 1157–1165. doi: 10.1073/pnas.1717617115

Gottel, N. R., Castro, H. F., Kerley, M., Yang, Z., Pelletier, D. A., Podar, M., et al. (2011). Distinct microbial communities within the endosphere and rhizosphere of *Populus deltoides* roots across contrasting soil types. *Appl. Environ. Microbiol.* 77, 5934–5944. doi: 10.1128/AEM.05255-11

Haas, D., and Keel, C. (2003). Regulation of antibiotic production in root-colonizing Pseudomonas spp. and relevance for biological control of plant disease. *Annu. Rev. Phytopathol.* 41, 117–153. doi: 10.1146/annurev.phyto.41.052002.095656

Hardoim, P. R., Andreote, F. D., Reinhold-Hurek, B., Sessitsch, A., van Overbeek, L. S., and van Elsas, J. D. (2011). Rice root-associated bacteria: insights into community structures across 10 cultivars. *FEMS Microbiol. Ecol.* 77, 154–164. doi: 10.1111/j.1574-6941.2011.01092.x

Hochholdinger, F., Yu, P., and Marcon, C. (2018). Genetic control of root system development in maize. *Trends Plant Sci.* 23, 79–88. doi: 10.1016/j.tplants.2017.10.004

Hussain, Q., Liu, Y., Zhang, A., Pan, G., Li, L., Zhang, X., et al. (2011). Variation of bacterial and fungal community structures in the rhizosphere of hybrid and standard rice cultivars and linkage to CO2 flux. *FEMS Microbiol. Ecol.* 78, 116–128. doi: 10.1111/j.1574-6941.2011.01128.x

Johnston-Monje, D., Mousa, W. K., Lazarovits, G., and Raizada, M. N. (2014). Impact of swapping soils on the endophytic bacterial communities of pre-domesticated, ancient and modern maize. *BMC Plant Biol.* 14:233. doi: 10.1186/s12870-014-0233-3

Johnston-Monje, D., and Raizada, M. N. (2011). Conservation and diversity of seed associated endophytes in Zea across boundaries of evolution, ethnography and ecology. *PLoS One* 6:e20396. doi: 10.1371/journal.pone.0020396

Kawasaki, A., Donn, S., Ryan, P. R., Mathesius, U., Devilla, R., Jones, A., et al. (2016). Microbiome and exudates of the root and rhizosphere of Brachypodium distachyon, a model for wheat. *PLoS ONE* 11:e0164533. doi: 10.1371/journal.pone.0164533

Knief, C., Delmotte, N., Chaffron, S., Stark, M., Innerebner, G., Wassmann, R., et al. (2012). Metaproteogenomic analysis of microbial communities in the phyllosphere and rhizosphere of rice. *ISME J.* 6, 1378–1390. doi: 10.1038/ismej.2011.192

Lakshmanan, V., Kitto, S. L., Caplan, J. L., Hsueh, Y. H., Kearns, D. B., Wu, Y. S., et al. (2012). Microbe-associated molecular patterns-triggered root responses mediate beneficial rhizobacterial recruitment in Arabidopsis. *Plant Physiol.* 160, 1642–1661. doi: 10.1104/pp.112.200386

Lebeis, S. L., Paredes, S. H., Lundberg, D. S., Breakfield, N., Gehring, J., McDonald, M., et al. (2015). Salicylic acid modulates colonization of the root microbiome by specific bacterial taxa. *Science* 349, 860–864. doi: 10.1126/science.aaa8764

Leff, J. W., Lynch, R. C., Kane, N. C., and Fierer, N. (2017). Plant domestication and the assembly of bacterial and fungal communities associated with strains of the common sunflower, *Helianthus annuus*. *New Phytol.* 214, 412–423. doi: 10.1111/nph.14323

Lundberg, D. S., Lebeis, S. L., Paredes, S. H., Yourstone, S., Gehring, J., Malfatti, S., et al. (2012). Defining the core *Arabidopsis thaliana* root microbiome. *Nature* 488, 86–90. doi: 10.1038/nature11237

Marschner, H. (1995). *Mineral Nutrition of Higher Plants*. London: Academic Press.

Naylor, D., DeGraaf, S., Purdom, E., and Coleman-Derr, D. (2017). Drought and host selection influence bacterial community dynamics in the grass root microbiome. *ISME J.* 11, 2691–2704. doi: 10.1038/ismej.2017.118

Ofek-Lalzar, M., Sela, N., Goldman-Voronov, M., Green, S. J., Hadar, Y., and Minz, D. (2014). Niche and host-associated functional signatures of the root surface microbiome. *Nat. Commun.* 5:4950. doi: 10.1038/ncomms5950

Peiffer, J. A., Spor, A., Koren, O., Jin, Z., Tringe, S. G., Dangl, J. L., et al. (2013). Diversity and heritability of the maize rhizosphere microbiome under field conditions. *Proc. Natl. Acad. Sci. U.S.A.* 110, 6548–6553. doi: 10.1073/pnas.1302837110

Pérez-Jaramillo, J. E., Carrión, V. J., Bosse, M., Ferrão, L. F., de Hollander, M., Garcia, A. A., et al. (2017). Linking rhizosphere microbiome composition of wild and domesticated *Phaseolus vulgaris* to genotypic and root phenotypic traits. *ISME J.* 11, 2244–2257. doi: 10.1038/ismej.2017.85

Pérez-Jaramillo, J. E., Mendes, R., and Raaijmakers, J. M. (2016). Impact of plant domestication on rhizosphere microbiome assembly and functions. *Plant Mol. Biol.* 90, 635–644. doi: 10.1007/s11103-015-0337-7

Picard, C., Baruffa, E., and Bosco, M. (2008). Enrichment and diversity of plant-probiotic microorganisms in the rhizosphere of hybrid maize during four growth cycles. *Soil Biol. Biochem.* 40, 106–115. doi: 10.1016/j.soilbio.2007.07.011

Picard, C., and Bosco, M. (2005). Maize heterosis affects the structure and dynamics of indigenous rhizospheric auxins-producing *Pseudomonas* populations. *FEMS Microbiol. Ecol.* 53, 349–357. doi: 10.1016/j.femsec.2005.01.007

Picard, C., and Bosco, M. (2006). Heterozygosis drives maize hybrids to select elite 2, 4-diacethylphloroglucinol-producing *Pseudomonas* strains among resident soil populations. *FEMS Microbiol. Ecol.* 58, 193–204. doi: 10.1111/j.1574-6941.2006.00151.x

Picard, C., Frascaroli, E., and Bosco, M. (2004). Frequency and biodiversity of 2,4-diacetylphloroglucinol-producing rhizobacteria are differentially affected by the genotype of two maize inbred lines and their hybrid. *FEMS Microbiol. Ecol.* 49, 207–215. doi: 10.1016/j.femsec.2004.03.016

Reinhold-Hurek, B., Bünger, W., Burbano, C. S., Sabale, M., and Hurek, T. (2015). Roots shaping their microbiome: global hotspots for microbial activity. *Ann. Rev. Phytopathol.* 53, 403–424. doi: 10.1146/annurev-phyto-082712-102342

Reinhold-Hurek, B., and Hurek, T. (2011). Living inside plants: bacterial endophytes. *Curr. Opin. Plant Biol.* 14, 435–443. doi: 10.1016/j.pbi.2011.04.004

Sasse, J., Martinoia, E., and Northen, T. (2017). Feed your friends: do plant exudates shape the root microbiome? *Trends Plant Sci.* 23, 25–41. doi: 10.1016/j.tplants.2017.09.003

Schlaeppi, K., Dombrowski, N., Oter, R. G., van Themaat, E. V. L., and Schulze-Lefert, P. (2014). Quantitative divergence of the bacterial root microbiota in Arabidopsis thaliana relatives. *Proc. Natl. Acad. Sci. U.S.A.* 111, 585–592. doi: 10.1073/pnas.1321597111

Schmidt, J. E., Bowles, T. M., and Gaudin, A. (2016). Using ancient traits to convert soil health into crop yield: impact of selection on maize root and rhizosphere function. *Front. Plant Sci.* 7:373. doi: 10.3389/fpls.2016.00373

Schreiter, S., Ding, G. C., Heuer, H., Neumann, G., Sandmann, M., Grosch, R., et al. (2014). Effect of the soil type on the microbiome in the rhizosphere of field-grown lettuce. *Front. Microbiol.* 5:144. doi: 10.3389/fmicb.2014.00144

Sessitsch, A., Reiter, B., Pfeifer, U., and Wilhelm, E. (2002). Cultivation-independent population analysis of bacterial endophytes in three potato varieties based on eubacterial and Actinomycetes-specific PCR of 16S rRNA genes. *FEMS Microbiol. Ecol.* 39, 23–32. doi: 10.1111/j.1574-6941.2002.tb00903.x

Smalla, K., Wieland, G., Buchner, A., Zock, A., Parzy, J., Kaiser, S., et al. (2001). Bulk and rhizosphere soil bacterial communities studied by denaturing gradient gel electrophoresis: plant-dependent enrichment and seasonal shifts revealed. *Appl. Environ. Microbiol.* 67, 4742–4751. doi: 10.1128/AEM.67.10.4742-4751.2001

Smith, K. P., Handelsman, J., and Goodman, R. M. (1999). Genetic basis in plants for interactions with disease-suppressive bacteria. *Proc. Natl. Acad. Sci. U.S.A.* 96, 4786–4790. doi: 10.1073/pnas.96.9.4786

Szoboszlay, M., Lambers, J., Chappell, J., Kupper, J. V., Moe, L. A., and McNear, D. H. Jr. (2015). Comparison of root system architecture and rhizosphere microbial communities of balsas teosinte and domesticated corn cultivars. *Soil Biol. Biochem.* 80, 34–44. doi: 10.1016/j.soilbio.2014.09.001

Tan, F. X., Wang, J. W., Chen, Z. N., Feng, Y. J., Chi, G. L., and Rehman, S. U. (2011). Assessment of the arbuscular mycorrhizal fungal community in roots and rhizosphere soils of Bt corn and their non-Bt isolines. *Soil Biol. Biochem.* 43, 2473–2479. doi: 10.1016/j.soilbio.2011.08.014

Turner, T. R., Ramakrishnan, K., Walshaw, J., Heavens, D., Alston, M., Swarbreck, D., et al. (2013). Comparative metatranscriptomics reveals kingdom level changes in the rhizosphere microbiome of plants. *ISME J.* 7, 2248–2258. doi: 10.1038/ismej.2013.119

Vacheron, J., Desbrosses, G., Bouffaud, M. L., Touraine, B., Moënne-Loccoz, Y., Muller, D., et al. (2013). Plant growth-promoting rhizobacteria and root system functioning. *Front. Plant Sci.* 4:356. doi: 10.3389/fpls.2013.00356

Walters, W. A., Jin, Z., Youngblut, N., Wallace, J. G., Sutter, J., Zhang, W., et al. (2018). Large-scale replicated field study of maize rhizosphere identifies heritable microbes. *Proc. Natl. Acad. Sci. U.S.A.* 115, 7368–7373. doi: 10.1073/pnas.1800918115

Yang, C. H., and Crowley, D. E. (2000). Rhizosphere microbial community structure in relation to root location and plant iron nutritional status. *Appl. Environ. Microbiol.* 66, 345–351. doi: 10.1128/AEM.66.1.345-351.2000

Yu, P., Gutjahr, C., Li, C., and Hochholdinger, F. (2016). Genetic control of lateral root formation in cereals. *Trends Plant Sci.* 21, 951–961. doi: 10.1016/j.tplants.2016.07.011

Yu, P., Wang, C., Baldauf, J. A., Tai, H., Gutjahr, C., Hochholdinger, F., et al. (2018). Root type and soil phosphate determine the taxonomic landscape of colonizing fungi and the transcriptome of field-grown maize roots. *New Phytol.* 217, 1240–1253. doi: 10.1111/nph.14893

Zachow, C., Müller, H., Tilcher, R., and Berg, G. (2014). Differences between the rhizosphere microbiome of *Beta vulgaris* ssp. *maritima*-ancestor of all beet crops-and modern sugar beets. *Front. Microbiol.* 5:415. doi: 10.3389/fmicb.2014.00415

Conflict of Interest Statement: The authors declare that the research was conducted in the absence of any commercial or financial relationships that could be construed as a potential conflict of interest.

frontiers in Microbiology

ORIGINAL RESEARCH
published: 26 September 2018
doi: 10.3389/fmicb.2018.02240

The Rootstock Regulates Microbiome Diversity in Root and Rhizosphere Compartments of *Vitis vinifera* Cultivar Lambrusco

*Federica D'Amico[1], Marco Candela[1], Silvia Turroni[1], Elena Biagi[1], Patrizia Brigidi[1], Alessia Bega[2], Davide Vancini[2] and Simone Rampelli[1]**

[1] Unit of Microbial Ecology of Health, Department of Pharmacy and Biotechnology, University of Bologna, Bologna, Italy, [2] Istituto d'Istruzione Superiore Ignazio Calvi, Modena, Italy

Plants belonging to *Vitis vinifera* varieties are usually grafted on different rootstocks to enhance the plant defenses against pathogens and increase productivity under harsh environmental conditions. Particularly, in Emilia-Romagna region (Italy), *Vitis vinifera* cultivar Lambrusco can be grafted on a hybrid of *V. berlandieri* × *V. riparia* (5BB) or *V. berlandieri* × *V. rupestris* (1103P). However, the latter shows potassium absorption problems, with a consequent reduction in grapevine production. Since it has recently been demonstrated that the rootstock has the potential to select for different microorganisms at the root-soil interface, here we hypothesized that the potassium deficiency of 1103P could be partially accounted for by the peculiarities of the rootstock microbiome. We thus employed 16S rRNA sequencing to compare root and rhizosphere microbiomes in plants of *V. vinifera* cultivar Lambrusco grafted on the two aforementioned rootstocks. According to our findings, 1103P shows a reduced diversity in root and rhizosphere microbiomes, including members of potassium-solubilizing microorganisms, possibly explaining the inadequate potassium absorption of this hybrid. Besides confirming the importance of the rootstock as a determinant of the composition of plant microbiomes, our data indicate the relevance of rootstock-selected microbiomes as possible regulators of potassium absorption by *V. vinifera*.

Keywords: microbiota, microbiome, soil-plant interface, grapevine, rootstock

OPEN ACCESS

Edited by:
Carsten W. Mueller, Technische Universität München, Germany

Reviewed by:
Hannes Schmidt, Universität Wien, Austria
Fei Gao, University of Missouri, United States

***Correspondence:**
Simone Rampelli
simone.rampelli@unibo.it

Specialty section:
This article was submitted to Plant Microbe Interactions, a section of the journal Frontiers in Microbiology

Received: *08 June 2018*
Accepted: *03 September 2018*
Published: *26 September 2018*

Citation:
D'Amico F, Candela M, Turroni S, Biagi E, Brigidi P, Bega A, Vancini D and Rampelli S (2018) The Rootstock Regulates Microbiome Diversity in Root and Rhizosphere Compartments of Vitis vinifera Cultivar Lambrusco. Front. Microbiol. 9:2240. doi: 10.3389/fmicb.2018.02240

INTRODUCTION

Multicellular organisms can no longer be considered individuals by the classical definitions of the term. Plants, as well as animals, are indeed holobionts, defined as meta-organisms including the host and its associated microbial communities, which are collectively referred to as the microbiota (Margulis, 1991; Hardoim et al., 2008; Ryan et al., 2008; Rosenberg and Zilber-Rosenberg, 2016). In particular, the plant microbiota includes the microorganisms that populate the thin layer of soil adhering to the roots (named as rhizosphere), those that inhabit the root surface (rhizoplane),

and those colonizing the root interior as well as other inner tissues of the plant (endosphere) (Kloepper et al., 1980; Kowalchuk et al., 2002; Bulgarelli et al., 2013).

The grape has a long winemaking history with archeological evidence indicating that also Etruscans and Romans cultivated the grapevine (Robinson, 1986). In Italy, the grapevine cultivation has a strong economic importance due to the valuable quality of the wine. Therefore, it is important to preserve the plant growth from any injury, in particular from the *Phylloxera* infection. Also for this reason, all *Vitis vinifera* varieties are cultivated as scions and grafted on rootstocks of other *Vitis* species (Whiting, 2003). In addition to the importance of rootstocks in enhancing the plant defenses against pathogens (Whiting, 2003; Wallis et al., 2013), they are strategic in increasing *V. vinifera* productivity under harsh environmental conditions, while simultaneously limiting agricultural inputs (irrigation, fertilizer, and pesticides) (Zarraonaindia et al., 2015; Warschefsky et al., 2016). Moreover, rootstocks are important to prevent problems due to soil conditions, such as salinity or poor mineral nutrition (Habran et al., 2016).

Perhaps not surprisingly, the rootstock choice plays a critical role in the winemaking process. A paradigmatic example of this phenomenon is the production of Lambrusco wine. In Emilia-Romagna, the Italian region leading Lambrusco's production globally[1], a dichotomy can be observed: grapevines are grafted on rootstock hybrids of either *V. berlandieri* × *V. rupestris* or *V. berlandieri* × *V. riparia*. The two hybrids show different characteristics and performance depending on the quality of the soil. Both are suitable for a clay soil, however, *V. berlandieri* × *V. rupestris* shows less absorption of potassium (K) that is the third most important nutrient of the plant, after nitrogen and phosphorus (Wolpert et al., 2005). When the defects in K absorption are such that the vigor of the grapevine can no longer be maintained, this deficiency leads to inhibition of photosynthesis and to sucrose being "trapped" in the leaves, which adversely affects the yield, the fruit ripening and the concentration of the sugar in the grapes. Moreover, an inadequate K absorption can lead to poor development of roots, slow growth and increased susceptibility to diseases and pest (Keller, 2010).

It is well known that rhizospheric microorganisms, particularly K-solubilizing microorganisms (KSMs), are able to solubilize insoluble minerals into soluble forms useful for plant metabolism (Meena et al., 2014; Etesami et al., 2017). Despite the molecular mechanisms by which microorganisms regulate the K solubilization are still not clear, a wide range of KSMs have been characterized, such as *Bacillus mucilaginosus*, *Bacillus edaphicus* (Meena et al., 2014), *Burkholderia*, *Aminobacter*, and *Sphingomonas* (Uroz et al., 2007; Zhang and Kong, 2014), as well as microorganisms belonging to *Rhizobiaceae*, *Cytophagaceae,* and *Micrococcaceae* families (Diep and Hieu, 2013; Zarjani et al., 2013; Zhang and Kong, 2014). Since the rootstock has recently been reported as a determinant of the bacterial composition in the root system compartments of *V. vinifera* (Liu et al., 2018; Marasco et al., 2018), we hypothesized that the different performance of *V. berlandieri* × *V. rupestris* and *V. berlandieri* × *V. riparia* rootstocks in K absorption is attributable to compositional differences in the microbiomes from the root compartments. In this scenario, here we characterized the bacterial community of soil, rhizosphere and root endosphere in *V. vinifera* cultivar Lambrusco grafted on the two aforementioned types of rootstock showing high or low performance in K absorption, i.e., *V. berlandieri* × *V. riparia* and *V. berlandieri* × *V. rupestris*, respectively. In order to avoid biases related to weather conditions and soil type, all plants were grown in the same field. Our data provides some glimpses on the microbial *terroir* of grapevines, highlighting the evolution of a specific relationship between rootstock, microbiota and plant physiology, and suggesting the possibility of improving grapevine physiology by complementing the rootstock microbiome through the supplementation of probiotic microbes to the soil.

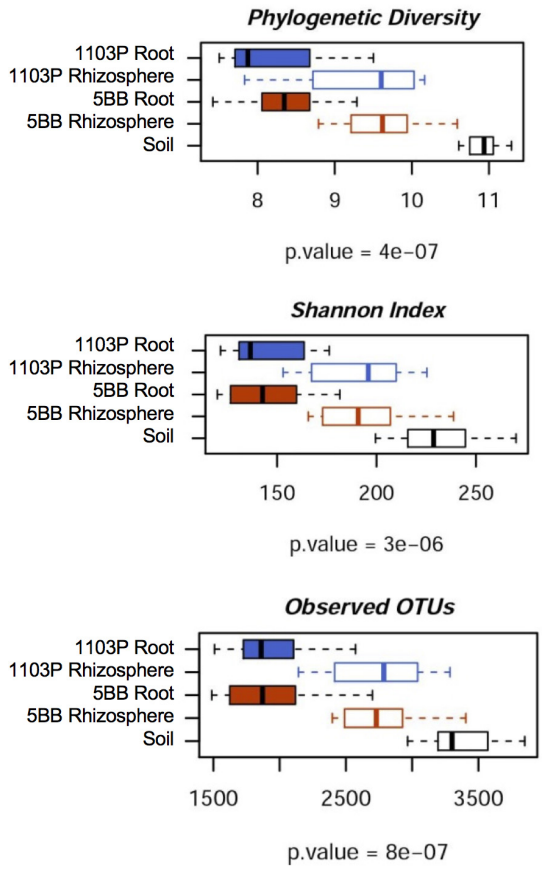

FIGURE 1 | Microbiota biodiversity in soil, rhizosphere, and root compartments for *V. vinifera* cultivar Lambrusco grafted onto different rootstocks. The OTU table at 0.03 similarity threshold was rarefied up to 10,277 reads per sample and analyzed using the following diversity metrics: Faith's Phylogenetic Diversity (PD whole tree), the Shannon index of biodiversity and observed OTUs. All metrics show greater microbiota diversity in the soil compared to rhizosphere and root compartments, for both *V. vinifera* 1103P and *V. vinifera* 5BB (Kruskal-Wallis test).

[1]https://www4.istat.it/it/archivio/207188

MATERIALS AND METHODS

Experimental Design and Sampling

Grafted Lambrusco grapevine plants (*Vitis vinifera* cultivar Lambrusco) were sampled at Istituto d'Istruzione Superiore (IIS) Ignazio Calvi (44.839 N/11.285 E, Finale Emilia, Modena, Italy) in November 2016. Specifically, two different rootstocks were selected: *V. berlandieri* × *V. rupestris* PAULSEN 1103 (1103P) and *V. berlandieri* × *V. riparia* KOBER 5BB (5BB) (**Table 1**). Eight 1103P and seven 5BB grapevine plants were randomly sampled from three rows of the same vineyard field. Physical and chemical properties of the soil from an unplanted area were determined (**Supplementary Table S1**).

For the microbiota analysis, for each plant, three compartments were analyzed: soil, rhizosphere and root endosphere for a total of 45 samples. The soil compartment was sampled next to each plant after removing the top 0.5–1 cm of soil. Roots were manually removed from the soil using sterile gloves and processed to separate the rhizosphere from the root endosphere, as previously described in Bulgarelli et al. (2012). Briefly, 3 cm of root segments, including the root tips, were dissected with a sterile scalpel, to standardize sampling. The root sections were collected in 15 mL Falcon tubes containing 2.5 mL of modified PBS buffer (130 mM NaCl, 7 mM Na_2HPO_4, 3 mM NaH_2PO_4, pH 7.0, 0.02% Silwet L-77) and washed on a shaking platform at 180 rpm for 20 min. The rhizosphere compartment was defined as the pellet resulting from the centrifugation of the washing buffer at 1.500 × *g* for 20 min. After a second washing step under the same conditions, roots were transferred to another Falcon tube with 2.5 mL of modified PBS buffer and subjected to 10 cycles of sonication consisting of 30-s pulses at 160 W with 30-s breaks in an ultrasonic bath (Branson 1800, Branson Ultrasonic Corporation, Danbury, CT, United States). Washed and sonicated roots were grinded with mortar and pestle, and defined as the root endosphere compartment. All samples were stored at −80°C until DNA extraction.

DNA Extraction and Sequencing

DNA was extracted from all the 45 samples from soil, rhizosphere and root endosphere compartments using the DNeasy PowerSoil Kit (QIAGEN, Hilden, Germany) as per the manufacturer's instructions, except for the homogenization step that was performed in a FastPrep instrument (MP Biomedicals, Irvine, CA, United States) by three 1-min steps at 5.5 movements per sec. The V3–V4 hypervariable region of the 16S rRNA gene was amplified using the 341F and 785R primers with added Illumina adapter overhang sequences as previously reported (Turroni et al., 2016). Briefly, the thermal cycle consisted of initial denaturation at 95°C for 3 min, 25 cycles of denaturation at 95°C for 30 s, annealing at 55°C for 30 s and extension at 72°C for 30 s, and a final extension step at 72°C for 5 min. PCR reactions were cleaned up with Agencourt AMPure XP magnetic beads (Beckman Coulter, Brea, CA, United States). Indexed libraries were prepared by limited-cycle PCR using Nextera technology. After a further clean-up step as described above, libraries were normalized to 4 nM and pooled. The sample pool was denatured with 0.2 N NaOH and diluted to 6 pM with a 20% PhiX control. Sequencing was performed on Illumina MiSeq platform using a 2 × 250 bp paired end protocol, according to the manufacturer's instructions (Illumina, San Diego, CA, United States). Sequencing reads were deposited in MG-RAST[2]

Bioinformatics and Statistical Analysis

Raw sequences were processed using a pipeline combining PANDAseq (Masella et al., 2012) and QIIME (Caporaso et al., 2011) using default parameters. Reads shorter than 350 bp or longer than 500 bp were discarded. Quality-filtered sequences were clustered into OTUs at 97% similarity threshold using UCLUST (Edgar, 2010), and taxonomy was assigned using the RDP classifier and the Greengenes database (May 2013 release). The filtering of chimeric OTUs was performed by using ChimeraSlayer (Haas et al., 2011). All singleton OTUs were discarded. We excluded the Cyanobacteria phylum from all analysis to prevent any problem due to the concomitant detection of plant chloroplasts (mean percentage of reads assigned to chloroplasts in root endosphere samples = 27.25%).

Alpha-diversity was evaluated using three different metrics: Shannon, PD whole tree, and observed OTUs. Weighted and

[2]https://www.mg-rast.org/mgmain.html?mgpage=token&token=rcSlcBTSY85CpNpN7552xeEBUUZYonG3TFqXfrYHH_f4ACrVPu

TABLE 1 | Characteristics of the two rootstocks used in the present study.

Rootstock	Parentage	Vigor	Drought resistance	Lime tolerance (%)†	Salt resistance	Wet feet‡	Soil preference§
1103P	*V. berlandieri* × *V. rupestris*	H	H	17	M	H	Adapted to drought, saline soils
5BB	*V. berlandieri* × *V. riparia*	M	L/M	20	L/M	Var	Moist clay

L = low; M = medium; H = high; Var = variable. †Tolerance to lime-induced chlorosis (percent by weight of finely divided calcium carbonate in soil that can be tolerated by the rootstock). ‡Tolerance to excessive moisture caused by poor soil drainage. §Actual performance characteristics on specific soils and scions may vary. Sources: Adapted from Lambert et al. (2008).

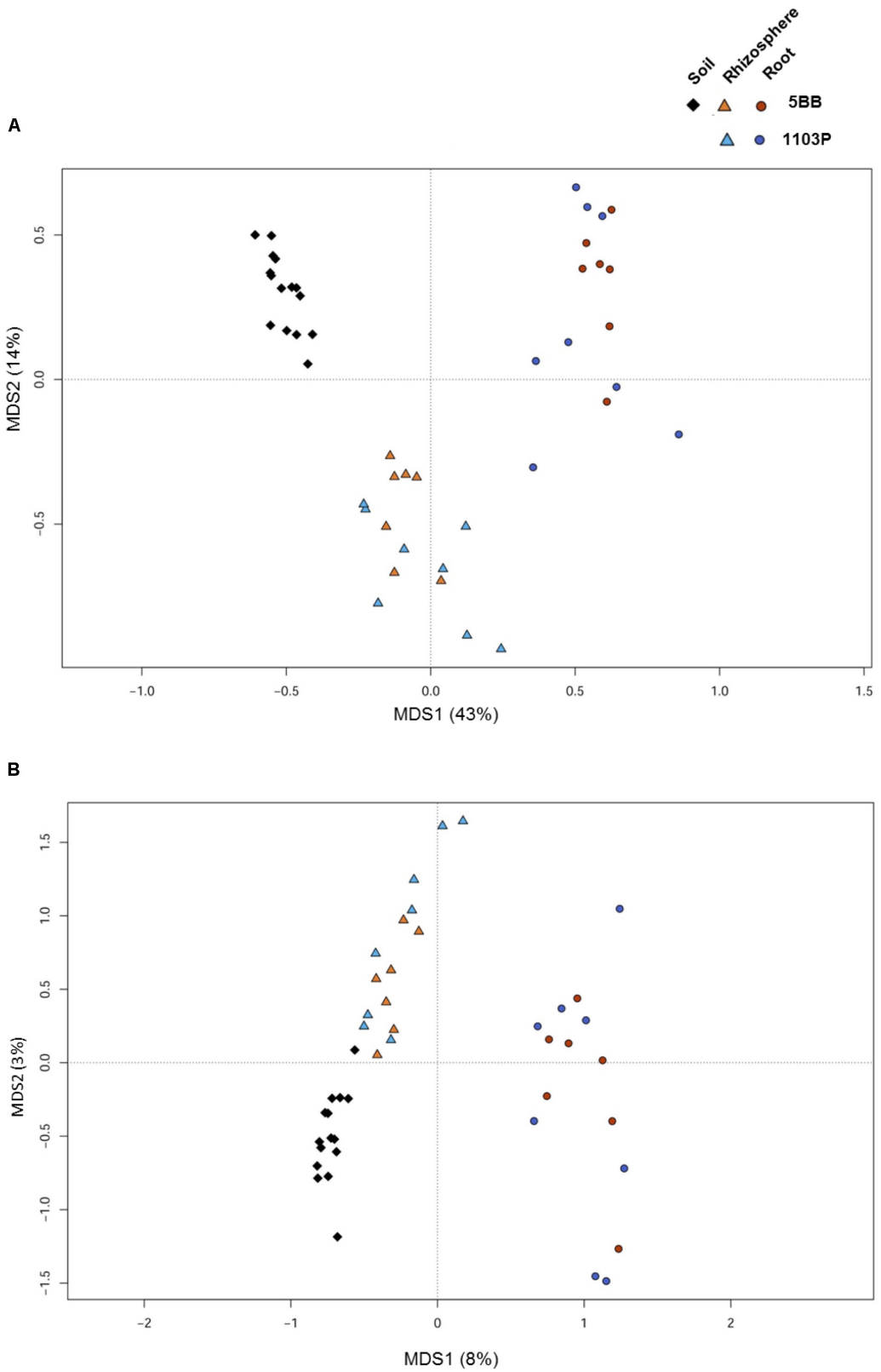

FIGURE 2 | Microbiota community structure in soil, rhizosphere, and root compartments for *V. vinifera* cultivar Lambrusco grafted onto different rootstocks. Weighted **(A)** and unweighted **(B)** UniFrac distance PCoA shows significant segregation among soil (diamonds), rhizosphere (triangles), and root (circles) samples for both *V. vinifera* 1103P and *V. vinifera* 5BB. Permutational multivariate ANOVA based on distance matrices (Adonis), $P = 0.0001$.

unweighted UniFrac distances were used to perform PCoA. PCoA and bar plots were built using the R packages "Made4" (Culhane et al., 2005) and "Vegan"[3]. Ternary plots were prepared using the R packages "vcd" (Meyer et al., 2017) and "ggtern" (Hamilton, 2017). The R packages "Stats" and "Vegan" were used to perform statistical analysis. In particular, to compare the microbiota structure among different groups for alpha and beta-diversity, we used a Mann-Whitney-Wilcoxon test. Data separation in the PCoA was tested using a permutation test with pseudo-F ratios (function "Adonis" in the "Vegan" package). Tropic groups [i.e., groups of OTUs enriched in the root endosphere (Ro_OTUs), in the rhizosphere (Rh_OTUs) or in both (RR_OTUs)] were defined based on OTU relative abundance values, as previously shown in Bulgarelli et al. (2012). Differentially abundant OTUs between microhabitats were detected using Mann-Whitney-Wilcoxon test. OTU niche differentiation (i.e., the OTU preference for the soil, the root endosphere and/or the rhizosphere) was defined based on the OTU differential representation among microhabitats. KSM-related OTUs were defined based on the literature available on microorganisms known for their K solubilization activity. Significant differences in bacterial relative abundance at different phylogenetic levels between microhabitats and plant groups, were assessed by Mann-Whitney-Wilcoxon test or Kruskal-Wallis test, and corrected for multiple comparisons using the Benjamini-Hochberg method when appropriate. False discovery rate (FDR) <0.05 was considered as statistically significant.

RESULTS

We worked on *Vitis vinifera* cultivar Lambrusco collected at Istituto d'Istruzione Superiore (IIS) Ignazio Calvi located in Finale Emilia (Modena, Italy). We analyzed two different groups of plants grafted onto different rootstocks: eight plants of *V. vinifera* grafted on the hybrid *V. berlandieri* × *V. rupestris* PAULSEN 1103 (1103P) and seven plants of *V. vinifera* grafted on the hybrid *V. berlandieri* × *V. riparia* KOBER 5BB (5BB). To exclude biases due to different soil characteristics (e.g., pH, moisture and temperature), as well as to a different soil microbiome layout, all plants were from the same vineyard (**Supplementary Table S1**). Although the cultivar was the same, the *V. vinifera* group 1103P showed problems of nutrient absorption, especially of potassium (K), as assessed by visual inspection of foliar symptoms, a standard approach to determine whether nutrient concentration is adequate for plant growth (Wolf, 2008). The leaves of *V. vinifera* 1103P were indeed characterized by widespread red spots, an established consequence of K deficiency (**Supplementary Figure S1**).

Overall Structure of Bacterial Communities Associated With the Root System of Grafted Grapevine

For each of the 15 plants of *V. vinifera* cultivar Lambrusco collected in this study, we analyzed the root endosphere

[3]https://cran.r-project.org/web/packages/vegan/index.html

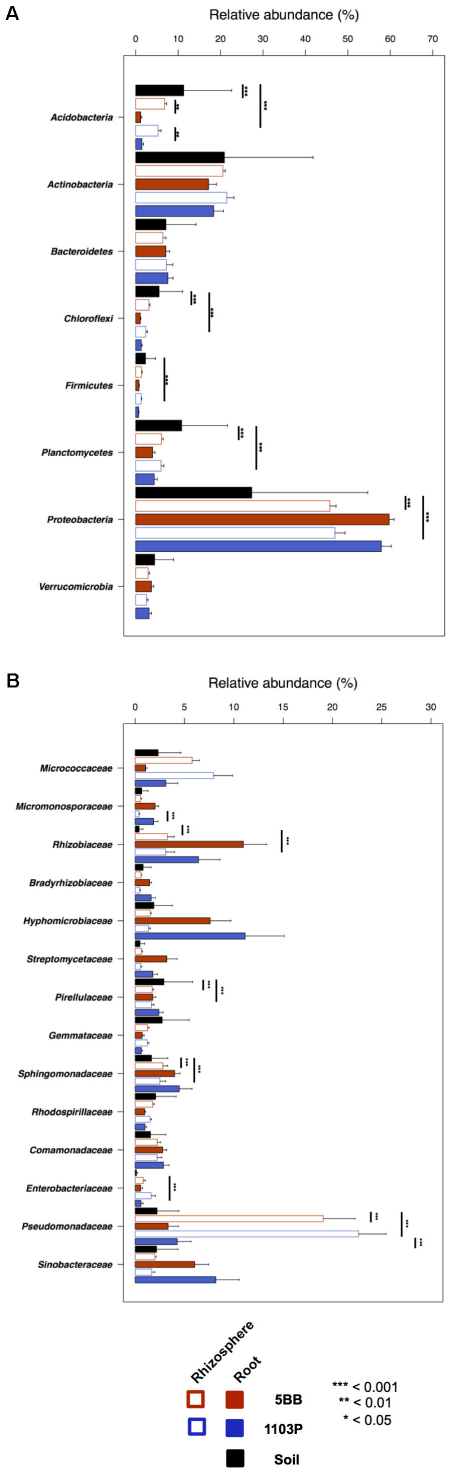

FIGURE 3 | Taxonomic composition of bacterial communities in soil, rhizosphere, and root compartments for *V. vinifera* cultivar Lambrusco grafted onto different rootstocks. Relative abundance (mean ± SEM) of the most abundant phyla **(A)** and families **(B)** in soil, rhizosphere, and root samples for both groups of plants analyzed (*V. vinifera* 1103P and *V. vinifera* 5BB). Stars indicate significant differences [Mann-Whitney-Wilcoxon test, false discovery rate (FDR)-adjustment]. Only taxa with relative abundance >0.5% in at least 15 samples were included.

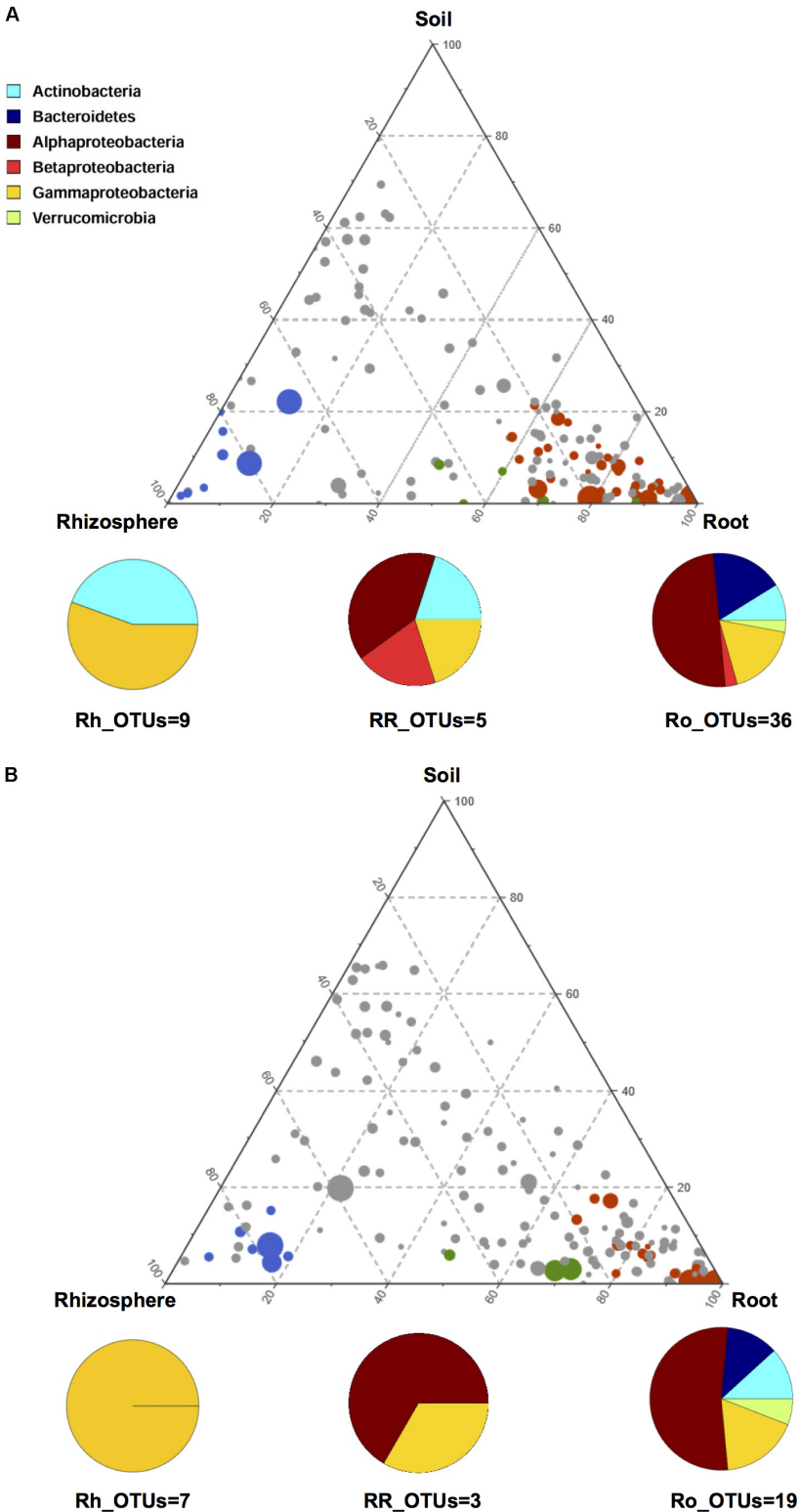

FIGURE 4 | OTU enrichment at the root-soil interface for *V. vinifera* cultivar Lambrusco grafted onto different rootstocks. Ternary plots of all OTUs detected in the dataset with relative abundance >0.5% in at least one sample, in *V. vinifera* 5BB **(A)** and *V. vinifera* 1103P **(B)**. Each circle represents one OTU, and the size is proportional to the weighted relative abundance. Red circles indicate OTUs significantly enriched in the root microhabitat (Ro_OTUs), blue circles indicate OTUs significantly enriched in the rhizosphere microhabitat (Rh_OTUs) and green circles indicate OTUs significantly enriched in both root and rhizosphere microhabitats (RR_OTUs). Mann-Whitney-Wilcoxon test, FDR-adjustment, $P < 0.05$. See also **Supplementary Table S2**.

(hereafter referred to as root), rhizosphere and soil compartments by next-generation sequencing of the V3-V4 hypervariable regions of 16S rDNA. The sequencing generated 5,444,065 high-quality reads (mean, 120,979; range, 34,386–2,683,522) that were clustered into 22,570 operational taxonomic units (OTUs) at 97% identity. We used different metrics to calculate alpha-diversity, including phylogenetic diversity, the Shannon index for biodiversity and observed OTUs (**Figure 1**). All measures indicate a significantly higher microbiota diversity in the soil compared to the rhizosphere and root microhabitats for both *V. vinifera* 1103P and *V. vinifera* 5BB (Kruskal-Wallis test, $P \leq 3 \times 10^{-6}$). Regardless of the rootstock type, the rhizosphere microbiota shows an intermediate diversity between soil and root samples ($P < 0.05$). Principal Coordinates Analysis (PCoA) of weighted and unweighted UniFrac distances reveals a significant segregation among the three different microhabitats analyzed (permutation test with pseudo-F ratios (Adonis), $P = 0.0001$) (**Figure 2**). Interestingly, soil samples show the lowest within-group variability, while greater dispersion is observed for rhizosphere and root samples (Mann-Whitney-Wilcoxon test, false discovery rate (FDR)-adjustment, unweighted UniFrac: soil vs. rhizosphere, $P = 9 \times 10^{-19}$; soil vs. root, $P = 6 \times 10^{-34}$; rhizosphere vs. root, $P = 7 \times 10^{-32}$; weighted UniFrac: soil vs. rhizosphere, $P = 4 \times 10^{-3}$; soil vs. root, $P = 4 \times 10^{-29}$; rhizosphere vs. root, $P = 3 \times 10^{-18}$). According to the taxonomic classification of OTU representative sequences, Proteobacteria, Actinobacteria and Bacteroidetes members dominate all microhabitats (**Figure 3**).

Differential OTUs Distribution in the Grapevine Root System

In order to gain further insights into the recruitment cues of the microbiota thriving at the root-soil interface, we employed a linear analysis of OTUs distribution in soil, rhizosphere and root samples, as previously described (Bulgarelli et al., 2015). Results from this analysis were used to build a ternary plot, highlighting the OTUs showing a specific propensity toward the three microhabitats at the root-soil interface. This approach allowed the identification of three distinct groups of OTUs, each characterized by a specific tropism for (i.e., enriched in) the rhizosphere, the root or both, compared to the other microhabitats (**Figure 4** and **Supplementary Table S2**). The first of these tropic groups, defined as root (Ro)_OTUs, is characterized by all the OTUs showing a preference for (i.e., significantly more abundant in) the root ecosystem, compared to the rhizosphere and the soil (Mann-Whitney-Wilcoxon test, FDR-adjustment, $P < 0.05$). The second tropic group, defined as root/rhizosphere (RR)_OTUs, is composed of OTUs with a tropism for both root and rhizosphere (i.e., enriched in both plant compartments, compared to the soil; $P < 0.05$). The last tropic group, named rhizosphere (Rh)_OTUs, includes all the OTUs more abundant in the rhizosphere ecosystem than in the soil or in the root ($P < 0.05$). According to our data, the Ro_OTUs group is enriched in Proteobacteria, Bacteroidetes and Actinobacteria, and shows a higher number of community-specific OTUs compared to the other groups. On the other hand, the RR_OTUs and Rh_OTUs groups are exclusively dominated by Proteobacteria and Actinobacteria. Interestingly, *V. vinifera* 5BB and *V. vinifera* 1103P show a different OTU compositional layout within the three tropic groups. In particular, members of Betaproteobacteria are included in the Ro_OTUs group of *V. vinifera* 5BB only. Analogously, the Rh_OTUs group only includes Gammaproteobacteria for *V. vinifera* 1103P, while also Actinobacteria for *V. vinifera* 5BB. Finally, the RR_OTUs group of *V. vinifera* 5BB includes bacteria assigned to Alphaproteobacteria, Betaproteobacteria, Gammaproteobacteria and Actinobacteria, while the corresponding group of *V. vinifera* 1103P only contains OTUs belonging to Alphaproteobacteria and Gammaproteobacteria. Strikingly, Ro_OTUs, RR_OTUs and Rh_OTUs groups from 5BB include several putative KSMs that are missing in the corresponding tropic groups from 1103P. In particular, members of *Micrococcaceae* (Rh_OTUs), *Comamonadaceae* (Ro_OTUs and RR_OTUs), *Cytophagaceae* (RR_OTUs), *Sphingomonadaceae*, *Rhizobiaceae*, *Xanthomonadaceae,* and *Microbacteriaceae* (Ro_OTUs) are among the KSMs exclusively present in 5BB (Diep and Hieu, 2013; Zarjani et al., 2013; Zhang and Kong, 2014). Consistently, when comparing the total load of KSMs between the two groups of plants analyzed, 5BB shows a significantly higher relative abundance of KSMs in the Ro_OTUs group compared to 1103P (mean ± SEM, 5BB vs. 1103P, 6.3 ± 1.4% vs. 0.2 ± 0.1%, Mann-Whitney-Wilcoxon test, $P < 0.05$). In addition, 5BB shows a higher number of OTUs assigned to KSMs compared to 1103P (**Supplementary Figure S2**).

Niche Differentiation of Microorganisms at the Root-Soil Interface

The assessment of the relative preferences of individual OTUs for the different niches in the root system allowed us to define four groups of microorganisms differentially represented at the root-soil interface (**Figure 5A**). The first one is characterized by OTUs (e.g., belonging to the *Hyphomicrobiaceae* family) with low relative abundance in the soil and in the rhizosphere, but highly represented in roots. A second group includes OTUs (e.g., from *Rhizobiaceae*) more abundant in the rhizosphere and in the root, than in the soil. The third comprises OTUs that show a higher percentage in the rhizosphere, compared to the root or the soil, such as members of the *Pseudomonadaceae* family. The last identified group is related to OTUs more represented in the soil and in the root, rather than in the rhizosphere compartment, including *Micromonosporaceae* members.

Next, we specifically explored the OTU niche differentiation by tropic group (Ro_OTUs; RR_OTUs; Rh_OTUs) (**Figure 5B**). Interestingly, according to our data, the same OTUs, even if sharing the same tropism, show different niche preferences based on the rootstock type. In particular, only in *V. vinifera* 5BB plants, 6 OTUs belonging to the *Micromonosporaceae*,*Caulobacteraceae*, *Hyphomicrobiaceae, Xanthomonadaceae,* and *Rhizobiaceae* families, show a higher relative abundance in the root compartment than in the soil and in the rhizosphere, suggesting the relevance of the root environment as a determinant of the bacterial niche preference at the root-soil interface.

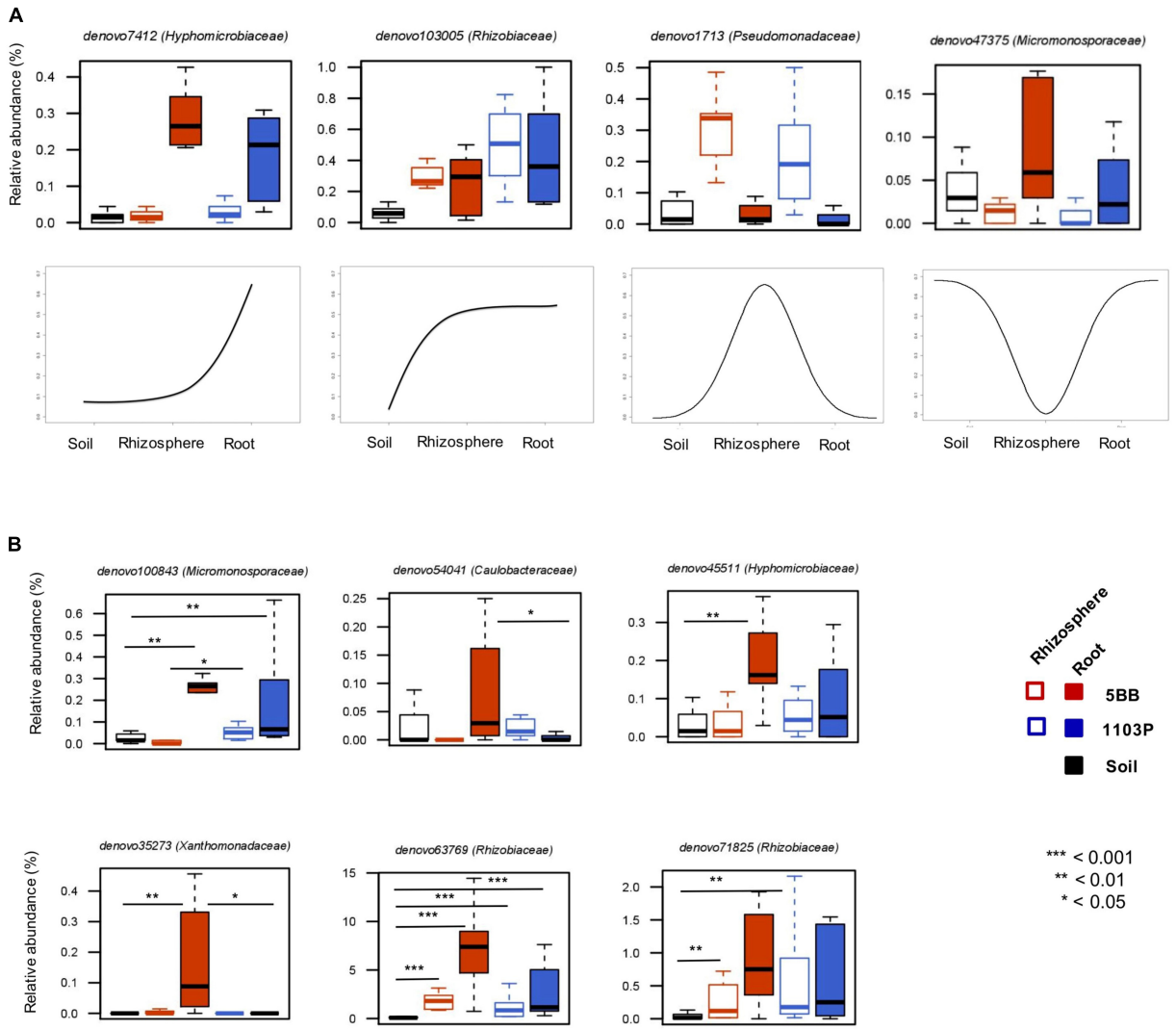

FIGURE 5 | Dynamic plots based on the relative abundance of OTUs with different preference for soil, rhizosphere, and root compartments of *V. vinifera* cultivar Lambrusco grafted onto different rootstocks. **(A)** Examples of OTU niche differentiation across the three microhabitats. **(B)** Differences between the two groups of plants (grafted on the 5BB or 1103P rootstock) in terms of OTU niche preference. *P*-values were assessed by Mann-Whitney-Wilcoxon test. See also **Supplementary Table S2**.

DISCUSSION

By means of next-generation sequencing of the 16S rRNA gene, here we profiled the compositional structure of the soil, rhizosphere and root endosphere microbiota from *V. vinifera* cultivar Lambrusco grafted on two different rootstock hybrids: PAULSEN 1103 (1103P) and KOBER 5BB (5BB). Even though both rootstocks are largely used for grafting Lambrusco cultivars, the 1103P group is prone to develop K absorption problems, with the consequent appearance of atypical red spots on the leaves and a reduction in grape production (Wolpert et al., 2005).

Our data highlight an overall different compositional layout among the three microbial ecosystems at the root-soil interface: soil, rhizosphere and root endosphere. Interestingly, we observed a progressive decrease of microbial diversity from soil to rhizosphere and root endosphere. Paralleled by a corresponding increase in individual specificity, this behavior reflects the typical organizing principle of holobionts microbiomes (Compant et al., 2010; Liu et al., 2017; Thompson et al., 2017). Thus, our data suggest that the enrichment in Actinobacteria, Bacteroidetes and Proteobacteria observed in the root endosphere-inhabiting microbiota is the result of a gated community assembled from the, taxonomically congruent, surrounding soil and rhizosphere biomes.

Through a ternary plot analysis, we were successful in discriminating microorganisms showing a specific tropic behavior for the plant ecosystems (i.e., rhizosphere and root endosphere), compared to the soil. Interestingly, the root endosphere-tropic microbial group is composed of the

largest number of microhabitat-characteristic OTUs, showing higher taxonomic diversity compared to the other two tropic groups. Strikingly, differences in specific tropisms for the plant ecosystems emerge from the comparison between the two rootstocks, with 1103P being depleted in several OTUs some of which belonging to KSMs, which are instead detected in 5BB. For instance, OTUs assigned to *Micrococcaceae* are represented only in the 5BB rhizosphere. However, the most severe depletion of KSMs-assigned OTUs is observed in the root endosphere of 1103P, with the absence of several well-known KSMs, including *Cytophagaceae*, *Rhizobiaceae, Xanthomonadaceae* and *Comamonadaceae* members (Diep and Hieu, 2013; Zarjani et al., 2013; Zhang and Kong, 2014), which are detected only in the 5BB root endosphere. This overall decrease in KSM diversity in the 1103P plant-associated microbiomes could account for the problems of K absorption characteristic of *V. vinifera* cultivar Lambrusco grafted on the 1103P rootstock. Indeed, the lack of KSMs – capable of easily metabolizing insoluble K into soluble forms, making it available to the plant – can compromise K absorption by the plant, leading to poor development of roots, slow growth and increased susceptibility to diseases and pest (Keller, 2010; Etesami et al., 2017). According to our findings, the two rootstocks differently modulate the niche preference of microorganisms at the root-soil interface. For instance, several microbes, belonging to the families *Micromonosporaceae, Caulobacteraceae*, *Hyphomicrobiaceae*, *Xanthomonadaceae,* and *Rhizobiaceae,* the latter two including KSMs, show only in 5BB plants a higher relative abundance in the root endosphere than in the soil and in the rhizosphere. Supposedly, these microorganisms are selected from the plant at the root interface as a result of the plant-bacteria cross-talk mediated by the rhizodeposition of metabolites (Bulgarelli et al., 2013). Growing up inside the root tissues, these microorganisms may provide a number of beneficial functions for the plant, such as indirect pathogen protection, phosphorus solubilization and nitrogen metabolism (Bulgarelli et al., 2013).

Taken together, our data indicate that different rootstocks result into different plant-associated microbiomes, as a result of different plant-bacteria interaction processes at the root-soil interface. In particular, compared to 1103P, the 5BB plants select for a higher diversity of KSMs in both the rhizosphere and root endosphere compartments, possibly explaining the inadequate K absorption observed in the 1103P group. Besides confirming the importance of the rootstock as a determinant of the composition of plant microbiomes (rhizosphere and root endosphere) (Samad et al., 2017; Marasco et al., 2018), our findings suggest the importance of rootstock-selected plant microbiomes as possible regulators of K absorption by *V. vinifera*.

In conclusion, different rootstocks used for grafting the same cultivar (i.e., the cultivar Lambrusco) select for different plant microbiotas in root endosphere and rhizosphere compartments. This process has strong repercussions in terms of plant physiology and health, such as the regulation of K absorption. Our results can provide the basis for future applications (e.g., microbial inocula) aimed at favoring a better microbiome composition in *V. vinifera* cultivar Lambrusco grafted onto 1103P, counteracting nutrient absorption deficiency when rootstock replacement is not possible. Further studies are needed to isolate and functionally characterize KSMs from the rhizosphere and root ecosystems, as well as to provide direct biological evidence of their impact on the rootstock performance in K absorption. Different K applications could be instrumental to unravel the mechanisms by which plant microbiomes regulate the plant nutrient status and its growth. Moreover, chemical mediators orchestrating the microbes-host cross-talk at the root-soil interface and eventually favoring the recruitment of KSMs, need to be discovered, opening the perspective to a knowledge-based chemical modulation of plant microbiomes to sustain the establishment of configurations promoting plant health and hence its productivity.

AUTHOR CONTRIBUTIONS

DV and AB carried out the field work. ST performed the DNA extraction and library preparation. FD run the sequencing. FD and SR performed the bioinformatics analysis. SR, ST, and MC designed the study. FD, SR, MC, and ST wrote the manuscript. EB and PB participated in the data interpretation and commented on the draft. All authors read and approved the final manuscript.

ACKNOWLEDGMENTS

We would like to thank Enrico Rampelli and Maura Zini from Istituto d'Istruzione Superiore (IIS) Ignazio Calvi (Finale Emilia, Modena, Italy) for collaboration, technical and scientific advice, and provision of experimental fields. We are thankful to Dr. Davide Bulgarelli (University of Dundee, United Kingdom) for the critical comments on the manuscript.

SUPPLEMENTARY MATERIAL

The Supplementary Material for this article can be found online at: https://www.frontiersin.org/articles/10.3389/fmicb.2018.02240/full#supplementary-material

FIGURE S1 | Location of experimental fields and leaves of *V. vinifera* cultivar Lambrusco with impaired potassium absorption. **(A)** Map of Italy and specifically of Emilia-Romagna region. The red dot localizes the experimental fields in Finale Emilia (Modena). **(B)** Images showing the leaves of *V. vinifera* cultivar Lambrusco grafted on the rootstock hybrid *V. berlandieri* × *V. rupestris* PAULSEN 1103, with the typical red spots caused by potassium deficiency.

FIGURE S2 | Number of OTUs assigned to potassium-solubilizing microorganisms (KSMs) in the root-tropic group (Ro_OTUs) for both 5BB and 1103P plant groups.

TABLE S1 | Physical and chemical characterization of the experimental soil substrates used in the study.

TABLE S2 | OTUs characterizing the root, the rhizosphere or both compartments for *V. vinifera* cultivar Lambrusco grafted onto the rootstock 5BB or 1103P. Ro, root; Rh, rhizosphere; RR, root/rhizosphere.

REFERENCES

Bulgarelli, D., Garrido-Oter, R., Münch, P. C., Weiman, A., Dröge, J., Pan, Y., et al. (2015). Structure and function of the bacterial root microbiota in wild and domesticated barley. *Cell Host Microbe* 17, 392–403. doi: 10.1016/j.chom.2015.01.011

Bulgarelli, D., Rott, M., Schlaeppi, K., Ver Loren van Themaat, E., Ahmadinejad, N., Assenza, F., et al. (2012). Revealing structure and assembly cues for *Arabidopsis* root-inhabiting bacterial microbiota. *Nature* 488, 91–95. doi: 10.1038/nature11336

Bulgarelli, D., Schlaeppi, K., Spaepen, S., Ver Loren van Themaat, E., and Schulze-Lefert, P. (2013). Structure and functions of the bacterial microbiota of plants. *Annu. Rev. Plant Biol.* 64, 807–838. doi: 10.1146/annurev-arplant-050312-120106

Caporaso, J. G., Kuczynski, J., Stombaugh, J., Bittinger, K., Bushman, F. D., Costello, E. K., et al. (2011). QIIME allows analysis of high-throughput community sequencing data. *Nat. Methods* 7, 335–336. doi: 10.1038/nmeth.f.303

Compant, S., Clément, C., and Sessitsch, A. (2010). Plant growth-promoting bacteria in the rhizo- and endosphere of plants: their role, colonization, mechanisms involved and prospects for utilization. *Soil Biol. Biochem.* 42, 669–678. doi: 10.1016/j.soilbio.2009.11.024

Culhane, A. C., Thioulouse, J., Perrière, G., and Higgins, D. G. (2005). MADE4: an R package for multivariate analysis of gene expression data. *Bioinformatics* 21, 2789–2790. doi: 10.1093/bioinformatics/bti394

Diep, C. N., and Hieu, T. N. (2013). Phosphate and potassium solubilizing bacteria from weathered materials of denatured rock mountain, Ha Tien, Kien Giang Province, Vietnam. *AJLS* 1, 88–92. doi: 10.11648/j.ajls.20130103.12

Edgar, R. C. (2010). Search and clustering orders of magnitude faster than BLAST. *Bioinformatics* 26, 2460–2461. doi: 10.1093/bioinformatics/btq461

Etesami, H., Emami, S., and Alikhani, H. A. (2017). Potassium solubilizing bacteria (KSB): mechanisms, promotion of plant growth, and future prospects - a review. *J. Soil Sci. Plant Nutr.* 17, 897–911. doi: 10.4067/S0718-95162017000400005

Haas, B. J., Gevers, D., Earl, A. M., Feldgarden, M., Ward, D. V., Giannoukos, G., et al. (2011). Chimeric 16S rRNA sequence formation and detection in Sanger and 454-pyrosequenced PCR amplicons. *Genome Res.* 21, 494–504. doi: 10.1101/gr.112730.110

Habran, A., Commisso, M., Helwi, P., Hilbert, G., Negri, S., Ollat, N., et al. (2016). Roostocks/scion/nitrogen interactions affect secondary metabolism in the grape berry. *Front. Plant Sci.* 7:1134. doi: 10.3389/fpls.2016.01134

Hamilton, N. (2017). ggtern: An Extension to 'ggplot2', for the Creation of Ternary Diagrams. R package version 2.2.1. Available at: https://CRAN.R-project.org/package=ggtern

Hardoim, P. R., van Overbeek, L. S., and Elsas, J. D. (2008). Properties of bacterial endophytes and their proposed role in plant growth. *Trends Microbiol.* 16, 463–471. doi: 10.1016/j.tim.2008.07.008

Keller, M. (2010). *The Science of Grapevines: Anatomy and Physiology*, 1st Edn. Cambridge, MA: Academic Press.

Kloepper, J. W., Leong, J., Teintze, M., and Schroth, M. N. (1980). Enhanced plant growth by siderophores produced by plant growth-promoting rhizobacteria. *Nature* 286, 885–886. doi: 10.1038/286885a0

Kowalchuk, G. A., Buma, D. S., de Boer, W., Klinkhamer, P. G. L., and van Veen, J. A. (2002). Effects of above-ground plant species composition and diversity on the diversity of soil-borne microorganisms. *Antonie Van Leeuwenhoek* 81, 509–520. doi: 10.1023/A:1020565523615

Lambert, J. J., Anderson, M. M., and Wolpert, J. A. (2008). Vineyard nutrient needs vary with rootstocks and soils. *Calif. Agric.* 62, 202–207. doi: 10.3733/ca.v062n04p202

Liu, H., Carvalhais, L. C., Crawford, M., Singh, E., Dennis, P. G., Pieterse, C. M. J., et al. (2017). Inner plant values: diversity, colonization and benefits from endophytic bacteria. *Front. Microbiol.* 8:2552. doi: 10.3389/fmicb.2017.02552

Liu, J., Abdelfattah, A., Norelli, J., Burchard, E., Schena, L., Droby, S., et al. (2018). Apple endophytic microbiota of different rootstock/scion combinations suggests a genotype-specific influence. *Microbiome* 6:18. doi: 10.1186/s40168-018-0403-x

Marasco, R., Rolli, E., Fusi, M., Michoud, G., and Daffonchio, D. (2018). Grapevine rootstocks shape underground bacterial microbiome and networking but not potential functionality. *Microbiome* 6:3. doi: 10.1186/s40168-017-0391-2

Margulis, L. (1991). "Symbiogenesis and symbionticism," in *Symbiosis as a Source of Evolutionary Innovation: Speciation and Morphogenesis*, eds L. Margulis and R. Fester (Cambridge, MA: MIT Press), 1–14.

Masella, A. P., Bartram, K. A., Truszkowski, J. M., Truszkowski, J. M., Brown, D. G., and Neufeld, J. D. (2012). PANDAseq: paired-end assembler for illumina sequences. *BMC Bioinformatics* 13:31. doi: 10.1186/1471-2105-13-31

Meena, V. S., Maurya, B. R., and Verma, J. P. (2014). Does a rhizospheric microorganism enhance K+ availability in agricultural soils? *Microbiol. Res.* 169, 337–347. doi: 10.1016/j.micres.2013.09.003

Meyer, D., Zeileis, A., and Hornik, K. (2017). *vcd: Visualizing Categorical Data. R package version* 1.4–4.

Robinson, J. (1986). *Vines, Grapes & Wines: The Wine Drinker's Guide to Grape Varieties*, 1st Edn. London: Mitchell Beazley.

Rosenberg, E., and Zilber-Rosenberg, I. (2016). Microbes drive evolution of animals and plants: the hologenome concept. *mBio* 7:e01395. doi: 10.1128/mBio.01395-15

Ryan, R. P., Germaine, K., Franks, A., Ryan, D. J., and Dowling, D. N. (2008). Bacterial endophytes: recent developments and applications. *FEMS Microbiol. Lett.* 278, 1–9. doi: 10.1111/j.1574-6968.2007.00918.x

Samad, A., Trognitz, F., Compant, S., Antonielli, L., and Sessitsch, A. (2017). Shared and host-specific microbiome diversity and functioning of grapevine and accompanying weed plants. *Environ. Microbiol.* 19, 1407–1424. doi: 10.1111/1462-2920.13618

Thompson, L. R., Sanders, J. G., McDonald, D., Amir, A., Ladau, J., Locey, K. J., et al. (2017). A communal catalogue reveals Earth's multiscale microbial diversity. *Nature* 551, 457–463. doi: 10.1038/nature24621

Turroni, S., Fiori, J., Rampelli, S., Schnorr, S. L., Consolandi, C., Barone, M., et al. (2016). Fecal metabolome of the Hadza hunter-gatherers: a host-microbiome integrative view. *Sci. Rep.* 6:32826. doi: 10.1038/srep32826

Uroz, S., Calvaruso, C., Turpault, M. P., Pierrat, J. C., Mustin, C., and Frey-Klett, P. (2007). Effect of the mycorrhizosphere on the genotypic and metabolic diversity of the bacterial communities involved in mineral weathering in a forest soil. *Appl. Environ. Microbiol.* 73, 3019–3027. doi: 10.1128/AEM.00121-07

Wallis, C. M., Wallingford, A. K., and Chen, J. (2013). Grapevine rootstock effects on scion sap phenolic levels, resistance to *Xylella fastidiosa* infection, and progression of Pierce's disease. *Front. Plant Sci.* 4:502. doi: 10.3389/fpls.2013.00502

Warschefsky, E. J., Klein, L. L., Frank, M. H., Chitwood, D. H., Londo, J. P., von Wettberg, E. J. B., et al. (2016). Rootstocks: diversity, domestication, and impacts on shoot phenotypes. *Trends Plant Sci.* 21, 418–437. doi: 10.1016/j.tplants.2015.11.008

Whiting, J. R. (2003). *Selection of Grapevine Rootstocks and Clones for Greater Victoria*. Melbourne, VIC: Dept. of Primary Industries.

Wolf, T. K. (2008). *Wine Grape Production Guide for Eastern North America*. Ithaca, NY: Natural Resource, Agriculture, and Engineering Service.

Wolpert, J. A., Smart, D. R., and Anderson, M. (2005). Lower petiole potassium concentration at bloom in rootstocks with *Vitis berlandieri* genetic backgrounds. *Am. J. Enol. Vitic.* 56, 163–169.

Zarjani, J. K., Aliasgharzad, N., Oustan, S., Emadi, M., and Ahmadi, A. (2013). Isolation and characterization of potassium-solubilizing bacteria in some Iranian soils. *Arch. Agron. Soil Sci.* 59, 1713–1723. doi: 10.1080/03650340.2012.756977

Zarraonaindia, I., Owens, S. M., Weisenhorn, P., West, K., Hampton-Marcella, J., Laxe, S., et al. (2015). The soil microbiome influences grapevine-associated microbiota. *mBio* 6:e02527-14. doi: 10.1128/mBio.02527-14

Zhang, C., and Kong, F. (2014). Isolation and identification of potassium-solubilizing bacteria from tobacco rhizospheric soil and their effect on tobacco plants. *Appl. Soil Ecol.* 82, 18–25. doi: 10.1016/j.apsoil.2014.05.002

Conflict of Interest Statement: The authors declare that the research was conducted in the absence of any commercial or financial relationships that could be construed as a potential conflict of interest.

frontiers in Microbiology

ORIGINAL RESEARCH
published: 29 June 2018
doi: 10.3389/fmicb.2018.01390

Cultivation of Drought-Tolerant and Insect-Resistant Rice Affects Soil Bacterial, but Not Fungal, Abundances and Community Structures

Peng Li[1,2], Shuifeng Ye[3], Hua Liu[1], Aihu Pan[1], Feng Ming[2] and Xueming Tang[1]**

[1] The Biotechnology Research Institute, Shanghai Academy of Agricultural Sciences, Shanghai, China, [2] State Key Laboratory of Genetic Engineering, Institute of Genetics–Institute of Plant Biology, School of Life Sciences, Fudan University, Shanghai, China, [3] Shanghai Agrobiological Gene Center, Shanghai, China

The impacts of rice varieties with stacked drought tolerance and insect resistance on soil microbiomes are poorly understood. Hence, the objective of this study was to investigate the effects resulting from the cultivation of the drought-tolerant and insect-resistant rice cultivar, Hanhui3T, on soil physical–chemical properties, and bacterial and fungal community composition. Soil samples of Hanhui3T and conventional rice varieties (Hanhui3 and Zhonghua11) were collected in triplicate at the booting stage, and bacterial and fungal population sizes and community structures were assessed using qPCR and Illumina MiSeq sequencing, respectively. The Bt protein concentration of Hanhui3T was significantly higher than that of Hanhui3 and Zhonghua11, while the pH of Hanhui3T was significantly lower. Bacterial population sizes and community composition were significantly different between Hanhui3T and Hanhui3 (or Zhonghua11), while no similar effects were observed for fungal communities. These differences suggest that the effect of Hanhui3T cultivation on bacterial community composition is stronger than the effect on fungal communities. Moreover, bacterial abundance was positively correlated to soil pH, while bacterial community structure variations were mainly driven by soil pH and Bt protein concentration differences. In conclusion, the abundances and structure of bacterial communities were altered in rhizosphere with Hanhui3T cultivation that changed soil pH and Bt protein concentrations, while fungal communities displayed no such responsiveness.

Keywords: drought-tolerant and insect-resistant rice, Illumina MiSeq sequencing, Bt proteins, bacterial community composition, fungal community composition

OPEN ACCESS

Edited by:
Christina Kaiser, Universität Wien, Austria

Reviewed by:
Mariusz Cycoń, Medical University of Silesia, Poland
Xuesong Luo, Huazhong Agricultural University, China

****Correspondence:***
Feng Ming
fming@fudan.edu.cn
Xueming Tang
sunsite@126.com

Specialty section:
This article was submitted to Plant Microbe Interactions, a section of the journal Frontiers in Microbiology

Received: *13 March 2018*
Accepted: *06 June 2018*
Published: *29 June 2018*

Citation:
Li P, Ye S, Liu H, Pan A, Ming F and Tang X (2018) Cultivation of Drought-Tolerant and Insect-Resistant Rice Affects Soil Bacterial, but Not Fungal, Abundances and Community Structures. Front. Microbiol. 9:1390. doi: 10.3389/fmicb.2018.01390

INTRODUCTION

The rhizosphere represents a hot spot for microbial activity and constitutes one of the most complex ecosystems on earth, with numerous complex interactions with neighboring plants and microbes (Mendes et al., 2013). Plant root exudates initiate and modulate the relationships between roots and soil microbes, whereby the quantity and quality of root exudates are determined by

plant genotypes (Badri and Vivanco, 2009). Consequently, these relationships are often specific, indicating that changes in plant genotypes impact the association of specific microbial groups with plants, and thus altering the abundance and composition of the rhizosphere microbiome. The alteration of plant genotypes by genetic modification have a potential bearing on the organisms that are targeted by the modification, in addition to other potential (collateral) effects resulting from the modification (Cotta et al., 2014). There has been a remarkable decline in crop planting area and food production in areas with continued deterioration of drought conditions brought about by climate change (Clive, 2016). Thus, the development of biotech crops with multiple favorable traits, such as drought and insect resistance, has increased dramatically, and rapid approval of these crops is needed.

A drought-tolerant and insect-resistant rice cultivar, Hanhui3T, has been developed by the Shanghai Agrobiological Gene Center of China. Field experiments have shown that Hanhui3T displays significant resistance to rice leaf roller, and apparently combines drought-tolerant traits (Ye et al., 2012). Importantly, the potential environmental effects of newly developed cultivars must be evaluated through environmental risk assessment before the cultivation of transgenic plants for commercial purposes (National Research Council, 2002). Environmental risk assessments are based on precautionary principles and they are practiced on a case-by-case basis by taking into consideration the nature of the plant, trait and the potential receiving environment (Khan et al., 2017). One of the major potential environmental risks associated with the use of drought- and insect-resistant rice varieties is the effect on soil and the inhabiting non-target organisms, including bacteria and fungi. The bacterial and fungal communities inhabiting the rhizosphere, that is the soil influenced by root metabolites, are influenced by soil types, plant species, local climates, and plant growth stages (Buée et al., 2009; Dohrmann et al., 2013). Sohn et al. (2016) suggest that the effects of drought-tolerant rice cultivation on soil microorganisms are not significant using plate counts and pyrosequencing. However, studies of the impact of transgenic rice with different genetic traits on rhizosphere microbial communities have revealed inconsistent results (Turrini et al., 2015). Moreover, considering the Bt protein that is released in root exudates from transgenic Bt plants (Saxena et al., 1999) and variation in drought stress-response gene expression, we hypothesized that drought- and insect-resistant rice varieties are likely to produce unintended effects on soil bacterial and the fungal communities. In addition, it is clear that factors, such as soil physical–chemical properties and plant genotypes, greatly influence the corresponding rhizosphere microbial community compositions (Khan et al., 2017). The extent to which these factors, including soil Bt protein exposure, influence and contribute to indigenous microbial community is not yet fully understood. Kennedy et al. (2004, 2005) hypothesized that bacterial communities are more sensitive to changes in environmental factors than fungal communities. However, additional studies are needed to evaluate whether bacterial and fungal community compositions differentially respond to the cultivation of drought and insect-resistant rice.

The objective of the present study was to characterize the effects of drought-tolerant and insect-resistant rice cultivation on the abundance and structure of soil bacterial and fungal communities. Bacterial and fungal population sizes were assessed with quantitative PCR (qPCR) of bacterial 16S rRNA genes and fungal internal transcribed spacer (ITS) genes, respectively. Changes in community structures (via 16S and 18S rRNA gene composition) between drought-tolerant and insect-resistant rice and conventional rice varieties were then assessed using Illumina MiSeq sequencing. Lastly, the relationships between soil bacterial and fungal community structures and soil physicochemical factors, including Bt protein exposure, were analyzed with redundancy analysis (RDA).

MATERIALS AND METHODS

Plants and Field Design

Hanhui3T is a rice hybrid that produces the insecticidal delta endotoxin protein Cry1Ab/Ac, which confers resistant to pests and combines drought-tolerance traits. The Hanhui3T is bred by introducing the *Cry1Ab/Ac* gene into the rice cultivar Hanhui3 by agrobacterium-mediated genetic transformation (Ye et al., 2012). A variety of the hybrid, Hanhui3, was included in this study that is a near isogenic parental counterpart to Hanhui3T, in addition to the conventional variety, Zhonghua11. Seeds of Hanhui3T, Hanhui3, and Zhonghua11 were obtained from the Shanghai Agrobiological Gene Center (Shanghai, China). Plants of the three rice varieties were grown in the same chambers within a glasshouse at the Shanghai Academy of Agricultural Sciences. The experiment consisted of a randomized block design with nine replicate chambers, where each chamber had a volume of 100 cm × 100 cm × 30 cm. Each chamber contained plants of all three varieties (36 plants of each), which were planted with a distance of 15 cm between plants. The soil was classified as Fluvio marine blue purple clay and contained 13.3 g/kg of organic matter, 1.2 g/kg of total nitrogen, 90.5 mg/kg available N, and a pH of 7.4 (soil:water ratio 1:5). The seedlings were planted on May 30, 2016 and rice rhizospheres were sampled at the booting stage on August 25, 2016. After weeds and litter were removed from the soil surface, two types of soil samples were harvested. Bulk soil was excised from at least 4 mm away from any roots, and soils within 2 mm of the root surface were considered rhizosphere soils (DeAngelis et al., 2009). Plants were gently removed from soils and rhizospheres were collected by gently shaking roots to dislodge small adhering soil clumps. To ensure representativeness of samples, each sample was a composite from three chambers with the same rice variety. The samples were placed on ice in a cooler and transported to the laboratory on the same day. Soils were passed through a 2.0-mm sieve, and then a portion of the soil sample (collected in triplicate for each rice variety) was stored at −80°C before DNA extraction, while the remainder was stored at 4°C prior to the analysis of soil properties.

Analysis of Soil Physicochemical Properties and Soil Microbial DNA Extraction

Soil Cry proteins were quantified by enzyme-linked immunosorbent assays as described by Dohrmann et al. (2013). Briefly, 0.5 g of soil sample was added to a 2-mL microcentrifuge tube. Next, 1.0 mL extraction buffer (0.1 M Na_2CO_3, 0.1 M $NaHCO_3$, 5.0 mM EDTA, 50 mM $Na_4P_2O_7.10H_2O$, 0.1%Triton X-100, pH10) was added to fill the tube and the sample was mixed for 30 min at room temperature, followed by centrifugation for 5 min at 4°C at 12,000 × *g*. The supernatant was collected to measure Bt protein content using a commercial ELISA kit (QuantiPlate^{TM} Kit for Cry1Ab/Cry1Ac, EnviroLogix Inc., Portland, ME, United States) according to the manufacturer's protocol. Soil pH was determined by preparing a suspension of air-dried soil sample in water at a ratio of 1:5 (w/v), and pH was measured using a digital pH meter. Organic matter was determined using the potassium dichromate oxidation method (Lu, 2000), total nitrogen with the Kjeldahl procedure (Kirk, 1950), and available nitrogen (AN) by the hot alkaline permanganate method (Subbiah and Asija, 1956). Soil microbial DNA was extracted from the soil samples collected in triplicates as previously described (Li et al., 2014). Total genomic DNA was extracted from 0.5 g of sample using the FastDNA SPIN Kit for soil (MP Biomedicals, LLC, Solon, OH, United States). Purified DNA was stored at −80°C for the analyses of qPCR and Illumina MiSeq sequencing.

Quantification of Bacterial and Fungal Community Abundances

Population sizes of soil bacterial and fungal communities were determined by qPCR assays according to methods described previously (Li et al., 2018), using the universal bacterial 16S rRNA gene primers 1369F (5′-CGG TGA ATA CGT TCY CGG-3′) and 1492R (5′-GGW TAC CTT GTT ACG ACT T-3′) (Suzuki et al., 2000), and fungal ITS genes primers NSI1 (5′-GAT TGA ATG GCT WAG TGA GG-3′) and 58A2R (5′-CTG CGT TCT TCA TCG AT-3′) (Mitchell and Zuccaro, 2006). The average bacterial and fungal qPCR efficiencies were 95.91 and 102.45%, respectively, with standard curve R^2 values of 0.998 and 0.997, respectively.

Illumina MiSeq Sequencing of Bacterial 16S rRNA and Fungal 18S rRNA Genes

Twelve independent samples of the rhizosphere from the three rice varieties Hanhui3T, Hanhui3, and Zhonghua11, and bulk soil as a control (with three replicates each) were selected for Illumina MiSeq sequencing. Bacterial 16S rRNA gene fragments were amplified with the primers 515F (5′-GTG CCA GCM GCC GCG G-3′)/907R (5′-CCG TCA ATT CMT TTR AGT TT-3′) and fungal 18S rRNA gene fragments were amplified with the primers SSU0817F (5′-TTA GCA TGG AAT AAT RRA ATA GGA-3′)/SSU1196R (5′-TCT GGA CCT GGT GAG TTT CC-3′) using a thermocycler PCR system (GeneAmp 9700, ABI, United States). PCR reactions were performed in triplicate in 20 μl reaction mixtures containing 4 μl of 5× FastPfu buffer, 2 μl of 2.5 mM dNTPs, 0.8 μl of each primer (5 μM), 0.2 μl of BSA, 0.4 μl of FastPfu polymerase, 10 ng of template DNA, and deionized, distilled water added up to a total volume of 20 μl. Bacterial PCRs comprised the following steps: 3 min of denaturation at 95°C, followed by 27 cycles of 95°C for 30 s, annealing at 55°C for 30 s, elongation at 72°C for 45 s, and a final extension at 72°C for 10 min. Fungal PCRs were conducted using the following program: 3 min of denaturation at 95°C, followed by 35 cycles of 95°C for 30 s, annealing at 53°C for 30 s, elongation at 72°C for 45 s, and a final extension at 72°C for 10 min. The resultant PCR products were visualized on a 2% agarose gel, and then extracted and purified using an AxyPrep DNA Gel Extraction Kit (Axygen Biosciences, Union City, CA, United States). PCR products were quantified using QuantiFluor^{TM}-ST (Promega, United States) according to the manufacturer's protocol. Equimolar amounts of the PCR products were pooled and prepared for sequencing on the Illumina MiSeq platform at Majorbio Bio-Pharm Technology Co., Ltd., Shanghai, China.

Raw sequence data were processed and analyzed using QIIME Pipeline version 1.8.0[1] (Caporaso et al., 2010). Briefly, low-quality sequences that were shorter than 200 bp and had an average quality score of less than 20 were removed prior to analysis. Chimeric sequences were detected and removed using the UCHIME algorithm (Edgar et al., 2011). The remaining high-quality sequences were clustered into operational taxonomic units (OTUs) at the 97% sequence similarity level using the program: Cluster Database at High Identity with Tolerance (CD-HIT) (Li and Godzik, 2006). The taxonomy of each OTU was assessed using the RDP Classifier algorithm[2] against the SILVA (128/16S Bacteria) 16S rRNA and SILVA (128/18S Eukaryota) 18S rRNA gene databases and a confidence threshold of 70%. All of the bacterial 16S rRNA and fungal 18S rRNA gene sequence data analyzed in this study have been deposited in the GenBank short-read archive SRA accessions: SRP130072 and SRP130195, respectively. In order to compare relative differences among samples, a subset of 11,620 and 21,723 bacterial and fungal sequences (the lowest value for a sample in each dataset), respectively, were randomly selected from each sample.

Statistical Analyses

Beta-diversity estimates (Bray–Curtis and Hellinger distances) were calculated using the QIIME pipeline (Caporaso et al., 2010). To estimate alpha-diversity, the Shannon–Wiener index *H*′, Simpson index *D*, Richness *R*, and Chao1 indices were calculated and rarefaction curves were generated using the mothur software package (v 1.35.1) (Schloss et al., 2009). Hierarchical cluster analysis of samples based on Hellinger distances was performed using the R software package[3]. The statistical significance of differences in soil properties, 16S rRNA and ITS gene copies, and bacterial and fungal alpha-diversity among samples were examined by one-way analysis of variance (ANOVA) using SPSS 19.0 (SPSS Institute, Inc., 2010), and the shortest significant range (SSR) test was employed for

[1]http://qiime.org/tutorials/tutorial.html

[2]http://rdp.cme.msu.edu/

[3]http://www.rproject.org/

multiple *post hoc* comparisons. In addition, the relationships between soil properties and 16S rRNA and ITS gene copies were tested by linear regression analyses using SPSS 19.0. Significant differences were considered as $P < 0.05$. An analysis of similarities (ANOSIM) was performed using QIIME 1.8.0 software (Caporaso et al., 2010) to determine whether different soil samples had significantly different microbial communities. RDA was conducted to determine the environmental variables that were most related to bacterial and fungal community compositional differences, and the results were used to construct a soil property matrix for variation partitioning analysis in R (v.2.8.1) using a Mantel test with the Pearson correlation method and 1,000 permutations through the "vegan" package (v.1.15-1) (R Core Team, 2006).

RESULTS

Soil Properties

The concentrations of soil Bt protein, organic matter, total N, and available N, in addition to pH are shown in **Table 1**. Cultivation of drought-tolerant and insect-resistant rice resulted in increased soil Bt protein content. The Bt protein content of the three rice varieties' rhizosphere and bulk soils were between 49.34 and 75.39 pg/g soil. The Bt protein content in the Hanhui3T rhizosphere was significantly higher than that in the other samples. In addition, the soil pH of Hanhui3T was significantly lower than that of Hanhui3 and Zhonghua11, but no significant difference was noted between Hanhui3T and bulk soils. No differences in organic matter, total N, or available N contents were found among all of the samples.

qPCR Estimates of the Total Bacterial and Fungal Population Sizes

qPCR estimates of bacterial population sizes, as determined by 16S rRNA genes, were between 8.32×10^9 and 15.44×10^9 copy numbers g^{-1} dry soil (**Figure 1A**). Fungal ITS rRNA gene copy numbers ranged from 4.59×10^7 to 5.78×10^7 copy numbers g^{-1} dry soil (**Figure 1B**). The population sizes of soil bacteria within Hanhui3T were significantly lower than those of Hanhui3 and Zhonghua11 soils, but higher than in bulk soils. In contrast, the population sizes of soil fungi were not significantly different between Hanhui3T and Hanhui3 (or Zhongua11), but bulk soils had significantly smaller populations. Consequently, the effect of Hanhui3T cultivation on soil bacterial population sizes was greater than the effect on soil fungal population sizes. A pairwise analysis indicated that the abundance of total bacteria was significantly positively correlated ($r = 0.741$, $p = 0.006$) with soil pH (7.41–7.55) (**Figure 2**), but it was not significantly correlated with other soil properties. In contrast, the total abundance of fungi was not significantly correlated to any soil properties.

Taxonomic Classification and Relative Abundance of Bacteria and Fungi by Illumina MiSeq Sequencing

In total, 171,013 and 333,361 high-quality sequences from 12 samples were obtained by Illumina MiSeq sequencing of bacterial 16S rRNA and fungal 18S rRNA genes, respectively. A total of 36 bacterial phyla, 92 classes, 187 orders, 325 families, and 533 genera were detected in the bacterial dataset. The most abundant bacterial phyla were *Proteobacteria* (44.10%), *Acidobacteria* (16.20%), *Bacteroidetes* (12.60%), *Actinobacteria* (6.70%), and *Chloroflexi* (5.00%), with relative abundances ranging from 36.97 to 50.40%, from 12.48 to 26.20%, from 6.14 to 17.37%, from 4.00 to 9.04% and from 3.33 to 6.14% across all samples, respectively (**Figure 3A**). A total of 26 fungal phyla, 42 classes, 64 orders, 79 families, and 90 genera were detected in the fungal dataset. The most abundant fungal phyla were *Ascomycota* (85.03%), *Ciliophora* (7.50%) and unclassified fungi/Eukaryotes (2.28%), with relative abundances ranging from 65.78 to 94.83%, from 1.51 to 25.27% and from 0.81 to 5.36% across all samples, respectively (**Figure 3B**). There were 2,053 and 219 OTUs that were identified at the 97% similarity level for 16S rRNA and 18S rRNA genes, respectively. Rarefaction curves for all of the soil samples, based on OTUs, reached asymptotes, indicating that the data generated in this study was adequate for the analysis of the bacterial and fungal diversity in the rhizosphere samples collected (Supplementary Figures S1A,B). Moreover, coverage (*C*) based on OTUs, confirmed the adequate sampling of diversity with estimates of 96.39% and 99.87% (Supplementary Table S1) for bacteria and fungi, respectively. The results, taken together, suggest that the sequencing depth used for all 12 of the samples was adequate to detect the total diversity of bacterial and fungal communities.

Bacterial and Fungal Community Diversity

The alpha-diversity indices represented by the Shannon index H', Simpson index *D*, Richness index *R*, and Chao1 estimate for bacterial communities, were not significantly different between Hanhui3T and Hanhui3 (or Zhonghua11)

TABLE 1 | Physical–chemical characteristics of the soil samples used in this study[a].

Rice Sample	pH (1:5 H_2O)	Bt protein (pg/g)	Organic matter (g/kg)	Total N (g/kg)	Available N (mg/kg)
Hanhui3T	7.46 ± 0.01^b	75.39 ± 9.95^a	14.03 ± 1.45^a	1.35 ± 0.04^a	90.90 ± 2.04^a
Hanhui3	7.53 ± 0.05^a	49.34 ± 2.41^b	14.46 ± 0.87^a	1.35 ± 0.08^a	91.84 ± 1.39^a
Zhonghua11	7.55 ± 0.06^a	53.00 ± 7.00^b	14.73 ± 0.55^a	1.39 ± 0.06^a	93.40 ± 0.95^a
BS	7.41 ± 0.06^b	49.67 ± 4.73^b	13.90 ± 0.56^a	1.28 ± 0.04^a	91.12 ± 1.90^a

[a] *Values represent the averages of three repetitions and the standard deviations. Different lowercase letters in the same column indicate a statistically significant difference at 0.05 level. BS indicates bulk soil control.*

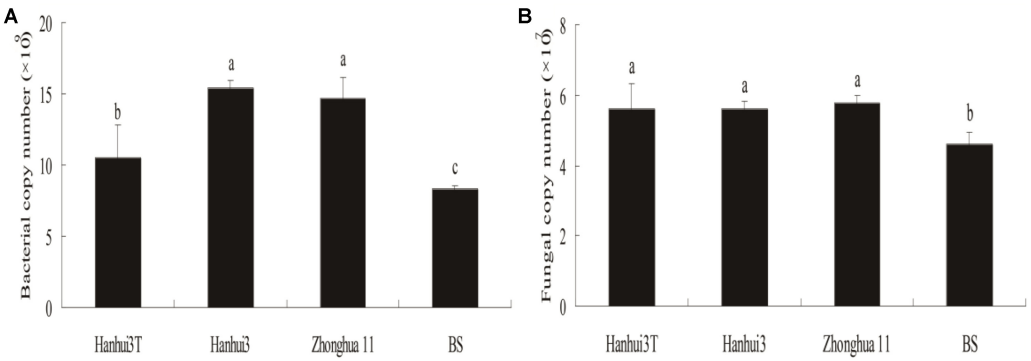

FIGURE 1 | Copy numbers of the 16S rRNA **(A)** and ITS **(B)** genes from the rhizosphere microbial DNA extracts (Mean ± Standard Deviation) as determined by qPCR. BS indicates bulk soil control.

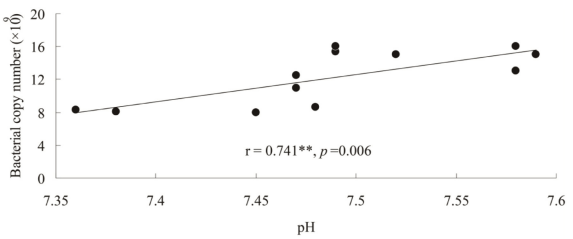

FIGURE 2 | Relationships between the abundance of total bacteria and the soil pH.

(**Table 2**). However, the Chao1 estimate of bacterial community richness significantly differed between the rhizosphere and bulk soil communities. Likewise, the Shannon index *H′*, Simpson index *D*, Richness index *R*, and Chao1 estimate for fungal communities were also not significantly different between Hanhui3T and Hanhui3 (or Zhonghua11) (**Table 3**). Notably, the abovementioned diversity index showed significant difference between rhizosphere and bulk soil fungal communities.

Hierarchical cluster analysis of the bacterial communities indicated that the rhizosphere communities from the three rice varieties and bulk soils belonged to two separate groups. This observation suggests an influence of root exudates on bacterial community composition (**Figure 4A**). In addition, the rhizosphere communities from the Hanhui3T and conventional rice variety (Hanhui3 and Zhonghua11) cultivar clustered into two separate groups, indicating that cultivation of insect-resistant and drought-tolerant rice considerably influenced bacterial community composition. Cluster analysis of fungal communities revealed similar clustering patterns between rhizosphere and bulk soil (**Figure 4B**). However, communities from Hanhui3T and Hanhui3 (or Zhonghua11) did not segregate into two distinct groups, suggesting that the cultivation of insect-resistant and drought-tolerant rice did not affect fungal community composition as drastically as that of bacteria. Analysis of

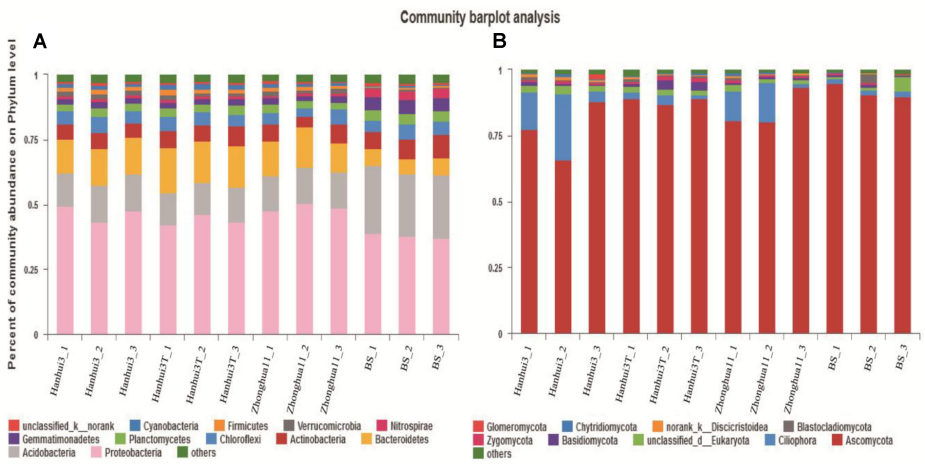

FIGURE 3 | Relative abundance of major bacterial phyla **(A)** and fungal phyla **(B)** in the soil samples. BS indicates bulk soil control.

TABLE 2 | The Shannon–Wiener index *H′*, Simpson index *D*, Richness *R*, and Chao1 of the soil bacterial communities of different rice varieties[a].

Rice sample	*H′*	*D*	*R*	Chao1
Hanhui3T	6.06 ± 0.07[a]	0.0066 ± 0.0009[a]	1508.33 ± 21.13[a]	1859.82 ± 44.07[a]
Hanhui3	6.01 ± 0.20[a]	0.0082 ± 0.0025[a]	1493.67 ± 184.08[a]	1807.04 ± 117.34[a]
Zhonghua11	5.88 ± 1.00[a]	0.0095 ± 0.0018[a]	1392.67 ± 43.25[a]	1759.45 ± 52.38[a]
BS	5.98 ± 0.07[a]	0.0060 ± 0.0005[a]	1304.67 ± 48.29[a]	1586.90 ± 34.44[b]

[a]*Values represent the averages of three repetitions and the standard deviations. Different lowercase letters in the same column indicate a statistically significant difference at 0.05 level. BS indicates bulk soil control.*

TABLE 3 | The Shannon–Wiener index *H′*, Simpson index *D*, Richness *R*, and Chao1 of the soil fungal communities of different rice varieties[a].

Rice sample	*H′*	*D*	*R*	Chao1
Hanhui3T	2.62 ± 0.04[ab]	0.1451 ± 0.0026[b]	133.33 ± 4.04[a]	146.61 ± 8.15[ab]
Hanhui3	2.71 ± 0.09[a]	0.1285 ± 0.0106[b]	141.33 ± 14.36[a]	150.14 ± 15.36[ab]
Zhonghua11	2.69 ± 0.20[a]	0.1302 ± 0.0306[b]	140.67 ± 4.73[a]	168.22 ± 10.82[a]
BS	2.36 ± 0.17[b]	0.1948 ± 0.0333[a]	111.67 ± 11.55[b]	125.20 ± 7.25[c]

[a]*Values represent the averages of three repetitions and the standard deviations. Different lowercase letters in the same column indicate a statistically significant difference at 0.05 level. BS indicates bulk soil control.*

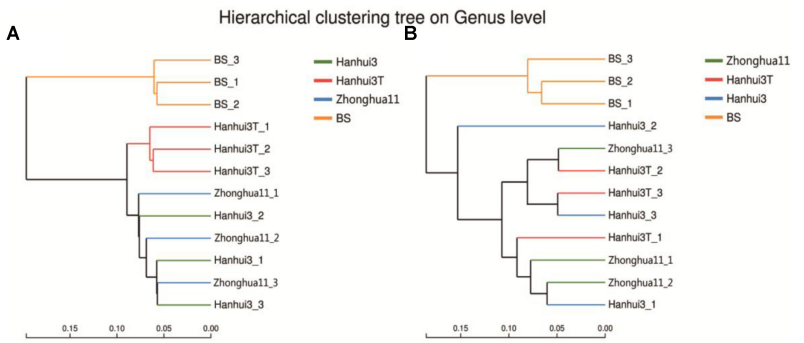

FIGURE 4 | Hierarchical cluster analysis of the bacterial **(A)** and fungal **(B)** communities from different rice varieties rhizosphere and bulk soil based on the Hellinger distances of microbial communities. BS indicates bulk soil control.

similarity (ANOSIM) showed that the difference in bacterial community composition in both Hanhui3 and Zhonghua11 compared to the Hanhui3T was significant (sample statistic (Hanhui3/Hanhui3T) = 0.719, p = 0.017; sample statistic (Zhonghua11/Hanhui3T = 0.724, p = 0.048), whereas the community composition of Hanhui3 and Zhonghua11 did not differ. However, the ANOSIM assay showed no significant difference among the fungal microbial communities from different soil samples.

Correlations Between Bacterial and Fungal Community Composition and Soil Properties

The relationships between soil properties and bacterial and fungal community compositions, at the genus level, were analyzed by RDA (**Figures 5A,B**). The first two RDA components explained 64.58% of the total variation in bacterial community composition and 68.43% of the total variation in fungal community composition. Soil pH was most correlated with variation in bacterial community composition (r = 0.75, p = 0.024), followed closely by Bt protein concentrations (r = 0.73, p = 0.024). However, the other environmental variables were not significantly correlated ($p > 0.05$) to bacterial community variation. In contrast, none of the aforementioned soil variables were significantly correlated ($p > 0.05$) to variation in fungal communities. Spearman's rank-order correlation was used to assess the response of specific bacterial and fungal genera to soil Bt protein concentrations (Supplementary Tables S2, S3). Thirty-four bacterial genera and seven fungal genera were correlated significantly with soil Bt protein concentrations. The relative abundances of bacterial genera, including *Coxiella*, *Blastopirellula*, *Sorangium,* and *Pseudomonas*, were positively correlated with Bt protein concentrations, while *Gemmatimonas*, *Flavisolibacter*, *Flavitalea,* and others, were negatively correlated with Bt protein concentrations. In addition, the relative abundance of unclassified fungal genera from the *Vampyrellidae*, *Agaricomycetes*, and *RM2-SGM5* groups, in addition to *Neourostylopsis,* were significantly positively correlated with Bt protein concentrations, whereas abundances

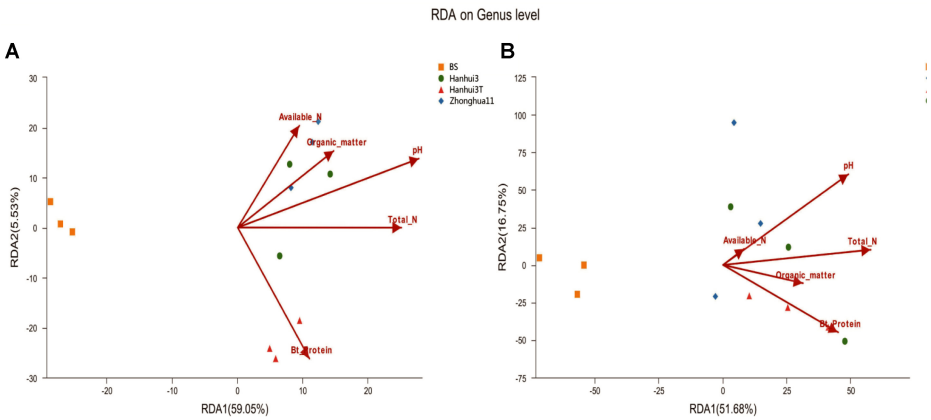

FIGURE 5 | RDA results of the soil properties and bacterial **(A)** and fungal **(B)** community compositions at the genus level. BS indicates bulk soil control. The number on each axis indicates the percentage of the total variation explained.

of unclassified genera from the *Craspedida*, *Malasseziales*, and *Savoryellales* were significantly negatively correlated with Bt protein concentrations.

DISCUSSION

Cultivation of Drought-Tolerant and Insect-Resistant Rice Altered Bt Protein Contents and Soil pH

It has been widely reported that Cry proteins can be released into soils in the root exudates of Bt plants during growth (Saxena and Stotzky, 2001; Rui et al., 2005; Knox et al., 2007). In the present study, the content of rhizosphere Bt protein was significantly higher in Hanhui3T soils compared to Hanhui3 and Zhonghua11 soils at the booting stage. Rhizosphere Bt protein concentrations from Hanhui3T were the highest at the booting stage of all of the growth stages, prompting our assessment of the rhizosphere microbial communities at this stage. Notably, we observed significantly lower pH in the Hanhui3T soils compared to Hanhui3 and Zhonghua11, while other soil factors were equivalent. This finding contrasts with a previous study that did not observe significant differences in soil pH between the cultivation of drought-tolerant transgenic rice and the parental rice cultivar (Sohn et al., 2016). The observed decrease in pH could have been caused by degradation of Bt proteins, which may lead to increased availability of amino acids, release of ammonia and subsequent nitrification (Dohrmann et al., 2013; Gundersen and Rasmussen, 2013). Hence, we characterized the proportion of Cry proteins in the total protein content of the rhizosphere, which was determined to be low (Supplementary Material and Methods). Consequently, we speculated that the increase of a small proportion of Cry protein due to genetic modification is unable to alter soil pH significantly, when considering the total protein content in the rhizosphere. Another explanation for the observed pH differences is related to differences in root exudates in the vicinities of roots from the different rice varieties (Somers et al., 2004). Thus, we cultured three rice varieties in International Rice Research Institute (IRRI) solution and found that the total amount of organic acids in root exudates from Hanhui3T was dramatically higher than compared to Hanhui3 and Zhonghua11 (Supplementary Table S4). Thus, the lower pH of rhizosphere soils of Hanhui3T may be related to the clear increase in organic acid abundances in its root exudates when compared to control varieties. Hartmann et al. (2009) found that root exudates containing particular organic acids can modulate local environmental conditions, such as pH, resulting in microbial community variation. However, whether other organic compounds of root exudates could also affect soil pH requires further investigation.

Effect of Drought-Tolerant and Insect-Resistant Rice Cultivation on Total Bacterial and Fungal Abundances

Cotta et al. (2014) suggested that microbial community abundances should be studied as bioindicators when monitoring for possible impacts of genetically modified plant cultivation. Sohn et al. (2016) did not detect significant differences in microbial community abundances in the soils of drought-tolerant transgenic rice and the parental rice cultivar using plate counts. However, considering that only a small fraction of soil microbial communities are cultured (Hill et al., 2000), we used real-time qPCR to accurately estimate bacterial and fungal abundances. Our results challenged the above conclusion based on the plate counting data. We found the abundance of bacteria in the drought and insect resistant rice rhizosphere was lower than those associated with the drought resistant only rice and conventional rice, although it was still higher than that in the bulk soil. In contrast, total fungal abundance of Hanhui3T was only significantly higher than that of bulk soils, and did not differ from the other two conventional rice varieties. Accordingly, correlation analysis was conducted

to quantify the relationships between soil characteristics and microbial community abundances. Among the soil parameters that were tested, only soil pH was positively correlated with bacterial 16S rRNA gene copy numbers, suggesting that pH was the main driver of bacterial abundances. These results are consistent with those of Rousk et al. (2010), who used qPCR and a bar-coded pyrosequencing technique, and found that both the relative abundance and diversity of bacteria were positively correlated to pH, while the relative abundance of fungi was unaffected by pH. However, it should be noted that the components of Bt protein that is released in root exudates could bind to soil humic acids rapidly, resulting in inefficient recovery and quantification of Bt protein concentrations (Crecchio and Stotzky, 1998; Valldor et al., 2015). Nevertheless, our results revealed that the abundance of bacteria and fungi was significantly different between rhizospheres and bulk soils, indicating that rice plants interacted with, and affected rhizosphere microbial communities. Furthermore, Badri and Vivanco (2009) found that the release of root exudates in the rhizosphere supported a highly specific diversity of microbes. Our results in combination with their findings suggested that there is a close co-evolutionary link between plant genotypes and rhizosphere population recruitment.

Effect of Drought-Tolerant and Insect-Resistant Rice Cultivation on Rhizosphere Bacterial and Fungal Community Diversity and Composition

In contrast to low-throughput sequencing methods, which typically limit analysis to the most dominant phylotypes in microbial communities (Lee et al., 2011; Li et al., 2014), the Illumina MiSeq sequencing approach applied here detected 533 bacterial genera and 90 fungal genera. Consequently, these high-throughput analyses allowed the detection of much less abundant members by a factor of more than two orders of magnitude relative to lower-throughput sequencing methods (Dohrmann et al., 2013). Although soil bacterial community diversity indices (H', D, R, and Chao1) did not differ significantly between Hanhui3T and Hanhui3 (or Zhonghua11), distinct bacterial community structures were present among these samples. Specifically, Hanhui3 and Zhonghua11 clustered together firstly, suggesting varieties related to the genetic modification had remarkable effect on bacterial community composition. No apparent changes in fungal community composition between drought-tolerant and insect-resistant rice and conventional varieties were found, supporting the hypothesis that bacterial communities are more sensitive to environmental factors than fungal communities (Taylor et al., 2010). Indeed, previous studies have indicated that fungal communities have greater resistance to changes in environmental factors compared to bacterial communities (Kennedy et al., 2004, 2005). Differences in the bacterial community structure between Hanhui3T and Hanhui3 (or Zhonghua11) were hypothesized to result from unintentional changes in root exudate composition or by direct effects resulting from soil chemical parameters on soil microorganisms. RDA indicated that soil pH and Bt protein concentrations were significantly related to variation in bacterial community composition, but that other soil parameters had no significant influences. Although soil pH is commonly regarded as the primary variable responsible for soil bacterial community changes, our results indicated that the impacts of other environmental variables on bacterial community composition varied with soil samples. However, owing to the difficult characterization of rhizosphere organic compounds within root exudates, more studies are required to further evaluate the ecological and co-evolutionary role of root exudates in shaping soil microbial communities. Valldor et al. (2015) demonstrated that the Bt protein of GM crops could be utilized by microorganism as a growth substrate using ^{14}C-tracer studies in two agricultural soils. In this study, we also found a total of 34 bacterial genera and 7 fungal genera that were significantly correlated to Bt protein concentrations. Whether these genera were real Bt utilized as growth sources remained unclear. This should be confirmed by future investigation. The other possibility is that bacteria from these genera utilized the dead insects killed by Bt toxins and thus statistically correlated with Bt contents.

CONCLUSION

In conclusion, this study represents the first ecological risk assessment of the potential effects of drought-tolerant and insect-resistant rice cultivation on rhizosphere microbial communities. Rhizosphere bacterial abundances and community structures were substantially different between drought-tolerant and insect-resistant rice cultivation and conventional rice variety cultivation at the booting stage. However, these effects were not observed for fungal community composition, indicating that the effects of drought-tolerant and insect-resistant rice cultivation were stronger for bacterial community composition compared to fungi community composition. Moreover, bacterial abundance was positively associated with soil pH, while bacterial community composition structure was primarily controlled by soil pH and Bt protein concentrations.

AUTHOR CONTRIBUTIONS

XT and FM designed the experiments. PL performed most of the experiments. AP performed some of the experiments. SY contributed materials and analysis tools. HL analyzed data and discussed the result. PL wrote the manuscript. FM edited the manuscript. XT analyzed the data and edited the manuscript.

FUNDING

This work was financially supported by the National Natural Science Foundation of China No. 31500461, the Key Technologies Program of Shanghai Agricultural Commission No. 2015 (4-3), the Shanghai Agriculture Committee Young

Talent Foundation No. 1-15 (2016), and the SAAS Program for Excellent Research Team No. 2017 (B-07).

ACKNOWLEDGMENTS

We would like to thank Christoph C. Tebbe and Anja B. Dohrmann (Institute of Biodiversity, Johann Heinrich von Thünen-Institute (vTI), Federal Research Institute for Rural Areas, Forestry and Fisheries, Braunschweig, Germany) for analytical method assistance. We gratefully acknowledge Yongchun Li (Zhejiang Agriculture and Forestry University, China) for interpretation of data for the work.

SUPPLEMENTARY MATERIAL

The Supplementary Material for this article can be found online at: https://www.frontiersin.org/articles/10.3389/fmicb.2018.01390/full#supplementary-material

REFERENCES

Badri, D. V., and Vivanco, J. M. (2009). Regulation and function of root exudates. *Plant Cell Environ.* 32, 666–681. doi: 10.1111/j.1365-3040.2009.01926.x

Buée, M., De Boer, W., Martin, F. M., van Overbeek, L., and Jurkevitch, E. (2009). The rhizosphere zoo: an overview of plant-associated communities of microorganisms, including phages, bacteria, archaea, and fungi, and of some of their structuring factors. *Plant Soil* 321, 189–212. doi: 10.1007/s11104-009-9991-3

Caporaso, J. G., Kuczynski, J., Stombaugh, J., Bittinger, K., Bushman, F. D., Costello, E. K., et al. (2010). QIIME allows analysis of high throughput community sequencing data. *Nat. Methods* 7, 335–336. doi: 10.1038/nmeth.f.303

Clive, J. (2016). *Global Status of Commercialized Biotech/GM Crops:2016. ISAAA Brief* 52. Ithaca, NY: ISAAA, 4–8.

Cotta, S. R., Franco Dias, A. C., Marriel, I. E., Andreote, F. D., Seldin, L., and van Elsas, J. D. (2014). Different effects of transgenic maize and nontransgenic maize on nitrogen-transforming archaea and bacteria in tropical soils. *Appl. Environ. Microbiol.* 80, 6437–6445. doi: 10.1128/AEM.01778-14

Crecchio, C., and Stotzky, G. (1998). Insecticidal activity and biodegradation of the toxin from *Bacillus thuringiensis* subsp. Kustuki bound to humic acids from soil. *Soil Biol Biochem.* 30, 463–470. doi: 10.1016/S0038-0717(97)00147-8

DeAngelis, K. M., Brodie, E. L., DeSantis, T. Z., Andersen, G. L., Lindow, S. E., and Firestone, M. K. (2009). Selective progressive response of soil microbial community to wild oat roots. *ISME J.* 3, 168–178. doi: 10.1038/ismej.2008.103

Dohrmann, A. B., Küting, M., Jünemann, S., Jaenicke, S., Schlüter, A., and Tebbe, C. C. (2013). Importance of rare taxa for bacterial diversity in the rhizosphere of Bt- and conventional maize. *ISME J.* 7, 37–49. doi: 10.1038/ismej.2012.77

Edgar, R. C., Haas, B. J., Clemente, J. C., Quince, C., and Knight, R. (2011). UCHIME improves sensitivity and speed of chimera detection. *Bioinformatics* 27, 2194–2200. doi: 10.1093/bioinformatics/btr381

Gundersen, P., and Rasmussen, L. (2013). Nitrification in forest soils: effects from nitrogen deposition on soil acidification and aluminum release. *Rev. Environ. Contam. Toxicol.* 113, 1–45.

Hartmann, A., Schmid, M., van Tuinen, D., and Berg, G. (2009). Plant-driven selection of microbes. *Plant Soil* 321, 235–257. doi: 10.1007/s11104-008-9814-y

Hill, G. T., Mitkowski, N. A., Aldrich-Wolfe, L., Emele, L. R., Jurkonie, D. D., Ficke, A., et al. (2000). Methods for assessing the composition and diversity of soil microbial communities. *Appl. Soil Ecol.* 15, 25–36. doi: 10.1016/S0929-1393(00)00069-X

Kennedy, N., Brodie, E., Connolly, J., and Clipson, N. (2004). Impact of lime, nitrogen and plant species on bacterial community structure in grassland microcosm. *Environ. Microbiol.* 6, 1070–1080. doi: 10.1111/j.1462-2920.2004.00638.x

Kennedy, N., Connolly, J., and Clipson, N. (2005). Impact of lime, nitrogen and plant species on fungal community structure in grassland microcosms. *Environ. Microbiol.* 7, 780–788. doi: 10.1111/j.1462-2920.2005.00748.x

Khan, M. S., Sadat, S. U., Jan, A., and Munir, I. (2017). Impact of transgenic *Brassica napus* harboring the antifungal synthetic chitinase (NiC) gene on rhizosphere microbial diversity and enzyme activities. *Front. Plant Sci.* 8:1307. doi: 10.3389/fpls.2017.01307

Kirk, P. L. (1950). Kjeldahl method for total nitrogen. *Anal. Chem.* 22, 354–358. doi: 10.1021/ac60038a038

Knox, O. G. G., Gupta, V. V. S. R., Nehl, D. B., and Stiller, W. N. (2007). Constitutive expression of Cry proteins in roots and border cells of transgenic cotton. *Euphytica* 154, 83–90. doi: 10.1007/s10681-006-9272-7

Lee, S. H., Kim, C. G., and Kang, H. J. (2011). Temporal dynamics of bacterial and fungal communities in a genetically modified (GM) rice ecosystem. *Microb. Ecol.* 61, 646–659. doi: 10.1007/s00248-010-9776-5

Li, P., Dong, J. Y., Yang, S. F., Bai, L., Wang, J. B., Wu, G. G., et al. (2014). Impact of beta-carotene transgenic rice with four synthetic genes on rhizosphere enzyme activities and bacterial communities at different growth stages. *Eur. J. Soil Biol.* 65, 40–46. doi: 10.1016/j.ejsobi.2014.09.002

Li, P., Li, Y. C., Zheng, X. Q., Ding, L. N., Ming, F., Pan, A. H., et al. (2018). Rice straw decomposition affects diversity and dynamics of soil fungal community, but not bacteria. *J. Soils Sediments* 18, 248–258. doi: 10.1007/s11368-017-1749-6

Li, W., and Godzik, A. (2006). Cd-hit: A fast program for clustering and comparing large sets of protein or nucleotide sequences. *Bioinformatics* 22, 1658–1659. doi: 10.1093/bioinformatics/btl158

Lu, R. K. (2000). *Analytical Methods for Soil and Agro-Chemistry*. Beijing: China Agricultural Science and Technology Press, 108–109.

Mendes, R., Garbeva, P., and Raaijmakers, J. M. (2013). The rhizosphere microbiome: significance of plant beneficial, plant pathogenic, and human pathogenic microorganisms. *FEMS Microbiol. Rev.* 37, 634–663. doi: 10.1111/1574-6976.12028

Mitchell, J. I., and Zuccaro, A. (2006). Sequences, the environment and fungi. *Mycologist* 20, 62–74. doi: 10.1016/j.mycol.2005.11.004

National Research Council (2002). *Environmental Effects of Transgenic Plants*. Washington, DC: National Academy Press.

R Core Team (2006). *R: A Language and Environment for Statistical Computing*. Vienna: R Foundation for Statistical Computing.

Rousk, J., Baath, E., Brookes, P. C., Lauber, C. L., Lozupone, C., Caporaso, J. G., et al. (2010). Soil bacterial and fungal communities across a pH gradient in an arable soil. *ISME J.* 4, 1340–1351. doi: 10.1038/ismej.2010.58

Rui, Y. K., Yi, G. X., Zhao, J., Wang, B. M., Li, Z. H., Zhai, Z. X., et al. (2005). Changes of Bt toxin in the rhizosphere of transgenic Bt cotton and its influence on soil functional bacteria. *World J. Microbiol. Biotechnol.* 21, 1279–1284. doi: 10.1007/s11274-005-2303-z

Saxena, D., Flores, S., and Stotzky, G. (1999). Insecticidal toxin in root exudates from Bt corn. *Nature* 402:480. doi: 10.1038/44997

Saxena, D., and Stotzky, G. (2001). *Bacillus thuringiensis* (Bt) toxin released from root exudates and biomass of Bt corn has no apparent effect on earthworms, nematodes, protozoa, bacteria, and fungi in soil. *Soil Biol Biochem.* 33, 1225–1230. doi: 10.1016/S0038-0717(01)00027-X

Schloss, P. D., Westcott, S. L., Ryabin, T., Hall, J. R., Hartmann, M., Hollister, E. B., et al. (2009). Introducing mothur: open-source, platform-independent, community-supported software for describing and comparing microbial communities. *Appl. Environ. Microbiol.* 75, 7537–7541. doi: 10.1128/AEM.01541-09

Sohn, S. I., Oh, Y. J., Kim, B. Y., and Cho, H. S. (2016). Effects of CaMSRB2-expressing transgenic rice cultivation on soil microbial communities. *J. Microbiol. Biotechnol.* 26, 1303–1310. doi: 10.4014/jmb.1601.01058

Somers, E., Vanderleyden, J., and Srinivisam, M. (2004). Rhizospherebacterial signaling: a love parade beneath our feet. *Crit. Microbiol.* 30, 205–240. doi: 10.1080/10408410490468786

Subbiah, B. V., and Asija, G. L. (1956). A rapid procedure for the estimation of available nitrogen in soils. *Curr. Sci.* 25, 518–522.

Suzuki, M. T., Taylor, L. T., and DeLong, E. F. (2000). Quantitative analysis of small subunit rRNA genes in mixed microbial populations via 5'-nuclease assays. *Appl. Environ. Microbiol.* 66, 4605–4614. doi: 10.1128/AEM.66.11.4605-4614.2000

Taylor, D. L., Herriott, I. C., Stone, K. E., McFarlan, J. W., Booth, M. G., and Leigh, M. B. (2010). Structure and resilience of fungal communities in Alaskan boreal forest soils. *Can. J. For. Res.* 40, 1288–1301. doi: 10.1139/X10-081

Turrini, A., Sbrana, C., and Giovannetti, M. (2015). Belowground environmental effects of transgenic crops: a soil microbial Perspective. *Res. Microbiol.* 166, 121–131. doi: 10.1016/j.resmic.2015.02.006

Valldor, P., Graff, R. M., Martens, R., and Tebbe, C. C. (2015). Fate of the insecticidal Cry1Ab protein of GM crops in two agricultural soils as revealed by 14C-tracer studies. *Appl. Microbiol. Biotechnol.* 99, 7333–7341. doi: 10.1007/s00253-015-6655-5

Ye, S. F., Li, T. F., Liu, G. L., and Luo, L. J. (2012). Production and identification of water-saving and drought-resistant transgenic indica-type rice with cry1C gene. *Acta Agric. Shanghai* 28, 1–3.

Conflict of Interest Statement: The authors declare that the research was conducted in the absence of any commercial or financial relationships that could be construed as a potential conflict of interest.

Advantages of publishing in Frontiers

OPEN ACCESS
Articles are free to read for greatest visibility and readership

FAST PUBLICATION
Around 90 days from submission to decision

HIGH QUALITY PEER-REVIEW
Rigorous, collaborative, and constructive peer-review

TRANSPARENT PEER-REVIEW
Editors and reviewers acknowledged by name on published articles

Frontiers
Avenue du Tribunal-Fédéral 34
1005 Lausanne | Switzerland

Visit us: www.frontiersin.org
Contact us: info@frontiersin.org | +41 21 510 17 00

REPRODUCIBILITY OF RESEARCH
Support open data and methods to enhance research reproducibility

DIGITAL PUBLISHING
Articles designed for optimal readership across devices

FOLLOW US
@frontiersin

IMPACT METRICS
Advanced article metrics track visibility across digital media

EXTENSIVE PROMOTION
Marketing and promotion of impactful research

LOOP RESEARCH NETWORK
Our network increases your article's readership